

DO NOT REMOVE FROM  
THE RESEARCH OFFICE

# **ANALYTICAL MODELING OF FOUNDATIONS FOR SEISMIC ANALYSIS OF BRIDGES**

WA-RD 328.2

Final Technical Report  
February 1994



**Washington State  
Department of Transportation**

Washington State Transportation Commission  
Transit, Research, and Intermodal Planning (TRIP) Division  
in cooperation with the U.S. Department of Transportation  
Federal Highway Administration

## TECHNICAL REPORT STANDARD TITLE PAGE

1. REPORT NO. <b>WA-RD 328.2</b>	2. GOVERNMENT ACCESSION NO.	3. RECIPIENT'S CATALOG NO.	
4. TITLE AND SUBTITLE <b>Analytical Modeling of Foundations for Seismic Analysis of Bridges</b>		5. REPORT DATE <b>February 1994</b>	
		6. PERFORMING ORGANIZATION CODE	
7. AUTHOR(S) <b>William F. Cofer, David I. McLean and Jeffrey W. McGuire</b>		8. PERFORMING ORGANIZATION REPORT NO.	
9. PERFORMING ORGANIZATION NAME AND ADDRESS <b>Washington State Transportation Center (TRAC) Civil and Environmental Engineering; Sloan Hall, Room 101 Washington State University Pullman, Washington 99164</b>		10. WORK UNIT NO.	
		11. CONTRACT OR GRANT NO. <b>T9234 Task 02</b>	
12. SPONSORING AGENCY NAME AND ADDRESS <b>Washington State Department of Transportation Transportation Building, MS 7370 Olympia, Washington 98504-4730</b>		13. TYPE OF REPORT AND PERIOD COVERED <b>Final Technical Report</b>	
		14. SPONSORING AGENCY CODE	
15. SUPPLEMENTARY NOTES <b>This study was conducted in cooperation with the U.S. Department of Transportation, Federal Highway Administration.</b>			
16. ABSTRACT <p>The response of bridges when subjected to seismic excitation may be significantly influenced by the dynamic properties of their foundations. With current design practice, foundation elements are typically considered as elastic springs without consideration of material and radiation damping.</p> <p>The objectives of this research were to identify general foundation models that are suitable for modeling soil-structure interaction in seismic bridge analysis, to modify an existing nonlinear seismic bridge analysis computer program to include a new element capable of representing such models, and to conduct a parametric study to assess the effect of the increased energy dissipation mechanisms on the response of bridge substructures.</p> <p>For spread footing foundations, three different models were identified and applied to a typical two-column bridge bent. For pile foundations, four models were derived and applied to a five-column bent. The seismic response for each model was compared with conventional elastic and fixed-base models. Several soil stiffness values and earthquake records were considered for analysis. Maximum values of displacement, plastic hinge rotation, and cumulative plastic hinge rotations were noted and compared.</p> <p>It was concluded that the use of the foundation models can produce an important change in the bridge response when compared to that of the fixed-base model, depending on the frequency content of the earthquake and the stiffness of the soil. The effects of radiation damping were observed to be insignificant for foundations on stiff soil, but important for those on soft soil. In addition, the performance of the simpler damped foundation models was found to be quite similar to that of the more complex models.</p>			
17. KEY WORDS <b>bridge, earthquakes, soil-structure interaction, foundation, analysis, modeling</b>		18. DISTRIBUTION STATEMENT <b>No restrictions. This document is available to the public through the National Technical Information Service, Springfield, VA 22616</b>	
19. SECURITY CLASSIF. (of this report) <b>None</b>	20. SECURITY CLASSIF. (of this page) <b>None</b>	21. NO. OF PAGES <b>339</b>	22. PRICE

**Final Technical Report**  
for  
Research Project T9234-02  
"Bridge Foundations - Seismic Analysis"

**ANALYTICAL MODELING OF FOUNDATIONS  
FOR SEISMIC ANALYSIS OF BRIDGES**

by

Dr. William F. Cofer, Dr. David I. McLean and Jeffrey W. McGuire  
**Washington State Transportation Center (TRAC)**  
Washington State University  
Department of Civil & Environmental Engineering  
Pullman, WA 99164-2910

Washington State Department of Transportation  
Technical Monitor  
Mark R. Wallace  
Bridge Design Engineer

Prepared for

**Washington State Transportation Commission**  
Department of Transportation  
and in cooperation with  
**U.S. Department of Transportation**  
Federal Highway Administration

February 1994

## **Disclaimer**

The contents of this report reflect the views of the authors, who are responsible for the facts and the accuracy of the data presented herein. The contents do not necessarily reflect the official views or policies of the Washington State Department of Transportation. This report does not constitute a standard, specification, or regulation.

# Table of Contents

Section	Page
<b>Disclaimer</b> .....	iii
<b>Table of Contents</b> .....	iv
<b>List of Figures</b> .....	vi
<b>Summary</b> .....	xi
<b>Chapter 1: Introduction</b> .....	1
1.1 Context and Problem Statement .....	1
1.2 Research Objectives .....	3
<b>Chapter 2: Research Approach</b> .....	5
2.1 Introduction .....	5
2.1.1 Soil–Structure Interaction .....	6
2.1.2 Half-Space Analogy .....	10
2.1.3 Spread Footing Foundation Models .....	11
2.1.4 Pile Foundation Models .....	27
2.2 Modification of NEABS .....	32
2.2.1 Description of NEABS .....	33
2.2.2 Discrete Foundation Element Capabilities .....	35
2.2.3 Discrete Foundation Element Implementation .....	43
2.2.4 Discrete Foundation Element Verification .....	43
<b>Chapter 3: Findings and Interpretation</b> .....	59
3.1 Parametric Study Approach and Objectives .....	59
3.2 Spread Footing Foundation Study .....	61
3.2.1 Description of Bridge and Site .....	61
3.2.2 Structure Model .....	66
3.2.3 Foundation Models .....	73
3.2.4 Seismic Excitation .....	75
3.2.5 Discussion of Results .....	80
3.3 Pile Foundation Study .....	94
3.3.1 Description of Bridge and Site .....	95
3.3.2 Structure Model .....	100
3.3.3 Foundation Models .....	104
3.3.4 Seismic Excitation .....	109
3.3.5 Discussion of Results .....	110

<b>Section</b>	<b>Page</b>
<b>Chapter 4: Conclusions</b> .....	125
4.1 Summary and Conclusions .....	125
4.2 Recommendations and Implementation .....	130
<b>Acknowledgments</b> .....	132
<b>References</b> .....	133
<b>Appendix A: NEABS User's Guide Supplement</b> .....	138
<b>Appendix B: Example NEABS Analysis     Incorporating DF Element</b> .....	141
<b>Appendix C: DF Element Subroutines Added     to NEABS Coding</b> .....	170
<b>Appendix D: Spread Footing Foundation Study</b> .....	194
<b>Appendix E: Pile Foundation Study</b> .....	300

## List of Figures

Figure	Page
2.1: Soil–structure interaction mechanisms: (a) modification of the site free-field motions due to the response of the soil layer; (b) kinematic interaction of the soil layer and foundation stiffness; (c) inertial response of the structure causing further interaction. Adapted from [25]. . . . .	7
2.2: Modeling the disk–half-space continuum system as a discrete system: (top) equivalent static spring produces the same static displacements; (bottom) selection of parameters $k$ , $c$ , and $m$ to produce the same displacement response to harmonic loading. . . . .	12
2.3: Graphs showing the dependence of Veletsos and Wei’s $\alpha$ and $\beta$ parameters (ordinates) on the applied harmonic loading frequency parameter, $a_0$ (abscissae). Graphs show $\alpha$ and $\beta$ for horizontal translation and rocking d.o.f. for two Poisson ratios (P.R. $\equiv \nu = 0.33$ and $\nu = 0.45$ ). . . . .	16
2.4: Four discrete models of the elastic half-space system: (a) spring–mass–dashpot model, three parameters; (b) Meek and Veletsos model, five parameters [31]; (c) Wolf and Paronesso model, nine parameters [32]; and (d) Jean <i>et al.</i> model, eleven parameters [33]. . . . .	20
2.5: Pais and Kausel embedded prismatic foundation [31]. . . . .	23
2.6: Shape factor and embedment factor functions, $s_i$ and $h_i$ , for the Pais and Kausel prismatic foundation model. . . . .	26
2.7: Soil–pile model proposed by Nogami <i>et al.</i> [37]: (top) Winkler foundation with three soil reaction models at each level: (bottom) soil near-field and far-field models. . . . .	28
2.8: Nogami and Konagai soil–pile model: (top) soil–pile interface model to represent gap development; (bottom) variation of the model stiffness/damping and mass parameters, $\xi_{sd}$ and $\xi_m$ , with Poisson’s ratio. . . . .	29

Figure	Page
2.9: Pictorial representation of the DF element. . . . .	36
2.10: DF element nonlinear stiffness capabilities: (a) bilinear hysteresis; (b) elastic stiffness degradation; (c) strain hardening options. . . . .	38
2.11: DF element nonlinear stiffness capabilities: gap development and in-gap hysteretic behavior. . . . .	41
2.12: NEABS subroutine organization diagram: shaded bubbles indicate the subroutines present in the code as-delivered; open bubbles indicate the subroutines added. . . . .	44
2.13: Elastic stiffness response verification test, force loads. . . . .	46
2.14: Elastic stiffness response verification test, moment loads. . . . .	47
2.15: Spatial orientation response invariance verification test, force loads. . . . .	48
2.16: Spatial orientation response invariance verification test, moment loads. . . . .	50
2.17: Mass-gravitational field modeling verification test. . . . .	51
2.18: Connectivity verification test. . . . .	53
2.19: Resonant harmonic excitation dynamic response verification test. . . . .	55
2.20: Nonlinear stiffness properties verification tests: (top) bilinear hysteresis with elastic stiffness degradation; (bottom) strain hardening options. . . . .	57
2.21: Nonlinear stiffness properties verification tests: (top) bilinear hysteresis with gap development; (bottom) bilinear hysteresis within gap. . . . .	58
3.1: Interstate 90 three-span bridge near Moses Lake: (top) photograph showing elevation view of bridge; (bottom) plan view drawing of bridge and site. Adapted from [40] and [39]. . . . .	62



Figure	Page
3.2: Moses Lake bridge bent column, crossbeam, and spread footing foundation details. Adapted from [39]. . . . .	64
3.3: Schematic of the NEABS models of the Moses Lake bridge bent and supports employed: (a) model of the bent structure, with beam elements forming columns and crossbeam; (b) five support models—fixed supports and four models representing spread footing foundations. . . . .	67
3.4: Calculated and assumed strength characteristics of Moses Lake bridge bent columns. Axial force–bending moment strength interaction curve taken at attainment of concrete strain of 0.003 in./in., and bending moment–curvature curve taken at static axial load of 236 kips. . . . .	70
3.5: Complete acceleration history plots of the El Centro and Olympia records. . . . .	77
3.6: El Centro record: acceleration plot of duration modeled and acceleration response spectra. . . . .	78
3.7: Olympia record: acceleration plot of duration modeled and acceleration response spectra. . . . .	79
3.8: Matrix of the 52 NEABS analysis runs for the study of spread footing models. Each run is identified by a name of the form “SF $nn$ – $fff$ . $see$ ,” where $nn$ is the run number, $fff$ is the foundation model code, $s$ is the soil stiffness code, and $ee$ is the applied seismic record code. . . . .	82
3.9: Typical results: time histories of column drift (relative lateral displacement between column top and bottom) and of the internal moment at the column top. . . . .	83
3.10: Typical results: Column moment–drift hysteresis and time history of the rotation of the plastic hinge at the column top. . . . .	84

Figure	Page
3.11: Comparison of effect of foundation model and soil stiffness on response of plastic hinge at column top during lower intensity El Centro record excitation: (top) maximum rotation attained (related to ductility demand); (bottom) total rotation sustained (related to energy demand). . . . .	87
3.12: Comparison of effect of foundation model and soil stiffness on response of plastic hinge at column top during higher intensity El Centro record excitation: (top) maximum rotation attained (related to ductility demand); (bottom) total rotation sustained (related to energy demand). . . . .	88
3.13: Comparison of effect of foundation model and soil stiffness on response of plastic hinge at column top during lower intensity Olympia record excitation: (top) maximum rotation attained (related to ductility demand); (bottom) total rotation sustained (related to energy demand). . . . .	89
3.14: Comparison of effect of foundation model and soil stiffness on response of plastic hinge at column top during higher intensity Olympia record excitation: (top) maximum rotation attained (related to ductility demand); (bottom) total rotation sustained (related to energy demand). . . . .	90
3.15: Interstate 90 bridge over Mercer Slough: (top) Aerial photograph showing the west- and eastbound Interstate 90 bridges and collector bridges; (bottom) Typical bridge longitudinal- and cross-sections. Adapted from [26] and [44]. . . . .	96
3.16: Mercer Slough: (top) approximate soil profile of Mercer Slough along alignment of Interstate 90, with seismic response zones as identified by Kramer [27]; (bottom) static pile head stiffness diagram for 8-inch diameter test pile as reported by Kramer [27]. . . . .	97
3.17: Mercer Slough bridge bent columns and pile cap details. Adapted from [44]. . . . .	99

Figure	Page
3.18: Schematic of NEABS models of Mercer Slough bridge bent and supports employed: (a) model of bent structure, with beam elements forming columns and crossbeam; (b) five support models—fixed supports and four models representing pile foundations. . . . .	101
3.19: Calculated and assumed strength characteristics of Mercer Slough bridge bent columns. Axial force–bending moment strength interaction curve taken at attainment of concrete strain of 0.003 in./in., and bending moment–curvature curve taken at static axial load of 60 kips. . . . .	102
3.20: El Centro, Zone 3 record: acceleration plot of duration modeled and acceleration response spectra. . . . .	111
3.21: El Centro, Zone 4 record: acceleration plot of duration modeled and acceleration response spectra. . . . .	112
3.22: Lake Hughes, Zone 1 record: acceleration plot of duration modeled and acceleration response spectra. . . . .	113
3.23: Lake Hughes, Zone 2 record: acceleration plot of duration modeled and acceleration response spectra. . . . .	114
3.24: Matrix of the 25 NEABS analysis runs for the study of pile foundation models. Each run is identified by a name of the form “PFnn-fff.eee,” where nn is the run number, fff is the foundation model code, and eee is the applied seismic record code. . . . .	116
3.25: Comparison of the effect of the foundation models on the response of the column when the subjected to the filtered seismic records: (top) column drift maxima; (bottom) column top internal moment maxima. . . . .	118
3.26: Comparison of the effect of foundation models on the response of the column top plastic hinge when subjected to the unfiltered seismic records: (top) maximum rotation attained (related to ductility demand); (bottom) total rotation sustained (related to energy demand). . . . .	119

## **Summary**

The response of bridges when subjected to seismic excitation may be significantly influenced by a number of mechanisms that are not currently incorporated into typical analysis methods. In particular, the dynamic interaction of the bridge foundations with the founding soil is the subject of the research presented in this report.

The objectives of the research were to determine foundation models suitable for incorporation into the seismic analysis of highway bridges, to modify the nonlinear seismic bridge analysis computer program NEABS to include a new element capable of representing the foundation models, and to conduct a parametric study to assess the performance of the foundation models relative to conventional fixed-base analysis in terms of their effects on the seismic response of two bridge bents.

Four models applicable to modeling spread footing foundations and four models applicable to modeling pile foundations were identified. A new element to represent these foundation models and other nonlinear soil reaction mechanisms, the "Discrete Foundation element," was designed and implemented within NEABS.

Two bents from Washington bridges were selected to be the subjects of the parametric study, one supported on the spread footing models, the other on the pile foundation models. Various seismic records were applied

to the bents in the transverse direction and the response of each bent was studied.

It was concluded that inclusion of the foundation models can produce a significant difference in predicted bridge response, depending on the frequency content of the earthquake and the stiffness of the soil. In some cases, the fixed-base bent models resulted in column demands that were unconservative compared with those obtained using the foundation models. Relatively simple models were found to be adequate for modeling both spread footing and pile foundations. NEABS, equipped with the Discrete Foundation element, is capable of being used to further explore the effects of soil–foundation interaction on the seismic response of bridges.

## **Chapter 1**

# **Introduction**

### **1.1 Context and Problem Statement**

The response of bridges when subjected to seismic excitation may be significantly influenced by a number of mechanisms that are not currently incorporated into typical analysis methods. The interaction of the bridge superstructure with the abutments has been the cause of significant damage in past earthquakes [1 and 2]. Although damage to other foundation elements, such as spread footings and pile caps, has been shown to be minimal, the dynamic characteristics of these components have important effects on the behavior of the bridge [3, 4, 5, and 2], especially when the founding soil is soft [6]. Current design practice does not consider the effects of soil–structure interaction [7], and little emphasis is placed upon studying the role of foundations in the seismic analysis of bridges [2 and 8]. Current design guidance is simplistic in that the foundation elements are considered to behave as linear springs [9 and 2], although research has shown that a significant amount of seismic energy is dissipated through the material and radiation damping associated with

the founding material [10]. The effects of expansion joint gaps and the material nonlinearity of the soil at the abutments are approximated by manually varying the support spring constants such that the soil strength is not exceeded. However, important additional nonlinearities at abutments result from the force developed in the abutment key [5] and the energy loss due to impact during expansion joint gap closure [11]. The assumption of elastic springs at the abutments has been reported to be unconservative [12].

The influence of pile foundations has been included through the use of coupled translational and rotational springs. Nonlinearities arise from inelastic soil behavior and connection details at the pile cap [3]. Other important effects include the dissipation of energy due to outward propagation of waves induced in the soil by the vibration of the structure (referred to as “radiation” damping), the degradation of soil stiffness that occurs during cyclic loading [13], the loss of strength in the soil due to liquefaction, and the influence of pile group behavior. In addition, hysteretic damping may be intentionally included in the bridge design through the use of base isolation techniques [14, 15, and 16].

For certain bridge configurations, the assumption that the seismic excitation is uniform at all supports is not valid [17]. Differential movements may be introduced that tend to alter, and possibly amplify, the response [18]. Typically, asynchronous ground motion, or ground motion which is not uniform at all supports, is important for long bridges, such as

suspension and some arch bridges [19, 20, 21, and 22]. However, this effect can also be significant for foundations in which soil properties vary greatly between supports.

Currently, Washington State Department of Transportation (WSDOT) engineers use the computer program, SEISAB-I [23], to perform the seismic analysis of bridges. SEISAB-I is convenient because it was developed specifically for bridges with features that correspond directly to field data and to design guidance documents. However, this program has the capability to perform elastic analyses only. Energy dissipation is accomplished through “Rayleigh”, or “proportional” damping, in which a unique damping coefficient is assigned to each of the structure’s modes of vibration. Concentrated dampers, such as those that would occur at foundations, are not documented.

As an alternative to SEISAB-I for the seismic analysis of bridges, the computer program NEABS [24] was obtained for this research project. As delivered, it has the ability to incorporate into the analysis plastic column end hinging, elastic supports, a nonlinear expansion joint element, and multiple support excitations.

## **1.2 Research Objectives**

The capability to more realistically model soil–foundation interaction mechanisms in the analysis of bridge seismic response is desired. Toward



that end, the objectives of this research were as follows:

1. To review and evaluate techniques that are employed to model soil-structure interaction and to identify models appropriate for representing typical bridge foundations.
2. To modify the nonlinear bridge analysis program NEABS, adding a new element capable of representing the foundation models and nonlinear soil mechanisms.
3. To evaluate the foundation models in terms of their effects on the predicted seismic response of bridges.

This report documents the findings of the research. Chapter Two, "Research Approach," discusses proposed foundation models, and describes the modification of NEABS to include the new "discrete foundation" (DF) element. A parametric study of the effects of the foundation models, using the DF element, on the predicted seismic response of two Washington bridges is presented in Chapter Three, "Findings and Interpretation." Based on the results of the parametric study, conclusions and recommendations pertinent to seismic bridge analysis needs of the Washington Department of Transportation (WSDOT) are developed in Chapter Four "Conclusions", as well as guidance on the implementation of NEABS for the seismic analysis of bridges.

## **Chapter 2**

# **Research Approach**

## **2.1 Introduction**

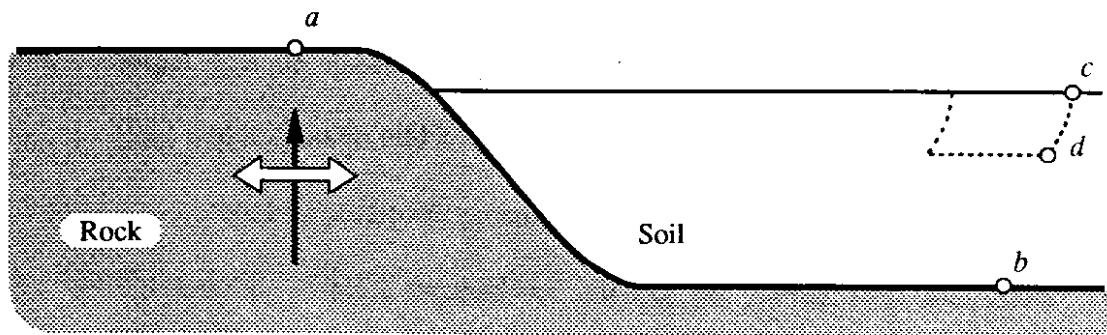
In this chapter, analytical models of foundations that have been used by various researchers are presented, and the modification of the bridge analysis program NEABS to accommodate these methods is described. First, the dynamic interaction of a structure and its founding soil is discussed qualitatively. Next, the soil–foundation modeling concept of the “half-space” is introduced. Various researchers have used this concept to construct discrete foundation models applicable to the dynamic analysis of structures founded on spread footing or pile foundations. The analysis program NEABS was used in the present research project to investigate the effects of these models on the seismic response of bridges. In order to incorporate the foundation models in NEABS analyses, the program was modified to include a new element capable of representing the models’ behavior. The NEABS program and the new element that was added are described, as well as the testing program undertaken to verify the new element’s performance.

### 2.1.1 Soil-Structure Interaction

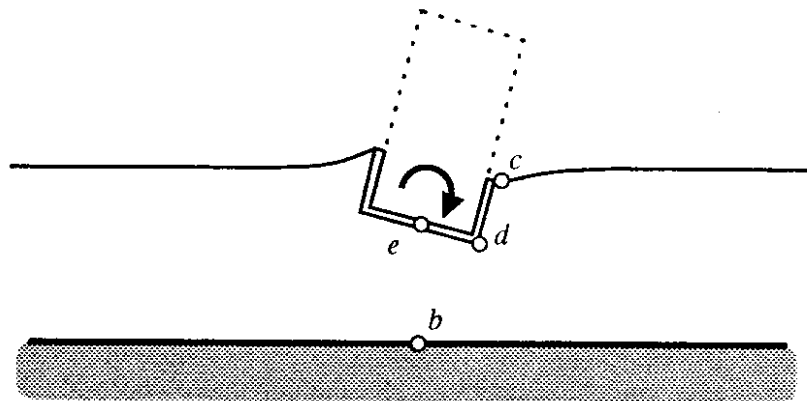
The influence of a bridge's foundations on the dynamic response of the bridge is an example of what is termed "soil-structure interaction." This phenomenon has been the subject of research dating from the early 1900's, but it has received increasing attention since the 1970's. To gain a general understanding of the issues involved in soil-structure interaction, the following discussion focuses on three component mechanisms of soil-structure interaction, following Wolf [25].

Figure 2.1 shows a structure founded on a soil layer which overlies bedrock. The bedrock, assumed to be essentially rigid, is subjected to vertically propagating horizontal excitations, which are recorded at point *a* of Figure 2.1(a). Point *b*, which lies on the bedrock-soil layer interface directly underneath the structure, may be expected to experience the same motions as point *a*. However, because of the response of the soil layer to the bedrock excitation, the ground motions at points *c* and *d* that would be recorded at the structure site without the presence of the structure, called the site "free-field" motions, would in general be different from each other, and often greater than those recorded at point *a*. Because it is the site free-field motions which are relevant to determining the response of the structure, recorded earthquake motions may not be applicable as seismic input to a discrete analysis of the structure if the structure's founding conditions are significantly different from those at the location of the

(a) Site Free-Field Motions



(b) Kinematic Interaction



(c) Inertial Interaction

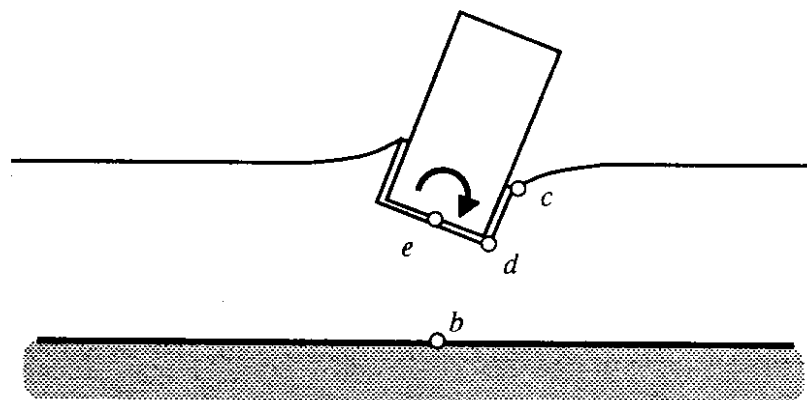


**Figure 2.1:** Soil–structure interaction mechanisms: (a) modification of the site free-field motions due to the response of the soil layer; (b) kinematic interaction of the soil layer and foundation stiffness; (c) inertial response of the structure causing further interaction. Adapted from [25].

recording instrument. As an example, in the study by McLean and Cannon of the seismic response of the westbound Interstate 90 bridge over the Mercer Slough [26], it was found necessary to use input excitation records obtained by a seismic analysis of the slough itself [27].

Kinematic interaction is caused by coupling the structure foundation with the soil layer, as shown in Figure 2.1(b). The stiffness of the foundation will modify the site free-field motions at points *c* and *d*, causing some averaging of the translational component and the introduction of a rotational component, as shown at point *e*. It is seen that this causes a different vertical distribution of lateral forces on the structure than would be experienced had the structure been founded on bedrock. Inertial interaction, shown in Figure 2.1(c), arises when the structure, with its stiffness, damping, and mass characteristics, is introduced. As the structure reacts to the imposition of the kinematic interaction-modified motions, forces are transmitted to the soil through the foundation, causing deformation of the soil and further modification of the motion at points *c*, *d*, and *e*.

Three commonly exhibited effects of these mechanisms may be identified [25]. First, the site free-field translational response is amplified and a rocking component is introduced. Second, the flexibility of the total dynamic system (which includes both the structure and the founding soil), and the corresponding natural period, is increased. Third, damping in the total system is increased, due to both the material hysteretic action of the

soil and to what is termed “radiation,” or “geometric” damping. This refers to the apparent damping of the system caused by the radiation of energy away from the structure in the form of outward-propagating waves.

To obtain the seismic response of a structure, it is common to employ analysis techniques that mathematically discretize the structure, such as computer programs using the finite element method. Two general approaches are available for rationally incorporating soil–structure interaction, or at least its effects, into this type of structural analysis [25]. In the “direct method,” the structure and the founding soil, or at least as much of the soil as is feasible, are incorporated into the finite element mesh. Conceptually, this is the simplest approach, but several drawbacks make its use prohibitive for all but the most extreme analysis demands. Because both the soil and the structure are modeled, the system may contain many more degrees-of-freedom than the structure alone, making the analysis computationally expensive. Developing appropriate soil elements based on available soil data may also be difficult. Additionally, the finite soil–structure system model restricts the outward propagation of soil waves that occurs in the essentially infinite real system, unless “boundary elements” or “infinite elements” are used at the system boundary to artificially model this effect. Failure to compensate for this boundary problem has the effect of unrealistically reducing the effective damping of the system model.

An approach more amenable for common structural analysis is the “substructure method.” In this method, the structure and the soil are analyzed separately. First, the soil is analyzed alone, loaded dynamically at the interface between the soil and the structure. This system is analyzed in terms of the response of the interface to determine the effective dynamic characteristics of the soil that the structure will experience. Next, a simplified model is used to reproduce, or approximate, the behavior of the soil at the interface. This simplified model is then coupled with the structure model at the interface, and the structure–simplified model system is analyzed.

Rather than developing simplified soil–structure interface models for every structure to be analyzed, it is more practical to use models that have already been developed for this purpose. A number of these models will be presented in the following sections.

### *2.1.2 Half-Space Analogy*

In order to create a simplified soil–structure interface model, the response of the soil at the interface must first be obtained. One of the most common analytical methods of doing this is to model the soil as an elastic or visco-elastic “half-space” continuum. The half-space continuum is a mathematical idealization of the soil as a medium with a flat surface extending horizontally in all directions to infinity, and having infinite depth. The half-space is assumed to have mechanical properties which

correspond to those of the soil; the elastic half-space is assigned a mass density,  $\rho$ , a shear modulus,  $G$ , and a Poisson's ratio,  $\nu$ . The half-space may be made visco-elastic (corresponding to an effective viscous soil material damping) by also giving it a viscous damping ratio,  $\xi$ .

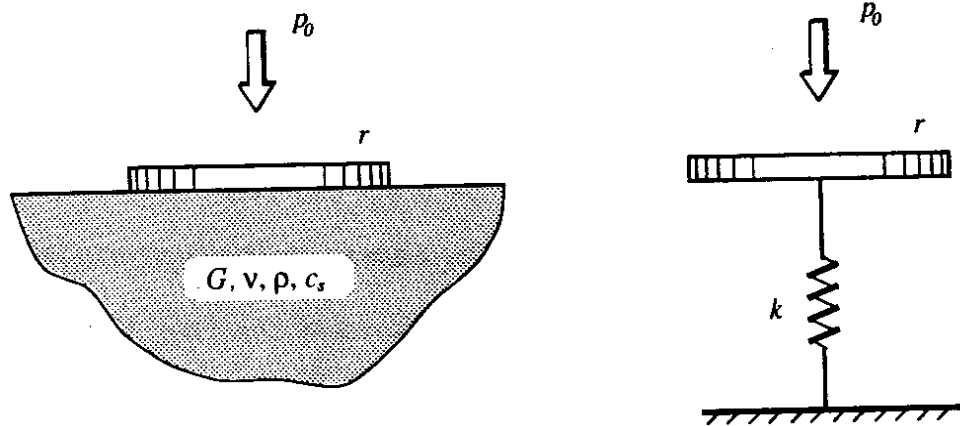
The response of the half-space may be analyzed using continuum mechanics, as will be discussed. Since the half-space continuum is a semi-infinite model, it does not have the energy reflecting boundary problem inherent in a finite element discretization of the soil. Thus, the elastic half-space correctly models radiation damping, given the assumption of soil linear elasticity. However, the constraint to elastic behavior renders the half-space continuum model more applicable for representing the soil away from the immediate vicinity of the structure (the soil "far-field"), since the behavior of the soil near the structure (the soil "near-field") is often nonlinear under seismic conditions.

### *2.1.3 Spread Footing Foundation Models*

The method in which the half-space continuum model is used to create simplified discrete interface models applicable to representing spread footing foundations is illustrated in Figure 2.2. As shown, a rigid disk of radius  $r$ , representing the structure foundation, is assumed to be bonded to the surface of the half-space. The half-space, or soil, is assigned



(a) Static



(b) Dynamic

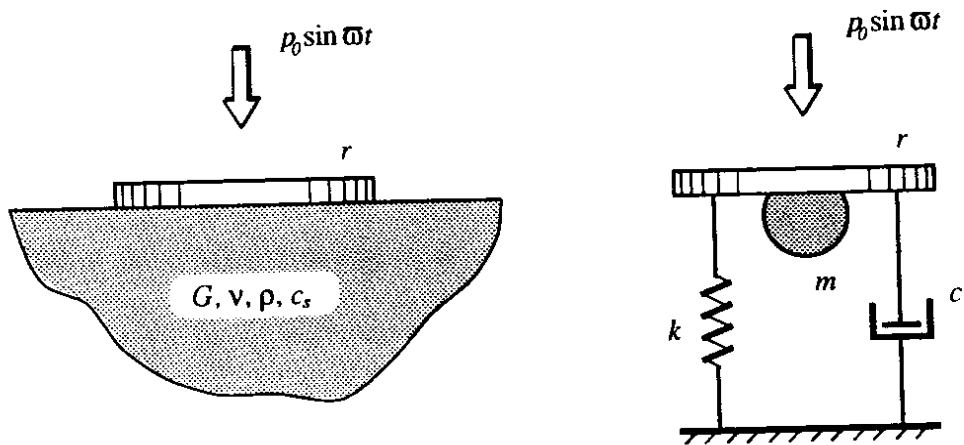


**Figure 2.2:** Modeling the disk-half-space continuum system as a discrete system: (top) equivalent static spring produces the same static displacements; (bottom) selection of parameters  $k$ ,  $c$ , and  $m$  to produce the same displacement response to harmonic loading.

the properties discussed earlier, as well as a shear wave velocity,  $c_s$ , which is related to the soil mass density and shear modulus as follows:

$$c_s = \sqrt{\frac{G}{\rho}} \quad (2.1)$$

The disk-half-space system is subjected to either a static or a dynamic load, and the disk response is obtained using continuum mechanics. The parameters of a discrete system are then selected to produce the same response. The discrete system serves as the interface model in the analysis of the structure itself, incorporating the effects of soil-structure interaction. This approach was used as early as 1904, as documented by Richart *et al.* [28]. This reference provides an excellent review of the development of the half-space model, as well as other soil-structure interaction issues, prior to 1970.

When the applied loading is static, the equivalent discrete model uses springs to represent the half-space static stiffness. Because the disk and the half-space are axially symmetric, the disk has four degrees-of-freedom: horizontal and vertical translation, rocking (rotation about a horizontal axis), and torsional rotation (rotation about the vertical axis). Four uncoupled springs are used to represent the half-space static stiffness, one spring being applied to each degree-of-freedom. Such a static discrete model is represented in Figure 2.2. The figure shows the vertical spring only, it being understood that the model's configuration is the same in each

of the four degrees-of-freedom. The stiffness of the springs are selected to produce the same static displacements as those experienced by the disk on the half-space. These static stiffnesses are well established in the literature as follows:

$$\begin{aligned}
 k_x^s &= \frac{8G}{2 - \nu} r && \text{horizontal translation} \\
 k_z^s &= \frac{4G}{1 - \nu} r && \text{vertical translation} \\
 k_{\theta_x}^s &= \frac{8G}{3(1 - \nu)} r^3 && \text{rocking rotation} \\
 k_{\theta_z}^s &= \frac{16}{3} Gr^3 && \text{torsional rotation}
 \end{aligned} \tag{2.2}$$

where  $k_i^s \equiv$  equivalent static spring stiffness for the  $i^{\text{th}}$  degree-of-freedom

$r \equiv$  radius of disk

$G \equiv$  shear modulus of the half-space (soil)

$\nu \equiv$  Poisson's ratio of the half-space (soil)

When the loading is dynamic, a more complicated discrete model is required. Because the continuum mechanics analysis of the dynamically loaded disk-half-space is typically carried out in the frequency domain, the dynamic load is formed as the superposition of a series of harmonic loads. Figure 2.2 shows a harmonic load being applied to the disk-half-space system and to a simple discrete system utilizing a spring, mass, and dashpot acting in the vertical degree-of-freedom. Again, the model's

configuration in the other three degrees-of-freedom is the same as in the vertical degree-of-freedom. Values for these three discrete model parameters are selected to produce the same displacement response as that experienced by the disk–half-space system. Veletsos and Verbič report that only two of these three discrete model parameters are independent, so the spring stiffness may arbitrarily, but conveniently, be set to the value of the static spring stiffness [29]. They then express the discrete system parameters as follows:

$$\begin{aligned}
 k_i &= k_i^s \\
 c_i &= \beta_i k_i^s \left( \frac{r}{c_s} \right)^2 \\
 m_i &= \gamma_i k_i^s \left( \frac{r}{c_s} \right)^2, \quad \gamma_i = \left( \frac{1 - \alpha_i}{a_0^2} \right)
 \end{aligned} \tag{2.3}$$

where  $c_s$   $\equiv$  shear wave velocity of the half-space (soil)

$a_0$   $\equiv$  dimensionless loading frequency parameter;  $a_0 \equiv \omega r / c_s$

$k_i, c_i, m_i$   $\equiv$  stiffness, damping, and mass parameters for the equivalent discrete system

$\alpha_i, \beta_i$   $\equiv$  dimensionless coefficients

The value of the coefficients  $\alpha_i$  and  $\beta_i$  depend upon Poisson's ratio of the soil and upon the frequency of the loading. As an example of this dependency, Figure 2.3 shows plots of  $\alpha_i$  and  $\beta_i$  versus the dimensionless loading frequency parameter,  $a_0$ , as determined by Veletsos and Wei [30],

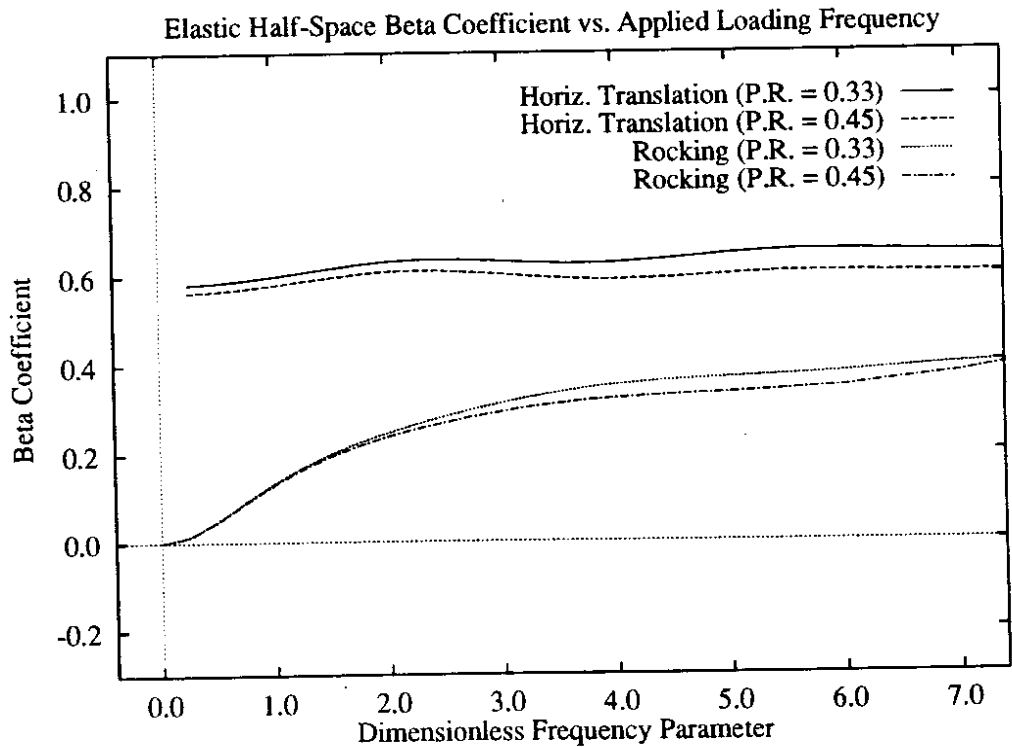
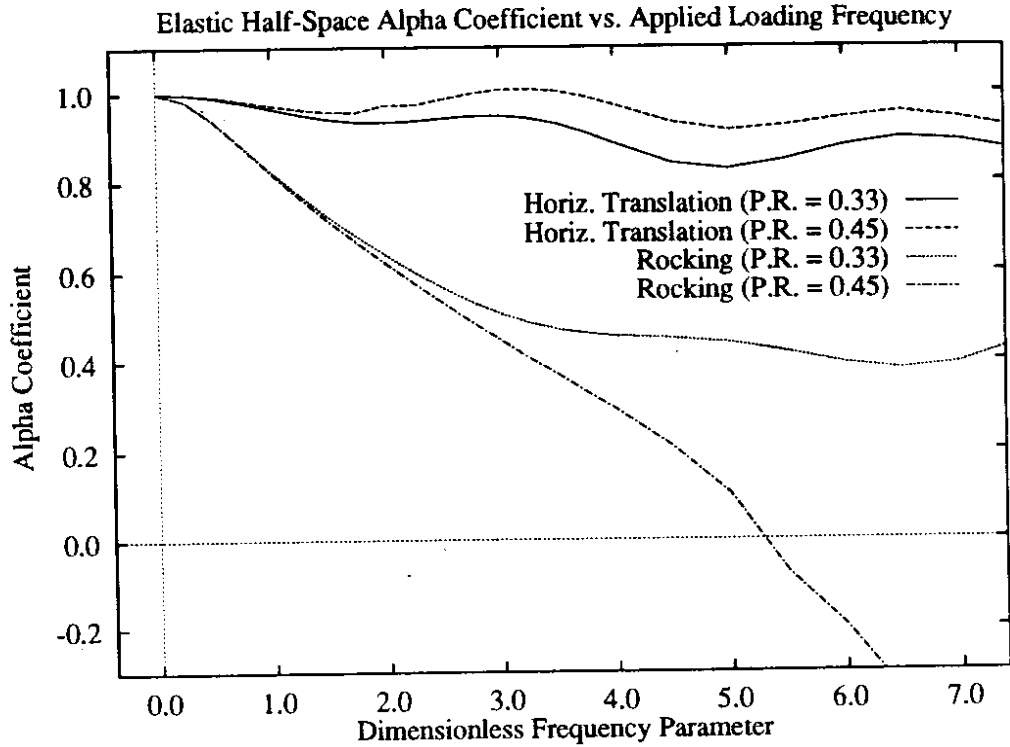


**Figure 2.3:** Graphs showing the dependence of Veletsos and Wei's  $\alpha$  and  $\beta$  parameters (ordinates) on the applied harmonic loading frequency parameter,  $a_0$  (abscissae). Graphs show  $\alpha$  and  $\beta$  for horizontal translation and rocking d.o.f. for two Poisson ratios (P.R.  $\equiv \nu = 0.33$  and  $\nu = 0.45$ ).

for two degrees-of-freedom at two different values of Poisson's ratio. Note also that  $a_0$  appears directly in the equation for  $m_i$ .

Veletsos and Verbič [29] report the following approximate analytical expressions for the coefficients  $\beta_i$  and  $\gamma_i$  appearing in equations (2.3):

$$\begin{aligned}\beta_i &= \rho_{i_4} q_2 + \rho_{i_1} \rho_{i_3}^3 s_i a_0^2 + 2 \frac{\xi}{a_0} \\ \gamma_i &= \rho_{i_3} + \rho_{i_1} \rho_{i_2}^2 t_i + \rho_{i_4} q_1 \frac{1}{a_0}\end{aligned}\quad (2.4)$$

where

$$\begin{aligned}s_i &\equiv \frac{q_2}{(q_1 + \rho_{i_2} a_0)^2 + q_2^2} \\ t_i &\equiv \frac{q_1 (q_1 + \rho_{i_2} a_0) + q_2^2}{(q_1 + \rho_{i_2} a_0)^2 + q_2^2} \\ q_1 &\equiv \left[ \frac{1}{2} (R - 1) \right]^{\frac{1}{2}} \\ q_2 &\equiv \left[ \frac{1}{2} (R + 1) \right]^{\frac{1}{2}} \\ R &\equiv [1 + (2\xi)^2]^{\frac{1}{2}}\end{aligned}\quad (2.5)$$

and  $\xi \equiv$  equivalent viscous damping ratio of the half-space (soil)  
 $\rho_{ij} \equiv$  coefficient  $j$  for degree-of-freedom  $i$ ; function of Poisson's ratio,  $\nu$ , of the half-space  
 $\beta_i, \gamma_i \equiv$  coefficients for use in equations (2.3)

Veletsos and Verbič report values for the coefficients  $\rho_{ij}$  for half-space Poisson's ratios of  $\nu = 0.00, 0.33, 0.45,$  and  $0.50$ .

If the equivalent viscous damping ratio is set to zero, ( $\xi = 0$ ), then the visco-elastic half-space becomes an elastic half-space, and equations (2.4) reduce to the following:

$$\beta_i = \rho_{i4} + \rho_{i1} \rho_{i2} \frac{(\rho_{i2} a_0)^2}{1 + (\rho_{i2} a_0)^2} \quad (2.6)$$

$$\gamma_i = \rho_{i3} + \frac{\rho_{i1} \rho_{i2}^2}{1 + (\rho_{i2} a_0)^2}$$

The dependency of the discrete model's parameters on the frequency of the applied loading introduces an analysis problem for nonharmonic loading, such as seismic excitation: a harmonic loading frequency must be chosen to determine the parameter values, and this is the only loading frequency at which the discrete model correctly reproduces the response of the half-space. This problem could be solved by performing the analysis in the frequency domain, expressing the seismic loading as a Fourier series, and using different parameter values for the discrete model in each component harmonic frequency. However, such an analysis relies upon the superposition of component responses, and therefore implicitly assumes linearity. To incorporate important nonlinearities in the system arising from the near-field soil behavior, yielding of structural members, gap development and closure, or other mechanisms, the analysis must be performed in the time domain. This restricts the analysis to a single set

of discrete model parameters; essentially, a loading frequency must be chosen for which the model is assumed to primarily respond.

One approach is to set this frequency to be equal to the fundamental frequency of the structure. The most damaging response of a structure frequently occurs when the fundamental mode of vibration is excited, and choosing this frequency as the basis for determining the discrete model parameter values ensures that the model is working best at this critical condition.

Another approach is to develop a more complicated discrete model. By incorporating more parameters in a model, more complicated response behavior can be achieved. This enables the model to acceptably reproduce the behavior of the half-space over a wider loading frequency range, thus reducing its frequency dependence. If a good fit can be achieved between the response of the discrete model and the half-space over the range of structure periods excited by earthquakes, then the model could be incorporated into analysis as though it was independent of frequency.

Figure 2.4 shows four such discrete models. It should again be pointed out that the figure shows the components of the model that appear in each degree-of-freedom. In a general three-dimensional analysis, incorporation of one of the models would require six of the component configurations shown for that model. It should also be noted that individual components do not necessarily represent real physical quantities. For example, the masses do not represent activated soil mass,



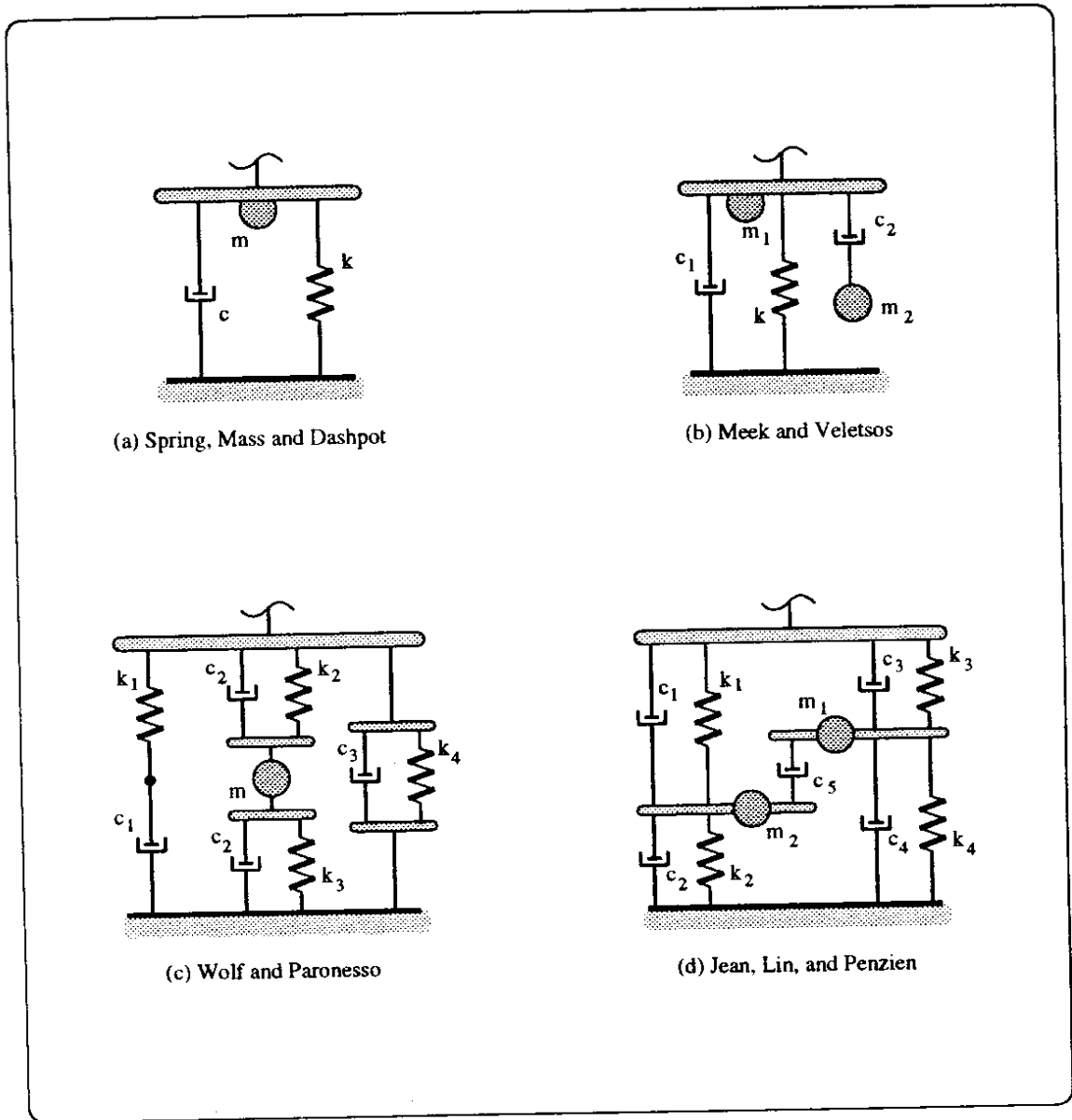


**Figure 2.4:** Four discrete models of the elastic half-space system: (a) spring–mass–dashpot model, three parameters; (b) Meek and Veletsos model, five parameters [31]; (c) Wolf and Paronesso model, nine parameters [32]; and (d) Jean *et al.* model, eleven parameters [33].

but are present simply to allow the model's behavior to better approximate the response of the half-space, and are thus called "virtual" masses. Additionally, springs and dampers with negative coefficients are sometimes utilized.

The first model shown, Figure 2.4(a), is the spring, mass, and dashpot model already discussed. It connects two nodes, one fixed, the other at the foundation–structure interface. This model will be referred to as a "three-parameter" model because it requires the specification of three parameters per degree-of-freedom. Of the three parameters, two are independent. This model has been used by numerous researchers, but the version presented by Veletsos and Verbič [29] was the one considered in this research. The second model shown was presented by Meek and Veletsos, and its inclusion in the report follows Wolf's discussion of this model [31]. This five-parameter model uses three nodes, one of the nodes being internal to the model. The third model, presented by Wolf and Paronesso [32], is a nine-parameter model, of which six parameters are independent. It uses two internal nodes, requiring four nodes total. The fourth model, presented by Jean, Lin, and Penzien [33], is an eleven-parameter model (ten independent parameters). This model also uses two internal nodes.

The number of independent parameters is directly related to the model's ability to reproduce the behavior of the half-space over a wide frequency band. On the other hand, the number of internal nodes and the

number of parameters that must be specified indicate the complexity involved in incorporating the model in analysis. The methods of determining the values of the discrete model parameters are relatively simple, and require such soil characteristics as mass density, shear modulus, Poisson's ratio, and shear wave velocity. In all cases, the parameter determination method for each model is specified in the reference cited.

Another required characteristic of the soil–foundation system is the disk radius. A foundation, such as a spread footing, may be rectangular rather than circular. For such cases, one approach is to use an effective radius,  $r^{eff}$ . Lam, Martin, and Imbsen [34] recommend using the radius of a disk having the same area as the actual foundation as the equivalent radius for the translational degrees-of-freedom, and the radius of a disk with the same spatial moment of inertia as the actual foundation as the equivalent radius for the rotational degrees-of-freedom. (Note that different degrees-of-freedom require different equivalent radii). These radii are additionally modified by “shape” factors. The change in the dynamic characteristics of the foundation due to embedment is also accounted for by modifying the effective radii. This is accomplished by applying “embedment” factors to the radii.

In another approach, Wolf [31] presents static spring stiffnesses developed by Pais and Kausel for the embedded rigid prismatic foundation shown in Figure 2.5. Spring stiffnesses for each of the six degrees-of-

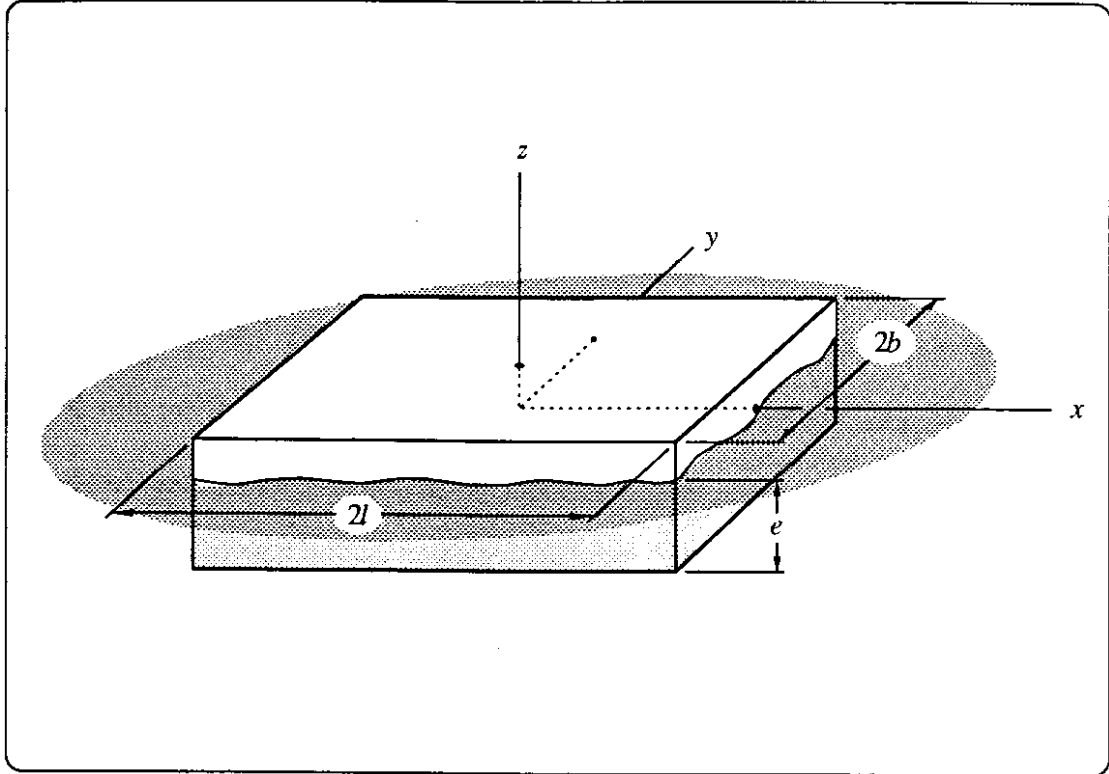


**Figure 2.5:** Pais and Kausel embedded prismatic foundation [31].

freedom of the foundation are given directly in terms of the dimensions of the foundation. Wolf also shows how the five-parameter Meek and Veletsos model may use these stiffnesses, and he gives values for the model parameters in terms of the foundation width  $b$ , instead of an effective radius. However, since most other models use a radius as their characteristic foundation dimension, it is useful to combine the Pais and Kausel stiffnesses with those stiffnesses presented in equations (2.2), and solve for the effective radii. In this manner, analytical expressions for the effective radii are obtained based implicitly on the Pais and Kausel stiffnesses. This allows the effects of foundation shape and embedment, as determined by Pais and Kausel, to be incorporated into each of the discrete models in a manner consistent with the model's development.

The approach presented by Lam *et al.* and the modified Pais and Kausel approach appear to yield comparable equivalent radii, at least over the common range of spread footing foundation dimensions and embedment depths. The Pais and Kausel equivalent radii are determined by the following equations, which assume that  $l \geq b$ , and that the  $x$ -axis is parallel

to the orientation of  $l$ , as shown in Figure 2.5:

$$r_i^{equiv} = q_i s_i h_i b \quad (2.7)$$

where

$$\begin{aligned} q_x &= 1.150 & s_x &= 0.739 \left( \frac{l}{b} \right)^{0.65} + 0.261 \\ q_y &= q_x & s_y &= 0.739 \left( \frac{l}{b} \right)^{0.65} + 0.087 \left( \frac{1}{b} \right) + 0.174 \\ q_z &= 1.175 & s_z &= 0.660 \left( \frac{l}{b} \right)^{0.75} + 0.340 \\ q_{\theta x} &= 1.145 & s_{\theta x} &= \left\{ 0.800 \left( \frac{l}{b} \right) + 0.200 \right\}^{\frac{1}{3}} \\ q_{\theta y} &= q_{\theta x} & s_{\theta y} &= \left\{ 0.993 \left( \frac{l}{b} \right)^{2.40} + 0.068 \right\}^{\frac{1}{3}} \\ q_{\theta z} &= 1.159 & s_{\theta z} &= \left\{ 0.511 \left[ \left( \frac{l}{b} \right)^{2.45} + 0.955 \right] \right\}^{\frac{1}{3}} \end{aligned} \quad (2.8)$$

$$\begin{aligned} h_x &= 1 + \left[ 0.33 + \frac{1.34}{1 + \left( \frac{l}{b} \right)} \right] \left( \frac{e}{b} \right)^{0.8} \\ h_y &= h_x \\ h_z &= 1 + 0.25 \left[ 1 + \frac{1}{\left( \frac{l}{b} \right)} \right] \left( \frac{e}{b} \right)^{0.8} \\ h_{\theta x} &= \left\{ 1 + \left( \frac{e}{b} \right) + \left[ \frac{1.6}{0.35 + \left( \frac{l}{b} \right)} \right] \left( \frac{e}{b} \right)^2 \right\}^{\frac{1}{3}} \\ h_{\theta y} &= \left\{ 1 + \left( \frac{e}{b} \right) + \left[ \frac{1.6}{0.35 + \left( \frac{l}{b} \right)^4} \right] \left( \frac{e}{b} \right)^2 \right\}^{\frac{1}{3}} \\ h_{\theta z} &= \left\{ 1 + \left[ 1.3 + \frac{1.32}{\left( \frac{l}{b} \right)} \right] \left( \frac{e}{b} \right)^{0.9} \right\}^{\frac{1}{3}} \end{aligned}$$

The shape and embedment functions,  $s_i$  and  $h_i$ , are plotted in Figure 2.6.

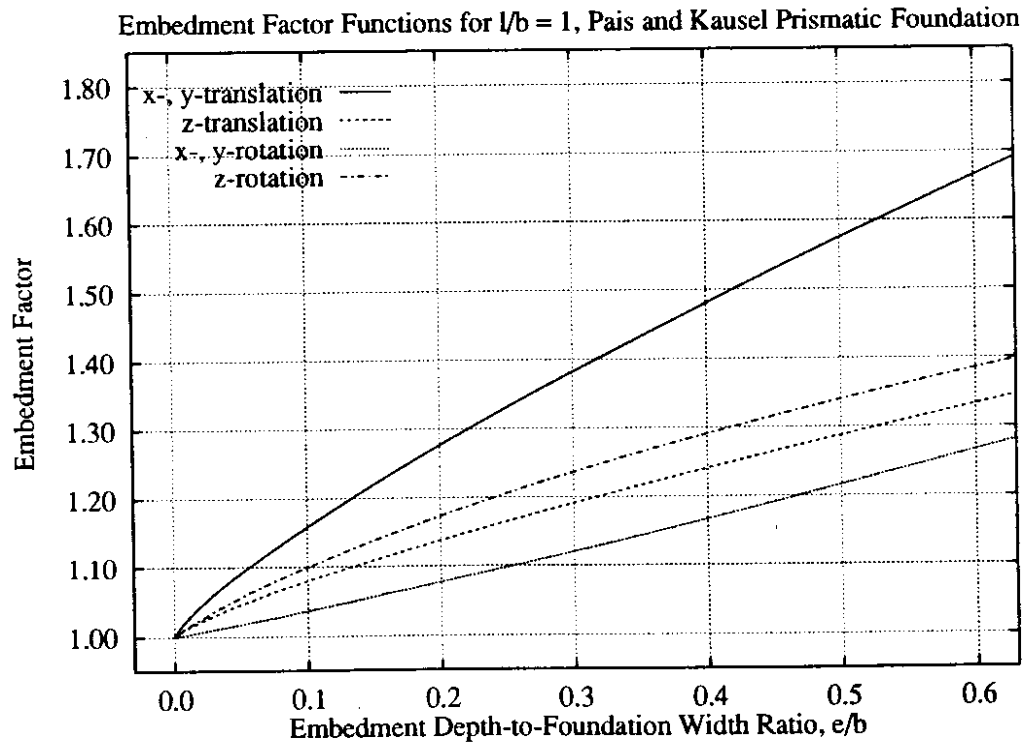
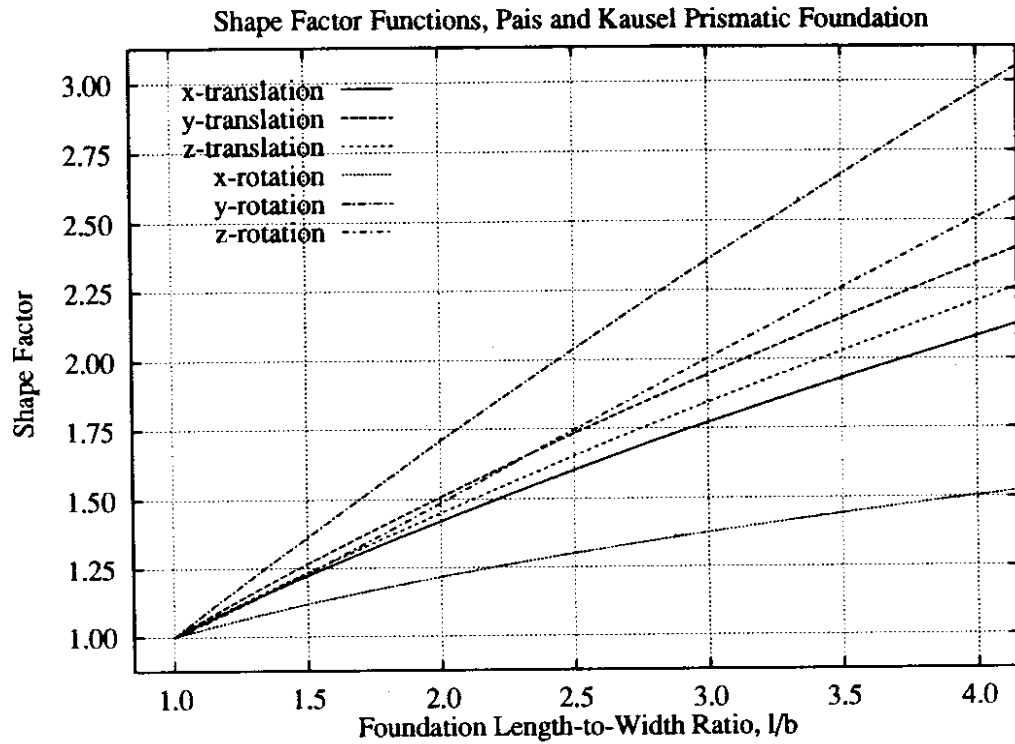


**Figure 2.6:** Shape factor and embedment factor functions,  $s_i$  and  $h_i$ , for the Pais and Kausel prismatic foundation model.

#### 2.1.4 Pile Foundation Models

The discrete models discussed thus far are based on the disk-half-space system shown in Figure 2.2, where the “foundation” is a rigid member bonded to the surface of the half-space. These discrete models are useful for modeling spread footing foundations, but the concept of representing the soil as a half-space has also been used to develop discrete models applicable for modeling pile foundations. Nogami and Konagai [35] represented the soil as a vertically-stratified series of plane-strain elastic layers to develop Winkler-type discrete models that could be applied along the length of pile models embedded in the soil. The concept was later extended by Nogami *et al.* [36] to include in the soil reaction model a nonlinear soil near-field sub-model, and a sub-model capable of representing the development of a gap between the pile shaft and the soil. This model is illustrated in Figures 2.7 and 2.8.

The Nogami far-field submodel consists of three linear spring-dashpot combinations placed in series, as shown in Figure 2.7. The



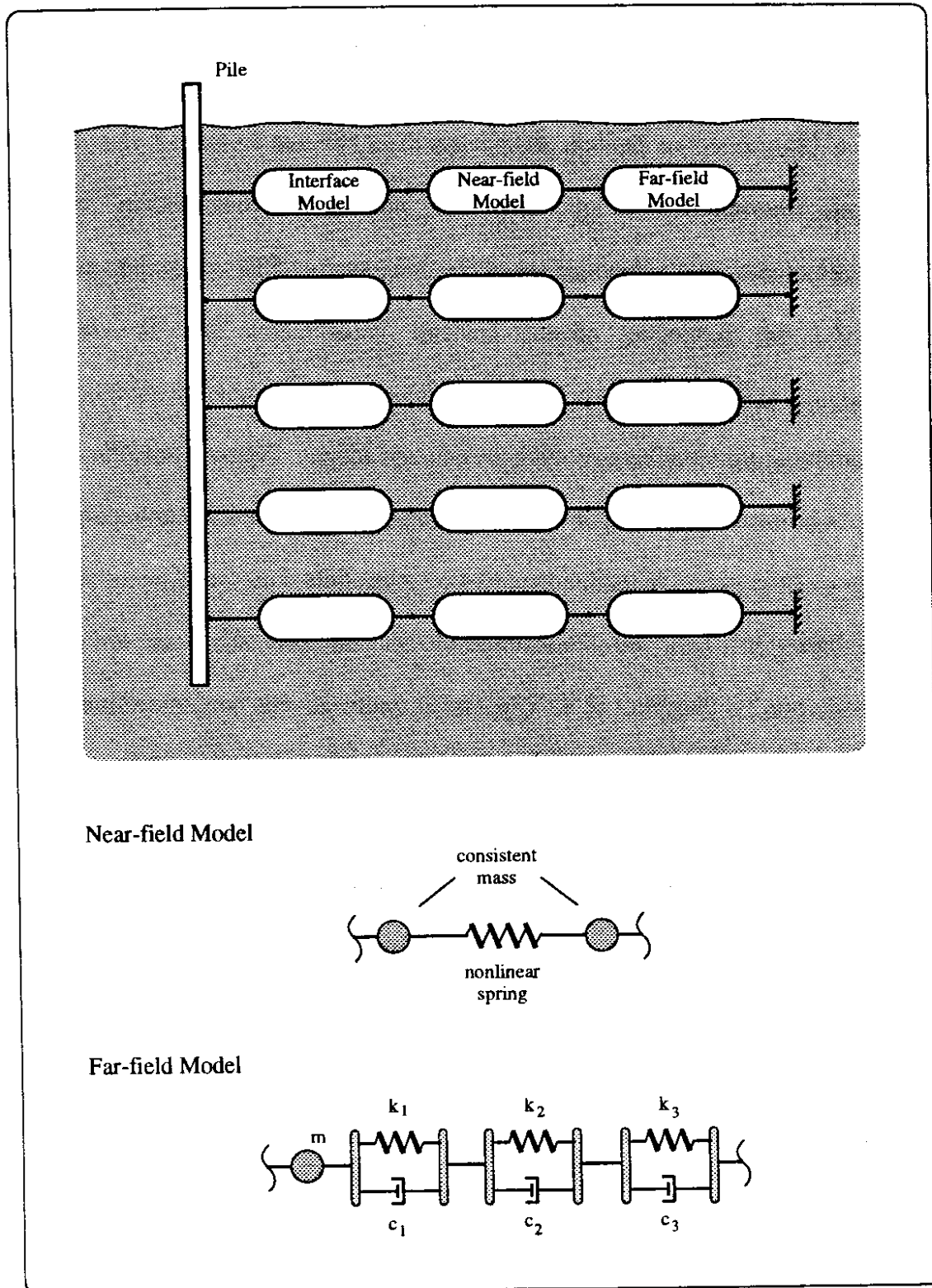


**Figure 2.7:** Soil-pile model proposed by Nogami *et al.* [37]: (top) Winkler foundation with three soil reaction models at each level: (bottom) soil far-field and near-field models.

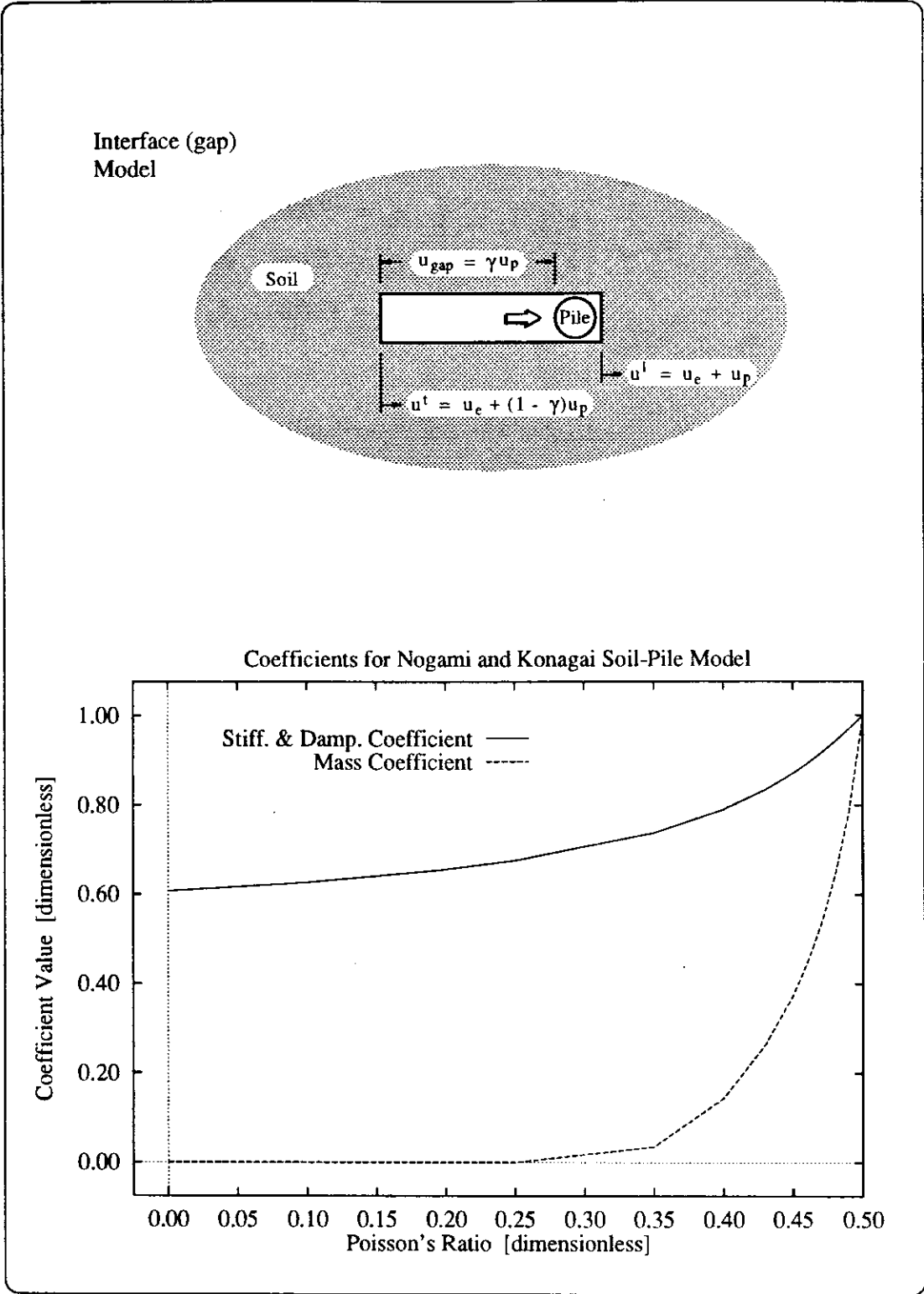


**Figure 2.8:** Nogami and Konagai soil–pile model: (top) soil–pile interface mechanism to model gap development; (bottom) variation of the model stiffness/damping and mass parameters,  $\xi_{sd}$  and  $\xi_m$ , with Poisson's ratio.

parameters of the far-field sub-model are determined by applying the following equations:

$$\begin{aligned}
 k_i &= q_i \xi_{sd} G \\
 c_i &= d_i \xi_{sd} G \left( \frac{r_n}{c_s} \right) \\
 m_i &= \pi \xi_m G \left( \frac{r_n}{c_s} \right)^2
 \end{aligned}
 \quad \left\{ \begin{array}{l}
 q_1 = 7.036, \quad d_1 = 226.1946 \\
 q_2 = 7.162, \quad d_2 = 50.266 \\
 q_3 = 11.058, \quad d_3 = 18.724
 \end{array} \right. \quad (2.9)$$

where  $r_n \equiv$  radius of the soil near-field

$\xi_{sd}, \xi_m \equiv$  dimensionless coefficients; functions of Poisson's ratio,  $\nu$ , of the soil, as shown in Figure 2.8

$q_i, d_i \equiv$  dimensionless coefficients

The far-field sub-model is intended to represent the reaction of the soil at a sufficient distance from the pile to ensure linear behavior of the soil. It also models radiation damping. Nogami *et al.* [37] report that this sub-model accurately reproduces the behavior of the plane-strain elastic half-space over a wide frequency range.

The near-field sub-model is intended to represent the nonlinear, hysteretic action of the soil in the immediate vicinity of the pile. A method is presented to determine the required behavior of the nonlinear spring; however, using standard “ $p$ - $y$ ” load-deflection curves as the backbone curve of a bilinear hysteretic spring would be consistent with the intended

function of this sub-model. The consistent mass matrix prescribed for the near-field sub-model is given by the following equation:

$$m_n = \frac{1}{6} \pi \rho_s r_p^2 \left( \frac{r_n}{r_p} - 1 \right) \begin{bmatrix} \frac{r_n}{r_p} + 3 & 3 \frac{r_n}{r_p} + 1 \\ 3 \frac{r_n}{r_p} + 1 & \frac{r_n}{r_p} + 1 \end{bmatrix} \quad (2.10)$$

where  $r_p \equiv$  radius of the pile  
 $\rho_s \equiv$  mass density of the soil  
 $m_{ij} \equiv$  inertial force at node  $i$  caused by a unit acceleration at node  $j$ ; node 1 is the “pile” end of near-field model, and node 2 is the “far-field” end of the near-field model.

The interface sub-model models the development of a gap between the pile and the surrounding soil. Referring to Figure 2.8, the displacement of the gap “leading” edge,  $u^l$ , is composed of an elastic component,  $u_e$ , and an accumulated plastic component,  $u_p$ . The gap displacement,  $u_{gap}$ , is taken to be a portion of  $u_p$ , and is controlled by the parameter  $\gamma$ . A gap parameter value of  $\gamma = 0$  corresponds to not developing any gap, in which case the pile remains in contact with the soil at all times. The displacement of the gap “trailing” edge,  $u^t$ , is the displacement of the leading edge,  $u^l$ , less the gap displacement,  $u_{gap}$ .

Nogami *et al.* [37] illustrate the use of this soil–pile discrete model and the selection of model parameters with several examples.

## 2.2 Modification of NEABS

The bridge analysis computer program NEABS (*Nonlinear Earthquake Analysis of Bridge Systems*) was chosen to be used in implementing the proposed methods to model mechanisms not currently incorporated into standard seismic analysis. The public domain source coding for NEABS was obtained and modified for this purpose [24]. As will be explained, it was already capable of modeling differential support excitation, nonlinear expansion joint behavior, and linear elastic spring supports. In order to implement the models discussed above to represent bridge spread footing and pile foundation interaction with the soil, NEABS was modified to include a new, discrete foundation element. In this section, NEABS is described and the development of the new foundation element is discussed.

### 2.2.1 Description of NEABS

The computer program NEABS was originally developed by Tseng and Penzien in 1973 as part of a study of the seismic performance of long, multiple-span bridges [38]. Using the finite element method (FEM), NEABS may be used to model a bridge by mathematically idealizing the structure as a discrete parameter system subjected to nodal dynamic loadings and/or to prescribed support motions. The discrete parameter system is composed of both linear and nonlinear elements. The program

was later modified in 1976 by Kawashima and Penzien, and again in 1978 by Imbsen, Nutt, and Penzien [38].

Four element types are available to model the structural members of a bridge. Deck sections and columns are modeled with a beam element that may be either elastic or elasto-plastic. In the case of the elasto-plastic beam, the ends are allowed to develop perfectly-plastic hinges. To define the beam's yield surface, axial force–bending moment strength interaction curves may be specified for bending about both principal axes, and biaxial bending moment strength interaction is included by using Bresler's "load contour" method. An elastic curved-beam element is available. Structure supports may be specified as fixed or free in each of the six degrees-of-freedom associated with a support node. Free supports may be given elastic stiffnesses (support springs) with the boundary spring element. A nonlinear expansion joint is included, which can model the opening and closing of the joint gap, the impact at gap closure, and elasto-plastic joint tie bars. An elastic truss element was originally included in the coding, but has since been discontinued.

Lumped masses, or mass moments of inertia for rotational degrees-of-freedom, may be assigned to structure nodes directly, or by specifying mass densities for both the straight- and the curved-beam elements. In the latter case, the total mass of the beam is computed and distributed equally to the two end nodes.

Energy dissipation not inherent in the material damping of the elasto-plastic elements is accomplished globally by using two-parameter Rayleigh damping. Rayleigh damping is a form of viscous damping (i.e., velocity-proportional damping force) in which the global damping matrix is assumed to be a linear combination of the global mass and stiffness matrices. For an elastic structure, this has the effect of assigning a unique damping ratio to each of the structure's modes of vibration; selection of desired damping ratios for two of the modes of vibration will uniquely determine the values of the two global damping parameters.

Both static and dynamic nodal loadings may be prescribed, as well as support motion. Dynamic nodal loads and support motions are specified by supplying load and acceleration time histories, respectively. Multiple dynamic load and/or support acceleration time histories can be applied, allowing NEABS to model differential support motions.

The equations of motion are solved in the time domain to allow nonlinear response, and they are numerically integrated directly at each time step using the Newmark method. Either constant or linear acceleration between successive time steps may be assumed in the integration, allowing for two numerical accuracy/stability tradeoff combinations. At each time step, the out-of-balance force vector (i.e., the difference between the applied equivalent force and the sum of the structure's restoring, damping, and inertial forces) from the previous time step is added to the current applied equivalent force to minimize the

accumulation of integration errors. Additionally, NEABS will iterate and/or subdivide the time step used in integration, using linear interpolation of applied load and acceleration time histories as necessary, to ensure that the Euclidean norm of the out-of-balance force vector is within prescribed tolerances. Output consists of both the forces and displacements of the initial static response and of time histories of the dynamic response. These time histories may consist of nodal displacements, nodal accelerations, member forces, and, for nonlinear elements, member “nonlinear” (plastic) displacements.

### *2.2.2 Discrete Foundation Element Capabilities*

The discrete foundation element (DF element) was designed and implemented within NEABS for this research project. It is intended to be a general purpose element to be used in incorporating a variety of discrete foundation models into NEABS analyses. These models may range in complexity from simple linear elastic spring supports to those employing a number of internal nodes, masses, dampers, and nonlinear springs.

A pictorial representation of the DF element may be seen in Figure 2.9. The DF element connects two nodes, nodes  $i$  and  $j$ . These two end nodes may actually occupy the same location, as in a simple foundation model using elastic supports, where node  $i$  might be fixed, and node  $j$  the connection point of a soil spring to the bridge foundation. Because of the possibility of having element lengths that are small, or even



Discrete Foundation  
Element

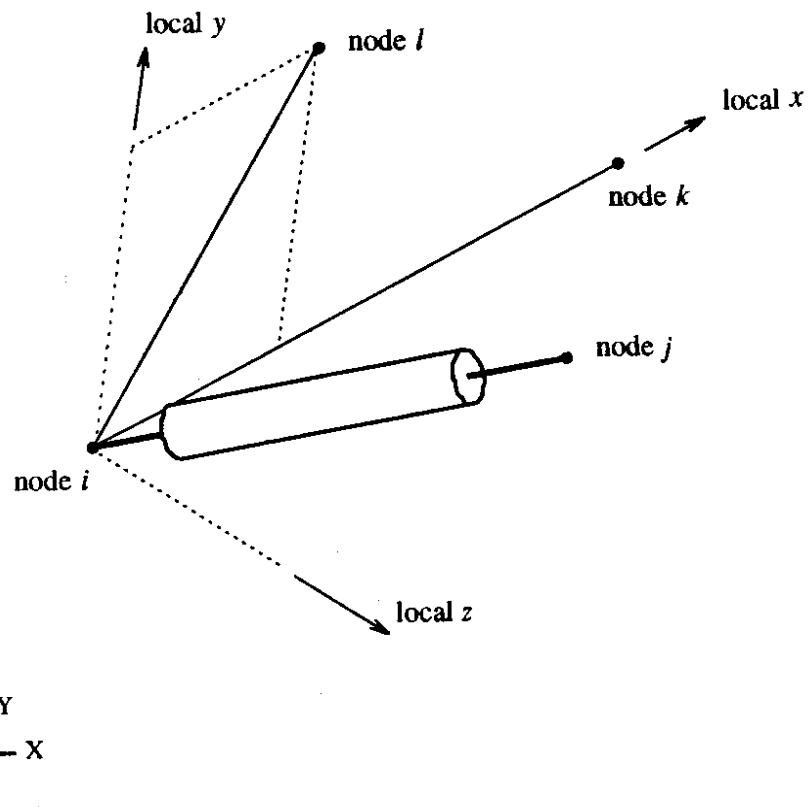
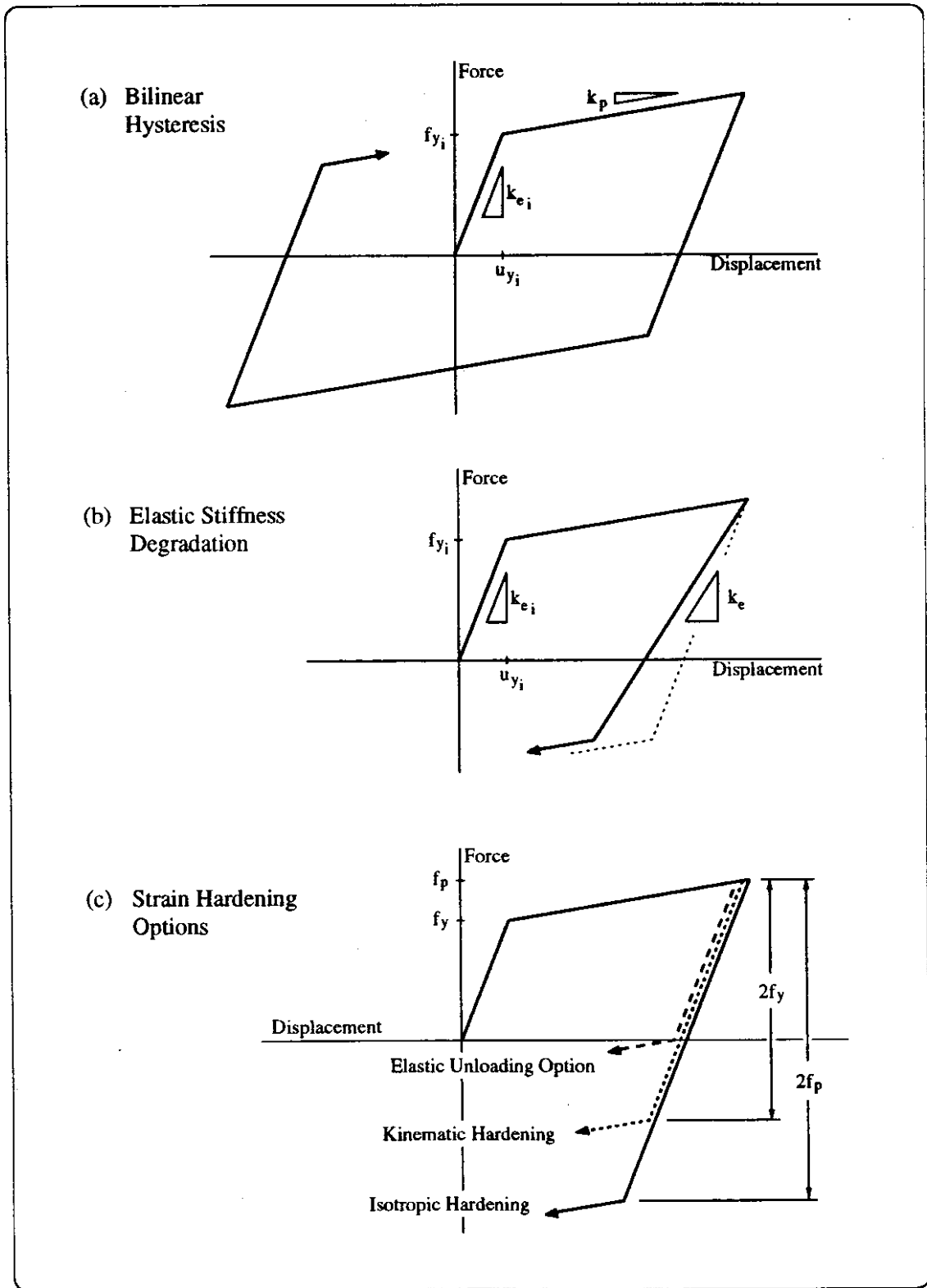


Figure 2.9: Pictorial representation of the DF element.

zero, the orientation of the local  $x$ -axis is determined by a vector originating at node  $i$  and terminating at node  $k$  (vector  $\overline{ik}$ ). The local  $y$ -axis is determined by specifying node  $l$ ; the component of the vector  $\overline{il}$  perpendicular to the vector  $\overline{ik}$  and lying in the plane defined by these vectors determines the direction of the local  $y$ -axis. The local  $z$ -axis is determined from the  $x$ - and  $y$ -axes, consistent with the requirements of a right-handed coordinate system. Nodes  $k$  and  $l$  serve only to determine the orientation of the local coordinate system, and need not be located on the structure.

The DF element connects the two end nodes with a spring and damper, or “dashpot,” for each of the six local degrees-of-freedom. There is no stiffness or damping coupling; thus, the response in each degree-of-freedom is independent. Mass and mass moments of inertia may be lumped to each end node and each degree-of-freedom independently. The dashpot is a linear viscous damper, while the spring may be nonlinear.

The spring incorporates a number of features to facilitate modeling many of the nonlinear characteristics of soil. These features may or may not be utilized, depending on the requirements of the foundation model and the availability of necessary input parameters. The spring stiffness is bilinear, to allow elastic-plastic behavior and hysteretic material damping. Referring to Figure 2.10(a), an initial elastic stiffness  $k_{e_i}$ , a plastic stiffness  $k_p$ , and an initial yield force  $f_{y_i}$  may be specified. The elastic stiffness may be allowed to degrade on the basis of strain, as shown in



**Figure 2.10:** DF element nonlinear stiffness capabilities: (a) bilinear hysteresis; (b) elastic stiffness degradation; (c) strain hardening options.

Figure 2.10(b), according to the following equation, used by Loh and Lee [17]:

$$k_e = k_{e_i} \left( \frac{|u|_{max}}{u_{y_i}} \right)^{-\alpha} \leq k_{e_i} \quad (2.11)$$

- where  $k_e$   $\equiv$  current elastic stiffness  
 $k_{e_i}$   $\equiv$  initial elastic stiffness  
 $|u|_{max}$   $\equiv$  maximum absolute displacement during plastic response that has been attained thus far;  $|u|_{max} \geq u_{y_i}$   
 $u_{y_i}$   $\equiv$  initial positive yield displacement  
 $\alpha$   $\equiv$  stiffness degradation parameter

Different forms of strain hardening may be incorporated, as illustrated in Figure 2.10(c). The DF element defaults to kinematic hardening (yield force limits remain at their initial values), but isotropic hardening (yield force limits expand to previously attained maximum force), or an intermediate combination of the two may be specified. Additionally, an option is supported to force yielding to occur if the element has elastically unloaded to zero force prior to attainment of the yield force in the opposite direction consistent with the prescribed strain hardening rule. The use of this option has the effect of preventing the positive and negative yield force envelopes from “crossing” the zero-force axis, as can happen at large strains with kinematic strain hardening.

The DF element can incorporate a gap, which is useful for modeling the soil reaction on a pile. This gap model is the one proposed by

Nogami *et al.* [37], discussed earlier. Referring to Figure 2.11(a), a gap can develop according to the equation:

$$u_{gap} = \gamma u_p \quad (2.12)$$

where  $u_{gap}$   $\equiv$  gap width, difference between displacements of gap “leading” and “trailing” edges,  $u^l$  and  $u^p$

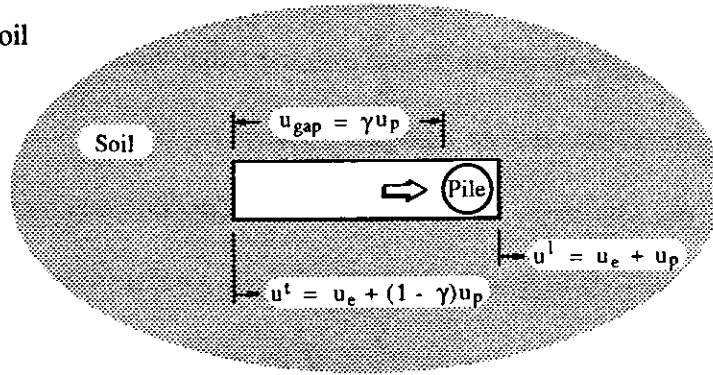
$u_p$   $\equiv$  accumulated plastic component of displacement at gap “leading” edge,  $u^l$

$\gamma$   $\equiv$  parameter governing gap development rate

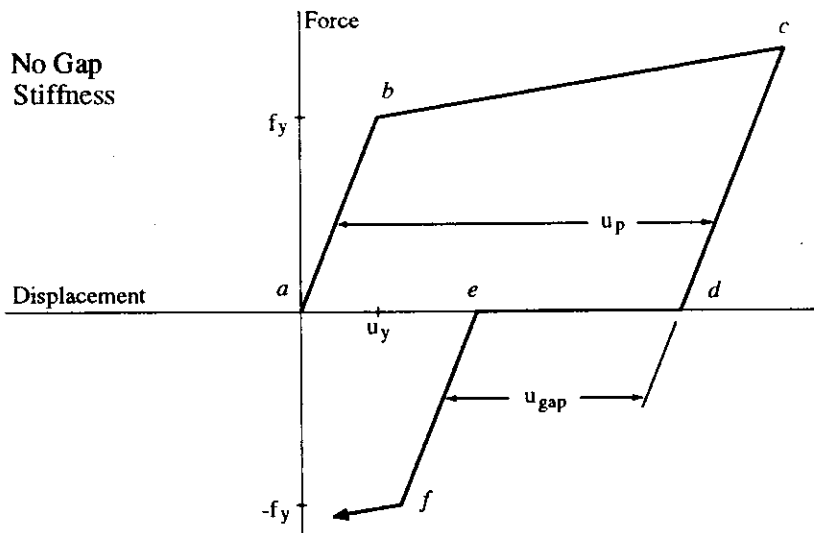
Thus, if  $\gamma = 0$ , no gap can develop, while a gap will develop for  $\gamma > 0$ . For the case of  $\gamma = 1/2$ , once the yield displacement is reached, the pile shown in Figure 2.11(a) will continue to “push” the “leading edge”, while the “trailing” edge will be “dragged” along at half the rate of the leading edge until the pile reverses direction (point *c* of Figure 2.11(b)). At that time, the pile may unload the leading edge to zero force (point *d*); during the elastic portion of the unloading, both edges will translate back in unison. The pile may now traverse the gap, contact the former trailing edge (point *e*), and load this side elastically up to the yield force consistent with the prescribed hardening rule (point *f*). When the elastic unloading option, discussed earlier, is used in conjunction with the gap option, the pile of Figure 2.11(a) will always unload elastically to zero force, whereupon it enters the gap.

Although a true gap, such as illustrated in Figure 2.11(b), has no stiffness, hysteretic bilinear behavior may be specified for the gap. As

(a) Pile-Soil Gap



(b) No Gap Stiffness



(c) Bilinear Gap Stiffness

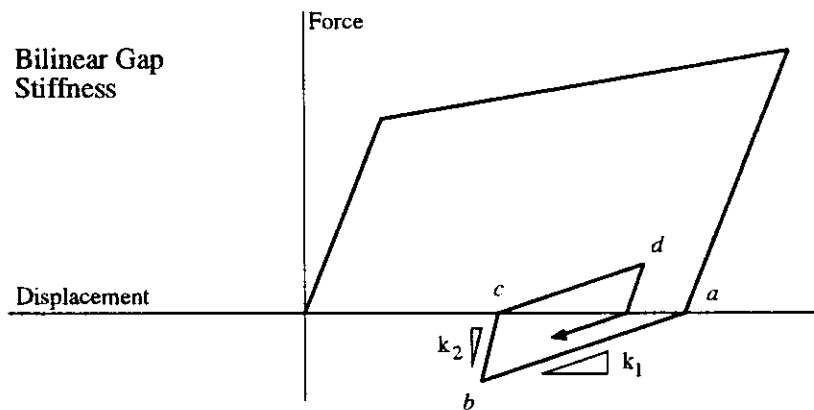


**Figure 2.11:** DF element nonlinear stiffness capabilities: gap development and in-gap hysteretic behavior.

illustrated in Figure 2.11(c), two stiffnesses may be specified. The first stiffness,  $k_1$ , applies when the gap is initially entered (point *a*). If the pile reverses direction within the gap (point *b*), it may unload at the second stiffness,  $k_2$ , to zero force (point *c*). Continuing on in the reversed direction, the pile will start loading again at the first stiffness. Thus, the in-gap behavior is similar to that of an elasto-plastic material, where the first stiffness is the plastic stiffness, and the second stiffness is the elastic stiffness. This feature is intended to provide versatile and rational behavior that may be utilized in modeling friction or other mechanisms which may give rise to stiffness within the gap.

The dashpot is a linear viscous damper. The coefficient of damping may be specified in all degrees-of-freedom independently, allowing concentrated dampers to be included in a foundation model. The DF element viscous damping is independent of the global Rayleigh viscous damping; the contribution of the DF element to the system's global mass and stiffness matrix is not considered when determining the Rayleigh damping contribution to the global damping matrix. Thus the Rayleigh damping concept may continue to be used for the majority of a bridge structure's components without affecting concentrated dampers present in the foundation models. The option of allowing the global damping parameters to apply to the DF element is supported, in which case the Rayleigh damping from the DF element is added to any specified dashpot damping in determining the element's total damping matrix.

### *2.2.3 Discrete Foundation Element Implementation*

Six main subroutines were added to the NEABS coding to include the DF element in the NEABS element family, as shown in Figure 2.12. The architecture of the DF element subroutines is similar to that of the existing elements. The coding for these subroutines is given in Appendix C. The form of the equation of motion that NEABS integrated had to be changed to accommodate the concentrated damping capability of the DF element. Since NEABS originally used only Rayleigh damping, in which the global damping matrix is a linear combination of the global mass and stiffness matrices, the equation of motion was cast in terms of the mass and stiffness matrices only without explicitly formulating the damping matrix. To prevent the DF element from (necessarily) including Rayleigh damping, and to allow it to include concentrated dampers, it was necessary to formulate the global damping matrix. The equation of motion was then recast to include the global damping matrix directly.

### *2.2.4 Discrete Foundation Element Verification*

Once the necessary coding was implemented in NEABS, verification tests were performed to ensure that the DF element behavior was correct; i.e., that the DF element response was sufficiently close numerically to the equations chosen to govern its behavior. These verification tests are described in this section. Static loading conditions were applied to test the DF element's elastic stiffness, the invariance of the elastic stiffness to



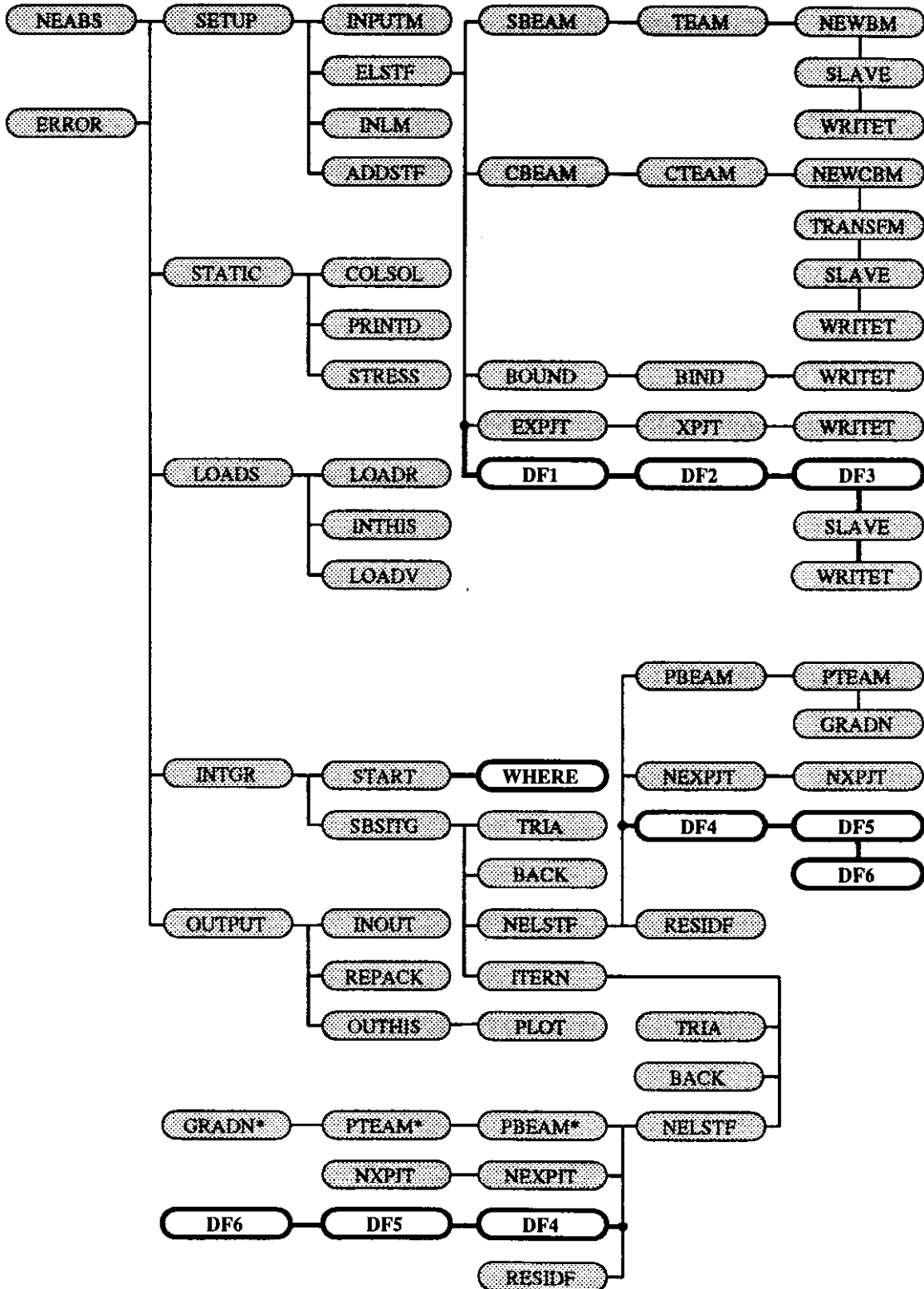


**Figure 2.12:** NEABS subroutine organization diagram: shaded bubbles indicate the subroutines present in the code as-delivered; open bubbles indicate the subroutines added.

spatial orientation, the DF element's ability to model weight (mass in a gravitational field), and its connectivity. Dynamic loading conditions were imposed to test the DF element's undamped and damped response, elastic stiffness degradation, strain hardening options, gap development, and in-gap hysteretic behavior.

To verify the DF element's correct elastic stiffness response, a single element was statically loaded as shown in Figure 2.13. The element was oriented such that its local coordinate system coincided with the global coordinate system. Different elastic stiffnesses were assigned to each translational degree-of-freedom. The element was fixed at one end, while the other was loaded in each translational degree-of-freedom. A variety of load force levels were applied, and the element forces and nodal displacements were recorded. The resulting load-displacement curves have slopes equal to the assigned stiffnesses, indicating correct static response. Figure 2.14 shows the setup and results of a corresponding test of the elastic response to moment loading applied to the rotational degrees-of-freedom.

To verify the invariance of the DF element behavior to its orientation relative to the global coordinate system, a test similar to the one above was performed, but with the element oriented as shown in Figure 2.15. Thus, a force applied in the local  $x$ -axis direction, acting against the element's  $x$ -axis translational stiffness, would produce nodal displacements in the global negative  $y$ -axis direction. Element stiffnesses were assigned

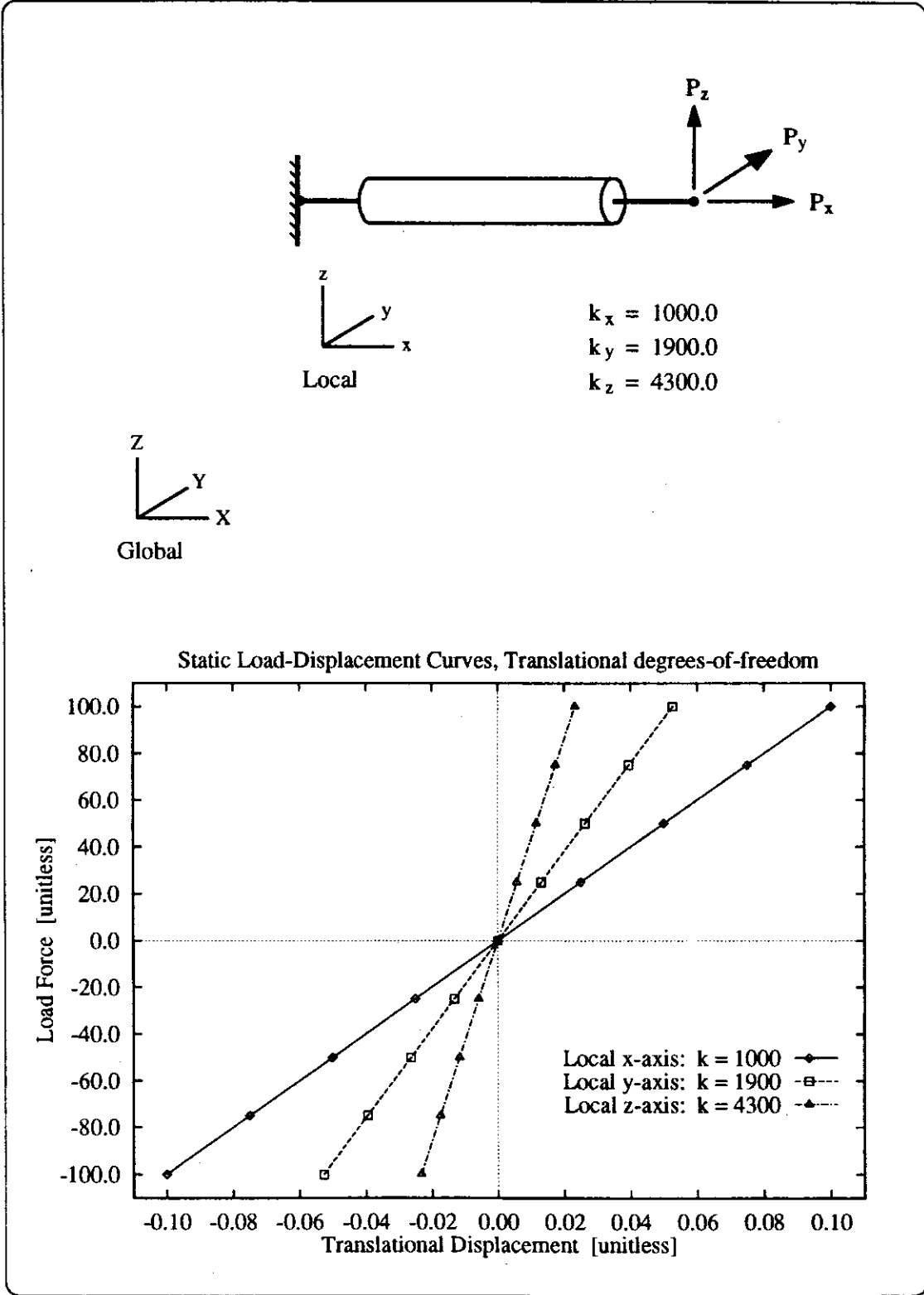


**Figure 2.13:** Elastic stiffness response verification test, force loads.

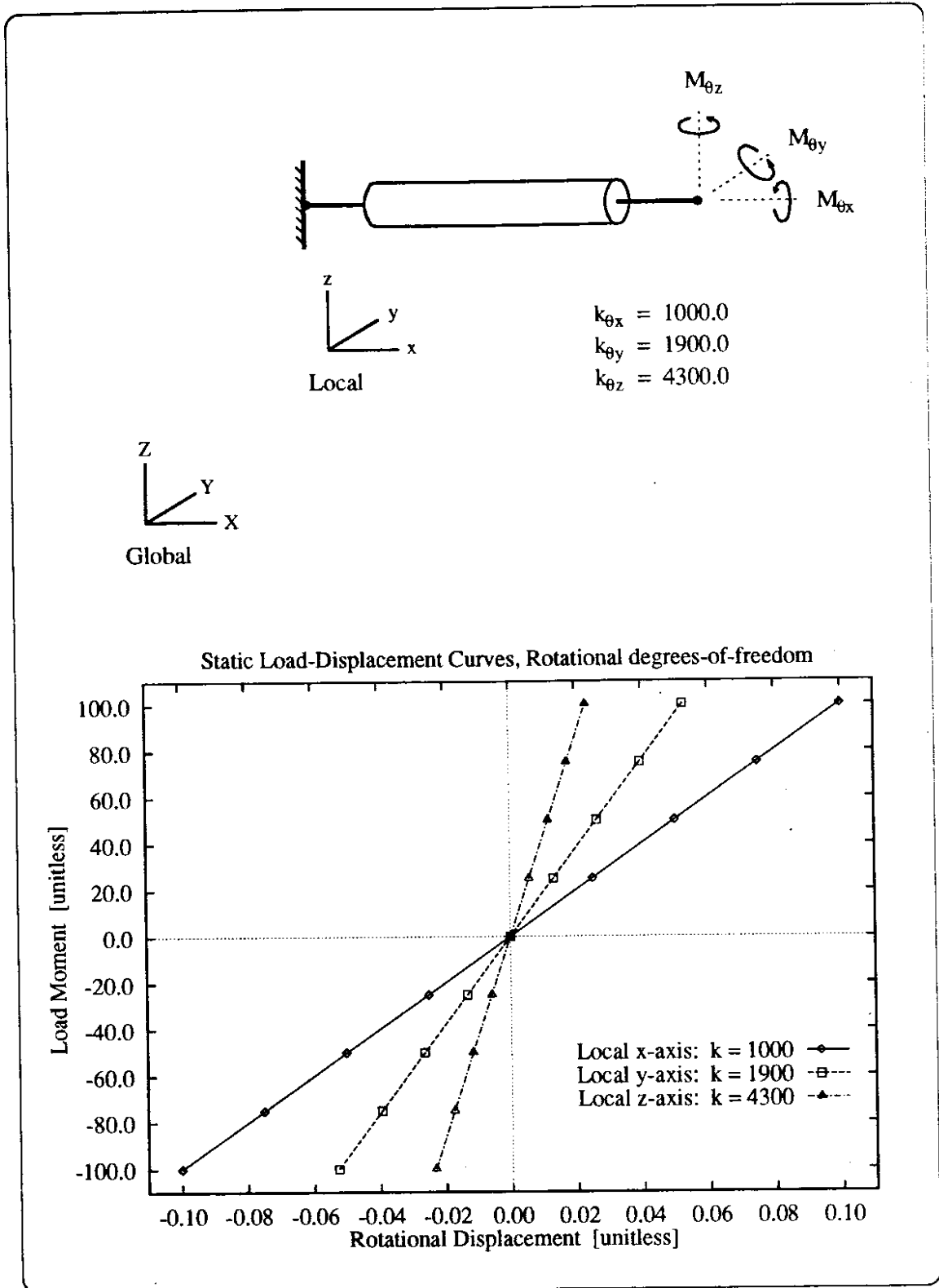


**Figure 2.14:** Elastic stiffness response verification test, moment loads.

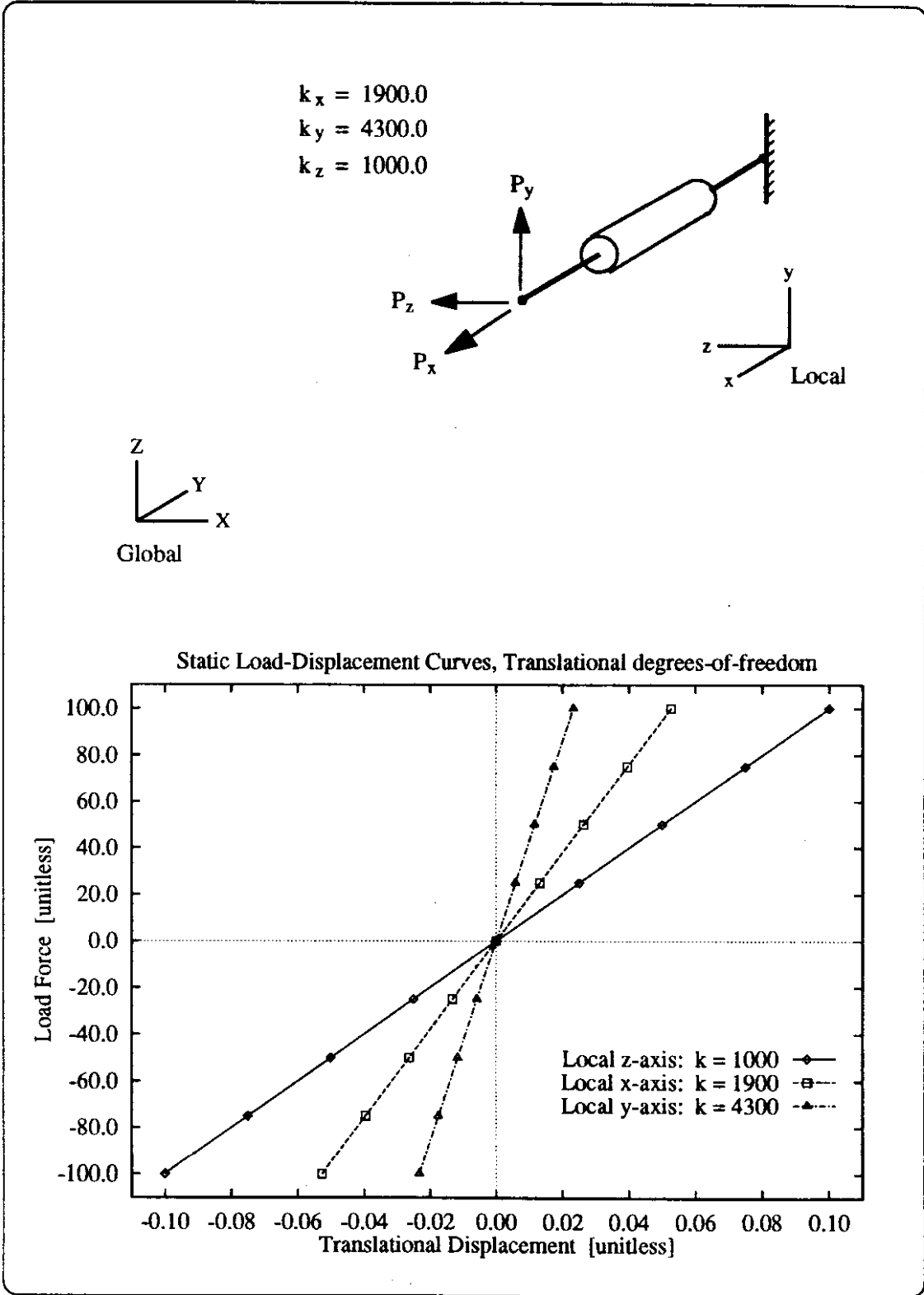


**Figure 2.15: Spatial orientation response invariance verification test, force loads.**

(specified relative to the local coordinate system), nodal loads were applied (assigned relative to the global system), and the resulting nodal displacements (reported relative to the global system) and element forces (reported relative to the local system) were recorded. Again, the load-displacement curve slopes corresponded directly with the stiffnesses assigned to each of the element's translational degrees-of-freedom. Figure 2.16 shows the setup and results of a corresponding test of the elastic response to loading applied to the rotational degrees-of-freedom.

Mass and mass moments-of-inertia may be assigned to each of the DF element's end nodes' translational and rotational degrees-of-freedom, respectively. Gravitational acceleration components in the global  $x$ -,  $y$ -, and  $z$ -axis directions may also be specified. These accelerations act on the nodal masses, resulting in static nodal forces. To verify the element's ability to model weight, which depends on its ability to apply a gravitational acceleration field to specified mass, the test illustrated in Figure 2.17 was conducted. A gravitational acceleration was applied in the global negative  $y$ -axis direction, which acted on the mass assigned to the free end of the element. The element was given a stiffness in the local  $x$ -axis direction, giving rise to a resisting force equal and opposite to the gravitational force, or weight. The mass was varied and plotted against the resulting resisting force, yielding a mass-weight curve with a slope equal to the gravitational acceleration.

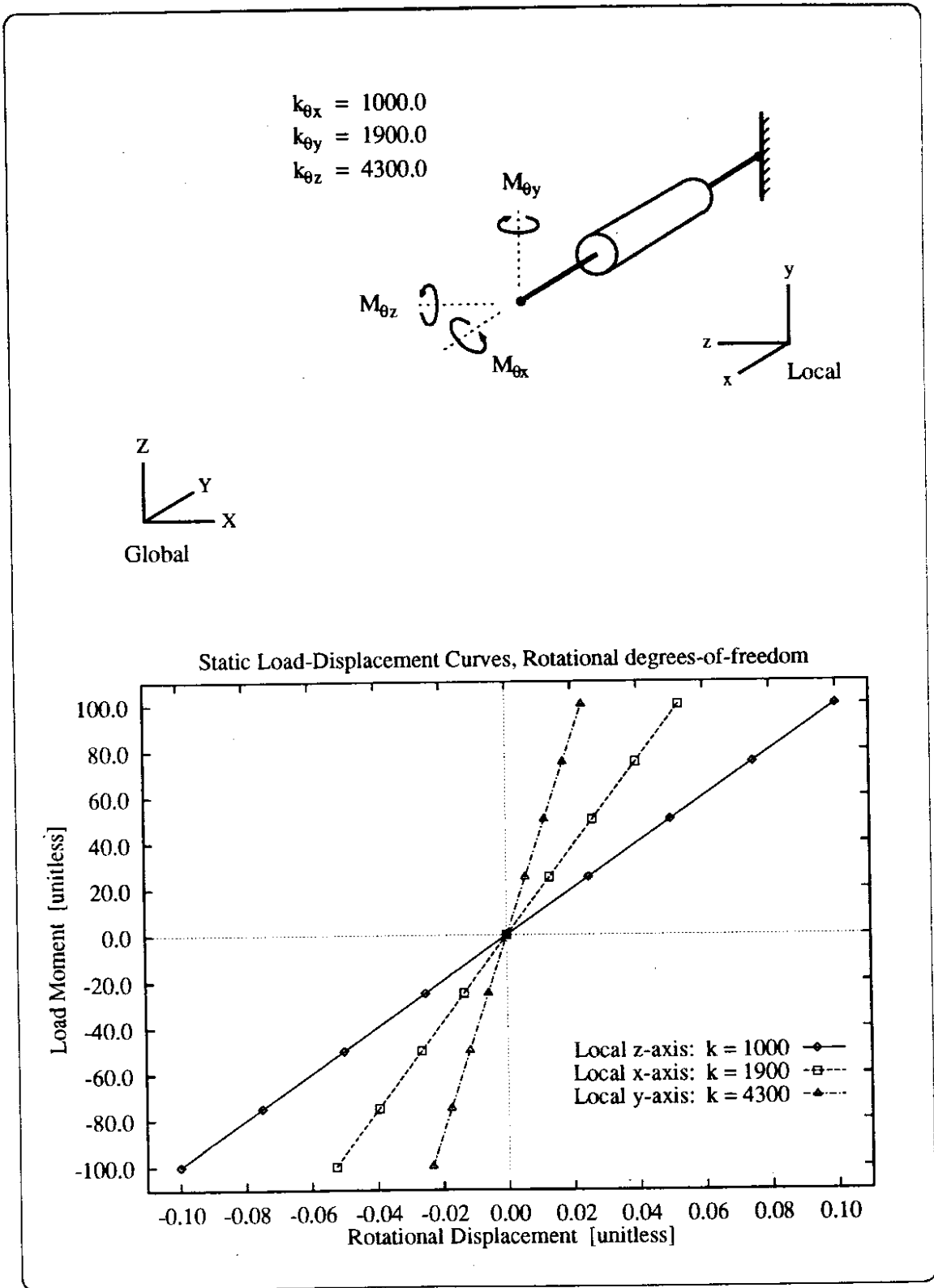


**Figure 2.16:** Spatial orientation response invariance verification test, moment loads.

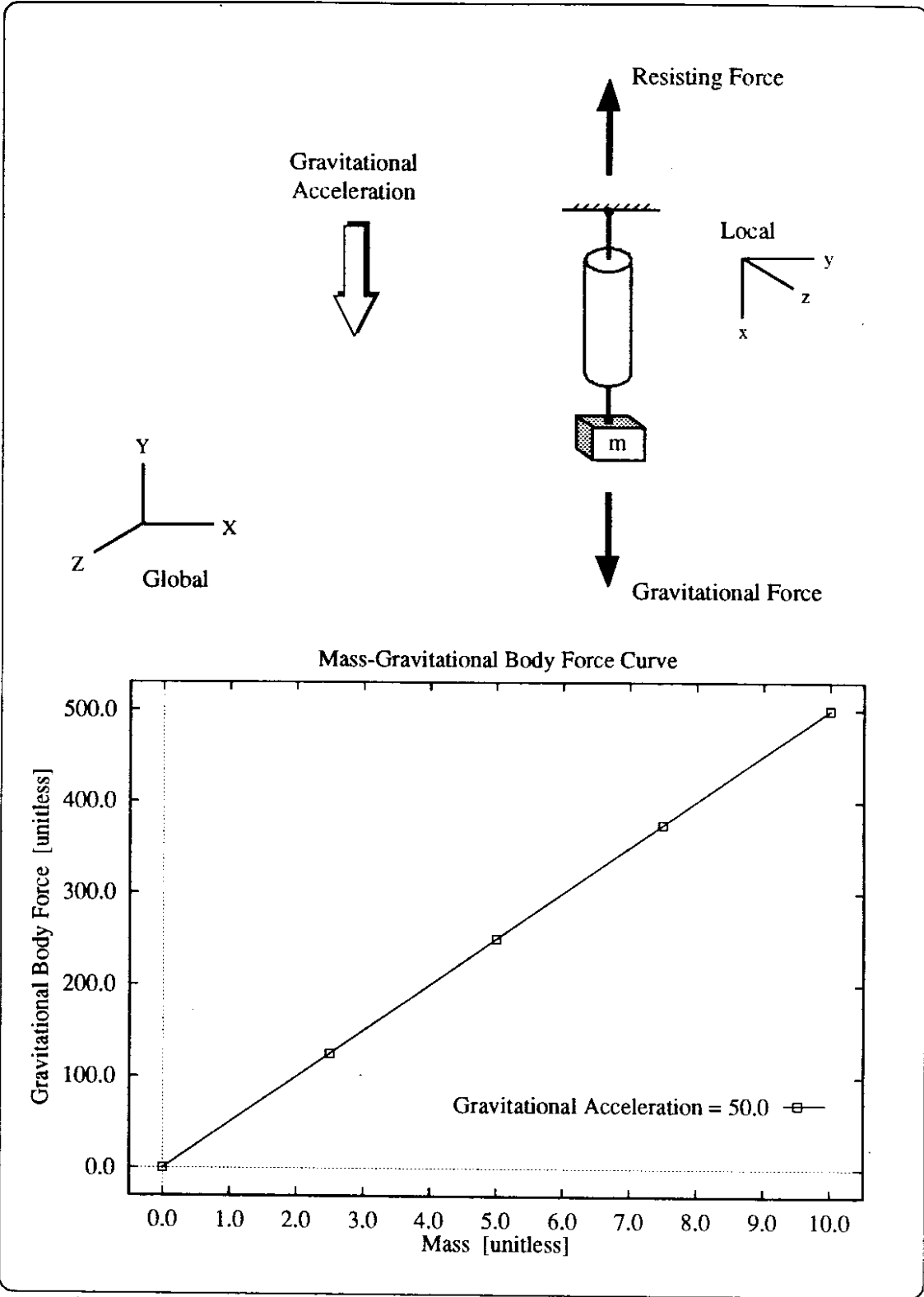


**Figure 2.17:** Mass-Gravitational field modeling verification test.



To verify the correct response of several DF elements interacting as a system, the “connectivity” test shown in Figure 2.18 was conducted. Two DF elements, having unitless stiffnesses  $k_1 = 1800$  and  $k_2 = 2250$ , were connected in both a series and a parallel arrangement. The effective stiffnesses of these systems are given by the following equation:

$$k_{eff}^{series} = \frac{1}{\frac{1}{k_1} + \frac{1}{k_2}} = 1000 \quad (2.13)$$

$$k_{eff}^{parallel} = k_1 + k_2 = 4050$$

The two systems were subjected to varying loads and the displacement of the end node was recorded. The slopes of the resulting load-displacement curves were found to be equal to their predicted values, providing verification of correct system behavior. Additionally, the distribution of the end node displacement to the elements in series, and the distribution of the load force to the elements in parallel, was found to be correct (inversely and directly proportional to element stiffness, respectively).

Correct undamped and damped dynamic response was verified by subjecting the DF element to resonant harmonic loading—sinusoidal loading at the natural period of the element. Without damping present,

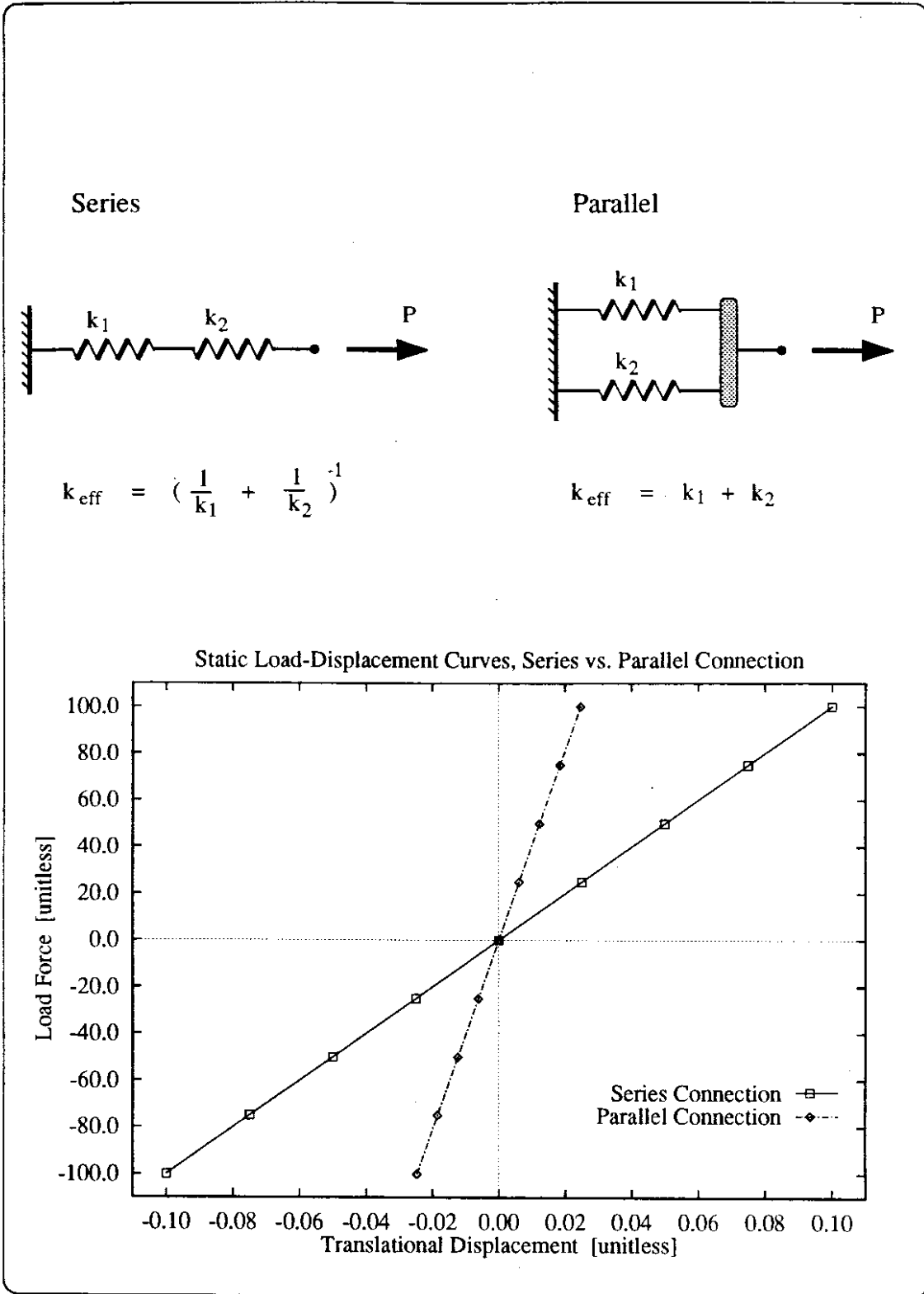


**Figure 2.18:** Connectivity verification test.

the displacement response should grow without bounds according to the equation:

$$u(t) = \frac{1}{2} \frac{P_0}{k} (\sin \omega t - \omega t \cos \omega t) \quad (2.14)$$

- where  $u(t) \equiv$  displacement at time  $t$
- $p_0 \equiv$  amplitude of resonant sinusoidal loading;  
load at time  $t$  is:  $p(t) \equiv p_0 \sin(\omega t)$
- $k \equiv$  elastic stiffness of DF element
- $\omega \equiv$  natural circular frequency of DF element,  
which is assumed to have mass  $m$

With damping present, the response will reach a steady-state amplitude,  $Q_0$ , according to the equation:

$$u(t) = Q_0 \left[ e^{-\xi \omega t} \left( \frac{\xi}{\sqrt{1 - \xi^2}} \sin \omega_d t + \cos \omega_d t \right) - \cos \omega t \right] \quad (2.15)$$

$$Q_0 = \frac{1}{2} \frac{P_0}{k} \frac{1}{\xi}$$

- where  $Q_0 \equiv$  steady-state response amplitude
- $\xi \equiv$  damping ratio; fraction of system critical damping
- $\omega_d \equiv$  damped natural circular frequency;  $\omega_d \equiv \omega(1 - \xi^2)^{1/2}$

Figure 2.19 shows the response plots of an undamped and a damped DF element subjected to resonant harmonic loading. They are numerically identical to equations (2.4) and (2.5) for the system/loading parameters chosen for the test, indicating correct element dynamic elastic behavior.

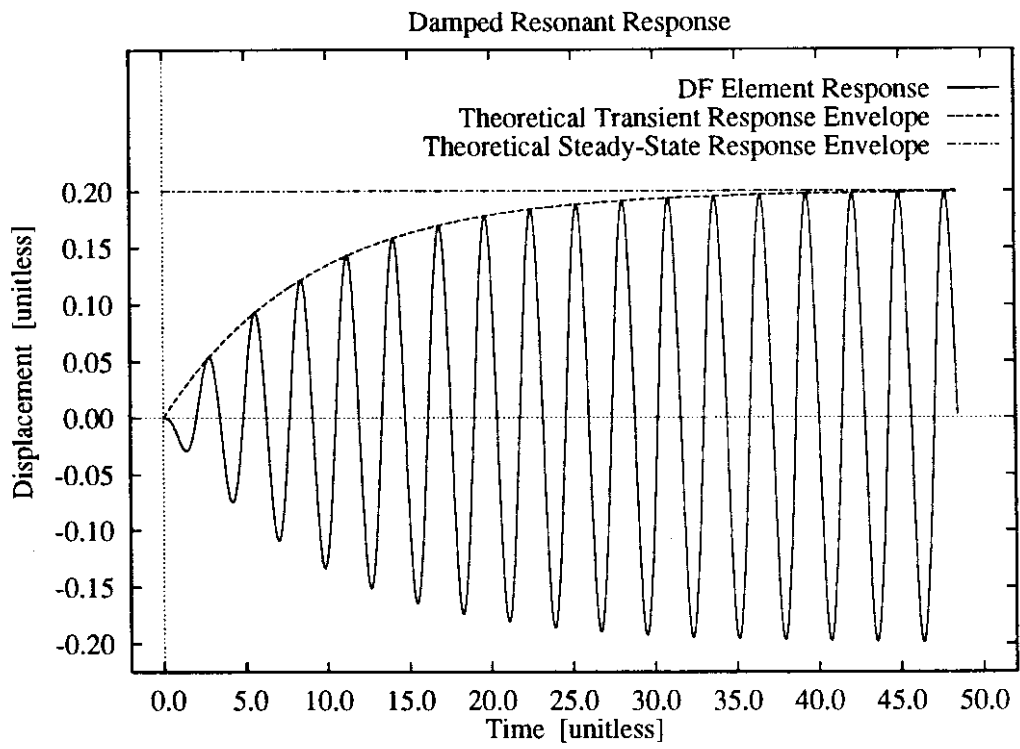
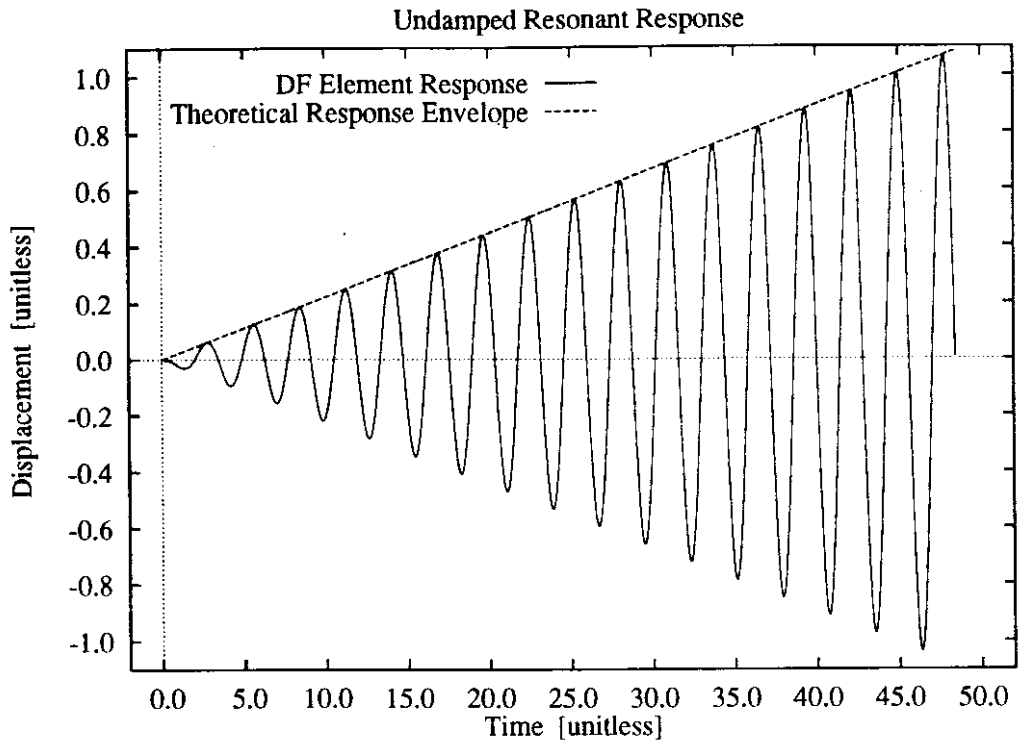


**Figure 2.19:** Resonant harmonic excitation dynamic response verification test.

Note also that the value of the steady-state response amplitude,  $Q_o$ , is dependent on the damping ratio  $\xi$ , providing a simple numerical check on the element's ability to correctly model viscous damping.

Sinusoidal loading was also used to test the DF element's nonlinear stiffness capabilities: bilinear hysteresis, elastic stiffness degradation, strain hardening options, gap development, and in-gap bilinear hysteresis. The results of these tests are presented in the four graphs of Figures 2.20 and 2.21. For these tests, no mass was assigned to the DF element, making the load quasi-static. In each of the four tests, the unitless elastic and plastic stiffnesses were  $k_{e_i} = 5000$  and  $k_p = 240$ , respectively. The first graph of Figure 2.20 shows the results of a test of the elastic stiffness degradation capability; here the parameter  $\alpha$  of equation (2.11) was taken to be  $\alpha = 0.12$ . Kinematic strain hardening, the default strain hardening rule, was used. In the second test, an identical sinusoidal load was applied to two DF elements, one using kinematic strain hardening, the other using isotropic strain hardening. The results of this test are shown in the second graph of Figure 2.20. The first graph of Figure 2.21 depicts the results of a test in which the DF element was allowed to develop a gap. No in-gap stiffness was specified (the default condition); the value of the  $\gamma$  parameter of equation (2.12) was  $\gamma = 0.30$ . In the fourth test, the same DF element was used, but with in-gap unitless stiffnesses of  $k_1 = 300$  and  $k_2 = 10100$ , where  $k_1$  and  $k_2$  are as defined in Figure 2.11(c). The results of this test are given in the second graph of Figure 2.21.

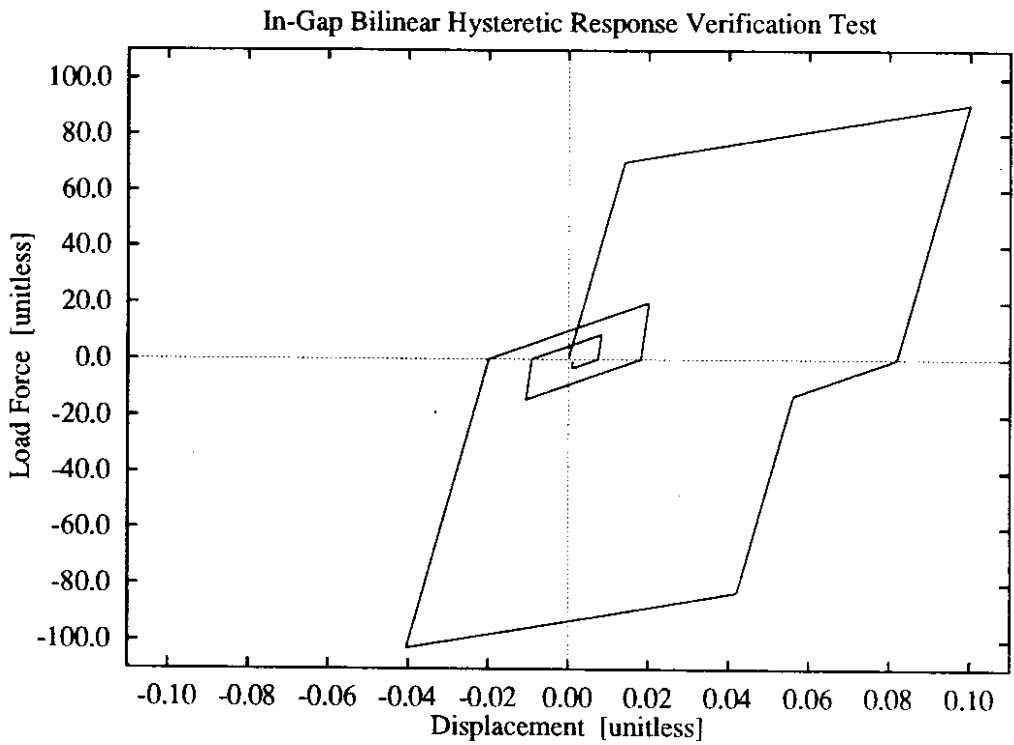
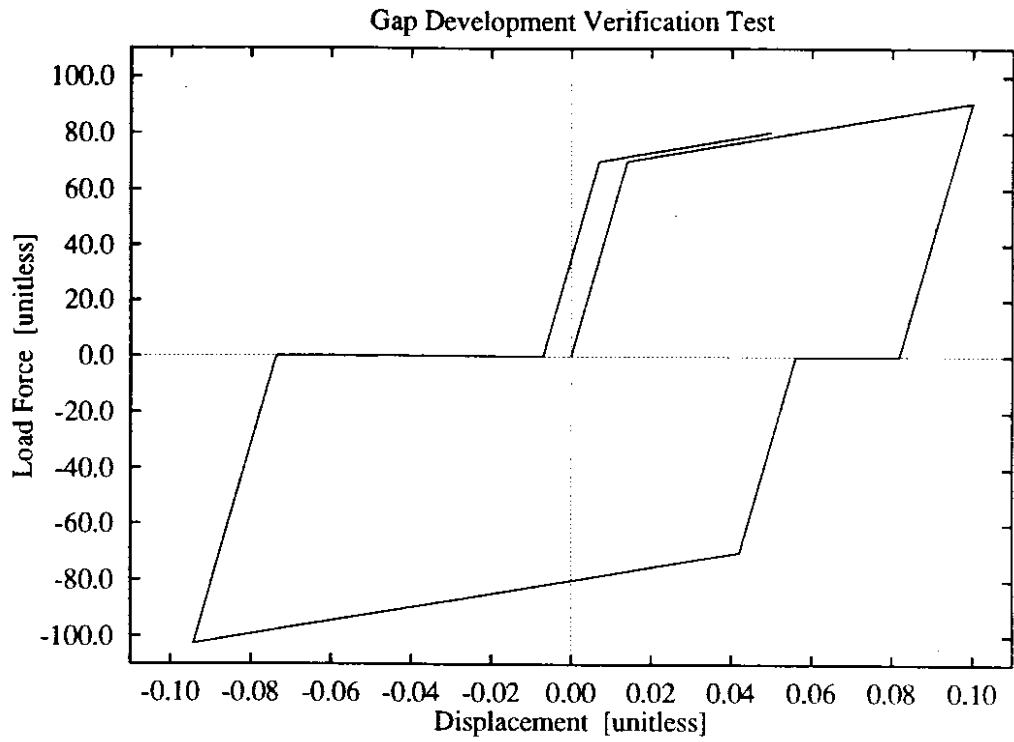


**Figure 2.20:** Nonlinear stiffness properties verification tests:  
 (top) bilinear hysteresis with elastic stiffness degradation;  
 (bottom) strain hardening options.

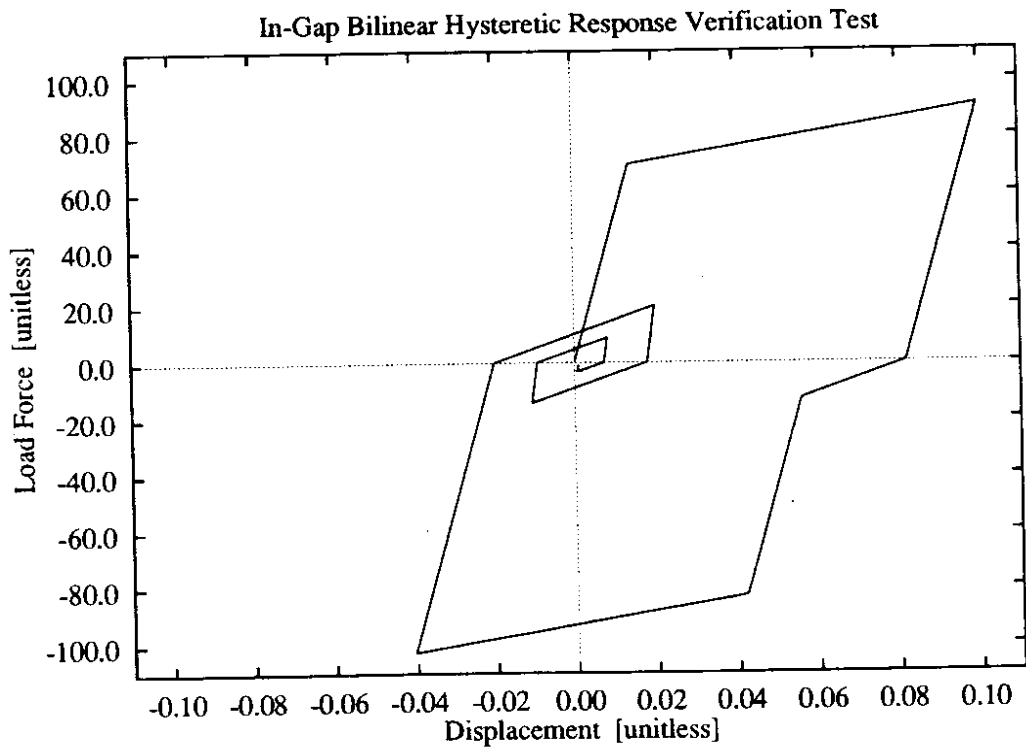
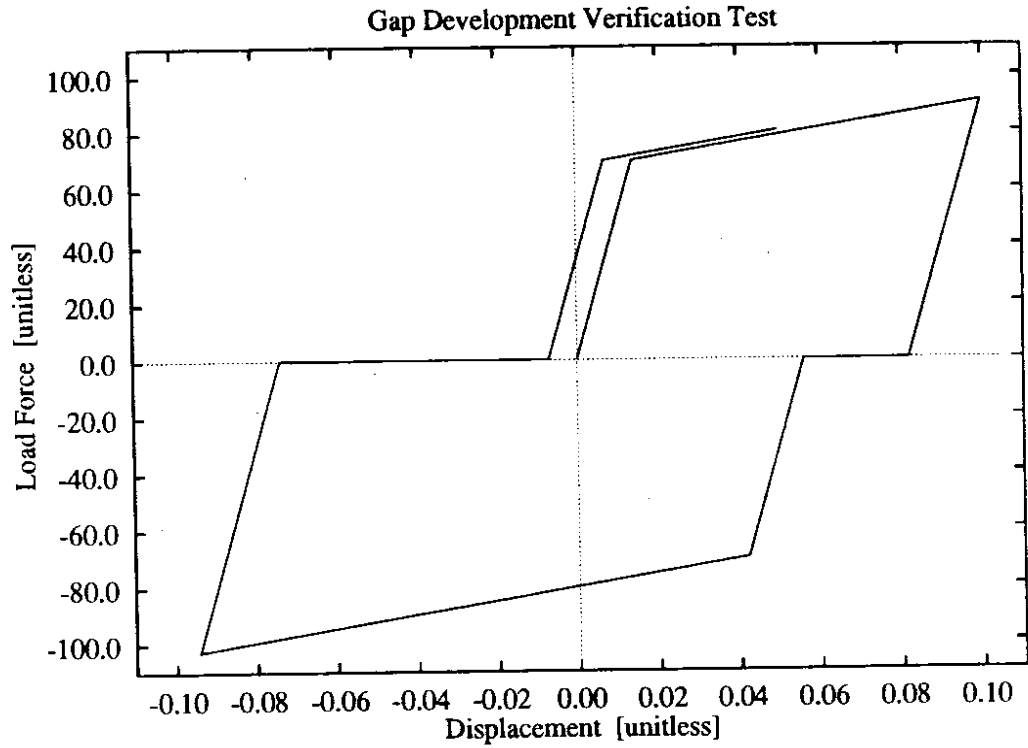


**Figure 2.21:** Nonlinear stiffness properties verification tests: (top) bilinear hysteresis with gap development; (bottom) bilinear hysteresis within gap.

## **Chapter 3**

# **Findings and Interpretation**

### **3.1 Parametric Study Approach and Objectives**

A parametric study was undertaken to investigate the effects of incorporating foundation models of varying complexity into the seismic analysis of a bridge. Specifically, models relevant to representing soil–structure interaction at spread footing foundations and pile foundations were analyzed. The purpose was to compare the various foundation models with each other and with standard support conditions, such as fixed or elastic supports, in terms of the effects on bridge structural response. It should be noted that since the study results were not correlated with experimental response data, the study does not constitute a verification test of these models' accuracy in modeling bridge supports. Rather, it is an exploration of the structural response effects of incorporating these models in seismic bridge analysis. The identified effects are consistent with the assumptions made in the models themselves; establishing consistency between these assumptions and real bridge–foundation–soil behavior is outside the scope of this project.



However, these are in general well accepted assumptions for rationally incorporating soil–structure interaction in analysis.

The parametric study was conducted in two portions, one addressing spread footing foundation modeling, and the other addressing pile foundation modeling. Two Washington State highway bridges were chosen to provide bridge design guidance for the development of NEABS structural analysis models: a three-span overpass on Interstate 90 near Moses Lake (now dismantled), and the multispan westbound Interstate 90 bridge over Mercer Slough near Seattle. Bridge design, soil parameters, and other pertinent data was readily available for both bridges, both having been the subject of previous WSDOT research projects.

The bent columns of the Moses Lake bridge were founded on spread footings, while the Mercer Slough bridge bents' columns are supported by a pile–pile cap foundation. As will be described, a bridge bent from both of these bridges was analyzed with NEABS using a variety of foundation models. These bridge bent–foundation systems were subjected to lateral seismic excitation, transverse to the long axis of the bridge. Several key parameters of the resulting bent responses were chosen to characterize different aspects of the overall bent response, and the effects of the different foundation models on these response parameters were compared.

In this chapter, the two studies are considered; first the spread footing foundation study for the Moses Lake bridge, and then the pile

foundation study for the Mercer Slough bridge. The approach used in each study is discussed in detail, and the results are presented.

## **3.2 Spread Footing Foundation Study**

The study using the Moses Lake bridge employed four different spread footing foundation models, along with a fixed-support “foundation.” The NEABS model of the bent was based on the actual bridge bent, but a selected variation of founding soil properties was assumed in developing the foundation models, and thus the properties do not represent the soil conditions particular to the bridge. Descriptions of the bridge and site, the NEABS model of the bridge bent, the foundation models employed, the seismic excitation applied, and the observed results are presented in the subsequent sections.

### *3.2.1 Description of Bridge and Site*

The bridge was located on Interstate 90, about 13 miles east of Moses Lake, and it was recently the subject of a WSDOT research project [39 and 40]. It was one of a pair of reinforced concrete bridges constructed in 1966 to span a now-abandoned railroad line. Figure 3.1 shows a photograph of the bridge, along with a plan-view drawing of the bridge and the site topography. The three-span bridge was 142 feet long. Two bents, skewed at 12.8°, supported the center span of 60 feet. The adjoining end spans

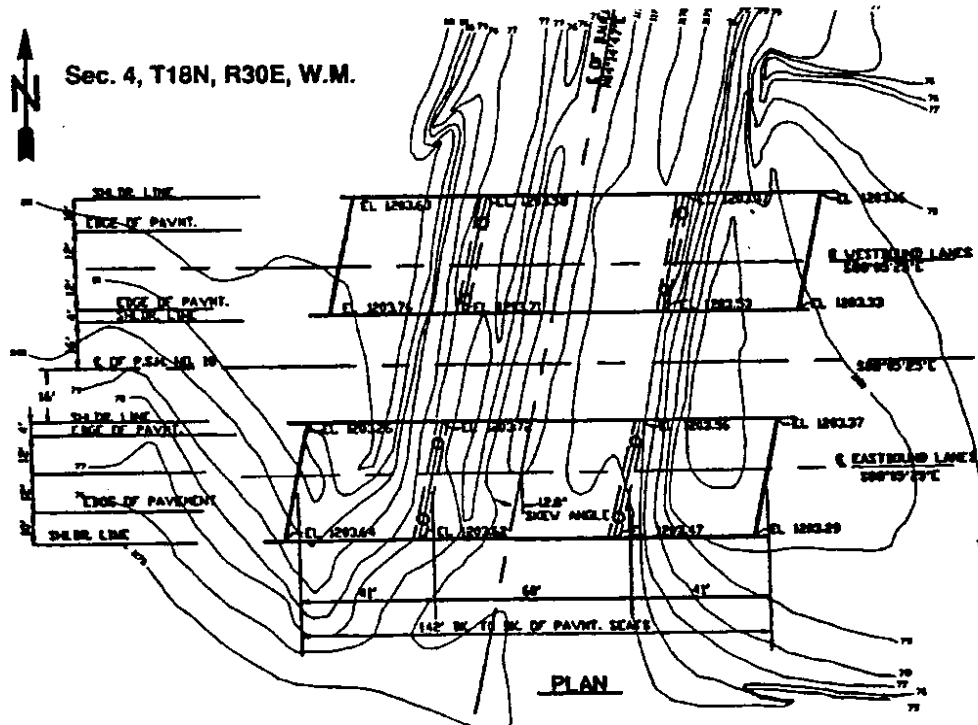
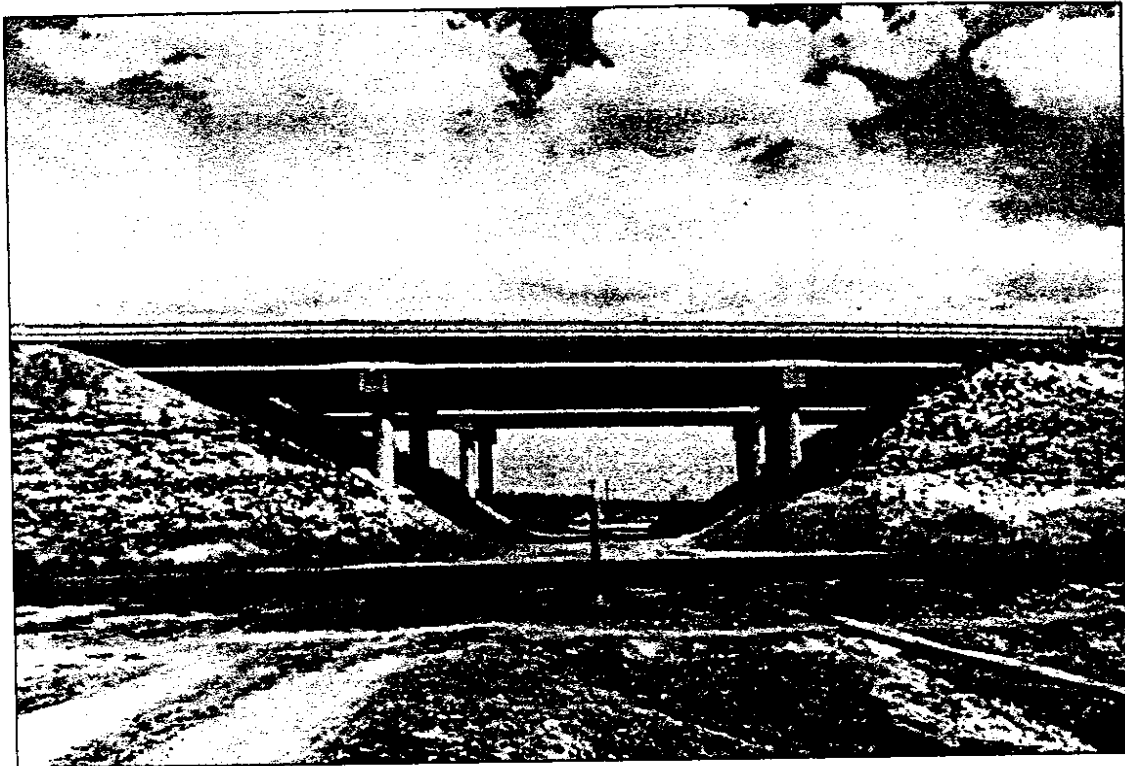


Figure 3.1: Interstate 90 three-span bridge near Moses Lake: (top) photograph showing elevation view of bridge; (bottom) plan view drawing of bridge and site. Adapted from [40] and [39].

were each 41 feet long, supported by the bents at one end and abutments at the other.

The reinforced concrete deck, 40 feet wide and 6.5 inches thick, was continuous over the two bents. The deck was supported by six prestressed concrete I-girders, 3 feet 6 inches deep and spaced at 6 feet 10 inches on center. These girders extended 2 inches into the 12-inch thick diaphragms at the bents and the cast-in-place abutments. At the bents, the heavily-reinforced diaphragm was cast monolithically with the slab and connected to the underlying bent crossbeam with No. 10 dowels. Eberhard *et al.* [39] report that, because of the heavy reinforcement and monolithic construction, the bridge was able to effectively transfer the high lateral test loading of the deck to the bents and the abutments. The abutments in particular were very stiff and strong. The bridge as a whole was therefore stiff and strong in the lateral direction, and tended to respond as a unit to lateral loads.

Figure 3.2 shows a detail of the bridge bents. The 42-inch wide, 36-deep crossbeam was reinforced longitudinally with ten No. 11 bars on the bottom and four No. 10 and six No. 11 bars on the top. Shear reinforcement was provided by No. 5 stirrups spaced at 12 inches. The crossbeam length was 39.5 feet, and it supported a static load of about 472 kips. The two supporting columns both had clear heights of about 25 feet, and their centerlines were spaced 24 feet apart. The circular columns had outside diameters of 36 inches. Eleven No. 9 bars provided

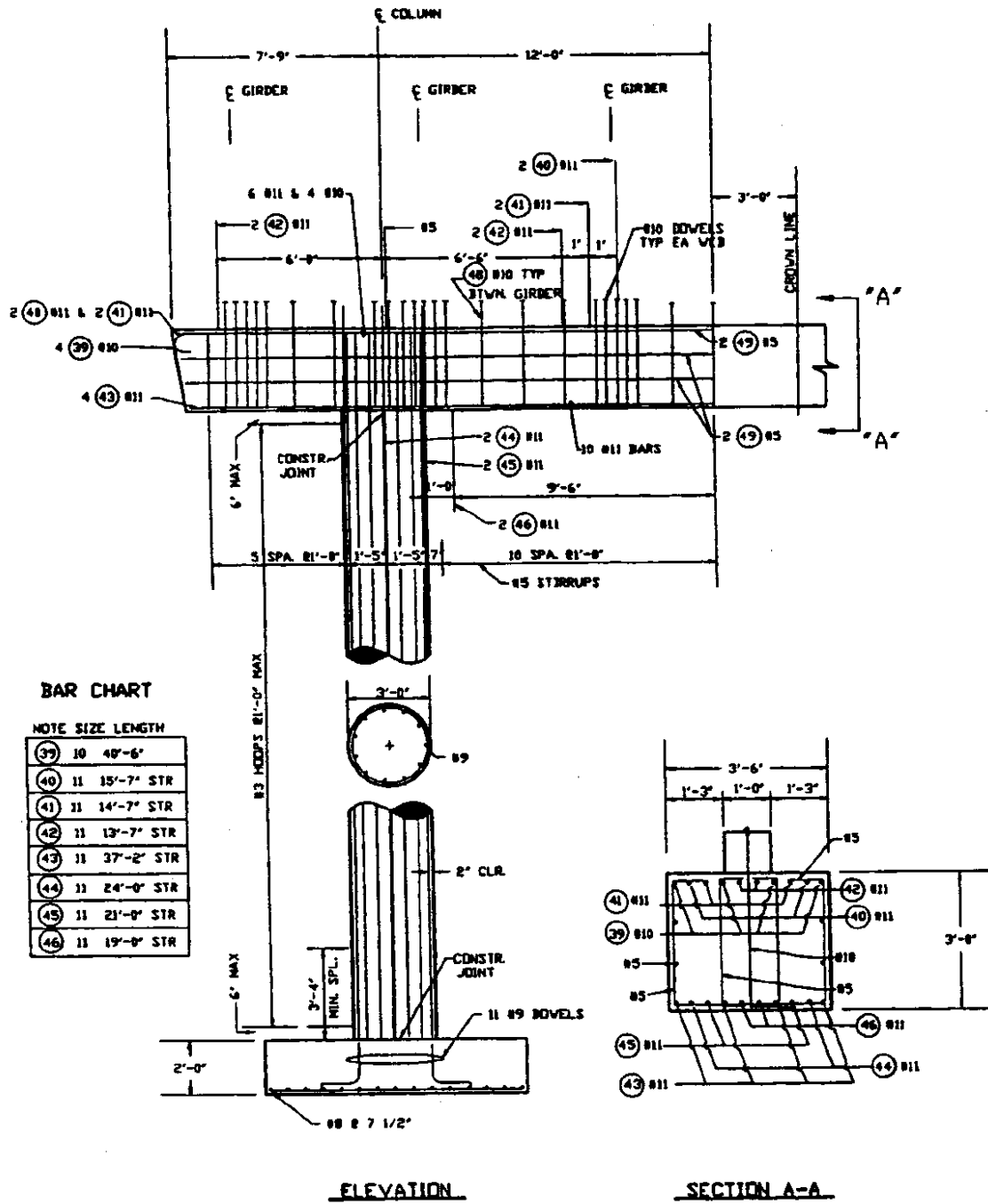


Figure 3.2: Moses Lake bridge bent column, crossbeam, and spread footing foundation details. Adapted from [39].

longitudinal reinforcement. The bars were spaced evenly around the cross-section perimeter and extended into the crossbeam with no splice. However, load transfer between the column bottom and the spread footing depended on a 40 inch lap splice (35 bar diameters). Column transverse reinforcement consisted of No. 3 hoops spaced at 12 inches; the hoops were closed with a 14-inch lap splice, but had no hooks into the column core. The spread footings were 9.5 feet square in plan and 24 inches deep. They were reinforced only at the bottom, by fourteen #8 bars in each direction. The footings and lower portions of the columns were embedded in compacted fill up to about half the column height, as shown in Figure 3.1.

The majority of the concrete used in the bridge was WSDOT class AX mix, which had a specified compressive strength at 28 days,  $f'_c$ , of 4000 psi. Eberhard *et al.* reports a measured in-situ compressive strength,  $f'_c$ , of  $6400 \pm 300$  psi, and a measured modulus of elasticity,  $E_c$ , of  $4700 \pm 200$  ksi, for twelve cores taken from the columns [39]. Two samples of the longitudinal steel were also taken from the column, and found to have a modulus of elasticity,  $E_s$ , of 29,500 ksi, a yield stress,  $f_y$ , of 50.6 ksi, and an ultimate strength,  $f_u$ , of 86.3 ksi. The spread footings and the abutment wall were constructed of WSDOT class B mix with a specified compressive strength of  $f'_c = 3000$  psi.

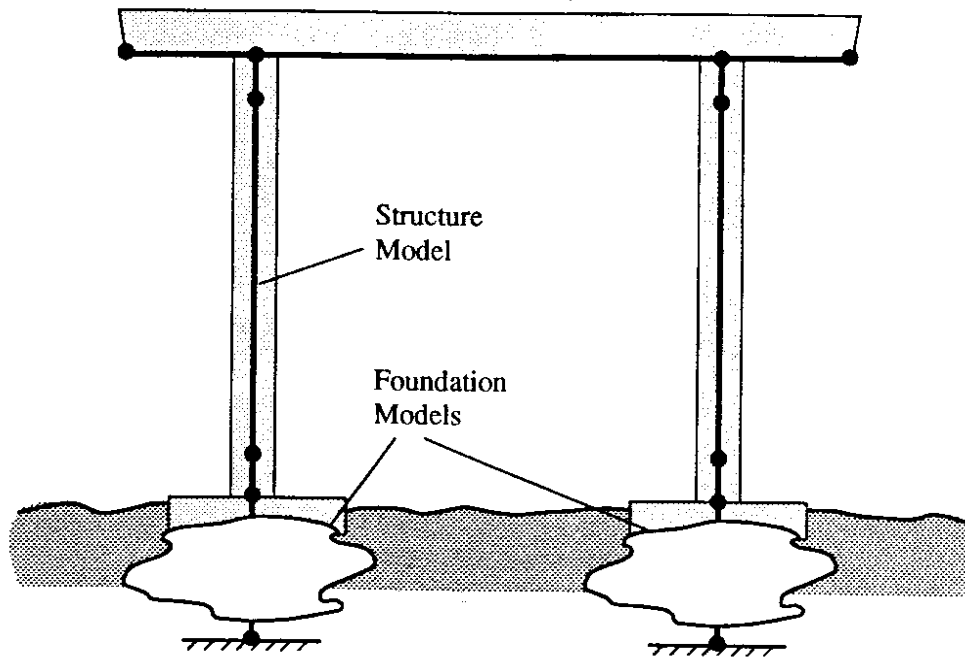
### 3.2.2 Structure Model

It was anticipated that the strength and stiffness of the bridge superstructure and abutments would minimize the dynamic participation of the soil-spread footing foundation in the overall seismic response of the bridge. To obtain a clearer understanding of the contribution to the structural response of the various foundation models, the spread footing study was confined to the analysis of an isolated bent. Additionally, the fill material surrounding the lower half of the columns was neglected. A schematic of the bent and foundation models used in the NEABS analyses is given in Figure 3.3. Note that the springs and dampers that are shown correspond to equivalent elastic half-space models for spread footings, as described in Section 2.1.3.

The bent structure itself was modeled with nine beam elements. This bent structure model was supported on various foundation models, which were comprised of DF elements. The crossbeam was modeled with elastic beam elements, while the columns used elasto-plastic beam elements. The modulus of elasticity used for the columns was  $E = 4600$  ksi, as used by Eberhard *et al.* in their analyses [39]. The moment of inertia,  $I$ , that was used was half of that of the gross column cross-section, as suggested by Buckle *et al.* [1]. Thus, for the columns, the elastic stiffness was proportional to  $EI_{eff} = 1/2EI_g$ .

To define the yield surface for the elasto-plastic beam column elements, NEABS requires that an axial force-yield moment interaction curve be specified for bending about both of the beam element's local axes.

(a) Structure Model



(b) Support Models

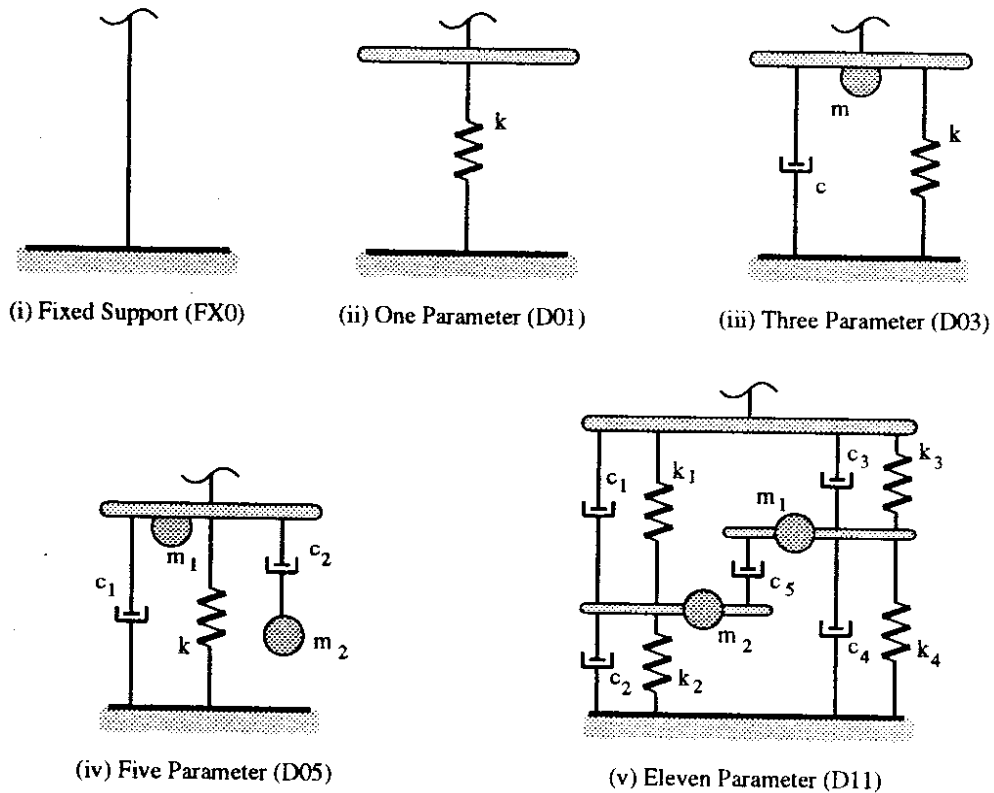


**Figure 3.3:** Schematic of the NEABS models of the Moses Lake bridge bent and supports employed: (a) model of the bent structure, with beam elements forming columns and crossbeam; (b) five support models—fixed supports and four models representing spread footing foundations.



NEABS uses the following cubic equation to represent these interaction curves:

$$M_y(P) = M_o \left[ a_0 + a_1 \left( \frac{P}{P_o} \right) + a_2 \left( \frac{P}{P_o} \right)^2 + a_3 \left( \frac{P}{P_o} \right)^3 \right] \quad (3.1)$$

where  $P \equiv$  axial force on beam element (tension positive)

$M_y \equiv$  yield moment under axial force  $P$

$M_o \equiv$  yield moment in pure bending ( $P = 0$ )

$P_o \equiv$  ultimate axial compressive capacity,  
defined to be positive

$a_0, a_1, a_2, a_3 \equiv$  required input coefficients

The required coefficients were determined by fitting a cubic curve to axial force-bending moment strength interaction data computed for the actual columns upon attainment of a maximum concrete strain of  $\epsilon_{cu} = 0.003$ . The computed interaction data was generated by a computer program developed by Marsh [41], which discretizes the column cross-section and utilizes material constitutive laws developed by Burns and Seiss for steel and by Park and Kent for concrete, as reported in Park and Paulay [42], in its force equilibrium calculations. To facilitate this curve

fitting, the following equations were developed, which force the curve to pass through  $M_0$  and  $P_0$ , and cause it to “peak” at  $M_m$ , as defined below:

$$\begin{aligned}
 a_0 &= 1 \\
 a_1 &= \frac{1}{\alpha} [r^4 - qr(2 - 3r)] \\
 a_2 &= \frac{1}{\alpha} [2r^3 - q(1 - 3r^2)] \\
 a_3 &= \frac{1}{\alpha} [r^2 - q(1 - 2r)] \\
 s &= \frac{1}{2a_3} [1 - a_1 - \sqrt{a_1^2 - 2a_1 - 4a_3 + 1}]
 \end{aligned} \tag{3.2}$$

where  $M_m \equiv$  maximum yield moment

$P_m \equiv$  compressive axial force at maximum yield moment (positive);  $M_m$  and  $P_m$  would typically occur at the balance point of an axial force–bending moment curve for a square cross-section

$q \equiv (M_m - M_0)/M_0$

$r \equiv P_m/P_0$ ,  $r \neq 1/2$

$\alpha \equiv r^2(1 - r)^2$

$s \equiv$  ratio  $P_t/P_0$ , required by NEABS, where  $P_t$  is the ultimate axial tensile capacity; in this method,  $s$ , and thus  $P_t$  also, are curve-dependent parameters

Figure 3.4 shows a comparison of the axial force–bending moment strength interaction data calculated for the column and the cubic curve used in the NEABS model, obtained by the above procedure; the fit is quite close. Since the column is axially symmetric, these curves apply to column

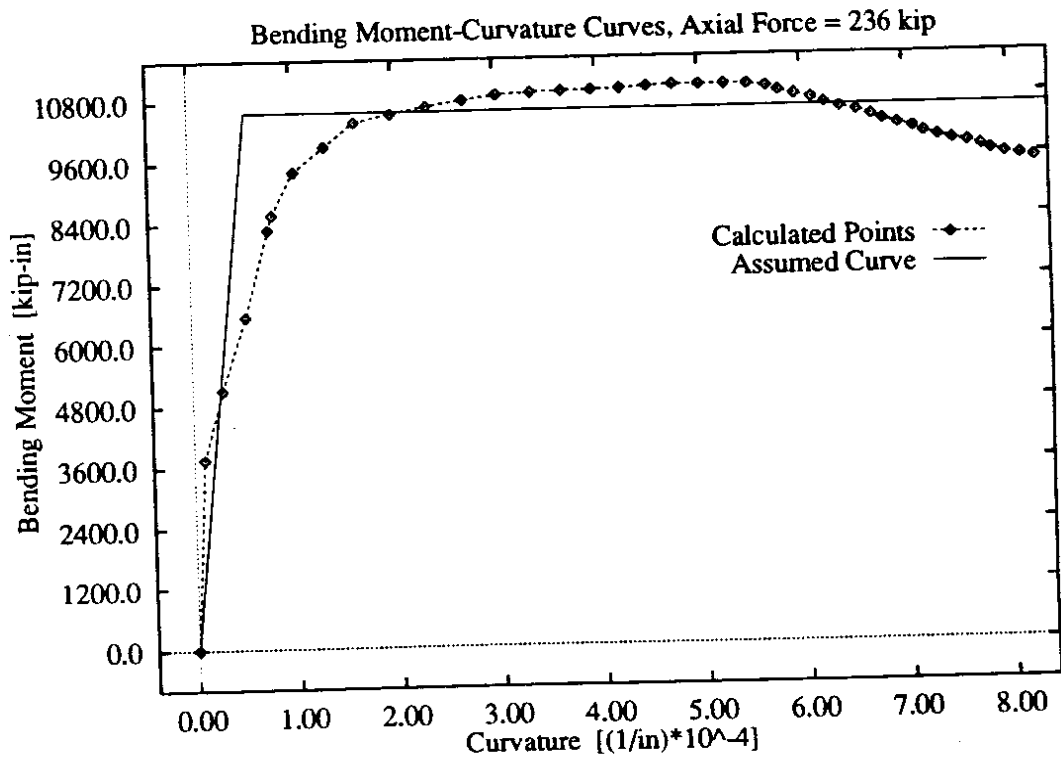
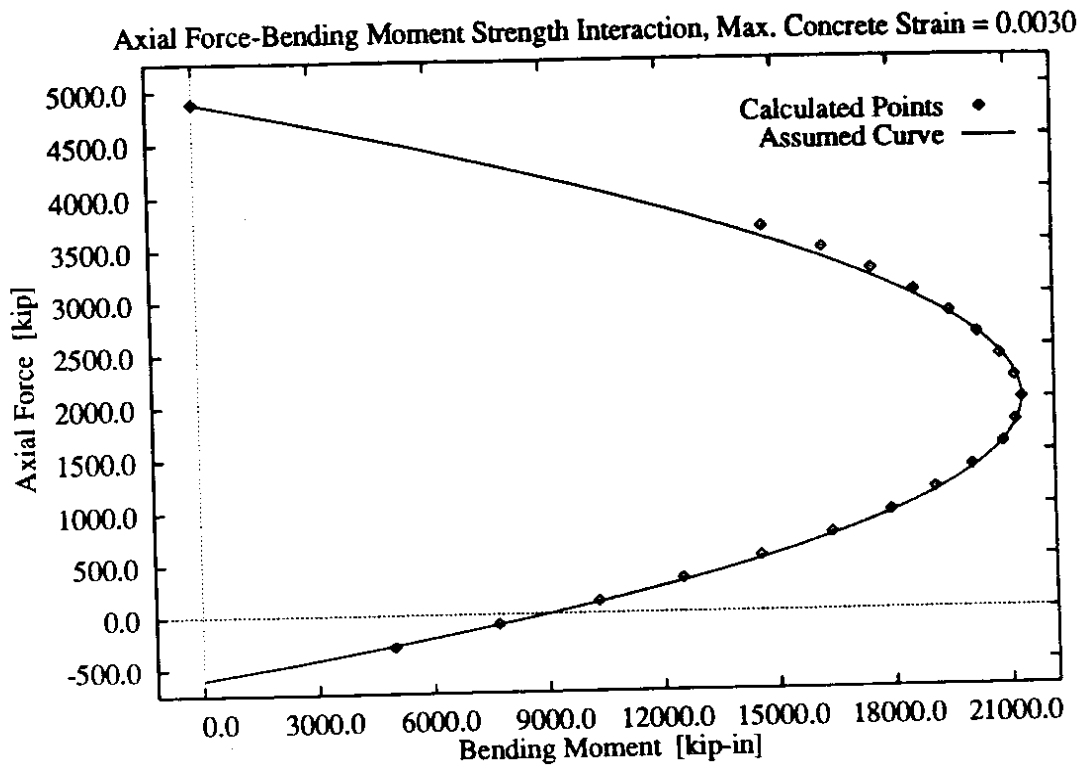


**Figure 3.4:** Calculated and assumed strength characteristics of Moses Lake bridge bent columns. Axial force–bending moment strength interaction curve taken at attainment of concrete strain of 0.003 in./in., and bending moment–curvature curve taken at static axial load of 236 kips.

bending about any axis. As another indication of this beam's accuracy in modeling the column's behavior, Figure 3.4 also shows a comparison of the bending moment–curvature relation calculated for the column under the static dead load of 236 kips and of the elasto-plastic curve used in the NEABS model. The bending moment–curvature data was calculated by a version of the computer program developed by Marsh [41] discussed earlier. The slope of the elastic portion of the NEABS curve is again  $EI_{eff} = \frac{1}{2}E_cI_g$ . The yield moment is determined by equation (3.1), the parameters of which were again determined by fitting a curve to the column's axial force–bending moment strength interaction diagram taken at attainment of a maximum concrete strain of  $\epsilon_{cu} = 0.003$ . This fit is also close.

The stiffness of the crossbeam was deemed to be quite high relative to that of the column because of the heavy reinforcement and its secure connection with the monolithic diaphragm–deck structure. The crossbeam was therefore modeled as an essentially rigid member, having a stiffness that was approximately four orders of magnitude larger than that of the columns. The mass supported by the bent was applied by specifying an appropriate density for the three beam elements forming the crossbeam. Because NEABS lumps beam mass to the nodes at the beam element ends, the mass supported by the bent was therefore distributed to four lumped masses, two larger masses at the column tops, and two smaller masses at the crossbeam ends. The mass moment of inertia of the crossbeam used

in the NEABS model was calculated to be sufficiently close to that of the actual crossbeam assuming a uniform distribution of the supported mass.

To apply damping to the bent structure, the following rationale was used. If the crossbeam was truly rigid, and the bent columns were fixed at their bases, the bent would be a single-degree-of-freedom system. Further, if the columns remained elastic, then the natural period of transverse vibration of this system may be calculated to be 0.53 seconds. Damping was applied to the members forming the columns and the crossbeam by assuming damping in this mode of vibration to be 5 percent of critical ( $\xi = 0.05$ ), and forcing damping in vibrational modes of all other periods to be higher. These constraints led to the following form of the Rayleigh damping coefficients:

$$\alpha = \xi \omega \tag{3.3}$$

$$\beta = \frac{\xi}{\omega}$$

- where
- $\omega$   $\equiv$  frequency of the uncoupled vibrational mode assumed to have minimum Rayleigh damping (taken here to be  $\omega = 2\pi/t$ , where  $t = 0.53$  seconds)
  - $\xi$   $\equiv$  fraction of critical damping to be applied to vibration at the above frequency,  $\omega$  (here  $\xi = 0.05$ )
  - $\alpha$   $\equiv$  Rayleigh damping coefficient; fractional multiplier to apply to the system mass matrix
  - $\beta$   $\equiv$  Rayleigh damping coefficient; fractional multiplier to apply to the system stiffness matrix

The NEABS models supported on the various foundation models are not single-degree-of-freedom systems, and their fundamental frequencies of vibration do not, in general, match the frequency used in the above method for determining the Rayleigh damping coefficients for the column–crossbeam portion of the system. However, by using these same  $\alpha$  and  $\beta$  coefficients for all the NEABS analyses, and by not allowing Rayleigh damping to apply to the DF elements forming the foundation models, the contribution to the system damping from the column–crossbeam structure’s Rayleigh damping was consistent for all of the analyses.

### *3.2.3 Foundation Models*

As previously discussed, four foundation models were compared, as well as fixed-base supports. The four foundation models were all discrete approximations of the elastic half-space continuum model, but incorporated varying levels of complexity. These five support conditions are shown in Figure 3.3.

The spring stiffnesses for the spring-only model were taken from the equivalent static stiffnesses of an elastic half-space, which are given in equations (2.2). It will be referred to as a “one parameter” model because it requires the specification of one parameter, the spring stiffness, in each degree-of-freedom. The three-parameter spring-mass-dashpot model was presented by Veletsos and Verbič [29]. The five-parameter model was

presented by Meek and Veletsos; here the parameters were taken from Wolf's discussion of this model [31]. The eleven-parameter model was presented by Jean *et al.* [33]. A nine-parameter model, presented by Wolf and Paronesso [32], was also tried, but it was not pursued because of apparent numerical instabilities when applied within NEABS, probably due to the model's numerous negative stiffness and damping parameters. As shown in Figure 3.3, these models are also assigned a name of the form "Dnn," where *nn* refers to the number of required parameters per degree-of-freedom. As discussed in Chapter Two, the more complex discrete models yield greater accuracy in representing the assumed half-space continuum soil model over a wider range of frequencies.

Since these discrete foundations are models of an *elastic* half-space, the damping present in those foundations incorporating dashpots models radiation damping only. Energy dissipation due to material damping, or to nonlinear action of the soil, is not modeled. These mechanisms would be expected to be significant only in the region of the soil in the immediate vicinity of the structure, the soil near-field. The elastic half-space foundation models are therefore better suited for capturing the effects of the far-field response than the near-field response. However, in the absence of applicable near-field models, the foundation models were applied directly to the bent base.

To obtain the equivalent radii for the square footings, the method discussed in conjunction with the Pais and Kausel prismatic foundation in

Chapter Two was used for all of the foundation models. Unlike the actual bridge bents, the footings and the columns were not assumed to be embedded, so no modification of the models to account for embedment was necessary.

Three soil stiffnesses were used in testing each model, making a total of twelve individual foundations in addition to the fixed-base bent. The stiffnesses were selected to span a range of soil stiffnesses commonly encountered. Based on soil tests reported by Eberhard *et al.* [39], the unit weight of the soil,  $\gamma_s$ , was taken to be 110 pcf. Three shear wave velocities,  $c_s$ , of 300, 700, and 1300 fps were selected to produce the three soil stiffnesses; for the given soil density, these corresponded to soil shear moduli,  $G$ , of 2140, 11,650, and 40,170 psi, respectively. These soils are identified as “soft,” “intermediate,” or “stiff,” referring to their relative stiffnesses. Poisson’s ratio for the soil was taken to be  $\nu = 0.33$ .

#### *3.2.4 Seismic Excitation*

Acceleration histories from actual earthquakes formed the basis of the seismic excitation applied to the bridge bent–foundation system. Two earthquake acceleration records were chosen to provide different frequency contents, and both records were scaled to two different intensities, providing four different frequency content–intensity combinations to be used as seismic input.



The two earthquake records chosen were the S00E component of the El Centro record of the 1940 Imperial Valley Earthquake (referred to as the "El Centro" record) and the N86E component of the Olympia record of the 1949 Western Washington earthquake (or "Olympia" record). The 1940 Imperial Valley earthquake was of 6.7 Richter magnitude, and the peak ground acceleration of the El Centro record was 0.35g. The 1949 Western Washington earthquake registered a magnitude 7.1 on the Richter scale, and 0.28g was the peak ground acceleration of the Olympia record. Acceleration history plots of the complete records are given in Figure 3.5.

As can be seen in Figure 3.5, it was not necessary to use the entire duration of either record. The method proposed by Trifunac and Brady (reported in [36]) for determining the strong-motion duration was employed to limit the record durations used as seismic input. The Trifunac and Brady duration lies between the accumulation of the first 5 and 95 percent of the quantity  $\int a^2 dt$ , where  $a$  is the earthquake acceleration and  $t$  is time. The duration used in this study began at the beginning of the record and ended at end of the Trifunac and Brady strong-motion duration (at 26.10 seconds and 24.42 seconds from the beginning of the record for the El Centro and Olympia records, respectively, as reported in [36]). Acceleration plots of the record durations that were modeled and elastic single-degree-of-freedom acceleration response spectra for the two records are given in Figures 3.6 and 3.7.

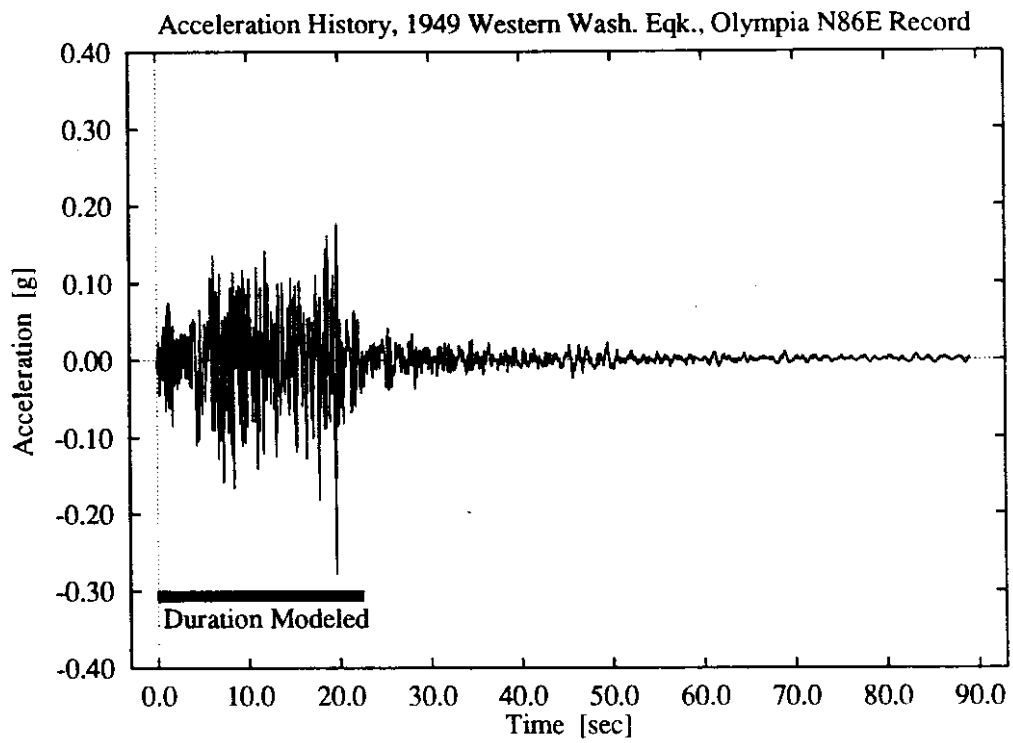
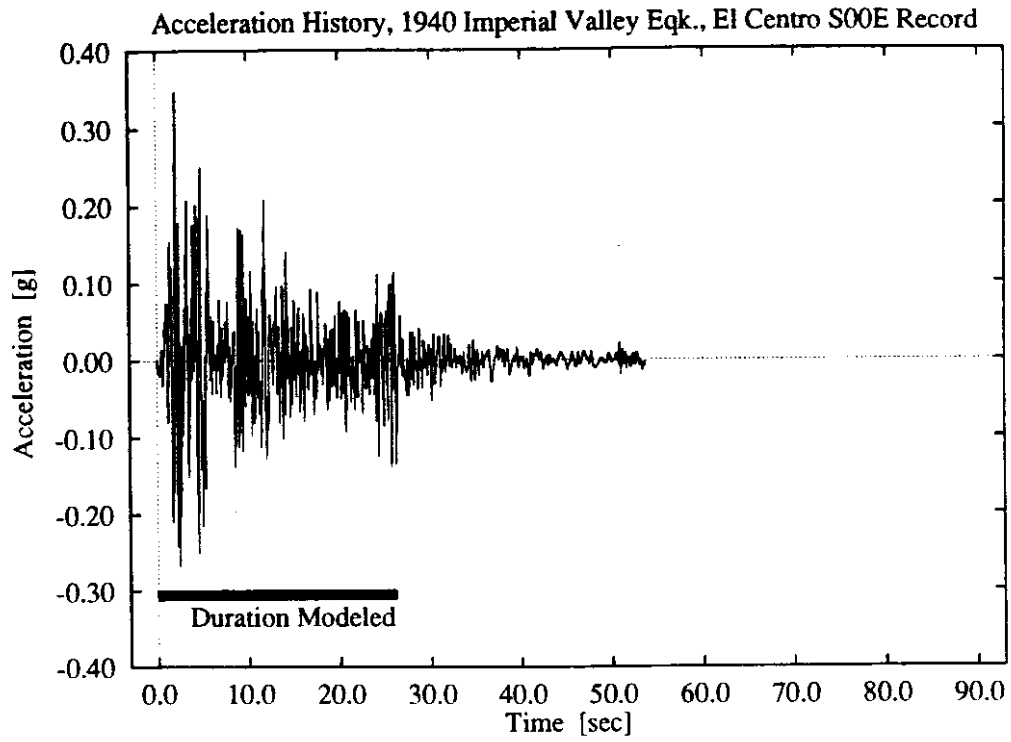


**Figure 3.5:** Complete acceleration history plots of the El Centro and Olympia records.

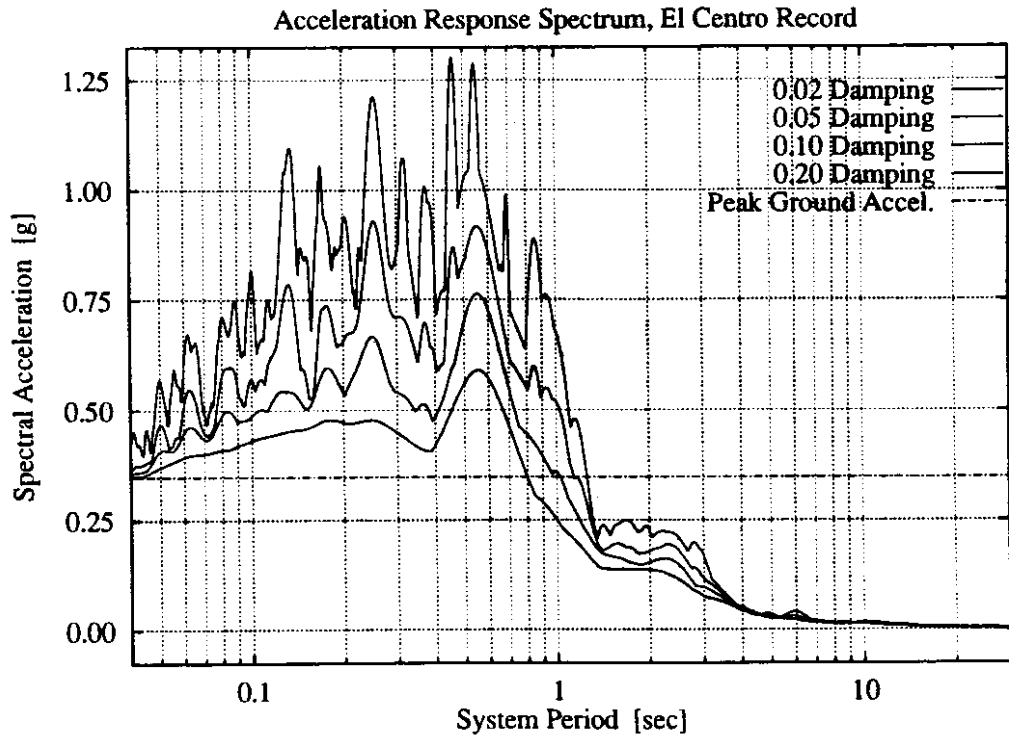
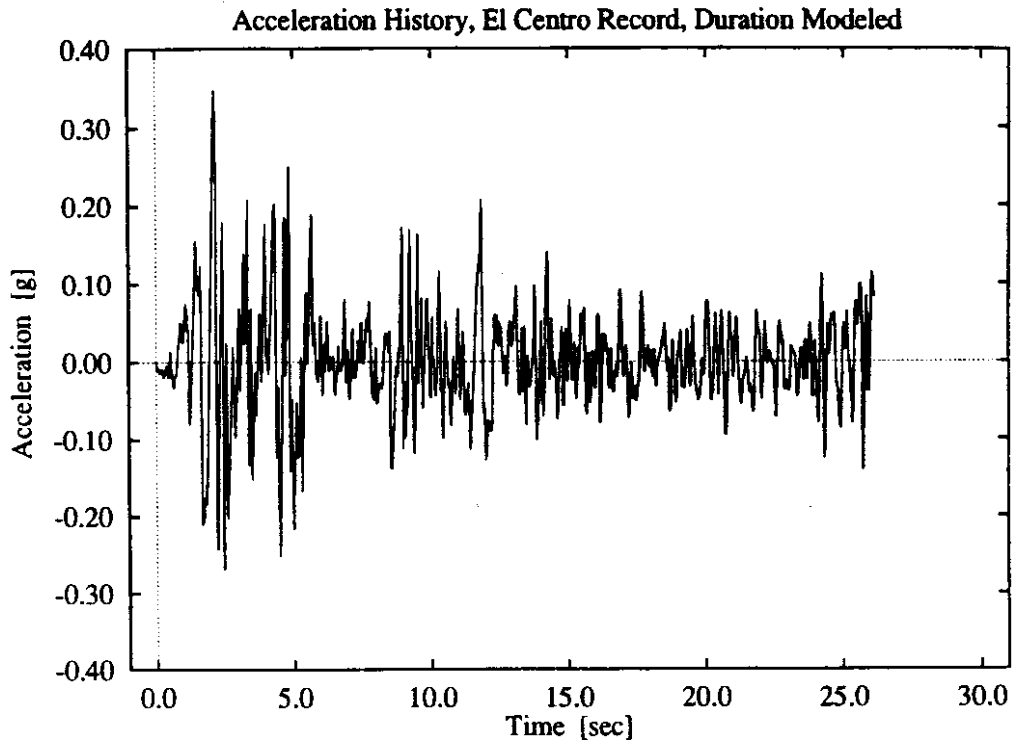


**Figure 3.6:** El Centro record: acceleration plot of duration modeled and acceleration response spectra.

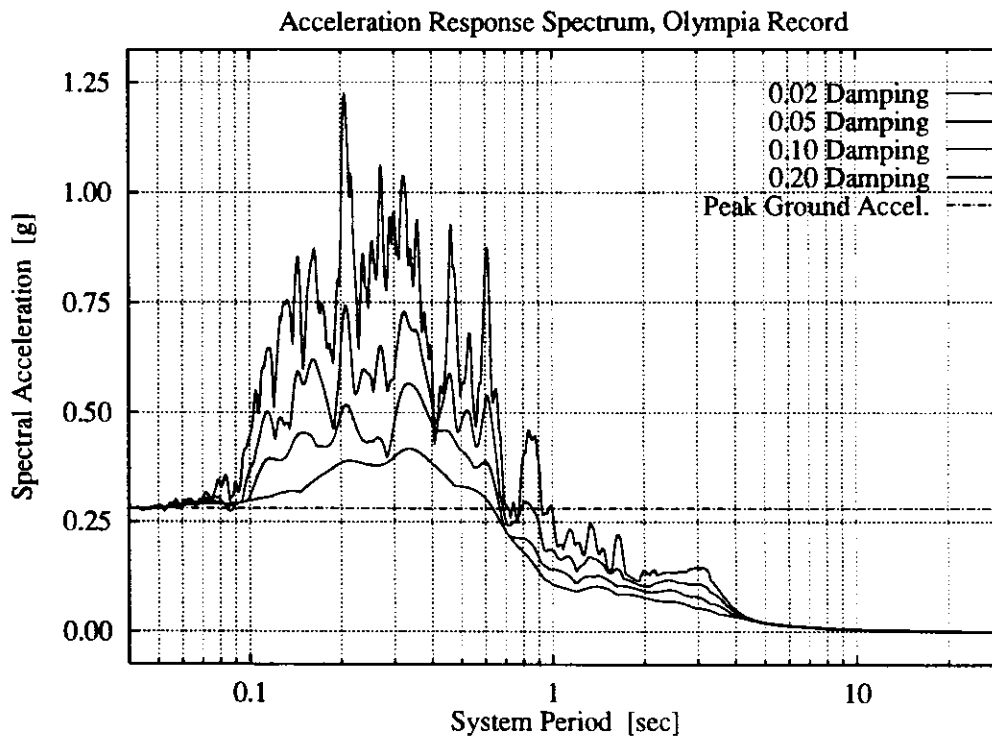
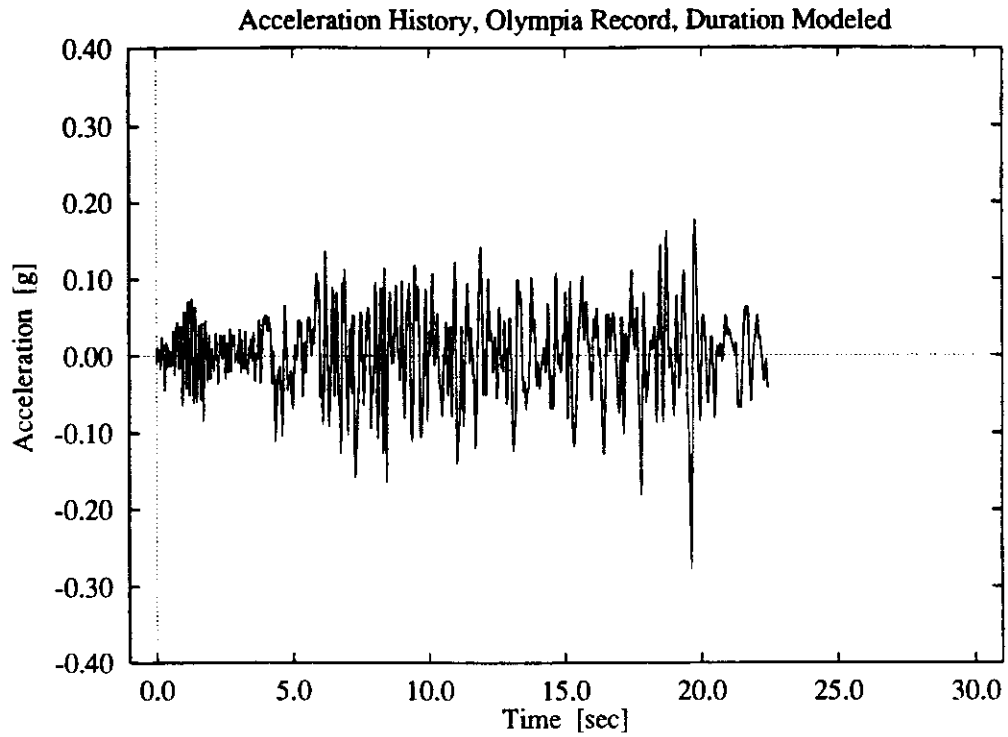


**Figure 3.7:** Olympia record: acceleration plot of duration modeled and acceleration response spectra.

The differences in the two acceleration response spectra are indicative of the different frequency content of these two records. To incorporate variations in record intensity in the study, both records were scaled to two different intensities, referred to as "lower" and "higher" intensities. The effective peak acceleration, or EPA, of each record was selected as the relevant intensity indicator. The EPA of a record is related to the average spectral acceleration the record produces over a certain system period range rather than to the ground motion itself. Thus, for engineering purposes, it is a more characteristic measure of intensity than peak ground acceleration [43]. The records were scaled such that the lower intensity El Centro and Olympia seismic inputs both had an intensity of 0.25g EPA, while the higher intensity inputs had an intensity of 0.40g EPA.

### *3.2.5 Discussion of Results*

The performance of the various foundation models was assessed in terms of their effects on the response of the bent structure. Specifically, three aspects of the bent's response were selected to be studied: column drift (the displacement of the column top relative to the bottom), the internal moment at the column top, and the rotation of the plastic hinge at the column top. NEABS provided this information in the form of time histories. The results were then interpreted in terms of their implications for column ductility and energy dissipation demands.

A total of 52 NEABS analyses were performed. As discussed, there were five supports modeled (four foundation models plus the fixed-base bent); three soil stiffnesses were applied to each of the four foundation models (thirteen individual support conditions); and each support condition was subjected to the four seismic input records. Figure 3.8 displays this information in a matrix form, and indicates the "name" by which each of the 52 runs is identified. The nomenclature used in Figure 3.8 to identify the foundation model, the soil, and the applied seismic record, is discussed in the previous sections.

To facilitate the study of these three response parameters, four different graphs of the data from each NEABS analysis were created. Figure 3.9 shows a typical example of the first two graphs, which are time histories of the column drift and of the column top moment. It should be noted that the moment reported by NEABS appears to be the sum of the internal moments produced by the column stiffness and damping actions. The third graph, shown in Figure 3.10, depicts column moment-drift hysteresis. If it is assumed that the column drift is roughly proportional to the rotation of the column top (it is exactly proportional only for the fixed-base model, which does not allow rotation at the column base), then the area enclosed by this hysteresis curve is roughly proportional to the energy dissipation demand. The fourth graph, also shown in Figure 3.10, is a time history of the plastic rotation of the column top. Horizontal lines on this graph indicate that the column top joint is elastic; vertical

## Spread Footing Parametric Study Matrix of NEABS runs

		El Centro Record		Olympia Record	
		Lower Intensity	Higher Intensity	Lower Intensity	Higher Intensity
Fixed		SF01-FX0_EL	SF02-FX0_EH	SF03-FX0_OL	SF04-FX0_OH
D01 Model (Springs only)	Soft Intermediate Stiff	SF05-D01.FEL SF09-D01.IEL SF13-D01.SEL	SF06-D01.FEH SF10-D01.IEH SF14-D01.SEH	SF07-D01.FOL SF11-D01.IOL SF15-D01.SOL	SF08-D01.FOH SF12-D01.IOH SF16-D01.SOH
D03 Model (Springs, Mass, & Dashpot)	Soft Intermediate Stiff	SF17-D03.FEL SF21-D03.IEL SF25-D03.SEL	SF18-D03.FEH SF22-D03.IEH SF26-D03.SEH	SF19-D03.FOL SF23-D03.IOL SF27-D03.SOL	SF20-D03.FOH SF24-D03.IOH SF28-D03.SOH
D05 Model (Meek & Veletsos)	Soft Intermediate Stiff	SF29-D05.FEL SF33-D05.IEL SF37-D05.SEL	SF30-D05.FEH SF34-D05.IEH SF38-D05.SEH	SF31-D05.FOL SF35-D05.IOL SF39-D05.SOL	SF32-D05.FOH SF36-D05.IOH SF40-D05.SOH
D11 Model (Jean et al.)	Soft Intermediate Stiff	SF41-D11.FEL SF45-D11.IEL SF49-D11.SEL	SF42-D11.FEH SF46-D11.IEH SF50-D11.SEH	SF43-D11.FOL SF47-D11.IOL SF51-D11.SOL	SF44-D11.FOH SF48-D11.IOH SF52-D11.SOH

**Figure 3.8:** Matrix of the 52 NEABS analysis runs for the study of spread footing models. Each run is identified by a name of the form "SF $nn$ - $fff$ . $see$ ," where  $nn$  is the run number,  $fff$  is the foundation model code,  $s$  is the soil stiffness code, and  $ee$  is the applied seismic record code.

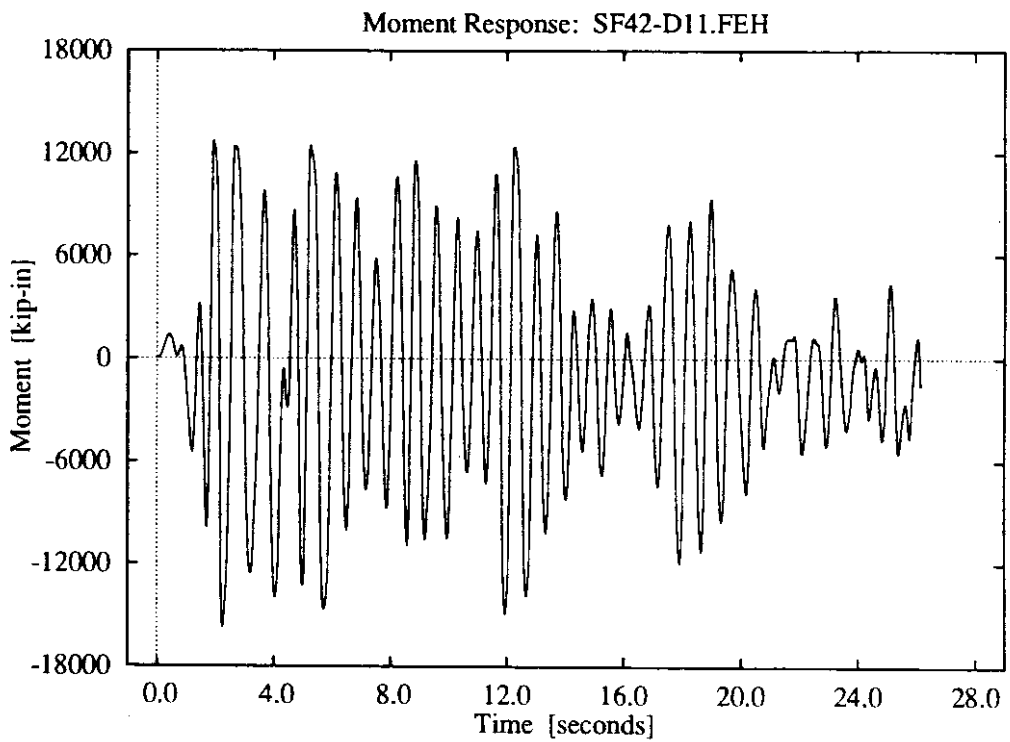
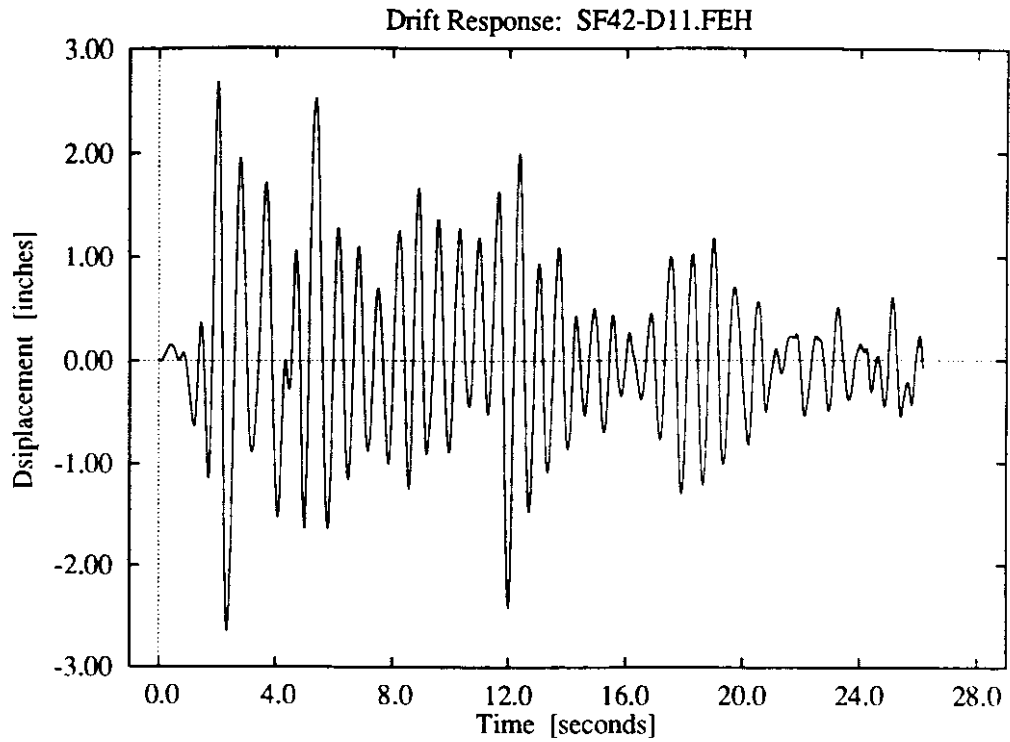


**Figure 3.9:** Typical results: time histories of column drift (relative lateral displacement between column top and bottom) and of the internal moment at the column top.



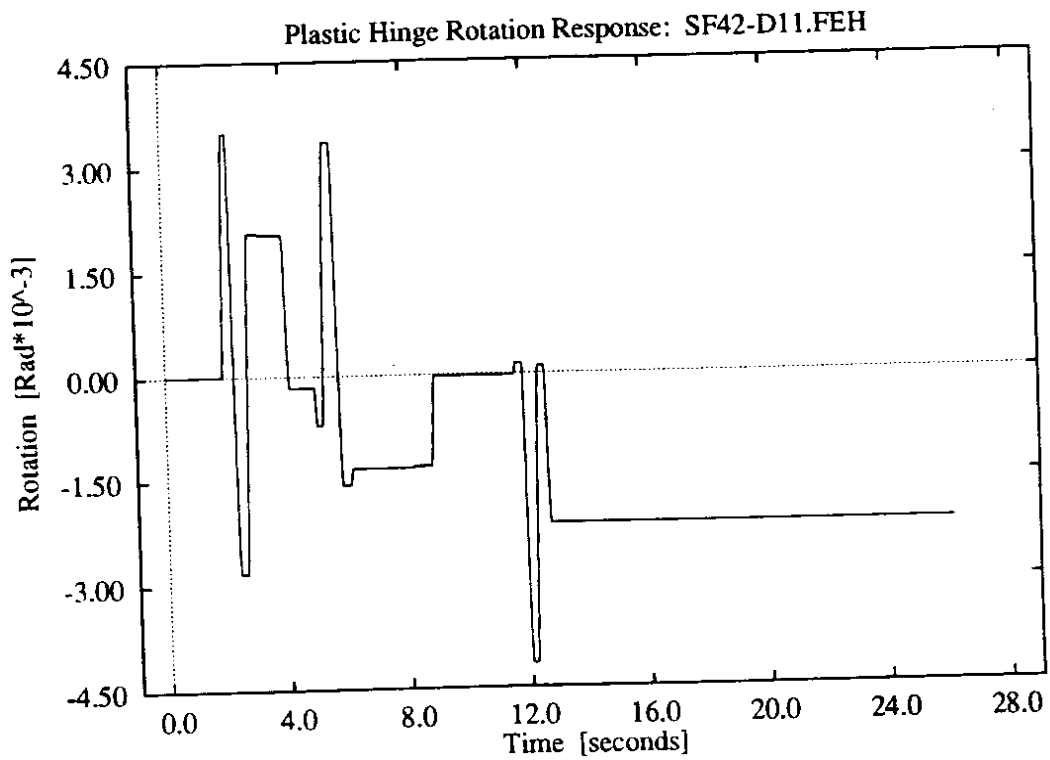
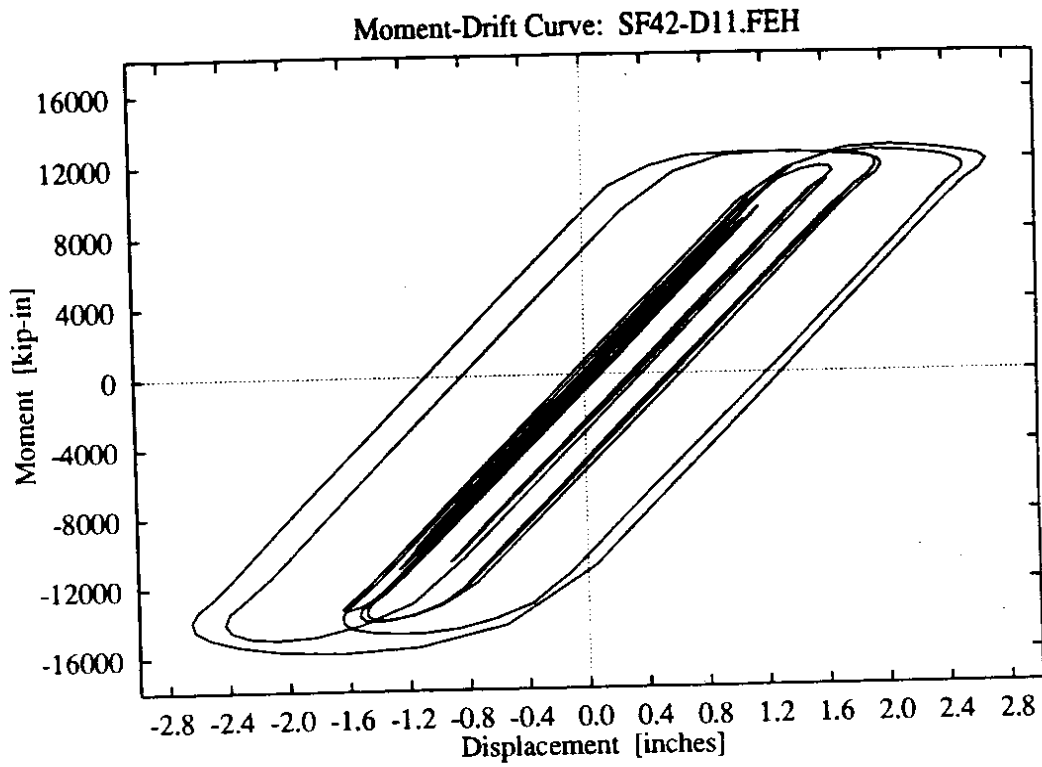


**Figure 3.10:** Typical results: Column moment–drift hysteresis and time history of the rotation of the plastic hinge at the column top.

movement indicates that a plastic hinge has formed at the column top, and it is being rotated by the internal moment. The lengths of these plastic rotation excursions are indicative of rotational ductility demand. Also, if the axial force on the columns is assumed to be constant, or nearly so, over the duration of the excitation, then the moment required to yield the column top will also be constant. If this is the case, then the work done on the column top over the excitation duration will be the yield moment multiplied by the sum of the vertical (absolute) lengths of all the plastic excursions indicated in the fourth graph (again, the second graph of Figure 3.10). Thus, for constant axial force, this plastic rotation “sum” is proportional to the energy dissipation demand of the column upper plastic hinge zone.

The column axial force observed in the analyses, however, was not nearly constant. The range of axial forces observed in the analyses with the more severe response resulted in a range of column top yield moments, as per equation (3.1), which varied approximately 20 percent from the median yield moment. Within the accuracy of assuming this varying yield moment to be constant, the plastic rotation sum obtained from the fourth graph provides an approximate indication of the energy dissipation demand of the upper plastic hinge zone. The four graphs discussed were compiled for all of the analyses and are given in Appendix D, along with the foundation model parameter values used in the analyses.

To summarize and compare these results, the maximum plastic rotation (measured from the initial orientation of the hinge) and the sum of all the plastic rotation was recorded for each run. As explained, these quantities are related to ductility and energy dissipation demands. This data is given in the form of bar charts in Figures 3.11 through 3.14. Each figure displays the bar charts of both the rotation maxima and rotation sums for the given seismic excitation record. Each chart shows the results of the four foundation models for each soil stiffness, and references them to the fixed-base results.

The response of the bridge bent to the two earthquakes is somewhat different, although the intensity of each record resulted in plastic hinge formation at the column top for almost all analyses. For the El Centro record, the models representing stiff and intermediate soil stiffness led to nearly the same ductility and energy dissipation demands at the column top as those observed for the fixed-base model. The models representing soft soil resulted in a significant increase in energy dissipation demand for both intensities, and they led to increased ductility demand for the lower intensity record. The ductility demand for the higher intensity El Centro record was approximately the same for all the foundation models.

As noted, the soft soil models caused an increase rather than a reduction in column demands. Comparing the El Centro record acceleration trace of Figure 3.6 with the plastic hinge rotation history of Figure 3.10 (D11 model of the soil, subjected to the higher intensity

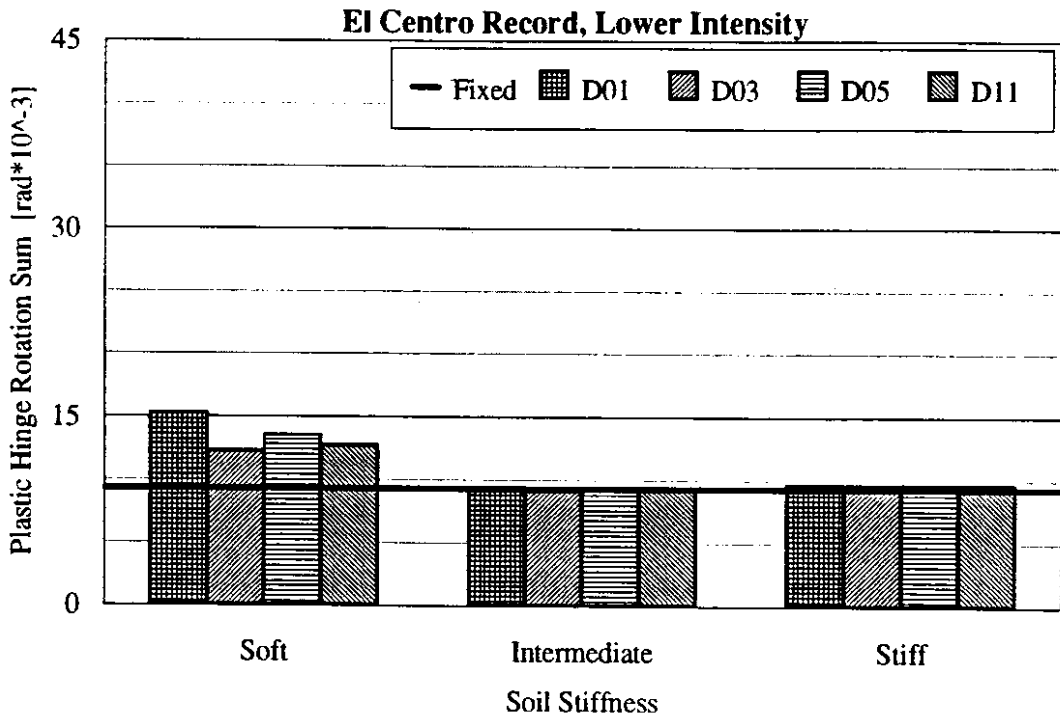
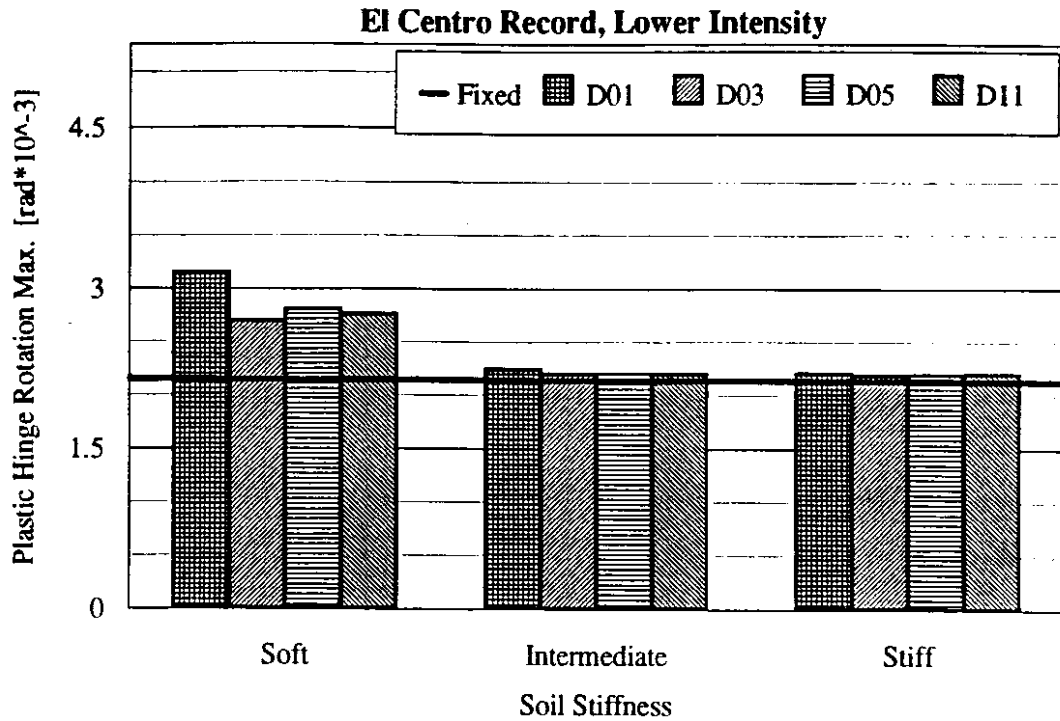


**Figure 3.11:** Comparison of effect of foundation model and soil stiffness on response of plastic hinge at column top during lower intensity El Centro record excitation: (top) maximum rotation attained (related to ductility demand); (bottom) total rotation sustained (related to energy demand).

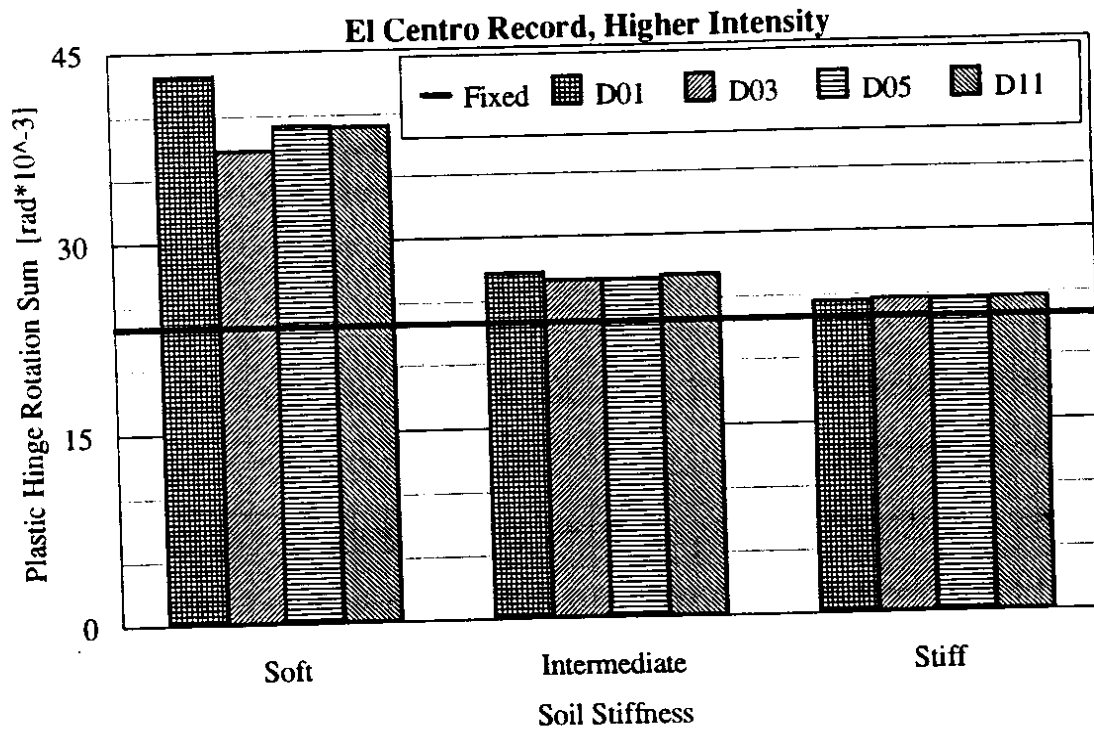
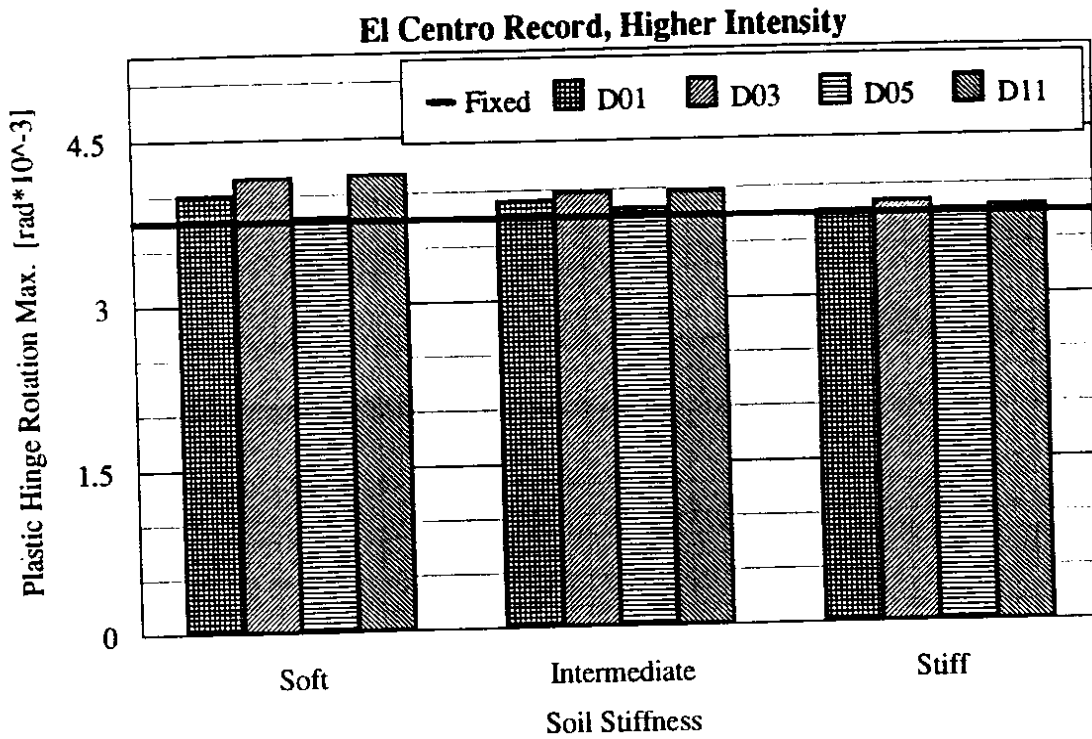


**Figure 3.12:** Comparison of effect of foundation model and soil stiffness on response of plastic hinge at column top during higher intensity El Centro record excitation: (top) maximum rotation attained (related to ductility demand); (bottom) total rotation sustained (related to energy demand).

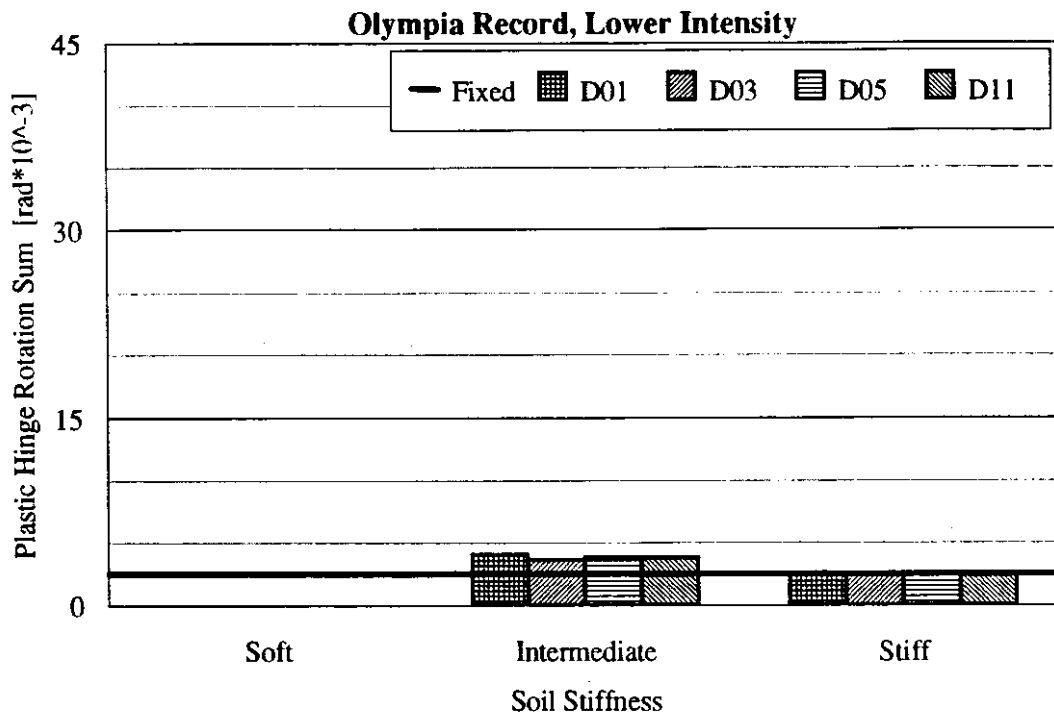
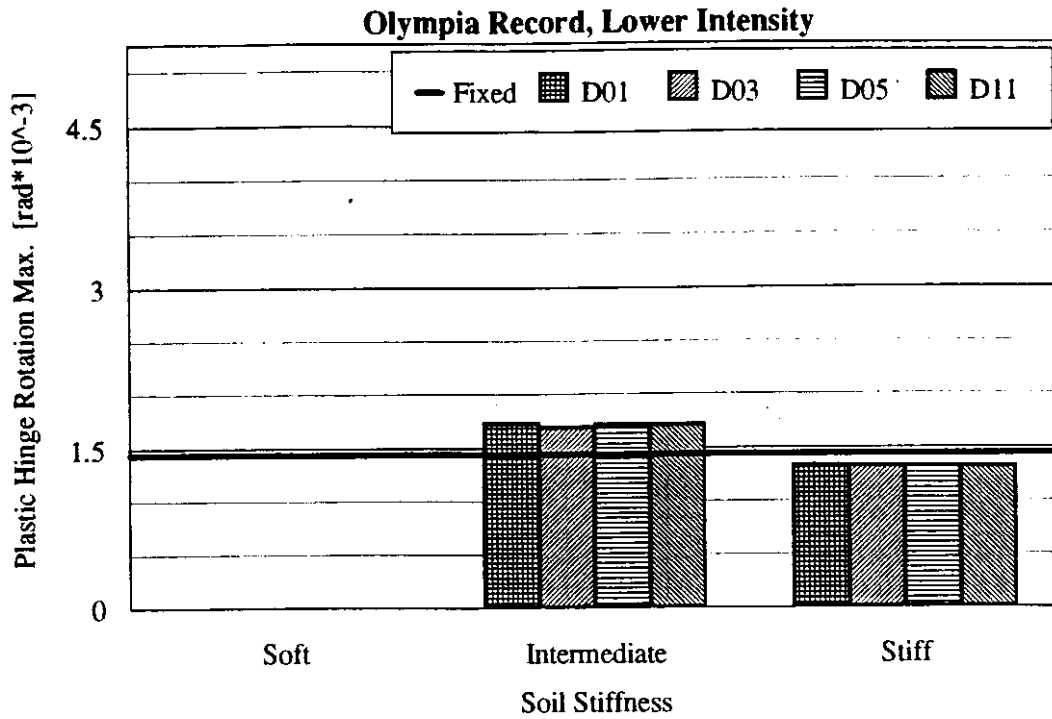


**Figure 3.13:** Comparison of effect of foundation model and soil stiffness on response of plastic hinge at column top during lower intensity Olympia record excitation: (top) maximum rotation attained (related to ductility demand); (bottom) total rotation sustained (related to energy demand).

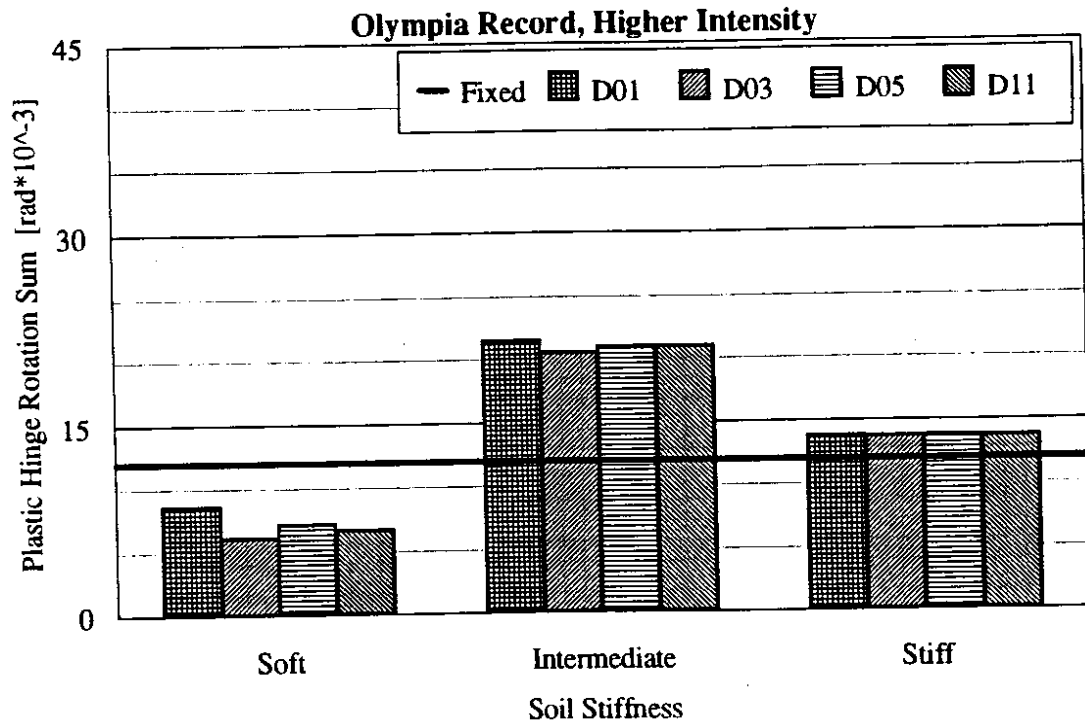
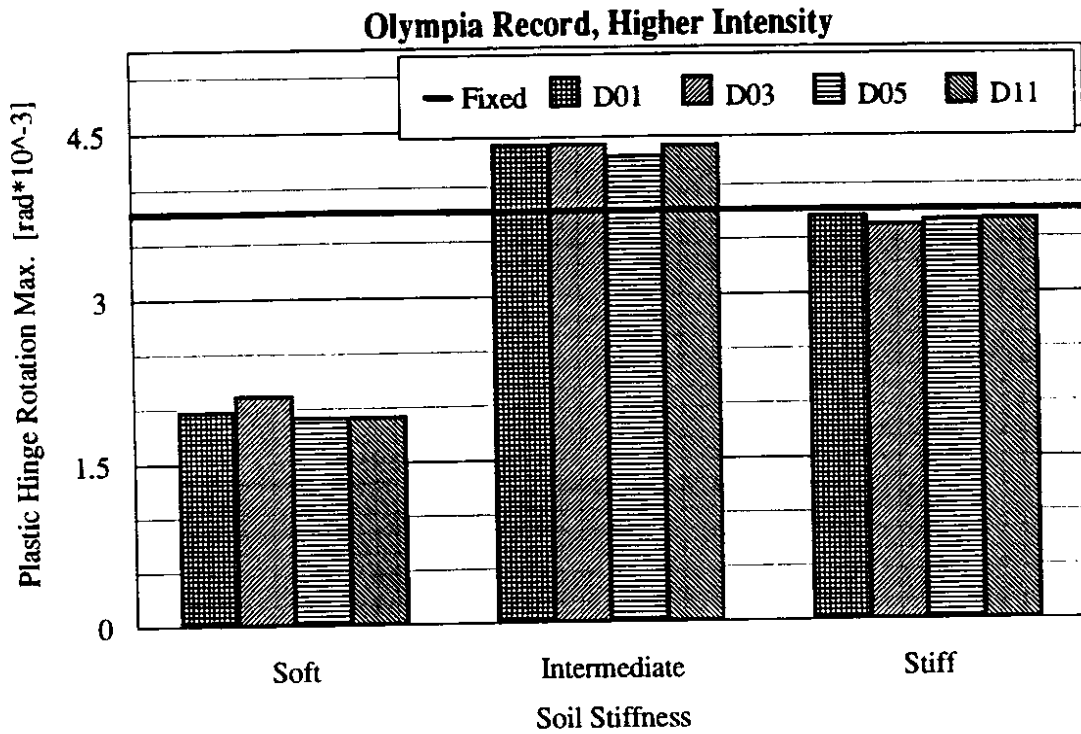


**Figure 3.14:** Comparison of effect of foundation model and soil stiffness on response of plastic hinge at column top during higher intensity Olympia record excitation: (top) maximum rotation attained (related to ductility demand); (bottom) total rotation sustained (related to energy demand).

El Centro record), it may be observed that much of the damage results from record acceleration peaks occurring at approximately 2 seconds, 5 seconds, and 12 seconds. The peak at 12 seconds is a major source of the increase in demand over the bents with the intermediate and stiff soil foundations. This may be caused by more excitation near the fundamental period of the soft soil-founded bent.

If only the lateral and rocking half-space static springs are applied to the column bases, neglecting the vertical springs, the equivalent lateral bent elastic stiffness may be calculated with the following equation:

$$k^{equiv} = \left[ \frac{1}{k_x} + \left\{ k_c \left[ 1 - \frac{3}{4} \left( 1 + 3 \frac{k_{\theta x}}{k_c} \right)^{-1} \right] \right\}^{-1} \right]^{-1} \quad (3.4)$$

where  $k_x$   $\equiv$  lumped stiffnesses of half-space translational springs  
 $k_{\theta x}$   $\equiv$  lumped stiffnesses of half-space rocking springs  
 $k_c$   $\equiv$  lumped equivalent lateral stiffness of columns with ends fixed

From this equivalent stiffness, the fundamental period of bent translational vibration may be approximated. It was calculated that this period was increased by 27 percent over the fixed-base period of 0.53 seconds for the bent founded on soft soil, as opposed to period increases of 6 and 2 percent for the other soil stiffnesses. The predominant period of excitation at the 12 second acceleration peak appears to be about



0.7 seconds, which is close to the soft soil-founded bent's approximate shifted period of 0.68 seconds.

Another possible reason for the increased column top response observed for the soft soil is the redistribution of column moment which occurs as the resistance to rotation of the column base is made more flexible. Even if the column moment experienced by a column with a flexible base was somewhat lower than that experienced by a column with a stiff base (and assuming the columns are responding elastically), proportionally more moment in the flexible-base column would be concentrated at the top, and a net increase in column top moment may be observed.

For the Olympia records, the column ductility demands were of the same order as those of the El Centro records for the bents using the intermediate and stiff foundation models, but much less for the soft soil-founded bent. Indeed, no column yielding was indicated for the bent when founded on the soft soil models and subjected to the lower intensity Olympia records. The energy dissipation demand, however, was significantly less for all foundations when compared to that of the El Centro records. The two earthquakes were scaled to the same effective peak accelerations, but from Figure 3.7, it is apparent that the Olympia record is dominated by a single peak occurring at approximately 20 seconds. Because the majority of the column damage is caused by this

peak, as opposed to several different peaks in the El Centro records, the total amount of plastic hinge rotation is reduced.

The results portrayed in Figures 3.11 through 3.14 indicate that the bent response, considered in terms of ductility and energy dissipation demands of the column top, are sensitive to the combination of frequency content of the seismic excitation and stiffness of the founding soil. The variation of response trends noted previously with soil stiffness was typically consistent between the higher and lower intensity records of either earthquake, but were not consistent between the two earthquakes.

If it is assumed that the elastic half-space represents the actual foundation conditions more realistically than a fixed-base model, and that the D11 foundation model most accurately represents the half-space, then the closeness of the response when using a given foundation model to that produced by the D11 model is a measure of the relative accuracy of that model. Using this criteria, the fixed-base model was at times significantly unconservative. Additionally, reasonably close agreement was observed between the three simpler foundation models and the D11 model. Of these three models, the most significant deviations from the response produced by the D11 model occurred when using the D01 (springs only) model to represent soft soil. In this case, the response produced by the D01 model was greater; otherwise it was in close agreement with the other foundation models. Since this trend was observed for all four records, it would appear

to indicate that radiation damping, which the D01 model neglects, is significant only for modeling soils considerably softer than the bridge structure, and that neglecting it is usually a conservative assumption.

The close agreement between the responses produced by the four foundation models indicates that relatively simple models are likely to be adequate for representing the soil as a half-space. The D01 model was in good agreement with the D11 model for the intermediate and stiff soils, and the D03 model agreed closely for all soil stiffnesses. Further, the response produced by the half-space models appeared to approach that of the fixed-base model for stiff soil, as expected, since the fixed-base model may be thought of as representing a soil of infinite stiffness.

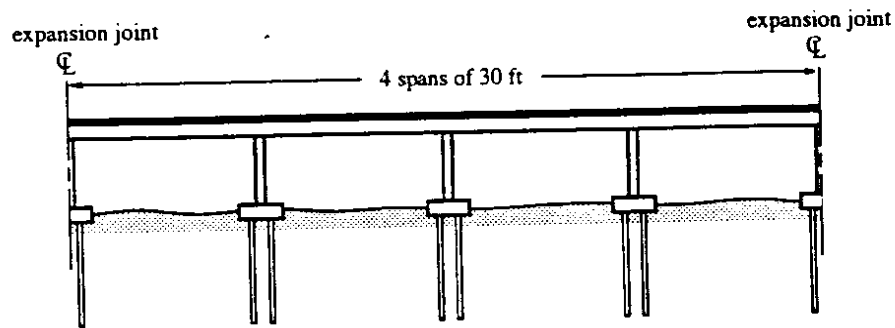
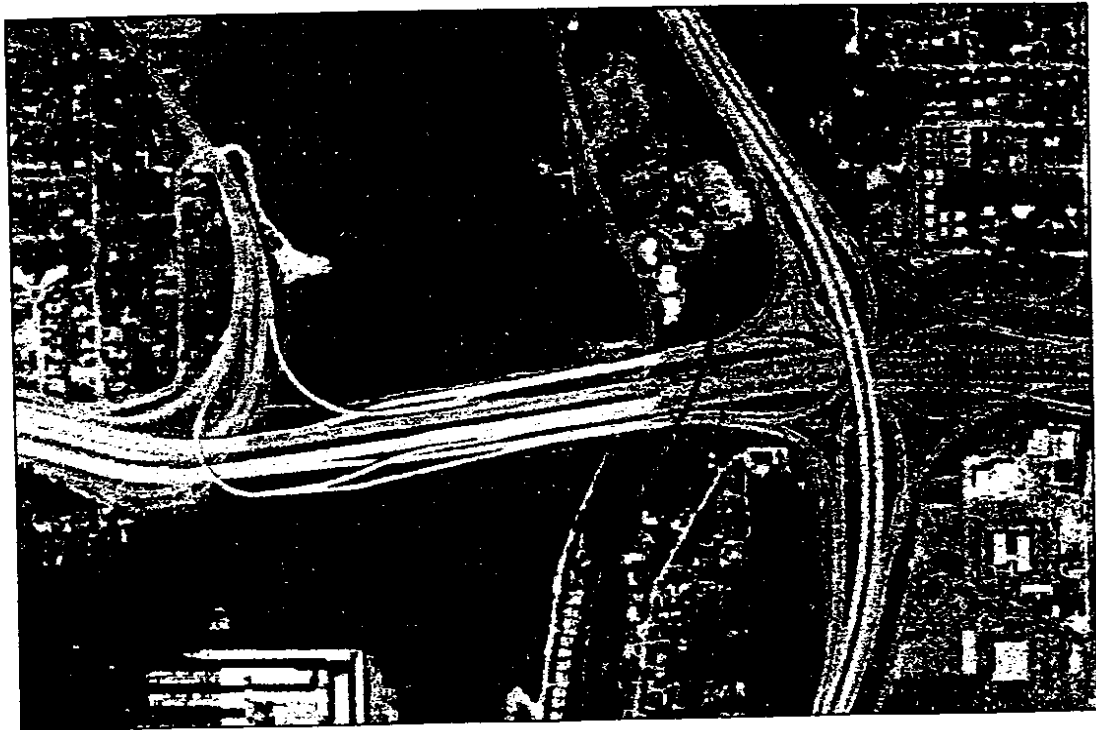
### **3.3 Pile Foundation Study**

The study using the Mercer Slough bridge employed four different pile foundation models, along with a fixed-support "foundation." The bridge bent model and pile foundation models used in NEABS were based on the dimensions and material properties of the actual bridge. Additionally, the applied seismic excitation incorporated the effects of the founding soil conditions unique to Mercer Slough. Descriptions of the bridge and site, the NEABS model of the bridge bent, the foundation models employed, the seismic excitation applied, and the observed results are presented in the subsequent sections.

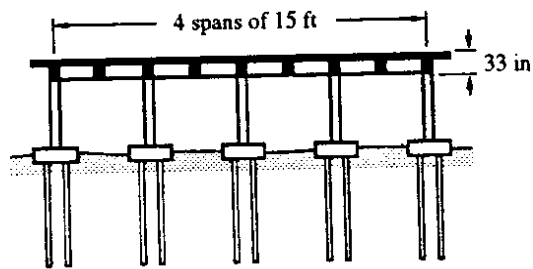
### *3.3.1 Description of Bridge and Site*

Interstate 90 crosses Mercer Slough in south Bellevue by means of four bridges, which carry two major roadways—one eastbound and one westbound—and several ancillary collectors and distributors. The structure carrying the westbound lanes was constructed in 1939, and it was recently the subject of a WSDOT research project [26 and 44]. This structure, referred to as the “Mercer Slough bridge”, is approximately 2800 feet long and contains 85 spans. The spans are typically supported on pile-founded, five column, reinforced concrete bents. Except for the longer end spans, the spans are 30 feet in length. The superstructure consists of reinforced concrete T-girders, which are continuous over four spans and separated by an expansion joint at every fourth bent. The span typically has a width of 60 feet, and incorporates a 6-inch thick slab and nine 16-inch wide T-girder webs at 7.5-foot centers. The section depth is typically 33 inches from the bottom of the web to the top of the slab. The bent caps form diaphragms between the T-girder webs. Figure 3.15 shows an aerial photograph of the Interstate 90 Mercer Slough crossing and drawings of typical bridge longitudinal- and cross-sections.

Mercer Slough is a marshy, peat-filled extension of Lake Washington. Figure 3.16 shows an approximate subsurface soil profile of Mercer Slough along the Interstate 90 alignment. In a WSDOT study of the slough by Kramer [27] conducted in parallel with the bridge studies cited above, the



Typical Side Elevation



Typical Cross Section

**Figure 3.15:** Interstate 90 bridge over Mercer Slough (top) Aerial photograph showing the west- and eastbound Interstate 90 bridges and collector bridges; (bottom) Typical westbound bridge longitudinal- and cross-sections. Adapted from [26] and [44].

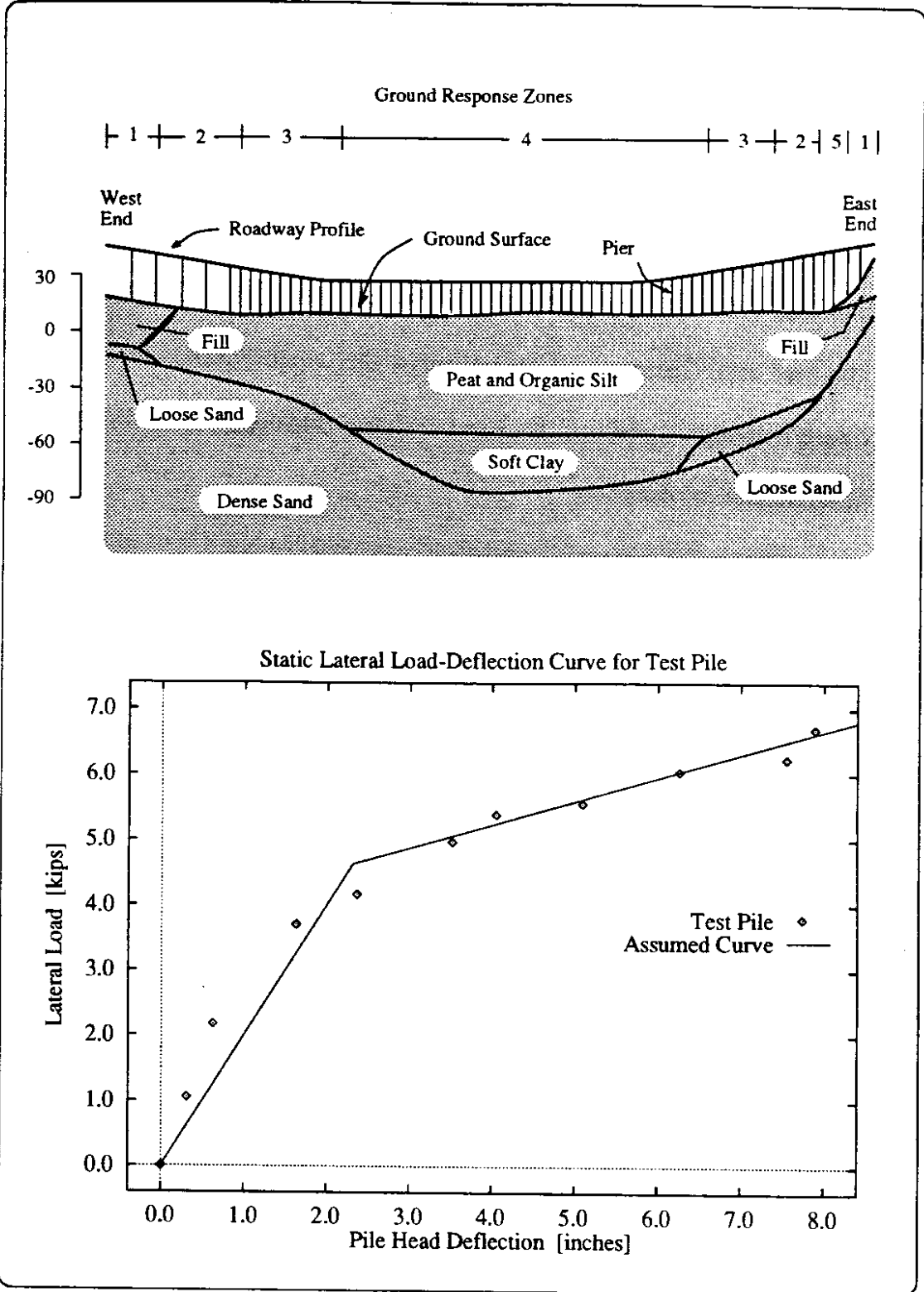


**Figure 3.16:** Mercer Slough: (top) approximate soil profile of Mercer Slough along alignment of Interstate 90, with seismic response zones as identified by Kramer [27]; (bottom) static pile head stiffness diagram for 8-inch diameter test pile as reported by Kramer [27].

soil was found, in general, to be very weak and soft. Because the seismic response of soft soils can change, and often amplify, ground free-field motions, free-field motions likely to occur at the Mercer Slough site were determined by Kramer. In addition to potentially amplifying ground motion, soft soils also provide little resistance to lateral bridge movement. McLean and Cannon [26] investigated the seismic response of the Mercer Slough bridge, applying as input seismic excitation the ground motions determined by Kramer.

Figure 3.17 shows a detail of a typical bridge bent column and pile cap. The column cross-section is 20 inches square, and contains eight No. 7 bars spaced evenly about the perimeter. The columns frame monolithically into both the foundation and the superstructure. The longitudinal reinforcement continues into the cross-beam or diaphragm at the column top, but it is lap spliced at the bottom with reinforcement from the pile cap. Column transverse reinforcement consists of No. 4 stirrups spaced 12 inches on center, which is insufficient to allow for the formation of a ductile plastic hinge [26]. The expected in-situ material strengths are  $f_c = 4500$  psi for the concrete and  $f_y = 45$  ksi for the steel [26].

Each of the five bent columns are supported on concrete pile caps, as shown for the column of Figure 3.17. Eight No. 8 bars in each direction provide the cap reinforcement. The pile cap, in turn, is supported on four timber piles. No mechanical connection is provided between the piles and the pile cap.

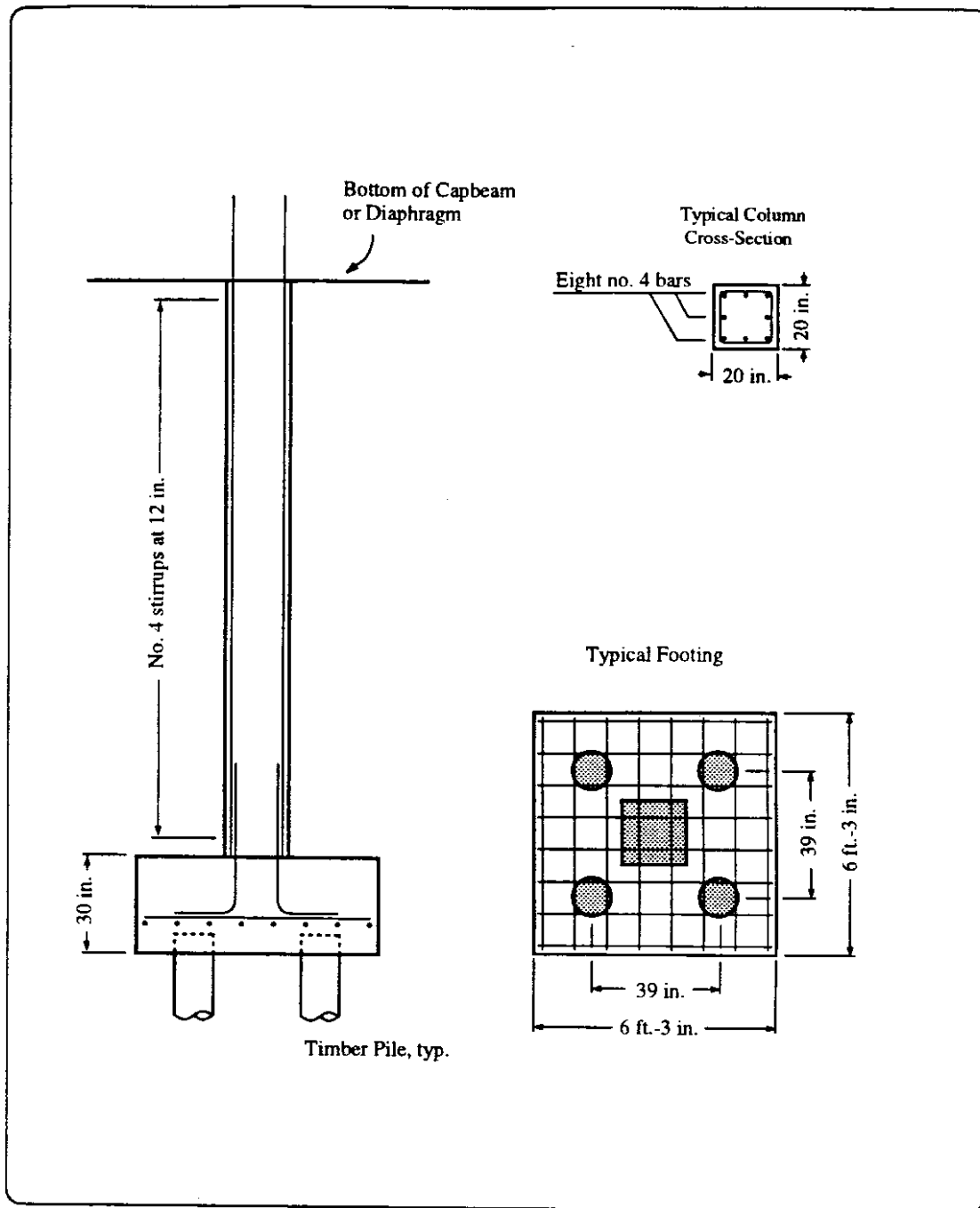


**Figure 3.17:** Mercer Slough bridge bent columns and pile cap details. Adapted from [44].



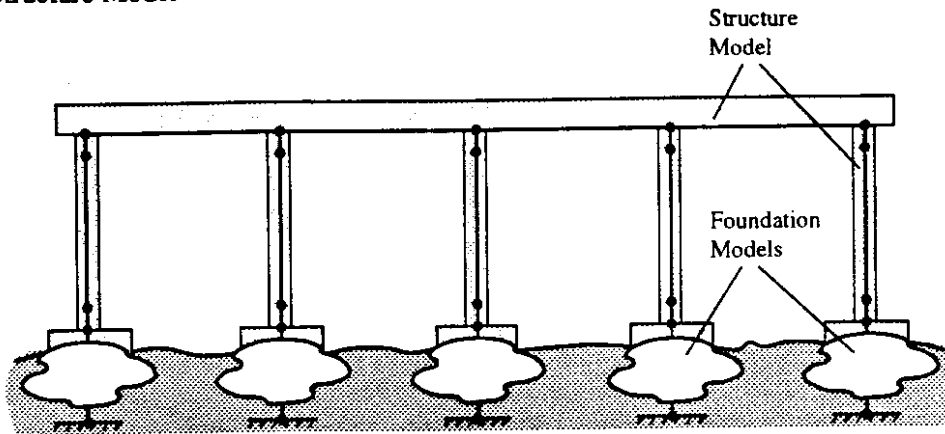
### 3.3.2 Structure Model

In the study by McLean and Cannon [26], it was observed that, away from the ends of the bridge, each four-span bridge section between expansion joints responded nearly independently to lateral seismic excitation. Therefore, as with the spread footing study on the Moses Lake bridge, the pile foundation study was confined to the analysis of an isolated bridge bent. A schematic of the bent and foundation models used in the NEABS analyses is given in Figure 3.18.

The bent structure was modeled with beam elements and the various foundation models with DF elements. The crossbeam was modeled with elastic beam elements, while the columns used elasto-plastic beam elements. The modulus of elasticity used for the columns was  $E = 3800 \text{ ksi} \approx 57 f_c^{1/2}$ , as per ACI 318-89 §8.5.1 [45]. The moment of inertia,  $I$ , that was used was half of that of the gross column cross-section [1]. Thus, for the columns, the elastic stiffness was proportional to  $EI_{eff} = 1/2 E_c I_g$ .

The same procedure described in the discussion the spread footing study was used for determining the NEABS yield surface of the columns. This procedure fits a cubic curve to the column's axial force-bending moment strength interaction diagram taken at attainment of a maximum concrete strain of  $\epsilon_{cu} = 0.003$ . Figure 3.19 shows a comparison of the axial force-bending moment strength interaction data calculated for the column

(a) Structure Model



(b) Support Models

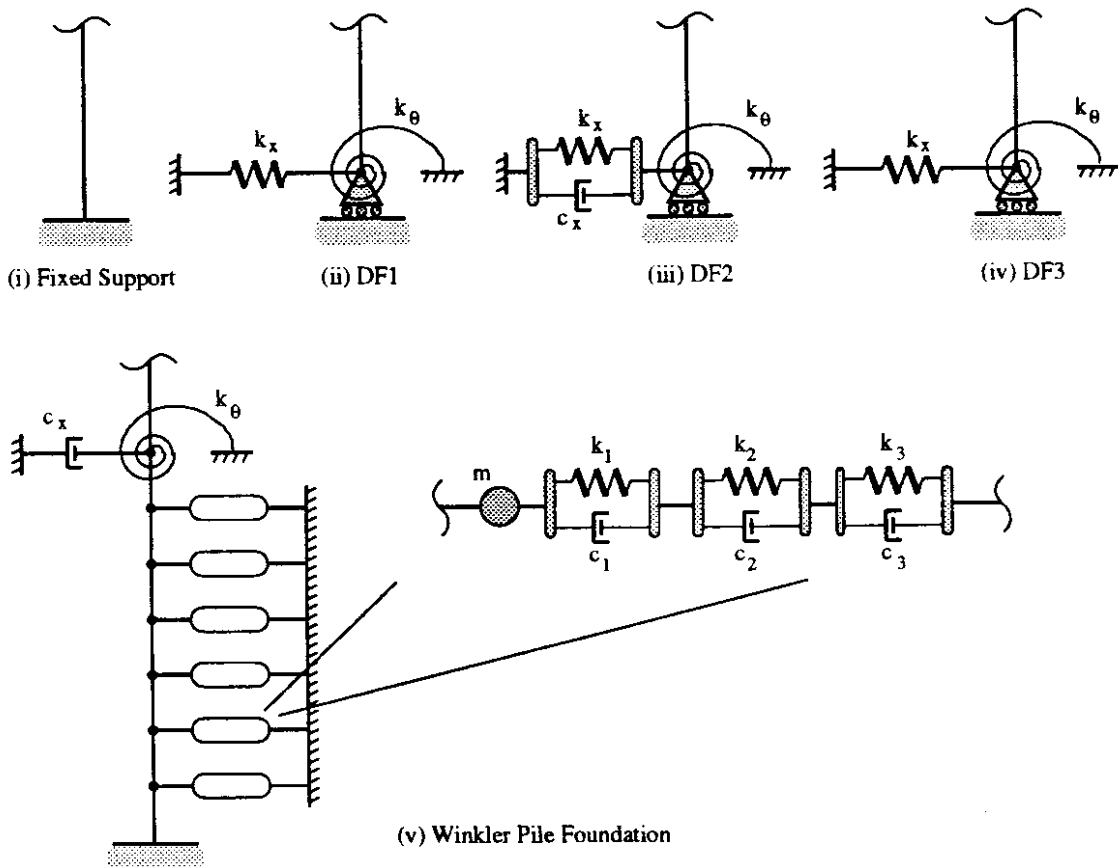


**Figure 3.18:** Schematic of NEABS models of Mercer Slough bridge bent and supports employed: (a) model of bent structure, with beam elements forming columns and crossbeam; (b) five support models—fixed supports and four models representing pile foundations.

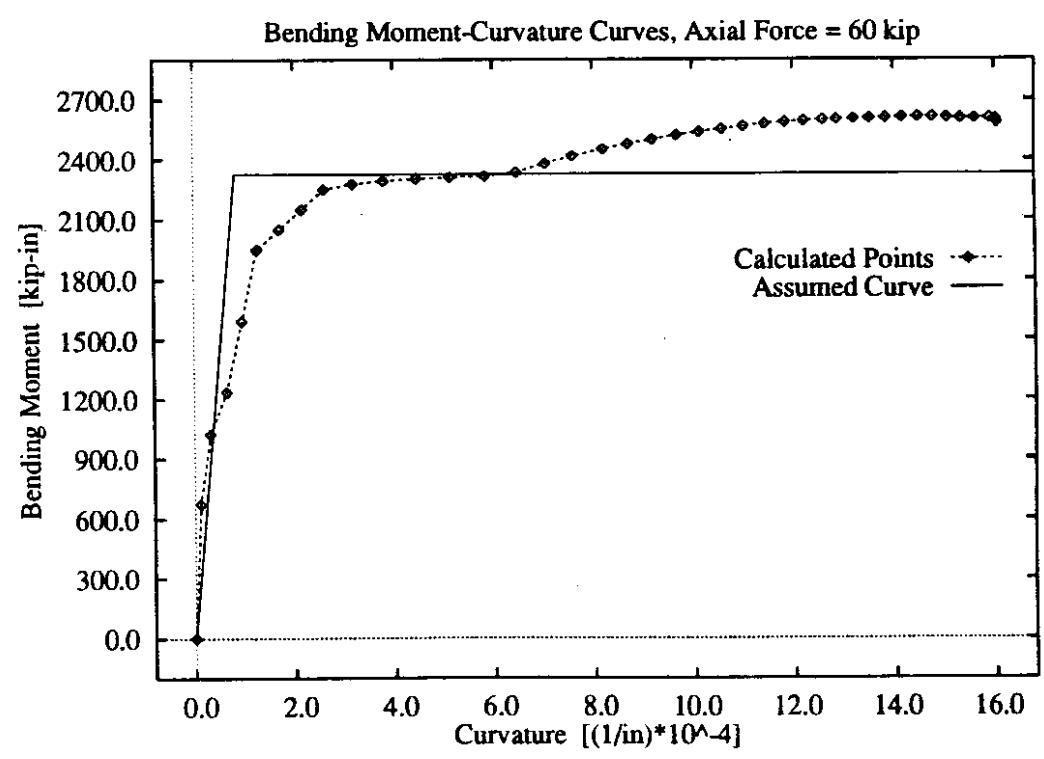
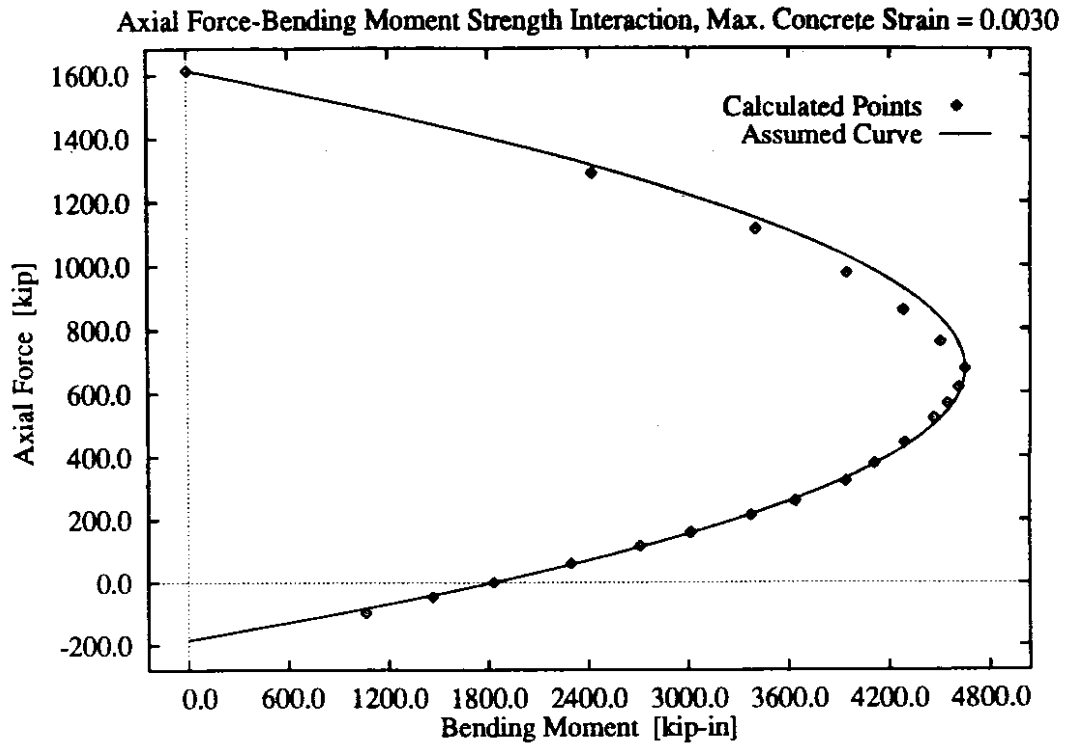


**Figure 3.19:** Calculated and assumed strength characteristics of Mercer Slough bridge bent columns. Axial force–bending moment strength interaction curve taken at attainment of concrete strain of 0.003 in./in., and bending moment–curvature curve taken at static axial load of 60 kips.

and the cubic curve used in the NEABS models. Also shown is a comparison of the bending moment–curvature relation calculated for the column under the static dead load of 60 kips. The slope of the elastic portion of the NEABS curve, again, is  $EI_{eff} = \frac{1}{2}EI_G$ . Both graphs show close agreement between calculated and assumed column strength characteristics.

Because the diaphragm forming the bent cap is constrained by the bridge T-girder superstructure, the stiffness of the crossbeam was deemed to be high relative to that of the column. As with the Moses Lake bridge model, the crossbeam was therefore modeled as an essentially rigid member. The mass supported by the bent was applied by specifying an appropriate density for the four crossbeam elements.

To apply consistent material damping to the bent elements, the same procedure described in the discussion of the spread footing study was used. The Rayleigh damping coefficients determined by this procedure are those necessary to produce a damping ratio of 5 percent of critical in a single-degree-of-freedom system having the same mass as the bridge bent and a stiffness equal to the total elastic stiffness of the columns, assuming the columns were fixed at the base and framed into a rigid crossbeam. The calculated period of this system is 0.33 seconds. The calculated coefficient values were used for all of the analyses.

### 3.3.3 Foundation Models

As previously discussed, four foundation models were compared, as well as fixed-base supports. Three of the four foundation models were discrete springs or spring/dashpot systems which modeled the pile cap behavior experienced by the column bases. The fourth foundation model was a Winkler-type pile foundation. These five support conditions are shown in Figure 3.18.

The first discrete pile cap model, referred to as the "DF1" model, used a lateral spring with a linear stiffness of  $k = 8.2$  kips/inch. This pile head stiffness was used by McLean and Cannon [26] in their modeling of the Mercer Slough bridge. A simplified half-space modeling procedure, used in conjunction with static pile head stiffness data obtained from the testing of an 8-inch diameter steel tube pile driven into Mercer Slough [27], was used to determine this stiffness. The pile head stiffness data for the 8-inch test pile is given in Figure 3.16.

Additionally, a rotational pile head spring was applied. The stiffness of this spring was determined by calculating the resistance to rotation of the center of the pile cap about a horizontal axis perpendicular to the plane of the bent which was afforded by the eccentric axial reaction of the piles. The piles were assumed to be elastic and end-bearing for this calculation. This rotational spring was used for all four foundation models.

The second discrete pile cap model, or "DF2" model, utilized a hysteretic bilinear lateral spring in conjunction with a viscous lateral damper. The DF2 model's stiffnesses were obtained by first modeling the 8-inch test pile with six Winkler-type soil reaction springs. Stiffnesses for the soil springs were determined by assuming values for the modulus of horizontal subgrade reaction,  $r_h$ , in the following equation:

$$p(z) = r_h z \quad (3.5)$$

where  $p(z) \equiv$  soil reaction stiffness per unit length of the pile at subsurface depth  $z$ .

$r_h \equiv$  modulus of horizontal subgrade reaction, [force/length<sup>3</sup>]

By subdividing the pile length and integrating equation (3.5) over the pile sublengths, discrete lateral soil spring stiffnesses were obtained. These soil springs were then applied to the pile at the depths of the "center-of-pressure" of the reaction  $p(z)$  on the pile sublengths to create a Winkler-type foundation.

Six such springs were applied to a fixed-base, beam element model of the 8-inch test pile. The value of  $r_h$  was then varied until the lateral pile head static stiffness, as determined by applying a static unit lateral load at the pile top, matched the elastic portion of the assumed bilinear stiffness curve shown in Figure 3.16. Pile head rotation was not constrained, as it was anticipated that little moment could be transferred between the actual piles and the pile cap. Similarly, the plastic stiffnesses

of the soil springs were determined by varying  $r_A$  until the pile head stiffness matched the plastic portion of the assumed bilinear stiffness curve. These six bilinear soil springs were then coupled to a fixed-base beam element model of a typical Mercer Slough bridge pile group (four Douglas fir timber piles of 12-inch diameter and 50-foot length), first scaling the stiffnesses up by a factor of 1.5, and then again by 4, to account for the larger diameter of the bridge piles and the lumping of the four piles into one pile model, respectively. This model of the bridge pile group was then analyzed statically, applying lateral loads at the pile head. The yield forces for the soil springs were obtained by requiring the soil springs to all yield simultaneously upon attainment of a lateral pile head deflection of 2.3 inches, the yield displacement of the bilinear stiffness curve assumed for the 8-inch test pile, under a laterally applied load at the pile head. By enforcing this yielding criteria, a bilinear pile head stiffness was obtained which has the same yield displacement as shown in Figure 3.16 for the 8-inch test pile, but with different elastic and plastic stiffnesses, and a different yield force. The bridge pile group model's pile head lateral elastic stiffness, yield force, and plastic stiffness were thus attained analytically, based on the 8-inch test pile data, but by an alternate method to that used by McLean and Cannon, and used as the lateral foundation spring for the DF2 model.

A lateral viscous damper was also used in the DF2 model. The damping coefficient was based on the lateral pile head damping coefficients

obtained by Kramer for the 8-inch test pile [27]. The damping coefficients reported by Kramer were obtained from a dynamic test conducted at low soil-strain amplitudes, so these coefficients account primarily for radiation damping. The damping was observed to be relatively independent of the frequency of applied vibration. Because radiation damping is a far-field phenomenon, and because it was deemed unlikely that the far-field effects would vary significantly between an 8-inch and a 12-inch pile, the damping coefficient used was obtained by multiplying the average coefficient reported by Kramer by four piles.

The third discrete pile head model, or “DF3” model, was not strictly a unique model, since it used a simple lateral spring like the DF1 model. However, it used a linear secant stiffness based on the results of the seismic analysis of the bridge bent utilizing the DF2 model, and in this respect, it represents a model of intermediate sophistication. It was employed to test the use of an elastic secant stiffness to approximate nonlinear pile head stiffness, and by comparison with the DF1 model results, to test the sensitivity of the bridge bent response to the elastic stiffness of the lateral pile head foundation spring. The secant stiffness was determined by recording the maximum pile head lateral deflection of the DF2 model under each of the applied seismic excitation records. The internal force of the bilinear spring used in the DF2 model at these recorded maximum pile head deflections, divided by these maximum deflections, defined the secant stiffness used in the DF3 model. However,



a practical secant stiffness could also be obtained without first performing an analysis using the more complicated DF2 model by iterating to a maximum pile head deflection on a standard pile “ $p-y$ ” curve. Like the DF1 model, no foundation damping was included in the DF3 model.

The fourth foundation model was a Winkler-type pile foundation, and it is referred to as the “WPF” model. The pile groups were each modeled as a single “pile” using beam elements coupled to the column bases. Six lateral soil reaction models were used with each of the pile group models. The soil reaction models that were used were based on the soil far-field sub-model proposed by Nogami and Konagai [35], illustrated in Figures 2.7 and 2.8. As discussed in Chapter Two, this model is derived from the representation of the soil as a vertically-stratified series of plane-strain elastic layers. The parameters of this model may be determined by use of equations (2.9) and Figure 2.8. For the Mercer Slough pile-soil foundation, the radius of the near field was taken as the timber pile radius,  $r_n = 6$  inches, and the resulting values of  $c_i$  and  $m_i$  of equations (2.9) were multiplied by four piles. The value of Poisson’s ratio was taken to be  $\nu = 1/2$ , and the value of the shear modulus,  $G = 149$  psi, was determined from average values of the soil weight density and shear wave velocity,  $\gamma_s = 69$  pcf and  $c_s = 100$  fps respectively, as measured by Kramer [27].

### *3.3.4 Seismic Excitation*

Six different acceleration time histories were applied to the bent models as seismic excitation. Four were ground motions determined by Kramer [27], which were obtained by applying recorded earthquake acceleration time histories to the base of the soil models of Mercer Slough. As the soft soil models responded to the seismic excitation, the ground motion changed, and thus these ground motions will be referred to as “filtered” records. The two “unfiltered” records are the lower and higher intensity El Centro records previously presented in the discussion of the spread footing foundation study. Since the unfiltered records are quite different from expected ground motions at the Mercer Slough site, using these records serves more as an exploratory exercise of the effects of the foundation models than as a study of the performance of the actual Mercer Slough bridge under probable seismic conditions.

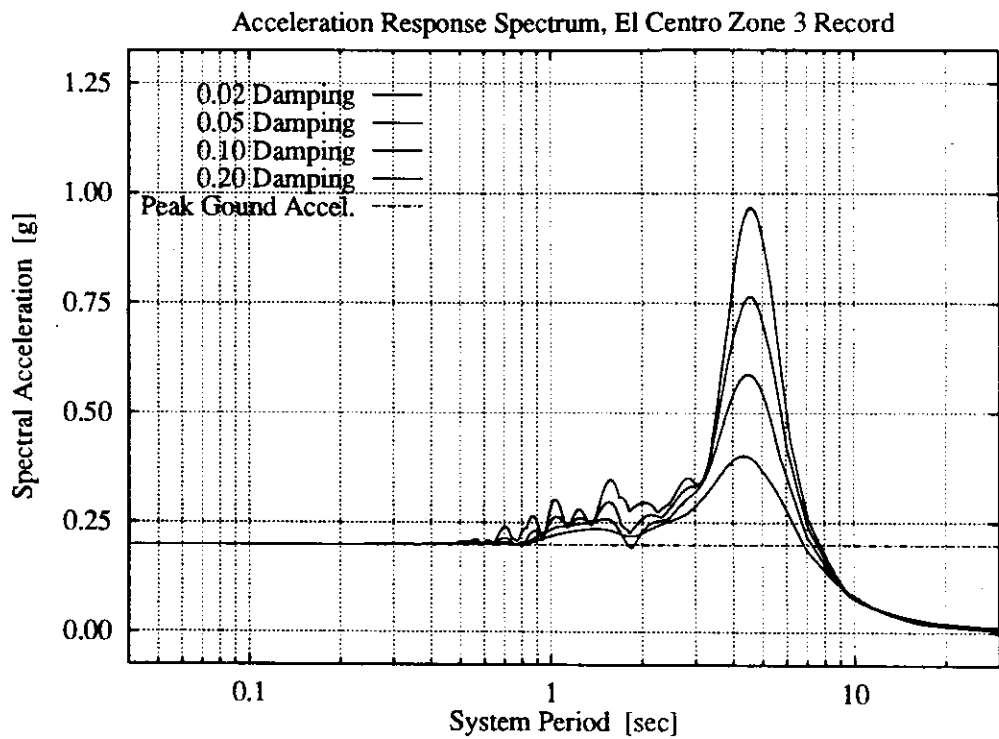
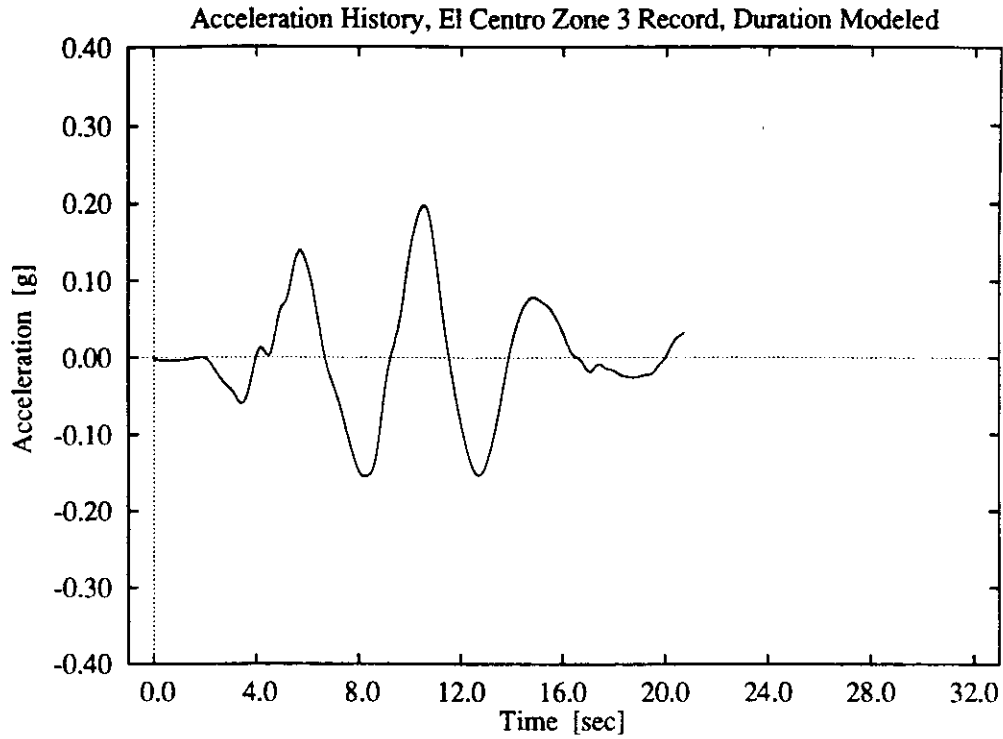
The four filtered records were determined by Kramer by first scaling the El Centro and Lake Hughes earthquake acceleration records to a peak acceleration of 0.25g and a predominant period of 0.36 seconds [27]. Then these scaled record were applied to the base of soil models representing Mercer Slough soil profiles at various positions along the length of the bridge, and the resulting surface ground motions were obtained. Based on similarities of the soil profiles and of the seismic response, the cross-section of Mercer Slough along the alignment of Interstate 90 shown in

Figure 3.16 was divided into five zones. The ground motions chosen to be used as seismic excitation for the pile foundation study were those resulting from applying the El Centro earthquake acceleration to zones three and four, and applying the Lake Hughes earthquake acceleration to zones one and two. These ground motions will be referred to as the "El Centro Z3," "El Centro Z4," "Lake Hughes Z1," and the "Lake Hughes Z2" records, respectively. They were chosen on the basis of the greater relative severity of their elastic spectral acceleration response spectra as compared with the other ground motions determined by Kramer.

As before, the beginning of the seismic excitation applied to the bent models was taken to be at the start of each record, and the end at the termination of the Trifunac and Brady duration for each record. These times were 20.77 seconds, 18.25 seconds, 32.68 seconds, and 33.05 seconds from the record beginnings for the El Centro Z3, El Centro Z4, Lake Hughes Z1, and the Lake Hughes Z2 records, respectively. Figures 3.20 through 3.23 show the acceleration time histories used in the pile foundation study, as well as the resulting elastic spectral acceleration response spectra.

### *3.3.5 Discussion of Results*

As with the spread footing study, the performance of the various foundations was assessed in terms their effects on the response of the bent structure. The same three aspects of the bent response were selected to



**Figure 3.20:** El Centro, Zone 3 record: acceleration plot of duration modeled and acceleration response spectra.

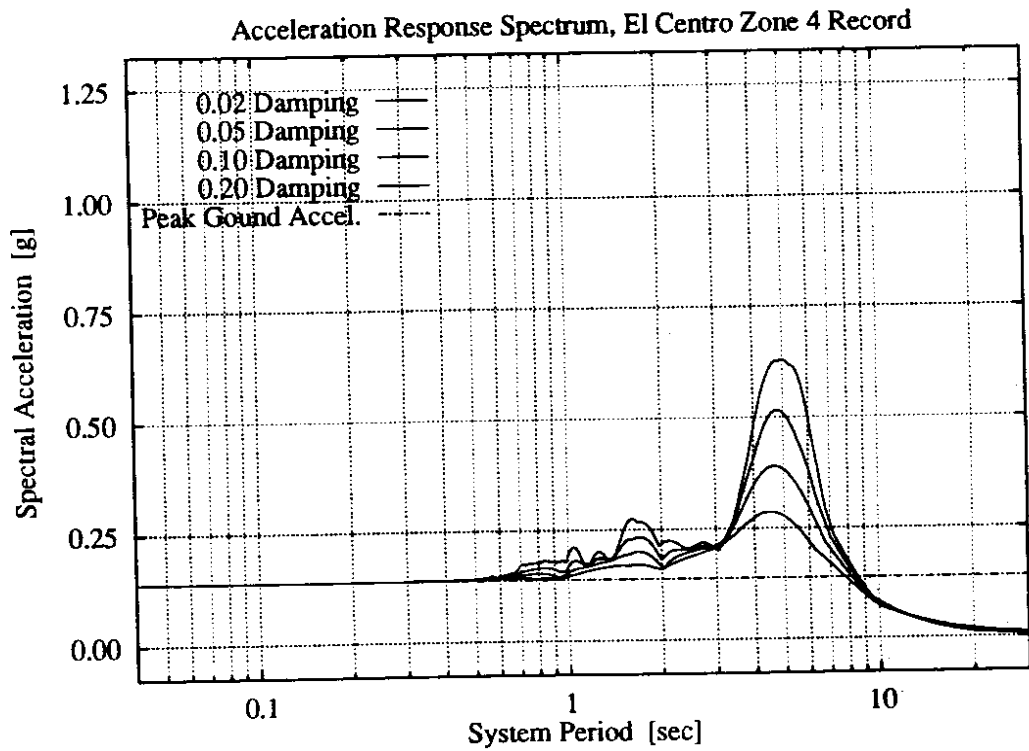
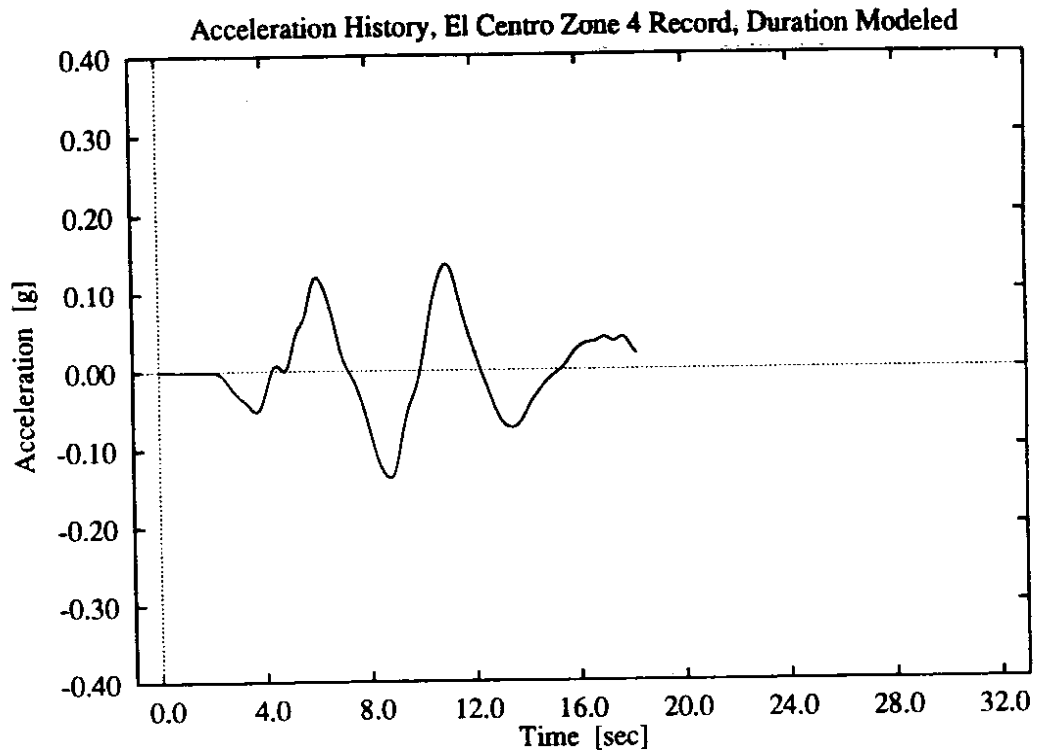


**Figure 3.21:** El Centro, Zone 4 record: acceleration plot of duration modeled and acceleration response spectra.

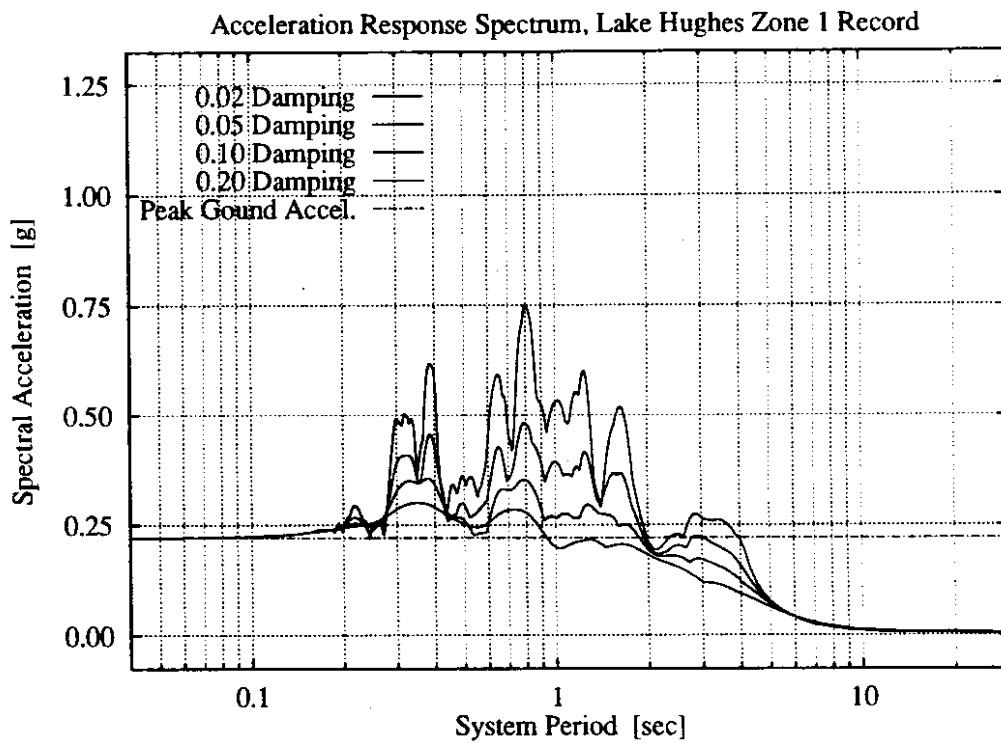
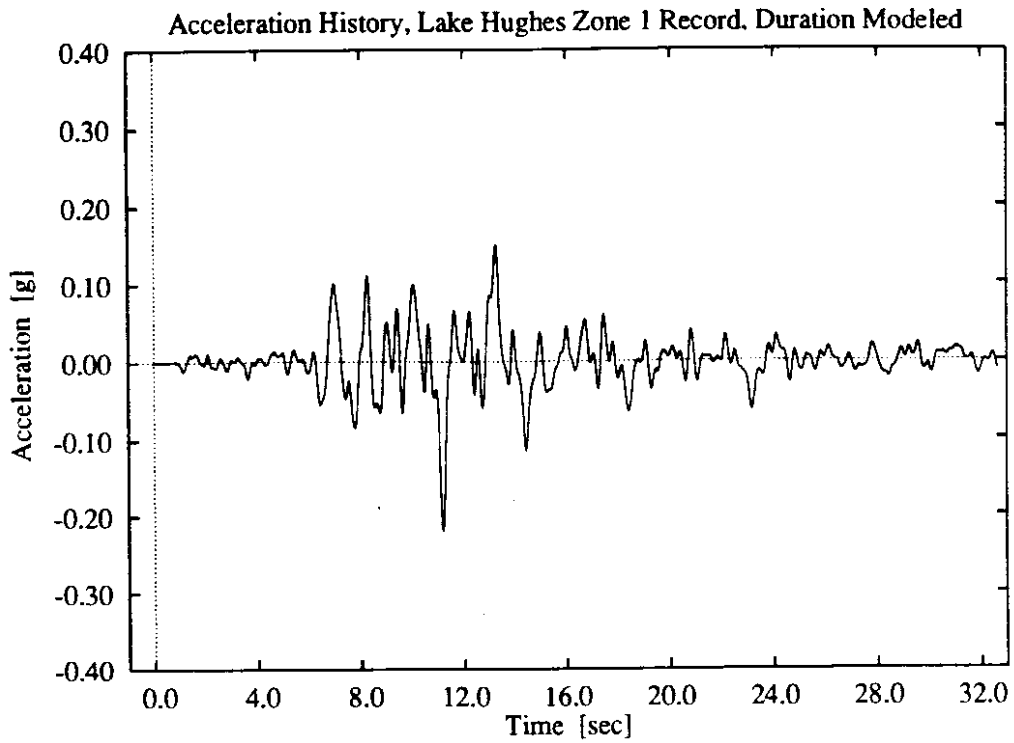


**Figure 3.22:** Lake Hughes, Zone 1 record: acceleration spectra plot of duration modeled and acceleration response spectra.

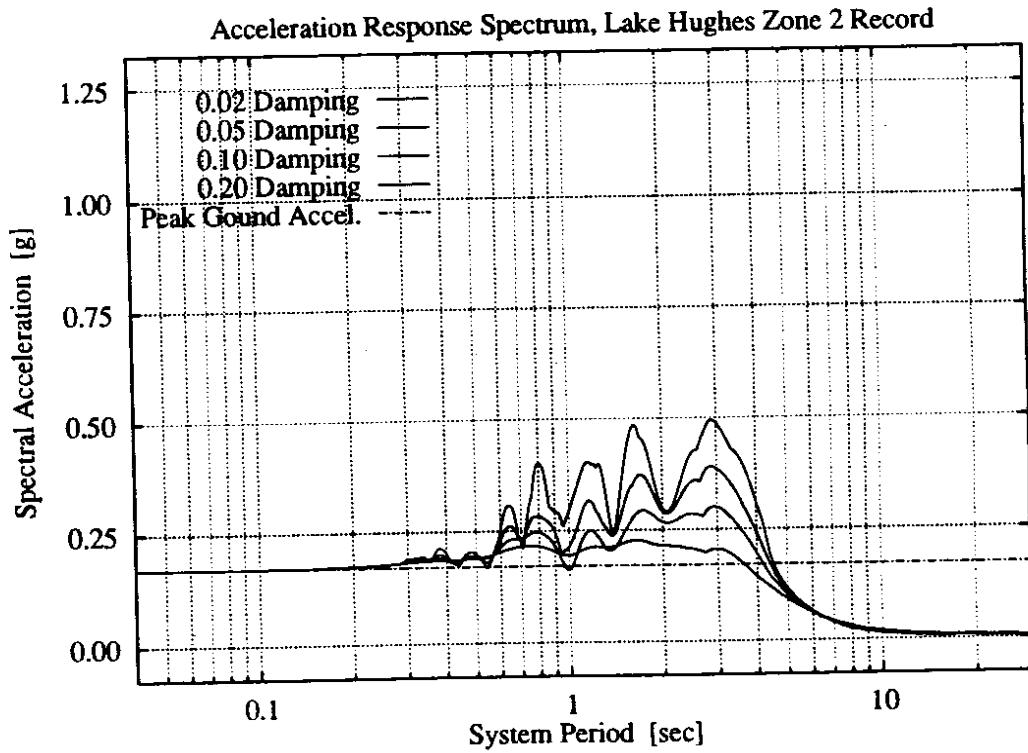
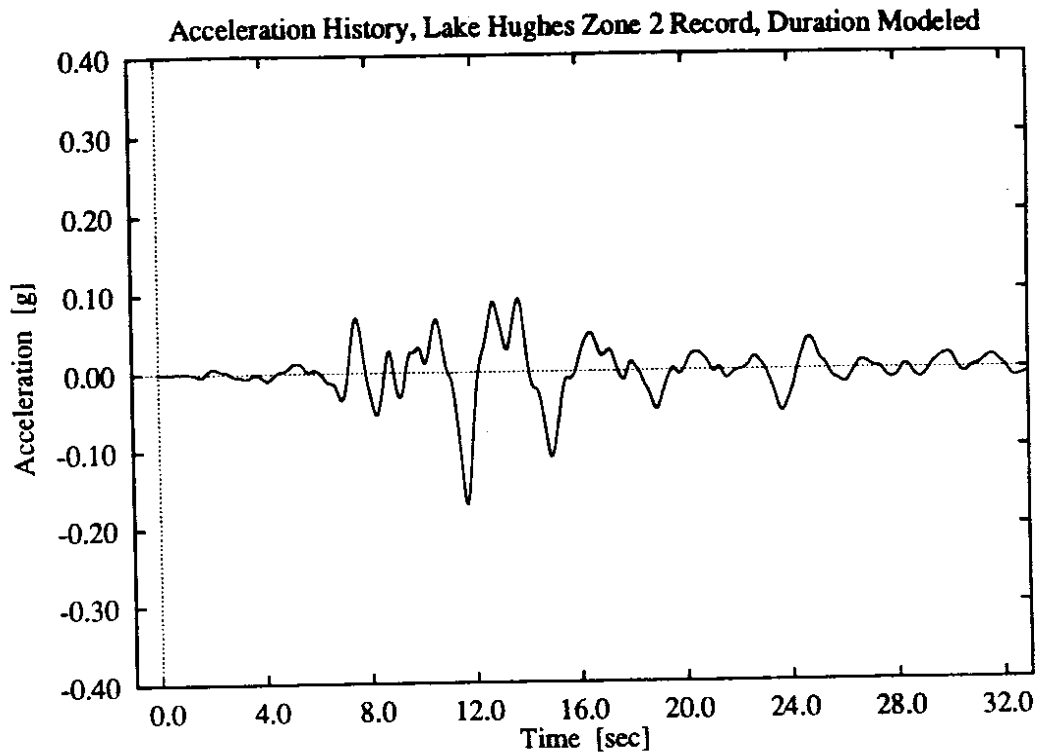


**Figure 3.23:** Lake Hughes, Zone 2 record: acceleration plot of duration modeled and acceleration response spectra.

be studied: column drift (the displacement of the column top relative to the bottom), the internal moment at the column top, and the rotation of the plastic hinge at the column top. Time histories of these parameters were obtained and studied in terms of their implications for column strength, ductility, and energy dissipation demands.

A total of 25 NEABS analyses were performed. As discussed, five supports were modeled, including the fixed-base bent. Four of these were subjected to all six ground motion records, while only the higher intensity El Centro record was applied to the fifth. Figure 3.24 displays this information in a matrix form, and indicates the “name” by which each of the 25 runs may be identified. The nomenclature used in Figure 3.24 to identify the foundation model and the applied seismic record is discussed in the previous sections.

Similar to the spread footing study, the three response parameters discussed were investigated by displaying the results of each analysis in up to four different graphs. The first two graphs are time histories of the column drift and the internal moment at the column top. These two graphs were created for each of the 25 runs. The second two graphs are a plot of the column moment–drift hysteresis and a time history of the plastic rotation of the column top. Examples of these four graphs are given in Figures 3.9 and 3.10, and interpretation of the physical significance of the type of data contained in these graphs may be found in the discussion of the spread footing study. The latter two graphs contain significant data



**Pile Foundation Parametric Study  
Matrix of NEABS runs**

	Filtered Records				Unfiltered Records	
	El Centro		Lake Hughes		El Centro	
	Zone 3	Zone 4	Zone 1	Zone 2	Lower Inten.	Higher Inten.
Fixed	PF01-FX_3EL	PF02-FX_4EL	PF03-FX_1LH	PF04-FX_2LH	PF05-FX_1EL	PF06-FX_HEL
DF1	PF07-DF1.3EL	PF08-DF1.4EL	PF09-DF1.1LH	PF10-DF1.2LH	PF11-DF1.LEL	PF12-DF1.HEL
DF2	PF13-DF2.3EL	PF14-DF2.4EL	PF15-DF2.1LH	PF16-DF2.2LH	PF17-DF2.LEL	PF18-DF2.HEL
DF3						PF19-DF3.HEL
WPF	PF20-WPF.3EL	PF21-WPF.4EL	PF22-WPF.1LH	PF23-WPF.2LH	PF24-WPF.LEL	PF25-WPF.HEL

**Figure 3.24:** Matrix of the 25 NEABS analysis runs for the study of pile foundation models. Each run is identified by a name of the form "PFnn-fff.eee," where nn is the run number, fff is the foundation model code, and eee is the applied seismic record code.

only when a plastic hinge forms at the column top. With one exception, the column remained elastic for the fixed-base bent model and for the three discrete pile head foundation models when subjected to the four filtered records. Because the plastic rotation of the one exception was very small, the second two graphs were not compiled for these runs. However, these graphs were created for all the analyses using the two unfiltered El Centro records, and for the six analyses using the Winkler-type pile foundation model. These graphs are presented in Appendix E, along with the foundation model parameter values used in the analyses.

To summarize and compare these results, the maxima of the three response parameters, column drift, column top internal moment, and column top plastic rotation, were recorded for each run. Additionally, as with the spread footing study, the sum of the absolute values of the plastic hinge rotations occurring over the duration of the seismic excitation were also recorded. It may be recalled that the plastic hinge rotation maxima and plastic rotation sums are related to ductility and energy dissipation demands, respectively. This data is presented in Figures 3.25 and 3.26. Each chart summarizes one of the four response parameters discussed above, the three maxima and the hinge rotation sum, for either the filtered or the unfiltered seismic records. For the four filtered records, bar charts are provided for drift and column top moment, while for the two unfiltered records, bar charts are given for the hinge rotation maxima and sums.

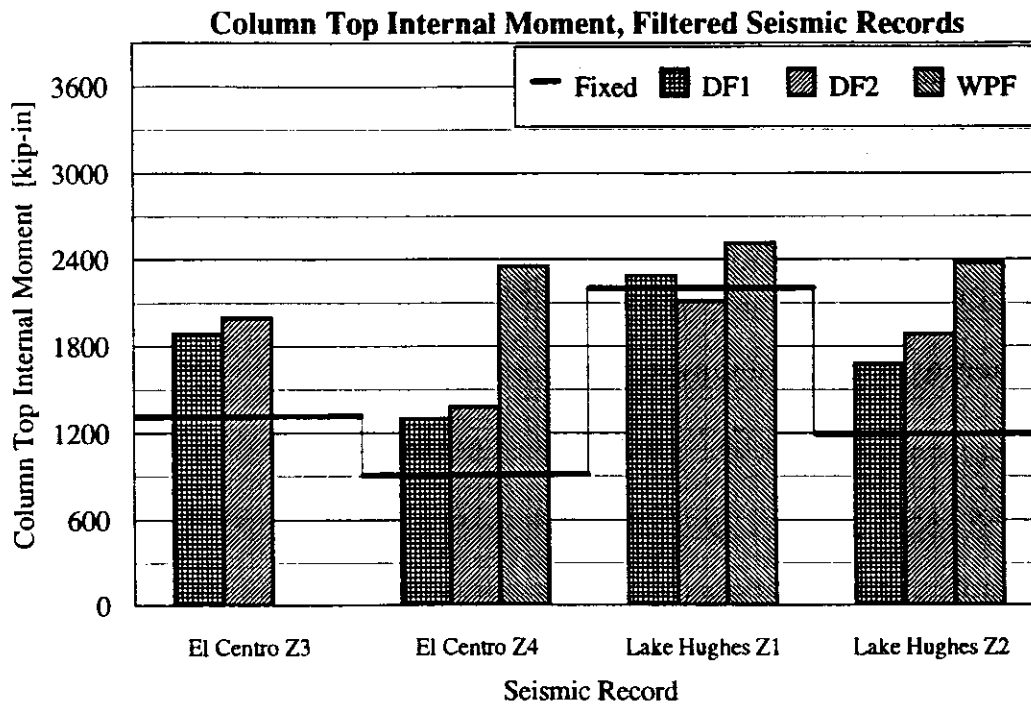
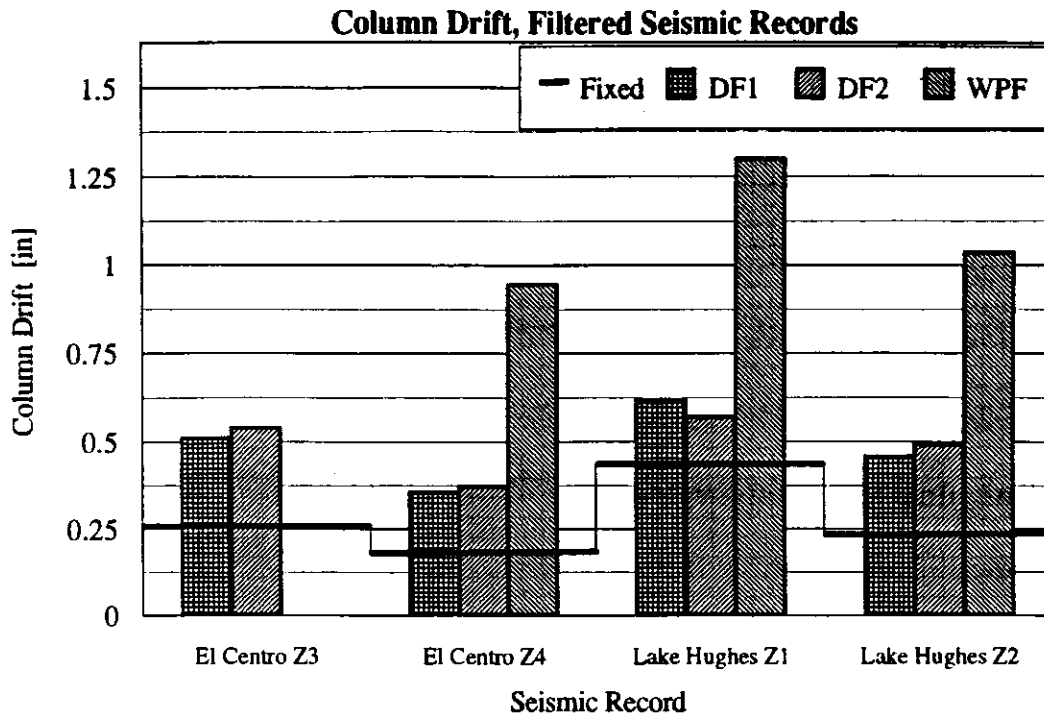


**Figure 3.25:** Comparison of the effect of the foundation models on the response of the column when the subjected to the filtered seismic records: (top) column drift maxima; (bottom) column top internal moment maxima.

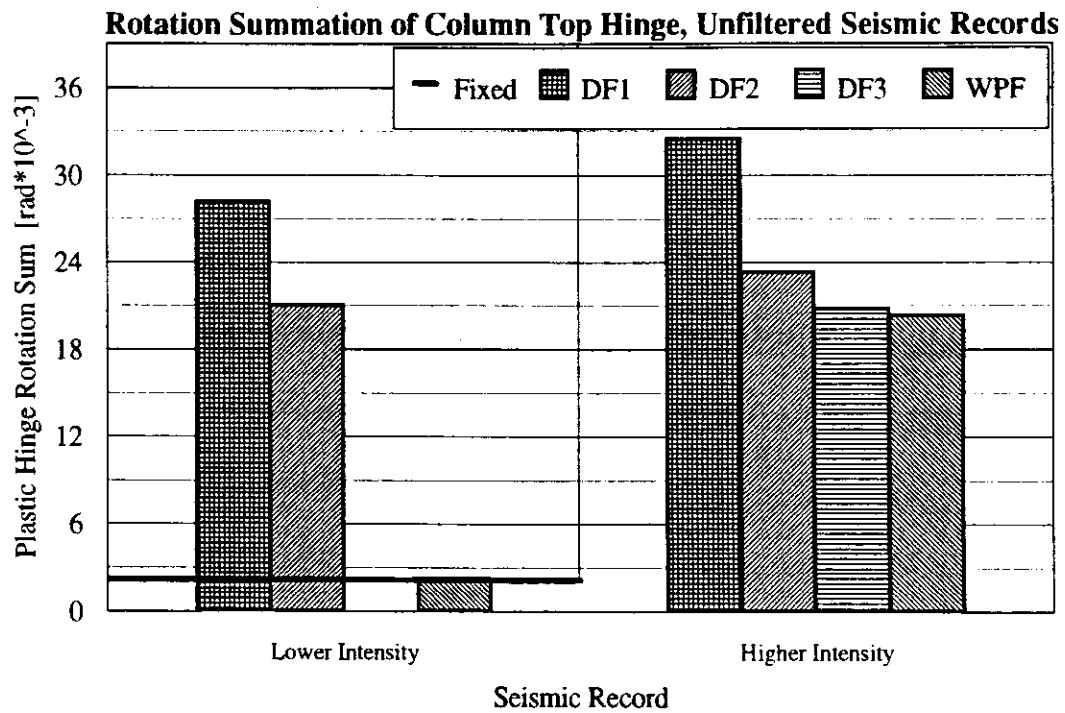
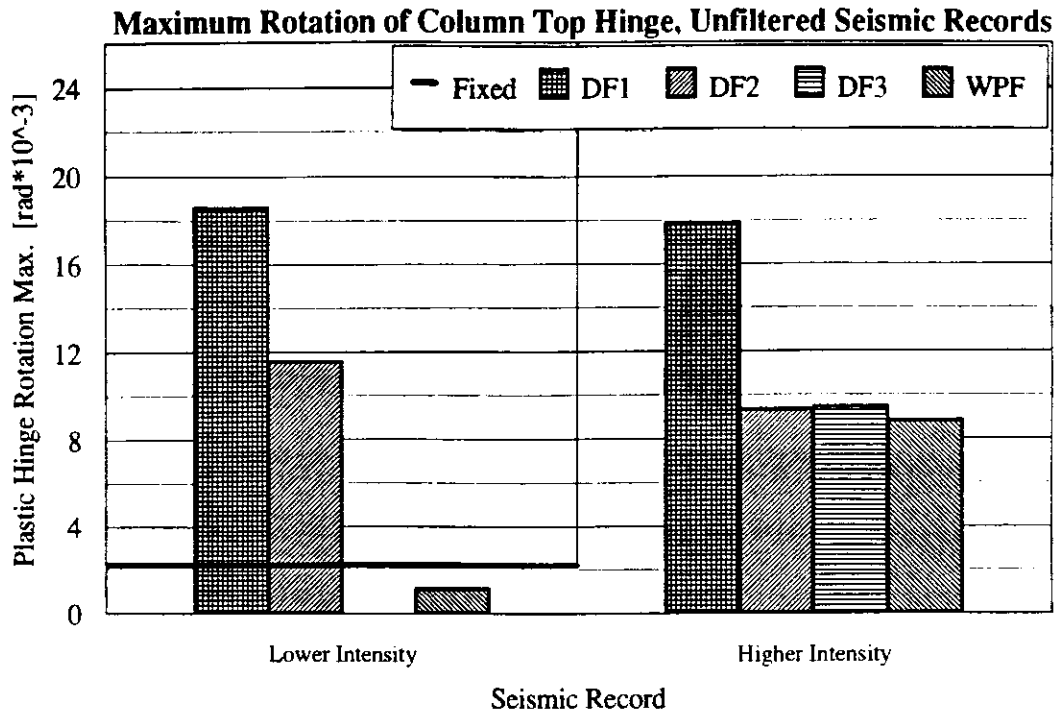


**Figure 3.26:** Comparison of the effect of foundation models on the response of the column top plastic hinge when subjected to the unfiltered seismic records: (top) maximum rotation attained (related to ductility demand); (bottom) total rotation sustained (related to energy demand).

Of the filtered records, the Lake Hughes Z1 record produced the highest values of all the measured response parameters for the fixed-base model, followed by the El Centro Z3 and Lake Hughes Z2 records (which produced very close results) and then by the El Centro Z4 record. This same ordering of response severity was observed for the bents using the DF1 and the DF2 foundation models. The column drift and column top moment response of these two models, as shown in Figure 3.25, were in close agreement with each other, and were both significantly more severe than the fixed-base response to each of these records. The DF1 model's response was slightly greater than the DF2 model's response for the Lake Hughes Z1 record, while the opposite was true for the other three records.

In no case was the response great enough to produce a maximum lateral pile head displacement in excess of 2.3 inches for the DF2 model, the yield displacement of the DF2 model's lateral spring. The only differences between the DF1 and the DF2 models were therefore the higher elastic stiffness of the DF2 model (approximately 40 percent stiffer) and the additional laterally-acting damper (which, as previously discussed, modeled primarily radiation damping). The closeness of the results of these two models appears to indicate that the column top moment is not especially sensitive to the stiffness of the pile head equivalent elastic springs, at least not in the stiffness range spanned by the DF1 and DF2 models. Further, the column top moment is not appreciably affected by radiation damping at the structure/excitation frequency combinations

analyzed, even though the Mercer Slough soil is very soft. Also, because the DF2 model's lateral spring did not yield during any of the analyses using the filtered records, the DF3 model's secant stiffness, as determined by the procedure described earlier, is the same as the elastic stiffness of the DF2 model's spring. Therefore, no unique DF3 model was created for these analyses.

The column top response is significantly more severe for the DF1 and the DF2 models than for the fixed-base model, contrary to the typical assumption that including the effects of soil-structure interaction in seismic analysis tends to reduce the predicted response. One probable reason for this increase is the redistribution of column moment, as was previously discussed for the spread footing study, which occurs when the fixed-base rotation constraint is removed for the addition of the foundation models. Even if the maximum column moment experienced by the column with the elastic base was somewhat lower than that experienced by the fixed-base column, proportionally more moment in the elastic base column would be concentrated at the top, and a net increase in column top moment may be observed.

The softest foundation model, in terms of lateral pile head stiffness, is the WPF model. The response it produced was significantly more severe than the DF1 or DF2 models, and yielding of the column top was observed for all the seismic records. This increased severity was most noticeable for the El Centro Z4 record. No results are reported for the WPF model

subjected to the El Centro Z3 record; an apparent numerical instability developed during this analysis, and caused the response to grow unreasonably.

It may also be noted that the increase in column drift between the bents with the fixed supports and those incorporating the WPF foundations is proportionally greater than the increase in column top moments between these models. This is consistent with the argument previously advanced regarding the redistribution of column moment between columns with fixed and elastic bases. In the limiting case of comparing elastic columns with fixed and pinned bases (and recalling that the column top is essentially fixed, since it frames into the crossbeam of very high relative stiffness), the proportional increase in column drift of the pinned base column relative to the fixed-base column is twice the proportional increase in column top moment.

The observed response of the bent models subjected to the two unfiltered records was more severe than that produced by the filtered records, and yielding of the column top was observed in all the analyses. The higher intensity El Centro record was the only record to produce yielding of the lateral pile head spring used in the DF2 model; thus, only one DF3 secant stiffness model was created. Using the procedure described earlier, based on the maximum pile head displacement observed in the DF2 model analysis, the secant stiffness was determined to be 9.0 kip/inch.

The responses of the column top plastic hinge for the DF1 and DF2 models, as shown in Figure 3.25, were quite different from each other. However, they were similar for each model between the lower and higher intensity records, despite the 60 percent greater EPA of the higher intensity record relative to that of the lower intensity record. For the lower intensity record, both the DF1 and the DF2 model produced much more severe response than did the fixed-base model. An apparent numerical instability developed during the analysis of the fixed-base model subjected to the higher intensity record, and caused the response to grow unreasonably at approximately 15 seconds.

The response of the DF1 model was significantly higher than the DF2 model for both records. The response of the one DF3 secant stiffness model was much closer to the response of the DF2 model (from which the DF3 model's stiffness is derived) than to the DF1 model, even though the DF3 model has an elastic spring stiffness only approximately 10 percent greater than the DF1 model. The DF3 model is apparently able to adequately reproduce the response of the bilinear DF2 model. The results of the analyses using the unfiltered records appear to indicate that the response is sensitive to the stiffness of elastic spring models of the pile cap lateral stiffness, contrary to the trend observed for the filtered records. However, this may again indicate that the effect of incorporating foundation models on the predicted response is very dependent on the



natural frequencies of the structure and the frequency content of the earthquake.

Also unlike the trend observed for the filtered record analyses, the response of the WPF model was the lowest of all the foundation models for the unfiltered record analyses. In examining the response histories given in Appendix E, the fundamental period of transverse vibration of the bent using the WPF model appears to be approximately 1.5 seconds. Comparing this period with the spectral acceleration response spectra of Figure 3.6, it appears probable that the lower predicted response for the WPF models is due to the lack of significant excitation of this period inherent in the El Centro record.

## **Chapter 4**

# **Conclusions**

### **4.1 Summary and Conclusions**

The seismic response of bridges may be significantly influenced by the dynamic interaction of the bridge foundations with the founding soil. This phenomenon, known as “soil–structure interaction,” is currently neglected, or included simplistically, in typical seismic analyses. Assuming a bridge to be fixed at its bases ignores the flexibility of the soil, while the use of elastic supports neglects energy dissipation which occurs through the soil’s material damping, “radiation” damping, and nonlinear response of the soil.

More sophisticated foundation models have been proposed to account for these mechanisms. For foundations in contact with the soil primarily at the soil surface, such as spread footings, the analogy of the foundation to a disk bonded to an elastic half-space has been used by researchers to develop discrete foundation models. Such models are expected to capture the effects of the soil far-field, away from the nonlinear action of the soil in the immediate vicinity of the structure, in a simple model which can be coupled with the structure at the soil–foundation interface. This approach

can also be extended further to develop discrete models which represent soil layers of finite depth and soil material viscous damping.

Enhanced soil-structure interface models have also been developed which can be used in Winkler-type pile foundations. These include models of the soil far-field (developed in a manner similar to the procedure for the spread footing far-field models), and the soil near-field (including soil nonlinear stiffness, inertial effects of mobilized soil, and the development of a gap between the pile and the soil).

In order to implement these foundation models in the seismic analysis of bridges, the computer program NEABS was modified to include a new element. NEABS performs time history analyses of bridges, using earthquake acceleration records as input. As delivered, NEABS provided four elements, which included nonlinear beam and expansion joint elements, as well as elastic foundations. The new element, called the "discrete foundation," or "DF" element, can be used to incorporate the foundation models developed by previous research that were identified as appropriate for including soil-structure interaction in NEABS analyses. The element has the properties required by these models, as well as nonlinear stiffness capabilities intended to make it versatile in modeling other nonlinear soil mechanisms. These nonlinear properties include bilinear hysteretic stiffness, elastic stiffness degradation, variable strain hardening rules, and gap development. The nonlinear characteristics may also be useful for modeling abutments and base isolation devices.

Two bridge bents were analyzed using several of the foundation models. The first bent used four spread footing foundation models of each of three soil stiffnesses (corresponding to shear wave velocities of  $c_s = 300$ , 700 and 1300 fps), and was subjected to four different seismic records. All four foundation models were discrete representations of a linear elastic half-space; three of the models included radiation damping. No near-field effects such as nonlinear soil stiffness or soil material damping were included in these models.

The second bridge bent used four models of piles embedded in very soft soil. Three of the models were variations of a simple equivalent pile head model, while the fourth was a Winkler-type pile foundation. The three pile head models were assigned properties based on the results of a pile test conducted at the site, while the Winkler pile foundation's properties were assigned in accordance with an analytical method proposed by Nogami and Konagai [35]. Seismic excitation included both acceleration records of relatively low intensity developed specifically for the soft soil (referred to as "filtered" records), and unmodified, or "unfiltered" records.

The foundation models were incorporated into the NEABS analyses of these bents using the DF element, and they exercised the bilinear stiffness with kinematic strain hardening, viscous damping, and mass features of the element. The elastic stiffness degradation, gap development, and alternate strain hardening options were not utilized in the parametric study, although their correct performance was verified during the development of the element.

The analysis results of the bents founded on spread footings were interpreted in terms of their implications for column top ductility and energy dissipation demands. The greatest change in these aspects of the bent response, compared with the fixed-base analyses, were observed for the spring-only model. However, all the models indicated that the fixed-base assumption was, occasionally, significantly unconservative in estimating column top demands. Except for the soft soil ( $c_s = 300$  fps), the spring-only foundation modeled the elastic half-space closely, using agreement with the response of the eleven parameter foundation model as a measure of adherence to the half-space soil representation. Models including radiation damping are probably warranted only for soft soil. The three-parameter model (spring-mass-dashpot) adequately modeled radiation damping, and the use of the more complex models does not appear to be justified. All the foundation models indicate that the response of the bent is very dependent on the frequency content of the earthquake. For the El Centro records, the soft soil models produced the highest column top demands, while the intermediate soil ( $c_s = 700$  fps) was critical for the Olympia records. As previously discussed, no soil near-field nonlinearities were included in these models. The behavior of the near-field is unknown, but could conceptually be accounted for by including a near-field model connected in series with the models based on the half-space, provided the appropriate model properties could be specified.

The analysis results of the bents founded on the pile foundations were also interpreted in terms of the response of the column top. For the analyses using the records filtered for the actual bridge conditions, the response was primarily elastic, and the column drift and column top moment were the aspects of the response that were considered. All the foundation models indicated higher column top moment demands than predicted for the fixed-base bent. The frequency content of the filtered records made the effective dynamic loading nearly quasi-static, so the higher demands predicted for the bents with the foundation models are likely the result of the redistribution of column moment caused by the inclusion of support flexibility. The quasi-static nature of the loading is probably also the reason that the inclusion of radiation damping in the pile head model did not appear to appreciably affect the response. The two pile head foundation models were in close agreement, even though the effective lateral spring stiffness of the model with the higher stiffness was approximately 40 percent greater than that of the lower stiffness model. This appears to indicate a relative insensitivity of the response to the selected pile head stiffness, at least in the stiffness range spanned by these two models.

The Winkler pile model, which had a much more flexible effective lateral pile head stiffness, predicted significantly higher column demands. In the one test using a secant pile head stiffness to approximate a bilinear pile head stiffness, the predicted responses were in close agreement.

Finally, the predicted response was again dependent on the intensity and frequency content of the earthquake, based on the differences in the results of the analyses using the filtered and unfiltered records.

## 4.2 Recommendations and Implementation

In view of these conclusions, it is recommended that the interaction of bridge foundations with the founding material be rationally included in seismic analysis. For spread footings, this can usually be accomplished (at least to account for soil far-field effects) by employing simple spring-only foundation models, with spring stiffnesses based on the static stiffness of an elastic half-space. For foundations that are soft in comparison with the bridge, however, neglecting radiation damping may cause an over-estimation of the response. The three parameter spring-mass-dashpot adequately models radiation damping, and may be used for soft soils, such as those with shear wave velocities in the vicinity of  $c_s = 300$  fps. Procedures for determining the three parameter model properties are presented by Veletsos and Verbič [29] and Wolf [31].

For pile foundations, either the Winkler pile or pile head models may be used, but the pile head models are recommended. The required properties may be determined from either field testing or finite element analysis data. Since they use far fewer elements than a Winkler pile foundation, the pile head models are particularly advantageous for large bridge models.

A few items may be suggested for future investigation. Additional parametric studies of the foundation models examined in the present study would prove useful in further identifying parameter sensitivity and bridge response trends. If undertaken, a greater number of earthquakes should be used to ensure a wide variety of frequency contents and to provide statistical significance to the observed results. However, they should be scaled to consistent intensities to better isolate frequency content-related effects.

Although the nonlinear stiffness properties of the DF element should make it versatile in soil–foundation modeling, these features should be further exercised to gain a better understanding of how they might realistically be employed in seismic analysis.

NEABS, equipped with the DF element, may be useful in developing and assessing new foundation models to represent the soil near-field, other bridge foundation substructures such as abutments and wall piers, and more refined pile models. One approach would be to identify the mechanisms that are exhibited in the response of these soil–foundation elements and determine if the DF element’s features are appropriate for their modeling. Another approach, similar to the method used to develop the spread footing foundation models, would be to determine the response of these elements by either experimental testing or detailed finite element analysis, and use NEABS as part of a curve-fitting procedure to obtain relatively simple models that can reproduce the observed behavior.



## **ACKNOWLEDGMENT**

The research project presented in this report was funded by the Washington State Transportation Center (TRAC). Mark Wallace served as the technical monitor at the Washington State Department of Transportation office of Bridges and Structures. Ed Henley and Richard Stoddard of the Washington State Department of Transportation also provided valuable guidance to the project.

The insight and critical review contributed by Dr. Lee Marsh and Dr. Carlton Ho of Washington State University is gratefully acknowledged. Tom Weber and Karl Hakimian were instrumental in getting the various computer systems at Washington State University to do what was needed.

## References

1. Ian. G. Buckle, Ronald L. Mayes, and M. R. Button, "Seismic Design and Retrofit Manual for Highway Bridges," *Final Report*, Federal Highway Administration, 1987.
2. John C. Wilson and Boon S. Tan, "Bridge Abutments: Formulation of a Simple Model for Earthquake Response Analysis," *Journal of Engineering Mechanics*, Vol. 116, No. 8, August, 1990, pp. 1828–1837.
3. Ignatius Po Lam and Geoffrey R. Martin, "Seismic Design for Highway Bridge Foundations," *Proceedings of Lifeline Earthquake Engineering: Performance, Design, and Construction*, ASCE Convention, October 1984, pp. 7–21.
4. Stuart D. Werner, J. L. Beck, and Marie B. Levine, "Seismic Response Evaluation of Meloland Road Overpass using 1979 Imperial Valley Earthquake Records," *International Journal of Earthquake Engineering and Structural Dynamics*, Vol. 15, 1987, pp. 249–274.
5. Weiming D. Liu, F. S. Nobari, and Roy A. Imbsen, "Dynamic Response Prediction for Earthquake Resistance Design of Bridge Structures," *Proceedings, ASCE Structures Congress, Seismic Engineering: Research and Practice*, 1989, pp. 1–10.
6. Joseph Penzien, "Soil–Pile Foundation Interaction," *Earthquake Engineering*, R. L. Weigel, ed., Prentice–Hall, Englewood Cliffs, New Jersey, 1970.
7. Constantine Chris Spyrakos, "Assessment of SSI on the Longitudinal Seismic Response of Short Span Bridges," *Engineering Structures*, Vol. 12, No. 1, January, 1990, pp. 60–66.
8. John B. Mander, "ERBS—Earthquake Resistant Bridge Systems/A Coordinated Research Initiative," *Proceedings of the Second Workshop on Bridge Engineering Research in Progress*, National Science Foundation and University of Nevada, Reno, October, 1990, pp. 197–200.

9. John C. Wilson, "Stiffness of Non-Skew Monolithic Bridge Abutments for Seismic Analysis," *Earthquake Engineering and Structural Dynamics*, Vol. 16, 1988, pp. 867–883.
10. C. B. Crouse, Behnan Hushmand, and Geoffrey R. Martin, "Dynamic Soil–Structure Interaction of a Single-Span Bridge," *International Journal of Earthquake Engineering and Structural Dynamics*, Vol. 15, 1987, pp. 711–729.
11. Emmanuel A. Maragakis, Bruce M. Douglas, and Spiros Vrontinos, "Analysis of the Effects of the Impact Energy Losses Occurring Between the Bridge Deck and Abutments," *Proceedings of Second Workshop on Bridge Engineering Research in Progress*, National Science Foundation and Civil Engineering Department of University of Nevada, Reno, October, 1990, pp. 201–204.
12. Michael E. Barenberg and Douglas A. Foutch,, "Evaluation of Seismic Design Procedures for Highway Bridges," *Journal of Structural Engineering*, Vol. 114, No. 7, July, 1988, pp. 1588–1605.
13. Gary Norris, "Lateral and Rotational Stiffness of Pile Foundation," *Structures Congress '91 Compact Papers*, Ninth Structures Congress, ASCE, 1991, pp. 749–752.
14. A. Ghobarah and H. M. Ali, "Seismic Performance of Highway Bridges," *Engineering Structures*, Vol. 10, No. 3, July, 1988, pp. 157–166.
15. A. Ghobarah, "Seismic Behavior of Highway Bridges with Base Isolation," *Canadian Journal of Civil Engineering*, Vol. 15, No. 1, February, 1988, pp. 72–78.
16. Ian G. Buckle and Ronald L. Mayes, "The Application of Seismic Isolation to Bridges," *Proceedings, ASCE Structures Congress, Seismic Engineering: Research and Practice*, 1989, pp. 633–642.
17. C. H. Loh and S. Z. Lee, "Aseismic Displacement Analysis of Multi-Supported Bridge to Multiple Excitations," *Soil Dynamics and Earthquake Engineering*, Vol. 9, No. 1, January, 1990, pp. 25–33.
18. Aspasia Zerva, "Effect of Spatial Variation of Ground Motions on Bridges," *Probabalistic Methods in Civil Engineering*, Proceedings of the Fifth ASCE Specialty Conference, May, 1988, pp. 253–256.

19. A. A. Dumanoglu and R. T. Severn, "Seismic Response of Modern Suspension Bridges to Asynchronous Vertical Ground Motion," *Proceedings of the Institution of Civil Engineers*, Vol. 83, Part 2, December, 1987, pp. 701–730.
20. Ahmed M. Abdel-Ghaffar, S. F. Masri, H. S. Sayed, and A. M. Niazy, "Performance of Suspension Bridges Subjected to Strong Earthquakes," *Proceedings of the Second Workshop on Bridge Engineering Research in Progress*, Reno, Nevada, October, 1990, pp. 15–18.
21. Weiming D. Liu, F. S. Nobari, R. Hamidi, and Roy A. Imbsen, "Modeling of the Golden Gate Bridge Tower Structure," *Proceedings, Ninth Structures Congress*, Indianapolis, Indiana, 1991, p. 838.
22. Ralph A. Dusseau and Robert K. Wen, "Seismic Response of Deck-Type Arch Bridges," *Earthquake Engineering and Structural Dynamics*, Vol. 18, 1989, pp. 701–715.
23. Roy A. Imbsen, J. Lea, V. N. Kalaikin, K. J. Perano, J. H. Gates, and S. L. Perano, *SEISAB-I Users Manual*, Imbsen & Associates, Sacramento, California, 1990.
24. Joseph Penzien, Roy A. Imbsen, and Weiming D. Liu, *NEABS (Nonlinear Earthquake Analysis of Bridge Systems)*, computer program source code and user's manual, National Information Service for Earthquake Engineering, EERC, University of California, Berkeley, 1981.
25. John P. Wolf, *Dynamic Soil-Structure Interaction*, Prentice-Hall, Inc., Englewood Cliffs, N. J., 1985.
26. David I. McLean and Ian B. S. Cannon, *Seismic Analysis of the I-90 Mercer Slough Westbound Lanes*, WSDOT Technical Report, 1992.
27. Steven L. Kramer, *Seismic Response—Foundations in Soft Soils*, WSDOT Draft Technical Report, July, 1992.
28. F. E. Richart, Jr., J. R. Hall, Jr., and R. D. Woods, *Vibrations of Soils and Foundations*, Prentice-Hall International, Inc., New Jersey, N.J., 1970.

29. Anestis S. Veletsos and B. Verbič, "Vibration of Viscoelastic Foundations," *International Journal of Earthquake Engineering and Structural Dynamics*, Vol. 2, No. 1, July–September, 1973, pp. 87–102.
30. Paul G. Somerville, James P. McLaren, Chandan K. Saikia, and Donald V. Helmberger, "Site-Specific Estimation of Spatial Incoherence of Strong Ground Motion," *Earthquake Engineering and Soil Dynamics II—Recent Advances in Ground-Motion Evaluation*, Geotechnical Special Publication No. 20, Geotechnical Engineering Division, ASCE, 1988, pp. 188–202.
31. John P. Wolf, *Soil–Structure-Interaction Analysis in Time Domain*, Prentice–Hall, Inc., Englewood Cliffs, N. J., 1988.
32. John P. Wolf and Antonio Paronesso, "Lumped-Parameter Model for a Rigid Cylindrical Foundation Embedded in a Soil Layer on Rigid Rock," *Earthquake Engineering and Structural Dynamics*, Vol. 21, 1992, pp. 1021–1038.
33. Wen-Yu Jean, Tsung-Wu Lin, and Joseph Penzien, "System Parameters of Soil Foundations for Time Domain Dynamic Analysis," *Earthquake Engineering and Structural Dynamics*, Vol. 19, 1990, pp. 541–553.
34. Ignatius Po Lam, Geoffrey R. Martin, and Roy A. Imbsen, "Modeling Bridge Foundations for Seismic Design and Retrofitting," *Transportation Research Record*, No. 1290, Vol. 2, 1991, pp. 113–126.
35. Toyooki Nogami and K. Konagai, "Time Domain Flexural Response of Dynamically Loaded Single Piles," *Journal of Engineering Mechanics*, ASCE, Vol. 114, No. 9, September, 1988, pp. 1512–1525.
36. Farzad Naeim, ed., *The Seismic Design Handbook*, Van Nostrand Reinhold, New York, 1989.
37. Toyooki Nogami, J. Otani, K. Konagai, and Hsiao-Lian Chen, "Nonlinear Soil–Pile Interaction Model for Dynamic Lateral Motion," *Journal of Geotechnical Engineering*, ASCE, Vol. 118, No. 1, January, 1992, pp. 89–106.

38. Roy A. Imbsen and Joseph Penzien, *Evaluation of Energy Absorption Characteristics of Highway Bridges under Seismic Conditions, Volume I*, Earthquake Engineering Research Center Report No. UBC/EERC-84/17, September, 1986.
39. Marc O. Eberhard, Jeffrey A. MacLardy, M. Lee Marsh, and Gaukur Hjartarson, *Lateral-Load Response of a Reinforced Concrete Bridge*, WSDOT Draft Technical Report, January, 1993.
40. Gaukur Hjartarson, *A Study of the Behavior of a Highway Bridge Under Lateral Loading / Phase I: Unaltered Conditions at the Abutments*, Master's Thesis, University of Washington, 1991.
41. M. Lee Marsh, *Effects of Flexural Strength Variations on the Seismic Performance of Reinforced Concrete Multiple Column Bridge Bents*, Doctoral Thesis, University of Washington, 1991.
42. R. Park and T. Paulay, *Reinforced Concrete Structures*, John Wiley and Sons, New York, 1975.
43. Federal Emergency Management Agency, *NEHRP Recommended Provisions for the Development of Seismic Regulations for New Buildings—Part 2: Commentary*, National Earthquake Hazards Reduction Program, 1991.
44. Ian B. S. Cannon, *Seismic Analysis of the Interstate 90 Mercer Slough Westbound Lanes*, Master's Thesis, Washington State University, August, 1992.
45. American Concrete Institute, *Building Code Requirements for Reinforced Concrete*, ACI Publication 318-89, 1989.
46. Kenji Kawano and Kouji Nagamitsu, "Random Seismic Response Analysis of High-Elevated Multi-Span Continuous Bridge," *Proceedings of the Eighth World Conference on Earthquake Engineering*, San Francisco, California, 1984, Vol. 5, pp. 167-174.

## Appendix A

# NEABS User's Guide Supplement

This appendix, "NEABS User's Guide Supplement", contains instructions for the use of NEABS, as modified to include the DF element (12/10/92). These instructions are supplementary to the instructions given in the user's guide provided with the program source code [24].

### *Changes/Additions to the required input data:*

1. The Rayleigh damping coefficients are no longer specified with Card VIII-A, but with Card II. The format of Card II has been changed to include the following:

Columns		
36-45	ALFA	damping factor proportional to mass
46-45	BETA	damping factor proportional to stiffness

The format of Card VIII-A has been changed to the following:

Columns		
1-10	DT	Time interval for integration in seconds
11-15	INTG	Integration method indicator

2. The following cards, which follow the expansion joint Card D and precede Card V, are required to specify DF element input data:

#### TYPE 6—Discrete Foundation (DF) Elements

- A. Control Data Card  
One card is required

Columns		
1-5	MTYPE	The number "6" for DF elements
6-10	NUMSSI	Number of DF elements
11-15	NPSET	Number of different element property sets

### B. Element Stiffness Parameter Cards

Supply one card for each degree-of-freedom for each element property set

#### Columns

1-5	NP	Element property set identification number (1 to NPSET)
6-10	IDOF	Local degree-of-freedom for which the following stiffness parameters apply (1 to 6)
11-20	RKEI	Initial elastic yield stiffness, as defined in Figure 2.10
21-30	FYI	Initial yield force, as defined in Figure 2.10
31-40	RKPI	Post-yield stiffness, as defined in Figure 2.10
41-50	RKG1	First in-gap stiffness, as defined in Figure 2.11
51-60	RKG2	Second in-gap stiffness, as defined in Figure 2.11
61-65	SD	Elastic stiffness degradation parameter; $SD \equiv \alpha$ , where $\alpha$ is as defined in equation (2.11)
66-70	RIK	Strain hardening parameter; $RIK = 0.0$ results in kinematic hardening (see Figure 2.10), $RIK = 1.0$ results in isotropic hardening. Intermediate values of $RIK$ are permitted.
71-75	RHOP	gap development parameter; $RHOP \equiv \gamma$ , where $\gamma$ is as defined in equation (2.12)
76-80	RIZ	Elastic unloading option parameter, as defined in Figure 2.10; $RIZ = 1$ turns option "on," $RIZ \neq 1$ leaves option "off"

### C. Element Damping Cards

Supply one card for each degree-of-freedom for each element property set

#### Columns

1-5	NP	Element property set identification number (1 to NPSET)
6-10	IDOF	Local degree-of-freedom for which the following damping parameter applies (1 to 6)
11-20	C	Linear viscous damping coefficient

### D. Element Mass Parameter Cards

Supply one card for each degree-of-freedom for each element property set

#### Columns

1-5	NP	Element property set identification number (1 to NPSET)
6-10	IDOF	Local degree-of-freedom for which the following mass parameters applies (1 to 6)
11-20	RMI	Mass to be lumped to node $i$ of element
21-30	RMJ	Mass to be lumped to node $j$ of element



### E. Element Data Cards

Supply one card for each DF element

Columns		
1-5	NE	Element number (1 to NUMSSI)
6-10	INI	Node <i>i</i> of element, as defined in Figure 2.9
11-15	INJ	Node <i>j</i> of element
16-20	INK	Node <i>k</i> of element
21-25	INL	Node <i>l</i> of element
26-30	PSNUM	Element property set number (1 to NPSET)
31-40	INELKI	End force release code at node <i>i</i> (works the same as for the NEABS beam element); using "000000" is recommended
41-50	INELKJ	End force release code at node <i>j</i>
51-55	-blank-	No data should be put in this field
56-60	IRD	Option to apply Rayleigh damping to element; IRD = 1 turns option "on," IRD ≠ 1 leaves option "off"

#### *Additional Notes:*

1. NEABS assumes input data to be contained in two files, "INPUT" and "RECORD". File INPUT contains all of the data specified by the users guide, including the changes/additions noted in this appendix, except for Cards VIII-F. These cards, which contain seismic acceleration and/or dynamic load data, are contained in file RECORD.
2. Results will be written to the file "OUTPUT". An execution error will result if a file named "OUTPUT" already exists when NEABS is executed.
3. If no input ground motion is to be specified, a blank line in the input should occupy the position of Card VIII-D. Failure to include a blank line will result in an execution error.
4. In the specification of requested element stress output (Cards IX-B-ii), output should be requested of at least one nonlinear element (elasto-plastic beam, expansion joint, or DF elements). Failure to do so will result in an execution error.
5. Appendix B contains the "INPUT", "RECORD", and "OUTPUT" files of an example NEABS analysis (specifically, the first 16 seconds of the SF42-D11.FEH analysis).

# Appendix B

## Example NEABS Analysis Incorporating DF Element

### System Model and Analysis Control Input File, "INPUT"

```

0      1      2      3      4      5      6      7      8
1234567890123456789012345678901234567890123456789012345678901234567890

Spread Footinge, Penzien ll model, soft soil, El Centro, high intensity
19  2  19  1  1  800  2  0.5869031  0.0042596
1  1  1  1  1  1  1  0.0  0.0  0.0
2  1  1  1  1  1  1  288.0  0.0  0.0
3  1  1  1  1  1  1  0.0  0.0  0.0
4  1  1  1  1  1  1  288.0  0.0  0.0
5  1  1  1  1  1  1  0.0  0.0  0.0
6  1  1  1  1  1  1  288.0  0.0  0.0
7  1  1  1  1  1  1  0.0  0.0  0.0
8  1  1  1  1  1  1  288.0  0.0  0.0
9  1  1  1  1  1  1  0.0  0.0  36.0
10 1  1  1  1  1  1  288.0  0.0  36.0
11 1  1  1  1  1  1  0.0  0.0  264.0
12 1  1  1  1  1  1  288.0  0.0  264.0
13 1  1  1  1  1  1  0.0  0.0  300.0
14 1  1  1  1  1  1  288.0  0.0  300.0
15 1  1  1  1  1  1  -92.0  0.0  300.0
16 1  1  1  1  1  1  380.0  0.0  300.0
17 1  1  1  1  1  1  0.0  0.0  600.0
18 1  1  1  1  1  1  288.0  0.0  600.0
19 1  1  1  1  1  1  576.0  0.0  600.0
2  9  2  0  2  1
1  4600.0  0.18  0.0
2  460000.0  0.18  1.000E-06
1  1076.0  968.0  968.0  82400.0  41200.0  41200.0
2  2590.0  96800.0  96800.0  8240000.0  4120000.0  4120000.0
0.0  0.0  0.0  0.0
-386.04  0.0  0.0  0.0
1  4884.0  9000.0  9000.0  0.1226
1  1.0  -6.9732  -9.4420  -1.4688  1.0  -6.9732  -9.4420  -1.4688
1  7  9  18  1  1
2  9  11  18  1  1
3  11  13  18  1  1
4  8  10  19  1  1
5  10  12  19  1  1
6  12  14  19  1  1
7  13  14  19  2  2
8  15  13  19  2  2
9  14  16  19  2  2
6  10  5
1  1  1392.526  1.0E+10  0.0  0.0  0.0  0.0  0.0  0.0
1  2  1699.802  1.0E+10  0.0  0.0  0.0  0.0  0.0  0.0
1  3  1699.802  1.0E+10  0.0  0.0  0.0  0.0  0.0  0.0
1  4  9458823  1.0E+10  0.0  0.0  0.0  0.0  0.0  0.0
1234567890123456789012345678901234567890123456789012345678901234567890
0      1      2      3      4      5      6      7      8

```

0 1 2 3 4 5 6 7 8  
 1234567890123456789012345678901234567890123456789012345678901234567890

1	5	5071944	1.0E+10	0.0	0.0	0.0	0.0	0.0	0.0	0.0
1	6	5071944	1.0E+10	0.0	0.0	0.0	0.0	0.0	0.0	0.0
2	1	1091.646	1.0E+10	0.0	0.0	0.0	0.0	0.0	0.0	0.0
2	2	591.1233	1.0E+10	0.0	0.0	0.0	0.0	0.0	0.0	0.0
2	3	591.1233	1.0E+10	0.0	0.0	0.0	0.0	0.0	0.0	0.0
2	4	2214651	1.0E+10	0.0	0.0	0.0	0.0	0.0	0.0	0.0
2	5	1306509	1.0E+10	0.0	0.0	0.0	0.0	0.0	0.0	0.0
2	6	1306509	1.0E+10	0.0	0.0	0.0	0.0	0.0	0.0	0.0
3	1	1777.904	1.0E+10	0.0	0.0	0.0	0.0	0.0	0.0	0.0
3	2	1798.386	1.0E+10	0.0	0.0	0.0	0.0	0.0	0.0	0.0
3	3	1798.386	1.0E+10	0.0	0.0	0.0	0.0	0.0	0.0	0.0
3	4	6646334	1.0E+10	0.0	0.0	0.0	0.0	0.0	0.0	0.0
3	5	3263418	1.0E+10	0.0	0.0	0.0	0.0	0.0	0.0	0.0
3	6	3263418	1.0E+10	0.0	0.0	0.0	0.0	0.0	0.0	0.0
4	1	450.1618	1.0E+10	0.0	0.0	0.0	0.0	0.0	0.0	0.0
4	2	571.5546	1.0E+10	0.0	0.0	0.0	0.0	0.0	0.0	0.0
4	3	571.5546	1.0E+10	0.0	0.0	0.0	0.0	0.0	0.0	0.0
4	4	7384009	1.0E+10	0.0	0.0	0.0	0.0	0.0	0.0	0.0
4	5	4552660	1.0E+10	0.0	0.0	0.0	0.0	0.0	0.0	0.0
4	6	4552660	1.0E+10	0.0	0.0	0.0	0.0	0.0	0.0	0.0
5	1	0.0	1.0E+10	0.0	0.0	0.0	0.0	0.0	0.0	0.0
5	2	0.0	1.0E+10	0.0	0.0	0.0	0.0	0.0	0.0	0.0
5	3	0.0	1.0E+10	0.0	0.0	0.0	0.0	0.0	0.0	0.0
5	4	0.0	1.0E+10	0.0	0.0	0.0	0.0	0.0	0.0	0.0
5	5	0.0	1.0E+10	0.0	0.0	0.0	0.0	0.0	0.0	0.0
5	6	0.0	1.0E+10	0.0	0.0	0.0	0.0	0.0	0.0	0.0
1	1	31.43207								
1	2	36.01573								
1	3	36.01573								
1	4	119823.6								
1	5	64412.38								
1	6	64412.38								
2	1	13.66794								
2	2	13.11395								
2	3	13.11395								
2	4	-32320.1								
2	5	-16789.4								
2	6	-16789.4								
3	1	24.47924								
3	2	24.75835								
3	3	24.75835								
3	4	7672.424								
3	5	3164.212								
3	6	3164.212								
4	1	7.306419								
4	2	1.983106								
4	3	1.983106								
4	4	65682.8								
4	5	39968.27								
4	6	39968.27								
5	1	27.95565								
5	2	30.38705								
5	3	30.38705								
5	4	63747.98								
5	5	33788.29								
5	6	33788.29								
1	1	0.0	0.0							
1	2	0.0	0.0							
1	3	0.0	0.0							
1	4	0.0	0.0							
1	5	0.0	0.0							
1	6	0.0	0.0							
2	1	0.0	0.0							
2	2	0.0	0.0							
2	3	0.0	0.0							
2	4	0.0	0.0							
2	5	0.0	0.0							
2	6	0.0	0.0							
3	1	0.0	0.0							
3	2	0.0	0.0							
3	3	0.0	0.0							
3	4	0.0	0.0							

12345678901234567890123456789012345678901234567890123456789012345678901234567890  
 0 1 2 3 4 5 6 7 8

0	1	2	3	4	5	6	7	8		
1234567890	1234567890	1234567890	1234567890	1234567890	1234567890	1234567890	1234567890	1234567890		
3	5	0.0	0.0							
3	6	0.0	0.0							
4	1	0.0	0.0							
4	2	0.0	0.0							
4	3	0.0	0.0							
4	4	0.0	0.0							
4	5	0.0	0.0							
4	6	0.0	0.0							
5	1	0.253735	0.393096							
5	2	0.297489	0.05269							
5	3	0.297489	0.05269							
5	4	790.8962	2420.943							
5	5	392.4067	1228.482							
5	6	392.4067	1228.482							
	0.0	0.0	0.0	0.0						
	0.0	0.0	0.0	0.0						
	-386.04	0.0	0.0	0.0						
1	1	5	17	18	1	000000	000000	0	0	0
2	5	7	17	18	2	000000	000000	0	0	0
3	1	3	17	18	3	000000	000000	0	0	0
4	3	7	17	18	4	000000	000000	0	0	0
5	3	5	17	18	5	000000	000000	0	0	0
6	2	6	18	19	1	000000	000000	0	0	0
7	6	8	18	19	2	000000	000000	0	0	0
8	2	4	18	19	3	000000	000000	0	0	0
9	4	8	18	19	4	000000	000000	0	0	0
10	4	6	18	19	5	000000	000000	0	0	0

	1.0								
	.02000	0							
5		0.050							
10	1		0.010	0.005					
1			1.433963						
1									
7	1	5							
13	1	5							
1									
2	3	7	8	12					

0	1	2	3	4	5	6	7	8
1234567890	1234567890	1234567890	1234567890	1234567890	1234567890	1234567890	1234567890	1234567890

**Applied Seismic Excitation File, "RECORD"**

0	1	2	3	4	5	6	7	8
1234567890	1234567890	1234567890	1234567890	1234567890	1234567890	1234567890	1234567890	1234567890

1940 Imperial Valley Eqk, El Centro S00E Rec: EPA = 0.279g

2689	135.0000	.0200	.0000						
.000000	-.004083	-.031496	-.029455	-.025663	-.027705	-.034996	-.041411	\$	1
-.037329	-.032079	-.024789	-.024789	-.038204	-.051327	-.056576	-.047244	\$	2
-.041995	-.031496	-.023914	-.012248	-.019248	-.038204	-.055410	-.057160	\$	3
-.019248	.008749	.041120	-.014290	-.037329	-.041995	-.059201	-.075824	\$	4
-.094780	-.089239	-.050160	-.057451	-.047536	-.047827	-.019539	.007291	\$	5
.043745	.068825	.073491	.097988	.135025	.143482	.122193	.104695	\$	6
.079032	.068533	.098863	.120152	.154564	.186352	.213473	.190143	\$	7
-.174686	.116652	.116652	.018373	-.150190	-.229513	-.175853	-.141149	\$	8
-.072908	-.017206	.039078	.089822	.145523	.207057	.290172	.355497	\$	9
.445903	.422572	.336833	-.272674	.260134	.270050	.244678	-.262759	\$	10
.289589	.352581	.095655	-.430155	-.602508	-.580052	-.593176	-.529600	\$	11
-.503062	-.510936	-.511228	-.526393	-.475357	-.392826	-.317002	-.228055	\$	12

0	1	2	3	4	5	6	7	8
1234567890	1234567890	1234567890	1234567890	1234567890	1234567890	1234567890	1234567890	1234567890

0 1 2 3 4 5 6 7 8  
12345678901234567890123456789012345678901234567890123456789012345678901234567890

-125109	-.004958	.104987	.228930	.339458	.466025	.571595	-.703412	\$ 13
.795859	.885389	.933217	.996500	.822689	.677749	-.349373	-.692038	\$ 14
-.478274	-.543890	-.319335	-.219598	-.050452	.032954	.155439	-.261009	\$ 15
.345873	.512394	.167979	-.767279	-.451152	-.504229	-.295130	-.168854	\$ 16
.069116	-.195392	-.577428	-.478565	-.491397	-.431904	-.358997	-.291922	\$ 17
-.219014	-.152523	-.079032	-.012832	.054826	-.027705	-.126276	-.244386	\$ 18
-.277340	-.208807	-.174686	-.097404	-.031496	.053952	.122485	.196267	\$ 19
-.028288	-.108486	-.011665	.003208	.100321	.164771	.257509	.329542	\$ 20
.397492	.063867	.070283	.199183	.200933	.384369	.394576	.594926	\$ 21
-.271508	-.381452	-.201808	-.159230	.020997	.196850	-.311169	-.433946	\$ 22
-.312336	-.338874	-.222222	-.163021	-.062700	-.036745	-.196559	-.094488	\$ 23
-.098279	-.031788	.004958	.087197	.142316	.177311	.064742	-.009332	\$ 24
-.071449	.022456	.061534	.165646	.240887	.351706	.431029	.506562	\$ 25
.122776	.008457	.075532	.085448	-.016040	-.042870	.041703	.060076	\$ 26
.145523	.188101	.279090	.328959	.421989	.475066	.567221	.541266	\$ 27
.578594	.515894	.364538	-.351998	-.158064	-.111986	-.090697	-.326043	\$ 28
-.484398	-.718577	-.590551	-.535141	-.384077	-.279965	-.094780	.044911	\$ 29
.237970	.384660	.530184	.016915	-.049286	.083115	.130359	.286672	\$ 30
.415281	.540391	.716244	.491397	-.402450	-.291339	-.317585	-.264509	\$ 31
-.136775	-.364538	-.615631	-.471566	-.493438	-.380869	-.324001	-.225430	\$ 32
-.148731	-.158647	-.349956	-.352581	-.337708	-.333917	-.209099	-.159230	\$ 33
.018664	-.234471	-.476524	-.250510	-.280257	-.115486	-.042870	.093030	\$ 34
.188976	.255468	.137649	.057743	-.007874	.085156	.129775	.228930	\$ 35
.301254	.394284	.468358	.542724	.373578	.186643	.059493	.091572	\$ 36
.108778	.144649	.068533	-.024497	-.048994	-.032954	-.066783	-.072324	\$ 37
-.045786	-.020122	.042870	.110528	.168854	.074366	-.011957	-.124818	\$ 38
-.038787	.027705	.067075	-.037620	-.014582	.023330	.061242	.110819	\$ 39
.148731	.045786	-.009332	-.032371	.001458	.022164	.010207	-.027705	\$ 40
-.010499	-.004666	.011082	.024789	-.016331	-.088656	-.122776	-.071158	\$ 41
-.068825	-.051619	-.037620	-.005249	.059201	-.031496	-.026538	-.009915	\$ 42
-.030913	-.032371	-.028871	-.000583	.021289	.068533	.103529	.205599	\$ 43
.227180	.053660	-.076699	-.036162	-.012248	.046369	.013998	-.063867	\$ 44
-.136191	-.124818	-.062992	-.012540	.046369	.093322	.122193	.035871	\$ 45
-.046661	-.059493	-.023914	-.060076	-.039953	-.016040	.015456	.039078	\$ 46
.077574	.067658	.023039	-.002333	.058326	.126859	.143482	.055701	\$ 47
.026830	-.006416	-.006124	.015165	.027122	.074366	.107320	.153106	\$ 48
.157772	.123943	.116069	.163021	.220472	.106445	.119860	.028580	\$ 49
-.059493	-.072616	-.118110	-.120443	-.137358	-.126276	-.133567	-.016623	\$ 50
.051910	-.060659	-.143482	-.154564	-.105570	-.118110	-.089822	-.092155	\$ 51
-.077282	-.077282	-.078449	-.100612	-.090114	-.063284	-.022747	.025372	\$ 52
.081948	.090405	.104404	.099446	.104404	.083698	.088947	.032663	\$ 53
.062409	.039662	.111986	-.251094	-.393409	-.391368	-.394867	-.347915	\$ 54
-.303879	-.241761	-.189851	-.129484	-.075241	-.017498	-.026538	-.053077	\$ 55
-.042870	.024789	.047536	.014582	.076990	.169729	.252843	.349956	\$ 56
-.494313	-.324001	-.320793	-.106737	-.129775	-.068825	-.279965	-.191309	\$ 57
-.174103	-.195392	-.160980	-.007874	.110236	.312628	.486731	.276174	\$ 58
.118985	.194517	.038495	-.027705	-.151648	-.241178	-.335958	-.335375	\$ 59
-.234179	-.107612	.008457	.158938	.343540	.469525	-.078740	.009915	\$ 60
-.016331	.005833	.042578	.156605	.232721	-.059784	-.172062	-.049286	\$ 61
-.051035	-.008166	.021581	.111403	.165354	.219598	.233596	.172645	\$ 62
.088656	.006707	.018664	-.118402	-.131525	-.023039	.048994	.165354	\$ 63
.027122	-.016040	.012832	-.035871	-.082240	-.127442	-.102654	-.074366	\$ 64
-.032371	.059784	.151356	.249052	.333625	.213765	.069116	-.107320	\$ 65
-.079032	-.063284	-.254593	-.283756	-.171770	-.097988	.022456	.075532	\$ 66
.148148	.105279	.023622	-.016331	-.060951	-.092447	-.069408	-.109653	\$ 67
-.160397	-.210557	-.234179	-.152523	-.099154	-.003208	.018956	-.010790	\$ 68
-.001458	-.048994	-.119568	-.023330	.023039	.109070	.179353	.193934	\$ 69
.074074	-.016623	-.138233	-.103820	-.070866	-.013998	.036745	.110528	\$ 70
.070283	-.066200	-.124818	-.198017	-.192768	-.172062	-.149606	-.118985	\$ 71
-.090114	-.077574	-.157772	-.183144	-.264800	-.322835	-.256926	-.224555	\$ 72
-.169729	-.137941	-.097113	-.058034	.005833	.061534	.125984	.178769	\$ 73
.223680	.272091	.310878	.329542	.346165	.363663	.389035	.464859	\$ 74
.524059	.594051	.360455	.128901	-.040828	-.194226	-.161855	-.202100	\$ 75
-.286964	-.363371	-.343832	-.306212	-.268300	-.216681	-.235929	-.247886	\$ 76
-.250802	-.251677	-.254593	-.253135	-.258093	-.156605	.015165	.062700	\$ 77
.071449	.169146	.091572	.068825	.141441	.171770	.153106	.103529	\$ 78
.057451	.058034	.143482	.100029	.083990	.125984	.069700	.025663	\$ 79
.022456	-.043161	-.022456	-.005541	.021872	.012832	-.042286	-.092155	\$ 80
-.070283	-.008166	.053077	.124234	.128026	.149315	.135900	.139691	\$ 81
.056285	.064742	.079907	.114611	.146982	.168271	.171479	.239720	\$ 82
.232429	.276757	.100612	.013123	-.035871	-.101196	-.124234	-.121318	\$ 83
-.080198	-.078740	.021581	.124818	-.067367	-.112861	-.024205	.040537	\$ 84

12345678901234567890123456789012345678901234567890123456789012345678901234567890  
0 1 2 3 4 5 6 7 8

0 1 2 3 4 5 6 7 8  
 12345678901234567890123456789012345678901234567890123456789012345678901234567890

.028288	.034412	.039370	.030621	.022456	.012832	.003500	-.006124	\$ 229
-.012248	-.019831	-.025372	-.034996	-.046369	-.057743	-.067950	-.075241	\$ 230
-.078740	-.081073	-.083698	-.081073	-.078740	-.075241	-.073199	-.063867	\$ 231
-.050452	-.037620	-.031788	-.030621	-.027705	-.026538	-.020997	-.017206	\$ 232
-.011665	-.006707	.005249	.010207	.012248	.013998	.012540	.012540	\$ 233
.011082	.010499	.009332	.013707	.018373	.024789	.032079	.039078	\$ 234
.046661	.052785	.050452	.048994	.046369	.042870	.031496	.019831	\$ 235
.009332	.002625	.005541	.008166	.011665	.015748	.020122	.027705	\$ 236
.034121	.041703	.041703	.036454	.035579	.036162	.036745	.037912	\$ 237
.038787	.030913	.023039	.013415	.005833	.001458	-.003208	-.007291	\$ 238
-.003208	.005249	.012540	.022164	.030038	.038787	.029455	.018081	\$ 239
.005249	-.007874	-.023330	-.025955	-.015748	-.009749	.001750	.003500	\$ 240
.006416	.007874	.009332	.013998	.020122	.025955	.032663	.038787	\$ 241
.040828	.039953	.040828	.039370	.040537	.029746	.008749	-.009332	\$ 242
-.018373	-.024789	-.032663	-.045786	-.057451	-.054826	-.053077	-.049577	\$ 243
-.045494	-.041411	-.037620	-.036454	-.034996	-.033829	-.033246	-.030913	\$ 244
-.018664	-.006124	.000583	-.001167	-.001167	-.004083	-.005541	-.002333	\$ 245
.003208	.007874	.014582	.015456	.012248	.008749	.003208	-.001458	\$ 246
-.006999	-.005833	-.002041	.001167	.005541	.009624	.013998	.016623	\$ 247
.018956	.021581	.023622	.026538	.037037	.049286	.041995	.030621	\$ 248
.020414	.010207	.000583	-.009332	-.018664	-.027705	-.026538	-.024205	\$ 249
-.021289	-.014873	-.008749	-.001167	.009624	.015165	.012832	.011665	\$ 250
.008749	.005833	.002916	.000292	.002916	-.004083	.000583	.004666	\$ 251
.008749	.006707	.004666	.004666	.007582	.009332	.013123	.013415	\$ 252
.006124	-.000875	-.008749	-.017498	-.025372	-.033829	-.031204	-.027413	\$ 253
-.022747	-.019831	-.018373	-.016623	-.014582	-.011957	-.009624	-.006999	\$ 254
-.004083	-.001458	.001167	.003791	.006124	.000292	-.005249	-.011665	\$ 255
-.018664	-.025372	-.032079	-.037620	-.044036	-.048119	-.050744	-.053660	\$ 256
-.056576	-.058909	-.062117	-.057743	-.050452	-.039370	-.018956	-.004083	\$ 257
.005833	.016040	.023914	.025955	.029746	.027122	.023330	.017789	\$ 258
.009624	.000875	-.006999	-.016623	-.013123	-.003791	.003791	.009624	\$ 259
.013998	.015748	.016915	.018081	.018956	.020122	.020997	.021872	\$ 260
.022456	.021289	.020122	.018664	.016915	.015748	.013998	.017789	\$ 261
.023039	.027997	.033246	.036745	.040537	.038204	.035871	.033246	\$ 262
.030038	.025372	.020997	.016331	.011665	.006999	.002041	.001167	\$ 263
.002333	.002625	.006707	.012248	.015165	.017789	.020997	.023039	\$ 264
.025955	.027705	.027705	.027122	.025955	.007291	.000000	-.001458	\$ 265
-.005833	-.006999	-.009624	-.013998	-.018664	-.023330	-.028288	-.033246	\$ 266
-.037329	-.030913	-.025955	-.019248	-.012540	-.005541	-.003208	-.002625	\$ 267
-.001458	-.001167	.001458	.004083	.006999	.010207	.012540	.012832	\$ 268
.011374	.003791	-.002333	-.010499	-.013707	-.016040	-.018081	-.019831	\$ 269
-.021289	-.023330	-.021872	-.018664	-.008166	.001458	.013415	.018956	\$ 270
.017498	.017498	.015748	.014290	.012832	.011374	.008457	.000000	\$ 271
-.007582	-.015165	-.012248	-.010790	-.007291	-.004374	-.000583	.000583	\$ 272
.000000	-.000292	-.001167	-.002041	-.001750	-.000292	.000875	.002041	\$ 273
-.000292	-.002041	-.004374	-.006999	-.008457	-.008166	-.008166	-.007291	\$ 274
-.006999	-.006124	-.007874	-.012832	-.016915	-.022164	-.024497	-.023914	\$ 275
-.024205	-.021872	-.014582	-.008166	-.000583	.005249	.005249	.006124	\$ 276
.006124	.006124	.009041	.012540	.014290	.014290	.014290	.013998	\$ 277
.013707	.015165	.019539	.023039	.027705	.028288	.027997	.027997	\$ 278
.027122	.026538	.025955	.025372	.024497	.023914	.023330	.022456	\$ 279
.018081	.013707	.010207	.010499	.009915	.010207	.010499	.009332	\$ 280
.005541	.004374	.004083	.003500	.003500	.003208	.000000	-.002916	\$ 281
-.005833	-.007291	-.008457	-.009624	-.010790	-.013998	-.018373	-.022456	\$ 282
-.026830	-.031204	-.035579	-.040245	-.041703	-.034996	-.030038	-.022747	\$ 283
-.019539	-.018373	-.016915	-.016331	-.015456	-.014582	-.013998	-.013123	\$ 284
-.012248	-.011374	-.009041	-.007582	-.003208	.002916	.009041	.013415	\$ 285
.013998	.015748	.016040	.018373	.024497	.029455	.024497	.020706	\$ 286
.015456	.009624	.008166	.008457	.008166	.007874	.003500	-.000292	\$ 287
-.002916	-.003208	-.004666	-.004374	-.009041	-.019831	-.028871	-.029746	\$ 288
-.030621	-.030913	-.028871	-.025955	-.023039	-.021581	-.020997	-.019831	\$ 289
-.019539	-.018373	-.011665	-.003791	.003791	.012540	.020706	.028871	\$ 290
.025080	.018373	.011957	.003791	-.004083	-.010207	-.010790	-.012832	\$ 291
-.013415	-.014290	-.014873	-.015748	-.016331	-.016915	-.013415	-.008457	\$ 292
-.003791	.002041	.004958	.005541	.007291	.007291	.010207	.014582	\$ 293
.018664	.023330	.027413	.028288	.029746	.030621	.031496	.032079	\$ 294
.030330	.028871	.027122	.025080	.023039	.020997	.018373	.016040	\$ 295
.013415	.011082	.009041	.007874	.006124	.004958	.003500	.002041	\$ 296
.000875	.002333	.003791	.005541	.006416	.002625	-.000875	-.004958	\$ 297
-.009041	-.013707	-.015456	-.013998	-.012540	-.011082	-.007291	-.002625	\$ 298
.002041	.004958	.006416	.016207	.017789	.024205	.032663	.031204	\$ 299
.025372	.020706	.013707	.007874	.001167	-.004666	-.006999	-.009624	\$ 300

12345678901234567890123456789012345678901234567890123456789012345678901234567890  
 0 1 2 3 4 5 6 7 8

0	1	2	3	4	5	6	7	8
1234567890123456789012345678901234567890123456789012345678901234567890123456789012345678901234567890								
-.013415	-.020122	-.024497	-.025663	-.027122	-.027705	-.028288	-.028871	\$ 301
-.029455	-.029746	-.028580	-.027705	-.026247	-.025372	-.025955	-.026538	\$ 302
-.027122	-.027997	-.028288	-.025663	-.023622	-.020706	-.019831	-.019831	\$ 303
-.019539	-.019539	-.019248	-.019248	-.018664	-.016331	-.014582	-.012540	\$ 304
-.009915	-.006707	-.003791	-.000583	.002916	.004958	.002625	.000875	\$ 305
-.001458	-.004083	-.002041	.001750	.004666	.003791	.003500	.002333	\$ 306
.001458	.000000	.000583	.002625	.004083	.006124	.006416	.002916	\$ 307
.000000	-.003500	-.006999	-.006999	-.005541	-.004666	-.005249	-.006416	\$ 308
-.007874	-.008749	-.007582	-.006416	-.006416	-.009332	-.011957	-.014873	\$ 309
-.013415	-.012540	-.011082	-.009332	-.007582	-.005833	-.005541	-.005249	\$ 310
-.004374	.003791	.011957	.019539	.020414	.022164	.022747	.023330	\$ 311
.023622	.024497	.022747	.017789	.013998	.009041	.008457	.008749	\$ 312
.009332	.010207	.010790	.006999	.002041	-.002333	-.008166	-.010207	\$ 313
-.006416	-.003791	.000292	.000875	.000292	-.000292	-.001458	-.002333	\$ 314
-.003208	-.004374	-.003500	-.002333	-.001167	.000292	.001458	.002333	\$ 315
.002333	.002625	.002916	.006416	.009624	.013415	.017206	.020997	\$ 316
.023039	.018081	.014582	.009332	.004666	-.001167	.000000	.008749	\$ 317
.015165	.025372	.023914	.009041	-.000583	-.018081	-.008166	.016915	\$ 318
.037912	.064450	.053952	.027413	.026538	.022456	.026247	.004666	\$ 319
-.024497	-.058326	-.043161	-.002041	.031204	.028871	.013998	.000875	\$ 320
-.020122	-.031204	-.004374	.020122	.040245	-.019539	.005833	.010207	\$ 321
.026247	.025080	.015165	.006999	.004666	.003791	-.003208	-.009915	\$ 322
-.019539	-.015748	-.005833	.004083	.013998	.028288	.016915	-.013998	\$ 323
-.034704	-.027705	-.017498	-.006999	.009332	.011082	.004083	-.000292	\$ 324
-.002041	.001750	.002916	.006999	.003791	.001167	-.002333	-.007874	\$ 325
-.016040	-.024497	-.027122	-.017789	-.010499	-.000583	.009624	.010790	\$ 326
-.004083	-.013123	-.030038	-.022456	-.006707	.009041	.011957	.007582	\$ 327
.003791	.004374	-.017789	.021289	.021581	.022164	.021289	.020706	\$ 328
.016623	.011082	.006124	-.000583	-.009624	-.018664	-.019831	-.014873	\$ 329
-.015748	-.015748	-.016623	-.009624	.000000	.009624	.020414	.027997	\$ 330
.024789	.023330	.019831	.021872	.022456	.024789	.017789	.010790	\$ 331
.002041	-.000292	.001167	.001458	-.002916	-.008457	-.013415	-.020122	\$ 332
-.018956	-.012832	-.008166	-.002041	-.006707	-.009624	-.014873	-.017498	\$ 333
-.016331	-.015748	-.014582	-.019248	-.026538	-.033246	-.040828	-.040245	\$ 334
-.040828	-.035287	-.027997	-.021581	-.013415	-.009915	-.012248	-.013123	\$ 335
-.016040	-.018373	-.020997	-.023330	-.021289	-.015165	-.010790	-.007582	\$ 336
-.004083								\$ 337

1234567890123456789012345678901234567890123456789012345678901234567890123456789012345678901234567890

### Analysis Results File, "OUTPUT"

0 1 2 3 4 5 6 7 8 9 10 11  
12345678901234567890123456789012345678901234567890123456789012345678901234567890123456789012345678901234

Spread Footings, Penzien 11 model, soft soil, El Centro, high intensity

number of nodal points = 19  
 number of element types = 2  
 number of total elements = 19  
 number of time functions = 1  
 ground motion input code = 1  
 number of time steps (dt) = 800  
 dt multiplier for output = 2  
 damping factor alpha = 5.869E-01  
 damping factor beta = 4.260E-03

Inodal point data as input.....

0node	boundary condition codes			nodal point coordinates		
number	x	y	z	xx	yy	zz

12345678901234567890123456789012345678901234567890123456789012345678901234567890123456789012345678901234

0 1 2 3 4 5 6 7 8  
 12345678901234567890123456789012345678901234567890123456789012345678901234567890

.129775	.007874	-.203266	-.232138	-.073199	-.039370	.023039	-.033537	\$ 85
-.073199	-.097113	-.078449	-.087781	-.058326	-.019539	-.011082	.030621	\$ 86
.086323	.100321	.279090	.261884	.052202	-.105570	-.289880	-.235346	\$ 87
-.216973	-.157189	-.096238	-.037329	.009041	.043161	.148148	-.006416	\$ 88
-.142607	-.104404	-.201516	-.150481	-.108195	.025663	.184310	.245261	\$ 89
.372120	.404783	.347915	.219014	.065617	-.025663	-.066200	.021581	\$ 90
.052785	.158647	.116360	.013123	-.023914	-.053952	-.005833	.001750	\$ 91
-.034121	-.061242	-.088364	-.149315	-.212015	-.168854	-.077574	-.051910	\$ 92
.011665	.028580	.039953	.064450	.127442	.026538	-.159813	-.161855	\$ 93
-.070866	-.023622	.072908	.119568	.053077	-.007874	-.070866	-.004374	\$ 94
.072033	.140566	.228346	.181394	.096530	-.004083	-.056868	-.072033	\$ 95
-.061826	-.032079	.014582	.070283	-.009915	-.062992	-.137358	-.105862	\$ 96
-.056868	-.005249	.049577	-.023330	.001458	.067075	.109070	.175270	\$ 97
.150481	.125984	.100321	.147273	.190435	.199183	.050160	-.049577	\$ 98
-.153689	-.193642	-.112861	-.064742	-.009624	.034704	-.037329	-.102362	\$ 99
-.149898	-.097696	-.063575	-.003500	.041411	.020414	-.018373	-.034996	\$ 100
-.093905	-.100904	-.026538	.021289	.090114	.137649	.175853	.167979	\$ 101
.096238	-.021289	-.226597	-.177311	-.127734	-.060951	.009041	.102071	\$ 102
.085448	.035287	.098571	.092447	.074074	.060076	.057743	.050744	\$ 103
.006124	-.041995	-.100029	-.098863	-.042286	-.008166	.049577	-.022997	\$ 104
-.074366	-.081365	-.113153	-.070575	-.062700	-.053077	-.050744	-.011082	\$ 105
-.007874	-.053952	-.035871	.025372	.100029	.202683	.265383	.248761	\$ 106
.221639	.149606	.054243	.004374	-.055410	-.044036	-.021289	.006124	\$ 107
.037620	.062700	.006999	-.036162	-.095946	-.151356	-.206474	-.168854	\$ 108
-.134733	-.089530	-.042286	-.002625	-.052493	-.092738	-.135608	-.114027	\$ 109
-.100612	-.092155	-.126859	-.143190	-.138524	-.122485	-.105279	-.080782	\$ 110
-.075241	-.040537	-.019831	.147857	.210557	.256051	.228055	.223097	\$ 111
.128026	.023330	.003791	-.036745	-.004374	.008749	.030330	.030330	\$ 112
.056285	.059784	.021581	-.016331	-.020997	.020414	.030913	.042870	\$ 113
-.002625	-.046369	-.054535	-.002041	.045203	.030621	-.033537	-.088072	\$ 114
-.090114	-.027705	-.016915	.001167	.005833	.014582	.016623	.028288	\$ 115
.039078	.051619	.063575	.076115	.088072	.100904	.112569	.138233	\$ 116
.114611	.069408	.033537	-.023039	-.036162	.015748	.007874	-.072908	\$ 117
-.165063	-.183727	-.172353	-.120443	-.019831	.079323	.080782	-.006124	\$ 118
-.017498	-.032079	-.064450	-.121318	-.151356	-.064742	.008749	-.023039	\$ 119
.040537	.049869	.073782	.094197	.114027	.047827	-.039662	-.094197	\$ 120
-.084864	-.083698	-.088656	-.098863	-.071449	-.022164	.036454	.109653	\$ 121
-.117235	.071449	.045494	-.011665	-.044619	-.084281	-.092155	-.032371	\$ 122
.027413	.097696	.167979	.123651	.041703	-.002041	-.039370	-.078740	\$ 123
-.099446	-.104112	-.115486	-.117235	-.142316	-.139983	-.118402	-.118693	\$ 124
-.102362	-.054535	-.016623	.012832	-.005541	-.020997	-.049286	-.033537	\$ 125
.036745	.104404	.190726	.208807	.222222	.215515	.183144	.141149	\$ 126
.076990	-.012832	-.083990	-.111986	-.143482	-.124818	-.121318	-.080490	\$ 127
-.015165	.069116	.124234	.176145	.131817	.082823	.036745	-.015748	\$ 128
-.080198	-.123360	-.051035	.000292	.074074	.140274	.186935	.161563	\$ 129
.120443	.053660	-.013998	-.088364	-.154856	-.206474	-.270633	-.251677	\$ 130
-.184019	-.109653	.025372	.090114	.171770	.179061	.112278	.102362	\$ 131
.090697	.071741	.005541	-.057743	-.046078	-.004374	.028871	.083406	\$ 132
.118985	.164188	.154856	.091572	.048119	-.006999	-.055118	-.080490	\$ 133
-.108195	-.131234	-.155731	-.140857	-.110528	-.086323	-.057160	-.053660	\$ 134
-.046369	-.034704	-.015456	.000583	.017206	-.006707	-.032663	-.059784	\$ 135
-.093905	-.113153	-.099446	-.083698	-.095655	-.118693	-.142024	-.164188	\$ 136
-.187810	-.161855	-.130067	-.002333	.073782	.119860	.187810	.168854	\$ 137
-.138233	-.111986	.112278	.099154	.104112	.002333	-.074074	-.134150	\$ 138
-.137358	-.064742	-.018956	.047827	.103529	.146982	.108195	.081656	\$ 139
.046078	.011957	-.007874	.006124	.012832	.028871	.039370	.027413	\$ 140
.016915	.006416	-.009041	-.009041	.001167	-.007291	-.036162	-.068533	\$ 141
-.118402	-.154564	-.204433	-.094197	-.015165	.027413	.095655	.139399	\$ 142
.148440	.104404	.099738	.089239	.083115	.076699	.048994	-.001458	\$ 143
-.061826	-.106445	-.090405	-.086614	-.081656	-.069116	-.077574	-.089822	\$ 144
-.106737	-.104112	-.089822	-.056285	.005541	.057160	.046661	.037620	\$ 145
.040828	.032079	.031496	.026830	.025955	.005541	-.038204	-.072033	\$ 146
-.127151	-.125984	-.087489	-.055993	-.013998	.028288	.048994	.043161	\$ 147
.050452	.022747	-.016915	-.062700	-.068241	.017498	.076407	.078449	\$ 148
.024497	-.011957	-.066200	-.022164	.009041	.053077	.090405	.139691	\$ 149
.133858	.048411	-.016915	-.115486	-.129484	-.070283	-.029455	.063284	\$ 150
.076115	.035287	.002333	-.048994	-.111403	-.165063	-.227763	-.180519	\$ 151
-.074657	.012832	.132983	.228346	.321668	.277924	.142607	.055579	\$ 152
-.112861	-.246719	-.357539	-.251969	-.179644	-.066492	.043745	.139108	\$ 153
.094197	.072324	.027705	.066200	.098571	.147273	.173228	.151356	\$ 154
.160980	.173520	.179936	.172937	.135900	.046678	-.022456	-.067075	\$ 155
-.088364	-.095946	-.106153	-.142899	-.192476	-.210849	-.228638	-.246719	\$ 156

12345678901234567890123456789012345678901234567890123456789012345678901234567890



0 1 2 3 4 5 6 7 8  
 1234567890123456789012345678901234567890123456789012345678901234567890

-.165063	-.060951	.037329	-.111111	.142316	-.105862	.072908	.046078	\$ 157
-.109945	.173228	.183727	-.107903	.063284	.011665	.006707	-.018081	\$ 158
-.083406	-.110819	-.133275	-.147273	-.226597	-.183144	-.055118	.055118	\$ 159
.148440	.216973	.218431	.163896	.132692	.153106	.185185	.213182	\$ 160
.248177	.270341	.284339	.270924	.237387	.076990	-.084281	-.262759	\$ 161
-.397784	-.250510	-.136483	.023622	.173228	.240012	.162146	.087781	\$ 162
-.003208	-.110819	-.101196	-.005833	.052493	.184602	.295421	.327209	\$ 163
.322835	.274132	.234762	.177311	.148148	.060076	-.058618	-.166812	\$ 164
-.297754	-.388451	-.357247	-.351998	-.293380	-.222222	-.159813	-.142607	\$ 165
-.118110	-.084864	-.051327	-.041120	-.028580	-.014582	.005541	.023330	\$ 166
.010207	-.008457	-.017789	-.009915	-.003791	.022164	.059784	.095363	\$ 167
.131234	.169271	.163896	.135316	.087489	.031204	-.001167	-.009624	\$ 168
-.020122	-.029455	-.058618	-.054826	.007291	.039078	.070866	.077574	\$ 169
.077282	.045203	-.005541	-.027705	-.062992	-.048702	-.034996	-.018664	\$ 170
-.037620	-.047536	-.056285	-.070575	-.068825	-.051035	-.036162	-.053952	\$ 171
-.077282	-.094197	-.097988	-.132400	-.125401	-.097404	-.062117	-.020122	\$ 172
.008749	.000875	-.027122	-.025955	-.043745	-.047827	-.069408	-.094197	\$ 173
-.122776	-.133275	-.115777	-.101779	-.075241	-.050160	-.005833	.045494	\$ 174
.082823	.105570	.103237	.078449	.029455	-.013123	.036454	-.071449	\$ 175
-.066783	-.036745	-.019831	.005249	.027122	.058326	.083406	.106445	\$ 176
.090697	.052785	.006999	-.045494	-.093030	-.063867	-.034412	.004374	\$ 177
.044619	.086906	.070866	.039662	.029746	.006999	-.002916	-.006707	\$ 178
-.010499	-.013998	-.025955	-.045203	-.043161	-.022164	.000000	-.005833	\$ 179
-.043161	-.065617	-.109070	-.106445	-.073199	-.047827	-.004083	.044619	\$ 180
.088072	.114611	.118402	.112278	.095946	.053368	.036454	.020414	\$ 181
-.000292	-.019831	-.037912	-.037329	-.033537	-.029746	-.024497	-.041120	\$ 182
-.059784	-.078449	-.102071	-.104695	-.086614	-.066200	.005249	.028871	\$ 183
.059201	.074657	.058034	.046661	.031204	.045494	.057743	.070575	\$ 184
.041120	.016040	-.019248	-.028288	-.007582	.004666	.029163	.027413	\$ 185
.011374	.000000	-.019248	-.028871	-.031788	-.033537	-.038204	-.048994	\$ 186
-.058034	-.030330	-.002916	.016040	.037620	.058326	.058034	.049286	\$ 187
.041703	.031788	.037329	.044328	.039953	.034121	.028288	.017498	\$ 188
-.008166	-.014582	-.024497	-.051910	-.093613	-.122485	-.151064	-.137649	\$ 189
-.114902	-.084573	-.032079	.014582	.038495	.045786	.051619	.056868	\$ 190
.074366	.096530	.095655	.073491	.050452	.013123	-.024789	-.055410	\$ 191
-.066783	-.088656	-.080782	-.066200	-.050744	-.035287	-.036745	-.037620	\$ 192
-.023330	-.007582	.011374	.018956	.016040	.014582	.018664	.036745	\$ 193
.052202	.070866	.089530	.086906	.073199	.062992	.047536	.055993	\$ 194
.068241	.082240	.087781	.057160	.030913	-.011374	-.047536	-.093905	\$ 195
-.097696	-.063867	-.043161	-.002916	.003208	-.015456	-.029455	-.036745	\$ 196
-.041703	-.037620	-.030330	-.020706	-.005249	.009624	.024789	.046078	\$ 197
.069700	.093030	.099446	.092738	.062117	.021289	.002625	-.004374	\$ 198
-.013707	-.021872	-.035287	-.045494	-.033829	-.016331	-.001750	-.000875	\$ 199
-.000875	.004083	.013415	.020997	.025080	.028580	.036162	.042870	\$ 200
.050160	.058326	.074657	.092447	.083698	.067367	.030621	-.000292	\$ 201
-.003208	-.010499	-.015456	-.024205	-.015165	-.002041	.010790	.027997	\$ 202
.045203	.059784	.041703	.021289	.006124	-.006416	-.020414	-.029163	\$ 203
-.021872	-.015748	-.008457	-.004374	.000000	-.000292	-.001750	-.003208	\$ 204
-.002916	-.000875	.000292	.004666	.015456	.025080	.036745	.044911	\$ 205
.038204	.029746	.016331	.001750	-.011665	-.028580	-.027997	-.013415	\$ 206
-.002041	.009041	.013123	.019831	.015165	.013123	.005249	-.000583	\$ 207
-.008457	-.008166	-.004958	-.001750	-.001458	-.004958	-.006416	-.010499	\$ 208
-.009332	-.002041	.004083	.011957	.018956	.018373	.015165	.001750	\$ 209
-.013123	-.022164	-.018664	-.018956	-.031204	-.046952	-.050744	-.034121	\$ 210
-.020414	-.010499	-.007291	-.000583	.001167	.010499	.023914	.033537	\$ 211
.020414	.011082	-.002916	-.007291	-.009915	-.011957	-.013123	-.018956	\$ 212
-.034996	-.034121	-.031496	-.028580	-.023622	-.022164	-.032079	-.040245	\$ 213
-.048411	-.041995	-.037912	-.032371	-.031496	-.028580	-.028580	-.018373	\$ 214
-.000583	.015748	.032079	.044328	.057451	.049577	.040828	.030038	\$ 215
.018664	.002916	-.019539	-.030621	-.035579	-.040245	-.048411	-.062700	\$ 216
-.078449	-.079907	-.063284	-.051910	-.033829	-.017789	.000000	.015748	\$ 217
.028871	.041995	.054535	.067658	.076407	.074366	.066200	.049869	\$ 218
.037037	.015748	-.013707	-.043453	-.061242	-.074074	-.073491	-.071449	\$ 219
-.065908	-.052202	-.039662	-.023914	-.004083	.012832	.025955	.028288	\$ 220
.029163	.029163	.030330	.039662	.035287	.029163	.020997	.005541	\$ 221
-.008166	-.024205	-.038204	-.055410	-.056576	-.040537	-.029163	-.012832	\$ 222
-.012832	-.011665	-.013123	-.014290	-.011374	-.006124	-.006416	-.004666	\$ 223
-.004666	-.003500	-.003500	.008166	.019831	.033537	.027997	.016331	\$ 224
.004958	-.009041	-.022747	-.026830	-.026830	-.027705	-.026830	-.025080	\$ 225
-.015165	-.006416	.004083	.011082	.009915	.009915	.008457	.011665	\$ 226
.015748	.019539	.024789	.025372	.022456	.020414	.017789	.021872	\$ 227
.025372	.029746	.032371	.026247	.021872	.015456	.018081	.023039	\$ 228

1234567890123456789012345678901234567890123456789012345678901234567890  
 0 1 2 3 4 5 6 7 8

0 1 2 3 4 5 6 7 8  
 12345678901234567890123456789012345678901234567890123456789012345678901234567890

.028288	.034412	.039370	.030621	.022456	.012852	.003500	-.006124	\$ 229
-.012248	-.019831	-.025372	-.034996	-.046369	-.057743	-.067850	-.075241	\$ 230
-.078740	-.081073	-.083698	-.081073	-.078740	-.075241	-.073199	-.063867	\$ 231
-.050452	-.037620	-.031788	-.030621	-.027705	-.026536	-.020997	-.017206	\$ 232
-.011665	-.006707	.005249	.010207	.012248	.013998	.012540	.012540	\$ 233
.011082	.010499	.009332	.013707	.018373	.024789	.032079	.039078	\$ 234
.046661	.052785	.050452	.048994	.046369	.042870	.031496	.019831	\$ 235
.009332	.002625	.005541	.008166	.011665	.015748	.020122	.027705	\$ 236
.034121	.041703	.041703	.036454	.035579	.036162	.036745	.037912	\$ 237
.038787	.030913	.023039	.013415	.005833	.001458	-.003208	-.007291	\$ 238
-.003208	.005249	.012540	.022164	.030038	.038787	.029455	.018081	\$ 239
.005249	-.007874	-.023330	-.025955	-.015748	-.008749	.001750	.003500	\$ 240
.006416	.007874	.009332	.013998	.020122	.025955	.032663	.038787	\$ 241
.040828	.039953	.040828	.039370	.040537	.029746	.008749	-.009332	\$ 242
-.018373	-.024789	-.032663	-.045786	-.057451	-.054826	-.053077	-.049577	\$ 243
-.045494	-.041411	-.037620	-.036454	-.034996	-.033829	-.033246	-.030913	\$ 244
-.018664	-.006124	.000583	-.001167	-.001167	-.004083	-.005541	-.002333	\$ 245
-.003208	.007874	.014582	.015456	.012248	.008749	.003208	.001458	\$ 246
-.006999	-.005833	-.002041	.001167	.005541	.009624	.013998	.016040	\$ 247
.018956	.021581	.023622	.026538	.037037	.049286	.041995	.030621	\$ 248
.020414	.010207	.000583	-.009332	-.018664	-.027705	-.026538	-.024205	\$ 249
-.021289	-.014873	-.008749	-.001167	.009624	.015165	.012832	.011665	\$ 250
.008749	.005833	.002916	.000292	-.002916	-.004083	.000583	.004666	\$ 251
.008749	.006707	.004666	.004666	.007582	.009332	.013123	.013415	\$ 252
.006124	-.000875	-.008749	-.017498	-.025372	-.033829	-.031204	-.027413	\$ 253
-.022747	-.019831	-.018373	-.016623	-.014582	-.011957	-.009624	-.006999	\$ 254
-.004083	-.001458	.001167	.003791	.006124	.000292	.005249	.011665	\$ 255
-.018664	-.025372	-.032079	-.037620	-.044036	-.048119	-.050744	-.053660	\$ 256
-.056576	-.058909	-.062117	-.057743	-.050452	-.039370	-.018956	-.004083	\$ 257
.005833	.016040	.023914	.025955	.029746	.027122	.023330	.017789	\$ 258
.009624	.000875	-.006999	-.016623	-.013123	-.003791	.003791	.009624	\$ 259
.013998	.015748	.016915	.018081	.018956	.020122	.020997	.021872	\$ 260
.022456	.021289	.020122	.018664	.016915	.015748	.013998	.017789	\$ 261
.023039	.027997	.033246	.036745	.040537	.038204	.035871	.033246	\$ 262
.030038	.025372	.020997	.016331	.011665	.006999	.002041	.001167	\$ 263
.002333	.002625	.006707	.012248	.015165	.017789	.020997	.023039	\$ 264
.025955	.027705	.027705	.027122	.025955	.007291	.000000	-.001458	\$ 265
-.005833	-.006999	-.009624	-.013998	-.018664	-.023330	-.028288	-.033246	\$ 266
-.037329	-.030913	-.025955	-.019248	-.012540	-.005541	-.003208	-.002625	\$ 267
-.001458	-.001167	.001458	.004083	.006999	.010207	.012540	.012832	\$ 268
.011374	.003791	-.002333	-.010499	-.013707	-.016040	-.018081	-.019831	\$ 269
-.021289	-.023330	-.021872	-.018664	-.008166	.001458	.017415	.018956	\$ 270
.017498	.017498	.015748	.014290	.012832	.011374	.008457	.000000	\$ 271
-.007582	-.015165	-.012248	-.010790	-.007291	-.004374	-.000583	.000583	\$ 272
.000000	-.000292	-.001167	-.002041	-.001750	-.000292	.000875	.002041	\$ 273
-.000292	-.002041	-.004374	-.006999	-.008457	-.008166	-.008166	-.007291	\$ 274
-.006999	-.006124	-.007874	-.012832	-.016915	-.022164	-.024497	-.023914	\$ 275
-.024205	-.021872	-.014582	-.008166	-.000583	.005249	.005249	.006124	\$ 276
.006124	.006124	.009041	.012540	.014290	.014290	.014290	.013998	\$ 277
.013707	.015165	.019539	.023039	.027705	.028288	.027997	.027997	\$ 278
.027122	.026538	.025955	.025372	.024497	.023914	.023330	.022456	\$ 279
.018081	.013707	.010207	.010499	.009915	.010207	.010499	.009332	\$ 280
.005541	.004374	.004083	.003500	.003500	.003208	.000000	-.002916	\$ 281
-.005833	-.007291	-.008457	-.009624	-.010790	-.013998	-.018373	-.022456	\$ 282
-.026830	-.031204	-.035579	-.040245	-.041703	-.034996	-.030038	-.022747	\$ 283
-.019539	-.018373	-.016915	-.016331	-.015456	-.014582	-.013998	-.013123	\$ 284
-.012248	-.011374	-.009041	-.007582	-.003208	.002916	.009041	.013415	\$ 285
.013998	.015748	.016040	.018373	.024497	.029455	.024497	.020706	\$ 286
.015456	.009624	.008166	.008457	.008166	.007874	.003500	-.000292	\$ 287
-.002916	-.003208	-.004666	-.004374	-.009041	-.019831	-.028871	-.029746	\$ 288
-.030621	-.030913	-.028871	-.025955	-.023039	-.021581	-.020997	-.019831	\$ 289
-.019539	-.018373	-.011665	-.003791	.003791	.012540	.020706	.028871	\$ 290
.025080	.018373	.011957	.003791	-.004083	-.010207	-.010790	-.012832	\$ 291
-.013415	-.014290	-.014873	-.015748	-.016331	-.016915	-.013415	-.008457	\$ 292
-.003791	.002041	.004958	.005541	.007291	.007291	.010207	.014582	\$ 293
-.018664	.023330	.027413	.028288	.029746	.030621	.031496	.032079	\$ 294
.030330	.028871	.027122	.025080	.023039	.020997	.018373	.016040	\$ 295
.013415	.011082	.009041	.007874	.006124	.004958	.003500	.002041	\$ 296
.000875	.002333	.003791	.005541	.006416	.002625	-.000875	-.004958	\$ 297
-.009041	-.013707	-.015456	-.013998	-.012540	-.011082	-.007291	-.002625	\$ 298
.002041	.004958	.006416	.010207	.017789	.024205	.032663	.031204	\$ 299
.025372	.020706	.013707	.007874	.001167	-.004666	-.006999	-.009624	\$ 300

12345678901234567890123456789012345678901234567890123456789012345678901234567890  
 0 1 2 3 4 5 6 7 8



```

0      1      2      3      4      5      6      7      8      9      10     11
12345678901234567890123456789012345678901234567890123456789012345678901234
-----
 1  1  1  1  1  1  1  1  1  .000  .000  .000  0
 2  1  1  1  1  1  1  1  1  288.000 .000 .000  0
 3  0  1  0  1  0  1  0  1  .000 .000 .000  0
 4  0  1  0  1  0  1  0  1  288.000 .000 .000  0
 5  0  1  0  1  0  1  0  1  .000 .000 .000  0
 6  0  1  0  1  0  1  0  1  288.000 .000 .000  0
 7  0  1  0  1  0  1  0  1  .000 .000 .000  0
 8  0  1  0  1  0  1  0  1  288.000 .000 .000  0
 9  0  1  0  1  0  1  0  1  .000 .000 36.000  0
10  0  1  0  1  0  1  0  1  288.000 .000 36.000  0
11  0  1  0  1  0  1  0  1  .000 .000 264.000  0
12  0  1  0  1  0  1  0  1  288.000 .000 264.000  0
13  0  1  0  1  0  1  0  1  .000 .000 300.000  0
14  0  1  0  1  0  1  0  1  288.000 .000 300.000  0
15  0  1  0  1  0  1  0  1  -92.000 .000 300.000  0
16  0  1  0  1  0  1  0  1  380.000 .000 300.000  0
17  1  1  1  1  1  1  1  1 .000 .000 600.000  0
18  1  1  1  1  1  1  1  1 288.000 .000 600.000  0
19  1  1  1  1  1  1  1  1 576.000 .000 600.000  0
incomplete nodal point data.....

```

```

Node boundary condition codes nodal point coordinates
number x y z xx yy zz x y z
 1  1  1  1  1  1  1  1  1  .000 .000 .000
 2  1  1  1  1  1  1  1  1  288.000 .000 .000
 3  0  1  0  1  0  1  0  1  .000 .000 .000
 4  0  1  0  1  0  1  0  1  288.000 .000 .000
 5  0  1  0  1  0  1  0  1  .000 .000 .000
 6  0  1  0  1  0  1  0  1  288.000 .000 .000
 7  0  1  0  1  0  1  0  1  .000 .000 .000
 8  0  1  0  1  0  1  0  1  288.000 .000 .000
 9  0  1  0  1  0  1  0  1  .000 .000 36.000
10  0  1  0  1  0  1  0  1  288.000 .000 36.000
11  0  1  0  1  0  1  0  1  .000 .000 264.000
12  0  1  0  1  0  1  0  1  288.000 .000 264.000
13  0  1  0  1  0  1  0  1  .000 .000 300.000
14  0  1  0  1  0  1  0  1  288.000 .000 300.000
15  0  1  0  1  0  1  0  1  -92.000 .000 300.000
16  0  1  0  1  0  1  0  1  380.000 .000 300.000
17  1  1  1  1  1  1  1  1 .000 .000 600.000
18  1  1  1  1  1  1  1  1 288.000 .000 600.000
19  1  1  1  1  1  1  1  1 576.000 .000 600.000
equation number of nodal degrees of freedom....

```

```

Node equation number node equation number
number x y z xx yy zz number x y z xx yy zz
 1  0  0  0  0  0  0  2  0  0  0  0  0  0
 3  1  0  2  0  3  0  4  4  0  5  0  6  0
 5  7  0  8  0  9  0  6  10 0 11 0 12 0
 7  13 0 14 0 15 0 8 16 0 17 0 18 0
 9  19 0 20 0 21 0 10 22 0 23 0 24 0
11  25 0 26 0 27 0 12 28 0 29 0 30 0
13  31 0 32 0 33 0 14 34 0 35 0 36 0
15  37 0 38 0 39 0 16 40 0 41 0 42 0
17  0  0  0  0  0  0  18  0  0  0  0  0  0
19  0  0  0  0  0  0
1.....three dimensional beam elements

```

```

number of beams = 9
number of geometric property sets = 2
number of fixed end force sets = 0
number of materials = 2
number of beam n/l property sets = 1
material properties....

```

```

material young's poisson's mass
number modulus ratio density
 1  4600. .18000 .00000
 2  460000. .18000 .00000

```

```

beam geometric properties....
element area area area inertia inertia inertia
type x y z x y z x y z
 1  1076.000 968.000 968.000 82400.000 41200.000 41200.000
 2  2590.000 96800.000 96800.000 8240000.000 4120000.000 4120000.000

```

```

element load multipliers....
a b c d
x-dir .000000E+00 .000000E+00 .000000E+00 .000000E+00
y-dir .000000E+00 .000000E+00 .000000E+00 .000000E+00
z-dir -.386040E+03 .000000E+00 .000000E+00 .000000E+00

```

```

123456789012345678901234567890123456789012345678901234567890123456789012345678901234
0      1      2      3      4      5      6      7      8      9      10     11

```

0 1 2 3 4 5 6 7 8 9 10 11  
 123456789012345678901234567890123456789012345678901234567890123456789012345678901234

1 beam element nonlinear parameters

npar no	axial pu	moment mu/y	moment mu/z	axial tu	a0	a1	yield a2	function a3	constants b0	b1	b2
1	.488E+04	.900E+04	.900E+04	.123E+00	1.000	-6.973	-9.442	-1.469	1.000	-6.973	-9.442

-1.469  
 lbeam element data.....

lbeam no	nodes i	nodes j	matl k	geom no	elem a	loads b	loads c	loads d	end i	codes j	l/nl ind
1	7	9	18	1	0	0	0	0	0	0	1
2	9	11	18	1	0	0	0	0	0	0	1
3	11	13	18	1	0	0	0	0	0	0	1
4	8	10	19	1	0	0	0	0	0	0	1
5	10	12	19	1	0	0	0	0	0	0	1
6	12	14	19	1	0	0	0	0	0	0	1
7	13	14	19	2	0	0	0	0	0	0	0
8	15	13	19	2	0	0	0	0	0	0	0
9	14	16	19	2	0	0	0	0	0	0	0

.....DF elements (Type 6)  
 number of DF elements: 10  
 number of element property sets: 5

STIFFNESS PARAMETER DATA

np dof	rke1	fyi	rkp1	rkg1	rkg2	sd	rik	rhop	r1z
1 1	.139E+04	.100E+11	.000E+00	.000E+00	.000E+00	.000	.000	.000	.000
1 2	.170E+04	.100E+11	.000E+00	.000E+00	.000E+00	.000	.000	.000	.000
1 3	.170E+04	.100E+11	.000E+00	.000E+00	.000E+00	.000	.000	.000	.000
1 4	.946E+07	.100E+11	.000E+00	.000E+00	.000E+00	.000	.000	.000	.000
1 5	.507E+07	.100E+11	.000E+00	.000E+00	.000E+00	.000	.000	.000	.000
1 6	.507E+07	.100E+11	.000E+00	.000E+00	.000E+00	.000	.000	.000	.000
2 1	.109E+04	.100E+11	.000E+00	.000E+00	.000E+00	.000	.000	.000	.000
2 2	.591E+03	.100E+11	.000E+00	.000E+00	.000E+00	.000	.000	.000	.000
2 3	.591E+03	.100E+11	.000E+00	.000E+00	.000E+00	.000	.000	.000	.000
2 4	.221E+07	.100E+11	.000E+00	.000E+00	.000E+00	.000	.000	.000	.000
2 5	.131E+07	.100E+11	.000E+00	.000E+00	.000E+00	.000	.000	.000	.000
2 6	.131E+07	.100E+11	.000E+00	.000E+00	.000E+00	.000	.000	.000	.000
3 1	.178E+04	.100E+11	.000E+00	.000E+00	.000E+00	.000	.000	.000	.000
3 2	.180E+04	.100E+11	.000E+00	.000E+00	.000E+00	.000	.000	.000	.000
3 3	.180E+04	.100E+11	.000E+00	.000E+00	.000E+00	.000	.000	.000	.000
3 4	.665E+07	.100E+11	.000E+00	.000E+00	.000E+00	.000	.000	.000	.000
3 5	.326E+07	.100E+11	.000E+00	.000E+00	.000E+00	.000	.000	.000	.000
3 6	.326E+07	.100E+11	.000E+00	.000E+00	.000E+00	.000	.000	.000	.000
4 1	.450E+03	.100E+11	.000E+00	.000E+00	.000E+00	.000	.000	.000	.000
4 2	.572E+03	.100E+11	.000E+00	.000E+00	.000E+00	.000	.000	.000	.000
4 3	.572E+03	.100E+11	.000E+00	.000E+00	.000E+00	.000	.000	.000	.000
4 4	.738E+07	.100E+11	.000E+00	.000E+00	.000E+00	.000	.000	.000	.000
4 5	.455E+07	.100E+11	.000E+00	.000E+00	.000E+00	.000	.000	.000	.000
4 6	.455E+07	.100E+11	.000E+00	.000E+00	.000E+00	.000	.000	.000	.000
5 1	.000E+00	.100E+11	.000E+00	.000E+00	.000E+00	.000	.000	.000	.000
5 2	.000E+00	.100E+11	.000E+00	.000E+00	.000E+00	.000	.000	.000	.000
5 3	.000E+00	.100E+11	.000E+00	.000E+00	.000E+00	.000	.000	.000	.000
5 4	.000E+00	.100E+11	.000E+00	.000E+00	.000E+00	.000	.000	.000	.000
5 5	.000E+00	.100E+11	.000E+00	.000E+00	.000E+00	.000	.000	.000	.000
5 6	.000E+00	.100E+11	.000E+00	.000E+00	.000E+00	.000	.000	.000	.000

DAMPING PARAMETER DATA

np dof	c
1 1	.3143E+02
1 2	.3602E+02
1 3	.3602E+02
1 4	.1198E+06
1 5	.6441E+05
1 6	.6441E+05
2 1	.1367E+02
2 2	.1311E+02
2 3	.1311E+02
2 4	-.3232E+05
2 5	-.1679E+05
2 6	-.1679E+05
3 1	.2448E+02
3 2	.2476E+02
3 3	.2476E+02
3 4	.7672E+04
3 5	.3164E+04
3 6	.3164E+04
4 1	.7306E+01
4 2	.1983E+01
4 3	.1983E+01
4 4	.6568E+05
4 5	.3997E+05
4 6	.3997E+05
5 1	.2796E+02
5 2	.3039E+02
5 3	.3039E+02
5 4	.6375E+05
5 5	.3379E+05

12345678901234567890123456789012345678901234567890123456789012345678901234567890123456789012345678901234

0 1 2 3 4 5 6 7 8 9 10 11  
1234567890123456789012345678901234567890123456789012345678901234

5 6 .3379E+05

MASS PARAMETER DATA

np	dof	mi	mj
1	1	.0000E+00	.0000E+00
1	2	.0000E+00	.0000E+00
1	3	.0000E+00	.0000E+00
1	4	.0000E+00	.0000E+00
1	5	.0000E+00	.0000E+00
1	6	.0000E+00	.0000E+00
2	1	.0000E+00	.0000E+00
2	2	.0000E+00	.0000E+00
2	3	.0000E+00	.0000E+00
2	4	.0000E+00	.0000E+00
2	5	.0000E+00	.0000E+00
2	6	.0000E+00	.0000E+00
3	1	.0000E+00	.0000E+00
3	2	.0000E+00	.0000E+00
3	3	.0000E+00	.0000E+00
3	4	.0000E+00	.0000E+00
3	5	.0000E+00	.0000E+00
3	6	.0000E+00	.0000E+00
4	1	.0000E+00	.0000E+00
4	2	.0000E+00	.0000E+00
4	3	.0000E+00	.0000E+00
4	4	.0000E+00	.0000E+00
4	5	.0000E+00	.0000E+00
4	6	.0000E+00	.0000E+00
5	1	.2537E+00	.3931E+00
5	2	.2975E+00	.5269E-01
5	3	.2975E+00	.5269E-01
5	4	.7909E+03	.2421E+04
5	5	.3924E+03	.1228E+04
5	6	.3924E+03	.1228E+04

ELEMENT LOAD FACTORS

Load Case:	a	b	c	d
Global X-dir:	.000000E+00	.000000E+00	.000000E+00	.000000E+00
Global Y-dir:	.000000E+00	.000000E+00	.000000E+00	.000000E+00
Global Z-dir:	-.386040E+03	.000000E+00	.000000E+00	.000000E+00

ELEMENT DATA

1	1	5	17	18	1	0	0	0	0	0
2	5	7	17	18	2	0	0	0	0	0
3	1	3	17	18	3	0	0	0	0	0
4	3	7	17	18	4	0	0	0	0	0
5	3	5	17	18	5	0	0	0	0	0
6	2	6	18	19	1	0	0	0	0	0
7	6	8	18	19	2	0	0	0	0	0
8	2	4	18	19	3	0	0	0	0	0
9	4	8	18	19	4	0	0	0	0	0
10	4	6	18	19	5	0	0	0	0	0

total number of nonlinear elements = 16

element type of 1/nl indicator.....

element number	ind type	element number	ind type	element number	ind type	element number	ind type	element number	ind type
1	2	2	2	3	2	4	2	5	2
6	2	7	-2	8	-2	9	-2	10	6
11	6	12	6	13	6	14	6	15	6
16	6	17	6	18	6	19	6		

system setup information...

total number of equations = 42

band width = 15

element load multiplier for static analysis.....

structure load case	element load multiplier a	b	c	d
1	1.000	.000	.000	.000

iprint of static displacements.....

1234567890123456789012345678901234567890123456789012345678901234  
0 1 2 3 4 5 6 7 8 9 10 11

0 1 2 3 4 5 6 7 8 9 10 11  
 12345678901234567890123456789012345678901234567890123456789012345678901234

node no.	node type	x	y	z	xx	yy	zz
1	fixe	0.000E+00	0.000E+00	0.000E+00	0.000E+00	0.000E+00	0.000E+00
2	fixe	0.000E+00	0.000E+00	0.000E+00	0.000E+00	0.000E+00	0.000E+00
3		-5.929E-07	0.000E+00	-4.908E-02	0.000E+00	-1.364E-07	0.000E+00
4		4.296E-07	0.000E+00	-4.903E-02	0.000E+00	-8.799E-08	0.000E+00
5		-6.344E-07	0.000E+00	-1.068E-01	0.000E+00	-4.798E-08	0.000E+00
6		4.597E-07	0.000E+00	-1.066E-01	0.000E+00	-3.094E-08	0.000E+00
7		-2.459E-06	0.000E+00	-2.429E-01	0.000E+00	-2.342E-07	0.000E+00
8		1.781E-06	0.000E+00	-2.427E-01	0.000E+00	-1.511E-07	0.000E+00
9		-1.320E-05	0.000E+00	-2.446E-01	0.000E+00	-3.577E-07	0.000E+00
10		-5.210E-06	0.000E+00	-2.444E-01	0.000E+00	-2.407E-07	0.000E+00
11		-1.565E-04	0.000E+00	-2.555E-01	0.000E+00	-7.990E-07	0.000E+00
12		-1.447E-04	0.000E+00	-2.552E-01	0.000E+00	-1.055E-06	0.000E+00
13		-1.856E-04	0.000E+00	-2.572E-01	0.000E+00	-8.150E-07	0.000E+00
14		-1.856E-04	0.000E+00	-2.569E-01	0.000E+00	-1.223E-06	0.000E+00
15		-1.856E-04	0.000E+00	-2.573E-01	0.000E+00	-8.827E-07	0.000E+00
16		-1.856E-04	0.000E+00	-2.568E-01	0.000E+00	-1.155E-06	0.000E+00
17	fixe	0.000E+00	0.000E+00	0.000E+00	0.000E+00	0.000E+00	0.000E+00
18	fixe	0.000E+00	0.000E+00	0.000E+00	0.000E+00	0.000E+00	0.000E+00
19	fixe	0.000E+00	0.000E+00	0.000E+00	0.000E+00	0.000E+00	0.000E+00

1 static stress output.....  
 0 ....straight beam forces and moments

beam no.	load no.	axial r1	shear r2	shear r3	torsion m1	bending m2	bending m3
1	1	2.359E+02	2.145E-03	0.000E+00	0.000E+00	0.000E+00	6.886E-01
		-2.359E+02	-2.145E-03	0.000E+00	0.000E+00	0.000E+00	-6.114E-01
2	1	2.359E+02	2.145E-03	0.000E+00	0.000E+00	0.000E+00	6.114E-01
		-2.359E+02	-2.145E-03	0.000E+00	0.000E+00	0.000E+00	-1.224E-01
3	1	2.359E+02	2.144E-03	0.000E+00	0.000E+00	0.000E+00	1.224E-01
		-2.359E+02	-2.144E-03	0.000E+00	0.000E+00	0.000E+00	-4.518E-02
4	1	2.356E+02	-1.554E-03	0.000E+00	0.000E+00	0.000E+00	4.441E-01
		-2.356E+02	1.554E-03	0.000E+00	0.000E+00	0.000E+00	-5.000E-01
5	1	2.356E+02	-1.554E-03	0.000E+00	0.000E+00	0.000E+00	5.000E-01
		-2.356E+02	1.554E-03	0.000E+00	0.000E+00	0.000E+00	-8.543E-01
6	1	2.356E+02	-1.554E-03	0.000E+00	0.000E+00	0.000E+00	8.543E-01
		-2.356E+02	1.554E-03	0.000E+00	0.000E+00	0.000E+00	-9.103E-01
7	1	1.770E-03	1.439E+02	0.000E+00	0.000E+00	0.000E+00	4.219E+03
		-1.770E-03	1.440E+02	0.000E+00	0.000E+00	0.000E+00	-4.233E+03
8	1	0.000E+00	-1.053E-01	0.000E+00	0.000E+00	0.000E+00	-2.999E+01
		0.000E+00	9.211E+01	0.000E+00	0.000E+00	0.000E+00	-4.214E+03
9	1	0.000E+00	9.239E+01	0.000E+00	0.000E+00	0.000E+00	4.245E+03
		0.000E+00	-3.872E-01	0.000E+00	0.000E+00	0.000E+00	8.852E+00

1 static stress output.....  
 ....ssi element forces and moments

beam no.	load no.	axial r1	shear r2	shear r3	torsion m1	bending m2	bending m3
1	1	1.487E+02	1.078E-03	0.000E+00	0.000E+00	0.000E+00	2.433E-01
		-1.487E+02	-1.078E-03	0.000E+00	0.000E+00	0.000E+00	-2.433E-01
2	1	1.487E+02	1.078E-03	0.000E+00	0.000E+00	0.000E+00	2.433E-01
		-1.487E+02	-1.078E-03	0.000E+00	0.000E+00	0.000E+00	-2.433E-01
3	1	8.726E+01	1.066E-03	0.000E+00	0.000E+00	0.000E+00	4.452E-01
		-8.726E+01	-1.066E-03	0.000E+00	0.000E+00	0.000E+00	-4.452E-01
4	1	8.726E+01	1.066E-03	0.000E+00	0.000E+00	0.000E+00	4.452E-01
		-8.726E+01	-1.066E-03	0.000E+00	0.000E+00	0.000E+00	-4.452E-01
5	1	0.000E+00	0.000E+00	0.000E+00	0.000E+00	0.000E+00	0.000E+00
		0.000E+00	0.000E+00	0.000E+00	0.000E+00	0.000E+00	0.000E+00
6	1	1.485E+02	-7.813E-04	0.000E+00	0.000E+00	0.000E+00	1.569E-01
		-1.485E+02	7.813E-04	0.000E+00	0.000E+00	0.000E+00	-1.569E-01
7	1	1.485E+02	-7.813E-04	0.000E+00	0.000E+00	0.000E+00	1.569E-01
		-1.485E+02	7.813E-04	0.000E+00	0.000E+00	0.000E+00	-1.569E-01
8	1	8.716E+01	-7.726E-04	0.000E+00	0.000E+00	0.000E+00	2.872E-01
		-8.716E+01	7.726E-04	0.000E+00	0.000E+00	0.000E+00	-2.872E-01
9	1	8.716E+01	-7.726E-04	0.000E+00	0.000E+00	0.000E+00	2.872E-01
		-8.716E+01	7.726E-04	0.000E+00	0.000E+00	0.000E+00	-2.872E-01
10	1	0.000E+00	0.000E+00	0.000E+00	0.000E+00	0.000E+00	0.000E+00
		0.000E+00	0.000E+00	0.000E+00	0.000E+00	0.000E+00	0.000E+00

1dynamic load input control data.....

time increment dt (sec) = .020

123456789012345678901234567890123456789012345678901234567890123456789012345678901234  
 0 1 2 3 4 5 6 7 8 9 10 11

```

0           1           2           3           4           5           6           7           8           9           10          11
12345678901234567890123456789012345678901234567890123456789012345678901234567890123456789012345678901234

```

```

total number of time steps = 800
output interval           = 2
number of time functions  = 1

```

step-by-step dynamic analysis control data.....

```

integration indicator      = 0
damping factor alpha      = 5.869E-01
damping factor beta       = 4.260E-03
subdivision of time increment control data .....

```

```

number of subdivision     = 5
relative tolerance of subdivision = .5000000E-01
equilibrium iteration control data .....

```

```

maximum number of iteration = 10
type of iteration          = 1
relative tolerance to use iteration = .1000000E-01
relative tolerance for convergence = .5000000E-02
ground motion input key.....

```

```

                    direction
                    x      y      z
function number...  1      0      0
scale factor.....  1.434  .000  .000
time history no.  1..... 940  per1  Val y Eq  El  ntro  00E  c: E = 0 79g

```

```

number of data point      = 2689
scaling factor            = 135.0000
time increment of data (sec) = .020000
zero correction           = .0000

```

1	.000	-5.51	-4.252	-3.976	-3.465	-3.740	-4.724	-5.590
2	-5.039	-4.331	-3.347	-3.347	-5.158	-6.929	-7.638	-6.378
3	-5.669	-4.252	-3.228	-1.653	-2.598	-5.158	-7.480	-7.717
4	-2.598	1.181	5.551	-1.929	-5.039	-5.669	-7.992	-10.236
5	-12.795	-12.047	-6.772	-7.756	-6.417	-6.457	-2.638	.984
6	5.906	9.291	9.921	13.228	18.228	19.370	16.496	14.134
7	10.669	9.252	13.347	16.221	20.866	25.158	28.819	25.669
8	23.583	15.748	15.748	2.480	-20.276	-30.984	-23.740	-19.055
9	-9.843	-2.323	5.276	12.126	19.646	27.953	39.173	47.992
10	60.197	57.047	45.472	36.811	35.118	36.457	33.032	35.472
11	39.095	47.598	12.913	-58.071	-81.339	-78.307	-80.079	-71.496
12	-67.913	-68.976	-69.016	-71.063	-64.173	-53.032	-42.795	-30.787
13	-16.890	-.669	14.173	30.906	45.827	62.913	77.165	94.961
14	107.441	119.528	125.984	134.527	111.063	91.496	-47.165	-93.425
15	-64.567	-73.425	-43.110	-29.646	-6.811	4.449	20.984	35.236
16	46.693	69.173	22.677	-103.583	-60.906	-68.071	-39.843	-22.795
17	9.331	-26.378	-77.953	-64.606	-66.339	-58.307	-48.465	-39.409
18	-29.567	-20.591	-10.669	-1.732	7.402	-3.740	-17.047	-32.992
19	-37.441	-28.189	-23.583	-13.150	-4.252	7.284	16.535	26.496
20	-3.819	-14.646	-1.575	.433	13.543	22.244	34.764	44.488
21	53.661	8.622	9.488	26.890	27.126	51.890	53.268	80.315
22	-36.654	-51.496	-27.244	-21.496	2.835	26.575	-42.008	-58.583
23	-42.165	-45.748	-30.000	-22.008	-8.465	-4.961	-26.535	-12.756
24	-13.268	-4.291	.669	11.772	19.213	23.937	8.740	-1.260
25	-9.646	3.032	8.307	22.362	32.520	47.480	58.189	68.386
26	16.575	1.142	10.197	11.535	-2.165	-5.787	5.630	8.110
27	19.646	25.394	37.677	44.409	56.969	64.134	76.575	73.071
28	78.110	69.646	49.213	-47.520	-21.339	-15.118	-12.244	-44.016
29	-65.394	-97.008	-79.724	-72.244	-51.850	-37.795	-12.795	6.063
30	32.126	51.929	71.575	-2.284	-6.654	11.221	17.598	38.701
31	56.063	72.953	96.693	66.339	-54.331	-39.331	-42.874	-35.709
32	-18.465	-49.213	-83.110	-63.661	-66.614	-51.417	-43.740	-30.433
33	-20.079	-21.417	-47.244	-47.598	-45.591	-45.079	-28.228	-21.496
34	2.520	-31.654	-64.331	-33.819	-37.835	-15.591	-5.787	12.559
35	25.512	34.488	18.583	7.795	-1.063	11.496	17.520	30.906
36	40.669	53.228	63.228	73.268	50.433	25.197	8.032	12.362
37	14.685	19.528	9.252	-3.307	-6.614	-4.449	-5.016	-9.764
38	-6.181	-2.716	5.787	14.921	22.795	10.039	-1.614	-16.850
39	-5.236	3.740	9.055	-5.079	-1.969	3.150	6.268	14.961
40	20.079	6.181	-1.260	-4.370	.197	2.992	1.378	-3.740
41	-1.417	-.630	1.496	3.347	-2.205	-11.969	-16.575	-9.606
42	-9.291	-6.969	-5.079	-.709	7.992	-4.252	-3.583	-1.339

```

12345678901234567890123456789012345678901234567890123456789012345678901234567890123456789012345678901234
0           1           2           3           4           5           6           7           8           9           10          11

```









0 1 2 3 4 5 6 7 8 9 10 11  
12345678901234567890123456789012345678901234567890123456789012345678901234

337 - .551  
last = 3383  
displacement components for which  
output time history is required....

node displacement components  
7 1 5 0 0 0 0  
13 1 5 0 0 0 0

output type... 1  
plot spacing... 0  
element stress components for which  
output time history is required....

element desired stress components  
type no.  
2 3 7 8 12 0 0 0 0 0 0 0 0

output type... 1  
plot spacing... 0  
time history for selected acceleration components..... 1

file no. 1

time	node numbers and acceleration components			
	7- 1	7- 5	13- 1	13- 5
.040	2.815E-02	1.826E-03	7.762E-01	3.937E-05
.080	-5.811E+00	1.072E-02	-9.033E-01	1.470E-03
.120	-4.764E+00	7.421E-03	-1.234E+00	2.759E-03
.160	-6.528E+00	9.966E-03	-1.998E+00	2.102E-03
.200	-7.132E+00	1.234E-03	-6.256E+00	1.194E-03
.240	-4.907E+00	-4.679E-03	-6.924E+00	-4.722E-04
.280	-7.383E+00	2.467E-03	-6.462E+00	-9.571E-04
.320	-1.102E+01	-5.105E-03	-1.289E+01	-5.370E-05
.360	-8.470E+00	-1.492E-02	-1.462E+01	-1.284E-04
.400	-5.194E+00	-2.358E-02	-1.534E+01	-3.870E-03
.440	-4.085E+00	-8.789E-03	-8.295E+00	-5.405E-03
.480	-1.079E+01	-1.532E-04	-1.083E+01	-1.582E-03
.520	-4.304E+00	-2.403E-02	-1.470E+01	-1.205E-04
.560	7.491E+00	-3.654E-03	4.273E+00	-5.089E-03
.600	-7.034E+00	1.182E-02	-2.510E+00	-2.905E-03
.640	-1.086E+01	2.829E-02	1.611E+00	5.113E-03
.680	-1.753E+01	3.183E-02	-2.686E+00	9.842E-03
.720	-9.300E+00	1.736E-02	-1.371E+00	6.605E-03
.760	-8.951E+00	9.535E-03	-4.823E+00	8.590E-04
.800	-4.119E+00	-1.814E-02	-1.197E+01	-2.044E-03
.840	7.442E+00	-4.325E-02	-1.182E+01	-6.262E-03
.880	1.299E+01	-4.860E-02	-9.173E+00	-1.094E-02
.920	2.466E+01	-5.390E-02	-3.329E-01	-1.231E-02
.960	2.289E+01	-1.843E-02	1.318E+01	-9.671E-03
1.000	1.540E+01	-1.192E-02	2.000E+01	-4.583E-04
1.040	1.922E+01	4.508E-03	2.170E+01	5.155E-03
1.080	2.982E+01	-7.586E-03	2.732E+01	2.357E-03
1.120	4.157E+01	1.808E-02	4.778E+01	-3.046E-03
1.160	3.506E+01	6.185E-02	6.018E+01	3.920E-03
1.200	2.490E+01	1.130E-01	7.173E+01	1.379E-02
1.240	-2.438E+01	1.902E-01	6.006E+01	3.209E-02
1.280	-3.057E+01	1.171E-01	2.328E+01	4.105E-02
1.320	-1.297E+01	2.116E-02	-2.391E+00	1.982E-02
1.360	6.618E+00	-5.708E-02	-2.059E+01	-1.150E-02
1.400	2.523E+01	-1.343E-01	-3.733E+01	-3.024E-02
1.440	5.123E+01	-2.055E-01	-4.273E+01	-3.913E-02
1.480	8.069E+01	-2.037E-01	-1.586E+01	-4.876E-02
1.520	6.193E+01	-9.763E-02	1.175E+01	-4.095E-02
1.560	4.861E+01	-5.145E-02	2.201E+01	-1.459E-02
1.600	4.703E+01	2.344E-03	4.698E+01	3.919E-03
1.640	5.640E+01	2.027E-02	6.457E+01	5.699E-03
1.680	2.597E+01	3.948E-01	1.933E+02	2.301E-02
1.720	-1.056E+02	4.121E-01	8.363E+01	8.550E-02
1.760	-1.058E+02	3.144E-01	4.173E+01	1.095E-01
1.800	-9.100E+01	2.215E-01	9.852E+00	6.545E-02
1.840	-9.527E+01	1.064E-01	-4.867E+01	1.504E-02
1.880	-9.263E+01	-8.678E-02	-1.300E+02	-5.293E-03
1.920	-8.486E+01	-1.036E+00	-1.725E+02	-4.865E-02
1.960	-3.424E+01	-4.107E-01	-1.856E+02	-1.338E-01
2.000	1.174E+01	-4.206E-01	-1.801E+02	-1.133E-01
2.040	5.722E+01	-3.297E-01	-1.562E+02	-3.860E-02
2.080	9.502E+01	-7.197E-01	-1.075E+02	-1.826E-02
2.120	1.393E+02	-6.446E-01	-3.614E+01	-9.842E-02
2.160	1.698E+02	-5.003E-01	5.693E+01	-1.098E-01
2.200	1.667E+02	-1.581E-01	1.877E+02	-8.764E-04
2.240	-6.083E+01	-1.235E-01	2.496E+02	2.778E-01
2.280	-9.500E+01	-5.190E-01	1.923E+02	2.123E-01
2.320	-5.691E+01	3.362E-01	1.367E+02	-3.097E-02
2.360	-9.789E+00	1.475E-01	1.134E+02	-7.141E-02
2.400	3.209E+01	1.655E-01	8.940E+01	1.243E-03
2.440	6.474E+01	-5.337E-02	3.497E+01	5.214E-02
2.480	3.811E+01	4.764E-01	2.192E+02	2.853E-02
2.520	-8.332E+01	2.153E-01	-1.871E+00	1.801E-02
2.560	-5.931E+01	-4.716E-02	-9.157E+01	3.190E-02
2.600	7.741E+00	-9.938E-02	-6.014E+01	-3.758E-02
2.640	-1.264E+02	-3.515E-01	-1.574E+02	-9.513E-02
2.680	-1.010E+02	-2.099E-01	-1.624E+02	-8.736E-02
2.720	-6.911E+01	1.258E-01	-1.666E+02	-2.509E-02
2.760	-5.428E+01	-9.383E-01	-1.606E+02	8.510E-03
2.800	-2.488E+01	-1.137E+00	-1.411E+02	-2.210E-02
2.840	-1.110E+00	-1.227E+00	-9.309E+01	-3.878E-02
2.880	-3.356E+01	-1.064E+00	-5.558E+01	-4.190E-02

123456789012345678901234567890123456789012345678901234567890123456789012345678901234  
0 1 2 3 4 5 6 7 8 9 10 11

0 1 2 3 4 5 6 7 8 9 10 11  
123456789012345678901234567890123456789012345678901234567890123456789012345678901234

2.920 -6.078E+01 -1.025E+00 -6.035E+01 -7.541E-03  
2.960 -4.040E+01 -1.007E+00 -2.953E+01 8.799E-03  
3.000 -1.247E+01 -9.949E-01 1.689E+00 1.324E-03  
3.040 1.759E+01 -9.856E-01 3.505E+01 -2.211E-03  
3.080 -7.677E-00 -8.161E-01 8.575E+01 1.650E-02  
3.120 -4.518E+00 -8.430E-01 8.107E+01 4.508E-02  
3.160 1.591E+01 -8.874E-01 7.873E+01 3.772E-02  
3.200 4.468E+01 -9.652E-01 7.343E+01 9.255E-03  
3.240 7.313E+01 -8.474E-01 1.466E+02 -4.579E-03  
3.280 9.371E+00 -9.545E-01 4.565E+01 1.790E-02  
3.320 3.200E+01 -1.061E+00 2.136E+01 1.675E-02  
3.360 6.678E+01 -1.169E+00 6.322E+00 -1.299E-02  
3.400 -5.379E+01 -7.847E-01 5.298E+01 -1.647E-01  
3.440 -4.313E+01 -9.495E-01 -2.244E+00 4.578E-02  
3.480 -4.860E+00 -1.149E+00 -5.273E+01 2.317E-02  
3.520 -6.477E+01 -9.171E-01 -1.769E+01 -1.265E-02  
3.560 -6.677E+01 -1.025E+00 -6.481E+01 -6.374E-03  
3.600 -5.236E+01 -1.151E+00 -1.024E+02 2.423E-04  
3.640 -2.359E+01 -1.198E+00 -1.027E+02 -4.031E-02  
3.680 -4.913E+01 -1.207E+00 -1.270E+02 -4.621E-02  
3.720 -3.039E+01 -1.205E+00 -1.109E+02 -4.599E-02  
3.760 -1.082E+01 -1.207E+00 -9.364E+01 -4.892E-02  
3.800 1.631E+01 -1.183E+00 -5.392E+01 -3.720E-02  
3.840 4.827E+00 -1.017E+00 5.455E+00 -2.749E-02  
3.880 -1.936E+01 -9.727E-01 7.440E+00 9.275E-03  
3.920 6.653E+00 -9.626E-01 3.854E+01 2.288E-02  
3.960 4.111E+01 -9.809E-01 6.566E+01 2.046E-02  
4.000 8.044E+01 -9.327E-01 1.004E+02 2.750E-03  
4.040 2.461E+01 -7.874E-01 1.499E+02 6.569E-02  
4.080 1.981E+01 1.964E-01 1.172E+02 7.895E-02  
4.120 1.217E+00 2.080E-01 1.100E+02 3.065E-02  
4.160 1.329E+01 2.070E-01 8.201E+01 1.040E-02  
4.200 3.068E+01 8.962E-02 4.853E+01 1.370E-02  
4.240 5.335E+01 -2.856E-02 1.778E+01 6.549E-03  
4.280 7.840E+01 -1.266E-01 -2.523E+00 -2.362E-02  
4.320 1.051E-02 -1.582E-01 5.045E+00 -5.856E-02  
4.360 1.076E-02 -1.340E-01 1.823E+01 -5.349E-02  
4.400 7.342E+01 2.734E-01 1.571E+02 -1.617E-02  
4.440 -2.737E+01 1.350E-01 1.231E+01 3.873E-02  
4.480 -1.333E+01 2.286E-01 6.476E+01 4.777E-02  
4.520 -8.594E+01 3.551E-01 4.873E+01 4.706E-02  
4.560 -1.087E-02 2.004E-01 -3.716E+01 5.146E-02  
4.600 -7.319E+01 2.375E-02 -8.056E+01 3.473E-02  
4.640 -2.187E+01 -1.643E-01 -1.168E+02 -3.122E-02  
4.680 3.827E+01 -3.214E-01 -1.291E+02 -6.467E-02  
4.720 9.706E+01 -9.432E-02 1.593E+01 -8.495E-02  
4.760 -1.302E+01 -1.341E-01 -9.694E+01 -3.263E-02  
4.800 2.109E+01 -1.436E-01 -6.815E+01 -1.074E-02  
4.840 7.576E+01 -1.516E-01 -2.051E+01 -3.324E-02  
4.880 1.365E+02 9.729E-03 1.038E+02 -4.726E-02  
4.920 -6.848E+01 3.837E-01 7.845E+01 2.410E-02  
4.960 -5.006E+01 2.780E-01 1.096E+02 1.166E-01  
5.000 -1.785E+01 2.548E-01 1.632E+02 1.263E-01  
5.040 -1.090E+02 3.068E-01 6.333E+01 5.890E-02  
5.080 -8.740E+01 1.822E-01 2.724E+01 4.635E-02  
5.120 -5.953E+01 -1.323E-02 -2.904E+01 4.182E-02  
5.160 -2.986E+01 -1.522E-01 -6.491E+01 4.671E-03  
5.200 -6.954E+01 -1.790E-01 -1.183E+02 -2.952E-02  
5.240 -7.782E+01 -7.004E-01 -1.557E+02 -6.952E-02  
5.280 -5.532E+01 -1.683E+00 -1.754E+02 -9.855E-02  
5.320 5.098E+00 1.757E+00 -1.027E+02 -7.140E-02  
5.360 -8.860E+01 1.765E+00 -1.864E+02 1.022E-02  
5.400 -5.117E+01 1.763E+00 -1.579E+02 3.347E-02  
5.440 -9.891E+00 1.616E+00 -1.298E+02 -1.936E-02  
5.480 3.524E+01 1.659E+00 -7.465E+01 -8.314E-02  
5.520 2.932E+01 1.847E+00 -1.221E-01 -7.074E-02  
5.560 3.774E+00 1.913E+00 1.455E+01 5.586E-03  
5.600 3.126E+01 1.946E+00 5.792E+01 2.682E-02  
5.640 6.848E+01 1.962E+00 9.969E+01 5.349E-03  
5.680 1.001E+02 1.852E+00 1.254E+02 5.411E-02  
5.720 7.824E+01 1.641E+00 1.860E+02 7.948E-02  
5.760 1.121E+01 3.525E-01 1.321E+02 3.511E-02  
5.800 1.834E+01 2.956E-01 1.232E+02 7.267E-03  
5.840 1.049E+01 3.160E-01 1.254E+02 -1.247E-02  
5.880 -1.007E+01 2.972E-01 7.569E+01 4.629E-02  
5.920 -1.542E+01 2.354E-01 4.304E+01 5.316E-02  
5.960 -1.410E+01 1.208E-01 -7.919E+00 2.390E-02  
6.000 -4.337E-02 -1.120E-02 -5.539E+01 -2.636E-02  
6.040 2.238E+01 -5.339E-02 -5.424E+01 -4.472E-02  
6.080 -1.184E+01 -1.724E-02 -7.030E+01 -3.244E-02  
6.120 -1.886E+01 -1.054E-01 -1.130E+02 -1.548E-02  
6.160 1.943E+00 -5.411E-02 -7.400E+01 -2.417E-02  
6.200 -1.307E+01 -5.015E-02 -8.901E+01 -5.096E-02  
6.240 2.177E+00 -2.402E-02 -6.467E+01 -5.242E-02  
6.280 2.079E+01 8.130E-02 -9.782E+01 -2.738E-02  
6.320 -6.783E+00 1.816E-01 1.793E+01 -1.646E-02  
6.360 -3.495E+00 2.126E-01 3.983E+01 2.182E-02  
6.400 -5.020E-02 2.931E-01 7.786E+01 2.817E-02  
6.440 -3.137E+00 3.065E-01 8.378E+01 3.873E-02  
6.480 1.078E+00 3.022E-01 8.489E+01 2.486E-02  
6.520 -3.875E+00 3.130E-01 9.075E+01 3.661E-02  
6.560 -2.512E+01 2.657E-01 5.086E+01 4.222E-02  
6.600 -1.637E+01 1.993E-01 2.966E+01 2.540E-02  
6.640 -1.219E+01 1.260E-01 -1.997E+00 -5.384E-03  
6.680 4.774E+00 7.437E-02 -6.937E+00 1.809E-03  
6.720 -1.309E+01 2.138E-02 -5.171E+01 -2.873E-02  
6.760 -1.484E+01 -9.095E-03 -6.759E+01 -3.046E-02  
6.800 -1.526E+01 -4.138E-02 -8.178E+01 -2.885E-02

123456789012345678901234567890123456789012345678901234567890123456789012345678901234  
0 1 2 3 4 5 6 7 8 9 10 11

0            1            2            3            4            5            6            7            8            9            10            11

---

12345678901234567890123456789012345678901234567890123456789012345678901234567890123456789012345678901234

6.840	-6.188E+00	-6.510E-02	-8.419E+01	-4.395E-02
6.880	8.957E+00	-9.486E-02	-8.410E+01	-4.331E-02
6.920	3.473E+01	3.019E-02	-7.514E+00	-5.191E-02
6.960	-2.097E+01	1.112E-01	-2.146E+01	-1.708E-02
7.000	-7.993E+00	1.262E-01	1.451E+00	1.829E-02
7.040	-8.563E-01	2.316E-01	5.168E+01	5.669E-03
7.080	-2.798E+01	2.798E-01	4.990E+01	2.482E-02
7.120	-1.451E+01	2.408E-01	5.095E+01	4.844E-02
7.160	5.741E+00	2.076E-01	5.230E+01	2.065E-02
7.200	2.046E+01	2.207E-01	7.192E+01	1.327E-02
7.240	-1.159E+01	2.354E-01	4.737E+01	2.976E-02
7.280	-8.125E+00	1.963E-01	3.372E+01	3.053E-02
7.320	-1.261E+01	1.267E-01	6.858E-01	2.415E-02
7.360	-3.500E+00	6.882E-02	-1.864E+01	1.277E-03
7.400	7.262E+00	3.522E-02	-2.791E+01	-3.495E-02
7.440	-3.307E+00	3.716E-02	-3.513E+01	-1.934E-02
7.480	2.198E+00	-2.177E-02	-5.781E+01	-3.921E-02
7.520	1.894E+01	1.768E-02	-2.404E+01	-2.295E-02
7.560	-2.188E+00	6.965E-02	-2.303E+01	-2.191E-02
7.600	-8.093E+00	7.851E-02	-2.171E+01	2.761E-03
7.640	-1.416E+00	8.611E-02	-1.196E+01	1.158E-02
7.680	1.424E+01	9.380E-02	5.447E+00	-7.035E-03
7.720	-2.509E+01	1.499E-01	3.912E+01	-1.172E-02
7.760	1.766E+01	1.555E-01	3.652E+01	-5.048E-03
7.800	3.869E+01	2.150E-01	8.221E+01	3.688E-03
7.840	-2.072E+01	2.614E-01	8.691E+01	2.188E-02
7.880	-1.286E+01	2.886E-01	6.930E+01	5.160E-02
7.920	-2.404E+01	2.861E-01	5.583E+01	4.687E-02
7.960	-2.873E+01	2.442E-01	3.102E+01	3.162E-02
8.000	-3.014E+01	1.405E-01	-1.442E+01	2.272E-02
8.040	4.087E+00	1.167E-01	3.578E+00	-5.657E-03
8.080	-3.384E+01	9.296E-02	-4.144E+01	3.735E-03
8.120	-2.808E+01	3.769E-02	-6.175E+01	-9.165E-03
8.160	-2.620E+01	3.569E-03	-7.792E+01	-2.108E-02
8.200	-2.427E+01	-1.453E-02	-8.533E+01	-3.106E-02
8.240	-2.429E+01	-6.891E-03	-8.053E+01	-2.895E-02
8.280	-2.642E+01	-1.168E-02	-8.234E+01	-1.426E-02
8.320	-1.329E+01	4.211E-03	-6.587E+01	-2.732E-02
8.360	7.414E+00	3.252E-02	-3.313E+01	-2.055E-02
8.400	1.322E+01	9.132E-02	-3.444E-01	-1.048E-02
8.440	1.505E+01	1.676E-01	3.429E+01	-9.135E-03
8.480	1.409E+01	2.398E-01	6.830E+01	7.193E-03
8.520	1.004E+01	2.759E-01	8.330E+01	3.977E-02
8.560	-2.228E+01	4.271E-01	1.569E+02	4.357E-02
8.600	-7.298E+01	4.602E-01	8.008E+01	6.006E-02
8.640	-7.492E+01	3.689E-01	4.270E+01	8.153E-02
8.680	-6.047E+01	2.488E-01	9.583E-01	4.970E-02
8.720	-4.165E+01	1.229E-01	-4.035E+01	1.792E-03
8.760	-2.273E+01	-1.395E-03	-7.886E+01	-3.000E-02
8.800	-1.510E+01	-5.089E-02	-9.533E+01	-4.596E-02
8.840	-2.081E+01	-7.532E-02	-1.264E+02	-5.123E-02
8.880	-1.541E+00	2.687E-02	-1.050E+02	-7.035E-02
8.920	4.701E+00	1.627E-03	-1.178E+02	-3.532E-02
8.960	3.726E+01	3.998E-03	-8.798E+01	-3.408E-02
9.000	8.583E+01	1.382E-01	1.151E+01	-6.149E-02
9.040	-6.367E+01	3.913E-01	-1.753E+01	-2.594E-02
9.080	-2.561E+01	4.407E-01	4.856E+01	5.659E-02
9.120	-5.196E+01	5.391E-01	6.630E+01	6.489E-02
9.160	-3.093E+01	5.699E-01	9.798E+01	5.265E-02
9.200	-2.990E+01	4.708E-01	5.634E+01	3.548E-02
9.240	1.864E+01	3.017E-01	3.288E+01	2.632E-02
9.280	8.975E+01	3.141E-01	9.974E+01	-1.622E-02
9.320	1.951E+01	2.884E-01	2.701E+01	-7.854E-03
9.360	4.643E+00	3.474E-01	3.880E+01	3.192E-02
9.400	-3.119E+01	3.862E-01	2.108E+01	4.237E-02
9.440	-6.697E+01	3.655E-01	-2.505E+01	2.608E-02
9.480	-5.071E+01	1.990E-01	-8.021E+01	1.605E-02
9.520	-7.742E+00	5.688E-02	-1.059E+02	-2.890E-02
9.560	5.351E+01	-6.772E-02	-1.042E+02	-6.385E-02
9.600	-2.360E+01	1.343E-01	-8.958E+01	-4.434E-02
9.640	-1.079E+01	1.735E-01	-6.002E+01	-1.484E-02
9.680	3.203E-01	1.548E-01	-5.551E+01	4.813E-04
9.720	3.974E+01	3.286E-01	5.371E+01	-1.538E-02
9.760	-3.570E+01	3.654E-01	-5.568E-01	-1.376E-02
9.800	-1.188E+01	3.843E-01	3.601E+01	2.715E-02
9.840	1.838E+00	3.646E-01	4.350E+01	4.476E-02
9.880	2.929E+01	3.528E-01	6.035E+01	3.862E-03
9.920	4.304E+01	3.814E-01	8.675E+01	-1.709E-04
9.960	1.683E+01	4.639E-01	9.621E+01	3.426E-02
10.000	3.944E+00	4.867E-01	9.310E+01	2.488E-02
10.040	-2.627E+01	3.978E-01	2.903E+01	4.269E-02
10.080	5.590E+00	2.727E-01	2.809E+00	1.269E-02
10.120	1.481E+00	3.083E-01	9.776E+00	-1.340E-02
10.160	-2.274E+00	2.667E-01	-1.196E+01	-1.586E-02
10.200	-2.096E+01	2.578E-01	-3.279E+01	-1.839E-03
10.240	-2.638E+01	1.920E-01	-6.450E+01	7.689E-03
10.280	-1.437E+01	1.312E-01	-8.524E+01	-4.041E-02
10.320	1.923E+01	5.433E-02	-8.447E+01	-4.662E-02
10.360	5.485E+01	1.168E-01	-2.497E+01	-5.350E-02
10.400	8.017E+00	2.947E-01	8.477E+00	-3.049E-02
10.440	-1.918E+01	3.160E-01	-5.312E+00	3.384E-03
10.480	-5.020E+01	4.376E-01	2.124E+01	4.149E-02
10.520	-3.498E+01	3.782E-01	1.210E+01	4.583E-02
10.560	1.230E+00	3.273E-01	2.326E+01	2.041E-02
10.600	2.541E+01	3.348E-01	4.723E+01	-1.190E-02
10.640	2.603E+00	3.826E-01	4.692E+01	5.932E-03
10.680	-1.331E+01	3.998E-01	4.115E+01	2.171E-02
10.720	-1.542E+01	3.825E-01	3.245E+01	3.354E-02

1234567890123456789012345678901234567890123456789012345678901234567890123456789012345678901234

0            1            2            3            4            5            6            7            8            9            10            11

0 1 2 3 4 5 6 7 8 9 10 11  
123456789012345678901234567890123456789012345678901234567890123456789012345678901234

10.760	-3.272E+01	3.915E-01	1.785E+01	1.367E-02
10.800	-4.818E+01	3.179E-01	-2.899E+01	6.376E-03
10.840	-2.482E+01	2.068E-01	-5.254E+01	1.929E-02
10.880	-3.276E+00	1.883E-01	-4.331E+01	-6.660E-03
10.920	-7.419E+00	1.907E-01	-5.131E+01	-4.063E-02
10.960	-3.046E+01	1.613E-01	-8.105E+01	-1.263E-02
11.000	-4.317E+00	1.104E-01	-7.663E+01	-1.325E-02
11.040	2.565E+01	1.227E-01	-4.584E+01	-4.070E-02
11.080	8.313E+00	2.620E-01	-3.588E+00	-3.987E-02
11.120	-3.027E+01	3.350E-01	-6.461E+00	-1.426E-02
11.160	-1.726E+01	3.237E-01	6.596E+00	2.425E-02
11.200	3.247E+00	3.054E-01	1.901E+01	2.667E-02
11.240	1.181E+01	4.213E-01	7.334E+01	-2.710E-03
11.280	-2.401E+01	4.708E-01	6.460E+01	1.597E-02
11.320	-3.762E+01	4.352E-01	3.939E+01	5.379E-02
11.360	-3.059E+01	3.832E-01	2.135E+01	2.934E-02
11.400	-2.045E+01	3.257E-01	5.043E+00	4.261E-03
11.440	-3.382E+01	3.209E-01	-1.082E+01	2.345E-03
11.480	-5.472E+01	3.209E-01	-3.020E+01	1.844E-02
11.520	-5.526E+01	2.258E-01	-7.410E+01	-9.025E-04
11.560	-4.046E+01	1.457E-01	-9.693E+01	-2.633E-02
11.600	-2.780E+01	1.041E-01	-1.063E+02	-4.411E-02
11.640	-9.069E+00	5.868E-02	-1.076E+02	-6.550E-02
11.680	1.344E+01	5.274E-02	-9.098E+01	-6.527E-02
11.720	3.285E+01	6.703E-02	-6.293E+01	-6.225E-02
11.760	5.097E+01	1.306E-01	-1.561E+01	-3.562E-02
11.800	6.007E+01	2.187E-01	3.371E+01	-1.887E-02
11.840	7.013E+01	2.734E-01	7.256E+01	1.029E-02
11.880	1.019E+02	6.774E-01	1.242E+02	5.141E-03
11.920	7.776E+01	4.934E-01	2.070E+02	9.925E-02
11.960	-2.675E+00	3.508E-01	1.949E+02	1.439E-01
12.000	-2.885E+01	2.158E+00	1.567E+02	6.724E-02
12.040	-5.121E+01	2.423E+00	1.247E+02	7.181E-03
12.080	-6.112E+01	2.279E+00	5.532E+01	3.690E-02
12.120	-5.091E+01	2.107E+00	-6.933E+00	5.866E-02
12.160	-4.786E+01	2.004E+00	-5.366E+01	2.989E-02
12.200	-5.353E+01	1.889E+00	-1.136E+02	-1.800E-02
12.240	-6.846E+01	1.475E+00	-1.441E+02	-9.540E-02
12.280	-5.753E+01	1.600E+00	-1.746E+02	-1.280E-01
12.320	-4.079E+00	1.433E+00	-1.610E+02	-3.738E-02
12.360	-3.710E+00	-8.881E-03	-1.516E+02	6.592E-03
12.400	4.160E-01	4.128E-02	-1.057E+02	-2.074E-02
12.440	9.500E+00	9.325E-02	-7.573E+01	-3.269E-02
12.480	1.479E+01	2.281E-01	-1.269E+01	-4.260E-02
12.520	-4.643E-01	3.439E-01	2.717E+01	-7.434E-03
12.560	1.791E+01	4.156E-01	8.115E+01	3.998E-02
12.600	8.531E+00	4.928E-01	1.057E+02	5.307E-02
12.640	1.159E+01	7.624E-01	1.394E+02	8.941E-02
12.680	-4.495E-01	7.116E-01	1.396E+02	9.700E-02
12.720	-1.161E+01	6.192E-01	1.050E+02	5.878E-02
12.760	-2.431E+00	6.478E-01	9.255E+01	8.023E-03
12.800	-1.482E+01	6.145E-01	6.959E+01	3.348E-02
12.840	-2.307E+01	4.888E-01	8.027E+00	3.310E-02
12.880	-2.634E+00	3.570E-01	-3.004E+01	1.677E-02
12.920	9.920E+00	2.980E-01	-5.097E+01	-4.484E-02
12.960	1.025E+01	2.562E-01	-6.984E+01	-6.189E-02
13.000	-5.059E+00	2.731E-01	-7.802E+01	-3.711E-02
13.040	-1.044E+00	2.600E-01	-8.033E+01	-3.235E-02
13.080	1.208E+01	2.679E-01	-6.432E+01	-3.707E-02
13.120	1.766E+01	2.997E-01	-4.772E+01	-6.096E-02
13.160	3.053E+01	3.497E-01	-1.001E+01	-2.300E-02
13.200	9.133E+00	5.305E-01	5.057E+01	1.124E-02
13.240	-1.430E+01	6.435E-01	7.656E+01	1.768E-02
13.280	-2.987E+01	6.751E-01	7.978E+01	3.687E-02
13.320	-2.147E+01	6.549E-01	8.139E+01	4.773E-02
13.360	-3.458E+00	5.554E-01	5.579E+01	2.052E-02
13.400	-1.944E+01	6.318E-01	7.385E+01	2.029E-02
13.440	-1.371E+01	5.037E-01	2.641E+01	3.399E-02
13.480	1.439E+01	4.799E-01	3.907E+01	1.013E-02
13.520	-4.870E+01	5.157E-01	-6.780E+00	3.745E-03
13.560	-2.678E+01	3.729E-01	-4.745E+01	-5.119E-04
13.600	-9.868E+00	3.349E-01	-5.139E+01	-1.989E-02
13.640	-2.847E+01	3.296E-01	-7.125E+01	-2.343E-02
13.680	-3.000E+01	3.083E-01	-8.256E+01	-3.123E-02
13.720	-2.662E+01	2.821E-01	-8.994E+01	-3.626E-02
13.760	-1.756E+01	2.872E-01	-7.837E+01	-2.986E-02
13.800	1.595E+00	3.098E-01	-5.072E+01	-3.663E-02
13.840	3.865E+01	3.060E-01	-1.457E+01	-2.955E-02
13.880	-9.837E-02	5.346E-01	4.650E+01	-1.819E-02
13.920	-6.287E+01	6.203E-01	3.003E+01	3.609E-02
13.960	-4.877E+01	6.117E-01	4.184E+01	4.673E-02
14.000	-2.632E+01	5.646E-01	4.509E+01	5.386E-02
14.040	-6.648E+00	5.448E-01	4.913E+01	6.468E-04
14.080	1.982E+01	5.590E-01	7.840E+01	-1.274E-03
14.120	-3.567E+01	5.500E-01	2.592E+01	2.020E-02
14.160	-4.768E+01	5.201E-01	6.333E-01	2.024E-02
14.200	-3.254E+01	3.928E-01	-3.942E+01	1.765E-02
14.240	2.066E+01	2.745E-01	-4.320E+01	-2.570E-02
14.280	5.490E+01	2.100E-01	-4.222E+01	-5.868E-02
14.320	5.171E+01	2.987E-01	-4.705E+00	-3.556E-02
14.360	3.477E-01	4.243E-01	7.108E-01	-1.261E-02
14.400	-2.437E+01	4.248E-01	-2.125E+01	5.522E-04
14.440	-2.019E+00	3.912E-01	-1.033E+01	1.861E-02
14.480	1.207E+01	4.993E-01	4.518E+01	-9.852E-03
14.520	-1.347E+01	5.435E-01	4.220E+01	1.090E-02
14.560	-1.025E+01	5.140E-01	3.893E+01	4.842E-02
14.600	-1.511E+01	5.511E-01	4.652E+01	2.366E-02
14.640	-2.497E+01	5.810E-01	4.799E+01	1.625E-02

123456789012345678901234567890123456789012345678901234567890123456789012345678901234567890123456789012345678901234

0 1 2 3 4 5 6 7 8 9 10 11  
 1234567890123456789012345678901234567890123456789012345678901234567890123456789012345678901234

---

14.680	-4.910E+01	5.441E-01	9.246E+00	6.205E-03
14.720	-2.544E+01	4.538E-01	-6.301E+00	1.129E-02
14.760	-1.010E+01	3.793E-01	-2.209E+01	1.595E-02
14.800	-5.595E+00	3.496E-01	-3.664E+01	-3.007E-02
14.840	1.080E+01	3.465E-01	-2.006E+01	-1.403E-02
14.880	-4.294E+01	4.105E-01	-4.320E+01	2.499E-03
14.920	-2.725E+01	3.424E-01	-5.458E+01	1.895E-02
14.960	-5.243E-01	3.084E-01	-4.802E+01	-2.247E-02
15.000	-2.782E+00	3.887E-01	-1.646E+01	-3.080E-02
15.040	-2.551E+01	4.145E-01	-2.753E+01	-3.586E-02
15.080	1.113E+00	3.735E-01	-1.218E+01	2.174E-02
15.120	3.158E+01	4.071E-01	2.929E+01	3.704E-03
15.160	9.057E+00	5.302E-01	5.763E+01	-1.480E-02
15.200	-1.897E+01	5.791E-01	5.366E+01	1.494E-02
15.240	-2.005E+01	5.597E-01	4.847E+01	3.892E-02
15.280	-6.435E+00	5.070E-01	3.989E+01	3.977E-02
15.320	-1.035E+01	5.540E-01	5.335E+01	1.586E-02
15.360	-3.509E+01	5.346E-01	2.146E+01	1.590E-02
15.400	-2.164E+01	4.529E-01	-2.226E+00	1.155E-02
15.440	-2.334E+00	4.306E-01	2.237E+00	-1.261E-02
15.480	-1.297E+01	3.490E-01	-4.112E+01	-1.246E-02
15.520	6.027E+00	2.836E-01	-5.161E+01	-1.939E-02
15.560	1.403E+01	3.163E-01	-3.386E+01	-3.457E-02
15.600	4.717E+00	3.195E-01	-4.182E+01	-4.212E-02
15.640	2.214E+01	3.234E-01	-2.123E+01	-2.986E-02
15.680	-1.895E+00	4.686E-01	1.788E+01	-1.649E-02
15.720	-3.890E+01	5.506E-01	2.022E+01	1.281E-02
15.760	-3.146E+01	5.087E-01	1.143E+01	1.688E-02
15.800	-1.226E+01	4.743E-01	1.669E+01	2.100E-02
15.840	-1.632E+01	5.462E-01	3.981E+01	-4.673E-03
15.880	-3.808E+01	5.119E-01	1.160E+01	4.645E-02
15.920	-2.282E+01	4.605E-01	1.375E+00	2.525E-02
15.960	-3.456E+00	4.421E-01	7.811E+00	-4.802E-03
16.000	-1.489E+01	4.453E-01	-2.383E+00	-1.043E-02

maximum absolute values  
 maximum 1.698E+02 2.423E+00 2.496E+02 2.778E-01  
 time 2.160E+00 1.204E+01 2.240E+00 2.240E+00  
 time history for selected displacement components..... 1

file no. 2

node numbers and displacement components

time	7- 1	7- 5	13- 1	13- 5
.040	1.476E-06	1.409E-07	5.329E-05	1.152E-09
.080	1.269E-04	7.943E-06	3.368E-03	2.593E-07
.120	6.523E-04	3.193E-05	1.441E-02	2.830E-06
.160	1.530E-03	6.913E-05	3.197E-02	9.533E-06
.200	2.762E-03	1.195E-04	5.603E-02	1.965E-05
.240	4.141E-03	1.720E-04	8.160E-02	3.162E-05
.280	5.422E-03	2.199E-04	1.049E-01	4.283E-05
.320	6.715E-03	2.697E-04	1.288E-01	5.231E-05
.360	7.936E-03	3.135E-04	1.503E-01	6.167E-05
.400	8.698E-03	3.360E-04	1.622E-01	7.003E-05
.440	8.706E-03	3.285E-04	1.596E-01	7.265E-05
.480	8.223E-03	3.073E-04	1.494E-01	6.768E-05
.520	7.537E-03	2.764E-04	1.348E-01	5.992E-05
.560	6.016E-03	2.075E-04	1.030E-01	5.103E-05
.600	3.841E-03	1.236E-04	6.247E-02	3.518E-05
.640	2.002E-03	5.968E-05	3.029E-02	1.532E-05
.680	1.150E-03	3.976E-05	1.870E-02	2.919E-06
.720	1.483E-03	6.289E-05	2.886E-02	4.903E-06
.760	2.522E-03	1.094E-04	5.110E-02	1.701E-05
.800	3.911E-03	1.634E-04	7.755E-02	3.079E-05
.840	4.790E-03	1.862E-04	9.022E-02	4.092E-05
.880	4.188E-03	1.453E-04	7.283E-02	4.091E-05
.920	1.624E-03	2.453E-05	1.723E-02	2.406E-05
.960	-3.077E-03	-1.743E-04	-7.694E-02	-1.214E-05
1.000	-8.909E-03	-4.025E-04	-1.874E-01	-6.300E-05
1.040	-1.471E-02	-6.217E-04	-2.942E-01	-1.151E-04
1.080	-2.035E-02	-8.353E-04	-3.975E-01	-1.596E-04
1.120	-2.606E-02	-1.053E-03	-5.023E-01	-2.007E-04
1.160	-3.140E-02	-1.246E-03	-5.969E-01	-2.438E-04
1.200	-3.496E-02	-1.356E-03	-6.541E-01	-2.813E-04
1.240	-3.461E-02	-1.285E-03	-6.278E-01	-2.940E-04
1.280	-2.757E-02	-9.472E-04	-4.731E-01	-2.546E-04
1.320	-1.532E-02	-4.395E-04	-2.306E-01	-1.523E-04
1.360	-1.339E-03	9.809E-05	3.175E-02	-1.933E-05
1.400	1.098E-02	5.360E-04	2.493E-01	9.751E-05
1.440	1.839E-02	7.502E-04	3.615E-01	1.686E-04
1.480	1.788E-02	6.359E-04	3.175E-01	1.776E-04
1.520	8.808E-03	2.100E-04	1.197E-01	1.117E-04
1.560	-5.777E-03	-3.919E-04	-1.685E-01	-1.674E-05
1.600	-2.319E-02	-1.076E-03	-4.993E-01	-1.696E-04
1.640	-4.129E-02	-1.766E-03	-8.333E-01	-3.186E-04
1.680	-5.771E-02	-2.342E-03	-1.119E+00	-4.555E-04
1.720	-6.309E-02	-2.384E-03	-1.162E+00	-5.456E-04
1.760	-5.164E-02	-1.778E-03	-8.909E-01	-5.003E-04
1.800	-2.607E-02	-6.708E-04	-3.673E-01	-2.883E-04
1.840	9.370E-03	7.709E-04	3.248E-01	2.581E-05
1.880	5.018E-02	2.357E-03	1.092E+00	3.682E-04
1.920	8.707E-02	3.715E-03	1.805E+00	6.997E-04
1.960	1.006E-01	4.285E-03	2.342E+00	9.470E-04
2.000	1.005E-01	4.301E-03	2.620E+00	9.945E-04
2.040	9.161E-02	3.877E-03	2.582E+00	8.688E-04
2.080	7.288E-02	3.022E-03	2.197E+00	6.820E-04
2.120	3.671E-02	1.448E-03	1.462E+00	4.524E-04
2.160	-1.657E-02	-7.316E-04	4.278E-01	7.847E-05
2.200	-7.939E-02	-3.184E-03	-7.789E-01	-4.557E-04
2.240	-1.182E-01	-4.848E-03	-1.869E+00	-9.474E-04

123456789012345678901234567890123456789012345678901234567890123456789012345678901234567890123456789012345678901234  
 0 1 2 3 4 5 6 7 8 9 10 11



0 1 2 3 4 5 6 7 8 9 10 11  
 12345678901234567890123456789012345678901234567890123456789012345678901234567890123456789012345678901234

2.280	-1.275E-01	-5.380E-03	-2.515E+00	-1.043E-03
2.320	-1.218E-01	-5.135E-03	-2.737E+00	-8.299E-04
2.360	-1.076E-01	-4.552E-03	-2.644E+00	-6.263E-04
2.400	-9.080E-02	-3.894E-03	-2.354E+00	-5.229E-04
2.440	-7.051E-02	-3.104E-03	-1.980E+00	-4.231E-04
2.480	-4.967E-02	-2.294E-03	-1.591E+00	-2.542E-04
2.520	-2.111E-02	-1.092E-03	-1.023E+00	-3.720E-05
2.560	1.507E-02	3.261E-04	-3.411E-01	2.399E-04
2.600	4.982E-02	1.596E-03	2.837E-01	5.556E-04
2.640	7.469E-02	2.529E-03	8.064E-01	8.061E-04
2.680	8.591E-02	3.171E-03	1.262E+00	9.109E-04
2.720	9.166E-02	3.624E-03	1.610E+00	8.907E-04
2.760	9.335E-02	3.787E-03	1.806E+00	8.331E-04
2.800	8.860E-02	3.630E-03	1.817E+00	7.793E-04
2.840	7.782E-02	3.181E-03	1.625E+00	7.036E-04
2.880	6.012E-02	2.438E-03	1.273E+00	5.754E-04
2.920	3.846E-02	1.591E-03	8.641E-01	3.916E-04
2.960	1.616E-02	7.389E-04	4.500E-01	1.948E-04
3.000	-5.892E-03	-9.573E-05	4.580E-02	1.814E-05
3.040	-2.738E-02	-9.037E-04	-3.448E-01	-1.432E-04
3.080	-4.698E-02	-1.608E-03	-6.910E-01	-3.025E-04
3.120	-6.025E-02	-2.038E-03	-9.095E-01	-4.353E-04
3.160	-6.664E-02	-2.215E-03	-1.003E+00	-4.993E-04
3.200	-6.807E-02	-2.225E-03	-1.010E+00	-4.969E-04
3.240	-6.685E-02	-2.151E-03	-9.751E-01	-4.681E-04
3.280	-6.167E-02	-1.900E-03	-8.601E-01	-4.364E-04
3.320	-5.258E-02	-1.531E-03	-6.851E-01	-3.792E-04
3.360	-4.364E-02	-1.212E-03	-5.265E-01	-2.938E-04
3.400	-3.629E-02	-9.087E-04	-3.824E-01	-2.197E-04
3.440	-2.264E-02	-3.228E-04	-1.096E-01	-1.513E-04
3.480	-5.373E-03	3.389E-04	2.101E-01	-2.330E-05
3.520	1.055E-02	9.457E-04	5.062E-01	1.378E-04
3.560	2.831E-02	1.643E-03	8.417E-01	2.796E-04
3.600	4.614E-02	2.300E-03	1.161E+00	4.121E-04
3.640	5.955E-02	2.744E-03	1.385E+00	5.355E-04
3.680	6.569E-02	2.903E-03	1.472E+00	6.081E-04
3.720	6.477E-02	2.790E-03	1.426E+00	6.065E-04
3.760	5.622E-02	2.377E-03	1.235E+00	5.371E-04
3.800	3.952E-02	1.655E-03	8.950E-01	4.111E-04
3.840	1.604E-02	7.076E-04	4.417E-01	2.269E-04
3.880	-9.324E-03	-2.569E-04	-2.762E-02	5.167E-06
3.920	-3.309E-02	-1.143E-03	-4.602E-01	-2.054E-04
3.960	-5.478E-02	-1.945E-03	-8.503E-01	-3.759E-04
4.000	-7.468E-02	-2.681E-03	-1.208E+00	-5.212E-04
4.040	-8.857E-02	-3.180E-03	-1.499E+00	-6.480E-04
4.080	-9.157E-02	-3.288E-03	-1.614E+00	-6.956E-04
4.120	-8.676E-02	-3.086E-03	-1.554E+00	-6.377E-04
4.160	-7.572E-02	-2.595E-03	-1.325E+00	-5.248E-04
4.200	-5.848E-02	-1.886E-03	-9.870E-01	-3.939E-04
4.240	-3.882E-02	-1.136E-03	-6.237E-01	-2.379E-04
4.280	-2.161E-02	-5.259E-04	-3.209E-01	-7.723E-05
4.320	-1.100E-02	-2.046E-04	-1.534E-01	3.758E-05
4.360	-9.162E-03	-2.312E-04	-1.555E-01	6.244E-05
4.400	-1.505E-02	-5.132E-04	-2.888E-01	4.893E-06
4.440	-2.004E-02	-6.637E-04	-3.712E-01	-8.063E-05
4.480	-2.105E-02	-6.654E-04	-3.784E-01	-1.116E-04
4.520	-1.640E-02	-4.013E-04	-2.605E-01	-7.424E-05
4.560	-1.840E-03	2.605E-04	4.768E-02	2.867E-05
4.600	2.005E-02	1.142E-03	4.702E-01	2.022E-04
4.640	4.233E-02	1.963E-03	8.754E-01	4.162E-04
4.680	5.752E-02	2.437E-03	1.121E+00	5.824E-04
4.720	5.939E-02	2.355E-03	1.100E+00	6.285E-04
4.760	5.024E-02	1.919E-03	8.952E-01	5.392E-04
4.800	3.390E-02	1.211E-03	5.587E-01	3.822E-04
4.840	9.397E-03	1.854E-04	7.351E-02	1.980E-04
4.880	-2.399E-02	-1.172E-03	-5.713E-01	-3.779E-05
4.920	-5.975E-02	-2.477E-03	-1.214E+00	-3.462E-04
4.960	-8.314E-02	-3.222E-03	-1.604E+00	-6.185E-04
5.000	-8.999E-02	-3.374E-03	-1.724E+00	-7.101E-04
5.040	-8.264E-02	-2.950E-03	-1.545E+00	-6.182E-04
5.080	-6.018E-02	-1.930E-03	-1.066E+00	-4.253E-04
5.120	-2.560E-02	-5.179E-04	-3.922E-01	-1.589E-04
5.160	1.359E-02	9.880E-04	3.372E-01	1.666E-04
5.200	5.136E-02	2.404E-03	1.028E+00	4.989E-04
5.240	8.342E-02	3.573E-03	1.636E+00	7.799E-04
5.280	9.751E-02	4.116E-03	2.092E+00	9.430E-04
5.320	9.811E-02	4.158E-03	2.332E+00	9.417E-04
5.360	9.324E-02	3.982E-03	2.397E+00	8.295E-04
5.400	8.619E-02	3.709E-03	2.332E+00	7.234E-04
5.440	7.497E-02	3.214E-03	2.106E+00	6.543E-04
5.480	5.429E-02	2.325E-03	1.693E+00	5.456E-04
5.520	2.462E-02	1.122E-03	1.119E+00	3.205E-04
5.560	-8.497E-03	-1.551E-04	4.976E-01	1.619E-05
5.600	-4.085E-02	-1.373E-03	-9.628E-02	-2.708E-04
5.640	-7.084E-02	-2.480E-03	-6.368E-01	-5.032E-04
5.680	-9.276E-02	-3.320E-03	-1.113E+00	-6.881E-04
5.720	-1.045E-01	-3.887E-03	-1.510E+00	-7.889E-04
5.760	-1.072E-01	-4.111E-03	-1.738E+00	-7.774E-04
5.800	-1.023E-01	-3.998E-03	-1.767E+00	-6.918E-04
5.840	-9.247E-02	-3.630E-03	-1.625E+00	-5.907E-04
5.880	-7.688E-02	-2.958E-03	-1.311E+00	-4.879E-04
5.920	-5.348E-02	-1.998E-03	-8.566E-01	-3.316E-04
5.960	-2.514E-02	-8.831E-04	-3.197E-01	-9.791E-05
6.000	3.896E-03	2.114E-04	2.150E-01	1.661E-04
6.040	2.876E-02	1.095E-03	6.520E-01	3.910E-04
6.080	4.669E-02	1.703E-03	9.539E-01	5.386E-04
6.120	5.798E-02	2.053E-03	1.130E+00	6.155E-04
6.160	6.070E-02	2.055E-03	1.143E+00	6.465E-04

12345678901234567890123456789012345678901234567890123456789012345678901234567890123456789012345678901234  
 0 1 2 3 4 5 6 7 8 9 10 11

0 1 2 3 4 5 6 7 8 9 10 11  
 123456789012345678901234567890123456789012345678901234567890123456789012345678901234

6.200	5.475E-02	1.747E-03	1.003E+00	6.191E-04
6.240	4.146E-02	1.164E-03	7.293E-01	5.132E-04
6.280	2.166E-02	3.454E-04	3.387E-01	3.477E-04
6.320	-1.865E-03	-5.680E-04	-1.029E-01	1.523E-04
6.360	-2.475E-02	-1.420E-03	-5.193E-01	-4.715E-05
6.400	-4.455E-02	-2.130E-03	-8.687E-01	-2.166E-04
6.440	-5.887E-02	-2.606E-03	-1.106E+00	-3.351E-04
6.480	-6.619E-02	-2.806E-03	-1.211E+00	-3.982E-04
6.520	-6.612E-02	-2.723E-03	-1.181E+00	-4.091E-04
6.560	-5.816E-02	-2.334E-03	-1.002E+00	-3.552E-04
6.600	-4.322E-02	-1.702E-03	-7.019E-01	-2.323E-04
6.640	-2.397E-02	-9.335E-04	-3.321E-01	-6.609E-05
6.680	-3.534E-03	-1.586E-04	4.446E-02	1.066E-04
6.720	1.534E-02	5.357E-04	3.839E-01	2.662E-04
6.760	3.081E-02	1.080E-03	6.525E-01	3.961E-04
6.800	4.132E-02	1.419E-03	8.234E-01	4.843E-04
6.840	4.551E-02	1.505E-03	8.733E-01	5.263E-04
6.880	4.224E-02	1.296E-03	7.823E-01	5.107E-04
6.920	3.065E-02	7.675E-04	5.361E-01	4.280E-04
6.960	1.346E-02	7.971E-05	2.051E-01	2.837E-04
7.000	-4.823E-03	-6.235E-04	-1.370E-01	1.140E-04
7.040	-2.275E-02	-1.293E-03	-4.634E-01	-3.617E-05
7.080	-3.736E-02	-1.796E-03	-7.133E-01	-1.618E-04
7.120	-4.597E-02	-2.058E-03	-8.477E-01	-2.398E-04
7.160	-4.911E-02	-2.124E-03	-8.846E-01	-2.623E-04
7.200	-4.823E-02	-2.050E-03	-8.521E-01	-2.494E-04
7.240	-4.330E-02	-1.813E-03	-7.429E-01	-2.138E-04
7.280	-3.375E-02	-1.406E-03	-5.511E-01	-1.463E-04
7.320	-2.094E-02	-9.901E-04	-3.037E-01	-3.989E-05
7.360	-6.904E-03	-3.534E-04	-4.287E-02	8.249E-05
7.400	5.794E-03	1.055E-04	1.833E-01	1.964E-04
7.440	1.535E-02	4.328E-04	3.457E-01	2.772E-04
7.480	2.121E-02	6.093E-04	4.362E-01	3.250E-04
7.520	2.179E-02	5.699E-04	4.243E-01	3.389E-04
7.560	1.741E-02	3.608E-04	3.275E-01	3.077E-04
7.600	1.012E-02	5.627E-05	1.814E-01	2.376E-04
7.640	8.731E-04	-3.152E-04	3.257E-03	1.604E-04
7.680	-9.945E-03	-7.422E-04	-2.013E-01	7.806E-05
7.720	-2.200E-02	-1.209E-03	-4.257E-01	-1.247E-05
7.760	-3.383E-02	-1.649E-03	-6.406E-01	-1.138E-04
7.800	-4.440E-02	-2.037E-03	-8.304E-01	-2.037E-04
7.840	-5.245E-02	-2.305E-03	-9.651E-01	-2.754E-04
7.880	-5.548E-02	-2.356E-03	-9.983E-01	-3.157E-04
7.920	-5.169E-02	-2.136E-03	-9.011E-01	-2.984E-04
7.960	-4.104E-02	-1.662E-03	-6.788E-01	-2.168E-04
8.000	-2.500E-02	-1.003E-03	-3.635E-01	-8.054E-05
8.040	-6.829E-03	-3.052E-04	-2.447E-02	8.032E-05
8.080	1.099E-02	3.696E-04	3.028E-01	2.283E-04
8.120	2.775E-02	9.847E-04	6.028E-01	3.602E-04
8.160	4.117E-02	1.450E-03	8.336E-01	4.757E-04
8.200	4.949E-02	1.707E-03	9.657E-01	5.556E-04
8.240	5.184E-02	1.732E-03	9.852E-01	5.829E-04
8.280	4.846E-02	1.544E-03	8.998E-01	5.550E-04
8.320	3.965E-02	1.149E-03	7.145E-01	4.830E-04
8.360	2.546E-02	5.514E-04	4.315E-01	3.718E-04
8.400	6.686E-03	-2.028E-04	7.083E-02	2.259E-04
8.440	-1.441E-02	-1.018E-03	-3.233E-01	5.267E-05
8.480	-3.501E-02	-1.785E-03	-6.980E-01	-1.260E-04
8.520	-5.225E-02	-2.395E-03	-9.996E-01	-2.788E-04
8.560	-6.418E-02	-2.783E-03	-1.195E+00	-3.824E-04
8.600	-6.669E-02	-2.747E-03	-1.194E+00	-4.225E-04
8.640	-5.605E-02	-2.207E-03	-9.493E-01	-3.644E-04
8.680	-3.453E-02	-1.290E-03	-5.145E-01	-1.894E-04
8.720	-6.817E-03	-1.885E-04	1.746E-02	5.845E-05
8.760	2.185E-02	8.909E-04	5.444E-01	3.129E-04
8.800	4.648E-02	1.768E-03	9.769E-01	5.256E-04
8.840	6.396E-02	2.344E-03	1.267E+00	6.743E-04
8.880	7.052E-02	2.502E-03	1.376E+00	7.386E-04
8.920	6.700E-02	2.291E-03	1.293E+00	7.036E-04
8.960	5.385E-02	1.668E-03	1.003E+00	5.895E-04
9.000	2.881E-02	5.899E-04	4.967E-01	4.101E-04
9.040	-3.377E-03	-6.492E-04	-1.037E-01	1.521E-04
9.080	-3.220E-02	-1.700E-03	-6.224E-01	-1.291E-04
9.120	-5.443E-02	-2.460E-03	-1.003E+00	-3.396E-04
9.160	-6.688E-02	-2.821E-03	-1.189E+00	-4.415E-04
9.200	-6.871E-02	-2.776E-03	-1.178E+00	-4.497E-04
9.240	-6.217E-02	-2.460E-03	-1.030E+00	-3.927E-04
9.280	-5.311E-02	-2.112E-03	-8.592E-01	-2.982E-04
9.320	-4.394E-02	-1.749E-03	-6.844E-01	-2.158E-04
9.360	-3.316E-02	-1.321E-03	-4.814E-01	-1.470E-04
9.400	-1.978E-02	-7.798E-04	-2.249E-01	-5.789E-05
9.440	-2.496E-03	-7.700E-05	1.099E-01	7.578E-05
9.480	1.802E-02	7.220E-04	4.961E-01	2.470E-04
9.520	3.686E-02	1.394E-03	8.289E-01	4.185E-04
9.560	4.760E-02	1.688E-03	9.878E-01	5.396E-04
9.600	4.681E-02	1.557E-03	9.357E-01	5.544E-04
9.640	3.928E-02	1.204E-03	7.689E-01	4.717E-04
9.680	2.645E-02	6.569E-04	5.083E-01	3.531E-04
9.720	8.284E-03	-8.677E-05	1.545E-01	2.170E-04
9.760	-1.144E-02	-8.209E-04	-2.035E-01	5.690E-05
9.800	-2.816E-02	-1.424E-03	-5.010E-01	-1.000E-04
9.840	-4.119E-02	-1.881E-03	-7.271E-01	-2.155E-04
9.880	-5.091E-02	-2.216E-03	-8.914E-01	-2.809E-04
9.920	-5.789E-02	-2.450E-03	-1.007E+00	-3.287E-04
9.960	-6.119E-02	-2.526E-03	-1.050E+00	-3.658E-04
10.000	-5.868E-02	-2.363E-03	-9.803E-01	-3.631E-04
10.040	-4.922E-02	-1.929E-03	-7.794E-01	-3.028E-04
10.080	-3.454E-02	-1.334E-03	-4.934E-01	-1.784E-04

123456789012345678901234567890123456789012345678901234567890123456789012345678901234  
 0 1 2 3 4 5 6 7 8 9 10 11

0 1 2 3 4 5 6 7 8 9 10 11  
 1234567890123456789012345678901234567890123456789012345678901234567890123456789012345678901234

10.120 -1.864E-02 -7.203E-04 -1.948E-01 -2.689E-05  
 10.160 -2.496E-03 -1.070E-04 1.030E-01 1.099E-04  
 10.200 1.280E-02 4.613E-04 3.787E-01 2.265E-04  
 10.240 2.647E-02 9.556E-04 6.199E-01 3.287E-04  
 10.280 3.656E-02 1.291E-03 7.888E-01 4.240E-04  
 10.320 4.033E-02 1.353E-03 8.299E-01 4.745E-04  
 10.360 3.495E-02 1.044E-03 6.933E-01 4.505E-04  
 10.400 2.135E-02 4.626E-04 4.172E-01 3.419E-04  
 10.440 5.196E-03 -1.625E-04 1.124E-01 1.856E-04  
 10.480 -9.846E-03 -7.082E-04 -1.580E-01 3.805E-05  
 10.520 -2.035E-02 -1.057E-03 -3.330E-01 -5.887E-05  
 10.560 -2.697E-02 -1.275E-03 -4.401E-01 -9.984E-05  
 10.600 -3.170E-02 -1.436E-03 -5.173E-01 -1.147E-04  
 10.640 -3.462E-02 -1.519E-03 -5.610E-01 -1.410E-04  
 10.680 -3.397E-02 -1.454E-03 -5.363E-01 -1.606E-04  
 10.720 -2.912E-02 -1.228E-03 -4.325E-01 -1.348E-04  
 10.760 -2.040E-02 -8.507E-04 -2.540E-01 -5.718E-05  
 10.800 -7.595E-03 -3.210E-04 -1.424E-03 4.886E-05  
 10.840 7.459E-03 2.574E-04 2.784E-01 1.682E-04  
 10.880 2.077E-02 7.304E-04 5.125E-01 2.877E-04  
 10.920 3.004E-02 1.039E-03 6.681E-01 3.806E-04  
 10.960 3.513E-02 1.189E-03 7.452E-01 4.200E-04  
 11.000 3.571E-02 1.152E-03 7.328E-01 4.205E-04  
 11.040 2.978E-02 8.499E-04 5.962E-01 3.869E-04  
 11.080 1.724E-02 3.181E-04 3.453E-01 3.010E-04  
 11.120 2.301E-03 -2.550E-04 6.615E-02 1.665E-04  
 11.160 -1.139E-02 -7.621E-04 -1.836E-01 2.931E-05  
 11.200 -2.351E-02 -1.208E-03 -4.006E-01 -6.704E-05  
 11.240 -3.413E-02 -1.587E-03 -5.852E-01 -1.377E-04  
 11.280 -4.059E-02 -1.770E-03 -6.818E-01 -2.001E-04  
 11.320 -4.003E-02 -1.674E-03 -6.464E-01 -2.272E-04  
 11.360 -3.289E-02 -1.340E-03 -4.908E-01 -1.718E-04  
 11.400 -2.111E-02 -8.482E-04 -2.554E-01 -6.232E-05  
 11.440 -6.531E-03 -2.663E-04 2.422E-02 6.160E-05  
 11.480 1.021E-02 3.917E-04 3.398E-01 1.897E-04  
 11.520 2.838E-02 1.087E-03 6.761E-01 3.330E-04  
 11.560 4.506E-02 1.691E-03 9.727E-01 4.766E-04  
 11.600 5.698E-02 2.082E-03 1.171E+00 5.912E-04  
 11.640 6.175E-02 2.178E-03 1.228E+00 6.454E-04  
 11.680 5.751E-02 1.912E-03 1.111E+00 6.199E-04  
 11.720 4.323E-02 1.263E-03 8.087E-01 5.180E-04  
 11.760 1.969E-02 2.740E-04 3.399E-01 3.335E-04  
 11.800 -1.096E-02 -9.545E-04 -2.489E-01 8.563E-05  
 11.840 -4.530E-02 -2.287E-03 -6.928E-01 -2.015E-04  
 11.880 -8.039E-02 -3.620E-03 -1.539E+00 -4.886E-04  
 11.920 -1.082E-01 -4.654E-03 -2.123E+00 -7.448E-04  
 11.960 -1.178E-01 -4.974E-03 -2.495E+00 -8.740E-04  
 12.000 -1.123E-01 -4.718E-03 -2.568E+00 -8.129E-04  
 12.040 -9.805E-02 -4.121E-03 -2.347E+00 -6.431E-04  
 12.080 -7.384E-02 -3.060E-03 -1.850E+00 -4.529E-04  
 12.120 -3.792E-02 -1.600E-03 -1.157E+00 -2.113E-04  
 12.160 3.409E-03 2.494E-06 -3.930E-01 1.262E-04  
 12.200 4.469E-02 1.559E-03 3.764E-01 4.981E-04  
 12.240 7.688E-02 2.747E-03 1.036E+00 8.032E-04  
 12.280 8.930E-02 3.440E-03 1.543E+00 9.378E-04  
 12.320 9.336E-02 3.765E-03 1.845E+00 8.929E-04  
 12.360 8.978E-02 3.644E-03 1.892E+00 7.825E-04  
 12.400 7.805E-02 3.156E-03 1.688E+00 6.687E-04  
 12.440 5.795E-02 2.290E-03 1.281E+00 5.352E-04  
 12.480 2.889E-02 1.108E-03 7.211E-01 3.328E-04  
 12.520 -4.648E-03 -1.939E-04 9.236E-02 5.157E-05  
 12.560 -3.786E-02 -1.443E-03 -5.186E-01 -2.509E-04  
 12.600 -6.755E-02 -2.519E-03 -1.047E+00 -5.066E-04  
 12.640 -8.795E-02 -3.220E-03 -1.432E+00 -6.857E-04  
 12.680 -9.456E-02 -3.481E-03 -1.625E+00 -7.488E-04  
 12.720 -9.106E-02 -3.320E-03 -1.613E+00 -6.906E-04  
 12.760 -8.101E-02 -2.889E-03 -1.419E+00 -5.752E-04  
 12.800 -6.416E-02 -2.185E-03 -1.078E+00 -4.502E-04  
 12.840 -4.038E-02 -1.204E-03 -6.214E-01 -2.854E-04  
 12.880 -1.378E-02 -1.859E-04 -1.277E-01 -6.345E-05  
 12.920 1.053E-02 7.005E-04 3.094E-01 1.662E-04  
 12.960 2.921E-02 1.343E-03 6.300E-01 3.395E-04  
 13.000 4.065E-02 1.696E-03 8.089E-01 4.285E-04  
 13.040 4.448E-02 1.754E-03 8.450E-01 4.518E-04  
 13.080 4.000E-02 1.493E-03 7.286E-01 4.244E-04  
 13.120 2.739E-02 9.322E-04 4.689E-01 3.383E-04  
 13.160 7.935E-03 1.247E-04 8.281E-02 1.827E-04  
 13.200 -1.591E-02 -8.085E-04 -3.680E-01 -1.704E-05  
 13.240 -3.857E-02 -1.635E-03 -7.746E-01 -2.201E-04  
 13.280 -5.532E-02 -2.196E-03 -1.057E+00 -3.790E-04  
 13.320 -6.384E-02 -2.428E-03 -1.180E+00 -4.610E-04  
 13.360 -6.435E-02 -2.368E-03 -1.158E+00 -4.606E-04  
 13.400 -5.857E-02 -2.078E-03 -1.024E+00 -4.069E-04  
 13.440 -4.607E-02 -1.538E-03 -7.703E-01 -3.178E-04  
 13.480 -3.000E-02 -9.075E-04 -4.656E-01 -1.836E-04  
 13.520 -1.234E-02 -2.076E-04 -1.293E-01 -3.236E-05  
 13.560 7.536E-03 5.562E-04 2.396E-01 1.213E-04  
 13.600 2.552E-02 1.201E-03 5.572E-01 2.738E-04  
 13.640 3.889E-02 1.660E-03 7.859E-01 3.975E-04  
 13.680 4.725E-02 1.921E-03 9.187E-01 4.697E-04  
 13.720 4.989E-02 1.956E-03 9.423E-01 4.932E-04  
 13.760 4.603E-02 1.737E-03 8.445E-01 4.688E-04  
 13.800 3.552E-02 1.266E-03 6.244E-01 3.907E-04  
 13.840 1.837E-02 5.406E-04 2.820E-01 2.638E-04  
 13.880 -4.275E-03 -3.532E-04 -1.480E-01 8.518E-05  
 13.920 -2.533E-02 -1.106E-03 -5.220E-01 -1.178E-04  
 13.960 -3.956E-02 -1.573E-03 -7.593E-01 -2.673E-04  
 14.000 -4.671E-02 -1.773E-03 -8.632E-01 -3.253E-04

1234567890123456789012345678901234567890123456789012345678901234567890123456789012345678901234





0 1 2 3 4 5 6 7 8 9 10 11  
12345678901234567890123456789012345678901234567890123456789012345678901234567890123456789012345678901234

5.480 -1.626E+02 1.960E-01 -8.274E+02 0.000E+00 -5.640E-03 -3.434E-03  
5.520 -1.968E+02 1.960E-01 -8.549E+02 0.000E+00 -9.059E-02 -3.434E-03  
5.560 -2.381E+02 1.960E-01 -8.840E+02 0.000E+00 4.082E-03 -3.434E-02  
5.600 -2.746E+02 1.960E-01 -9.119E+02 0.000E+00 8.856E+03 -3.434E-03  
5.640 -3.162E+02 1.964E-01 -9.272E+02 0.000E+00 1.292E-04 -3.293E-03  
5.680 -4.717E+02 2.038E-01 -9.041E+02 0.000E+00 1.428E+04 -2.651E-03  
5.720 -5.066E+02 2.153E-01 -9.245E+02 0.000E+00 1.461E-04 -1.427E-03  
5.760 -4.733E+02 2.264E-01 -9.399E+02 0.000E+00 1.430E+04 -2.413E-04  
5.800 -3.976E+02 2.345E-01 -9.573E+02 0.000E+00 1.355E+04 5.911E-04  
5.840 -3.022E+02 2.375E-01 -9.751E+02 0.000E+00 1.256E+04 8.757E-04  
5.880 -2.813E+02 2.375E-01 -9.626E+02 0.000E+00 1.000E+04 8.757E-04  
5.920 -2.584E+02 2.375E-01 -9.407E+02 0.000E+00 6.206E+03 8.757E-04  
5.960 -2.239E+02 2.375E-01 -9.152E+02 0.000E+00 1.830E+03 8.757E-04  
6.000 -1.884E+02 2.375E-01 -8.902E+02 0.000E+00 -2.459E+03 8.757E-04  
6.040 -1.606E+02 2.375E-01 -8.697E+02 0.000E+00 -5.941E+03 8.757E-04  
6.080 -1.449E+02 2.375E-01 -8.555E+02 0.000E+00 -8.359E+03 8.757E-04  
6.120 -1.378E+02 2.375E-01 -8.471E+02 0.000E+00 -9.788E+03 8.757E-04  
6.160 -1.352E+02 2.375E-01 -8.467E+02 0.000E+00 -9.829E+03 8.757E-04  
6.200 -1.414E+02 2.375E-01 -8.536E+02 0.000E+00 -8.619E+03 8.757E-04  
6.240 -1.587E+02 2.375E-01 -8.667E+02 0.000E+00 -6.355E+03 8.757E-04  
6.280 -1.832E+02 2.375E-01 -8.853E+02 0.000E+00 -3.159E+03 8.757E-04  
6.320 -2.099E+02 2.375E-01 -9.062E+02 0.000E+00 4.337E+02 8.757E-04  
6.360 -2.359E+02 2.375E-01 -9.258E+02 0.000E+00 3.785E+03 8.757E-04  
6.400 -2.571E+02 2.375E-01 -9.422E+02 0.000E+00 6.591E+03 8.757E-04  
6.440 -2.705E+02 2.375E-01 -9.534E+02 0.000E+00 8.490E+03 8.757E-04  
6.480 -2.762E+02 2.375E-01 -9.582E+02 0.000E+00 9.303E+03 8.757E-04  
6.520 -2.753E+02 2.375E-01 -9.566E+02 0.000E+00 8.998E+03 8.757E-04  
6.560 -2.653E+02 2.375E-01 -9.479E+02 0.000E+00 7.488E+03 8.757E-04  
6.600 -2.465E+02 2.375E-01 -9.336E+02 0.000E+00 5.020E+03 8.757E-04  
6.640 -2.236E+02 2.375E-01 -9.162E+02 0.000E+00 2.017E+03 8.757E-04  
6.680 -2.005E+02 2.375E-01 -8.984E+02 0.000E+00 -1.032E+03 8.757E-04  
6.720 -1.795E+02 2.375E-01 -8.824E+02 0.000E+00 -3.770E+03 8.757E-04  
6.760 -1.641E+02 2.375E-01 -8.697E+02 0.000E+00 -5.926E+03 8.757E-04  
6.800 -1.545E+02 2.375E-01 -8.617E+02 0.000E+00 -7.285E+03 8.757E-04  
6.840 -1.506E+02 2.375E-01 -8.595E+02 0.000E+00 -7.644E+03 8.757E-04  
6.880 -1.556E+02 2.375E-01 -8.640E+02 0.000E+00 -6.847E+03 8.757E-04  
6.920 -1.692E+02 2.375E-01 -8.759E+02 0.000E+00 -4.784E+03 8.757E-04  
6.960 -1.899E+02 2.375E-01 -8.916E+02 0.000E+00 -2.085E+03 8.757E-04  
7.000 -2.132E+02 2.375E-01 -9.076E+02 0.000E+00 6.573E+02 8.757E-04  
7.040 -2.326E+02 2.375E-01 -9.231E+02 0.000E+00 3.298E+03 8.757E-04  
7.080 -2.479E+02 2.375E-01 -9.348E+02 0.000E+00 5.296E+03 8.757E-04  
7.120 -2.557E+02 2.375E-01 -9.410E+02 0.000E+00 6.343E+03 8.757E-04  
7.160 -2.567E+02 2.375E-01 -9.427E+02 0.000E+00 6.625E+03 8.757E-04  
7.200 -2.536E+02 2.375E-01 -9.411E+02 0.000E+00 6.356E+03 8.757E-04  
7.240 -2.482E+02 2.375E-01 -9.359E+02 0.000E+00 5.439E+03 8.757E-04  
7.280 -2.374E+02 2.375E-01 -9.266E+02 0.000E+00 3.839E+03 8.757E-04  
7.320 -2.219E+02 2.375E-01 -9.149E+02 0.000E+00 1.820E+03 8.757E-04  
7.360 -2.051E+02 2.375E-01 -9.026E+02 0.000E+00 -2.866E+02 8.757E-04  
7.400 -1.911E+02 2.375E-01 -8.920E+02 0.000E+00 -2.094E+03 8.757E-04  
7.440 -1.823E+02 2.375E-01 -8.844E+02 0.000E+00 -3.393E+03 8.757E-04  
7.480 -1.762E+02 2.375E-01 -8.802E+02 0.000E+00 -4.110E+03 8.757E-04  
7.520 -1.760E+02 2.375E-01 -8.809E+02 0.000E+00 -3.969E+03 8.757E-04  
7.560 -1.830E+02 2.375E-01 -8.856E+02 0.000E+00 -3.153E+03 8.757E-04  
7.600 -1.935E+02 2.375E-01 -8.924E+02 0.000E+00 -1.975E+03 8.757E-04  
7.640 -2.035E+02 2.375E-01 -9.009E+02 0.000E+00 -5.225E+02 8.757E-04  
7.680 -2.149E+02 2.375E-01 -9.106E+02 0.000E+00 1.158E+03 8.757E-04  
7.720 -2.272E+02 2.375E-01 -9.213E+02 0.000E+00 3.002E+03 8.757E-04  
7.760 -2.404E+02 2.375E-01 -9.315E+02 0.000E+00 4.735E+03 8.757E-04  
7.800 -2.517E+02 2.375E-01 -9.404E+02 0.000E+00 6.264E+03 8.757E-04  
7.840 -2.611E+02 2.375E-01 -9.467E+02 0.000E+00 7.331E+03 8.757E-04  
7.880 -2.645E+02 2.375E-01 -9.481E+02 0.000E+00 7.544E+03 8.757E-04  
7.920 -2.594E+02 2.375E-01 -9.433E+02 0.000E+00 6.695E+03 8.757E-04  
7.960 -2.459E+02 2.375E-01 -9.326E+02 0.000E+00 4.847E+03 8.757E-04  
8.000 -2.257E+02 2.375E-01 -9.176E+02 0.000E+00 2.274E+03 8.757E-04  
8.040 -2.040E+02 2.375E-01 -9.017E+02 0.000E+00 -4.607E+02 8.757E-04  
8.080 -1.849E+02 2.375E-01 -8.862E+02 0.000E+00 -3.113E+03 8.757E-04  
8.120 -1.685E+02 2.375E-01 -8.720E+02 0.000E+00 -5.553E+03 8.757E-04  
8.160 -1.541E+02 2.375E-01 -8.612E+02 0.000E+00 -7.397E+03 8.757E-04  
8.200 -1.449E+02 2.375E-01 -8.551E+02 0.000E+00 -8.422E+03 8.757E-04  
8.240 -1.436E+02 2.375E-01 -8.543E+02 0.000E+00 -8.536E+03 8.757E-04  
8.280 -1.496E+02 2.375E-01 -8.584E+02 0.000E+00 -7.817E+03 8.757E-04  
8.320 -1.612E+02 2.375E-01 -8.673E+02 0.000E+00 -6.286E+03 8.757E-04  
8.360 -1.777E+02 2.375E-01 -8.808E+02 0.000E+00 -3.953E+03 8.757E-04  
8.400 -1.981E+02 2.375E-01 -8.980E+02 0.000E+00 -9.893E+02 8.757E-04  
8.440 -2.220E+02 2.375E-01 -9.166E+02 0.000E+00 2.218E+03 8.757E-04  
8.480 -2.458E+02 2.375E-01 -9.343E+02 0.000E+00 5.236E+03 8.757E-04  
8.520 -2.644E+02 2.375E-01 -9.484E+02 0.000E+00 7.644E+03 8.757E-04  
8.560 -2.760E+02 2.375E-01 -9.575E+02 0.000E+00 9.193E+03 8.757E-04  
8.600 -2.782E+02 2.375E-01 -9.572E+02 0.000E+00 9.095E+03 8.757E-04  
8.640 -2.660E+02 2.375E-01 -9.452E+02 0.000E+00 6.987E+03 8.757E-04  
8.680 -2.381E+02 2.375E-01 -9.244E+02 0.000E+00 3.408E+03 8.757E-04  
8.720 -2.032E+02 2.375E-01 -8.993E+02 0.000E+00 -8.939E+02 8.757E-04  
8.760 -1.698E+02 2.375E-01 -8.746E+02 0.000E+00 -5.133E+03 8.757E-04  
8.800 -1.436E+02 2.375E-01 -8.543E+02 0.000E+00 -8.599E+03 8.757E-04  
8.840 -1.429E+02 2.377E-01 -8.452E+02 0.000E+00 -1.076E+04 8.567E-04  
8.880 -1.610E+02 2.403E-01 -8.482E+02 0.000E+00 -1.097E+04 6.387E-04  
8.920 -1.295E+02 2.413E-01 -8.423E+02 0.000E+00 -1.037E+04 5.498E-04  
8.960 -1.481E+02 2.413E-01 -8.560E+02 0.000E+00 -7.984E+03 5.498E-04  
9.000 -1.759E+02 2.413E-01 -8.803E+02 0.000E+00 -3.761E+03 5.498E-04  
9.040 -2.127E+02 2.413E-01 -9.089E+02 0.000E+00 1.143E+02 5.498E-04  
9.080 -2.489E+02 2.413E-01 -9.330E+02 0.000E+00 5.245E+03 5.498E-04  
9.120 -2.738E+02 2.413E-01 -9.507E+02 0.000E+00 8.246E+03 5.498E-04  
9.160 -2.828E+02 2.413E-01 -9.594E+02 0.000E+00 9.713E+03 5.498E-04  
9.200 -2.806E+02 2.413E-01 -9.587E+02 0.000E+00 9.584E+03 5.498E-04  
9.240 -2.701E+02 2.413E-01 -9.517E+02 0.000E+00 8.358E+03 5.498E-04  
9.280 -2.562E+02 2.413E-01 -9.437E+02 0.000E+00 7.003E+03 5.498E-04  
9.320 -2.461E+02 2.413E-01 -9.355E+02 0.000E+00 5.594E+03 5.498E-04  
9.360 -2.372E+02 2.413E-01 -9.257E+02 0.000E+00 3.899E+03 5.498E-04

1234567890123456789012345678901234567890123456789012345678901234567890123456789012345678901234  
0 1 2 3 4 5 6 7 8 9 10 11



0 1 2 3 4 5 6 7 8 9 10 11  
 123456789012345678901234567890123456789012345678901234567890123456789012345678901234

13.320	-2.729E+02	3.328E-01	-1.343E+01	0.000E+00	9.832E-03	1.568E-03
13.360	-2.701E+02	3.328E-01	-1.231E+01	0.000E+00	9.626E+03	1.568E-03
13.400	-2.616E+02	3.328E-01	-5.936E+00	0.000E+00	8.519E+03	1.568E-03
13.440	-2.476E+02	3.328E-01	6.277E+00	0.000E+00	6.402E+03	1.568E-03
13.480	-2.279E+02	3.328E-01	2.072E+01	0.000E+00	3.922E+03	1.568E-03
13.520	-2.076E+02	3.328E-01	3.660E+01	0.000E+00	1.194E+03	1.568E-03
13.560	-1.869E+02	3.328E-01	5.417E+01	0.000E+00	-1.828E+03	1.568E-03
13.600	-1.678E+02	3.328E-01	6.913E+01	0.000E+00	-4.382E+03	1.568E-03
13.640	-1.532E+02	3.328E-01	7.976E+01	0.000E+00	-6.189E+03	1.568E-03
13.680	-1.450E+02	3.328E-01	8.595E+01	0.000E+00	-7.236E+03	1.568E-03
13.720	-1.437E+02	3.328E-01	8.697E+01	0.000E+00	-7.397E+03	1.568E-03
13.760	-1.493E+02	3.328E-01	8.220E+01	0.000E+00	-6.557E+03	1.568E-03
13.800	-1.623E+02	3.328E-01	7.162E+01	0.000E+00	-4.722E+03	1.568E-03
13.840	-1.808E+02	3.328E-01	5.523E+01	0.000E+00	-1.884E+03	1.568E-03
13.880	-2.061E+02	3.328E-01	3.473E+01	0.000E+00	1.642E+03	1.568E-03
13.920	-2.339E+02	3.328E-01	1.732E+01	0.000E+00	4.601E+03	1.568E-03
13.960	-2.506E+02	3.328E-01	6.462E+00	0.000E+00	6.430E+03	1.568E-03
14.000	-2.542E+02	3.328E-01	1.642E+00	0.000E+00	7.244E+03	1.568E-03
14.040	-2.512E+02	3.328E-01	1.617E+00	0.000E+00	7.247E+03	1.568E-03
14.080	-2.463E+02	3.328E-01	5.045E+00	0.000E+00	6.654E+03	1.568E-03
14.120	-2.389E+02	3.328E-01	1.228E+01	0.000E+00	5.39E+03	1.568E-03
14.160	-2.262E+02	3.328E-01	2.408E+01	0.000E+00	3.348E+03	1.568E-03
14.200	-2.077E+02	3.328E-01	3.864E+01	0.000E+00	8.422E+02	1.568E-03
14.240	-1.868E+02	3.328E-01	5.139E+01	0.000E+00	-1.322E+03	1.568E-03
14.280	-1.754E+02	3.328E-01	5.792E+01	0.000E+00	-2.408E+03	1.568E-03
14.320	-1.767E+02	3.328E-01	5.642E+01	0.000E+00	-2.122E+03	1.568E-03
14.360	-1.883E+02	3.328E-01	4.990E+01	0.000E+00	-1.002E+03	1.568E-03
14.400	-2.021E+02	3.328E-01	4.229E+01	0.000E+00	2.912E+02	1.568E-03
14.440	-2.115E+02	3.328E-01	3.403E+01	0.000E+00	1.708E+03	1.568E-03
14.480	-2.201E+02	3.328E-01	2.470E+01	0.000E+00	3.322E+03	1.568E-03
14.520	-2.306E+02	3.328E-01	1.693E+01	0.000E+00	4.650E+03	1.568E-03
14.560	-2.394E+02	3.328E-01	1.253E+01	0.000E+00	5.385E+03	1.568E-03
14.600	-2.401E+02	3.328E-01	1.128E+01	0.000E+00	5.587E+03	1.568E-03
14.640	-2.366E+02	3.328E-01	1.390E+01	0.000E+00	5.127E+03	1.568E-03
14.680	-2.288E+02	3.328E-01	2.130E+01	0.000E+00	3.840E+03	1.568E-03
14.720	-2.152E+02	3.328E-01	3.223E+01	0.000E+00	1.953E+03	1.568E-03
14.760	-1.990E+02	3.328E-01	4.350E+01	0.000E+00	2.501E+01	1.568E-03
14.800	-1.838E+02	3.328E-01	5.287E+01	0.000E+00	-1.565E+03	1.568E-03
14.840	-1.768E+02	3.328E-01	5.890E+01	0.000E+00	-2.586E+03	1.568E-03
14.880	-1.761E+02	3.328E-01	6.214E+01	0.000E+00	-3.146E+03	1.568E-03
14.920	-1.753E+02	3.328E-01	6.390E+01	0.000E+00	-3.449E+03	1.568E-03
14.960	-1.745E+02	3.328E-01	6.216E+01	0.000E+00	-3.131E+03	1.568E-03
15.000	-1.798E+02	3.328E-01	5.620E+01	0.000E+00	-2.088E+03	1.568E-03
15.040	-1.915E+02	3.328E-01	4.847E+01	0.000E+00	-7.607E+02	1.568E-03
15.080	-2.052E+02	3.328E-01	3.976E+01	0.000E+00	7.289E+02	1.568E-03
15.120	-2.170E+02	3.328E-01	2.882E+01	0.000E+00	2.616E+03	1.568E-03
15.160	-2.292E+02	3.328E-01	1.697E+01	0.000E+00	4.657E+03	1.568E-03
15.200	-2.427E+02	3.328E-01	8.141E+00	0.000E+00	6.157E+03	1.568E-03
15.240	-2.509E+02	3.328E-01	4.076E+00	0.000E+00	6.829E+03	1.568E-03
15.280	-2.497E+02	3.328E-01	4.277E+00	0.000E+00	6.784E+03	1.568E-03
15.320	-2.427E+02	3.328E-01	7.787E+00	0.000E+00	6.178E+03	1.568E-03
15.360	-2.342E+02	3.328E-01	1.566E+01	0.000E+00	4.812E+03	1.568E-03
15.400	-2.217E+02	3.328E-01	2.702E+01	0.000E+00	2.848E+03	1.568E-03
15.440	-2.048E+02	3.328E-01	3.887E+01	0.000E+00	8.181E+02	1.568E-03
15.480	-1.898E+02	3.328E-01	4.967E+01	0.000E+00	-1.025E+03	1.568E-03
15.520	-1.800E+02	3.328E-01	5.746E+01	0.000E+00	-2.348E+03	1.568E-03
15.560	-1.755E+02	3.328E-01	6.024E+01	0.000E+00	-2.805E+03	1.568E-03
15.600	-1.773E+02	3.328E-01	5.822E+01	0.000E+00	-2.445E+03	1.568E-03
15.640	-1.866E+02	3.328E-01	5.167E+01	0.000E+00	-1.308E+03	1.568E-03
15.680	-2.011E+02	3.328E-01	4.155E+01	0.000E+00	4.321E+02	1.568E-03
15.720	-2.154E+02	3.328E-01	3.216E+01	0.000E+00	2.030E+03	1.568E-03
15.760	-2.232E+02	3.328E-01	2.589E+01	0.000E+00	3.093E+03	1.568E-03
15.800	-2.261E+02	3.328E-01	2.196E+01	0.000E+00	3.764E+03	1.568E-03
15.840	-2.277E+02	3.328E-01	2.001E+01	0.000E+00	4.098E+03	1.568E-03
15.880	-2.285E+02	3.328E-01	2.160E+01	0.000E+00	3.810E+03	1.568E-03
15.920	-2.224E+02	3.328E-01	2.625E+01	0.000E+00	3.000E+03	1.568E-03
15.960	-2.129E+02	3.328E-01	3.185E+01	0.000E+00	2.043E+03	1.568E-03
16.000	-2.056E+02	3.328E-01	3.751E+01	0.000E+00	1.073E+03	1.568E-03

maximum absolute values  
 maximum 6.319E+02 3.328E-01 1.609E+03 0.000E+00 1.573E+04 3.798E-03  
 time 2.240E+00 1.276E+01 2.400E+00 0.000E+00 2.240E+00 1.204E+01

123456789012345678901234567890123456789012345678901234567890123456789012345678901234  
 0 1 2 3 4 5 6 7 8 9 10 11



## Appendix C

# Discrete Foundation Element Subroutines Added to NEABS Coding

```

0          1          2          3          4          5          6          7
12345678901234567890123456789012345678901234567890123456789012345678
-----
c          ***** DF1 subroutine ***** jm
c          subroutine df1 jm
c          implicit double precision(a-h,o-z), integer(i-n) jm
c          common/big/a(99000) jm
          common/epar/ npar(14),numnp,neltyp,numel,nelcount,numnel, jm
          +          neq,mband,mtot,nnn(7) jm
c          ** Subroutine DF1 by W. Cofer & J. McGuire, 12/10/92 ** jm
c          ** This subroutine allocates space in the global 'a' matrix ** jm
c          ** for temporary storage of discrete foundation (DF) element ** jm
c          ** data prior to its permanent storage on tape. ** jm
c          ** Variable list: ** jm
c          ** 'mtype' = 6 (for element type 6--DF element ** jm
c          ** 'numssi' = number of DF elements ** jm
c          ** 'npset' = number of element property sets ** jm
c          ** 'n1' = location in 'a' of beginning of nodal fixity ** jm
c          ** codes (n1=1 set in SETUP) ** jm
c          ** 'n2' = location in 'a' of beginning of nodal x-coord** jm
c          ** 'n3' = location in 'a' of beginning of nodal y-coord** jm
c          ** 'n4' = location in 'a' of beginning of nodal z-coord** jm
c          ** 'n5' = location in 'a' of beginning of element ** jm
c          ** linear/nonlinear indicators ** jm
c          ** 'n6' = location in 'a' of beginning of element ** jm
c          ** stiffness data ** jm
c          ** 'n7' = location in 'a' of beginning of element ** jm
c          ** damping data ** jm
c          ** 'n8' = location in 'a' of beginning of element ** jm
c          ** mass data ** jm
c          ** 'n9' = location in 'a' just after end of element ** jm
c          ** mass data, (end of DF data storage in 'a') ** jm
c          write(*,7777) 1 jm
c          numdof = 6 jm
c          nkpar = 9 jm
c          ncpair = 1 jm
c          nmpair = 2 jm
c          nelpar = 10 jm
c          nlsv1 = 11 jm
c          nlsv2 = 17 jm
c          mtype = npar(1) jm
c          numssi = npar(2) jm
c          npset = npar(3) jm
          if ((mtype.ne.6).or.(numssi.lt.1).or.(npset.lt.1)) then jm
-----
12345678901234567890123456789012345678901234567890123456789012345678
0          1          2          3          4          5          6          7

```

0 1 2 3 4 5 6 7  
 123456789012345678901234567890123456789012345678901234567890123456789012345678

```

      write (31,4010)
      stop
    end if
    if (numssi+nelcount.gt.numel) then
      write (31,4020)
      stop
    end if
  c
  n1 = nnn(1)
  n2 = nnn(2)
  n3 = nnn(3)
  n4 = nnn(4)
  n5 = nnn(5)
  n6 = nnn(6)
  n7 = n6 + npset *numdof*nkpar
  n8 = n7 + npset *numdof*ncpar
  n9 = n8 + npset *numdof*nmpar
  n10 = n9 + numssi*nelpar
  n11 = n10 + numdof*nlsv1
  n12 = n11 + numdof*nlsv2
  last = n12
  c
  if (last.ge.mtot) then
    iover = last - mot
  c   write(*,7778) 3
    call error (1,iover,7hbeam )
  c   write(*,7777) 4
  end if
  c
  c   write(*,7778) 4
  call df2 (numnp,      numel,      nelcount, mband,
+          mtype,      numssi,      npset,      nlsv1,      nlsv2,
+          numdof,      nkpar,      ncpar,      nmpar,      nelpar,
+          a(n1),      a(n2),      a(n3),      a(n4),      a(n5),
+          a(n6),      a(n7),      a(n8),      a(n9),
+          a(n10),     a(n11)
  c   write(*,7777) 5
  c
  c   write(*,7778) 5
  return
  c
  4010 format (1x,'ERROR:  1')
  4020 format (1x,'ERROR:  2')
  7777 format (1x,'DF1 enter ',i2)
  7778 format (1x,'DF1 exit ',i2)
  7779 format (1x,'DF1 stop ',i2)
  c
  end
  c
  c
  c
  c   ***** DF2 subroutine *****
  c
  subroutine df2 ( numnp,      numel,      nelcount, mband,
+                mtype,      numssi,      npset,      nlsv1,      nlsv2,
+                numdof,      nkpar,      ncpar,      nmpar,      nelpar,
+                id,          x,          y,          z,          ind,
+                qssi,      cssi,      wssi,      iessi,
+                rnlm1,      rnlm2
  c
  c   implicit      double precision(a-h,o-z), integer(i-n)
  c   dimension     id(numnp,numdof),x(numnp),y(numnp),z(numnp),ind(numel)
+                ,qssi(npset,numdof,nkpar), cssi(npset,numdof,ncpar),
+                wssi(npset,numdof,nmpar), iessi(numssi,nelpar),
+                rnlm1(numdof,nlsv1), rnlm2(numdof,nlsv2),
+                told(3,3), emul(3,4)
  c   common/emtx/lm(24),nd,ns,asa(24,24),rf(24,4),xm(24),sa(12,24),
+                sf(12,4),enpar(24),s(12,12),f(48),
+                lms(12),ec(12),t(3,3),q(45),
+                aca(24,24),ca(12,24),c(12,12)
  c   common/misc/nfn,ngm,nt,not,dt,alfa,beta,intg,igm(3),fgm(3),
+                kk1,kk2,nrflg

```

1234567890123456789012345678901234567890123456789012345678901234567890123456789012345678  
 0 1 2 3 4 5 6 7

0 1 2 3 4 5 6 7  
 12345678901234567890123456789012345678901234567890123456789012345678

```

c      ** Subroutine DF2 by W. Cofer & J. McGuire, 12/10/92      ** jm
c      ** This subroutine reads DF element data from the input file, ** jm
c      ** manages the creation of DF element stiffness, damping, and ** jm
c      ** mass matrices (performed in subroutine DF3), and writes ** jm
c      ** element data to tape for permanent storage.            ** jm
c      write (*,7777) 1
c      ** INITIALIZE VARIABLES
c      rewind (13)
c      rewind (14)
c      rewind (15)
c      rewind (16)
c      iflag1 = 0
c      iflag2 = 0
c      iflag3 = 0
c      igen = 0
c      nind = 1
c      nd = 12
c      ns = 12
c      ndeclare = 3
c      ldeclare = numssi
c      do 310 i = 1,24
c         lm(i) = 0
c      310 continue
c      do 320 i = 1,1352
c         stif(i) = 0.0
c      320 continue
c      do 370 i = 1,(npset+1)
c         do 360 j = 1,numdof
c            do 330 k = 1,nkpar
c               qssi(i,j,k) = 0.0
c      330          continue
c            do 340 k = 1,nmpar
c               cssi(i,j,k) = 0.0
c      340          continue
c            do 350 k = 1,nmpar
c               wssi(i,j,k) = 0.0
c      350          continue
c      360          continue
c      370          continue
c         do 390 i = 1,(numssi+1)
c            do 380 j = 1,nelpar
c               iessi(i,j) = 0
c      380          continue
c      390          continue
c      ** PRINT DF ELEMENT CONTROL DATA      ** jm
c      write (31,2010) numssi, npset
c      ** READ & PRINT DF ELEMENT PROPERTIES: STIFFNESS PARAMETERS ** jm
c      do 410 il=1,npset*numdof
c         iflag1 = 0
c         read (21,1010) np,idof
c         if ((np.lt.1).or.(np.gt.npset)) then
c            if ((il.eq.1).or.((idof.lt.1).or.(idof.gt.numdof))) then
c               ERROR: DF element property set number or degree-of-
c                  freedom number outside of applicable range.
c            write (31,4010)
c            stop
c         end if
c         if (np.eq.0) then
c            np = npp
c         end if
c         end if
c         do 400 k=1,nkpar
c            if ((qssi(np,idof,k).ne.0.0).and.(iflag1.eq.0)) then

```

12345678901234567890123456789012345678901234567890123456789012345678  
 0 1 2 3 4 5 6 7

0 1 2 3 4 5 6 7  
 123456789012345678901234567890123456789012345678901234567890123456789012345678

```

    iflag1 = 1
    WARNING: the stiffness properties of this degree-of-
    freedom for this element property set number
    have already been specified; will now overwrite.
    write (31,3010) np,idof
  end if
400 continue
  backspace (21)
  read (21,1010) np,idof,(qssi(np,idof,k),k=1,nkpar)
  npp = np
410 continue
  write (31,2020)
  do 430 i=1,npset
    do 420 j=1,numdof
      write (31,2030) i,j,(qssi(i,j,k),k=1,nkpar)
    end do
  end do
420 continue
430 continue
c
c ** READ & PRINT DF ELEMENT PROPERTIES: DAMPING PARAMETERS **
c
do 450 il=1,npset*numdof
  iflag1 = 0
  read (21,1020) np,idof
  if ((np.lt.1).or.(np.gt.npset)) then
    if ((il.eq.1).or.((idof.lt.1).or.(idof.gt.numdof))) then
      ERROR: DF element property set number or degree-of-
      freedom number outside of applicable range.
      write (31,4020)
      stop
    end if
    if (np.eq.0) then
      np = npp
    end if
  end if
  do 440 k=1,nkpar
    if ((cssi(np,idof,k).ne.0.0).and.(iflag1.eq.0)) then
      iflag1 = 1
      WARNING: the damping properties of this degree-of-
      freedom for this element property set number
      have already been specified; will now overwrite.
      write (31,3020) np,idof
    end if
  end do
440 continue
  backspace (21)
  read (21,1020) np,idof,(cssi(np,idof,k),k=1,nkpar)
  npp = np
450 continue
  write (31,2040)
  do 470 i=1,npset
    do 460 j=1,numdof
      write (31,2050) i,j,(cssi(i,j,k),k=1,nkpar)
    end do
  end do
460 continue
470 continue
c
c ** READ & PRINT DF ELEMENT PROPERTIES: MASS PARAMETERS **
c
do 490 il=1,npset*numdof
  iflag1 = 0
  read (21,1030) np,idof
  if ((np.lt.1).or.(np.gt.npset)) then
    if ((il.eq.1).or.((idof.lt.1).or.(idof.gt.numdof))) then
      ERROR: DF element property set number or degree-of-
      freedom number outside of applicable range.
      write (31,4030)
      stop
    end if
    if (np.eq.0) then
      np = npp
    end if
  end if
  do 480 k=1,nkpar
    if ((wssi(np,idof,k).ne.0.0).and.(iflag1.eq.0)) then

```

123456789012345678901234567890123456789012345678901234567890123456789012345678  
 0 1 2 3 4 5 6 7

0 1 2 3 4 5 6 7  
 123456789012345678901234567890123456789012345678901234567890123456789012345678

```

    iflag1 = 1
c      WARNING: the mass properties of this element property set
c      number have already been specified; will overwrite.
    write (31,3030) np, idof
    end if
480  continue
    backspace (21)
    read (21,1030) np, idof, (wssi(np, idof, k), k=1, nmpar)
490  continue
    write (31,2060)
    do 500 i=1, npset
      do 505 j = 1, numdof
        write (31,2070) i, j, (wssi(i, j, k), k=1, nmpar)
505  continue
500  continue
c
c      ** READ & PRINT ELEMENT LOAD FACTORS
c
c      read (21,1035) ((emul(i, j), j=1, 4), i=1, 3)
c      write(31,2075) ((emul(i, j), j=1, 4), i=1, 3)
c
c      ** READ DF ELEMENT DATA
c
c      do 530 i1=1, numssi
c      read (21,1040) ne
c      if ((ne.lt.1).or.(ne.gt.numssi)) then
c      if (ne.eq.-999) then
c      go to 540
c      else
c      ERROR: element number outside of range.
c      write (31,4040)
c      stop
c      end if
c      end if
c      if (iessi(ne,1).ne.0) then
c      WARNING: the element data for this DF element have
c      already been specified; will now overwrite.
c      write (31,3040) ne
c      end if
c      backspace (21)
c      read (21,1040) ne, (iessi(ne, j), j=1, nelpar)
c      if ((iessi(ne,5).lt.1).or.(iessi(ne,5).gt.npset)) then
c      ERROR: element property set number outside of range.
c      write (31,4050)
c      stop
c      end if
c      isupt = iessi(ne,8)
c      if ((isupt.ne.0).and.(isupt.ne.1).and.(isupt.ne.-1)) then
c      iessi(ne,8) = 0
c      WARNING: unspecified change of support indicator
c      to 0 (neither end supported condition).
c      write (31,3050) ne
c      end if
c      do 520 i2 = 1, 4
c      if ((iessi(ne, i2).lt.1).or.(iessi(ne, i2).gt.numnp)) then
c      ERROR: node number outside of range.
c      write (31,4060)
c      stop
c      end if
c      do 510 i3=1, 4
c      if ((i2.ne.i3).and.(iessi(ne, i2).eq.iessi(ne, i3))) then
c      ick = i2*i3
c      if ((ick.ne.6).and.(ick.ne.8).and.(ick.ne.12)) then
c      ERROR: i- and j-node nos. not different, or i-, k-,
c      & l-node nos. not different.
c      write (31,4070)
c      stop
c      end if
c      end if
510  continue
520  continue
530  continue

```

123456789012345678901234567890123456789012345678901234567890123456789012345678  
 0 1 2 3 4 5 6 7

0 1 2 3 4 5 6 7  
 12345678901234567890123456789012345678901234567890123456789012345678

```

540 continue jm
c jm
c ** AUTOMATIC MESH GENERATION ALGORITHM ** jm
c jm
do 550 il=numssi,1,-1 jm
  if (iessi(il,1).eq.0) ldeclare = il - 1 jm
550 continue jm
  if (ldeclare.eq.0) then jm
    ERROR: first DF element data not explicitly specified. jm
    write (31,4080) jm
    stop jm
  end if jm
  if ((numssi.ge.2).and.(ldeclare.lt.numssi)) then jm
    do 560 il=1,(numssi-1) jm
      if ((iessi(il,1).ne.0).and.(iessi(il+1,1).ne.0)) then jm
        if (iessi(il,nelpar).ne.0) then jm
          iessi(il,nelpar) = 0 jm
          WARNING: unspecified mesh generation de-invokation. jm
          write (31,3060) il,il+1 jm
        end if jm
      end if jm
560 continue jm
      do 640 il=ldeclare,(numssi-1) jm
        if ((iessi(il,1).eq.0).and.(iflag2.eq.0)) then jm
          iflag2 = 1 jm
          igen = 0 jm
          if (iessi(ldeclare,nelpar).eq.0) then jm
            iessi(ldeclare,nelpar) = 1 jm
            WARNING: unspecified mesh generation invokation. jm
            write (31,3070) ldeclare,il jm
          end if jm
          incr = iessi(ldeclare,nelpar) jm
          if (numssi.ge.3) then jm
            do 570 i2=(il+1),numssi jm
              if (iessi(i2,1).ne.0) then jm
                go to 580 jm
              end if jm
570 continue jm
              i2 = numssi + 1 jm
580 continue jm
              ndeclare = i2 jm
            end if jm
            do 630 i2=il,(ndeclare-1) jm
              igen = igen + 1 jm
              do 590 i3=1,2 jm
                iessi(i2,i3) = iessi(ldeclare,i3) + igen*incr jm
                if ((iessi(i2,i3).lt.1).or.(iessi(i2,i3).gt.numnp)) then jm
                  ERROR: generated node number outside of range. jm
                  write (31,4090) jm
                  stop jm
                end if jm
590 continue jm
                do 600 i3=3,(nelpar-1) jm
                  iessi(i2,i3) = iessi(ldeclare,i3) jm
600 continue jm
                do 620 i3=1,4 jm
                  do 610 i4=1,4 jm
                    if((i3.ne.i4).and.(iessi(i2,i3).eq.iessi(i2,i4))) then jm
                      ick = i3*i4 jm
                      if ((ick.ne.6).and.(ick.ne.8).and.(ick.ne.12)) then jm
                        ERROR: i- and j-node nos. not different, or i-, jm
                        k-, & l-node nos. not different jm
                        write (31,4100) jm
                        stop jm
                      end if jm
                    end if jm
610 continue jm
620 continue jm
630 continue jm
                  else jm
                    iflag2 = 0 jm
                    ldeclare = il jm
  
```

1234567890123456789012345678901234567890123456789012345678901234567890123456789012345678  
 0 1 2 3 4 5 6 7

0 1 2 3 4 5 6 7  
123456789012345678901234567890123456789012345678901234567890123456789012345678

```
        end if
640     continue
        end if
c
c      ** PRINT DF ELEMENT DATA
c
      write (31,2080)
      do 650 i=1,numssi
        write (31,2090) i, (iessi(i,j), j=1,nelpar)
650    continue
      write (31,2100)
c
c
c      ***** LOOP THROUGH DF ELEMENTS TO GENERATE ELEMENT *****
c      ***** STIFFNESS, MASS, DAMPING, AND LOADING MATRICIES. *****
c
c      ** FORM GLOBAL TO LOCAL COORDINATE TRANSFORMATION
c
do 730 il=1,numssi
  iflag3 = 0
  ni = iessi(il,1)
  nj = iessi(il,2)
  nk = iessi(il,3)
  nl = iessi(il,4)
  np = iessi(il,5)
  ireli = iessi(il,6)
  irelj = iessi(il,7)
  isupt = iessi(il,8)
  ird = iessi(il,9)
  dx = x(nj) - x(ni)
  dy = y(nj) - y(ni)
  dz = z(nj) - z(ni)
  dl = sqrt(dx*dx + dy*dy + dz*dz)
  a1 = x(nk) - x(ni)
  a2 = y(nk) - y(ni)
  a3 = z(nk) - z(ni)
  b1 = x(nl) - x(ni)
  b2 = y(nl) - y(ni)
  b3 = z(nl) - z(ni)
  ab = a1*b1 + a2*b2 + a3*b3
  aa = a1*a1 + a2*a2 + a3*a3
  bb = b1*b1 + b2*b2 + b3*b3
  c1 = aa*b1 - ab*a1
  c2 = aa*b2 - ab*a2
  c3 = aa*b3 - ab*a3
  cc = c1*c1 + c2*c2 + c3*c3
  if ((aa.le.0.0).or.(bb.le.0.0).or.(cc.le.0.0)) then
    write (31,4110)
    stop
  end if
  da = sqrt(aa)
  dc = sqrt(cc)
  t(1,1) = a1/da
  t(1,2) = a2/da
  t(1,3) = a3/da
  t(2,1) = c1/dc
  t(2,2) = c2/dc
  t(2,3) = c3/dc
  t(3,1) = t(1,2)*t(2,3) - t(1,3)*t(2,2)
  t(3,2) = t(1,3)*t(2,1) - t(1,1)*t(2,3)
  t(3,3) = t(1,1)*t(2,2) - t(1,2)*t(2,1)
c
c      ** CHECK IF NEW ELEMENT STIFFNESS IS NEEDED
c
  if (il.ne.1) then
    if (abs(dlnew-dlold).lt.dlnew/100.0) then
      if (np.eq.npold) then
        if (ireli.eq.ireliold) then
          if (irelj.eq.ireljold) then
            if (isupt.eq.isuptold) then
              do 670 i2=1,3
                do 660 i3=1,3
```

1234567890123456789012345678901234567890123456789012345678901234567890123456789012345678

0 1 2 3 4 5 6 7  
 123456789012345678901234567890123456789012345678901234567890123456789012345678

```

        check1 = abs(told(i2,i3) - t(i2,i3))           jm
        check2 = abs(t(i2,i3)/100.0)                   jm
        if (check1.lt.check2) then                      jm
            iflag3 = 1                                  jm
        end if                                          jm
660      continue                                       jm
670      continue                                       jm
        end if                                          jm
        end if                                          jm
        end if                                          jm
        end if                                          jm
        end if                                          jm
        end if                                          jm
        dlold = dl                                       jm
        npold = np                                       jm
        ireliold = ireli                                   jm
        ireljold = irelj                                   jm
        isuptold = isupt                                   jm
        do 690 i2 = 1,3                                    jm
            do 680 i3 = 1,3                                jm
                told(i2,i3) = t(i2,i3)                  jm
680      continue                                       jm
690      continue                                       jm
        iflag3 = 0                                       jm
c
c      ** GENERATE NEW STIFFNESS MATRIX                  ** jm
c
c      if (iflag3.ne.1) then                             jm
c          write(*,7778) 13                               jm
c          call df3 (i1, np, alfa, beta,                 jm
+             numssi, npset, numdof, nkpar, ncpar, nmpar, nelpar, jm
+             emul, t, qssi, cssi, wssi, iessi,          jm
+             s, sa, asa, c, ca, aca,                   jm
+             xm, sf, rf, nlsvl, rnml, nlsv2, rnlm2)      jm
c          write(*,7777) 14                               jm
c          end if                                         jm
c
c      ** FORM ELEMENT LOCATION MATRIX                  ** jm
c
c          do 700 i2=1,6                                   jm
c              lm(i2) = id(ni,i2)                         jm
c              lm(i2+6) = id(nj,i2)                       jm
700      continue                                       jm
c
c      ** TRANSFORM TO MASTER DEGREES OF FREEDOM      ** jm
c
c          write(*,7778) 14                               jm
c          call slave (x, y, z, id, numnp, ni, nj)        jm
c          write(*,7777) 15                               jm
c
c      ** WRITE ELEMENT DATA ON TAPE (LINEAR PORTION) ** jm
c
c          write(*,7778) 15                               jm
c          call writet (mband, ndif)                       jm
c          write(*,7777) 16                               jm
c
c      ** WRITE ELEMENT DATA ON TAPE (NON-LINEAR PORTION) ** jm
c
c          if (nind.gt.0) then                             jm
c              nlmult = 1                                  jm
c              write (3) mtype, nd, ns, lm, asa, sa, s    jm
c              write (3) lms, ec, t                       jm
c              write (3) numdof, nlsvl, nlsv2             jm
c              write (13) rnml                             jm
c              write (14) rnlm2                             jm
c              write (15) rnlm2                             jm
c              write (16) rnlm2                             jm
c          else                                           jm
c              nlmult = -1                                  jm
c              ERROR: element failed test for nonlinearity jm
c              (DF element assumed to always be nonlinear). jm
c              write (31,4120)                             jm

```

1234567890123456789012345678901234567890123456789012345678901234567890123456789012345678  
 0 1 2 3 4 5 6 7



0 1 2 3 4 5 6 7  
 123456789012345678901234567890123456789012345678901234567890123456789012345678

```

    stop
    end if
    nn = nelcount + il
    ind(nn) = nlmult*mtype
c
730 continue
    rewind (13)
    rewind (14)
    rewind (15)
    rewind (16)
c
c write(*,7778) 17
return
c
1010 format (2i5, 5f10.0, 4f5.0)
1020 format (2i5, 1f10.0)
1030 format (2i5, 2f10.0)
1035 format (4f10.0)
1040 format (6i5, 2i10, 3i5)
2010 format ( ///, '.....DF elements (Type 6)', //
+ 'number of DF elements: ', 2x, i5, /,
+ 'number of element property sets:', 2x, i5, )
2020 format (///, 1x, 'STIFFNESS PARAMETER DATA', //,
+ 'np dof rkei fyi rkpi rkgl ',
+ 'rkq2 sd rik rhop riz' )
2030 format (i2,i3,5(e10.3),4(1x,f5.3))
2040 format (///, 1x, 'DAMPING PARAMETER DATA', //,
+ 'np dof c' )
2050 format (i2,i3,1(e11.4))
2060 format (///, 1x, 'MASS PARAMETER DATA', //,
+ 'np dof mi mj' )
2070 format (i2,i3,2(e11.4))
2075 format (///, 1x, 'ELEMENT LOAD FACTORS', //,
+ 1x, ' Load Case:', 9x, 'a', 14x, 'b', 14x, 'c', 14x, 'd', /,
+ 1x, ' Global X-dir: ', 4e15.6, /,
+ 1x, ' Global Y-dir: ', 4e15.6, /,
+ 1x, ' Global Z-dir: ', 4e15.6 )
2080 format (///, 1x, 'ELEMENT DATA', //)
2090 format (6(i5),2(i6),3(i5))
2100 format ( /// )
3010 format (1x, 'WARNING: The stiffness properties for property set ',
+ 'number ', i5, ', degree-of-freedom ', i5, ', have', //,
+ 1x, ' been specified more than once, ',
+ 'and will be overwritten.')
3020 format (1x, 'WARNING: The damping properties for property set ',
+ 'number ', i5, ', degree-of-freedom ', i5, ', have', //,
+ 1x, ' been specified more than once, ',
+ 'and will be overwritten.')
3030 format (1x, 'WARNING: The mass properties for property set ',
+ 'number ', i5, ', degree-of-freedom ', i5, ', have', //,
+ 1x, ' been specified more than once, ',
+ 'and will be overwritten.')
3040 format (1x, 'WARNING: The element data for DF element ', i5, ' have'
+ ', /, 1x, ' been specified more than once, ',
+ 'and will be overwritten.')
3050 format (1x, 'WARNING: Wrong support indicator specified ',
+ 'on DF element ', i5, '; changed to 0.')
3060 format (1x, 'WARNING: Unspecified mesh generation de-invokation ',
+ 'on DF element ', i5, ';', //,
+ 1x, ' DF element ', i5, ' data already declared.')
3070 format (1x, 'WARNING: Unspecified mesh generation invoked ',
+ 'on DF element ', i5, ';', //,
+ 1x, ' DF element ', i5, ' data undeclared.')
4010 format (1x, 'ERROR: 1')
4020 format (1x, 'ERROR: 2')
4030 format (1x, 'ERROR: 3')
4040 format (1x, 'ERROR: 4')
4050 format (1x, 'ERROR: 5')
4060 format (1x, 'ERROR: 6')
4070 format (1x, 'ERROR: 7')
4080 format (1x, 'ERROR: 8')
4090 format (1x, 'ERROR: 9')

```

123456789012345678901234567890123456789012345678901234567890123456789012345678  
 0 1 2 3 4 5 6 7

```

0          1          2          3          4          5          6          7
12345678901234567890123456789012345678901234567890123456789012345678

```

```

4100 format (ix,'ERROR: 10')
4110 format (ix,'ERROR: 11')
4120 format (ix,'ERROR: 12')
7777 format (ix,'DF2 enter ',i2)
7778 format (ix,'DF2 exit ',i2)
7779 format (ix,'DF2 stop ',i2)
c
c   end
c
c
c
c   ***** DF3 subroutine *****
c
c   subroutine df3( il,      np,      alfa,      beta,
+                 numssi, npset, numdof, nkpar, ncpars, nmpars, nelpars)
+                 ,emul,  t,      qssi,  cssi,  wssi,  iessi,
+                 s,      sa,  asa,  c,      ca,  aca,
+                 xm,      sf,  rf,      nlsv1, rnlm1, nlsv2, rnlm2)
c
c   implicit double precision(a-h,o-z), integer(i-n)
c   dimension      qssi(npset,numdof,nkpar),  cssi(npset,numdof,ncpar),
+                 wssi(npset,numdof,nmpar),  iessi(numssi,nelpar),
+                 s(12,12), sa(12,24), asa(24,24), emul(3,4), t(3,3),
+                 c(12,12), ca(12,24), aca(24,24),
+                 xm(24),  xml(12),  sf(12,4),  rf(24,4),
+                 rs(12),  rc(12),  qs(12),  qc(12),
+                 gl(3,4),  kkk(6,2),
+                 rnlm1(numdof,nlsv1),  rnlm2(numdof,nlsv2)
c   level 2,e,g,ro,coprop,sft
c
c   ** Subroutine DF3 by W. Cofer & J. McGuire, 12/10/92
c
c   ** This subroutine receives input data for a single DF
c   ** element and forms element stiffness, damping, and mass
c   ** matrices in local and global coordinates, determines
c   ** fixed end forces, and initializes the "rnlm1" and
c   ** "rnlm2" arrays.
c
c   write(*,7777) 1
c
c   ** initialize variables.
c
c   pi = 4.0*atan(1.0)
c   do 7 i=1,3
c     do 5 j=1,4
c       gl(i,j) = 0.0
c     5 continue
c   7 continue
c     do 40 i=1,12
c       xml(i) = 0.0
c       rs(i) = 0.0
c       rc(i) = 0.0
c       qs(i) = 0.0
c       qc(i) = 0.0
c       do 10 j=1,4
c         sf(i,j) = 0.0
c       10 continue
c     do 20 j=1,12
c       s(i,j) = 0.0
c       c(i,j) = 0.0
c     20 continue
c     do 30 j=1,24
c       sa(i,j) = 0.0
c       ca(i,j) = 0.0
c     30 continue
c   40 continue
c     do 70 i=1,24
c       xm(i) = 0.0
c       do 50 j=1,4
c         rf(i,j) = 0.0
c       50 continue
c     do 60 j=1,24

```

```

12345678901234567890123456789012345678901234567890123456789012345678
0          1          2          3          4          5          6          7

```

0 1 2 3 4 5 6 7  
12345678901234567890123456789012345678901234567890123456789012345678

```
        asa(i,j) = 0.0
        aca(i,j) = 0.0
60 continue
70 continue
c
c ** form element stiffness, damping, and mass
c ** matrices in local coordinates
c
do 80 ij = 1, 6
  qk0 = qssi(np,ij,1)
  s(ij, ij) = qk0
  s(ij+6,ij) = -qk0
  s(ij, ij+6) = -qk0
  s(ij+6,ij+6) = qk0
  qc0 = cssi(np,ij,1)
  c(ij, ij) = qc0
  c(ij+6,ij) = -qc0
  c(ij, ij+6) = -qc0
  c(ij+6,ij+6) = qc0
80 continue
do 85 i = 1, 3
  xml(i) = wssi(np,i,1)
  xml(i+6) = wssi(np,i,2)
85 continue
c
c ** Modify damping matrix for Proportional Damping Option
c
ird = iessi(np,9)
if (ird.eq.1) then
  do 100 i = 1, 12
    c(i,i) = c(i,i) + alfa*xml(i)
    do 90 j = 1, 12
      c(i,j) = c(i,j) + beta*s(i,j)
90 continue
100 continue
end if
c
c ** determine gravitational acceleration components
c ** in local directions for load cases A-D.
c
do 135 j=1,4
  do 130 i=1,3
    sum = 0.0
    do 125 k=1,3
      sum = sum + t(i,k)*emul(k,j)
125 continue
    gl(i,j) = sum
130 continue
135 continue
c
c ** determine fixed end forces in local coordinates.
c
virtual = 0.0
do 140 j=1,4
  do 138 i = 1, 3
    glc = gl(i,j)
    sf(i, j) = -virtual*xml(i)*glc
    sf(i+6,j) = -virtual*xml(i+6)*glc
138 continue
140 continue
c
c ** modify stiffness, damping, and fixed end forces for
c ** zero end conditions
c
inelki = iessi(il,6)
inelkj = iessi(il,7)
isupt = iessi(il,8)
if ((inelki.ne.0).or.(inelkj.ne.0)) then
  do 160 j = 1, 2
    if (j.eq.1) then
      cd = real(inelki)
    else
```

12345678901234567890123456789012345678901234567890123456789012345678  
0 1 2 3 4 5 6 7

```

0          1          2          3          4          5          6          7
12345678901234567890123456789012345678901234567890123456789012345678

```

```

      cd = real(inelkj)
      end if
      cd = cd/1000000.0
      do 142 i = 1, 6
        qq = anint(10.0**i)
        ic1 = nint(qq*cd)
        ic2 = nint(nint(ic1/10.0)*10.0)
        icq = ic1 - ic2
        if ((icq.eq.0).or.(icq.eq.1)) then
          kkk(i,j) = icq
        else
          stop
        end if
142      continue
        do 154 n = 1, 6
          i = 6*(j-1) + n
          if (kkk(n,j).eq.1) then
            sii = s(i,i)
            cii = c(i,i)
            do 144 k = 1, 12
              rs(k) = s(i,k)
              rc(k) = c(i,k)
144          continue
              do 148 k = 1, 12
                qs(k) = s(k,i)/sii
                qc(k) = c(k,i)/cii
                do 146 m = 1, 12
                  s(k,m) = s(k,m) - qs(k)*rs(m)
                  c(k,m) = c(k,m) - qc(k)*rc(m)
146          continue
148          continue
              do 152 k = 1, 4
                sfi = sf(i,k)
                do 150 m = 1, 12
                  sf(m,k) = sf(m,k) - qs(m)*sfi
150          continue
152          continue
              end if
154          continue
160          continue
        end if
c
c      ** perform local to global transformation
c
      do 180 la = 1, 10, 3
        lb = la + 2
        do 178 ma = 1, 10, 3
          mb = ma - 1
          do 176 i = la, lb
            do 174 jm = 1, 3
              j = jm + mb
              xs = 0.0
              xc = 0.0
              do 170 k = 1, 3
                xs = xs + s(i,k+mb)*t(k,jm)
                xc = xc + c(i,k+mb)*t(k,jm)
170          continue
              sa(i,j) = xs
              ca(i,j) = xc
174          continue
176          continue
178          continue
180          continue
c
c      ** elem stiffness asa(12,12), damping aca(12,12), and
c      ** fixed end forces rf(12) in global coordinates
c
      do 200 la = 1, 10, 3
        lb = la - 1
        do 198 ma = 1, 10, 3
          mb = ma + 2
          do 196 il = 1, 3

```

```

12345678901234567890123456789012345678901234567890123456789012345678
0          1          2          3          4          5          6          7

```

0 1 2 3 4 5 6 7  
 12345678901234567890123456789012345678901234567890123456789012345678

```

    i = il + lb
    do 194 j = ma, mb
      xs = 0.0
      xc = 0.0
      do 190 k = 1, 3
        xs = xs + t(k,il)*sa(k+lb,j)
        xc = xc + t(k,il)*ca(k+lb,j)
190      continue
        asa(i,j) = xs
        aca(i,j) = xc
194      continue
196      continue
198      continue
200      continue
c
    do 220 la = 1, 10, 3
      lb = la - 1
      do 218 il = 1, 3
        i=il + lb
        do 216 n = 1, 4
          xf = 0.0
          xw = 0.0
          do 210 k = 1, 3
            xf = xf - t(k,il)*sf(k+lb,n)
            xw = xw + t(k,il)*xml(k+lb)
210          continue
            rf(i,n) = xf
            xm(i) = xw
216          continue
218          continue
220          continue
c
c      *** Determine *rnlm1* and *rnlm2* matrices ***
c
c      do 250 n = 1, numdof
c
c        rkei = qssi(np,n,1)
c        fyi = qssi(np,n,2)
c        rkp = qssi(np,n,3)
c        rkg1 = qssi(np,n,4)
c        rkg2 = qssi(np,n,5)
c        sd = qssi(np,n,6)
c        rik = qssi(np,n,7)
c        rhoe = 0.0
c        rhop = qssi(np,n,8)
c        riz = qssi(np,n,9)
c
c        if (rkei.ne.0.0) then
c          ruyi = fyi/rkei
c        else
c          if (fyi.eq.0.0) then
c            ruyi = 0.0
c          else
c            ruyi = 1.0e+12
c          end if
c        end if
c
c        elflag = 1.0
c        xorigin = 0.0
c        yorigin = 0.0
c        rke = rkei
c        fy = fyi
c        ruy = ruyi
c        rub = 0.0
c        drub = 0.0
c        rkfb = rke
c        pb = 0.0
c        grt = 0.0
c        glt = 0.0
c        gap = 0.0
c        rubmax = 0.0
c        pbmax = 0.0
c        right = 0.0

```

12345678901234567890123456789012345678901234567890123456789012345678  
 0 1 2 3 4 5 6 7

```

0          1          2          3          4          5          6          7
12345678901234567890123456789012345678901234567890123456789012345678

```

```

      first = 1.0
c
c      rnlm1(n, 1) = rkei
c      rnlm1(n, 2) = fyi
c      rnlm1(n, 3) = ruyi
c      rnlm1(n, 4) = rkp
c      rnlm1(n, 5) = rkg1
c      rnlm1(n, 6) = rkg2
c      rnlm1(n, 7) = sd
c      rnlm1(n, 8) = rik
c      rnlm1(n, 9) = rhoe
c      rnlm1(n,10) = rhop
c      rnlm1(n,11) = riz
c
c      rnlm2(n, 1) = elflag
c      rnlm2(n, 2) = xorigin
c      rnlm2(n, 3) = yorigin
c      rnlm2(n, 4) = rke
c      rnlm2(n, 5) = fy
c      rnlm2(n, 6) = ruy
c      rnlm2(n, 7) = rub
c      rnlm2(n, 8) = drub
c      rnlm2(n, 9) = rkttb
c      rnlm2(n,10) = pb
c      rnlm2(n,11) = grt
c      rnlm2(n,12) = glt
c      rnlm2(n,13) = gap
c      rnlm2(n,14) = rubmax
c      rnlm2(n,15) = pbmax
c      rnlm2(n,16) = right
c      rnlm2(n,17) = first
c
c      250 continue
c
c      write(*,7778) 1
c      return
c
c      7777 format (1x,'DF3 enter ',i2)
c      7778 format (1x,'DF3 exit ',i2)
c      7779 format (1x,'DF3 stop ',i2)
c
c      end
c
c
c
c      ***** DF4 subroutine *****
c      subroutine df4 ( nel,icond,nind,last,mtot,asa,sa,s,lms,ec,t,
c      +               assa,ssa,df,f,up,ex,dex,efi,ndof,nlsv1,nlsv2 )
c
c      implicit double precision (a-h, o-z), integer (i-n)
c      dimension   asa(24,24),sa(12,24),s(12,12),lms(12),ec(12),t(3,3),
c      +           assa(24,24),ssa(12,24),df(24),f(12),up(12),
c      +           ex(24),dex(24),efi(12)
c      common/big/ a(99000)
c
c      ** Subroutine DF4 by W. Cofer & J. McGuire, 12/10/92
c
c      ** This subroutine allocates space in the global *a* matrix
c      ** for temporary storage of DF element data for use by
c      ** subroutines DF5 and DF6.
c
c      write (*,7777) 1
c
c      nn1 = last
c      nn2 = nn1 + ndof*nlsv1
c      nn3 = nn2 + ndof*nlsv2
c      nn4 = nn3 + ndof*nlsv2
c      final = nn4
c      if (final.gt.mtot) then
c        write (*,7778) 1
c        call error (1, last-mtot, 7hstepc )

```

```

12345678901234567890123456789012345678901234567890123456789012345678
0          1          2          3          4          5          6          7

```

```

0          1          2          3          4          5          6          7
12345678901234567890123456789012345678901234567890123456789012345678

```

```

      write (*,7777) 2
      end if
c
      call df5(      nel, icond, nind, asa, sa, s, lms, ec, t,
+                assa, ssa, df, f, up, ex, dex, efi,
+                ndof, nlsv1, nlsv2, a(nn1), a(nn2), a(nn3) )
c
c      write (*,7778) 2
c      return
c
7777 format (1x,'DF4 enter ',i2)
7778 format (1x,'DF4 exit ',i2)
7779 format (1x,'DF4 stop ',i2)

      end

c      ***** DF5 subroutine *****
c
      subroutine df5 ( nel, icond, nind, asa, sa, s, lms, ec, t,
+                    assa, ssa, df, f, up, ex, dex, efi,
+                    ndof, nlsv1, nlsv2, rnlm1, rnlm2, rnlm3 )
c
c      implicit double precision(a-h,o-z), integer(i-n)
c      dimension      asa(24,24),sa(12,24),s(12,12),lms(12),ec(12),t(3,3),
+                    assa(24,24),ssa(12,24),df(24),f(12),up(12),
+                    ex(24),dex(24),efi(12),
+                    rnlm1(ndof,nlsv1),rnlm2(ndof,nlsv2),rnlm3(ndof,nlsv2)
+                    ss(12,12),u(12),du(12),p(12),dp(12),x(12),dx(12)
c
c      *** Subroutine DF5 by W. Cofer & J. McGuire, 12/10/92
c
c      *** This subroutine receives and processes data for the DF
c      *** elements for the current time step, manages the
c      *** calculation of the tangential stiffness matrix and
c      *** element force vectors for each DF element (performed
c      *** in subroutine DF6).
c
c      write (*,7777) 1
c
c      *** Initialize variables; setting *nind* not equal to zero
c      *** indicates that element is responding nonlinearly.
c
      nind = 1
      do 120 i = 1, 12
        x(i)      = ex(i)
        dx(i)     = dex(i)
        u(i)      = 0.0
        du(i)     = 0.0
        up(i)     = 0.0
        p(i)      = 0.0
        dp(i)     = 0.0
        f(i)      = 0.0
        efi(i)    = 0.0
        df(i)     = 0.0
        do 110 j = 1, 12
          ss (i, j) = 0.0
          ssa (i, j) = 0.0
          ssa (i, j+12) = 0.0
          assa(i, j) = 0.0
          assa(i+12, j) = 0.0
          assa(i, j+12) = 0.0
          assa(i+12, j+12) = 0.0
110      continue
120      continue
c
c      *** Transform to master degrees-of-freedom ***
c
      kk = 1
      .kd = 13
      do 140 nf = 1, 2

```

```

12345678901234567890123456789012345678901234567890123456789012345678
0          1          2          3          4          5          6          7

```

```

0          1          2          3          4          5          6          7
12345678901234567890123456789012345678901234567890123456789012345678

```

```

do 130 k = 1, 3
  i = 6*(nf-1) + k
  if (lms(i).gt.0) then
    d1 = ec(kk)
    d2 = ec(kk+1)
    dx(i) = dx(i) + dex(kd)*d1 + dex(kd+1)*d2
    x(i) = x(i) - dex(i) + dx(i)
    kk = kk + 2
    kd = kd + 2
  end if
130 continue
140 continue
c
c *** Convert elmnt displacement from global to local coords. ***
c
do 170 n = 0, 9, 3
  do 160 i = 1, 3
    sum1 = 0.0
    sum2 = 0.0
    do 150 j = 1, 3
      sum1 = sum1 + t(i,j)* x(n+j)
      sum2 = sum2 + t(i,j)*dx(n+j)
150 continue
    u(n+i) = sum1
    du(n+i) = sum2
    up(n+i) = u(n+i)
160 continue
170 continue
c
c *** Determine following elmnt variables in local coords ***
c *** ss: tangential stiffness matrix ***
c *** p, dp: "true" force & "nonlinear restoring" force ***
c
call df6 ( icond, ndof, nlsv1, nlsv2, rnlm1, rnlm2, rnlm3,
+         u, du, ss, p, dp )
c
c *** Convert elemental tangential stiffnes matrix from ***
c *** local to global coords. ***
c
do 220 la = 1, 10, 3
  lb = la + 2
  do 210 ma = 1, 10, 3
    mb = ma - 1
    do 200 i = la, lb
      do 190 jm = 1, 3
        j = jm + mb
        sum = 0.0
        do 180 k = 1, 3
          sum = sum + t(k,jm)*ss(i,k+mb)
180 continue
        ssa(i,j) = sum
190 continue
200 continue
210 continue
220 continue
c
do 270 la = 1, 10, 3
  lb = la - 1
  do 260 ma = 1, 10, 3
    mb = ma + 2
    do 250 il = 1, 3
      i = il + lb
      do 240 j = ma, mb
        sum = 0.0
        do 230 k = 1, 3
          sum = sum + t(k,il)*ssa(k+lb,j)
230 continue
        assa(i,j) = sum
240 continue
250 continue
260 continue
270 continue

```

```

12345678901234567890123456789012345678901234567890123456789012345678
0          1          2          3          4          5          6          7

```



```

0          1          2          3          4          5          6          7
12345678901234567890123456789012345678901234567890123456789012345678

```

```

c                                     jm
c *** Transform to master degrees-of-freedom ***                             jm
c                                     jm
c                                     jm
c kk = 1                               jm
c kd = 13                              jm
c do 310 nf = 1, 2                      jm
c   do 300 k = 1, 3                    jm
c     i = 6*(nf-1) + k                 jm
c     if (lms(i).gt.0) then            jm
c       d1 = ec(kk )                   jm
c       d2 = ec(kk+1)                  jm
c       do 280 ii = 1, 12              jm
c         ssa(ii,kd ) = ssa(ii,i)*d1    jm
c         ssa(ii,kd+1) = ssa(ii,i)*d2  jm
280   continue                          jm
c       do 290 ii = 1, kd              jm
c         assa(kd ,ii ) = assa(i, ii)*d1 jm
c         assa(kd+1,ii ) = assa(i, ii)*d2 jm
c         assa(ii, kd ) = assa(ii,i )*d1 jm
c         assa(ii, kd+1) = assa(ii,i )*d2 jm
290   continue                          jm
c       assa(kd, kd ) = assa(i,i)*(d1**2) jm
c       assa(kd+1,kd+1) = assa(i,i)*(d2**2) jm
c       assa(kd, kd+1) = assa(i,i)*(d1*d2) jm
c       assa(kd+1,kd ) = assa(kd, kd+1) jm
c       kk = kk + 2                    jm
c       kd = kd + 2                    jm
c     end if                            jm
c   300 continue                        jm
c   310 continue                        jm
c *** Set elemental force vector, local coordinates. ***                   jm
c                                     jm
c do 320 n = 1, 12                      jm
c   f(n) = p(n)                         jm
320 continue                             jm
c *** Convert true elemental 'nonlinear restoring force' ***               jm
c *** vector from local to global coordinates. ***                         jm
c                                     jm
c do 350 n = 0, 9, 3                    jm
c   do 340 i = 1, 3                     jm
c     sum = 0.0                          jm
c     do 330 j = 1, 3                   jm
c       sum = sum + t(j,i)*dp(n+j)      jm
330   continue                          jm
c     efi(n+i) = sum                    jm
340   continue                          jm
350 continue                             jm
c write (*,7778) 1                       jm
c return                                 jm
c                                     jm
c 7777 format (lx,'DF5 enter ',i2)      jm
c 7778 format (lx,'DF5 exit ',i2)       jm
c 7779 format (lx,'DF5 stop ',i2)       jm
c end                                     jm
c                                     jm
c *** DF6 subroutine *****                                                  jm
c subroutine df6 ( icond, ndof, nlsv1, nlsv2, rnlm1, rnlm2, rnlm3,          jm
+   u, du, ss, p, dp )                 jm
c implicit double precision (a-h,o-z), integer (i-n)                       jm
c dimension u(12),du(12),ss(12,12),p(12),dp(12),                          jm
+   rnlm1(ndof,nlsv1),rnlm2(ndof,nlsv2),rnlm3(ndof,nlsv2)                  jm
c dimension tmp(6,3), tmp2(6,14)                                              jm
c *** Subroutine DF6 by W. Cofer & J. McGuire, 12/10/92 ***                jm

```

```

12345678901234567890123456789012345678901234567890123456789012345678
0          1          2          3          4          5          6          7

```

0 1 2 3 4 5 6 7  
12345678901234567890123456789012345678901234567890123456789012345678

```
end if
if (jswitch.eq.-1) then
  ielflag = -2
  xorigin = ru0
  yorigin = 0.0
elseif (jswitch.eq.1) then
  if (abs(eru).gt.ruy) then
    if (iz.eq.1) then
      if (fy-abs(yorigin).ge.0.0) then
        ielflag = -1
        ixyalg = 1
      elseif ((iptrial.ne.iyorigin).or.
+         (yorigin.eq.0.0) ) then
        ielflag = -1
        ixyalg = 2
      elseif ((iptrial.eq.iyorigin ) .and.
+         (abs(ptrial).ge.abs(yorigin)) ) then
        ielflag = -1
        ixyalg = 1
      else
        continue
      end if
    else
      ielflag = -1
      ixyalg = 1
    end if
  if (ielflag.eq.-1) then
    if (ixyalg.eq.1) then
      if (eru.gt.0.0) then
        xorigin = xorigin + ruy
        yorigin = yorigin + fy
      else
        xorigin = xorigin - ruy
        yorigin = yorigin - fy
      end if
    elseif (ixyalg.eq.2) then
      if ((pb.eq.ptrial).or.(pb.eq.0.0)) then
        ratio = 0.0
      elseif (ptrial.eq.0.0) then
        ratio = 1.0
      else
        ratio = pb/(pb-ptrial)
      end if
      ru0 = rub + ratio*dru
      xorigin = ru0
      yorigin = 0.0
    end if
    delta = rhoe*(xorigin - rub) + rhop*(ru - xorigin)
  end if
  if (ptrial.ge.0.0) then
    gap = gap + delta
    gr = ru
    gl = gr - gap
  elseif (ptrial.lt.0.0) then
    gap = gap - delta
    gl = ru
    gr = gl + gap
  end if
end if
c
c
c
*** DF element currently plastic ***
elseif (ielflag.eq.-1) then
  delta = rhop*dru
  jswitch = 1
  if (iptrial.ne.ipb) then
    if ((pb.eq.ptrial).or.(pb.eq.0.0)) then
      ratio = 0.0
    elseif (ptrial.eq.0.0) then
      ratio = 1.0
    else
      ratio = 0.0
    end if
  end if

```

12345678901234567890123456789012345678901234567890123456789012345678  
0 1 2 3 4 5 6 7

0 1 2 3 4 5 6 7  
 12345678901234567890123456789012345678901234567890123456789012345678

```

    ratio = pb/(pb -ptrial)
  end if
  ru0 = rub + ratio*dru
  if (ptrial.ge.0.0) then
    glt = ru0
    grt = glt + (gap - ratio*delta)
    if (ru.le.grt) then
      jswitch = -1
      gap = gap - ratio*delta
      gl = glt
      gr = grt
    end if
  elseif (ptrial.lt.0.0) then
    grt = ru0
    glt = grt - (gap + ratio*delta)
    if (ru.ge.glt) then
      jswitch = -1
      gap = gap + ratio*delta
      gr = grt
      gl = glt
    end if
  end if
  end if
  if (jswitch.eq.-1) then
    ielflag = -2
    xorigin = ru0
    yorigin = 0.0
  elseif (jswitch.eq.1) then
    if (iswitch.eq.-1) then
      ielflag = 1
      if (rubmax.le.ruyi) then
        rke = rkei
      elseif (rubmax.ne.0.0) then
        rke = rkei*( ruyi/rubmax)**sd )
      else
        stop
      end if
    end if
    fy = fyi + rik*(pbmax - fyi)
    if (rke.ne.0.0) then
      ruy = fy/rke
    else
      if (fy.eq.0.0) then
        ruy = 0.0
      else
        ruy = 1.0e+12
      end if
    end if
    delta = rhoe*dru
    if (dru.le.0.0) then
      xorigin = rub - ruy
      yorigin = pb - fy
    else
      xorigin = rub + ruy
      yorigin = pb + fy
    end if
  end if
  if (ptrial.ge.0.0) then
    gap = gap + delta
    gr = ru
    gl = gr - gap
  elseif (ptrial.lt.0.0) then
    gap = gap - delta
    gl = ru
    gr = gl + gap
  end if
end if

c
c
c
*** DF element currently within gap at rkgl stiffness ***
elseif( ielflag.eq.-2) then
  if (iswitch.eq.-1) then
    ielflag = 2
  
```

12345678901234567890123456789012345678901234567890123456789012345678  
 0 1 2 3 4 5 6 7

```

0          1          2          3          4          5          6          7
12345678901234567890123456789012345678901234567890123456789012345678

```

```

c
c   *** This subroutines receives current data for a single DF   *** jm
c   *** DF element and determines the element tangential       *** jm
c   *** stiffness matrix and element force vectors for current *** jm
c   *** time step.                                             *** jm
c
c   data nthru / 0 /
c   save nthru
c   nthru = nthru + 1
c
c   write (*,7777) 1
c
c   read (13) rnlm1
c   if (icond.eq.2) then
c     read (16) rnlm3
c     backspace (16)
c     write (14) rnlm3
c     backspace (14)
c   end if
c   read (14) rnlm2
c   backspace (14)
c   read (15) rnlm3
c   if (icond.ne.3) then
c     backspace (15)
c     write (15) rnlm2
c     write (16) rnlm3
c   end if
c
c   do 110 i = 1, ndof
c
c     rkei = rnlm1(i, 1)
c     fyi = rnlm1(i, 2)
c     ruyi = rnlm1(i, 3)
c     rkp = rnlm1(i, 4)
c     rkg1 = rnlm1(i, 5)
c     rkg2 = rnlm1(i, 6)
c     sd = rnlm1(i, 7)
c     rik = rnlm1(i, 8)
c     rhoe = rnlm1(i, 9)
c     rhop = rnlm1(i,10)
c     riz = rnlm1(i,11)
c
c     elflag = rnlm2(i, 1)
c     xorigin = rnlm2(i, 2)
c     yorigin = rnlm2(i, 3)
c     rke = rnlm2(i, 4)
c     fy = rnlm2(i, 5)
c     ruy = rnlm2(i, 6)
c     rub = rnlm2(i, 7)
c     drub = rnlm2(i, 8)
c     rkbtb = rnlm2(i, 9)
c     pb = rnlm2(i,10)
c     gr = rnlm2(i,11)
c     gl = rnlm2(i,12)
c     gap = rnlm2(i,13)
c     rubmax = rnlm2(i,14)
c     pbmax = rnlm2(i,15)
c     right = rnlm2(i,16)
c     first = rnlm2(i,17)
c
c     ielflag = nint( elflag )
c     iz = nint(riz )
c     ifirst = nint(sign(1.0,first ))
c
c     ru = u(i) - u(i+6)
c     dru = ru - rub
c     if (icond.eq.3) then
c       trub = rnlm3(i,7)
c       tdru = ru - trub
c     else
c       trub = rub
c       tdru = dru

```

```

12345678901234567890123456789012345678901234567890123456789012345678
0          1          2          3          4          5          6          7

```

0 1 2 3 4 5 6 7  
12345678901234567890123456789012345678901234567890123456789012345678

```
end if jm  
c eru = ru - xorigin jm  
ptrial = yorigin + rktb*eru jm  
c if (icond.ne.3) then jm  
c *** Determine if a change of state (elastic, *** jm  
c *** plastic, or in-gap) has occurred; if so, *** jm  
c *** update 'ielflag', 'xorigin', and 'yorigin'. *** jm  
c *** 1. Update maximum displacement and force *** jm  
c if (abs(rub).gt.rubmax) then jm  
c rubmax = abs(rub) jm  
c end if jm  
c if (abs(pb).gt.pbmax) then jm  
c pbmax = abs(pb) jm  
c end if jm  
c *** 2. Check for reversal of direction; if *** jm  
c *** continuing in present direction, *** jm  
c *** 'iswitch' = 1; if reverse, 'iswitch' = -1. *** jm  
c iswitch = 1 jm  
c idru = nint(sign(1.0,dru )) jm  
c idrub = nint(sign(1.0,drub)) jm  
c if (idru.ne.idrub) then jm  
c iswitch = -1 jm  
c end if jm  
c *** 3. Determine if a change of state has occurred *** jm  
c ieru = nint(sign(1.0,eru )) jm  
c iright = nint(sign(1.0,right )) jm  
c ipb = nint(sign(1.0,pb )) jm  
c iptrial = nint(sign(1.0,ptrial )) jm  
c iyorigin = nint(sign(1.0,yorigin)) jm  
c *** DF element currently elastic *** jm  
c if (ielflag.eq.1) then jm  
c delta = rhoe*dru jm  
c jswitch = 1 jm  
c if ((iptrial.ne.ipb).and.(ifirst.lt.0)) then jm  
c if ((pb.eq.ptrial).or.(pb.eq.0.0)) then jm  
c ratio = 0.0 jm  
c elseif (ptrial.eq.0.0) then jm  
c ratio = 0.0 jm  
c else jm  
c ratio = pb/(pb -ptrial) jm  
c end if jm  
c ru0 = rub + ratio*dru jm  
c if (ptrial.ge.0.0) then jm  
c glt = ru0 jm  
c grt = glt + (gap - ratio*delta) jm  
c if (ru.le.grt) then jm  
c jswitch = -1 jm  
c gap = gap - ratio*delta jm  
c gl = glt jm  
c gr = grt jm  
c end if jm  
c elseif (ptrial.lt.0.0) then jm  
c grt = ru0 jm  
c glt = grt - (gap + ratio*delta) jm  
c if (ru.ge.glt) then jm  
c jswitch = -1 jm  
c gap = gap + ratio*delta jm  
c gr = grt jm  
c gl = glt jm  
c end if jm  
end if jm
```

12345678901234567890123456789012345678901234567890123456789012345678  
0 1 2 3 4 5 6 7

0 1 2 3 4 5 6 7  
 12345678901234567890123456789012345678901234567890123456789012345678

```

    xorigin = rub
    yorigin = pb
    if (drub.ge.0.0) then
      right = 1.0
    else
      right = -1.0
    end if
  end if
  if ((ru.gt.gr).or.(ru.lt.gl)) then
    ielflag = 1
    if (ru.gt.gr) then
      rout = gr
      delta = rhoe*(ru - rout)
      gap = gap + delta
      gr = ru
      gl = gr - gap
    elseif (ru.lt.gl) then
      rout = gl
      delta = rhoe*(ru - rout)
      gap = gap - delta
      gl = ru
      gr = gl + gap
    end if
    yorigin = yorigin + rkg1*(rout - xorigin)
    xorigin = rout
  end if

c
c
c
  *** DF element currently within gap at rkg2 stiffness ***
  elseif( ielflag.eq.2) then
    if ((iptrial.ne.ipb).or.(ieru.eq.iright)) then
      ielflag = -2
      if (iptrial.ne.ipb) then
        if ((pb.eq.ptrial).or.(pb.eq.0.0)) then
          ratio = 0.0
        elseif (ptrial.eq.0.0) then
          ratio = 1.0
        else
          ratio = pb/(pb - ptrial)
        end if
        ru0 = rub + ratio*dru
        xorigin = ru0
        yorigin = 0.0
      end if
    end if
    if ((ru.gt.gr).or.(ru.lt.gl)) then
      ielflag = 1
      if (ru.gt.gr) then
        rout = gr
        delta = rhoe*(ru - rout)
        gap = gap + delta
        gr = ru
        gl = gr - gap
      elseif (ru.lt.gl) then
        rout = gl
        delta = rhoe*(ru - rout)
        gap = gap - delta
        gl = ru
        gr = gl + gap
      end if
      yorigin = yorigin + rkg2*(rout - xorigin)
      xorigin = rout
    end if
  end if

c
c
  elseif (icond.eq.3) then
    if ((ielflag.eq.1).or.(ielflag.eq.-1)) then
      if (ielflag.eq.1) then
        delta = rhoe*dru
      elseif (ielflag.eq.-1) then
        delta = rhop*dru
      end if
    end if
  end if

```

1234567890123456789012345678901234567890123456789012345678901234567890123456789012345678  
 0 1 2 3 4 5 6 7



```

0          1          2          3          4          5          6          7
12345678901234567890123456789012345678901234567890123456789012345678
-----
      rnlm2(i,13) = gap
      rnlm2(i,14) = rubmax
      rnlm2(i,15) = pbmax
      rnlm2(i,16) = right
      rnlm2(i,17) = first
c
c 110 continue
      do 112 i = 1, ndof
          xx1 = -tmp2(i,4)
          xx2 = -tmp2(i,5)
          xx3 = -tmp2(i,2)
          xx4 = tmp2(i,1)
          xx5 = -tmp2(i,13)
          xx6 = -tmp2(i,14)
c      write (32,6000) nthru, i, xx1, xx2, xx3, xx4, xx5, xx6
c 112 continue
c      write (32,6010)
c
c      write (14) rnlm2
c
c      *** Elmnt. tangential stiffness matrix, local coords. ***
c
      do 120 i = 1, 6
          rkt = tmp(i,1)
          ss(i, i) = rkt
          ss(i+6,i) = -rkt
          ss(i, i+6) = -rkt
          ss(i+6,i+6) = rkt
c 120 continue
c
c      *** Determine elmnt force vector in local coords. if element ***jm
c      *** had remained elastic (pe), the "true" elmnt force vector ***jm
c      *** (p), also in local coords, and the element "nonlinear ***jm
c      *** restoring force" vector (dp = p - pe). ***jm
c
      do 130 i = 1, 6
          pp = tmp(i,2)
          dpp = tmp(i,3)
          p(i) = pp
          dp(i) = dpp
          p(i+6) = -pp
          dp(i+6) = -dpp
c 130 continue
c
c      write (*,7778) 2
c      return
c
c 6000 format ( i5,1x,i2,1x,
+          f9.6,1x,f9.6,1x,f12.6,1x,f8.2,1x,f9.6,1x,f12.6 )
c 6010 format ( ' ' )
c
c 7777 format (1x,'DF6 enter ',i2)
c 7778 format (1x,'DF6 exit ',i2)
c 7779 format (1x,'DF6 stop ',i2)
c
c      end
-----
12345678901234567890123456789012345678901234567890123456789012345678
0          1          2          3          4          5          6          7

```



## Appendix D

### Spread Footing Foundation Study

The 52 NEABS analyses performed in the parametric study of spread footing foundations are presented below in matrix form. Each run is identified by a name of the form "SF $nn$ - $fff$ . $see$ ," where  $nn$  is the run number,  $fff$  is the foundation model code,  $s$  is the soil stiffness code, and  $ee$  is the applied seismic record code. The values of the foundation model parameters are given in this appendix, in terms of the model configurations shown in Figure 3.3 of Chapter Three. References of the publications which describe the procedures used to determine these parameters accompany the values. The results of the NEABS analyses are also presented in this appendix; the presentation order of the results follows the numbering of the analyses given in the matrix below.

		El Centro Record		Olympia Record	
		Lower Intensity	Higher Intensity	Lower Intensity	Higher Intensity
Fixed		SF01-FX0_EL	SF02-FX0_EH	SF03-FX0_OL	SF04-FX0_OH
D01 Model (Springs only)	Soft Intermediate Stiff	SF05-D01.FEL SF09-D01.IEL SF13-D01.SEL	SF06-D01.FEH SF10-D01.IEH SF14-D01.SEH	SF07-D01.FOL SF11-D01.IOL SF15-D01.SOL	SF08-D01.FOH SF12-D01.IOH SF16-D01.SOH
D03 Model (Springs, Mass, & Dashpot)	Soft Intermediate Stiff	SF17-D03.FEL SF21-D03.IEL SF25-D03.SEL	SF18-D03.FEH SF22-D03.IEH SF26-D03.SEH	SF19-D03.FOL SF23-D03.IOL SF27-D03.SOL	SF20-D03.FOH SF24-D03.IOH SF28-D03.SOH
D05 Model (Meek & Veletsos)	Soft Intermediate Stiff	SF29-D05.FEL SF33-D05.IEL SF37-D05.SEL	SF30-D05.FEH SF34-D05.IEH SF38-D05.SEH	SF31-D05.FOL SF35-D05.IOL SF39-D05.SOL	SF32-D05.FOH SF36-D05.IOH SF40-D05.SOH
D11 Model (Jean et al.)	Soft Intermediate Stiff	SF41-D11.FEL SF45-D11.IEL SF49-D11.SEL	SF42-D11.FEH SF46-D11.IEH SF50-D11.SEH	SF43-D11.FOL SF47-D11.IOL SF51-D11.SOL	SF44-D11.FOH SF48-D11.IOH SF52-D11.SOH

## Spread Footing Foundation Models: Parameter Values\*

		Soft Soil				Intermediate Soil				Stiff Soil			
		D01	D03	D05	D11	D01	D03	D05	D11	D01	D03	D05	D11
Lateral Translation	k1	866.5	866.5	866.5	591.1	4718	4718	4718	3218	16271	16271	16271	11100
	k2				1700				9254				31919
	k3				571.6				3112				10733
	k4				1798				9791				33770
	c1		11.78	10.29	13.11		27.49	24.01	30.6		51.06	44.59	56.83
	c2			0.0	36.02			0.0	84.04			0.0	156.1
	c3				1.983				4.627				8.593
	c4				24.75				57.77				107.3
	c5				30.39				70.90				131.7
	m1		0.0452	0.0	0.0527		0.0452	0.0	0.0527		0.452	0.0	0.0527
m2			0.0	0.2975			0.0	0.2975			0.0	0.2975	
Vertical Translation	k1	983.1	983.1	983.1	1091	5353	5353	5353	5943	18461	18461	18461	20499
	k2				1393				7582				26149
	k3				450.2				2451				8453
	k4				1778				9680				33385
	c1		17.78	14.01	13.67		41.49	32.69	31.89		77.05	60.71	59.23
	c2			4.700	31.43			10.90	73.34			20.24	136.2
	c3				7.306				17.04				31.66
	c4				24.48				57.12				106.1
	c5				27.96				65.23				121.1
	m1		0.1202	0.0	0.3931		0.1202	0.0	0.3931		0.1202	0.0	0.3931
m2			0.0345	0.2537			0.0345	0.2537			0.0345	0.2537	
Rocking	k1	3.00E6	3.00E6	3.00E6	1.31E6	16.34E6	16.34E6	16.34E6	7.113E6	56.37E6	56.37E6	56.37E6	24.53E6
	k2				5.07E6				27.61E6				95.24E6
	k3				4.55E6				24.79E6				85.49E6
	k4				3.26E6				17.77E6				61.28E6
	c1		16553	0.0	-16789		38624	0.0	-39175		71732	0.0	-72754
	c2			21389	64412			49909	150.3E6			92688	279.1E3
	c3				39968				93259				173.2E6
	c4				3164				7383				13712
	c5				33788				78839				146.4E3
	m1		276.6	0.0	1228		276.6	0.0	1228		276.6	0.0	1228
m2			255.9	392.4			255.9	392.4			255.9	392.4	

\* unit of force = kip; unit of length = inch; unit of rotation = radian; unit of time = second

D01 Model: John P. Wolf, *Soil-Structure Interaction Analysis in Time Domain*, Prentice-Hall, Inc., Englewood Cliffs, N.J., 1988.

D03 Model: Anestis S. Veletsos and B. Verbič, "Vibration of Viscoelastic Foundations," *International Journal of Earthquake Engineering and Structural Dynamics*, Vol. 2, No. 1, July-September, 1973, pp. 87-102.

D05 Model: John P. Wolf, *Soil-Structure Interaction Analysis in Time Domain*, Prentice-Hall, Inc., Englewood Cliffs, N.J., 1988.

D11 Model: Wen-Ye Jean, Tsung-Wu Lin, and Joseph Penzien, "System Parameters of Soil Foundations for Time Domain Dynamic Analysis," *Earthquake Engineering and Structural Dynamics*, Vol 19, 1990, pp. 541-553.

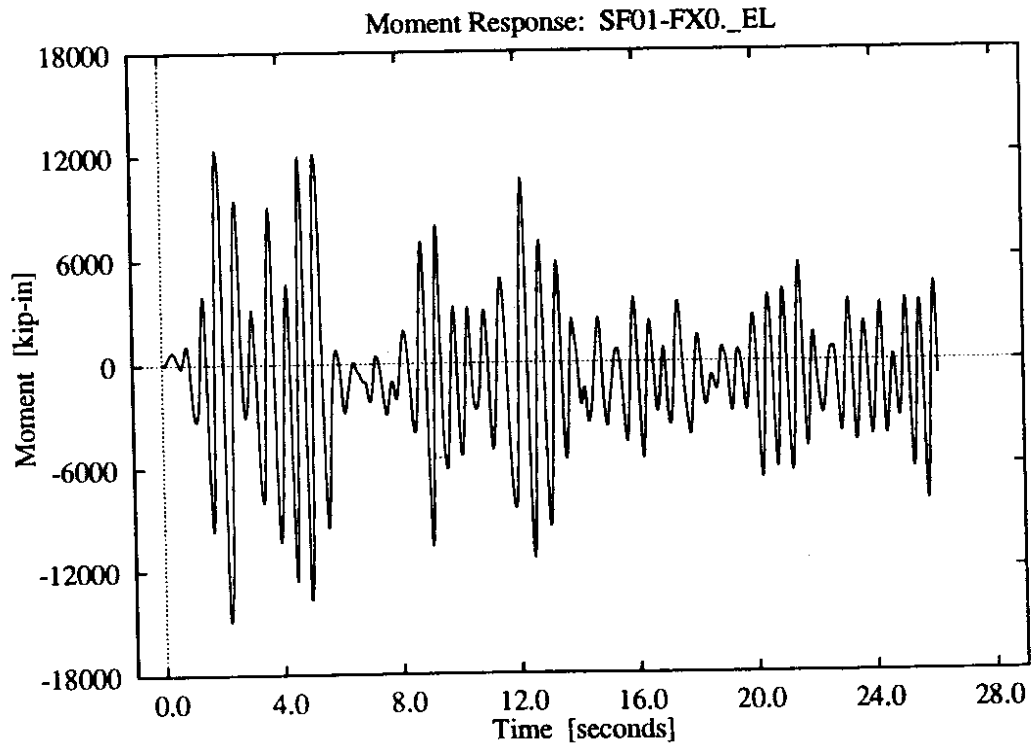
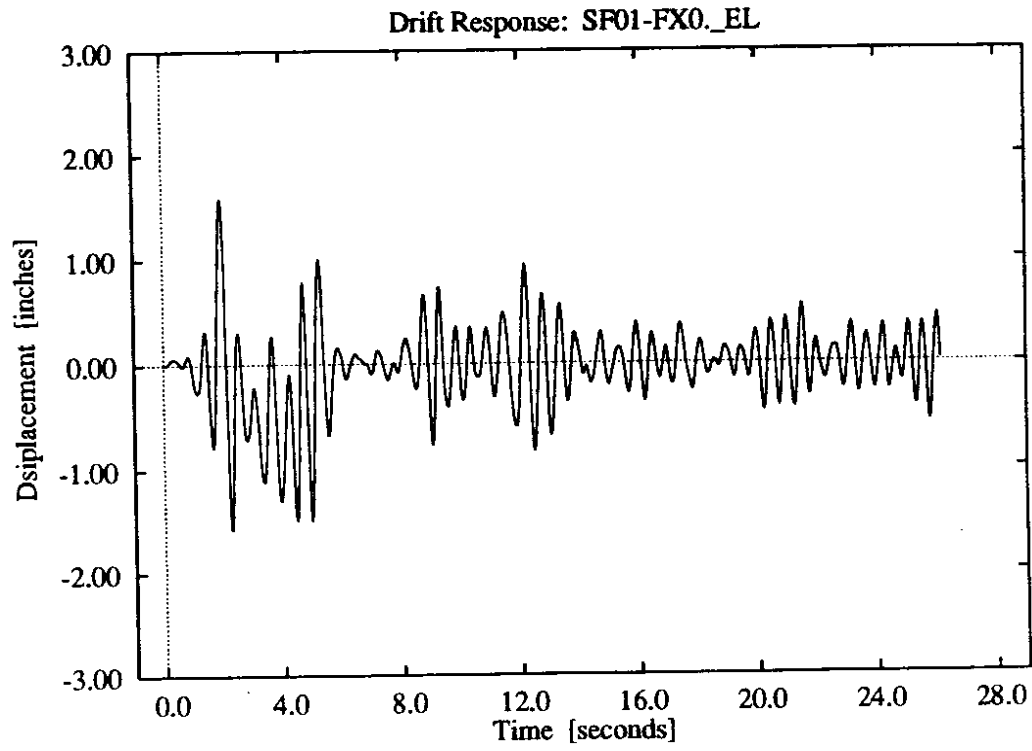


**Figure D-1: Fixed-base foundation,  
lower intensity El Centro record.**

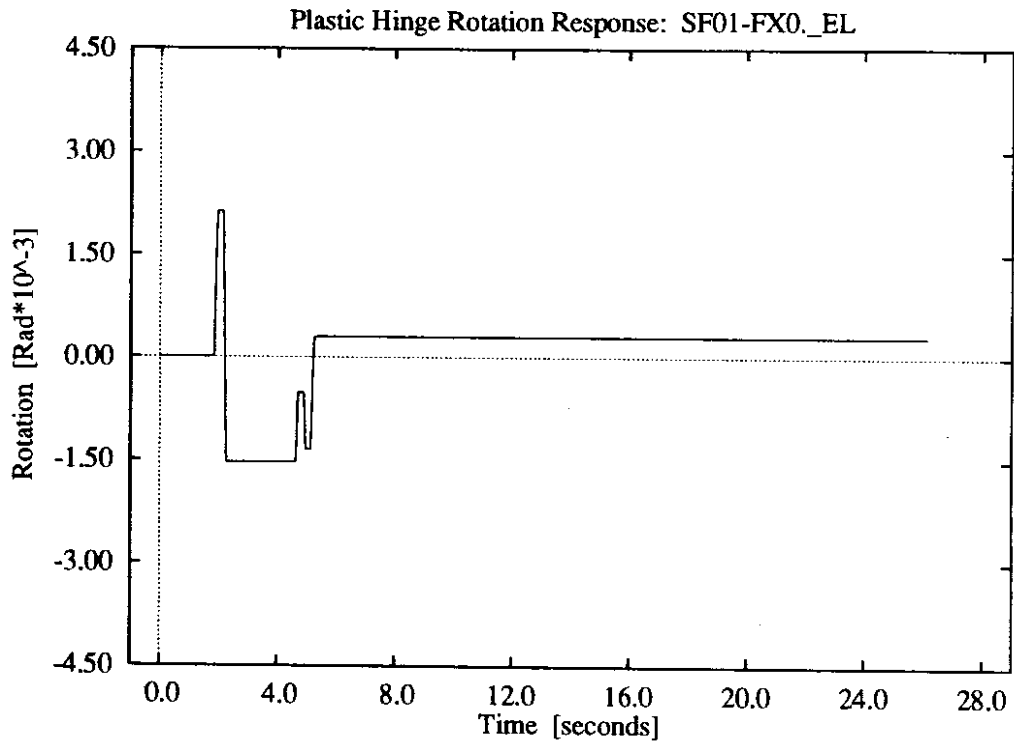
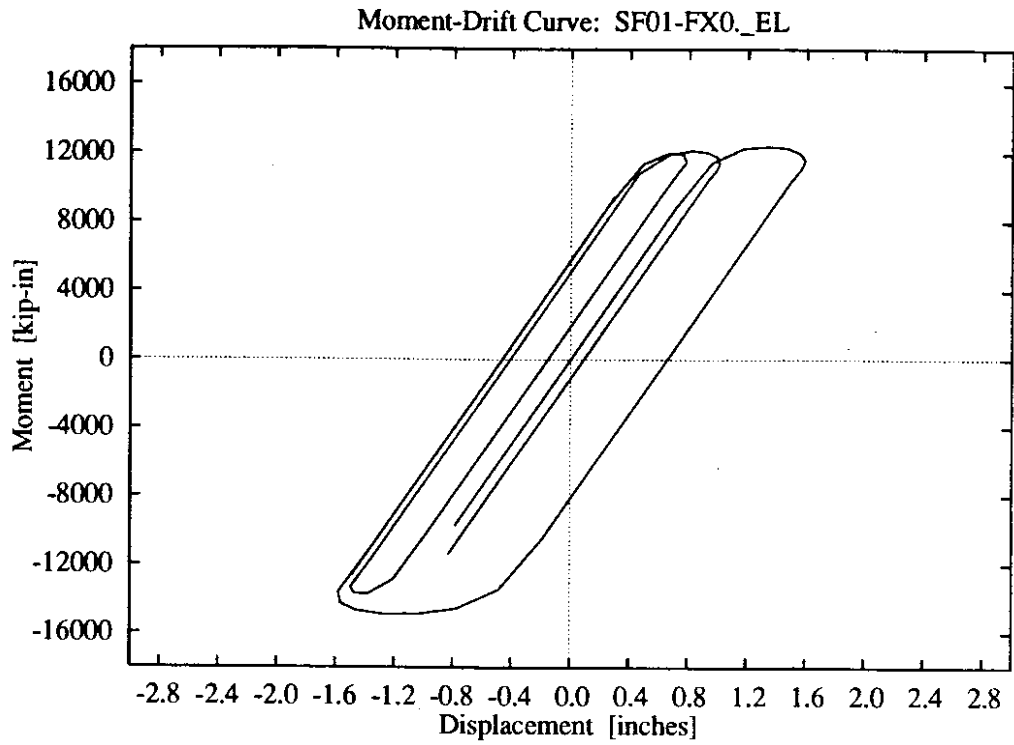


**Figure D-2:** Fixed-base foundation,  
lower intensity El Centro record.

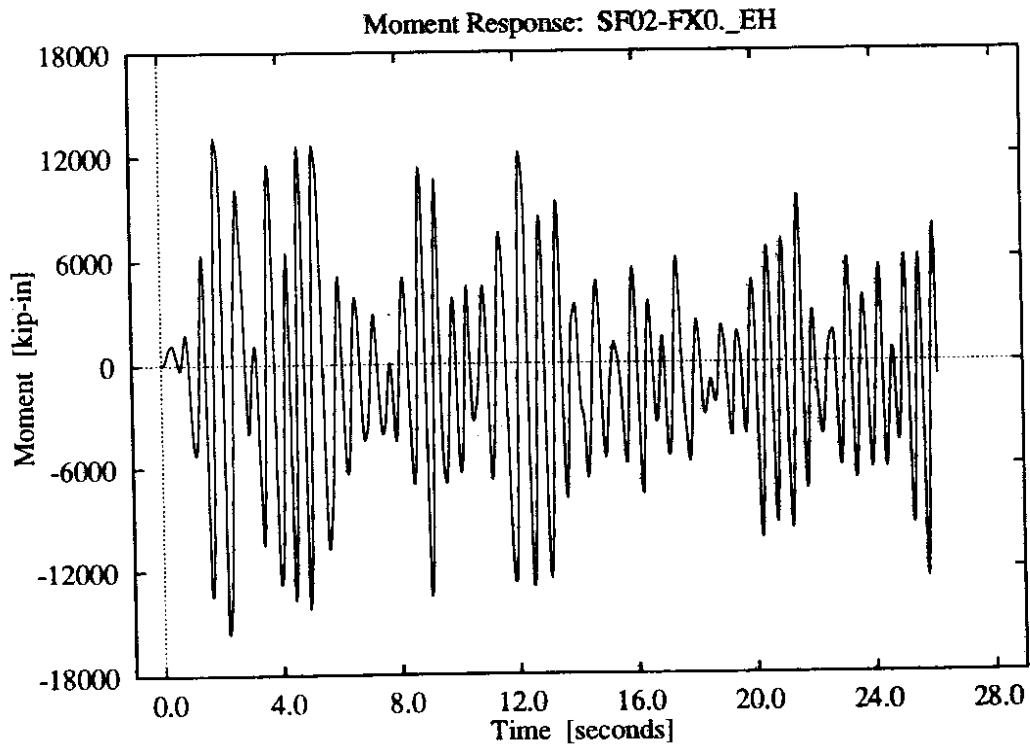
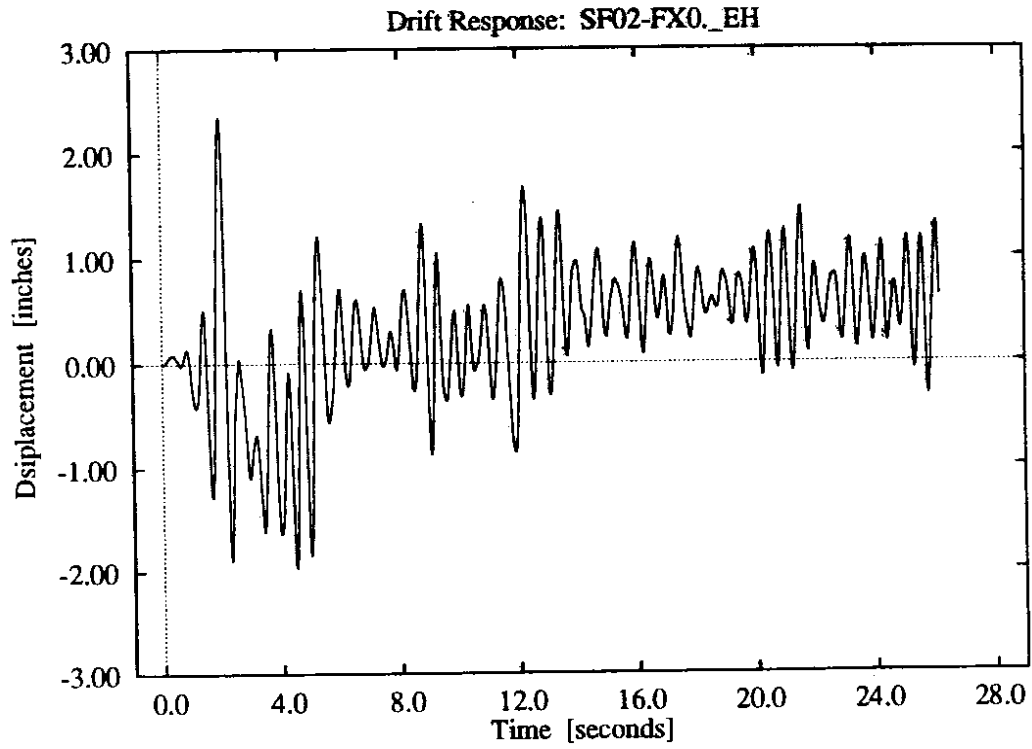


**Figure D-3: Fixed-base foundation,  
higher intensity El Centro record.**

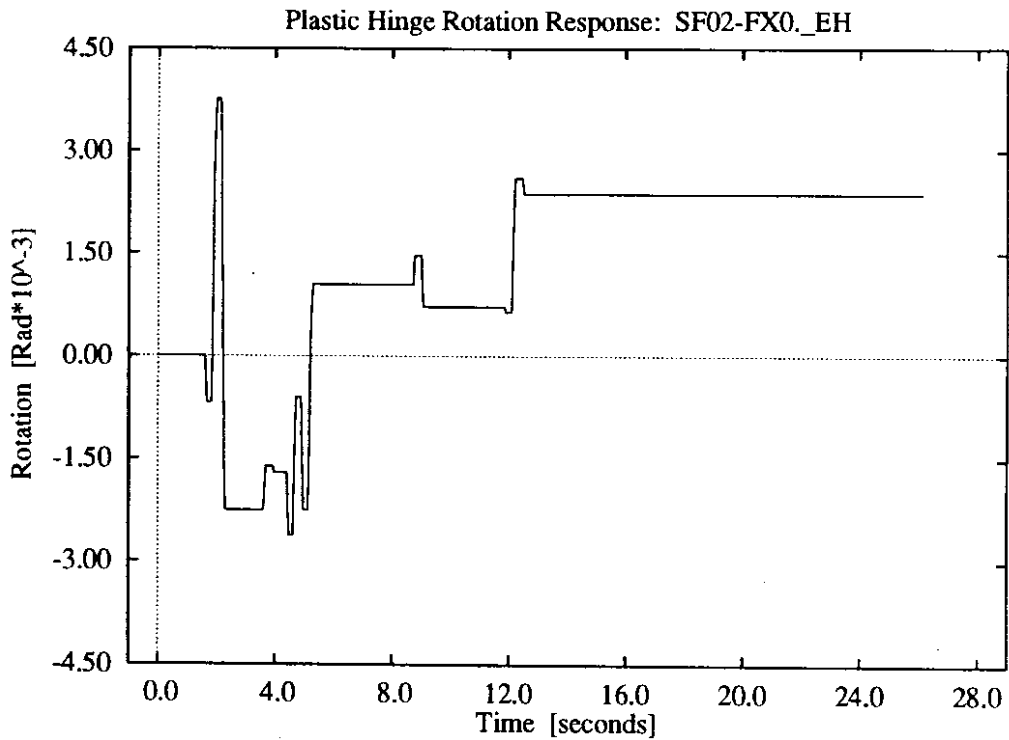
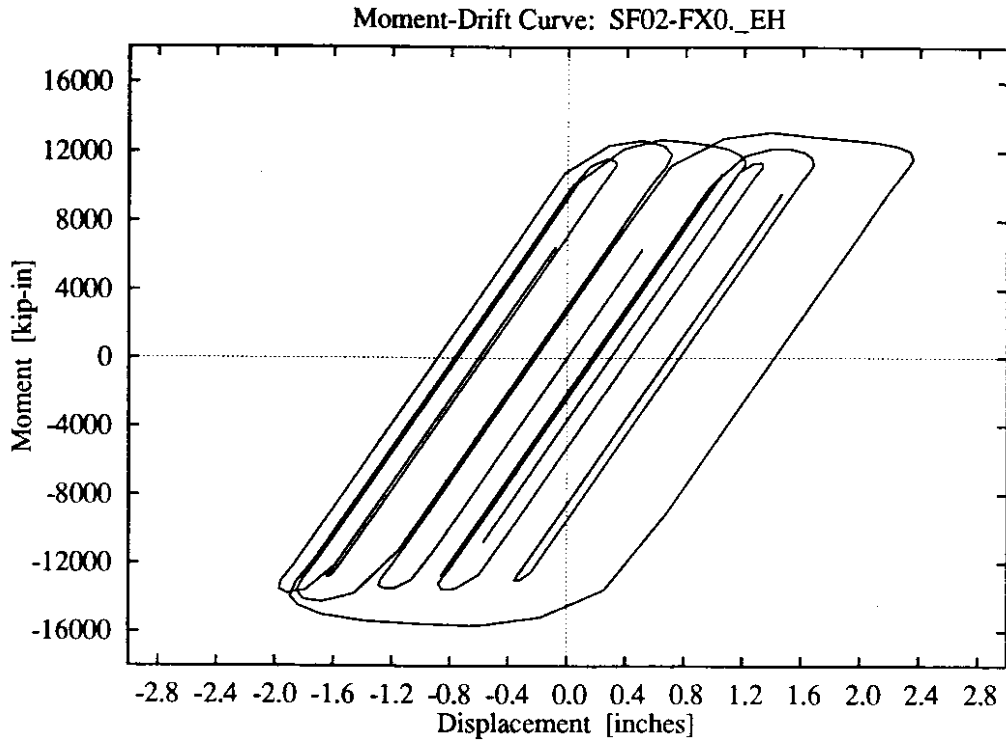


**Figure D-4:** Fixed-base foundation, higher intensity El Centro record.

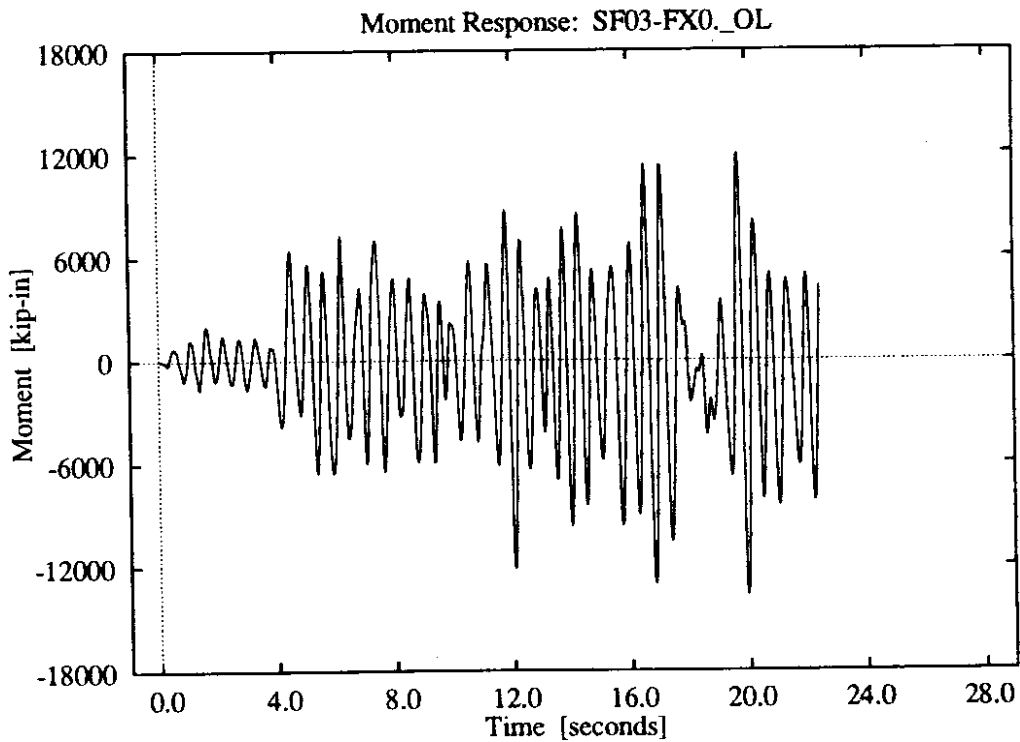
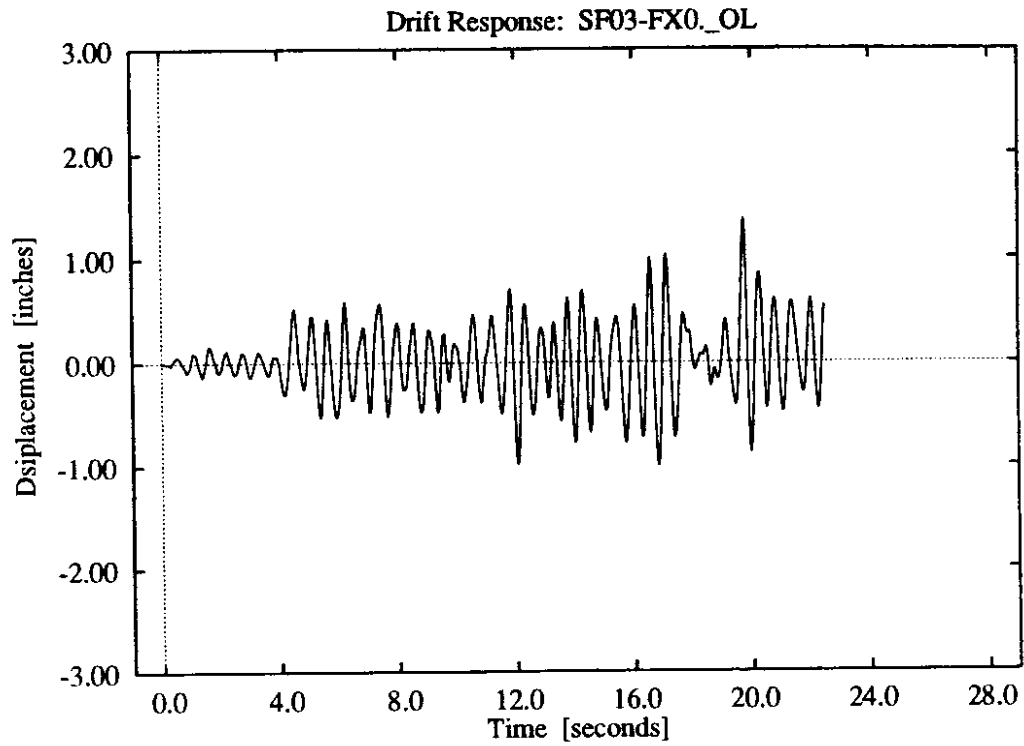


**Figure D-5: Fixed-base foundation,  
lower intensity Olympia record.**

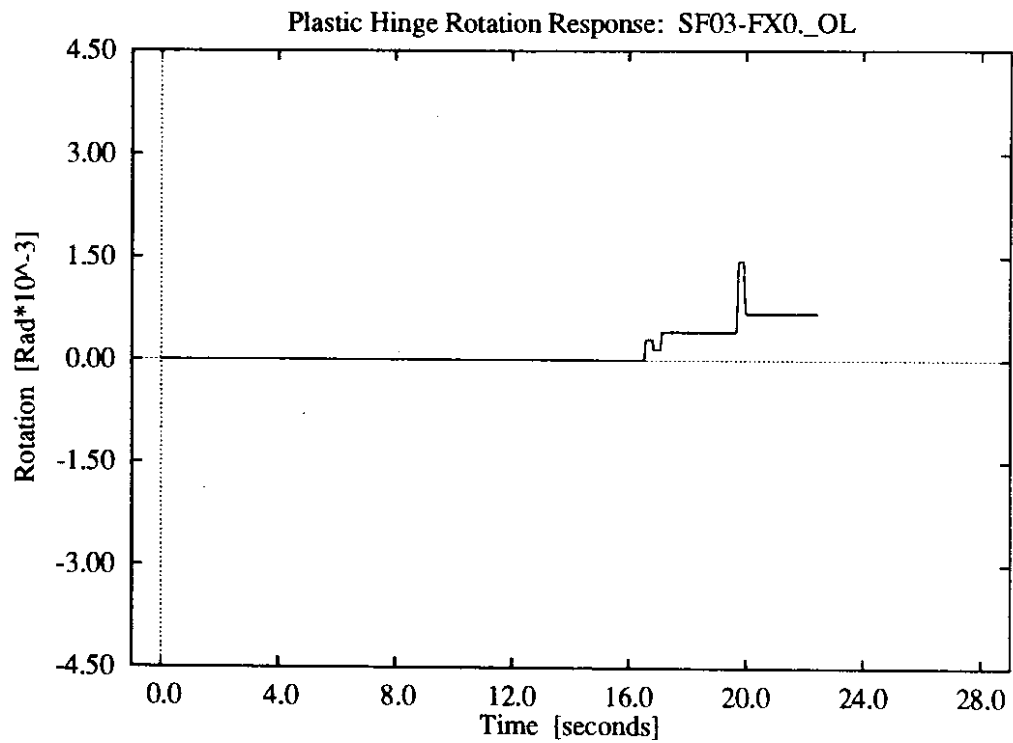
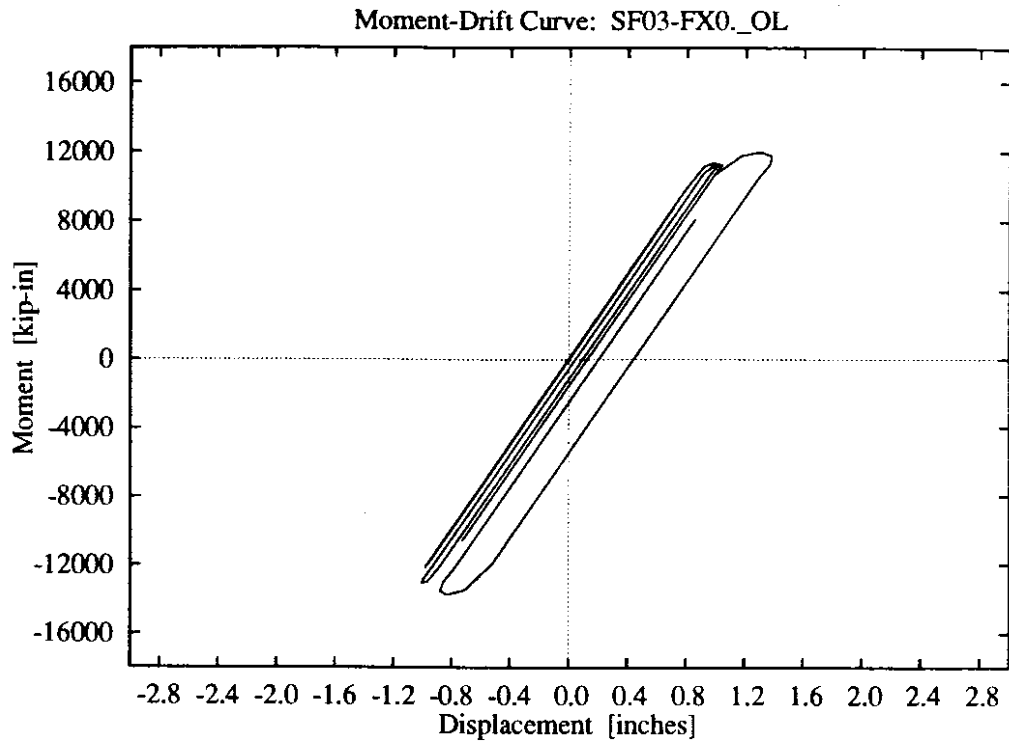


**Figure D-6:** Fixed-base foundation,  
lower intensity Olympia record.



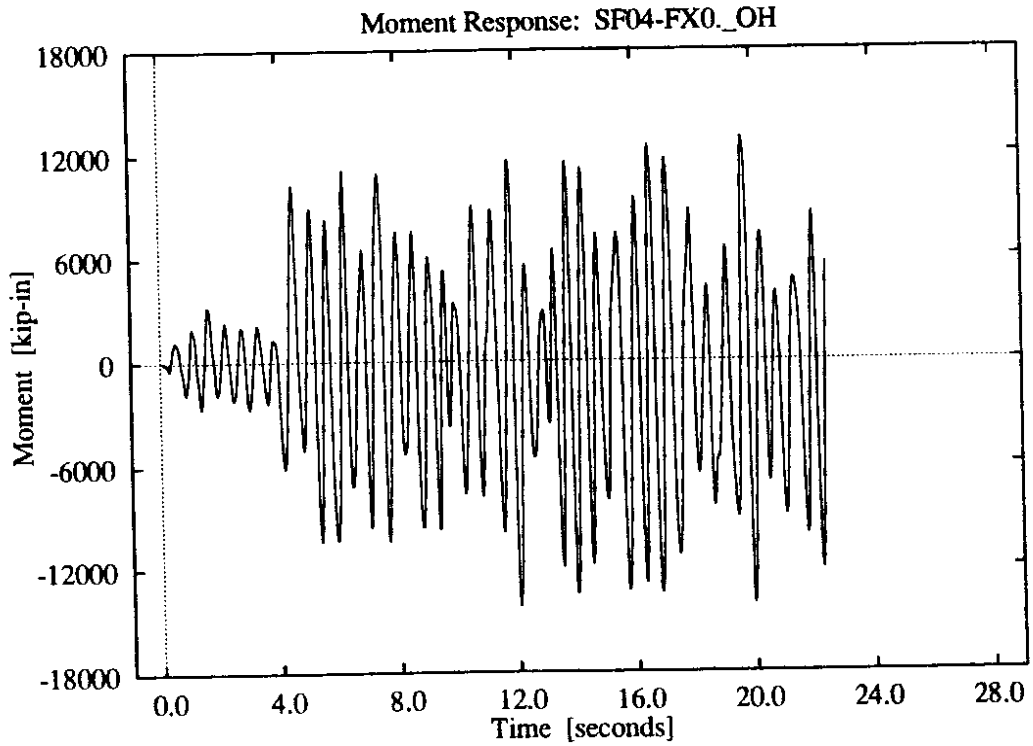
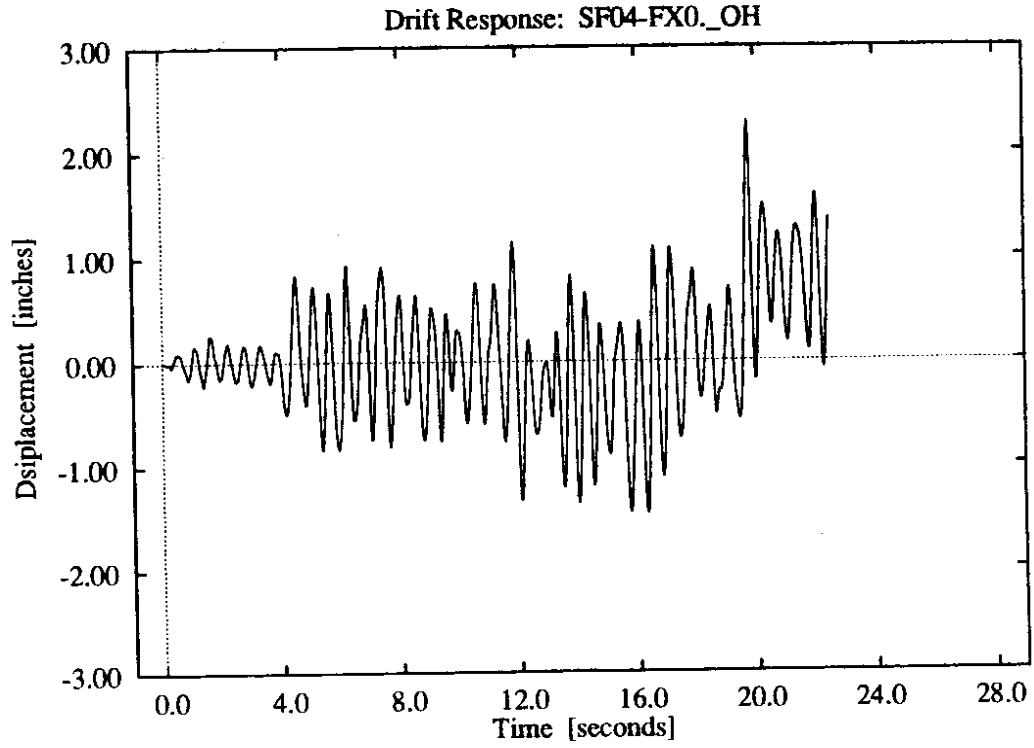


**Figure D-7: Fixed-base foundation,  
higher intensity Olympia record.**

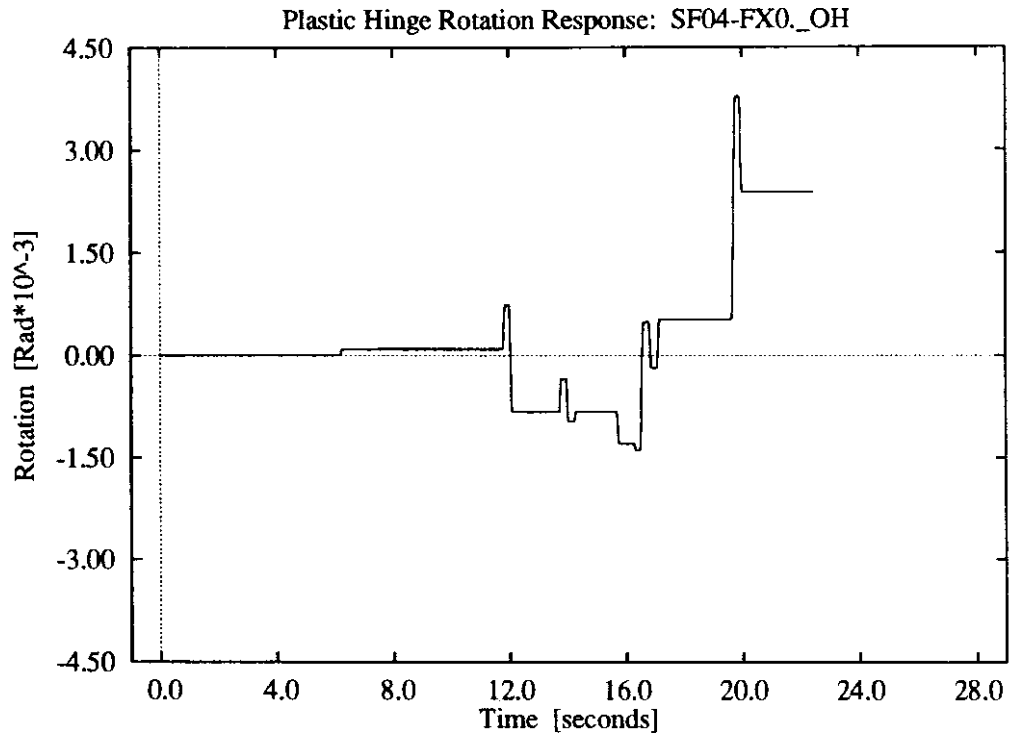
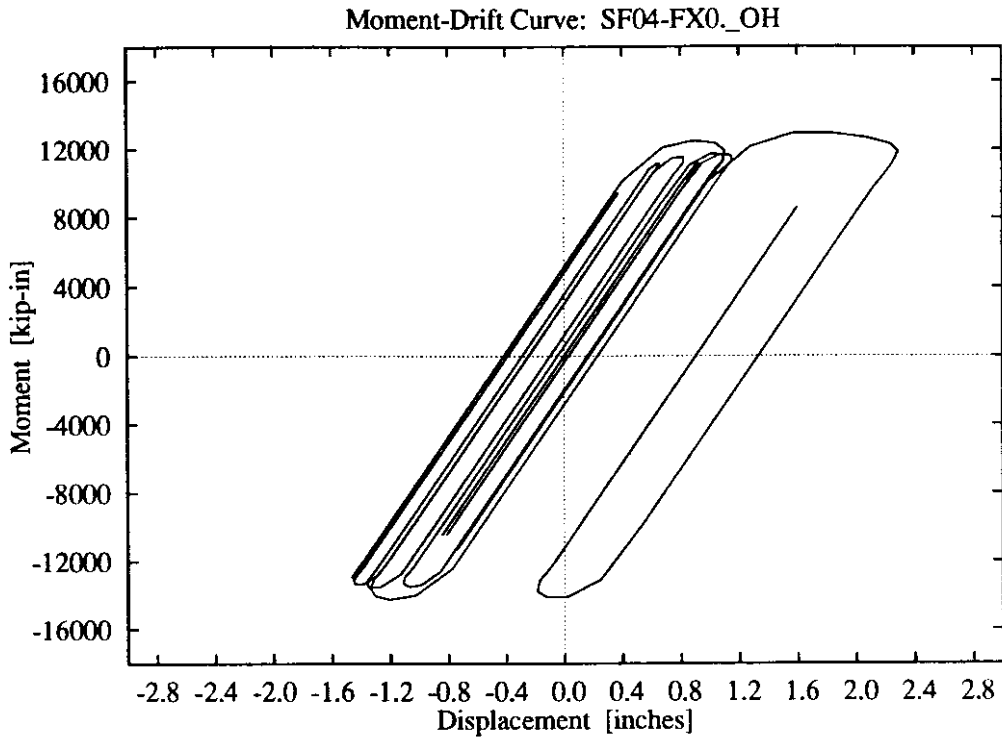


**Figure D-8:** Fixed-base foundation, higher intensity Olympia record.

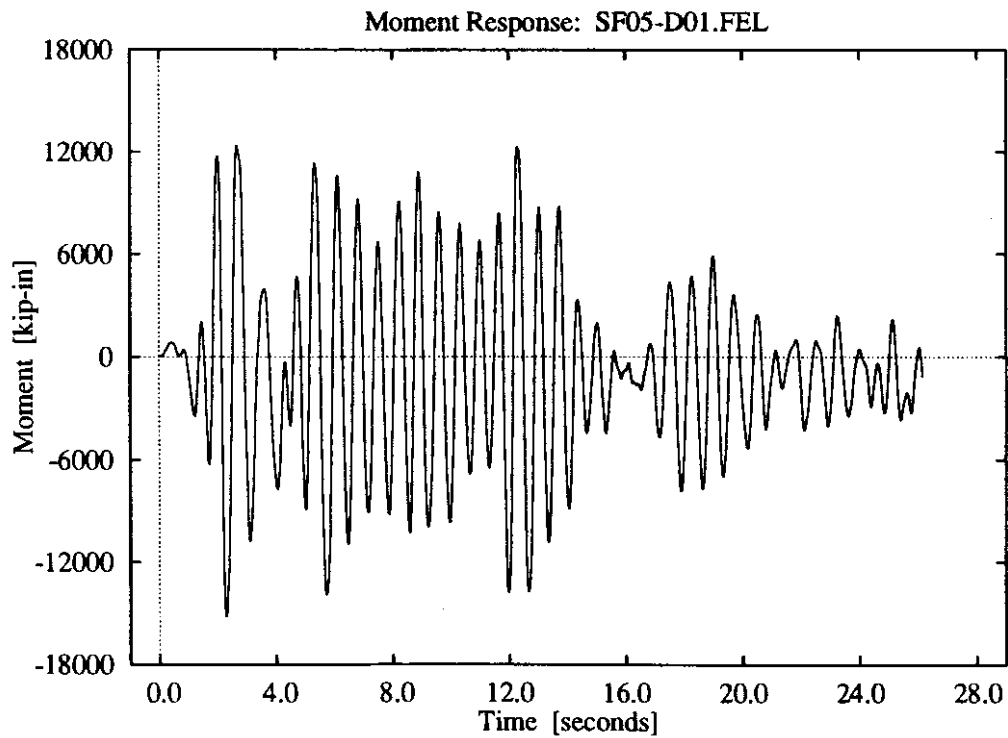
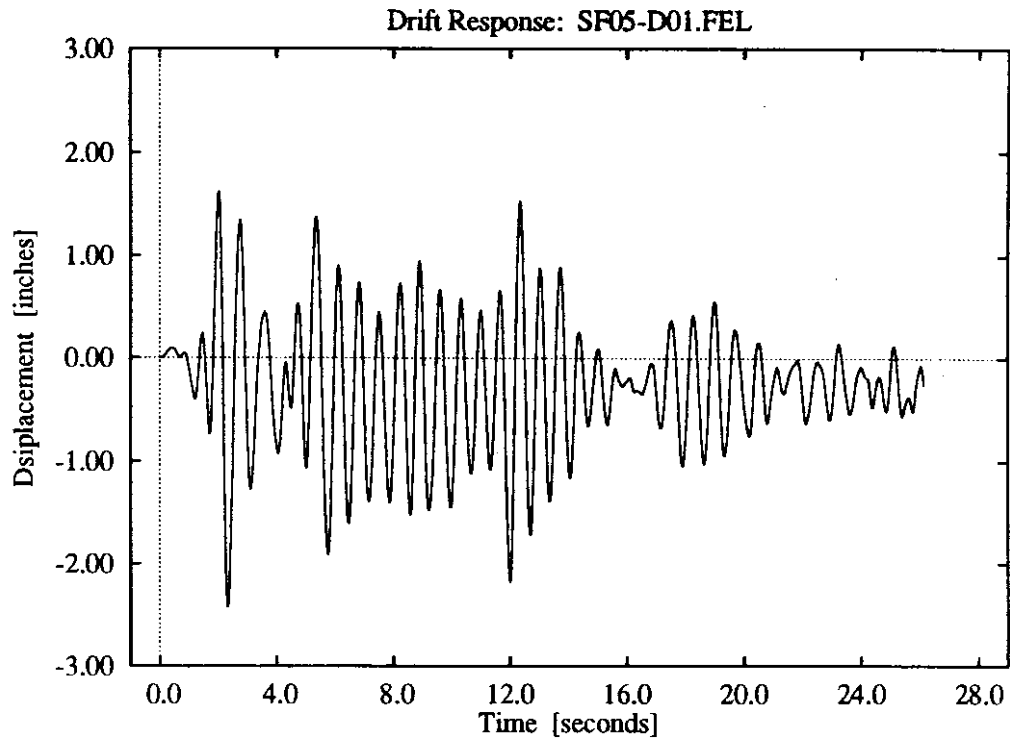


**Figure D-9:** 1 parameter foundation model, low soil stiffness, lower intensity El Centro record.

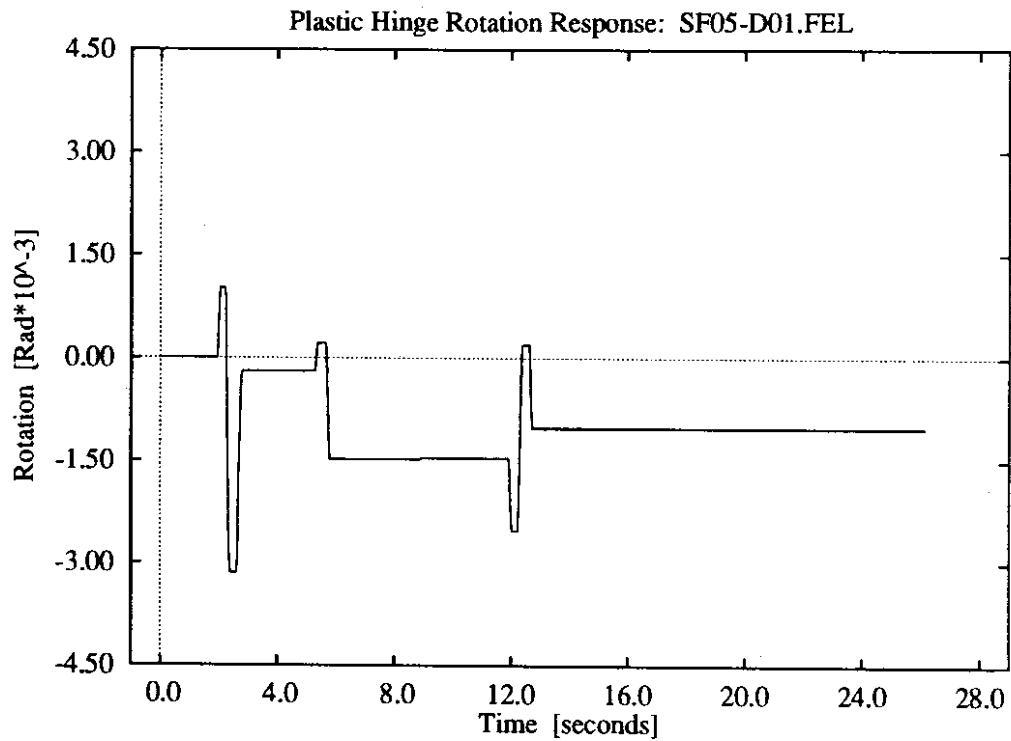
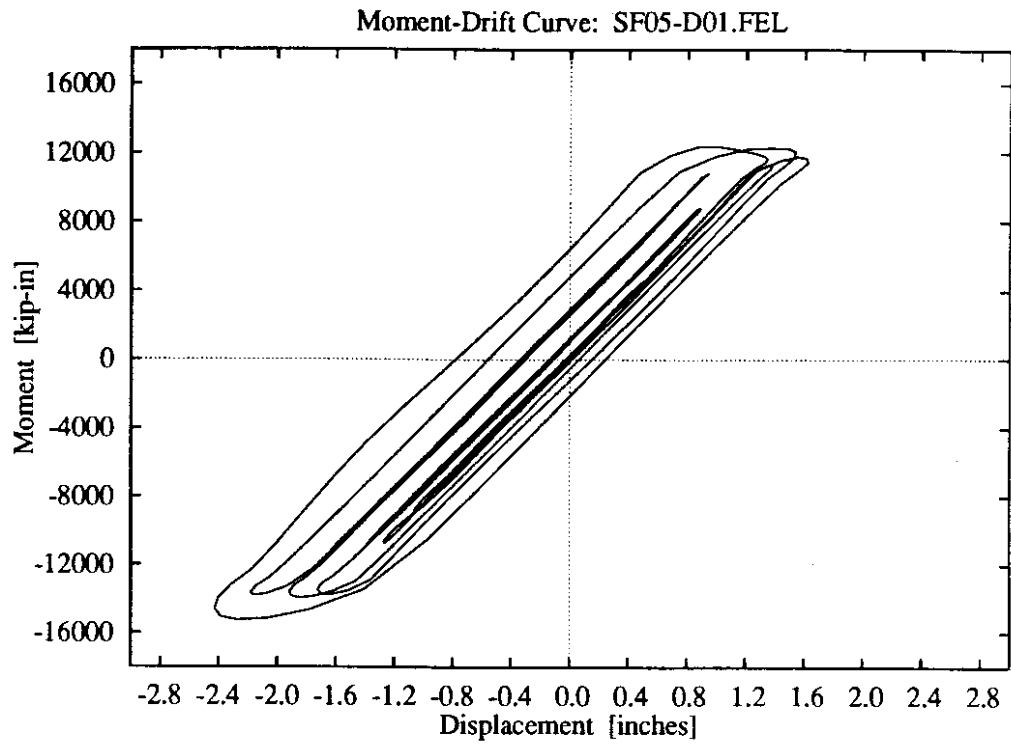


**Figure D-10:** 1 parameter foundation model, low soil stiffness, lower intensity El Centro record.

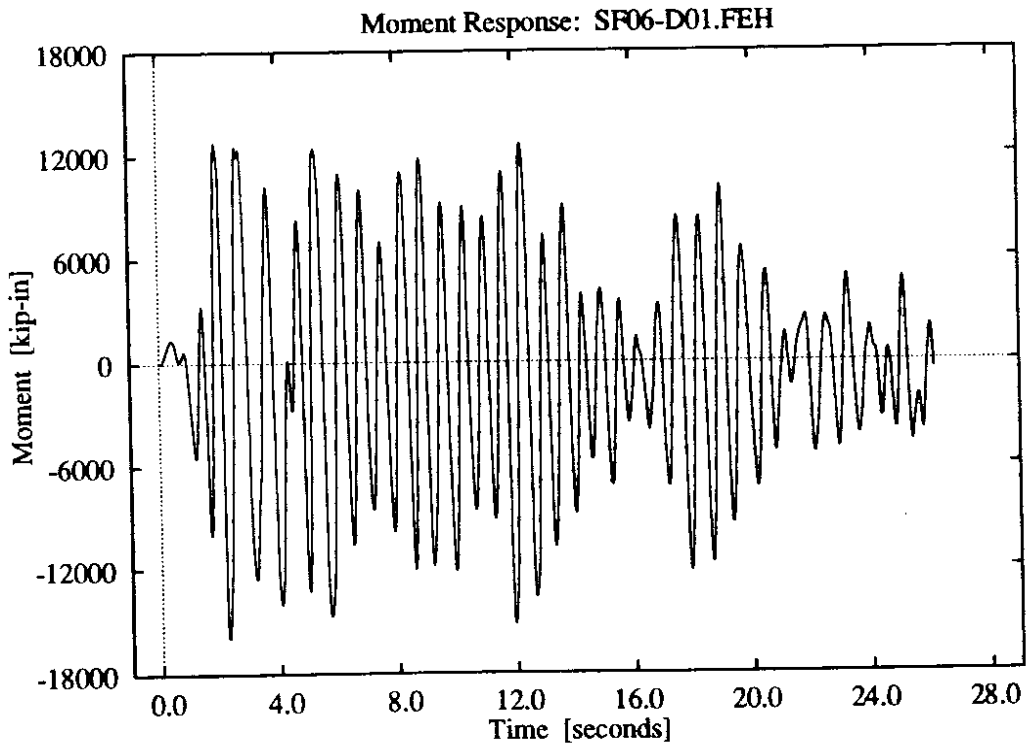
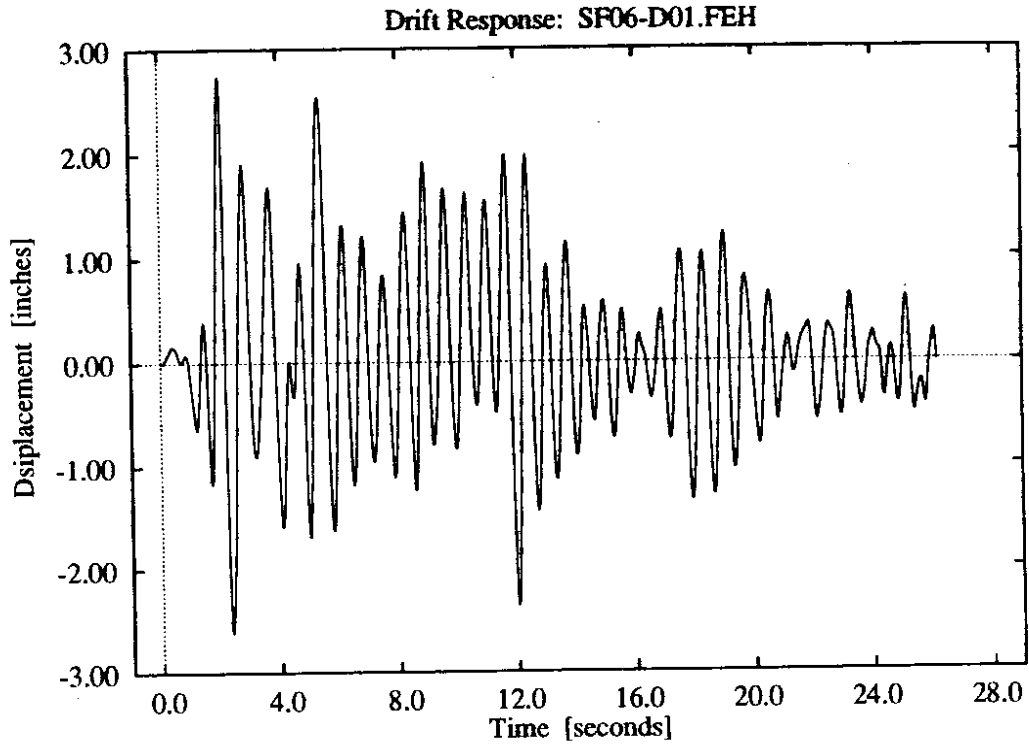


**Figure D-11: 1 parameter foundation model, low soil stiffness, higher intensity El Centro record.**

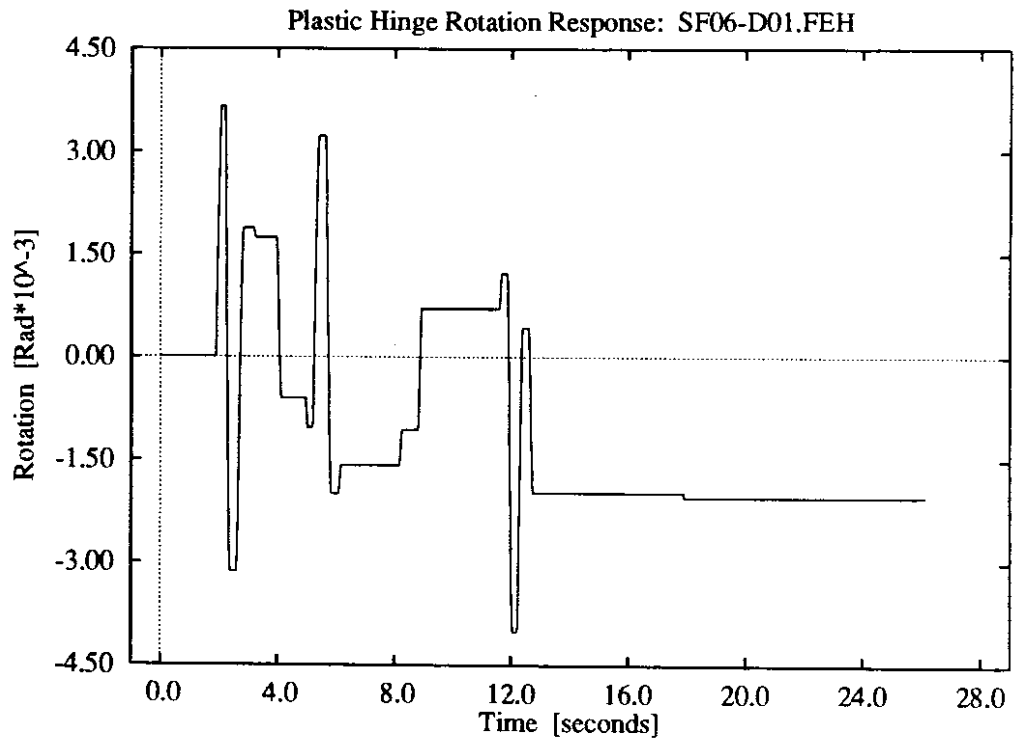
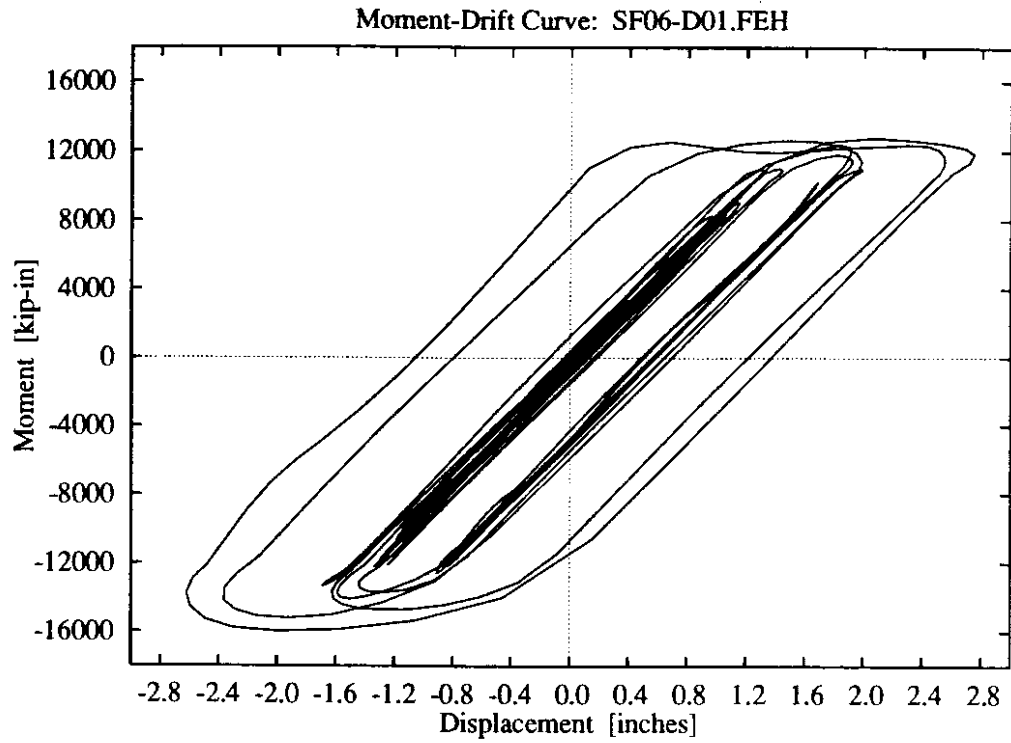


**Figure D-12:** 1 parameter foundation model, low soil stiffness, higher intensity El Centro record.

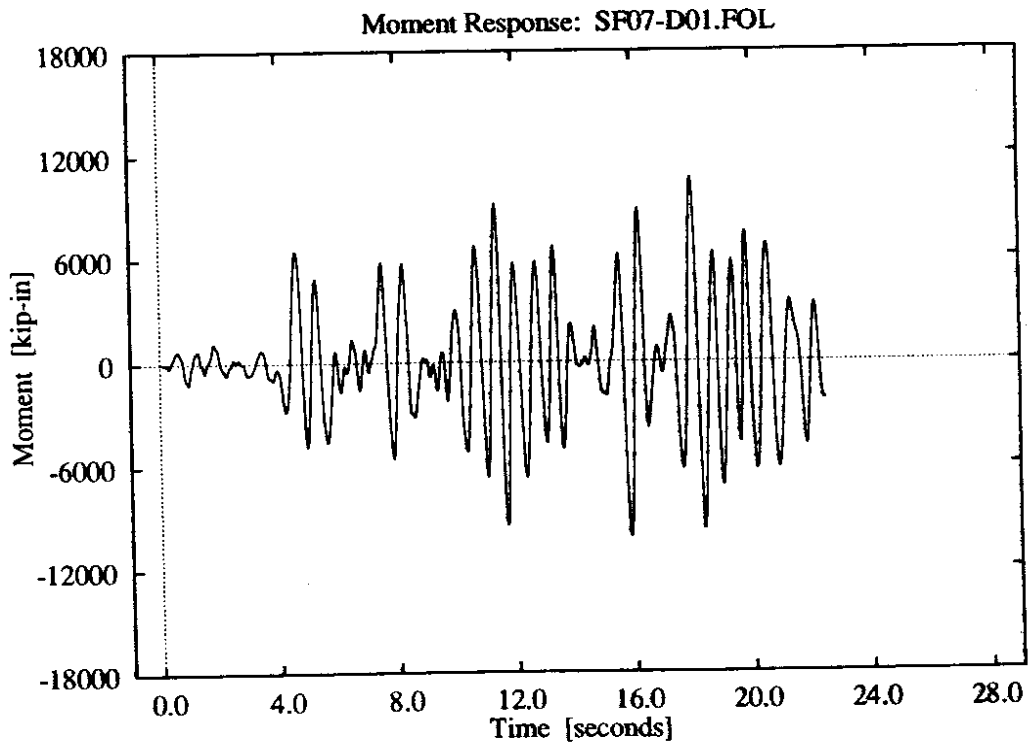
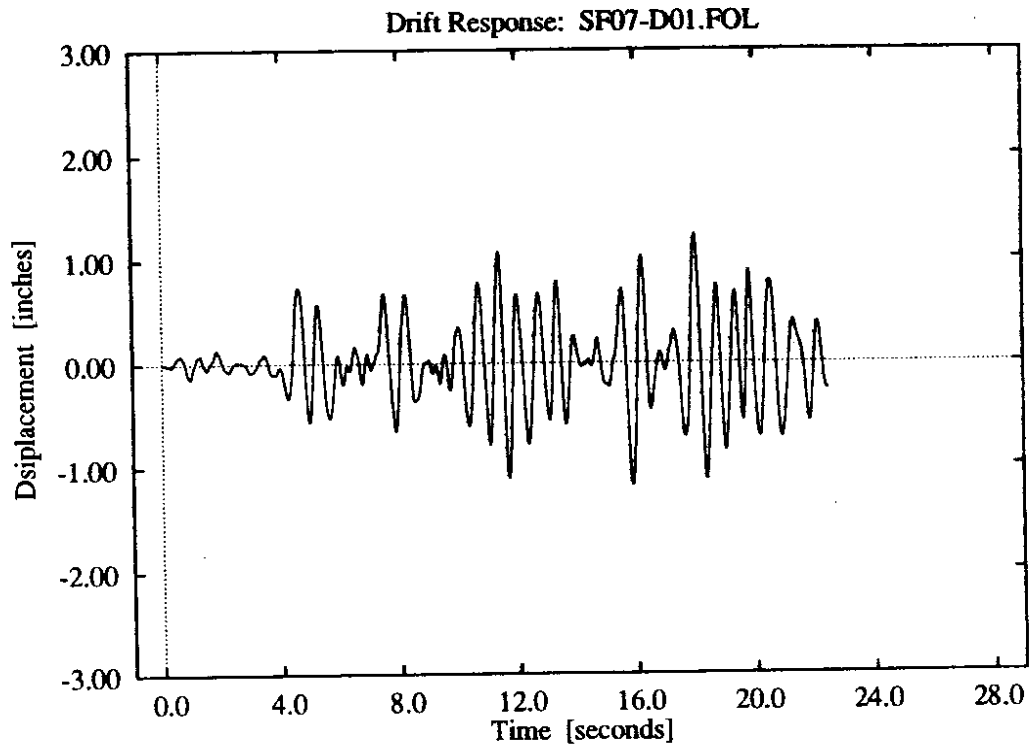


**Figure D-13:** 1 parameter foundation model, low soil stiffness, lower intensity Olympia record.

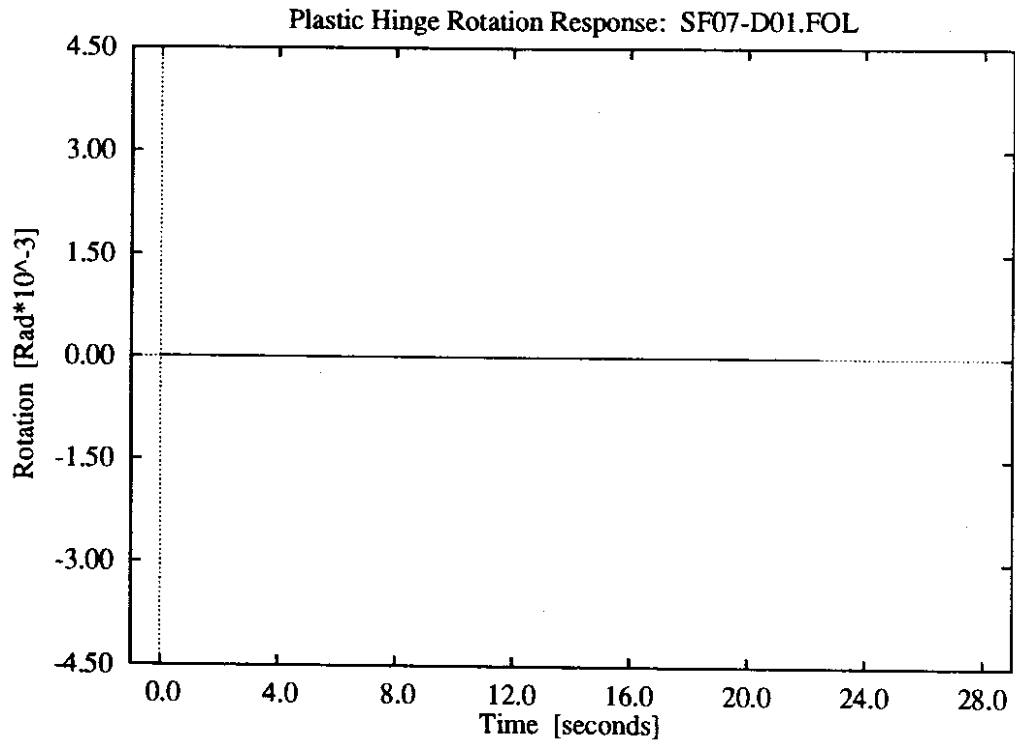
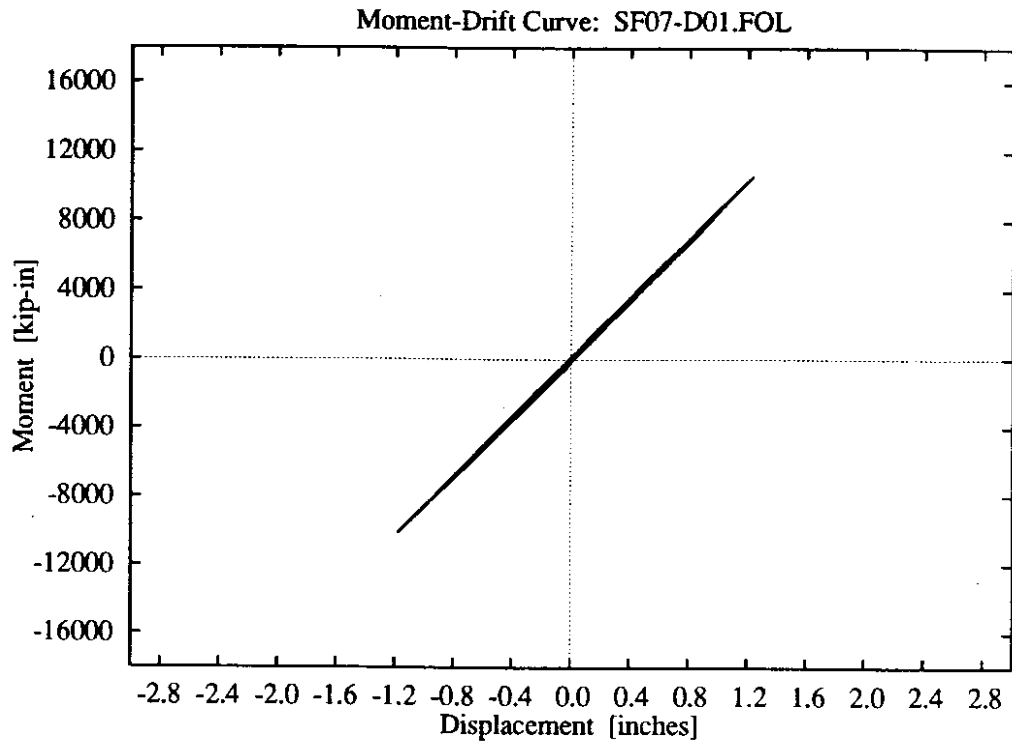


**Figure D-14:** 1 parameter foundation model, low soil stiffness, lower intensity Olympia record.



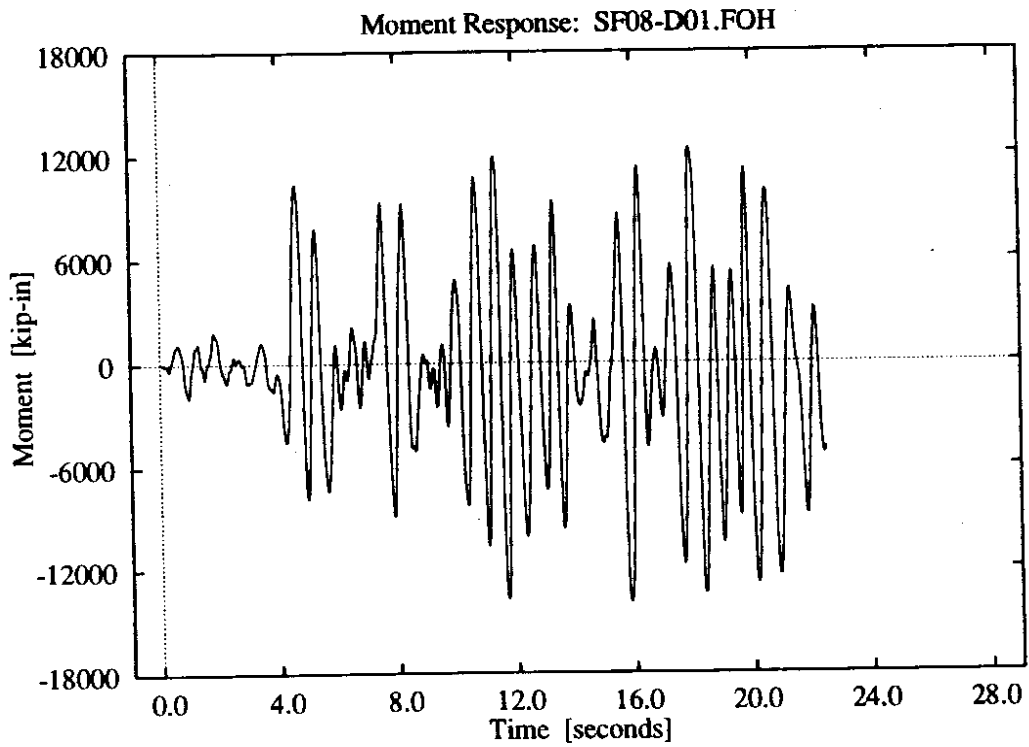
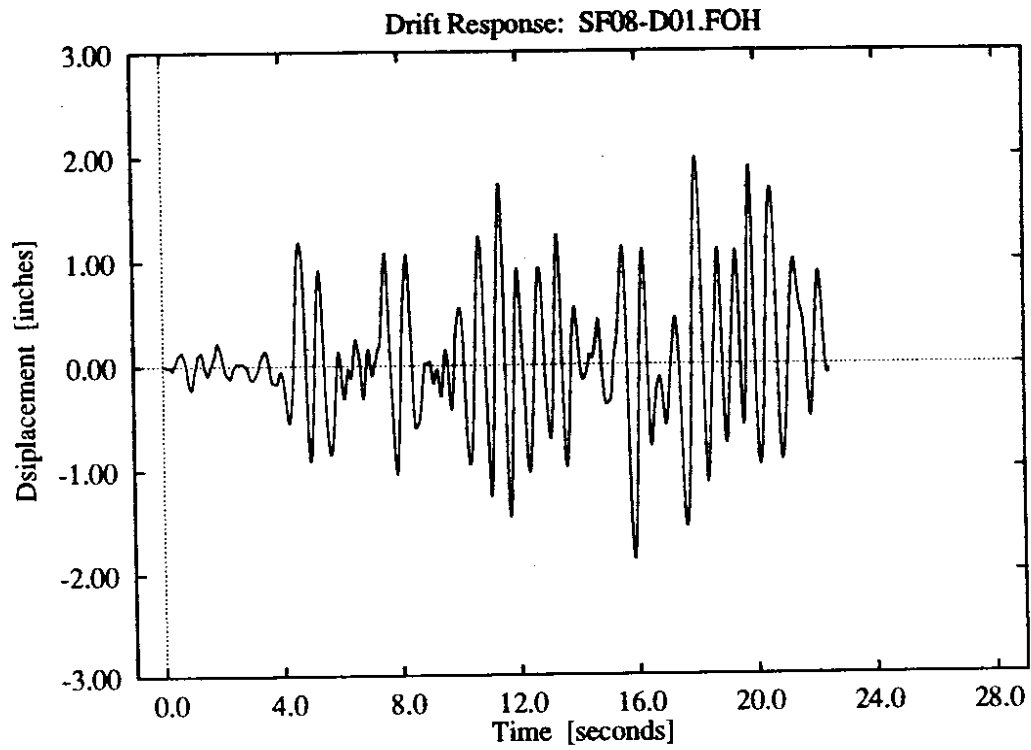


**Figure D-15:** 1 parameter foundation model, low soil stiffness, higher intensity Olympia record.

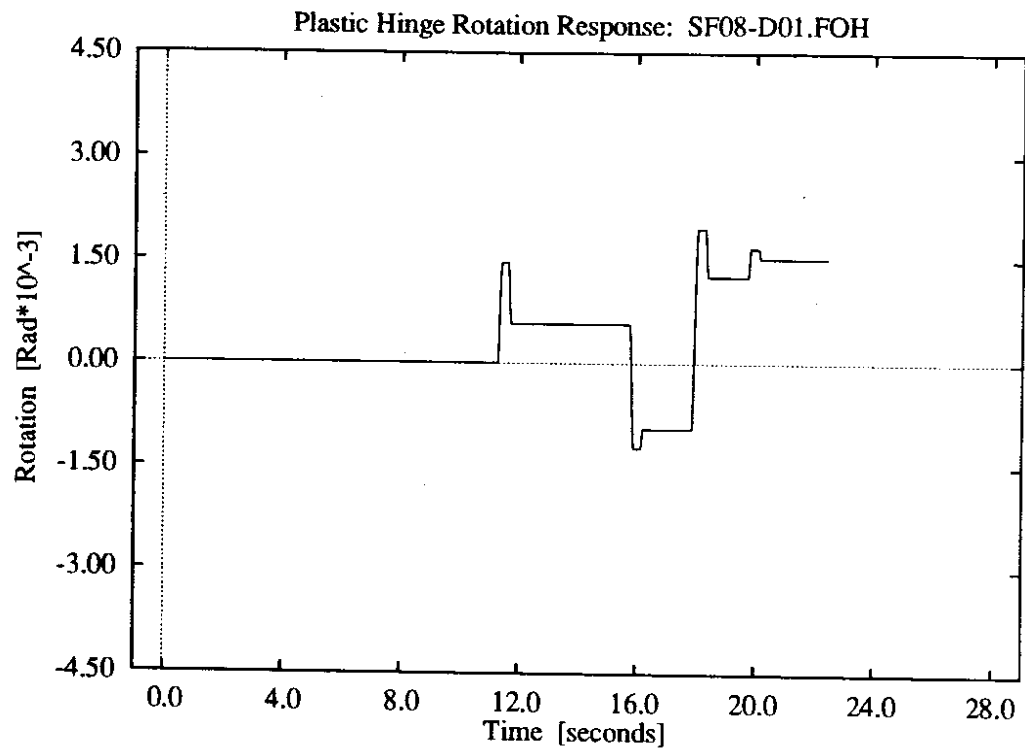
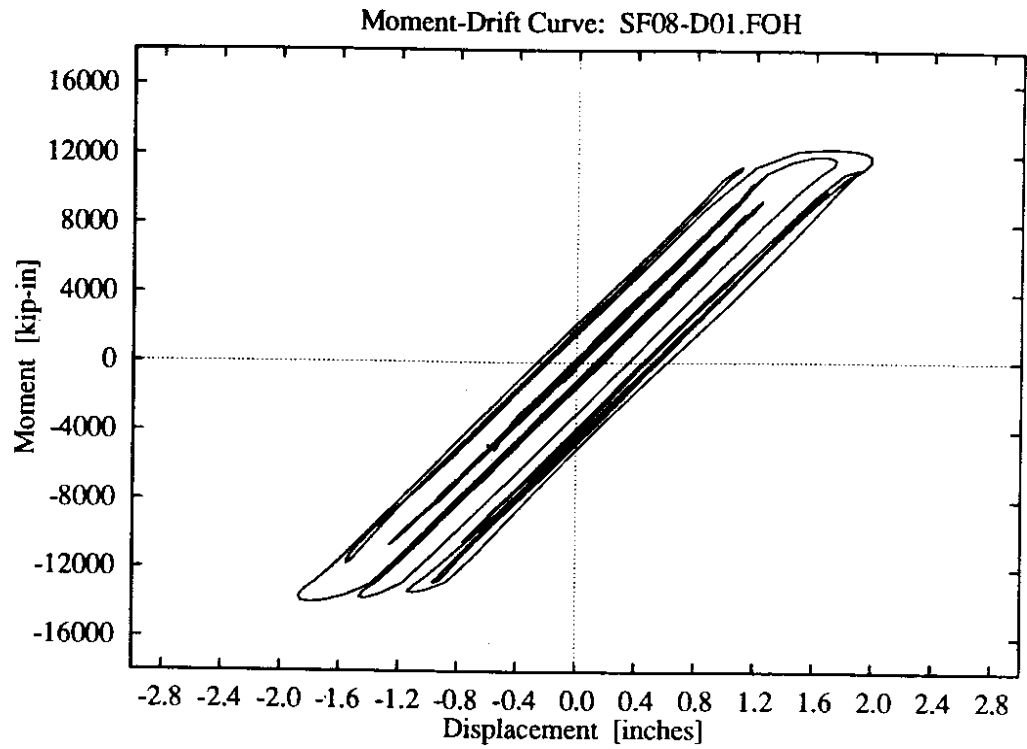


**Figure D-16:** 1 parameter foundation model, low soil stiffness, higher intensity Olympia record.

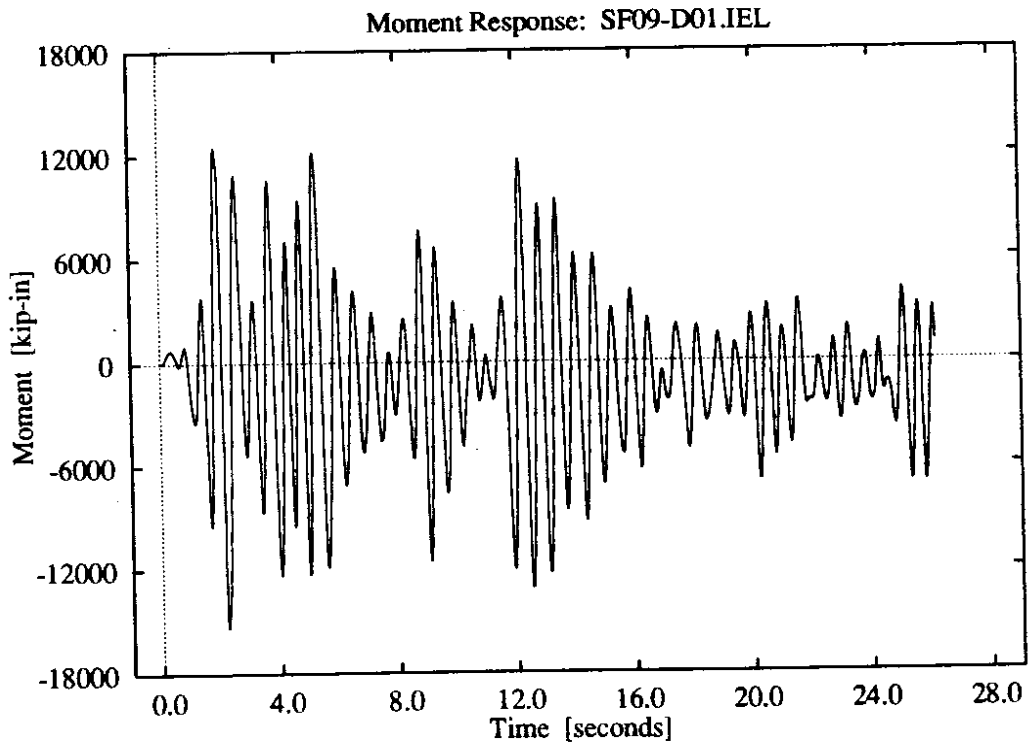
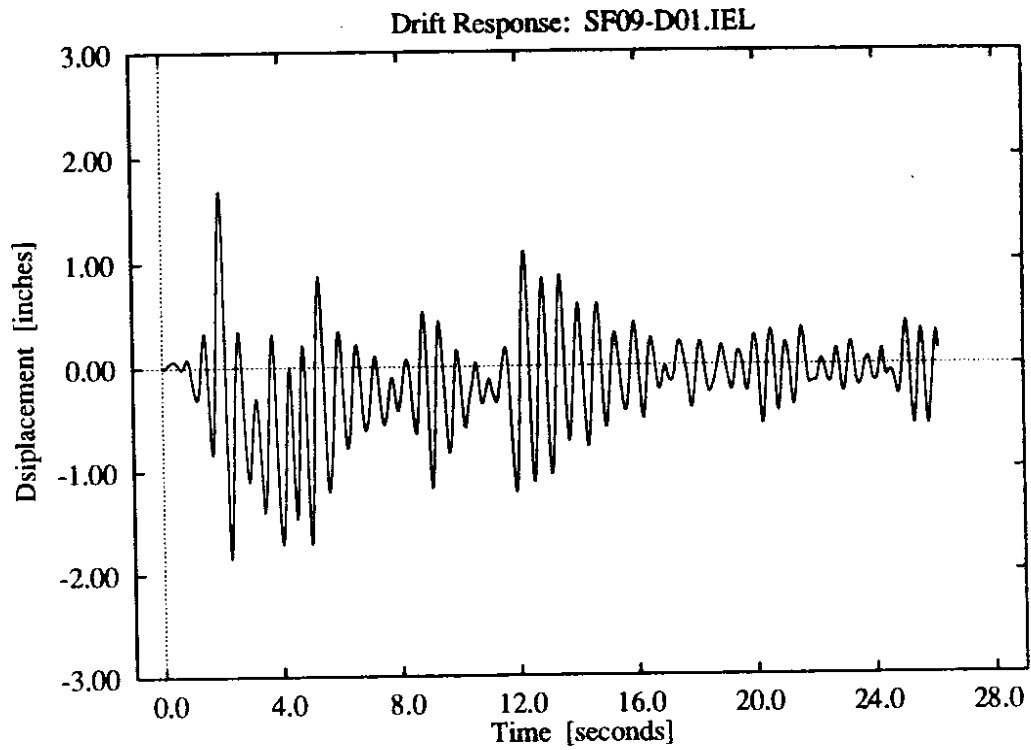


**Figure D-17: 1 parameter foundation model, intermediate soil stiffness, lower intensity El Centro record.**

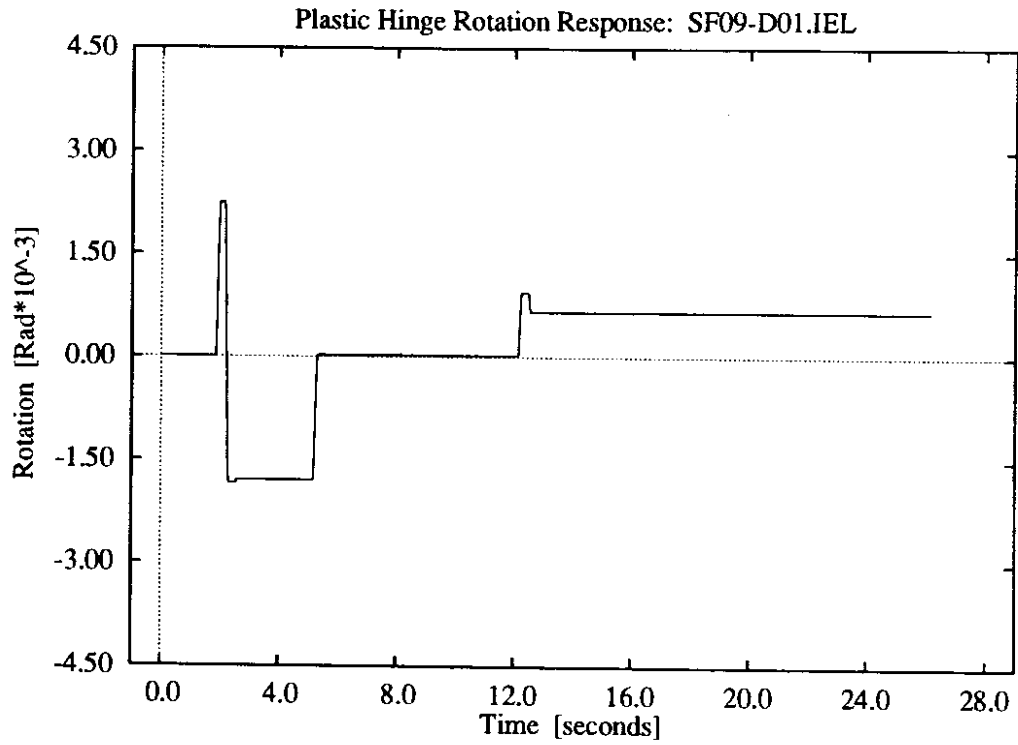
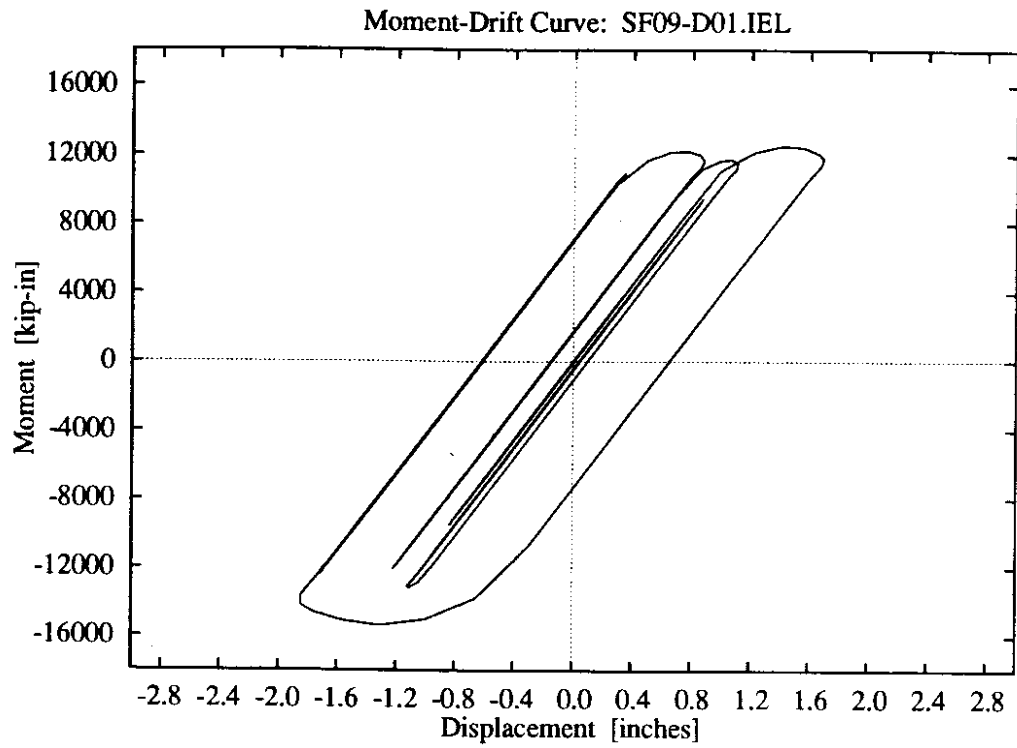


**Figure D-18:** 1 parameter foundation model, intermediate soil stiffness, lower intensity El Centro record.

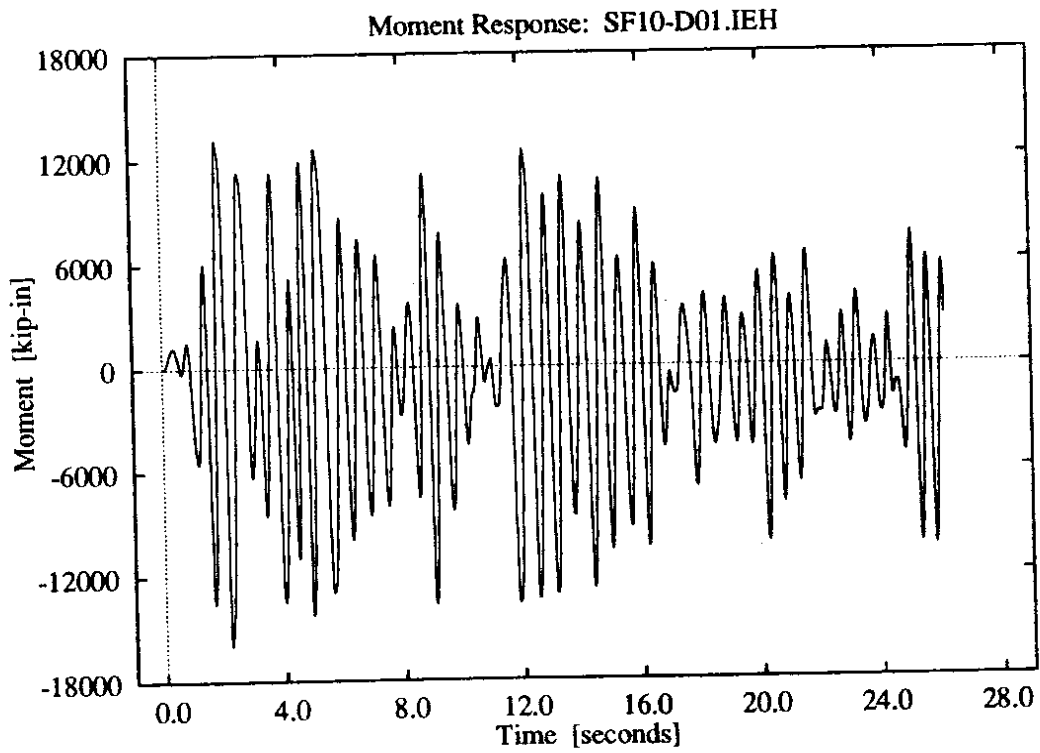
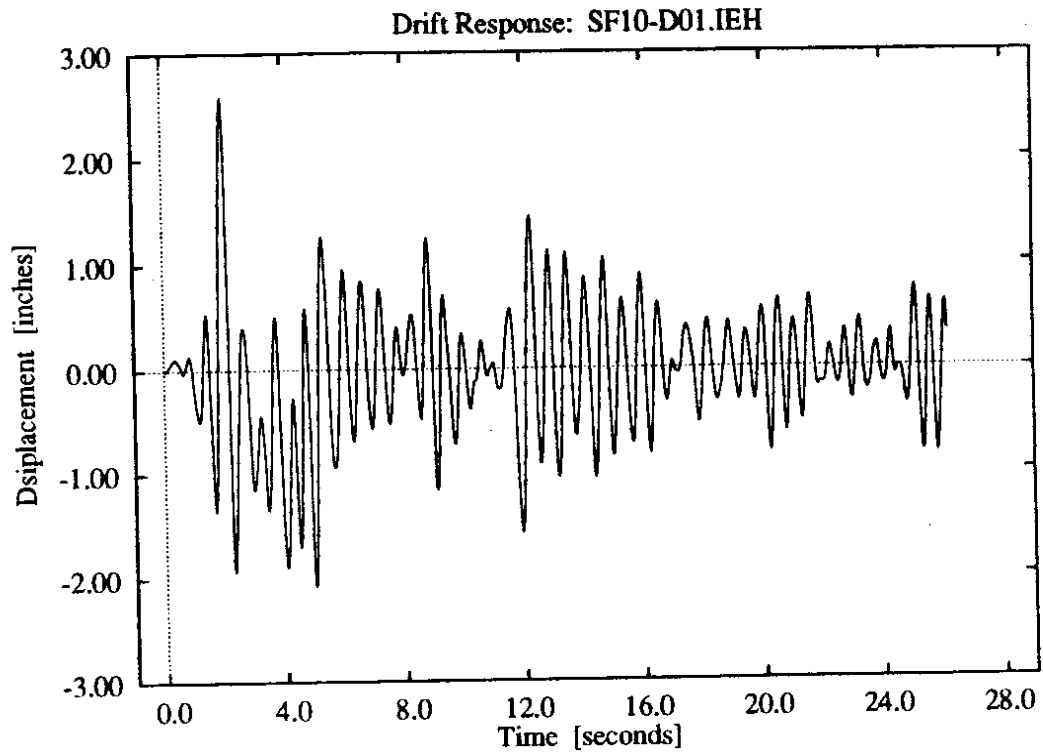


**Figure D-19: 1 parameter foundation model, intermediate soil stiffness, higher intensity El Centro record.**

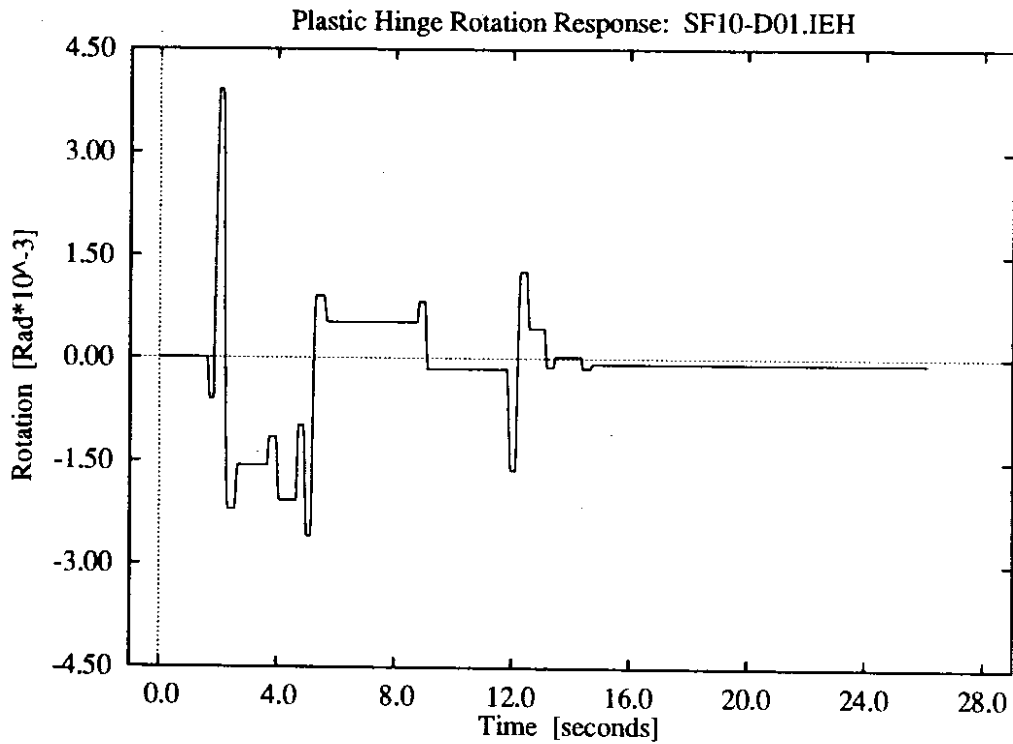
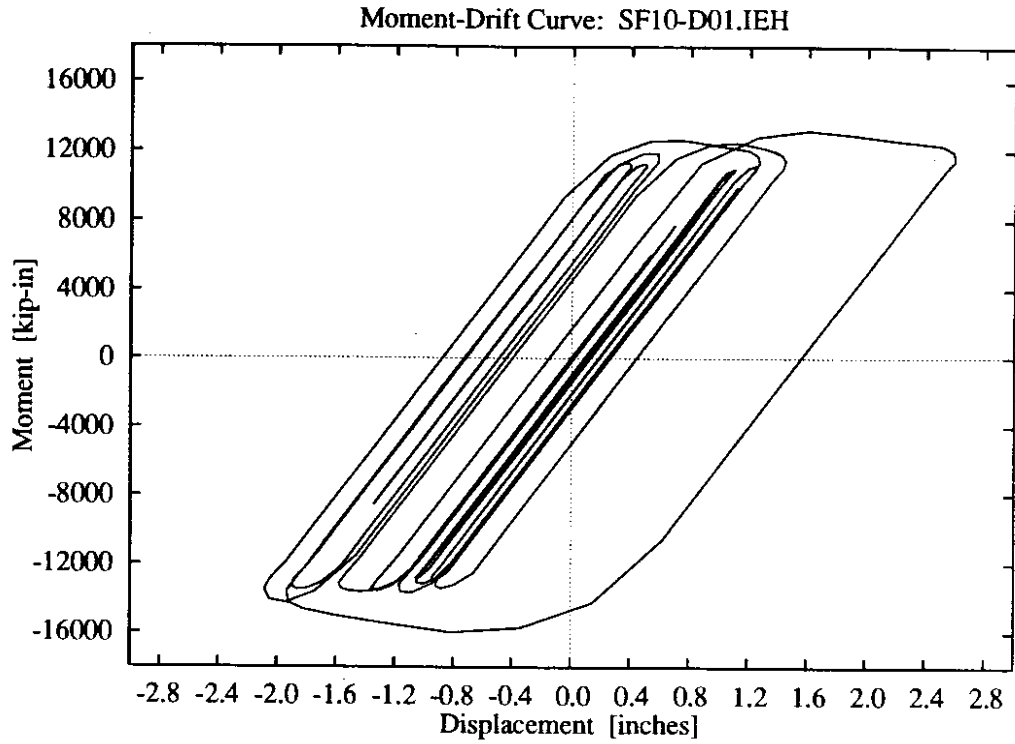


**Figure D-20:** 1 parameter foundation model, intermediate soil stiffness, higher intensity El Centro record.

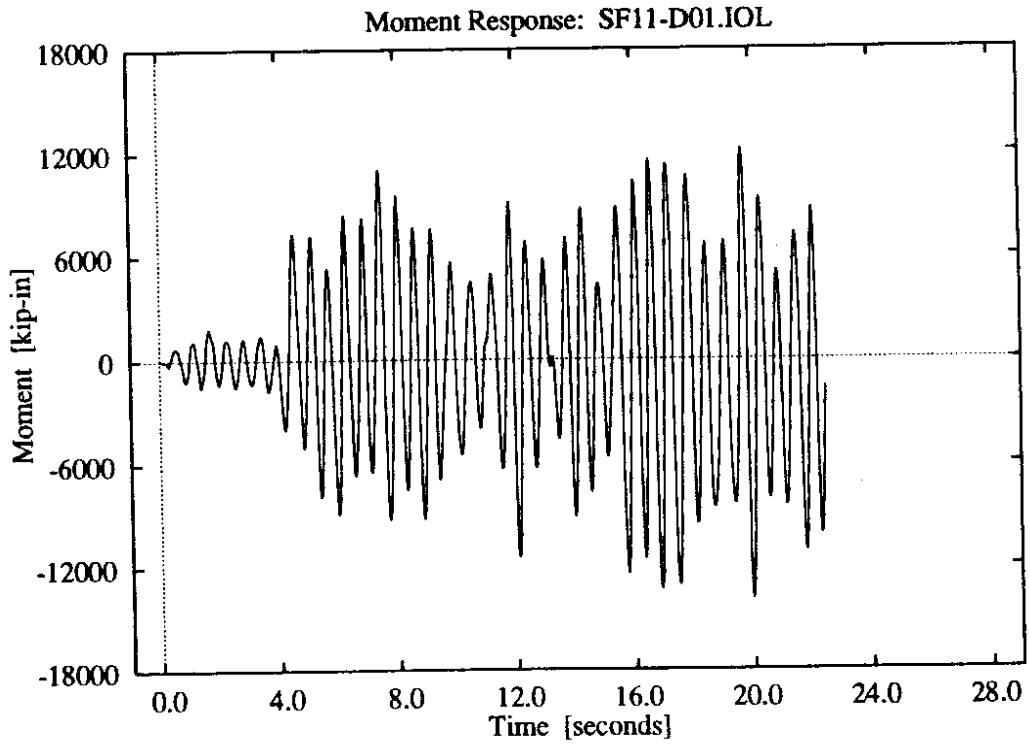
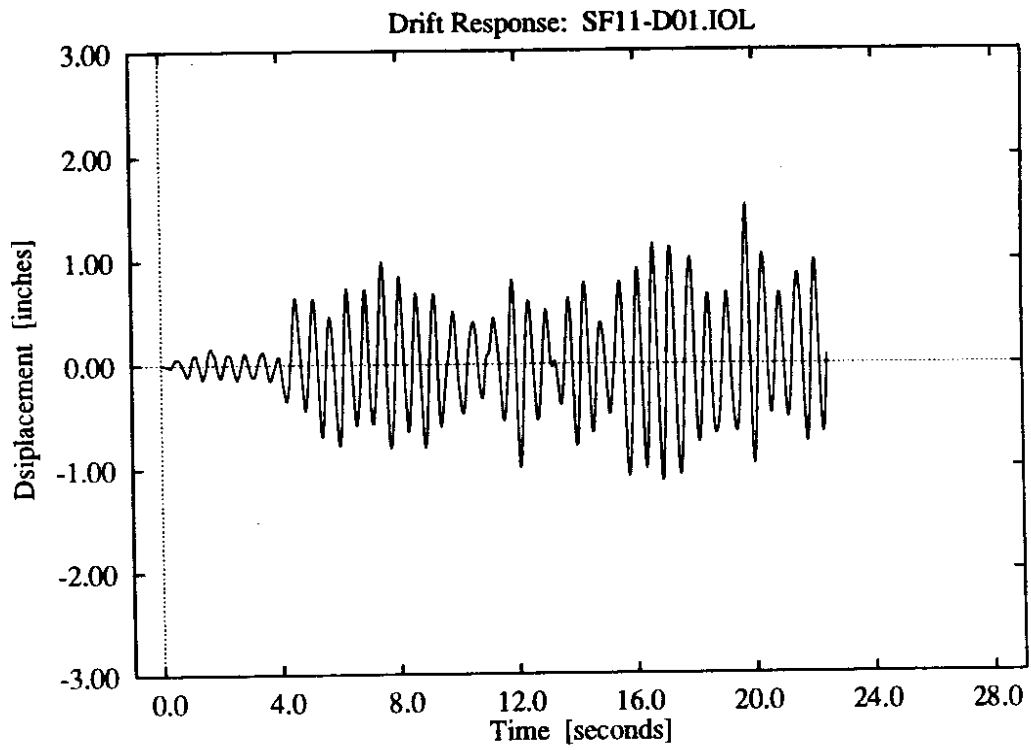


**Figure D-21: 1 parameter foundation model, intermediate soil stiffness, lower intensity Olympia record.**

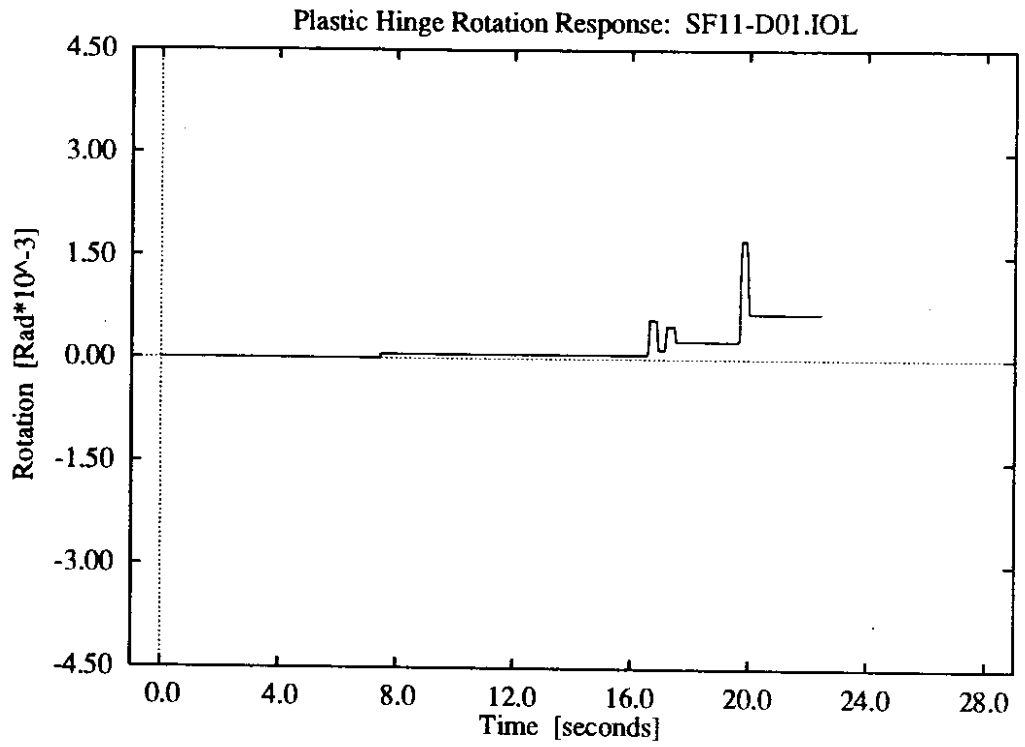
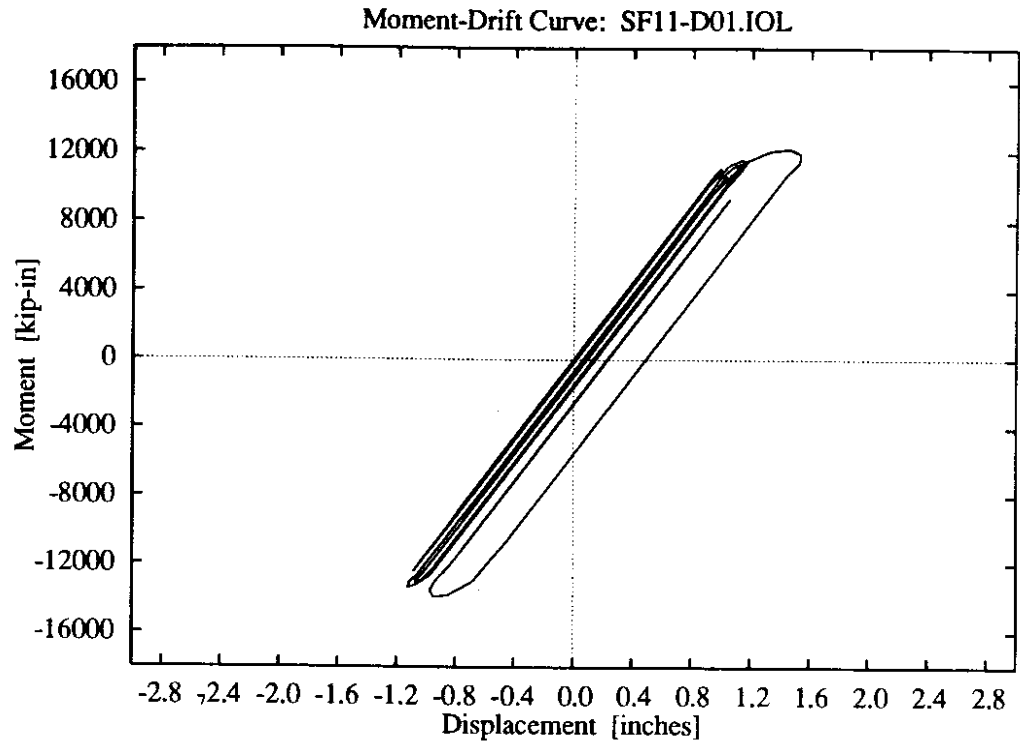


**Figure D-22:** 1 parameter foundation model, intermediate soil stiffness, lower intensity Olympia record.



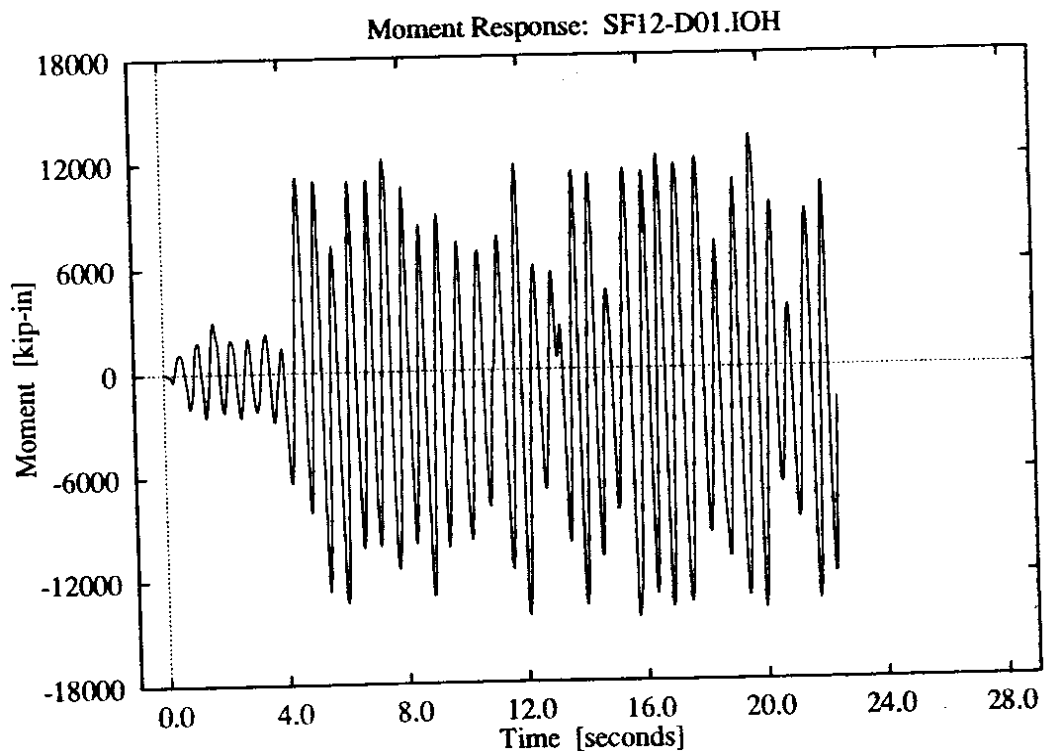
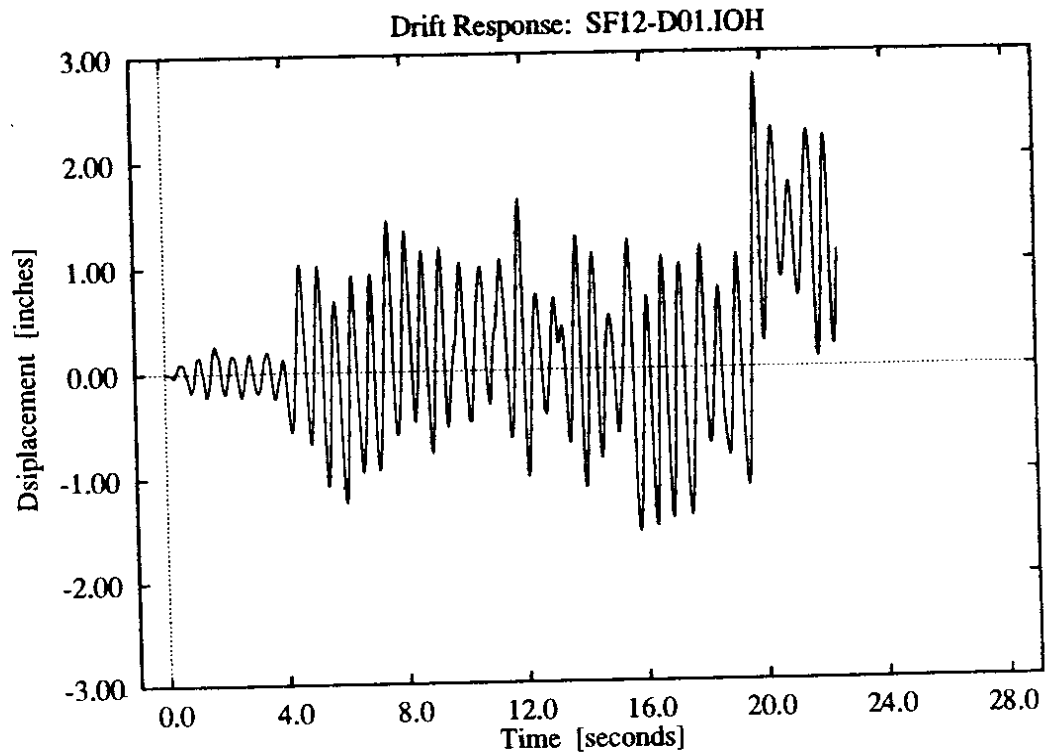


**Figure D-23:** 1 parameter foundation model, intermediate soil stiffness, higher intensity Olympia record.

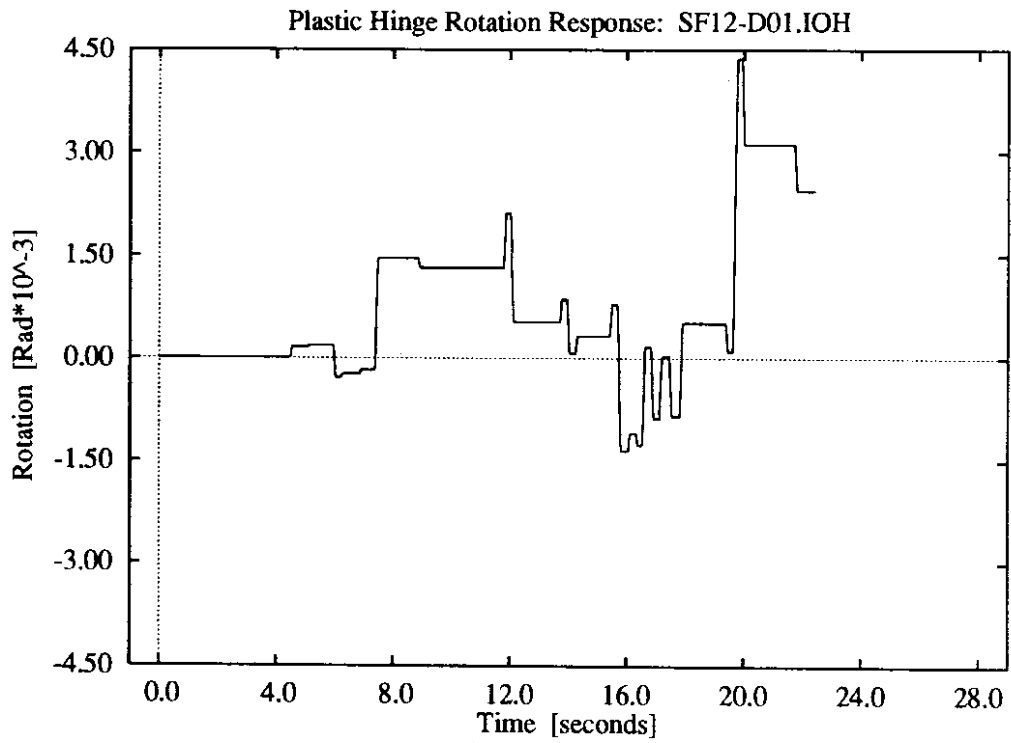
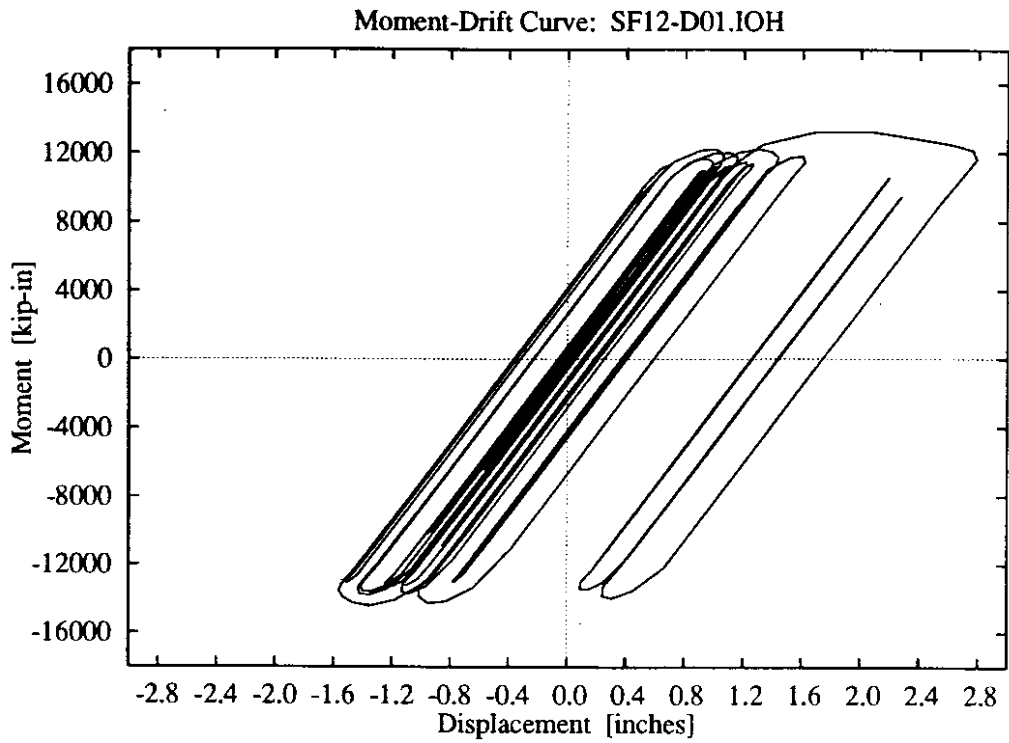


**Figure D-24:** 1 parameter foundation model, intermediate soil stiffness, higher intensity Olympia record.

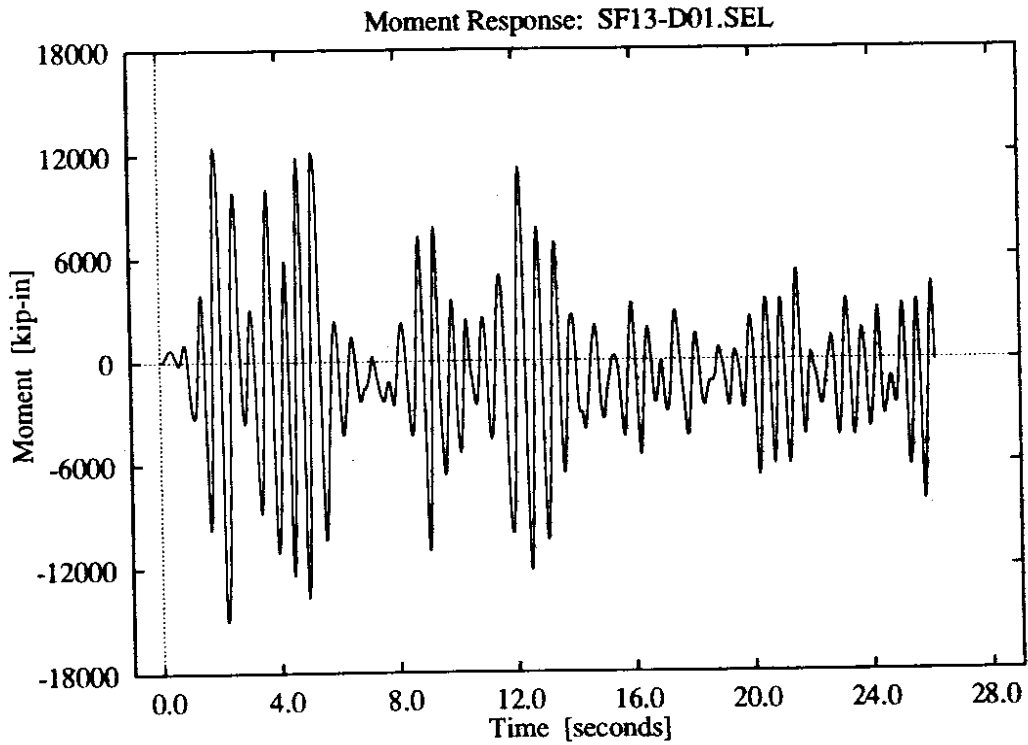
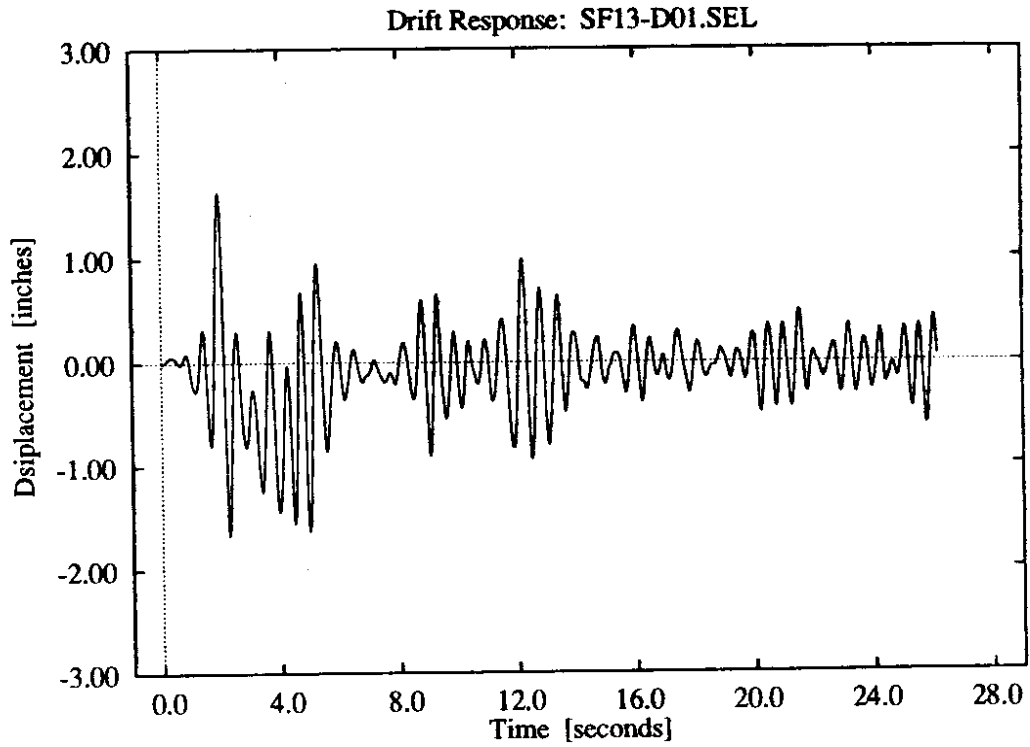


**Figure D-25: 1 parameter foundation model, high soil stiffness, lower intensity El Centro record.**

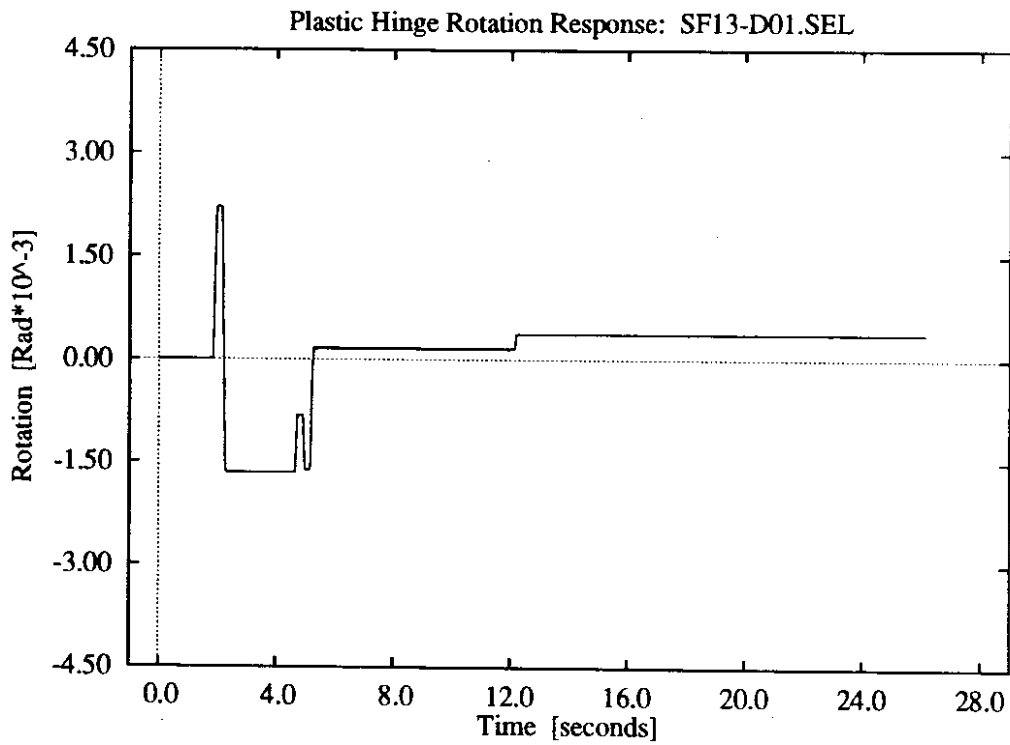
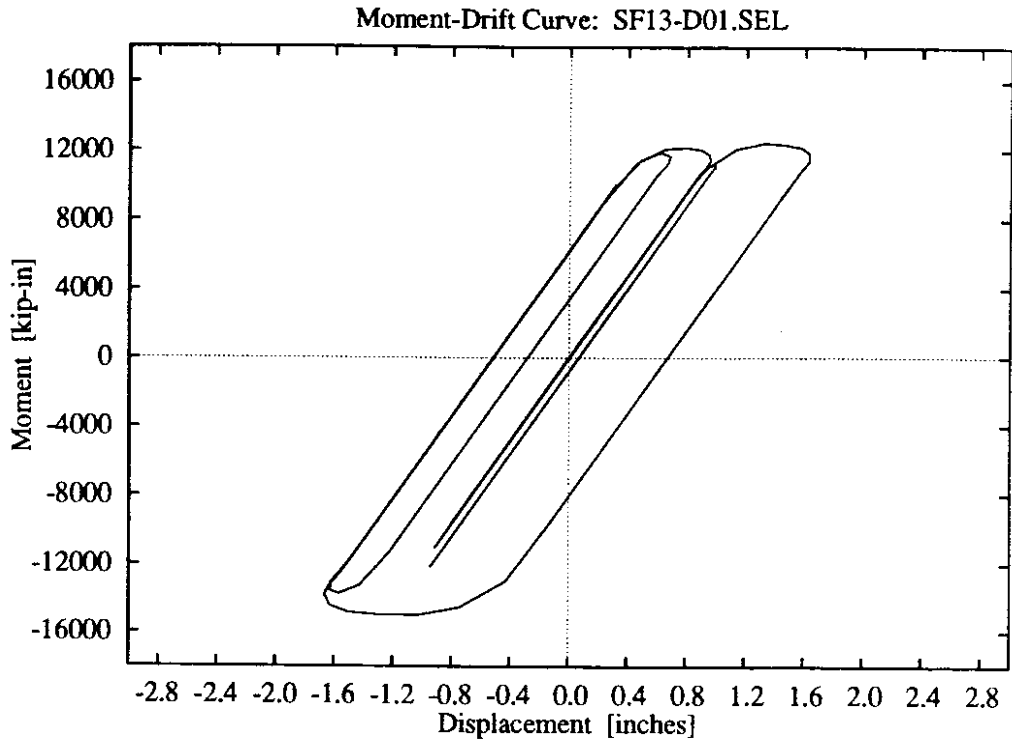


**Figure D-26:** 1 parameter foundation model, high soil stiffness, lower intensity El Centro record.

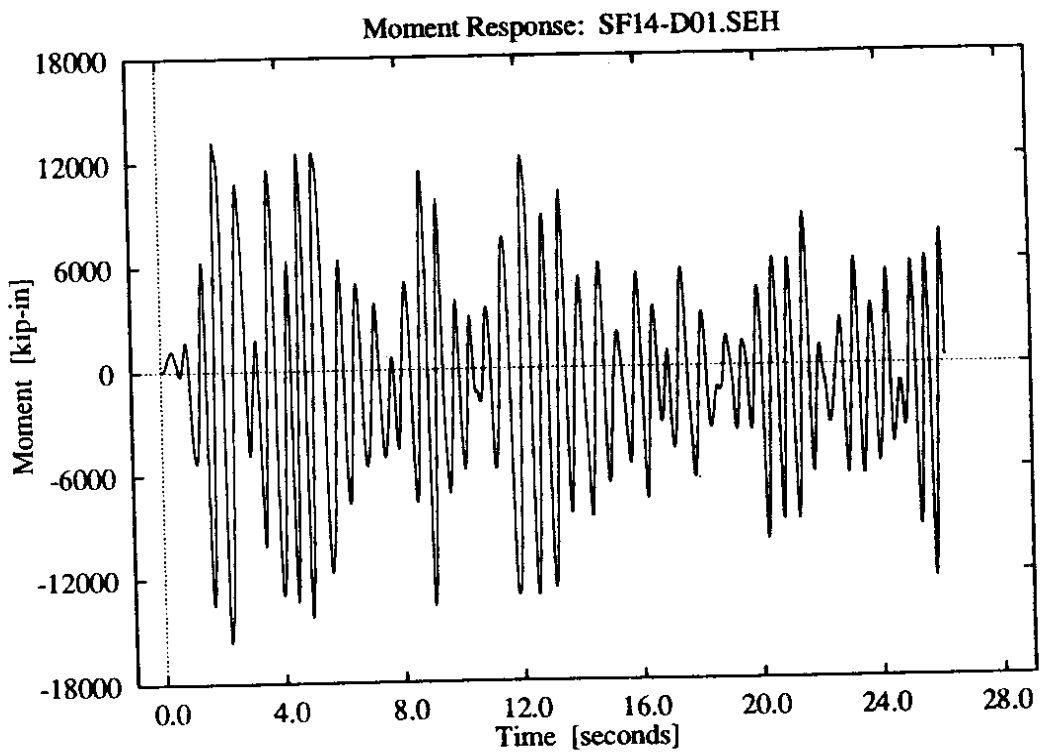
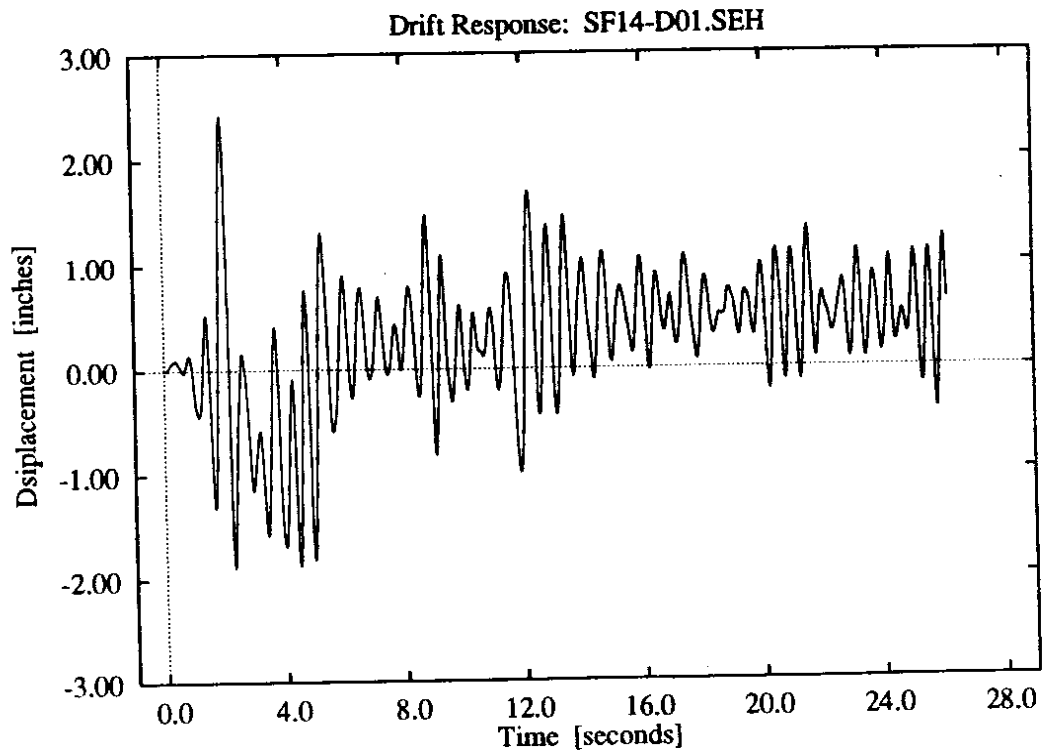


**Figure D-27:** 1 parameter foundation model, high soil stiffness, higher intensity El Centro record.

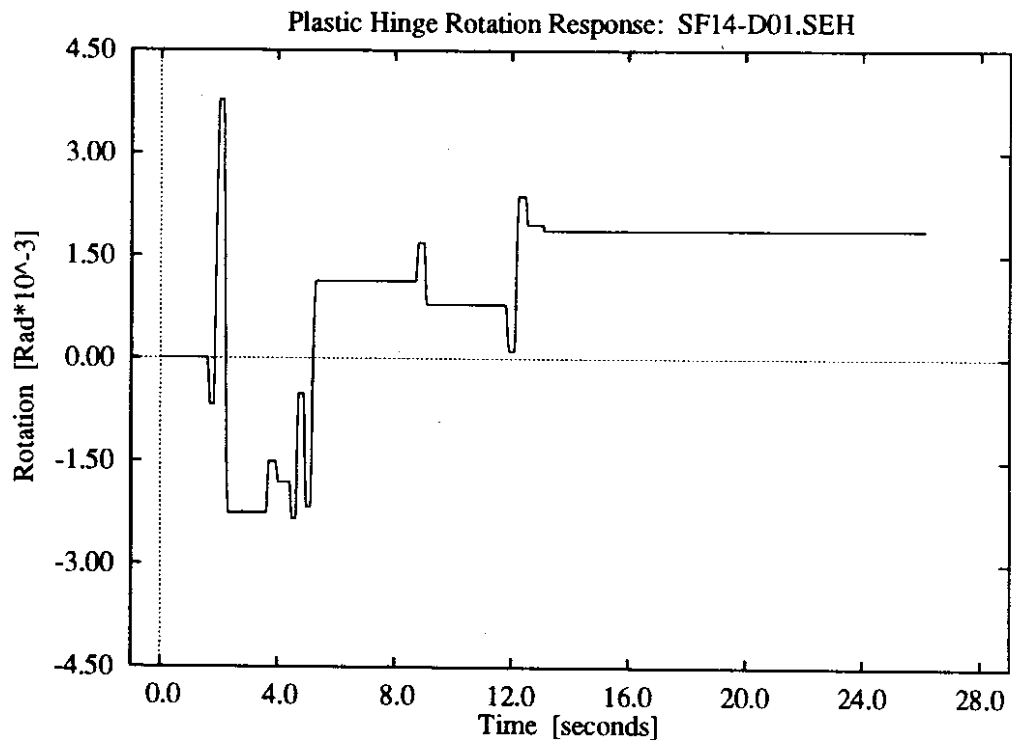
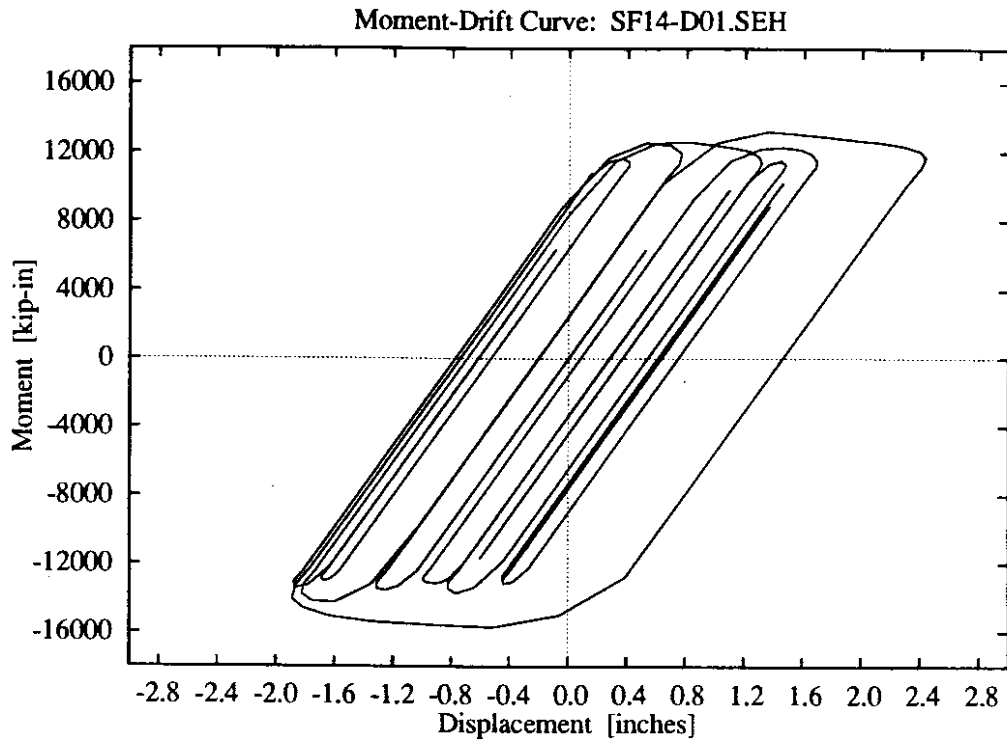


**Figure D-28:** 1 parameter foundation model, high soil stiffness, higher intensity El Centro record.

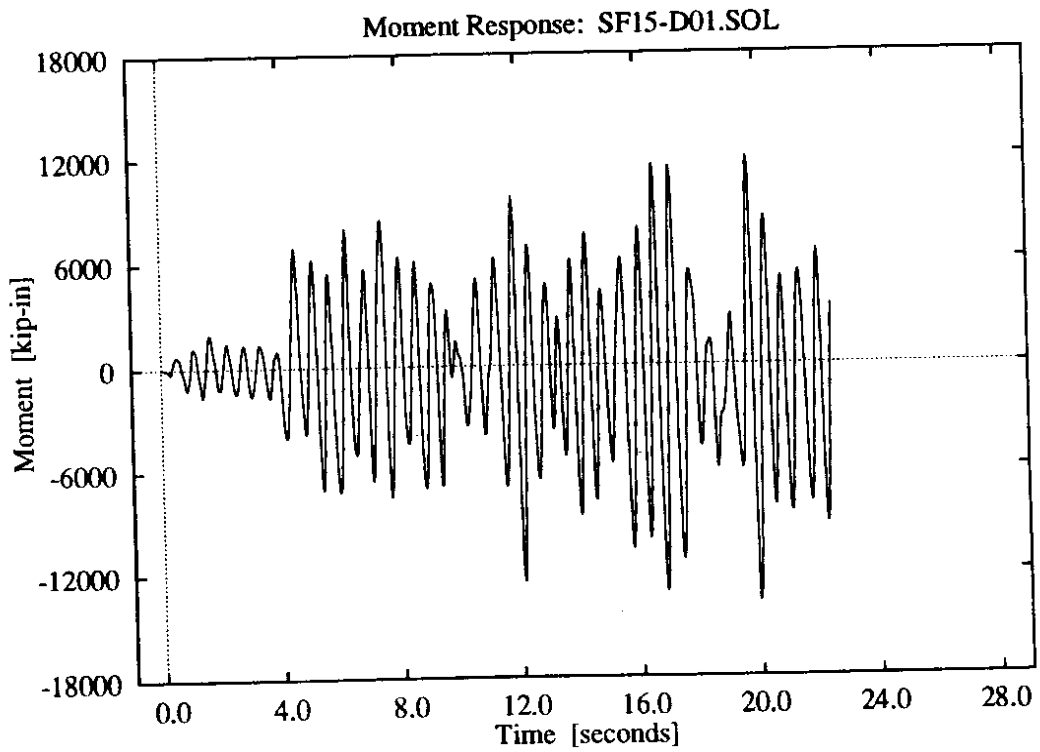
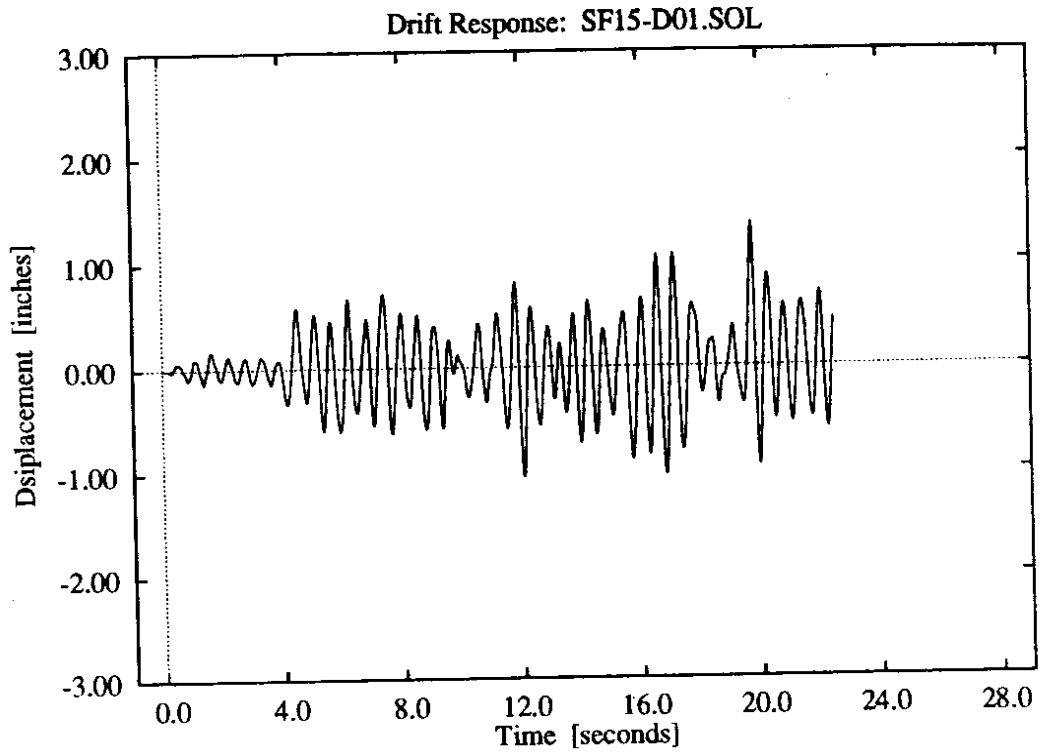


**Figure D-29:** 1 parameter foundation model, high soil stiffness, lower intensity Olympia record.

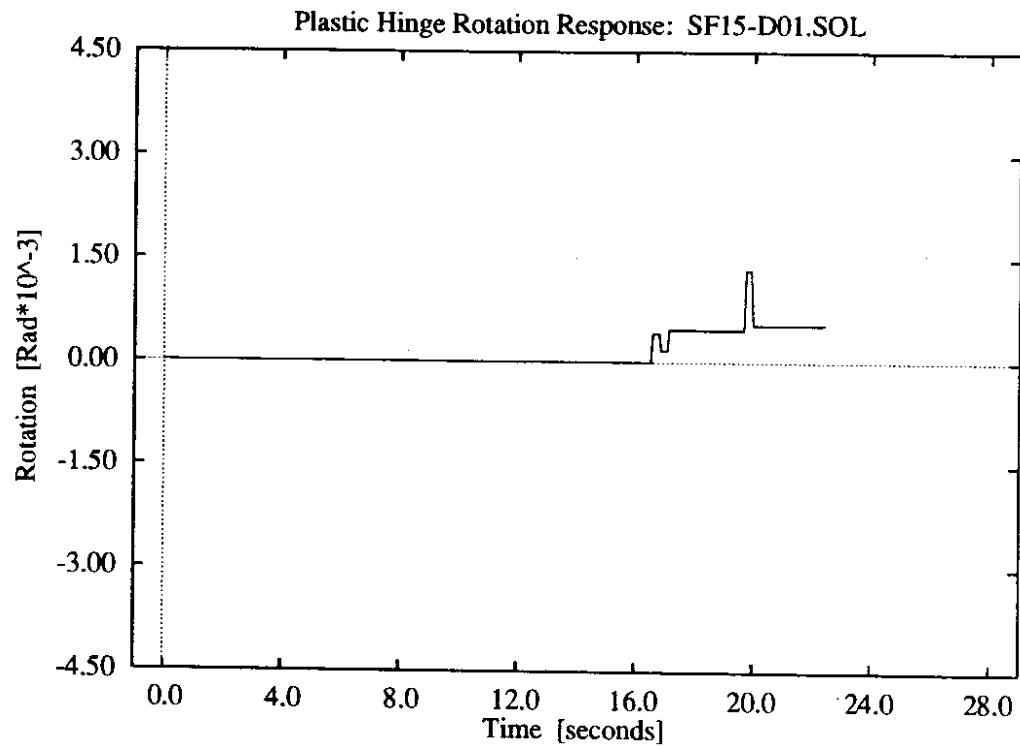
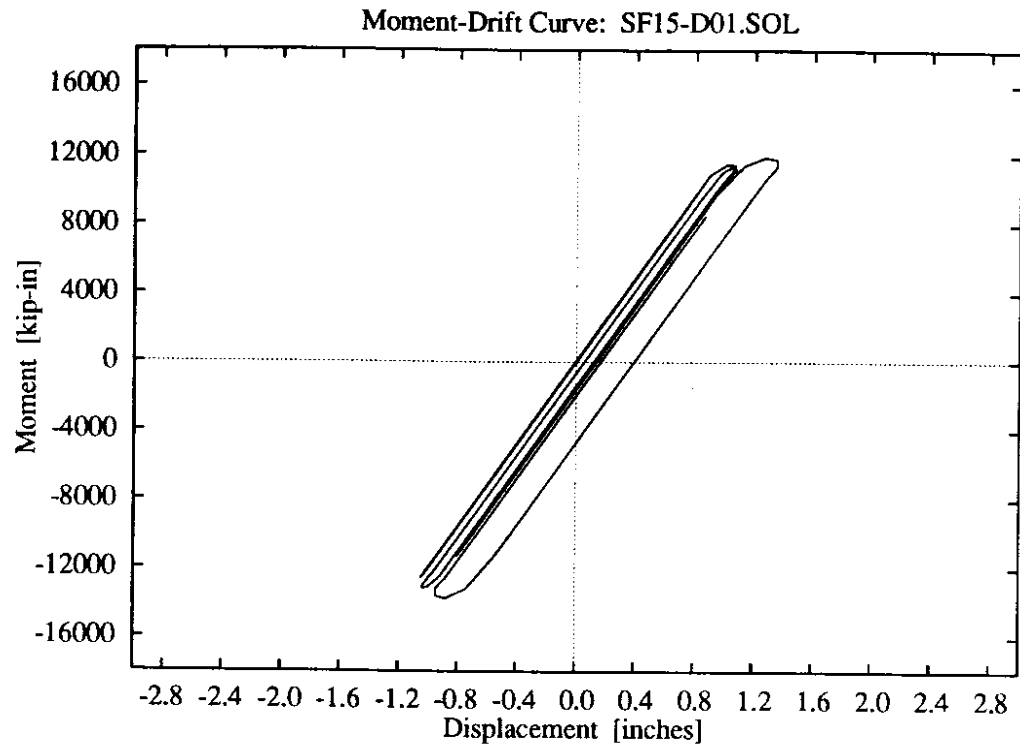


**Figure D-30:** 1 parameter foundation model, high soil stiffness, lower intensity Olympia record.



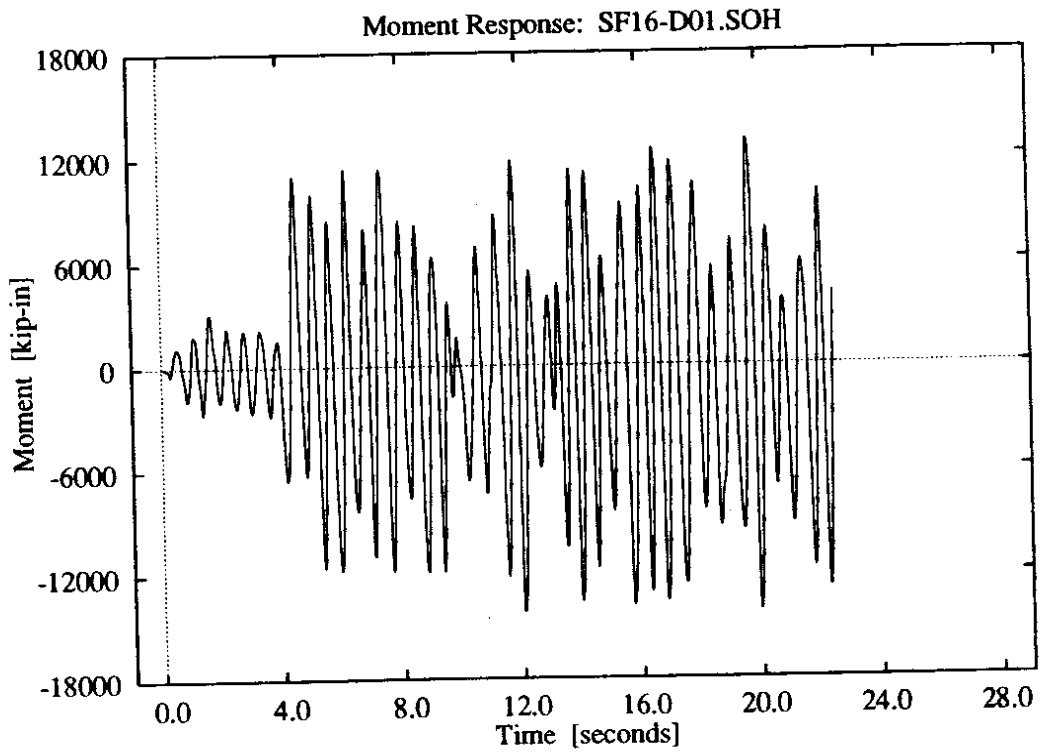
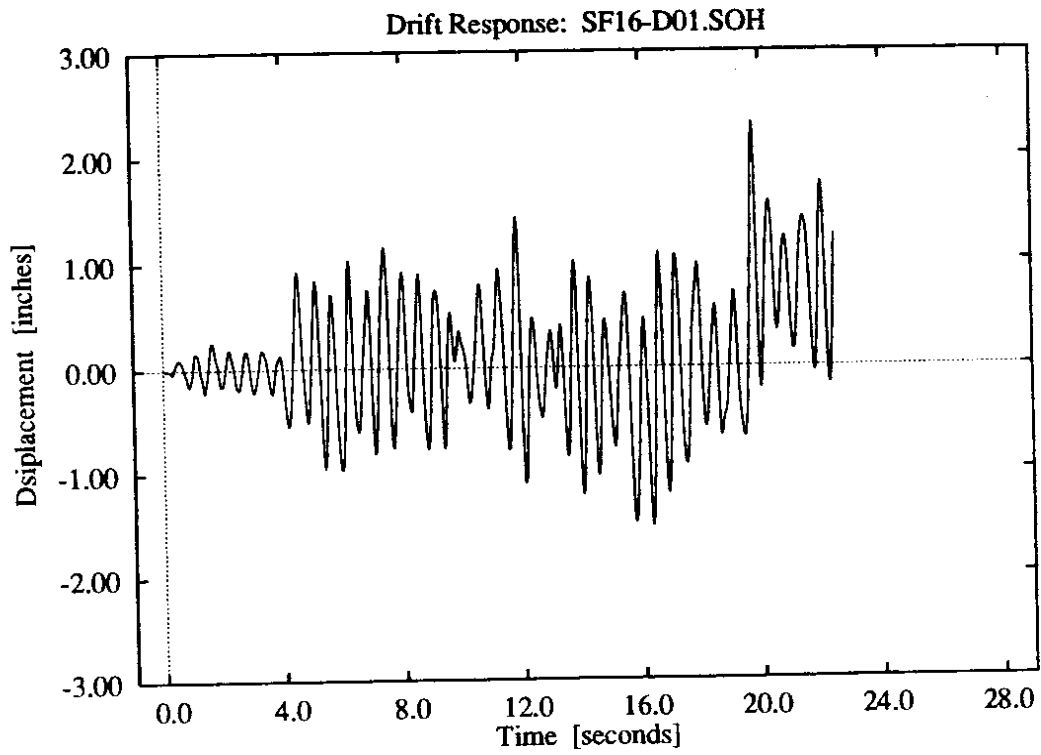


**Figure D-31:** 1 parameter foundation model, high soil stiffness, higher intensity Olympia record.

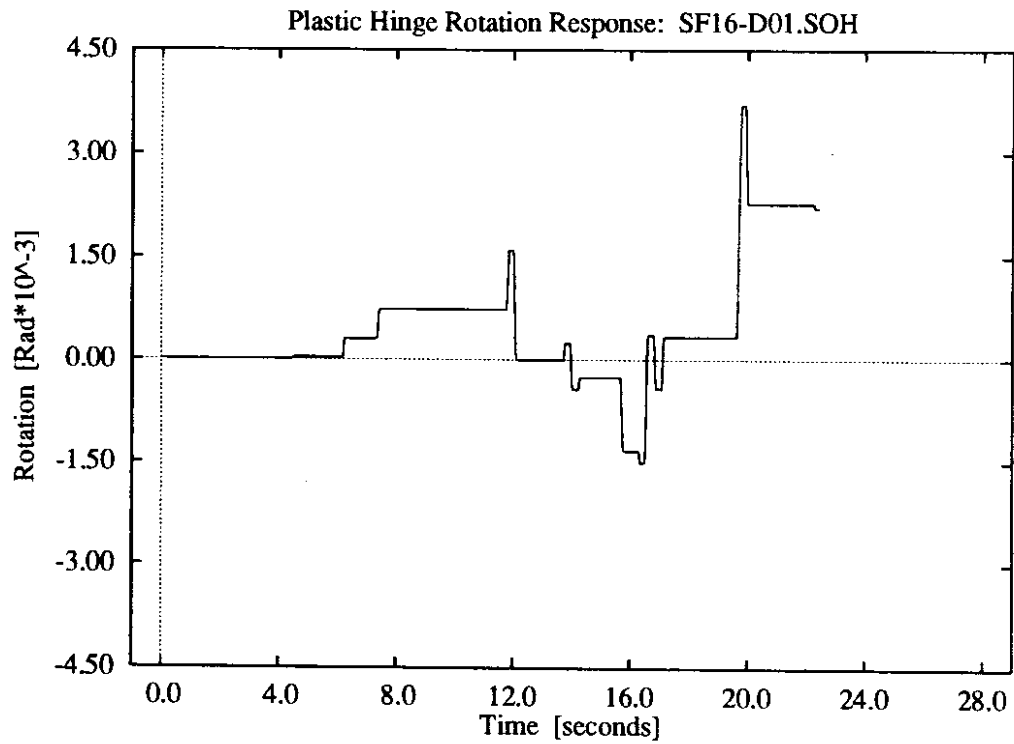
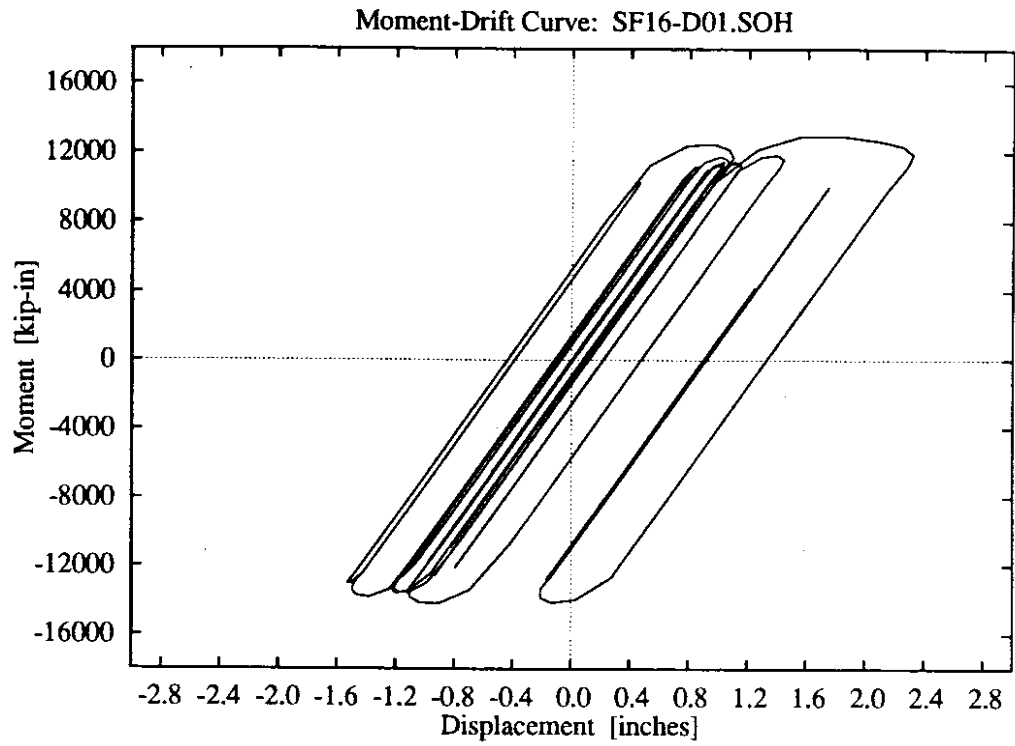


**Figure D-32: 1 parameter foundation model, high soil stiffness, higher intensity Olympia record.**

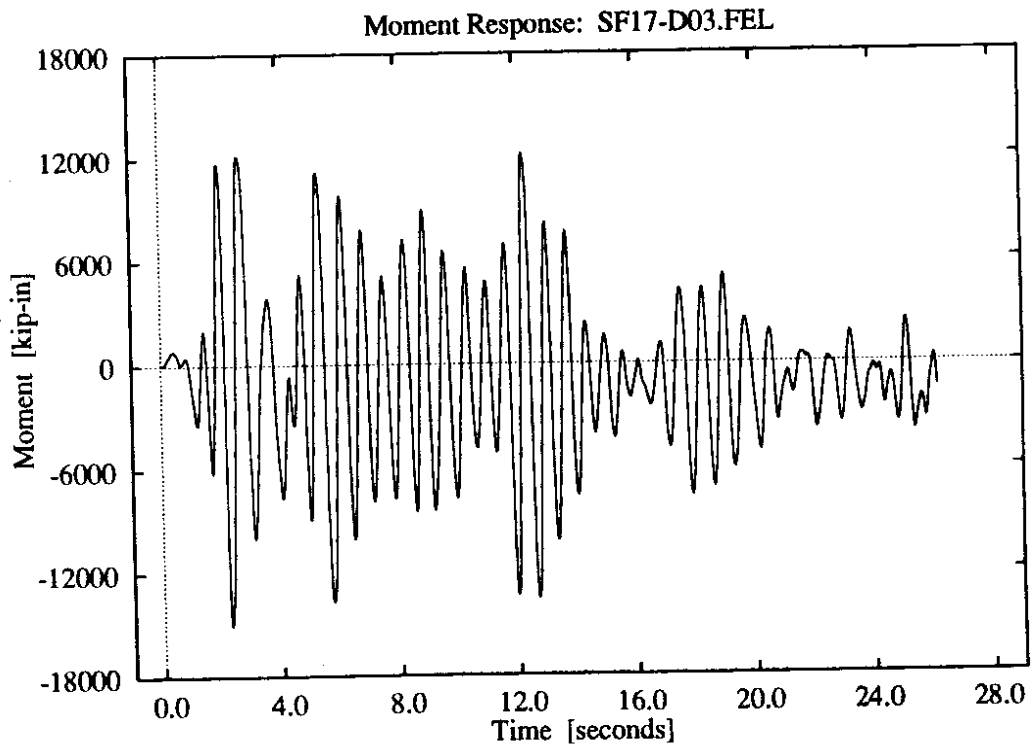
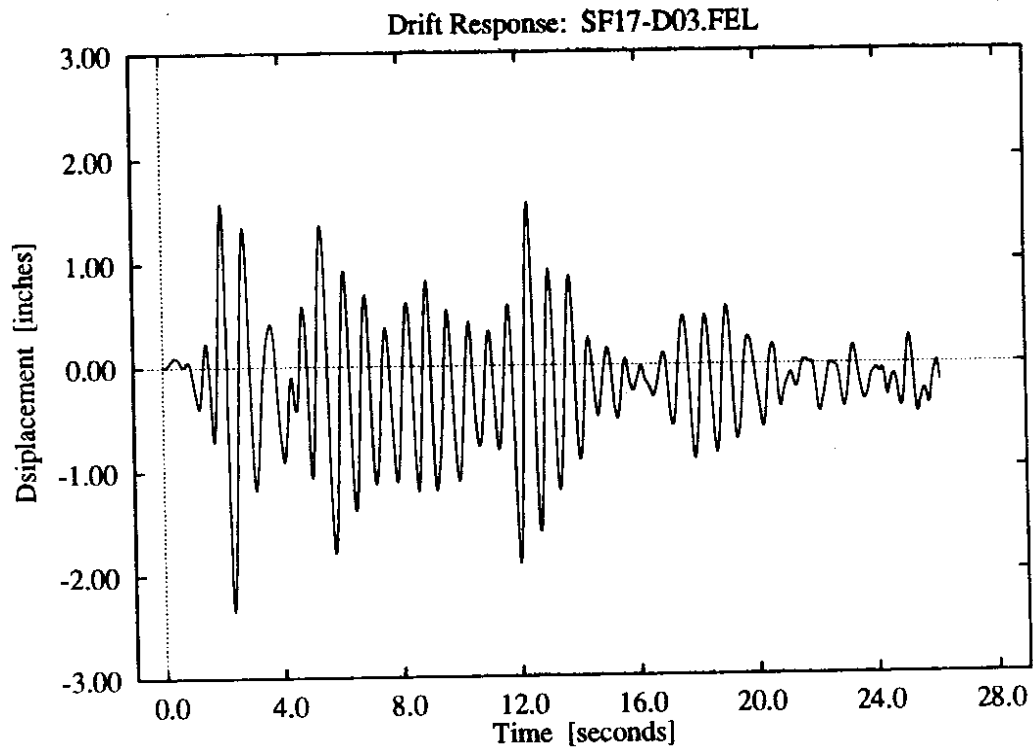


**Figure D-33:** 3 parameter foundation model, low soil stiffness, lower intensity El Centro record.

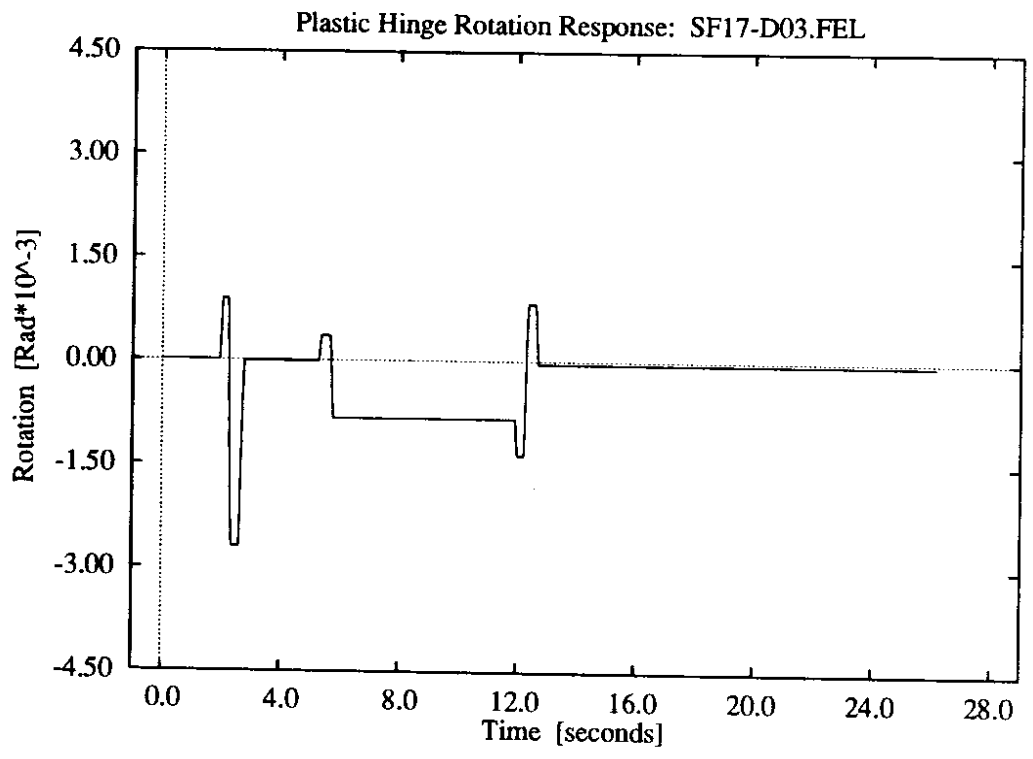
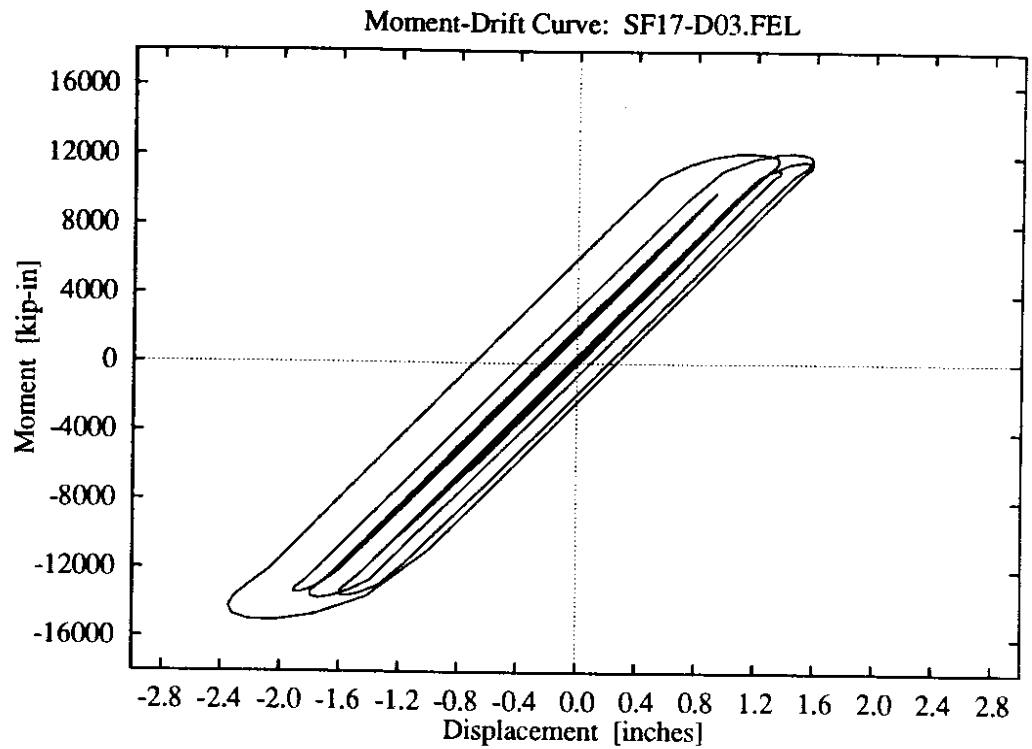


**Figure D-34:** 3 parameter foundation model, low soil stiffness, lower intensity El Centro record.

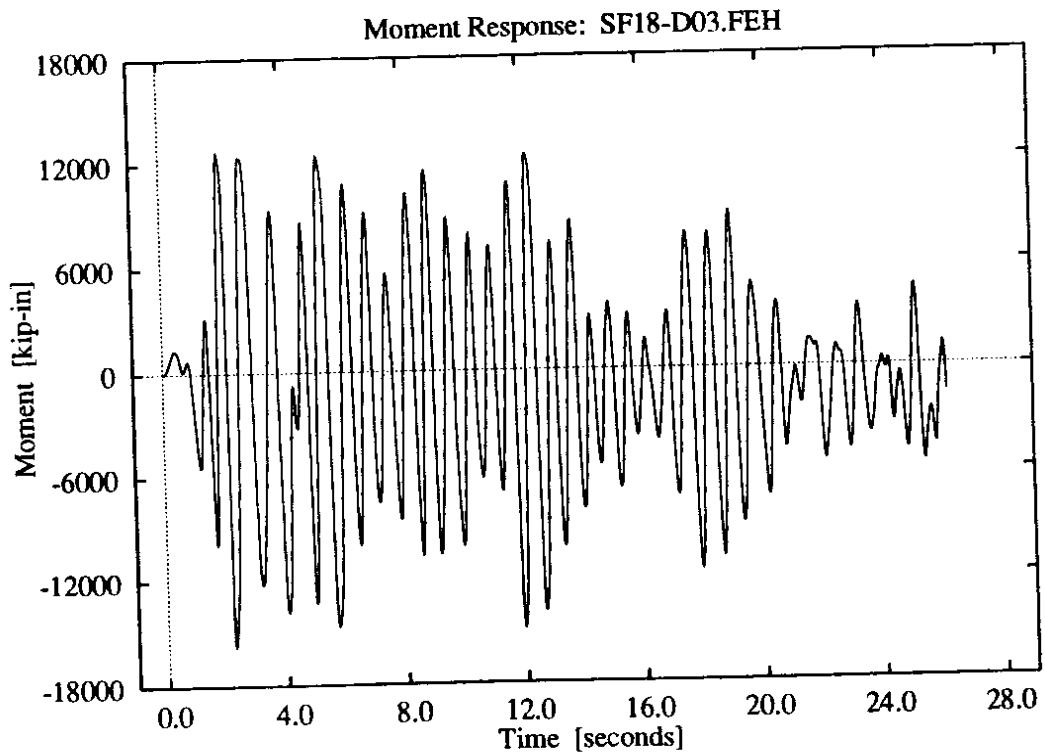
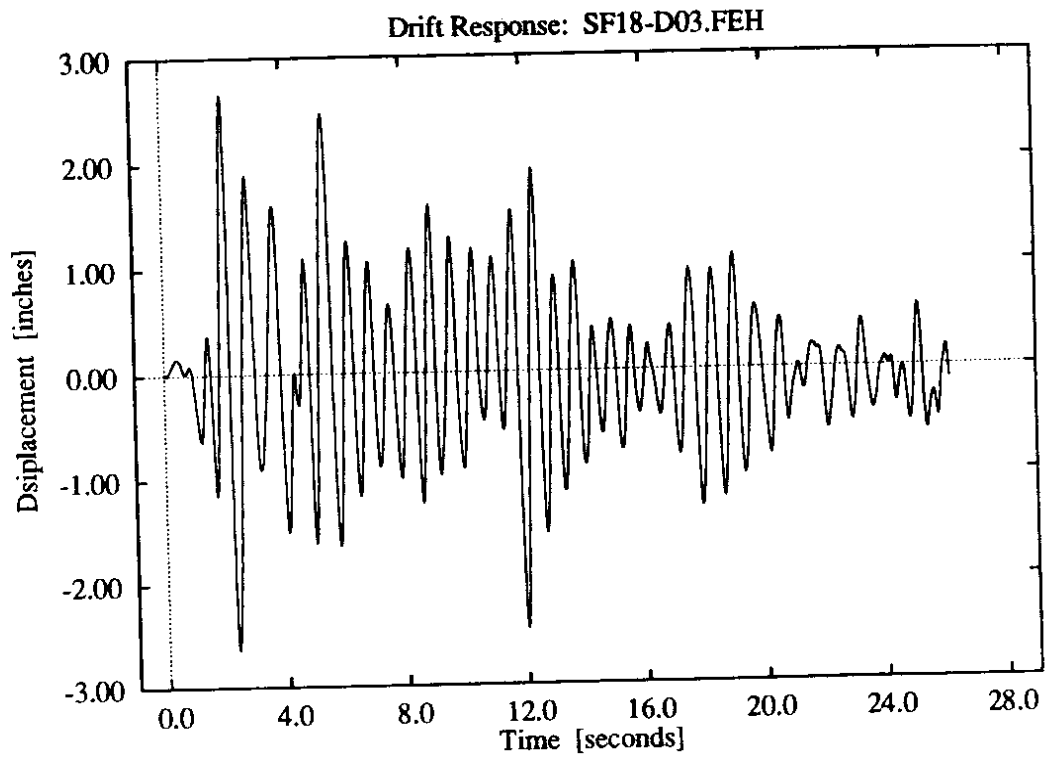


**Figure D-35:** 3 parameter foundation model, low soil stiffness, higher intensity El Centro record.

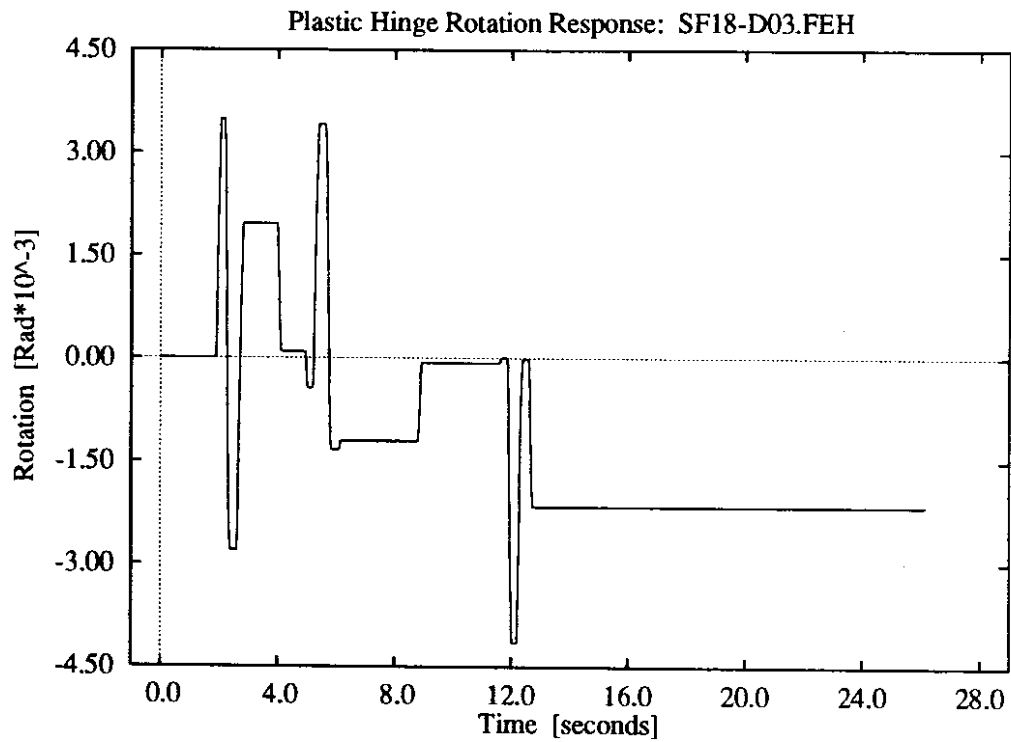
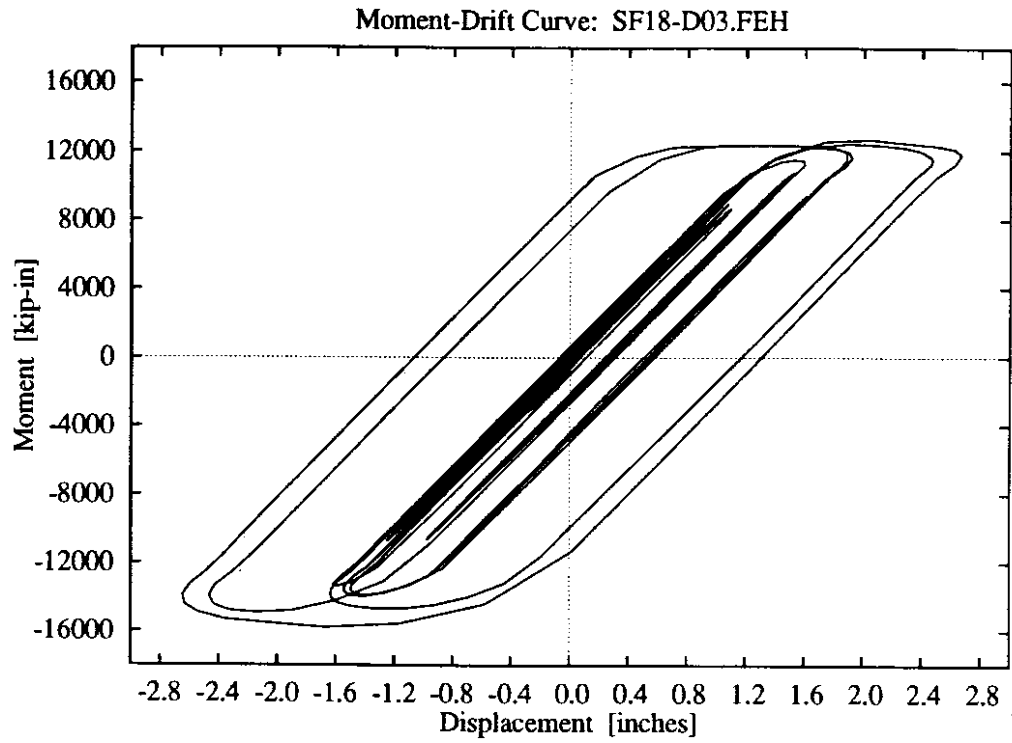


**Figure D-36:** 3 parameter foundation model, low soil stiffness, higher intensity El Centro record.

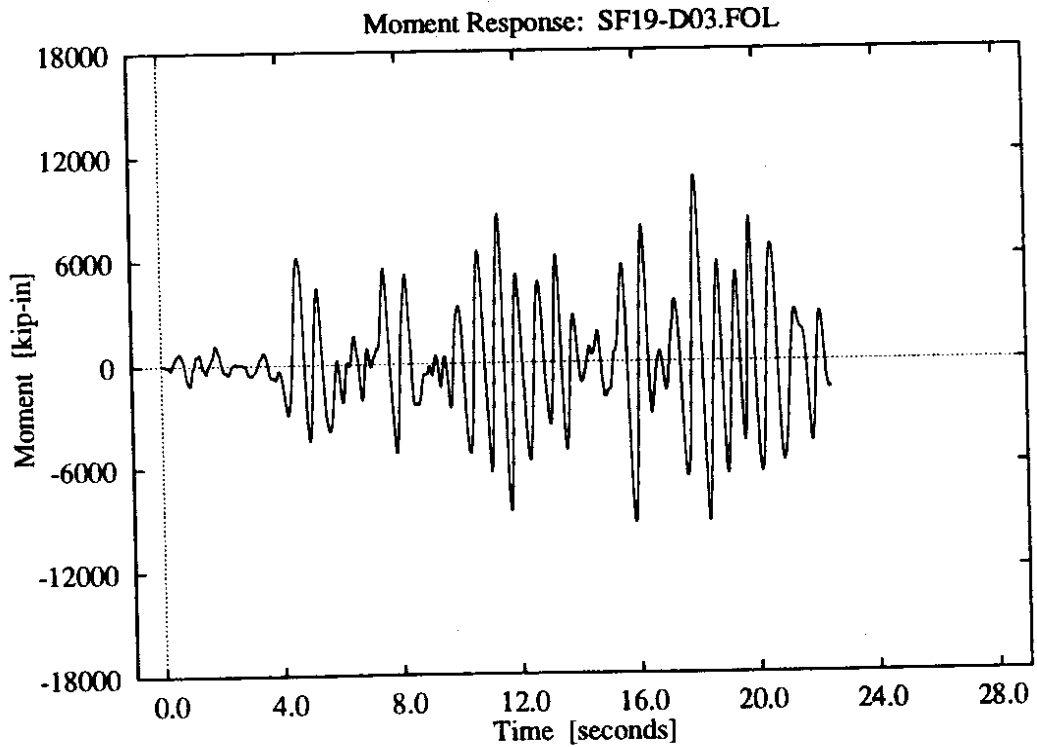
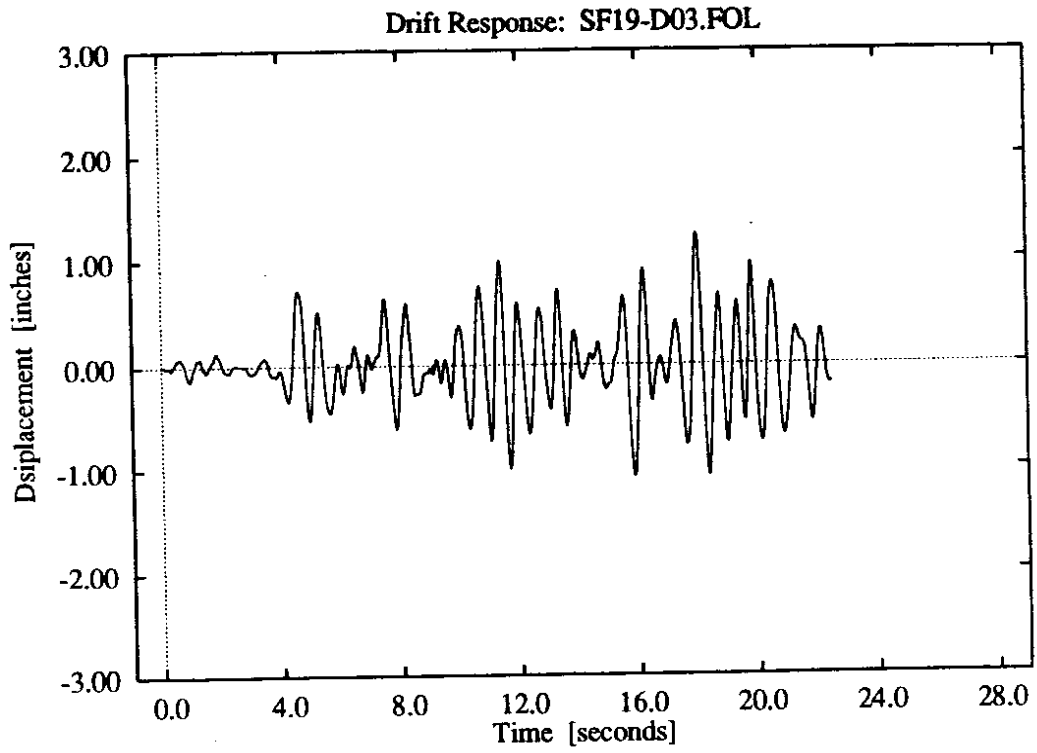


**Figure D-37: 3 parameter foundation model, low soil stiffness, lower intensity Olympia record.**

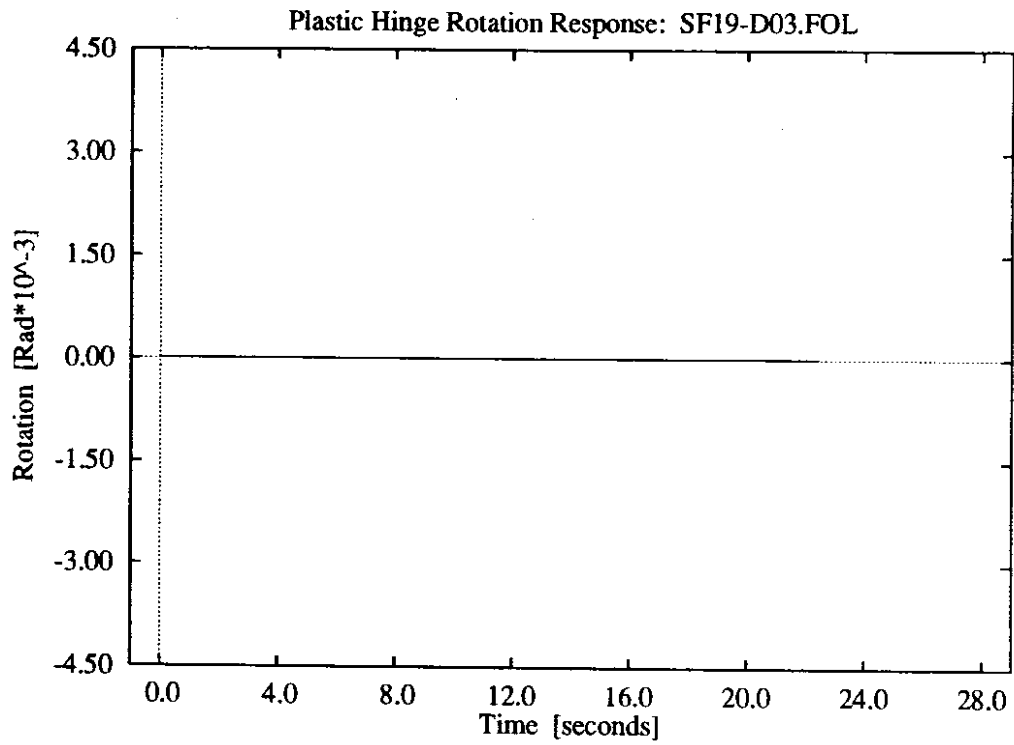
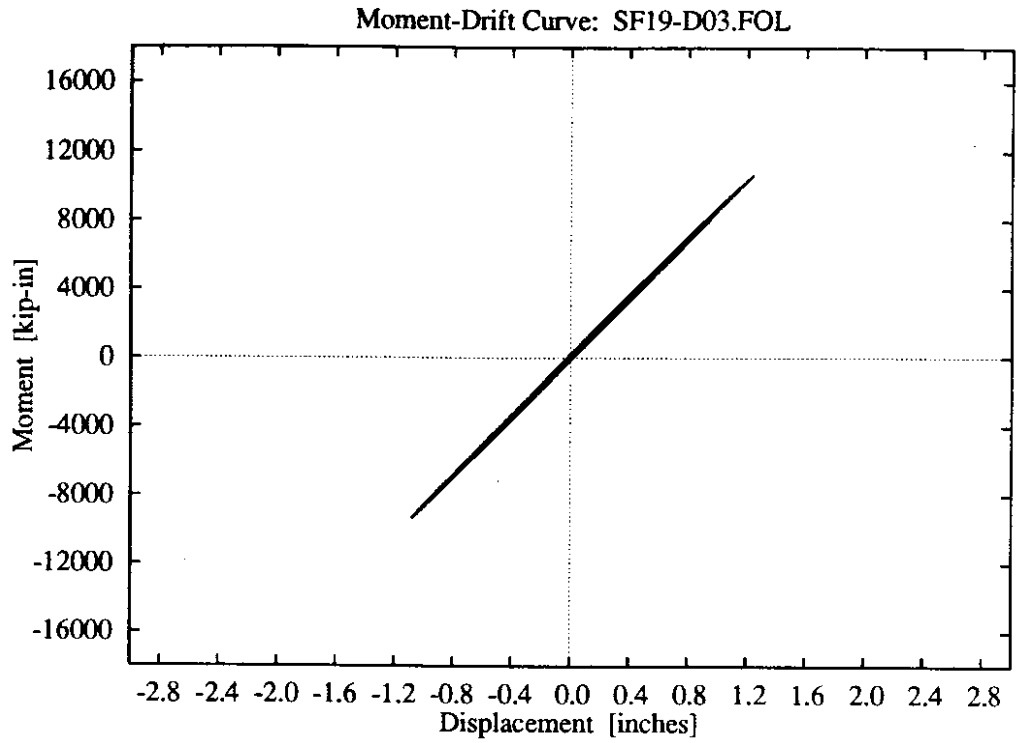


**Figure D-38:** 3 parameter foundation model, low soil stiffness, lower intensity Olympia record.



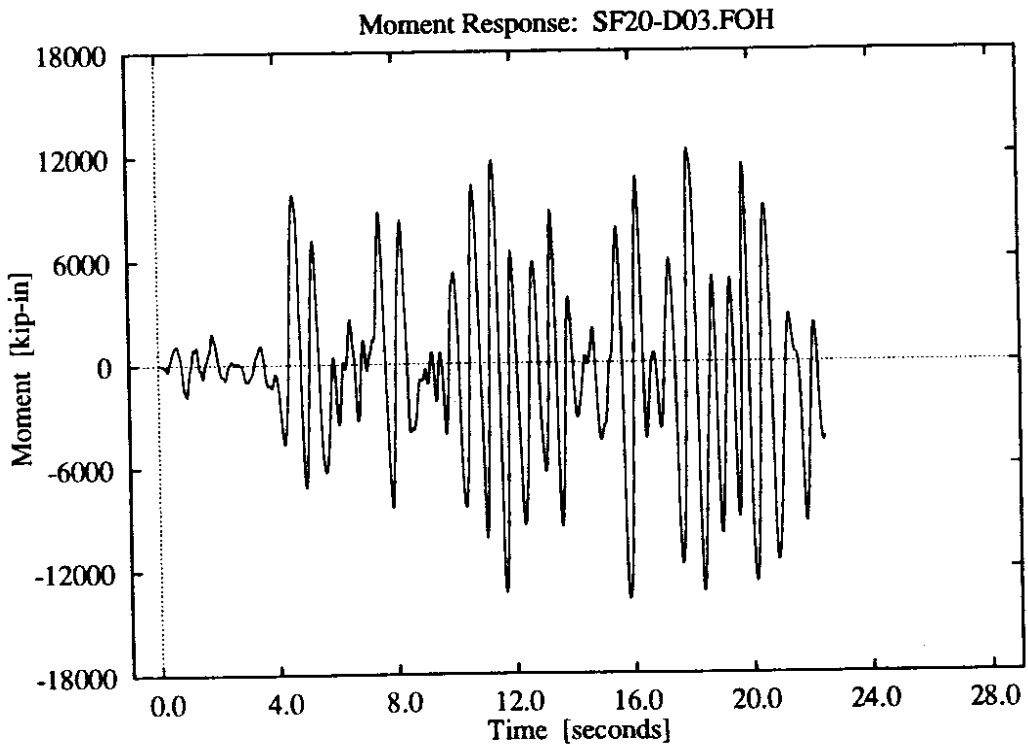
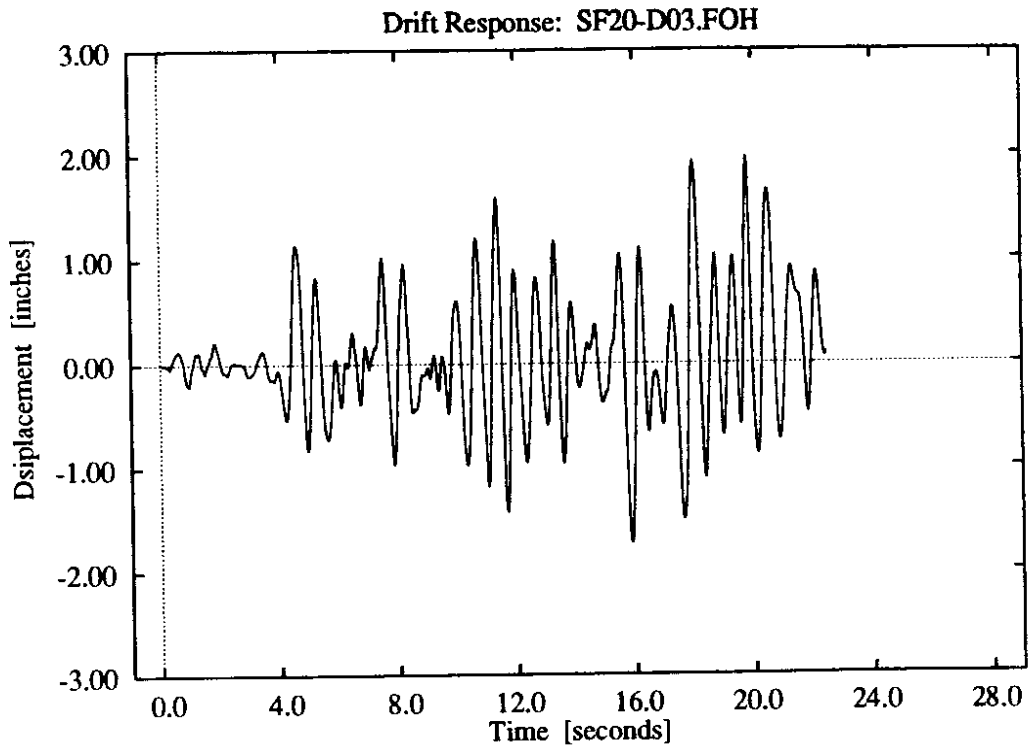


**Figure D-39:** 3 parameter foundation model, low soil stiffness, higher intensity Olympia record.

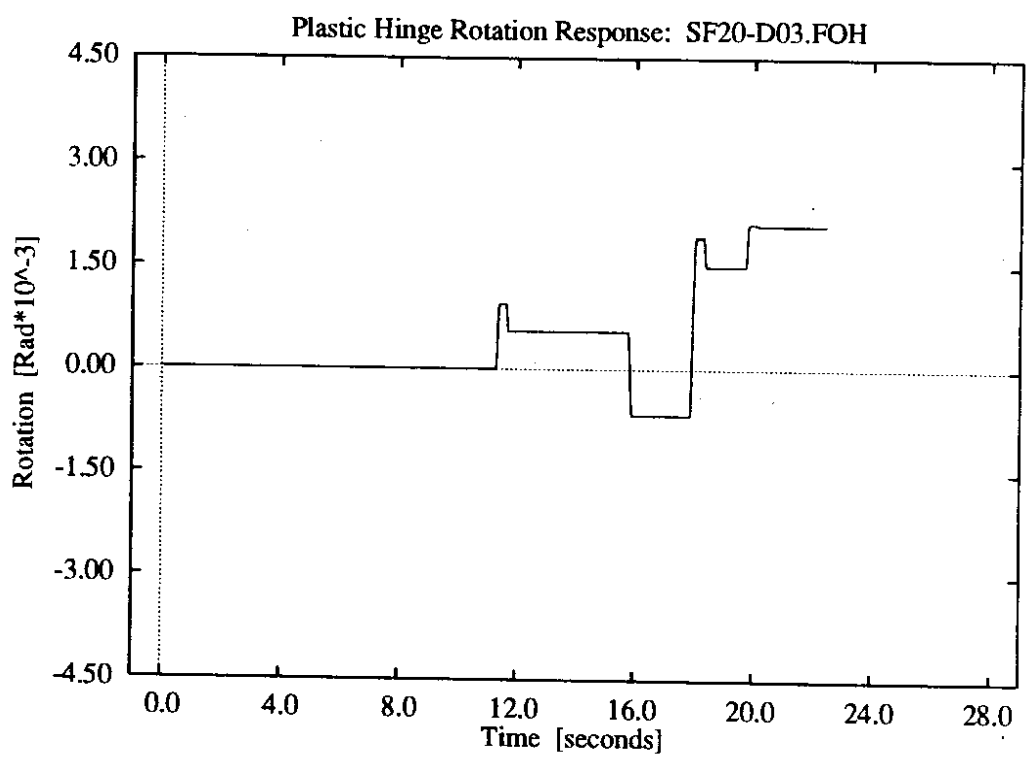
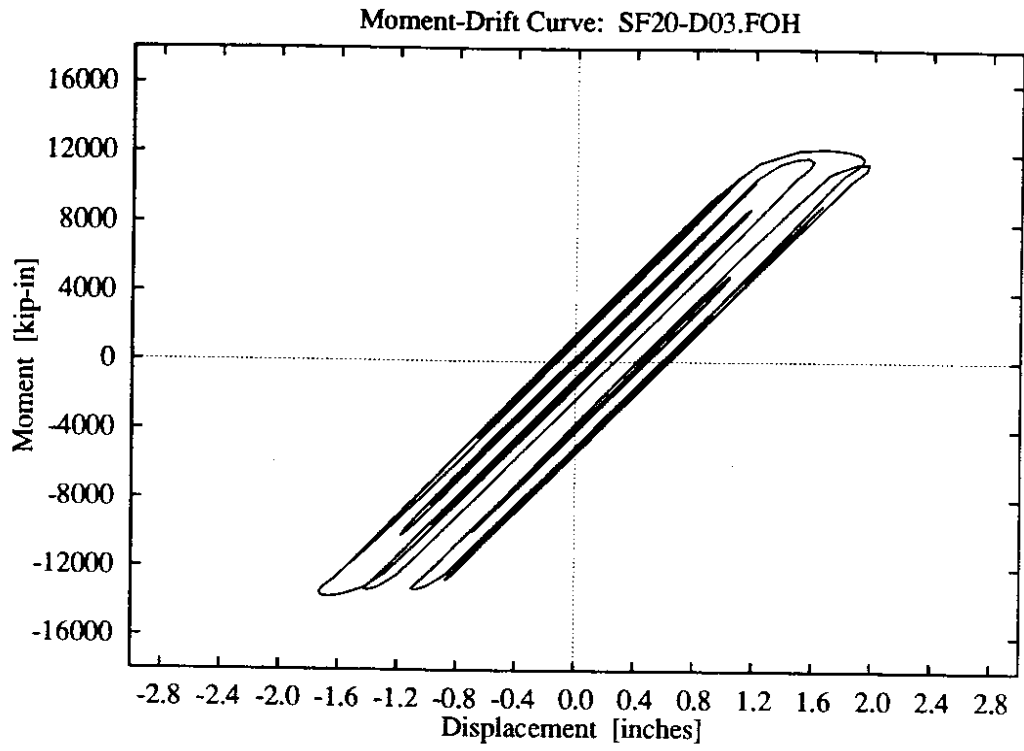


**Figure D-40:** 3 parameter foundation model, low soil stiffness, higher intensity Olympia record.

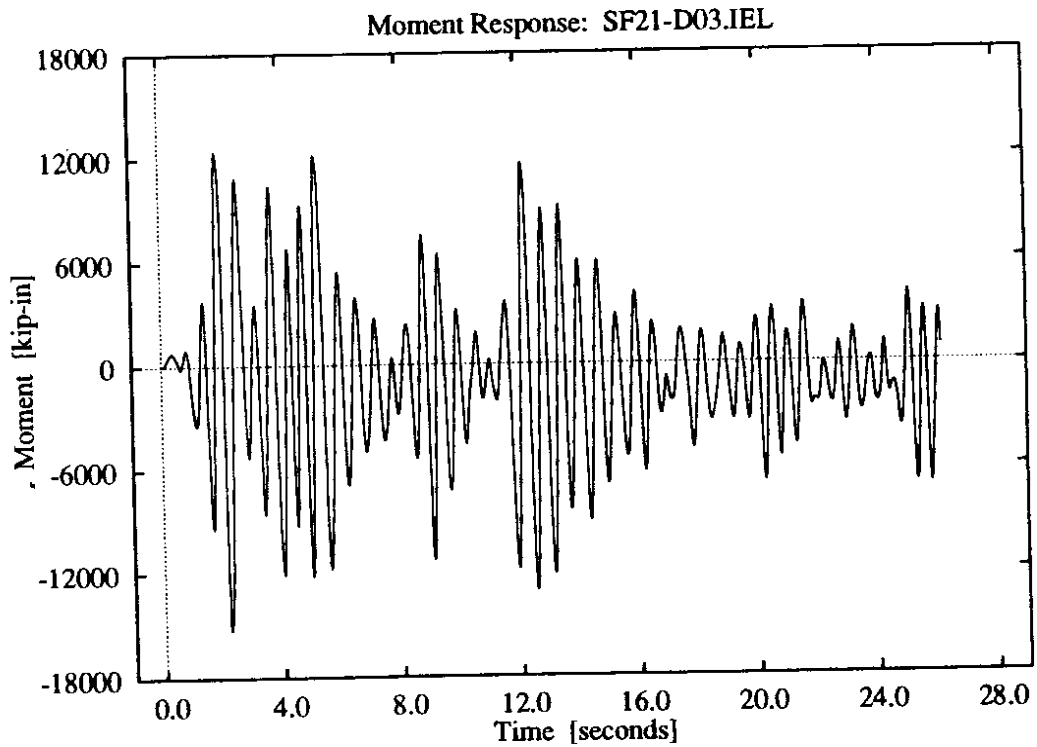
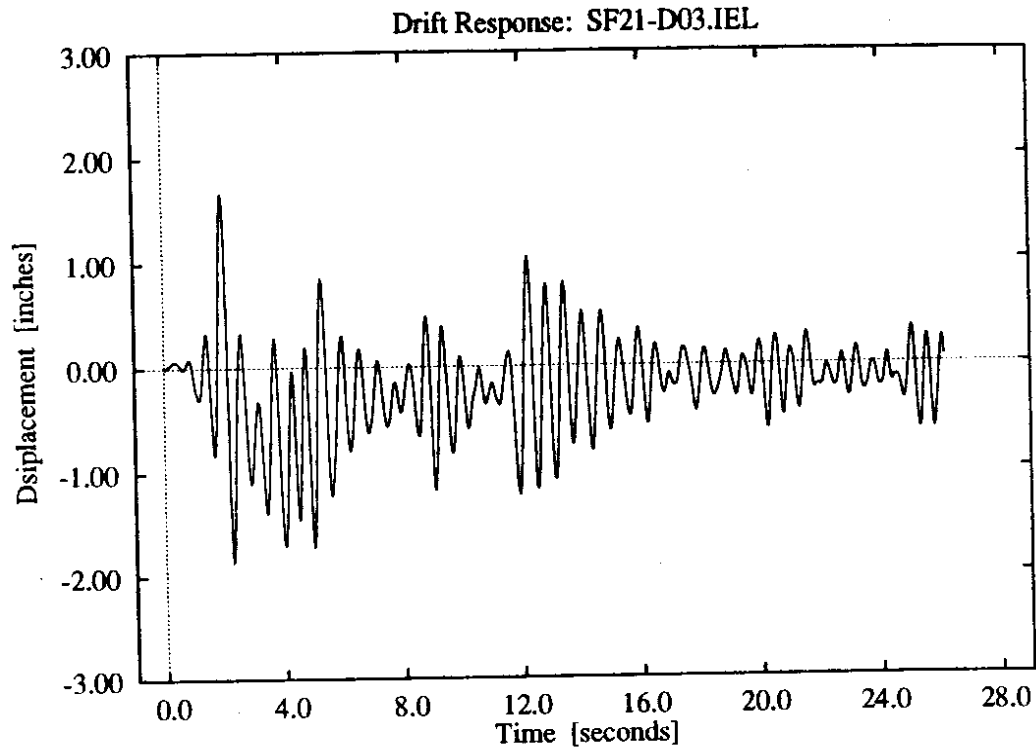


**Figure D-41:** 3 parameter foundation model, intermediate soil stiffness, lower intensity El Centro record.

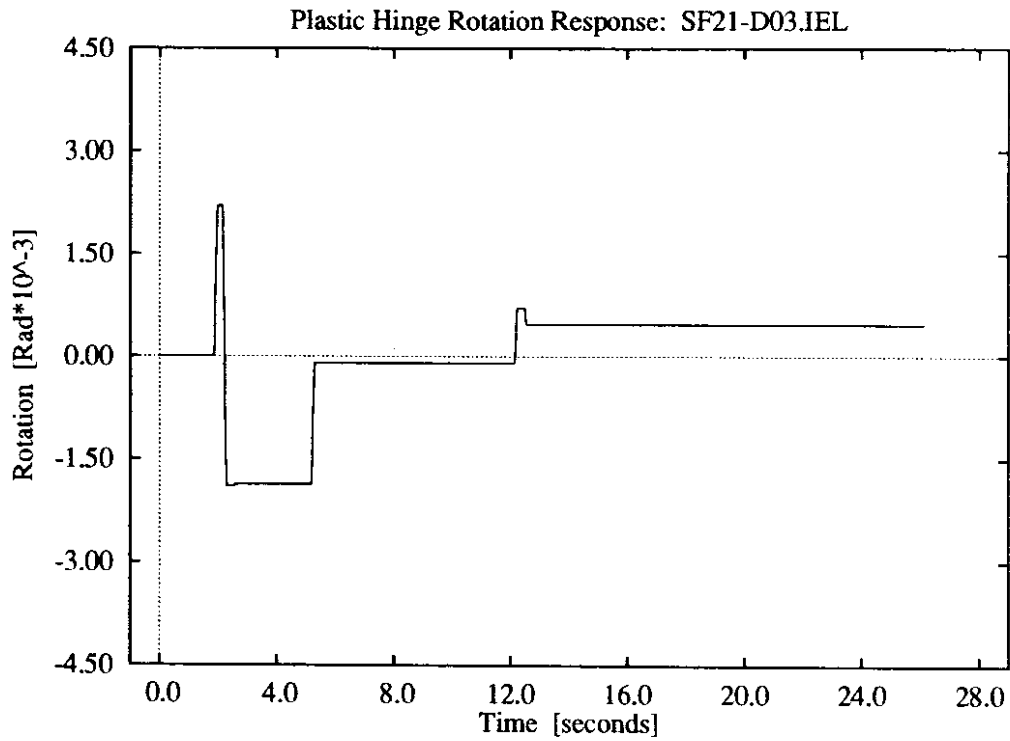
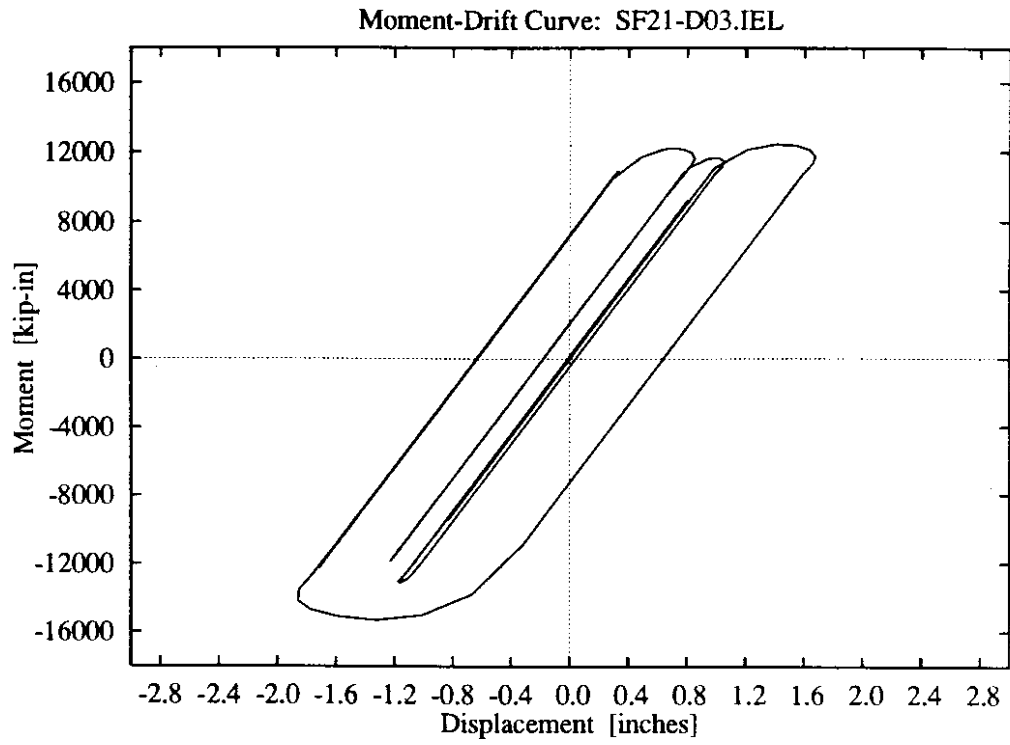


**Figure D-42:** 3 parameter foundation model, intermediate soil stiffness, lower intensity El Centro record.

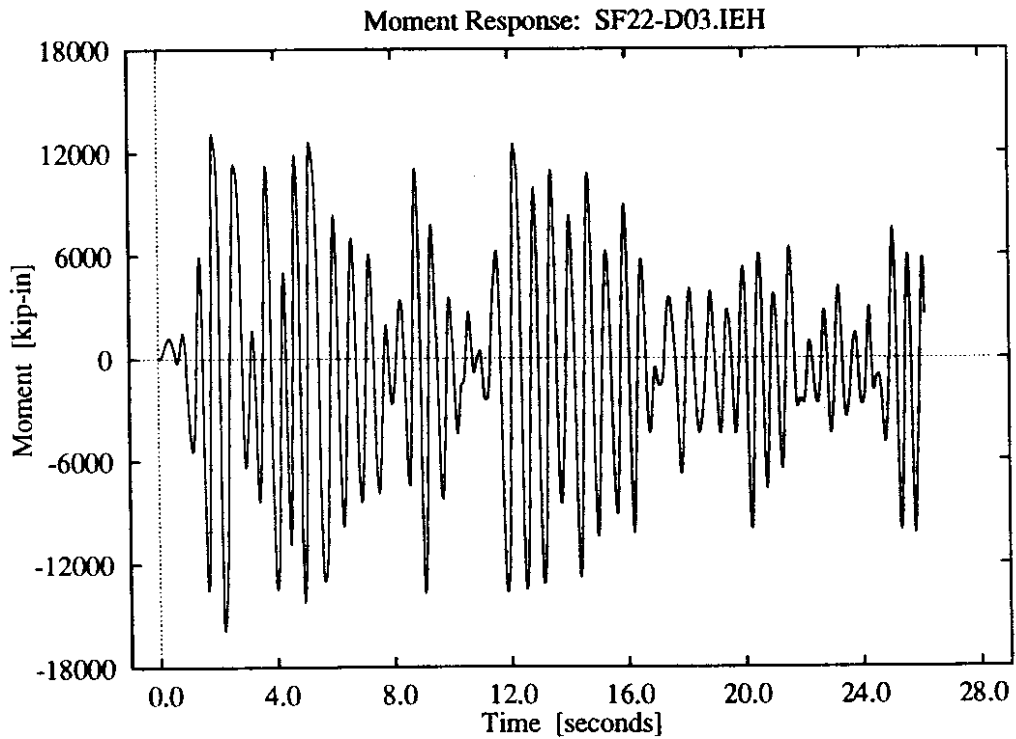
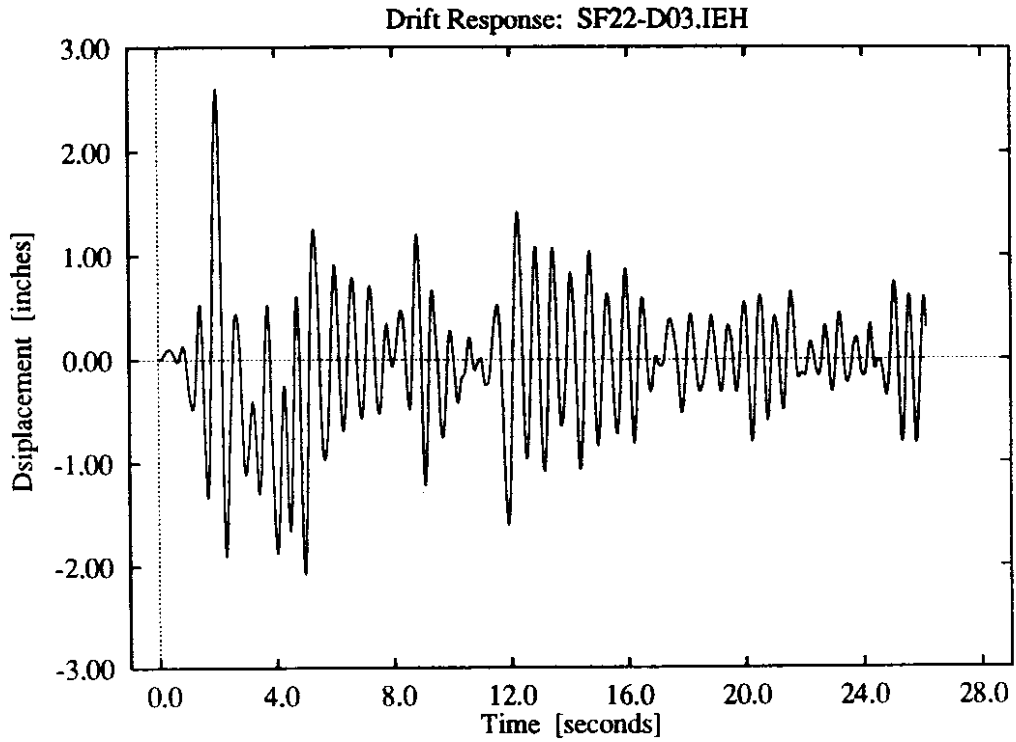


**Figure D-43:** 3 parameter foundation model, intermediate soil stiffness, higher intensity El Centro record.

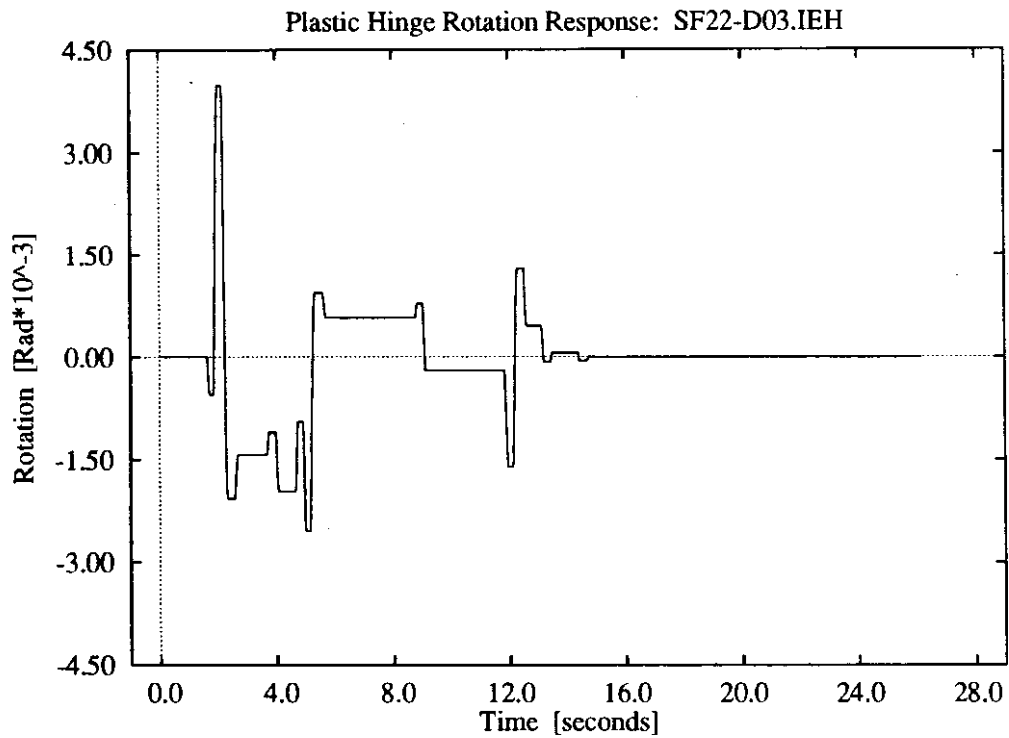
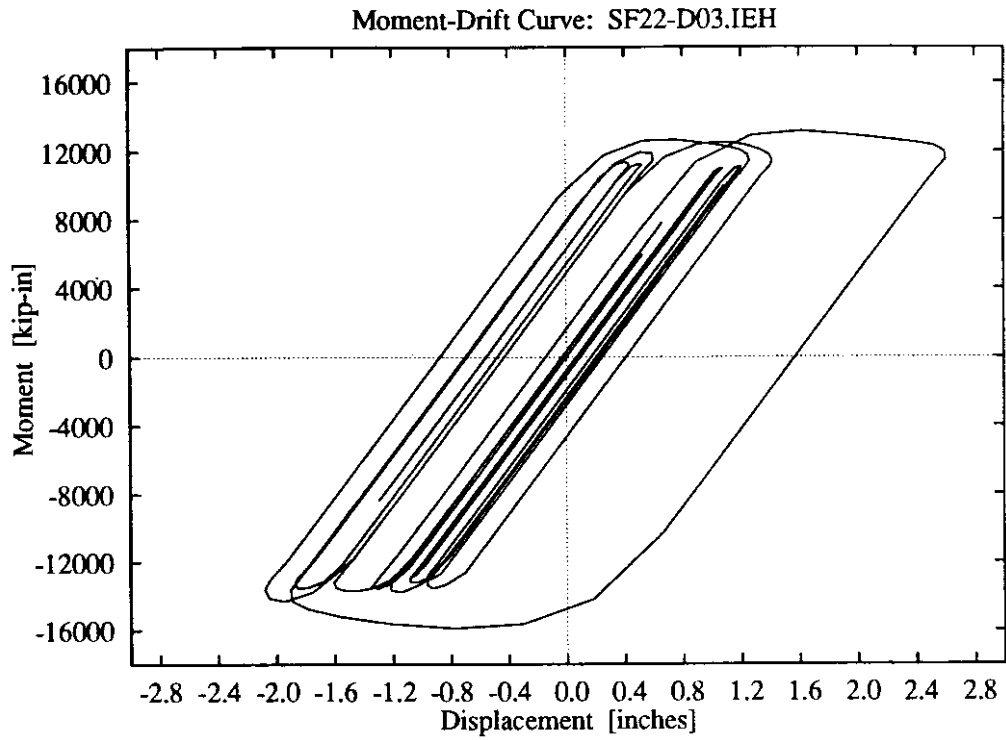


**Figure D-44:** 3 parameter foundation model, intermediate soil stiffness, higher intensity El Centro record.

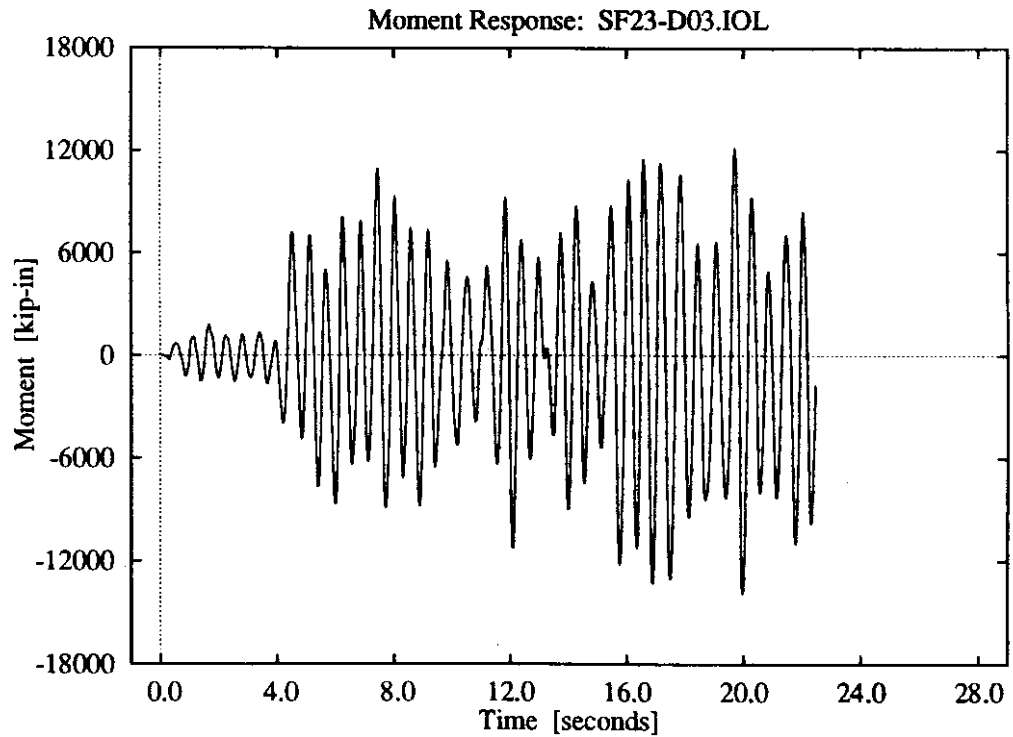
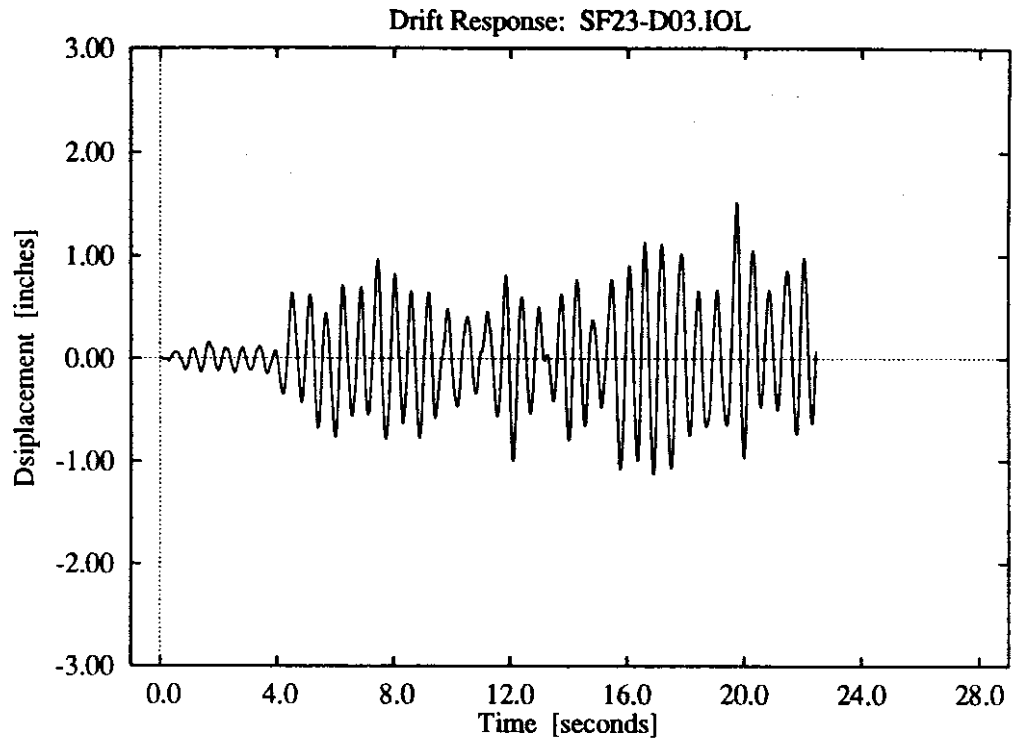


**Figure D-45: 3 parameter foundation model, intermediate soil stiffness, lower intensity Olympia record.**

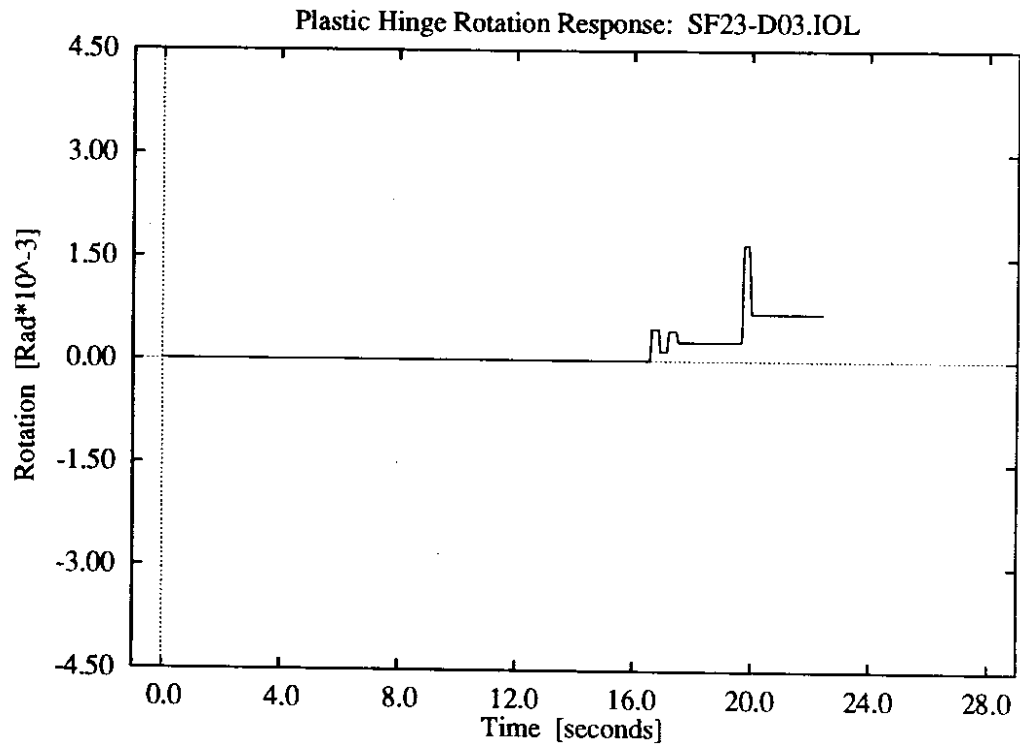
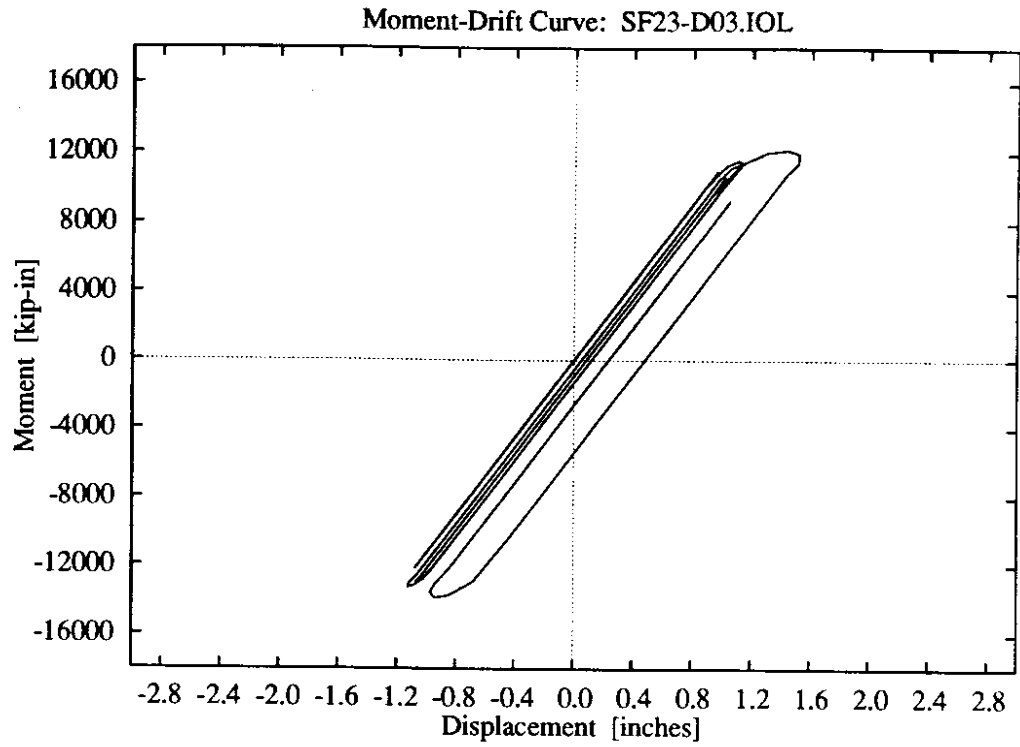


**Figure D-46:** 3 parameter foundation model, intermediate soil stiffness, lower intensity Olympia record.



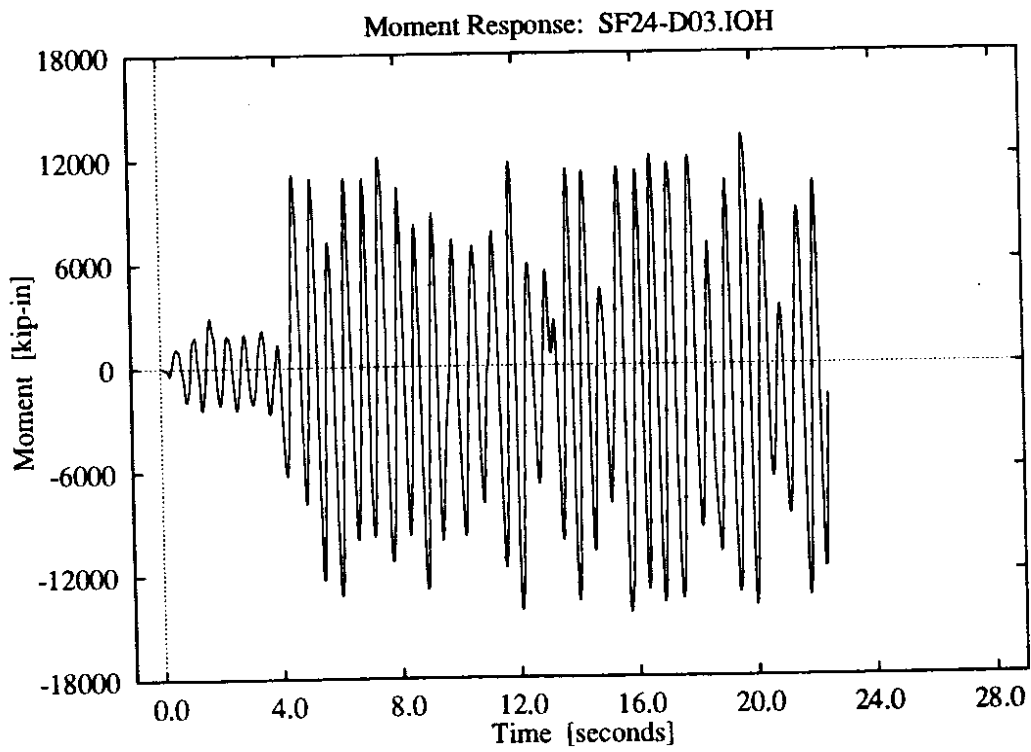
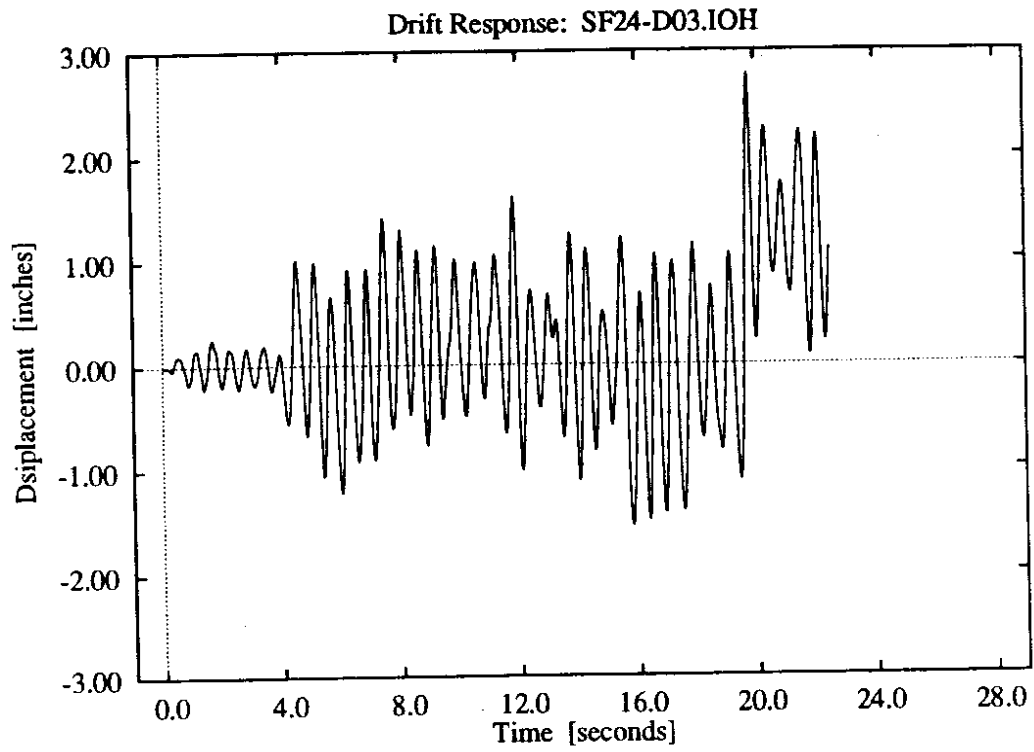


**Figure D-47:** 3 parameter foundation model, intermediate soil stiffness, higher intensity Olympia record.

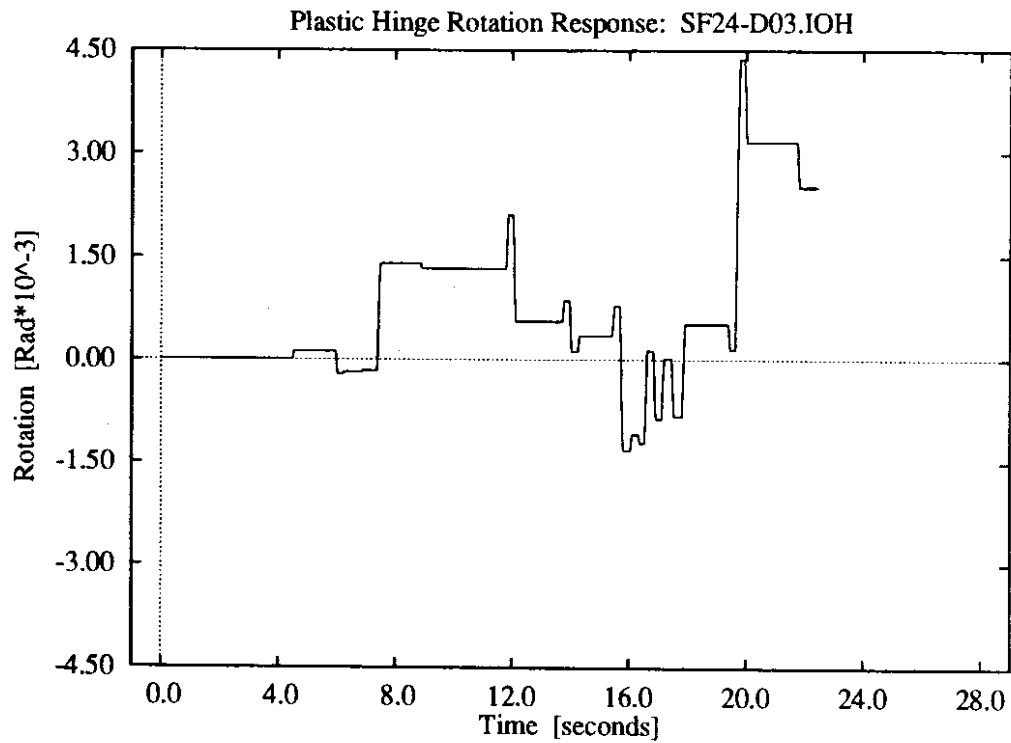
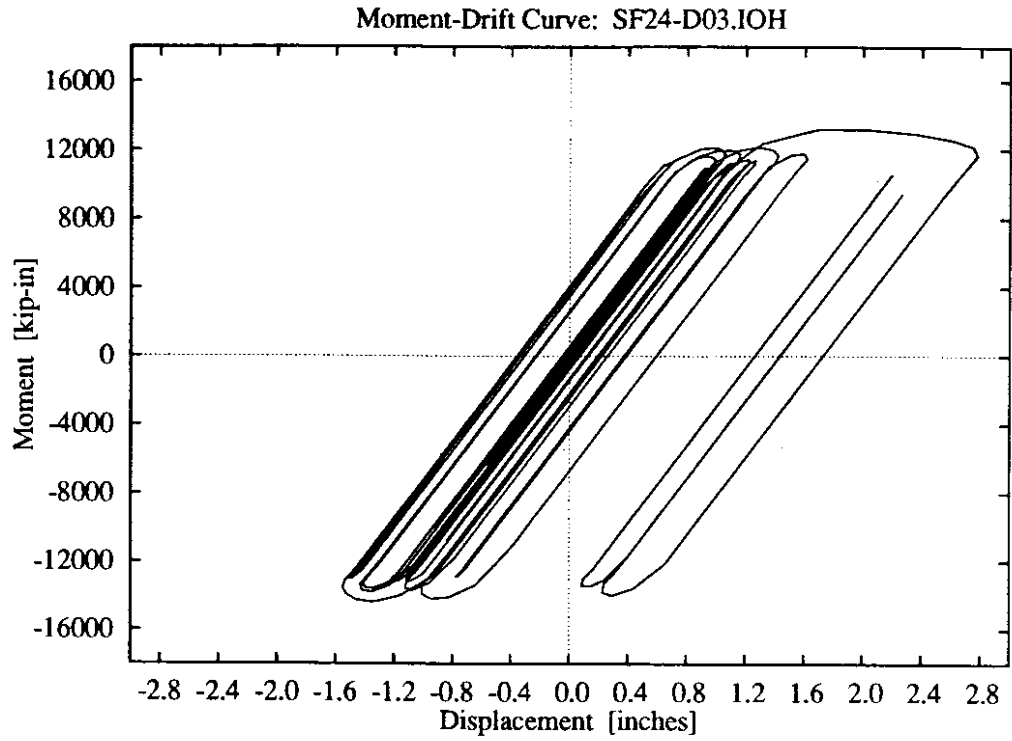


**Figure D-48:** 3 parameter foundation model, intermediate soil stiffness, higher intensity Olympia record.

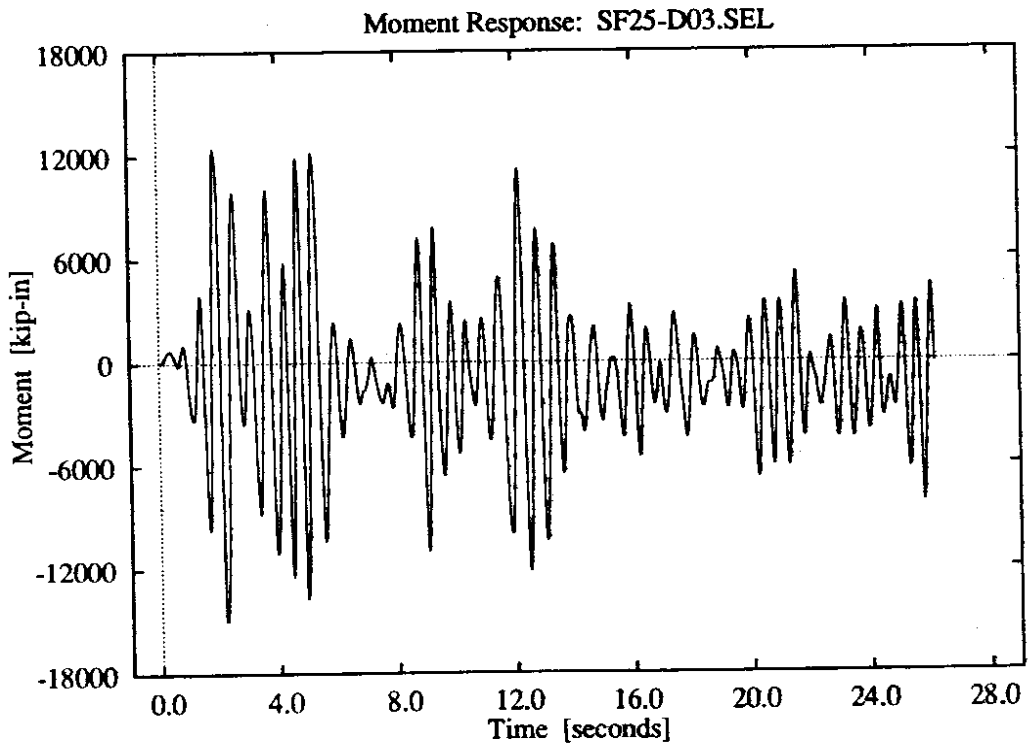
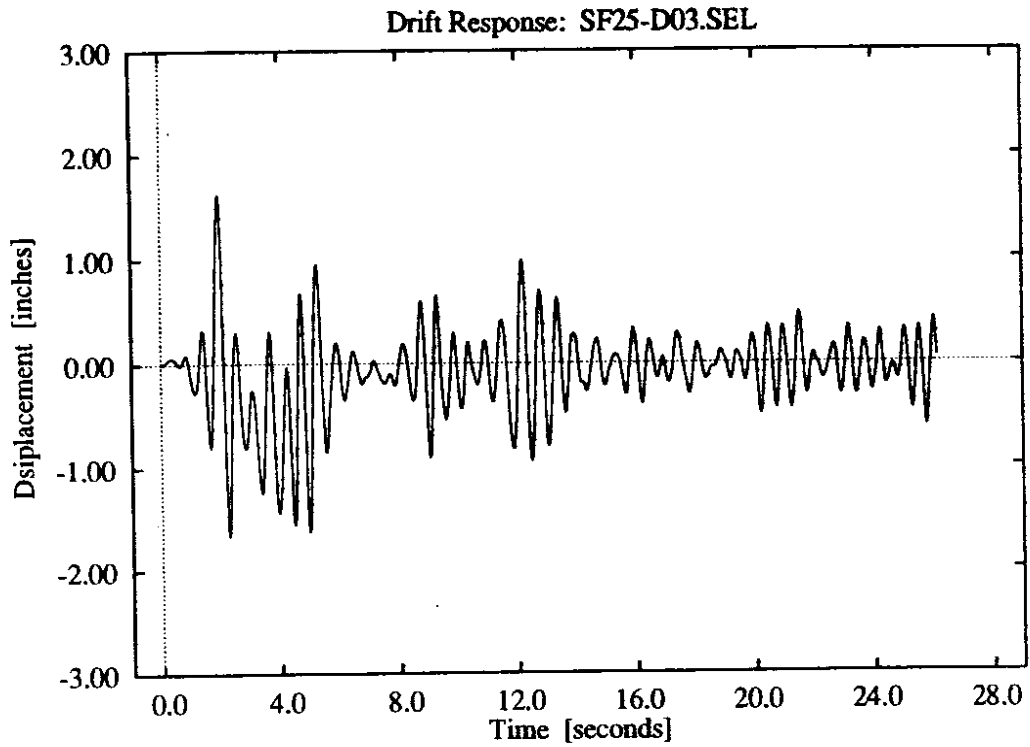


**Figure D-49:** 3 parameter foundation model, high soil stiffness, lower intensity El Centro record.

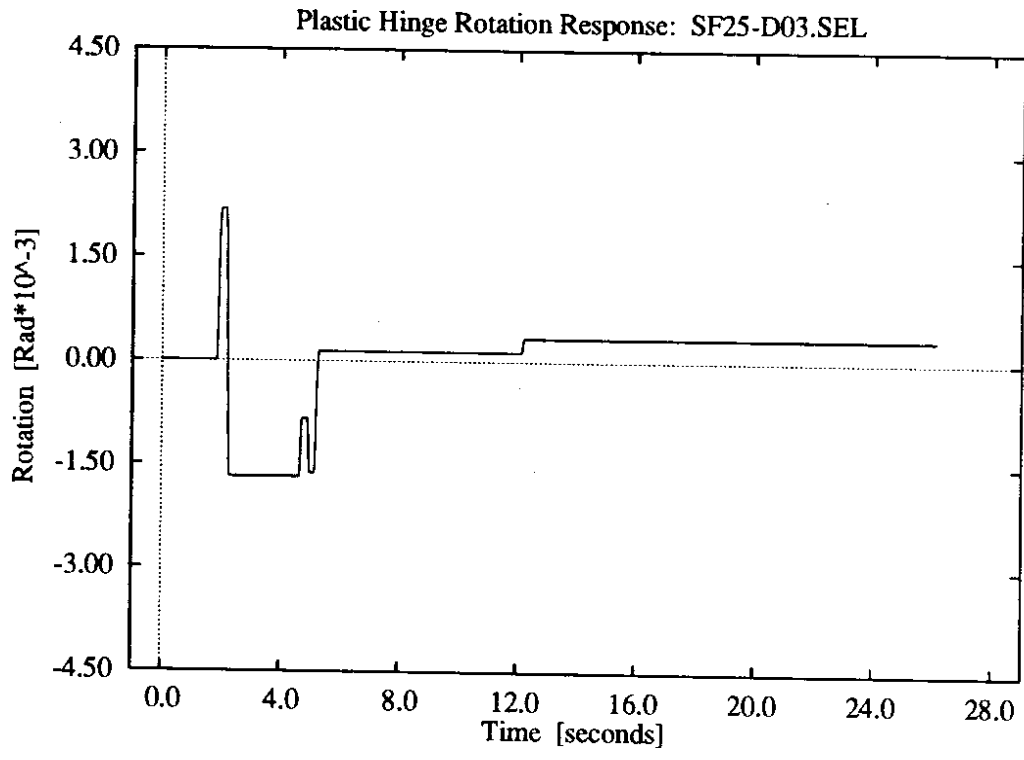
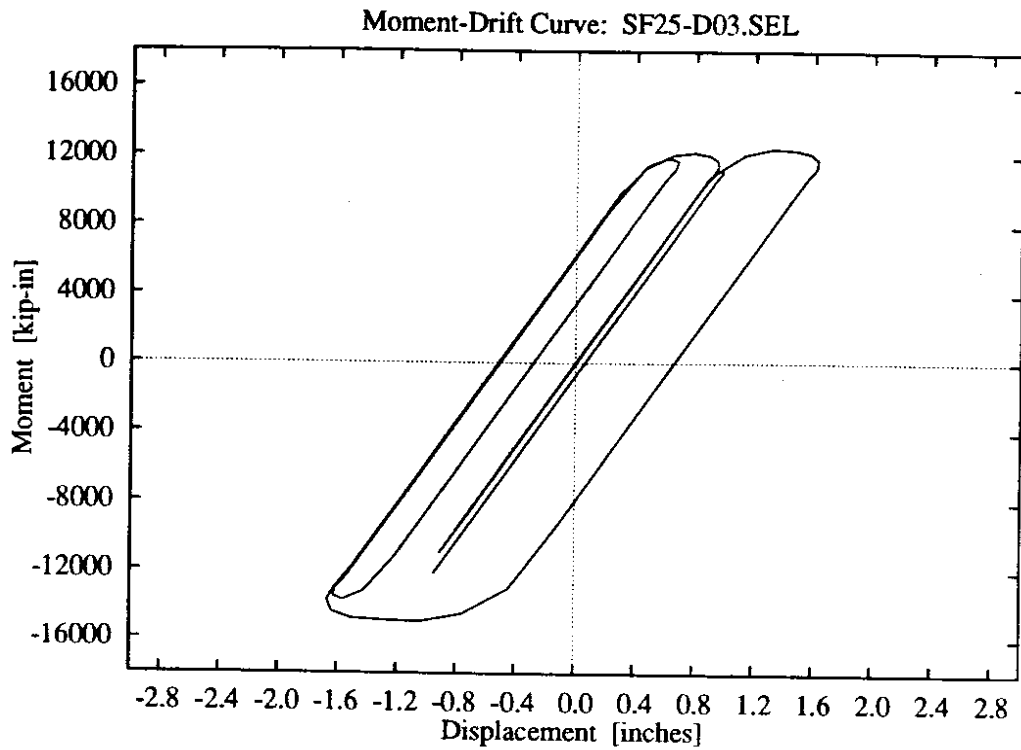


**Figure D-50: 3 parameter foundation model, high soil stiffness, lower intensity El Centro record.**

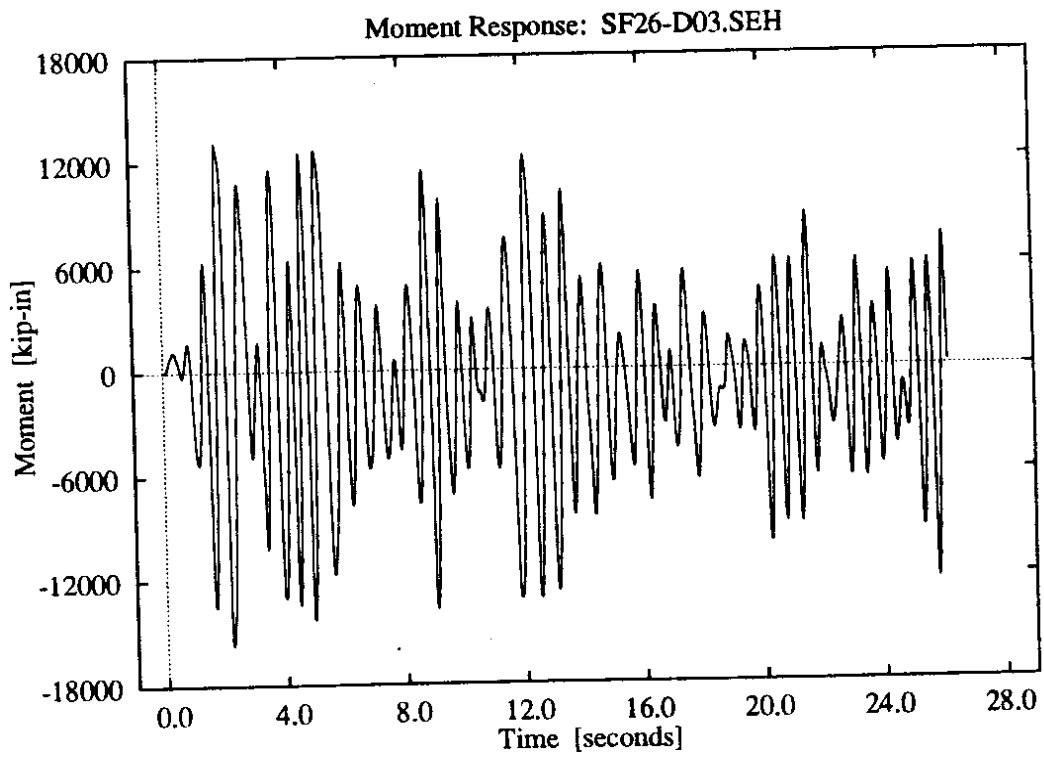
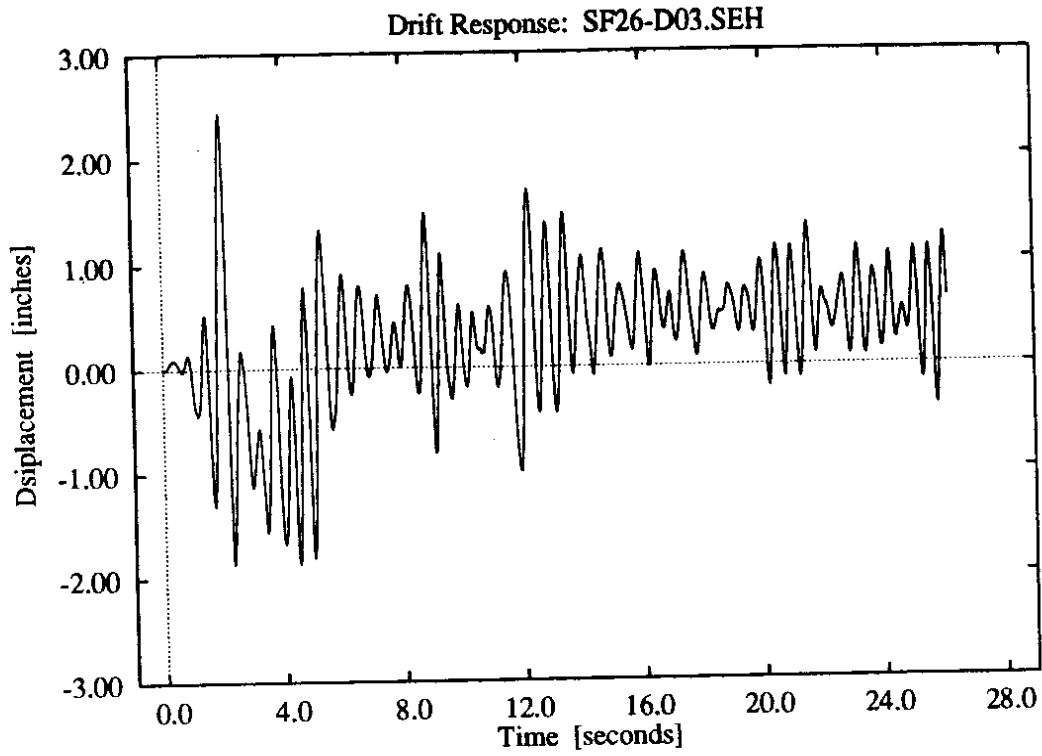


**Figure D-51: 3 parameter foundation model, high soil stiffness, higher intensity El Centro record.**

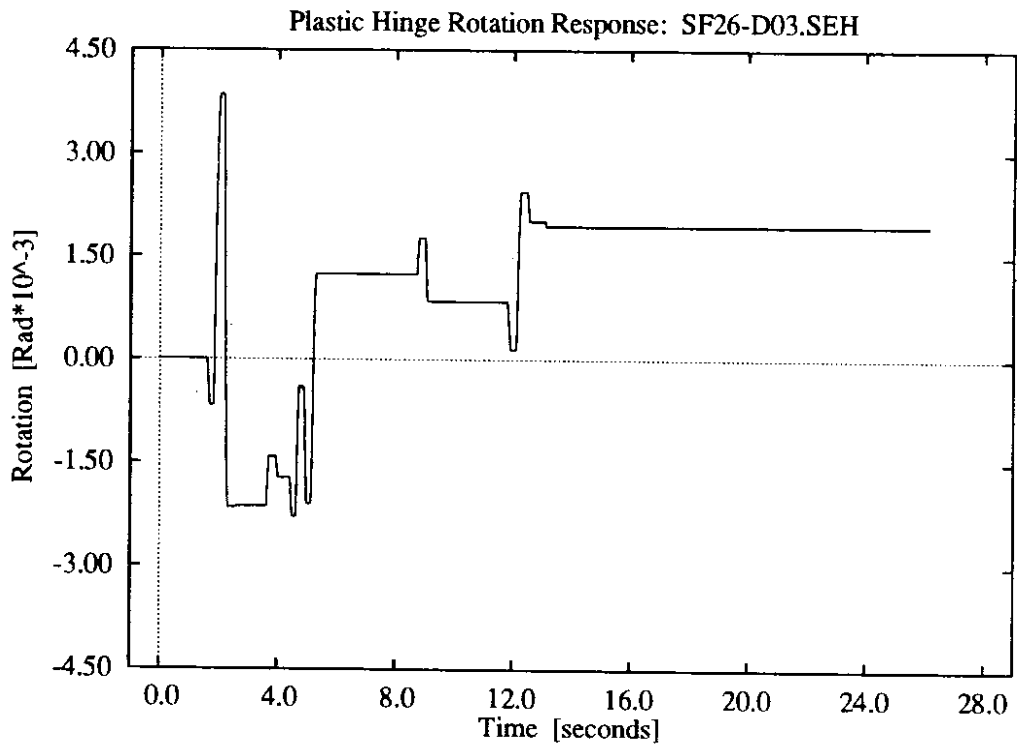
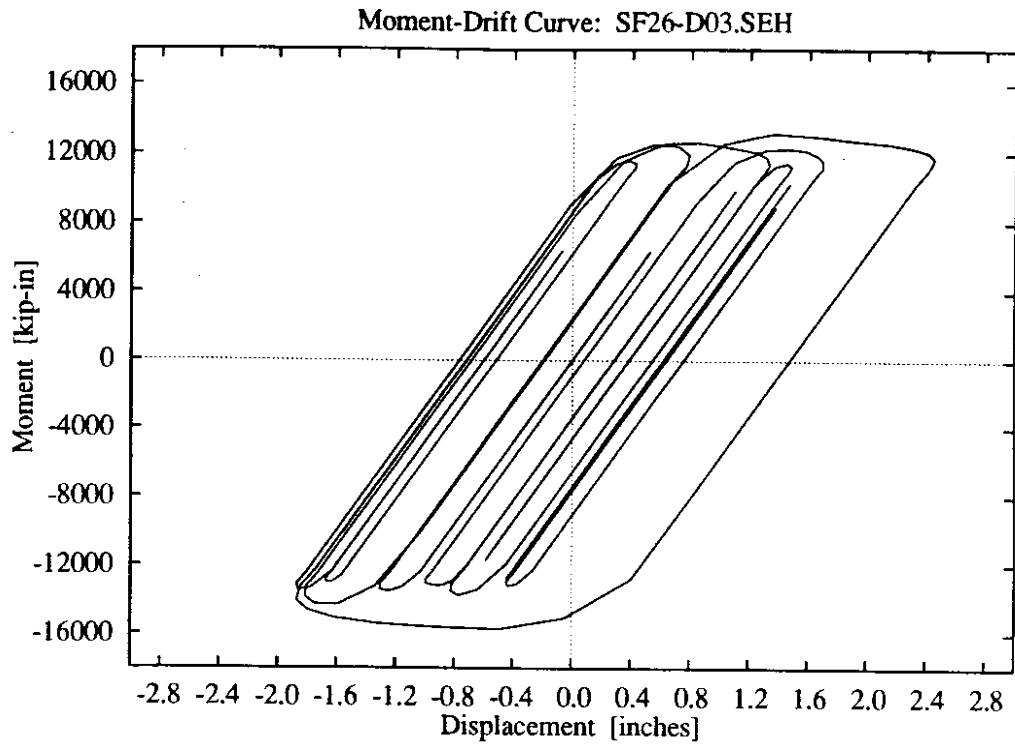


**Figure D-52:** 3 parameter foundation model, high soil stiffness, higher intensity El Centro record.

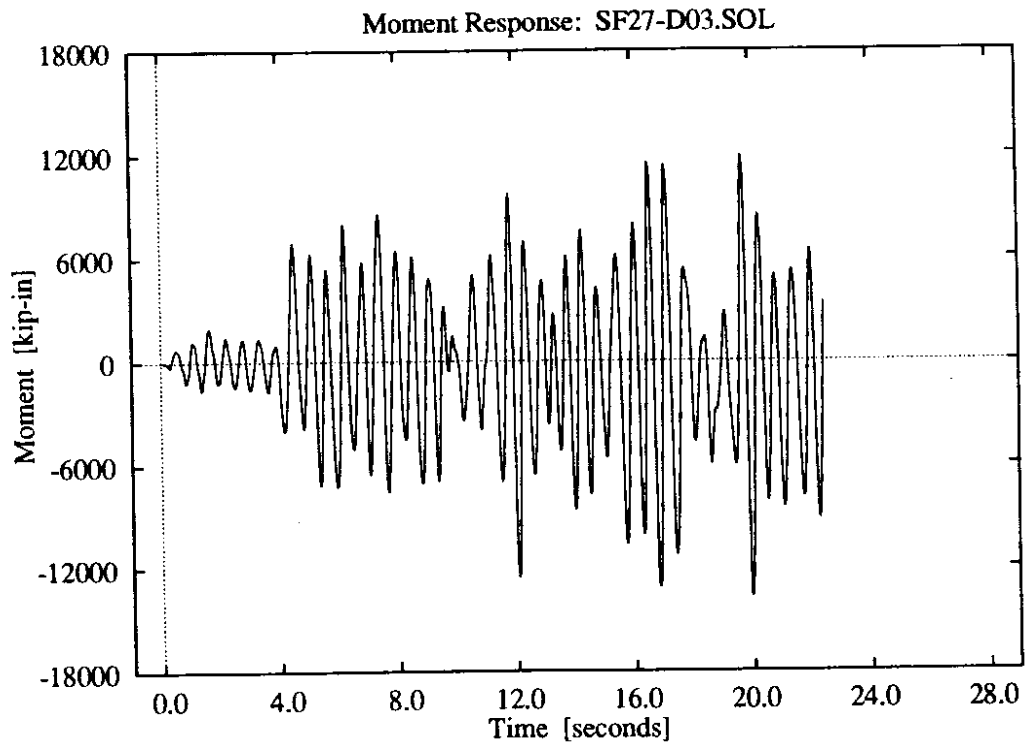
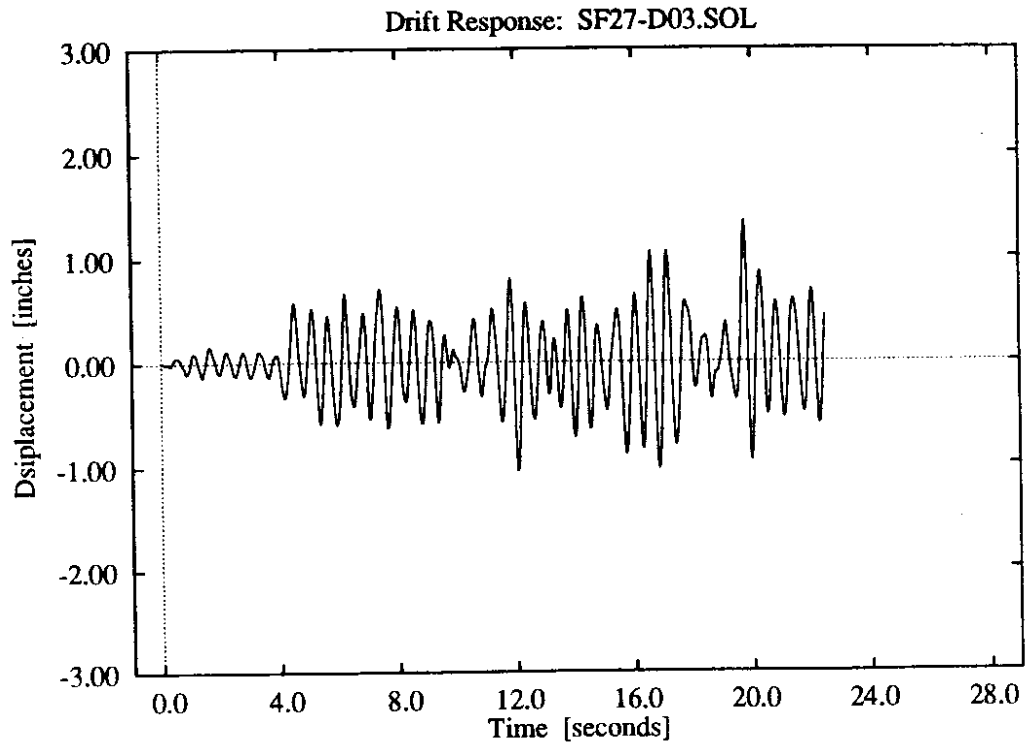


**Figure D-53:** 3 parameter foundation model, high soil stiffness, lower intensity Olympia record.

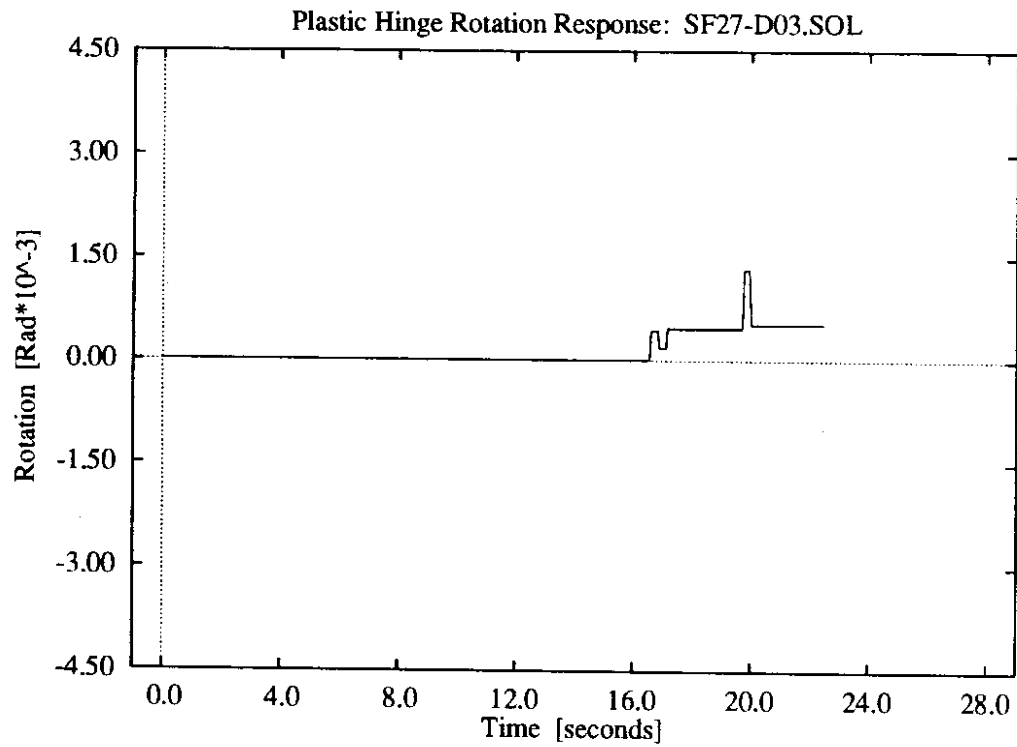
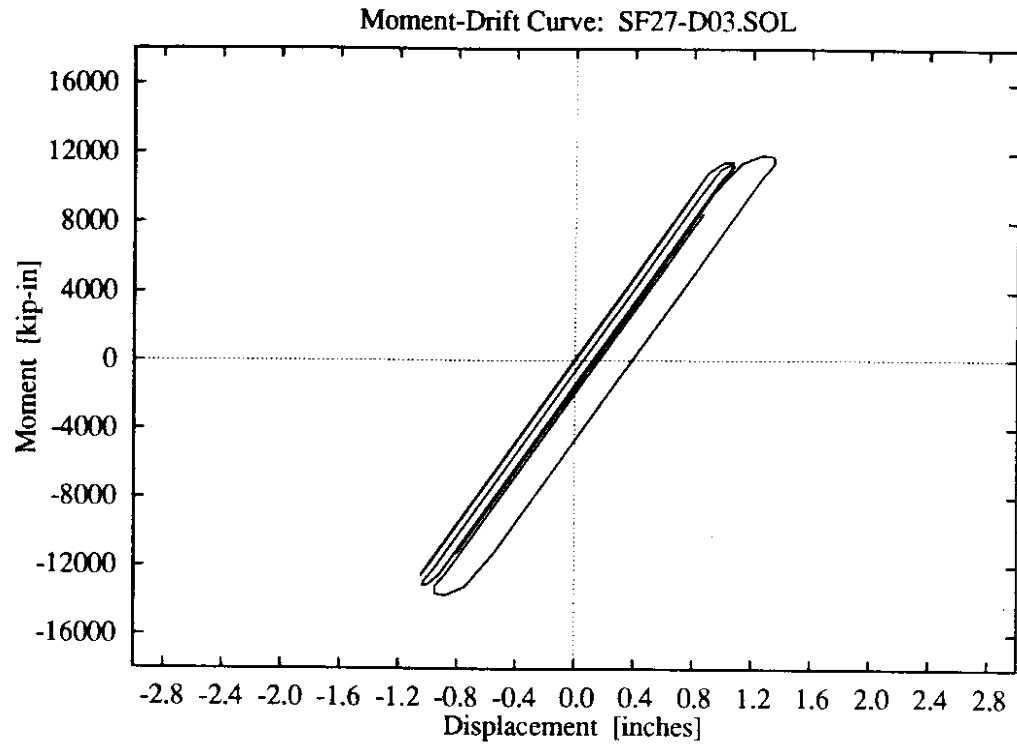


**Figure D-54:** 3 parameter foundation model, high soil stiffness, lower intensity Olympia record.



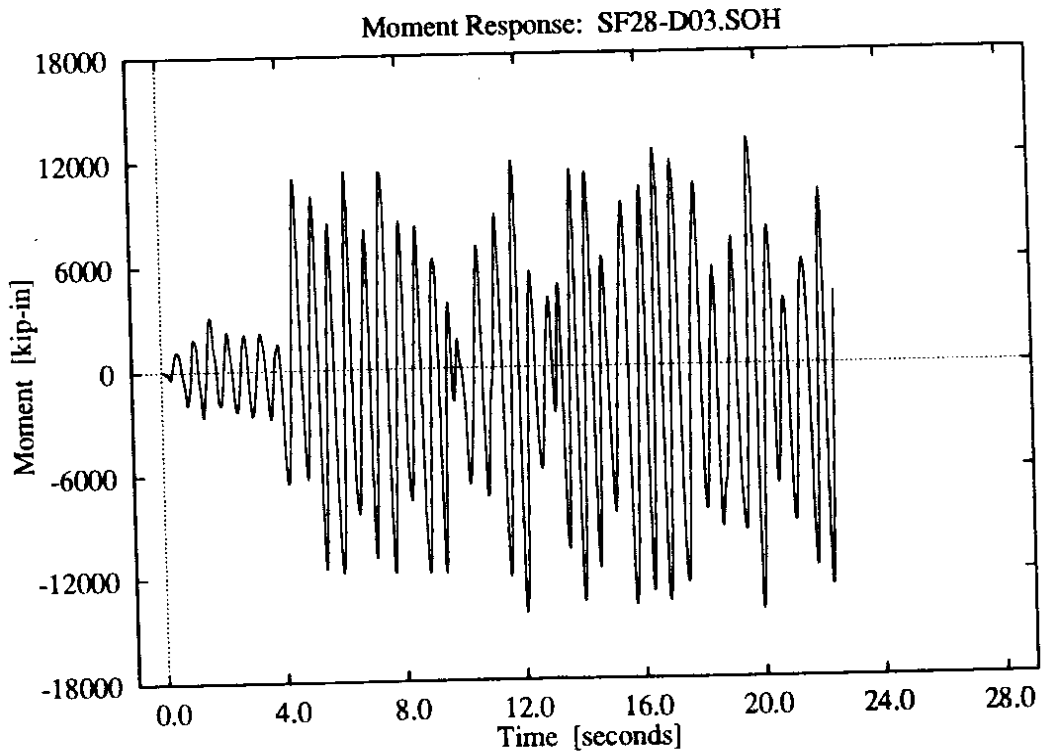
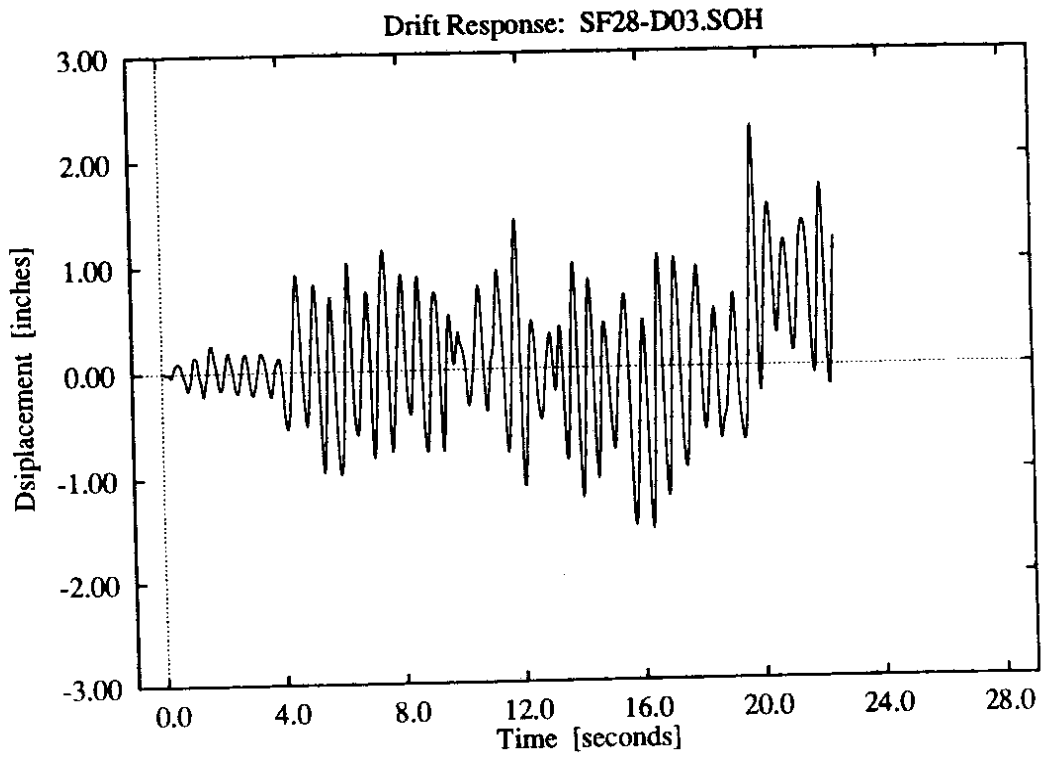


**Figure D-55: 3 parameter model, high soil stiffness, higher intensity Olympia record.**

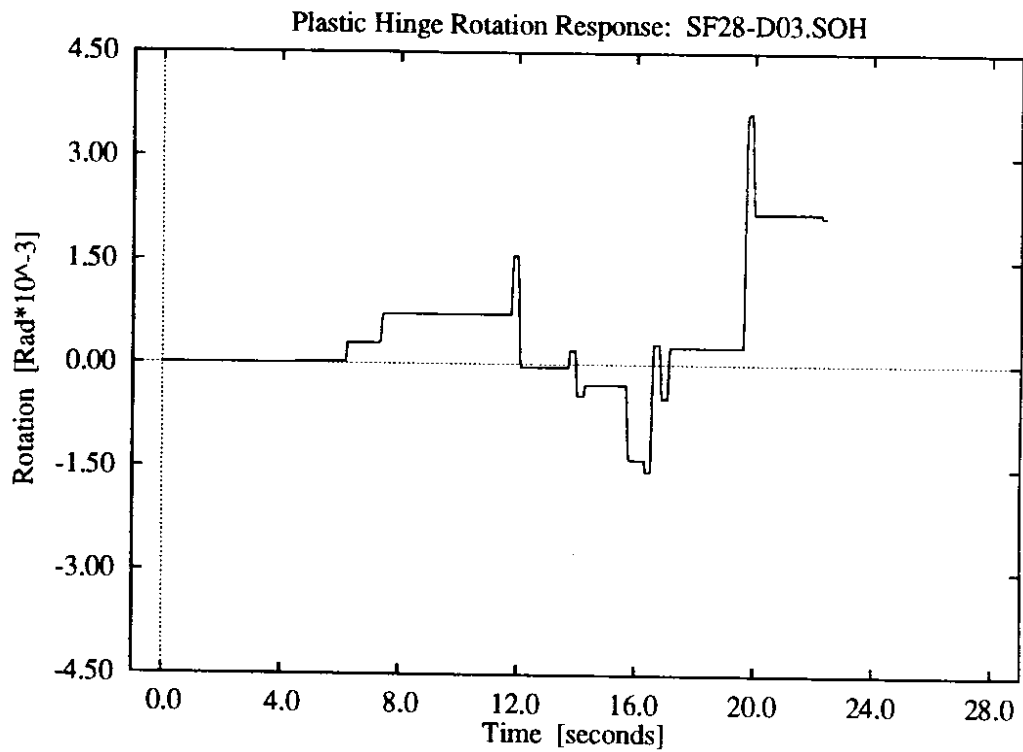
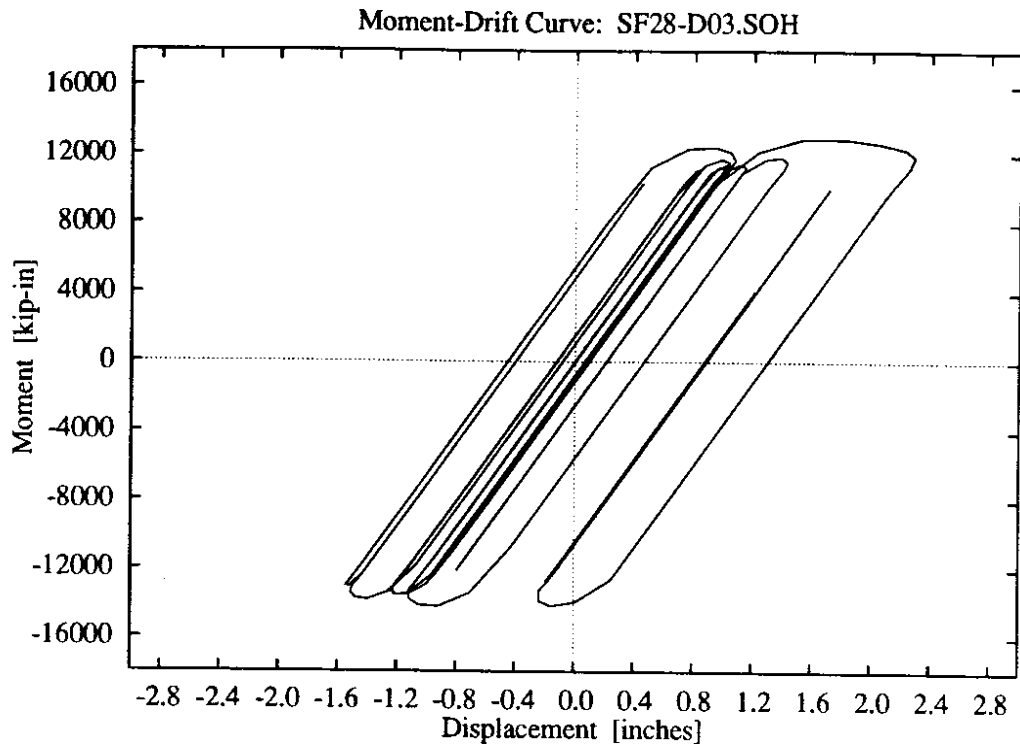


**Figure D-56: 3 parameter model, high soil stiffness, higher intensity Olympia record.**

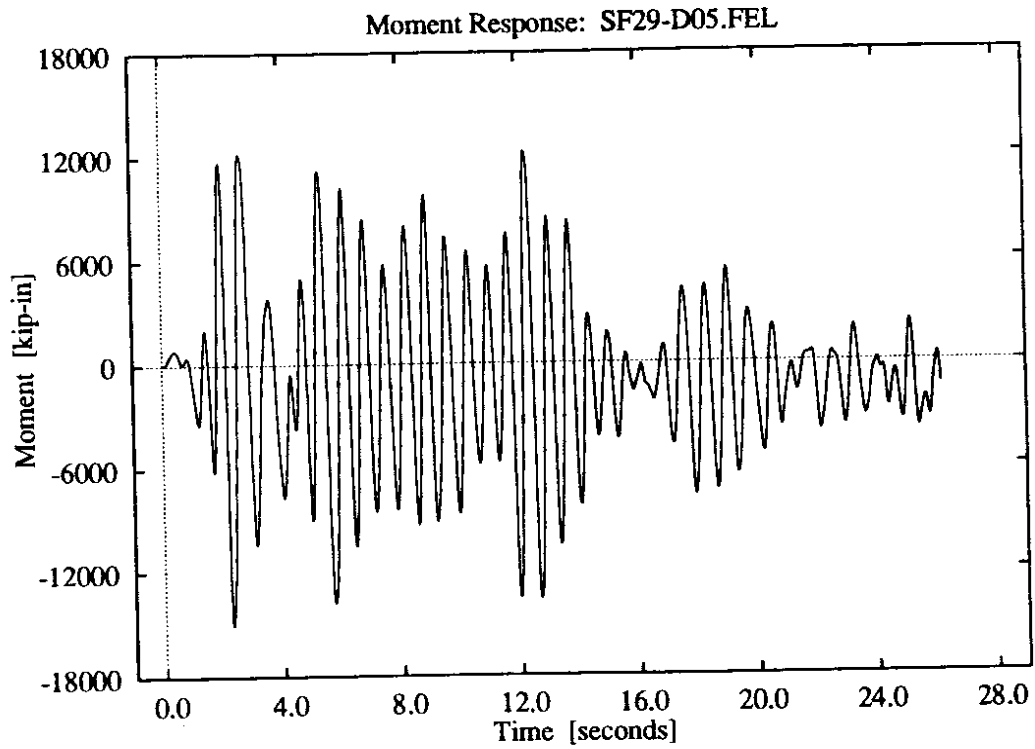
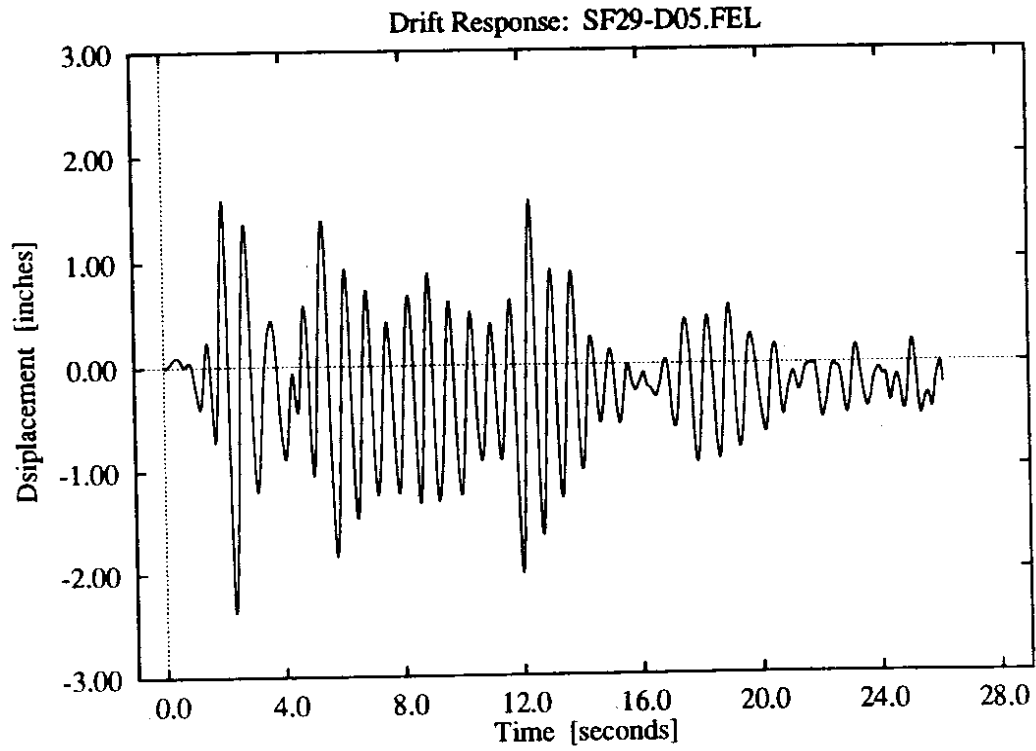


**Figure D-57:** 5 parameter foundation model, low soil stiffness, lower intensity El Centro.

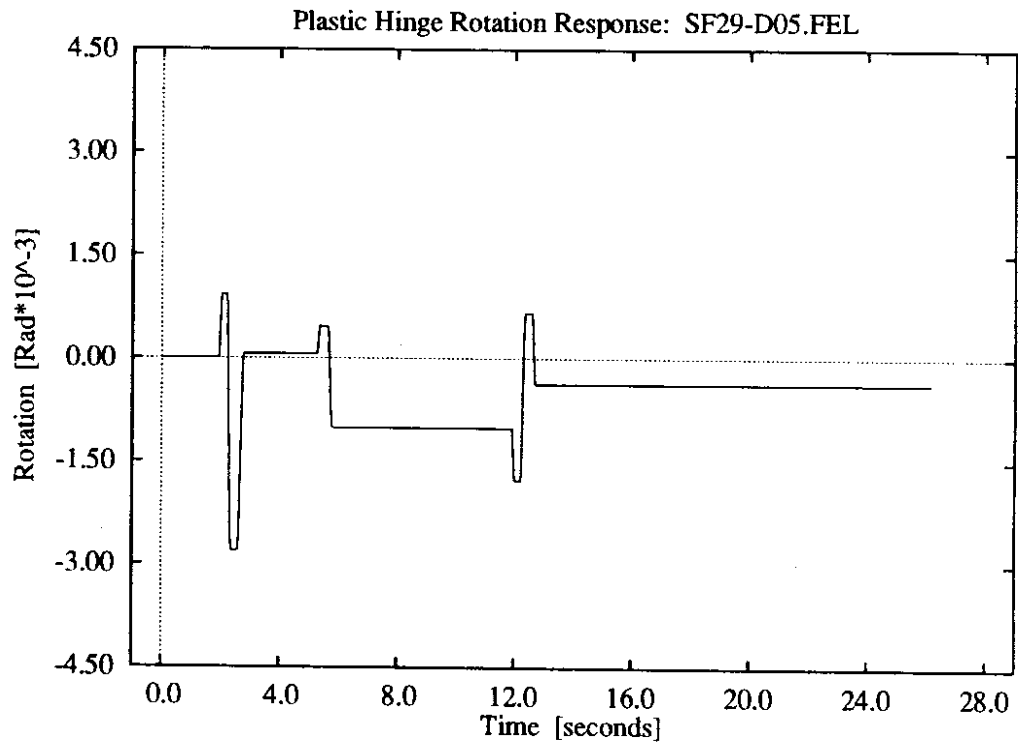
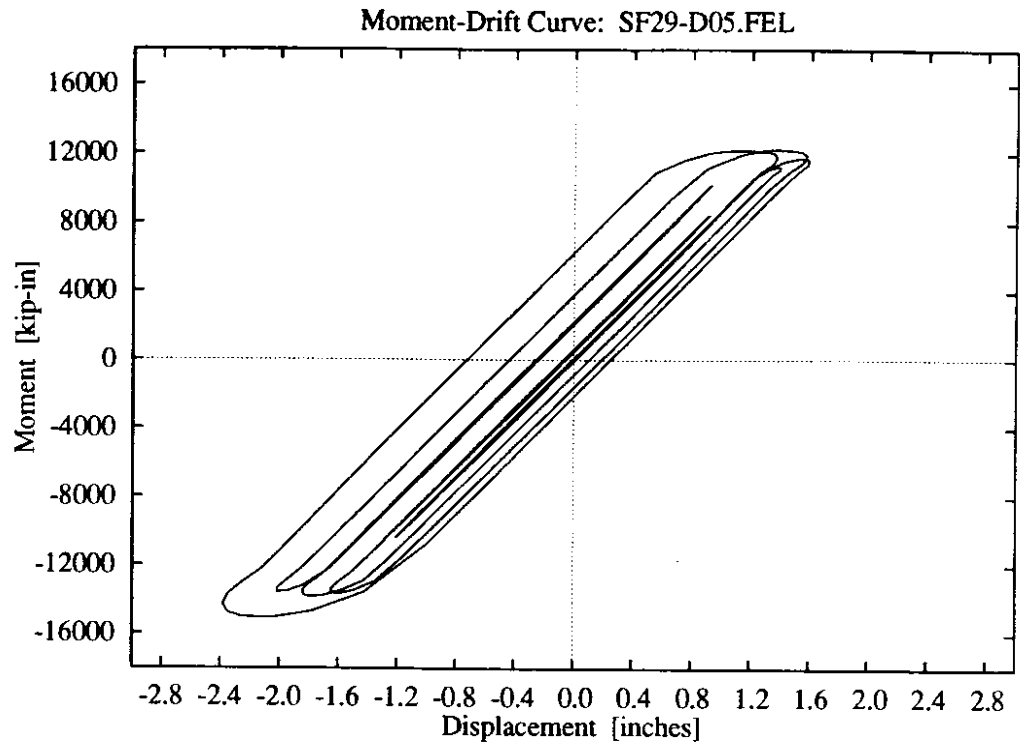


**Figure D-58:** 5 parameter foundation model, low soil stiffness, lower intensity El Centro.

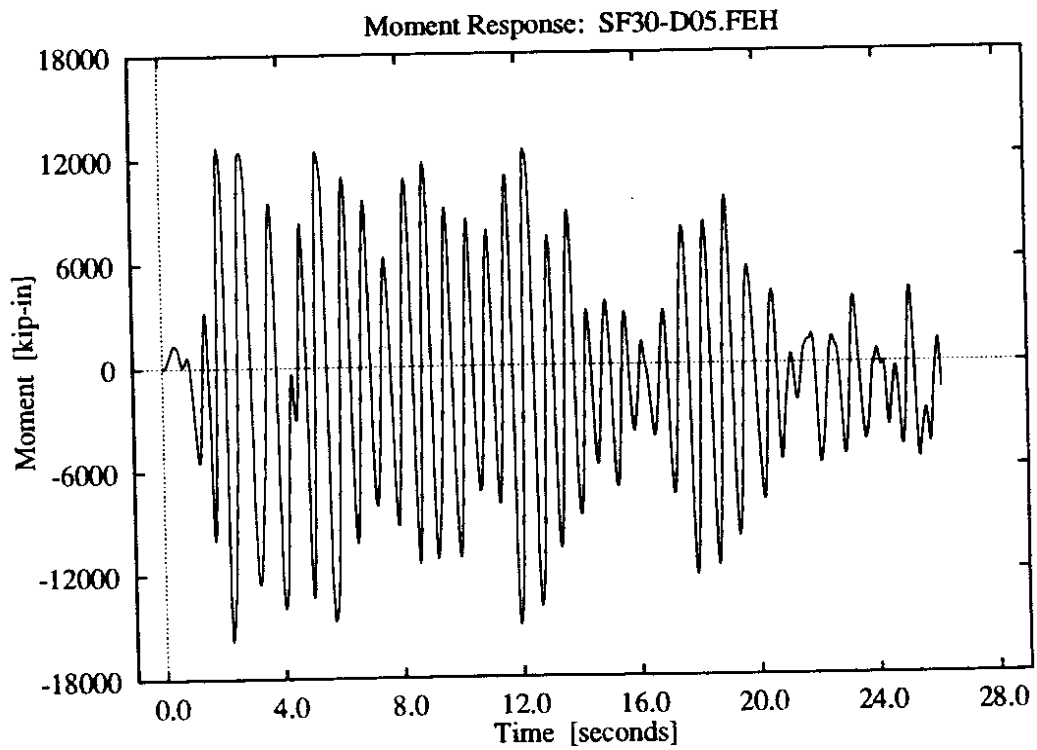
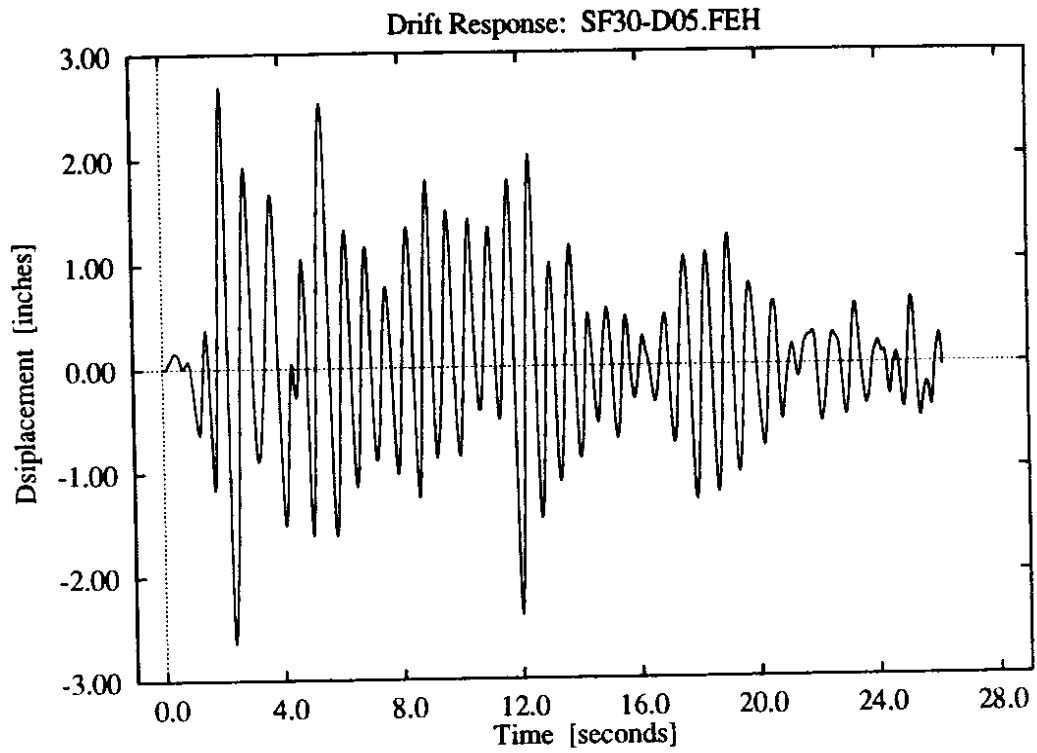


**Figure D-59:** 5 parameter foundation model, low soil stiffness, higher intensity El Centro.

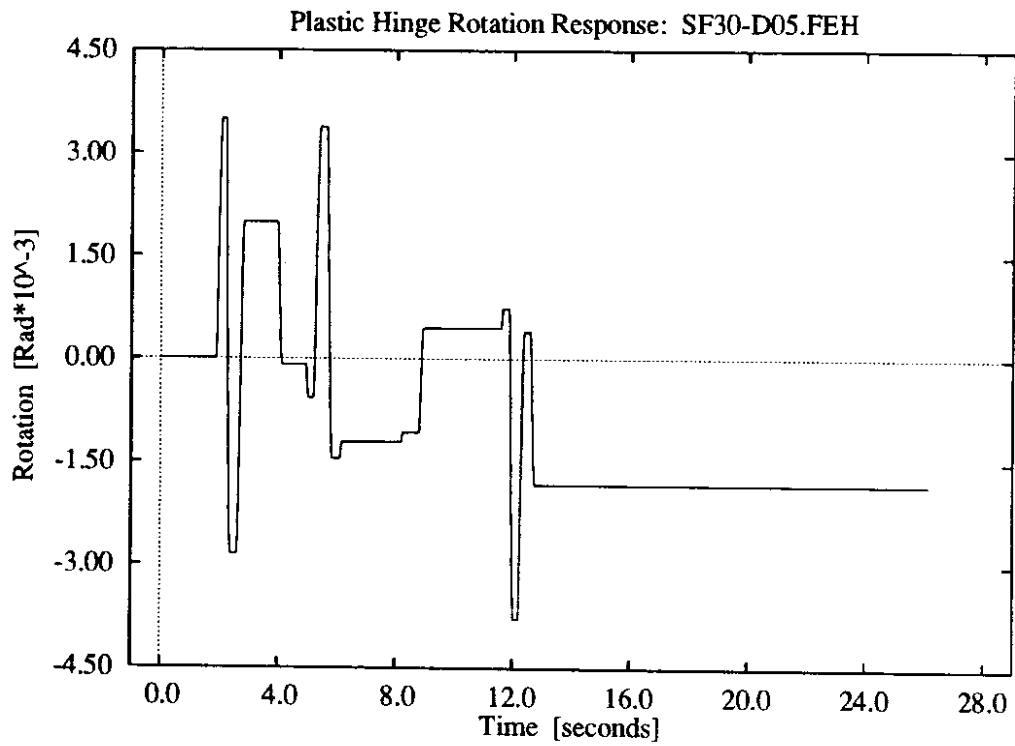
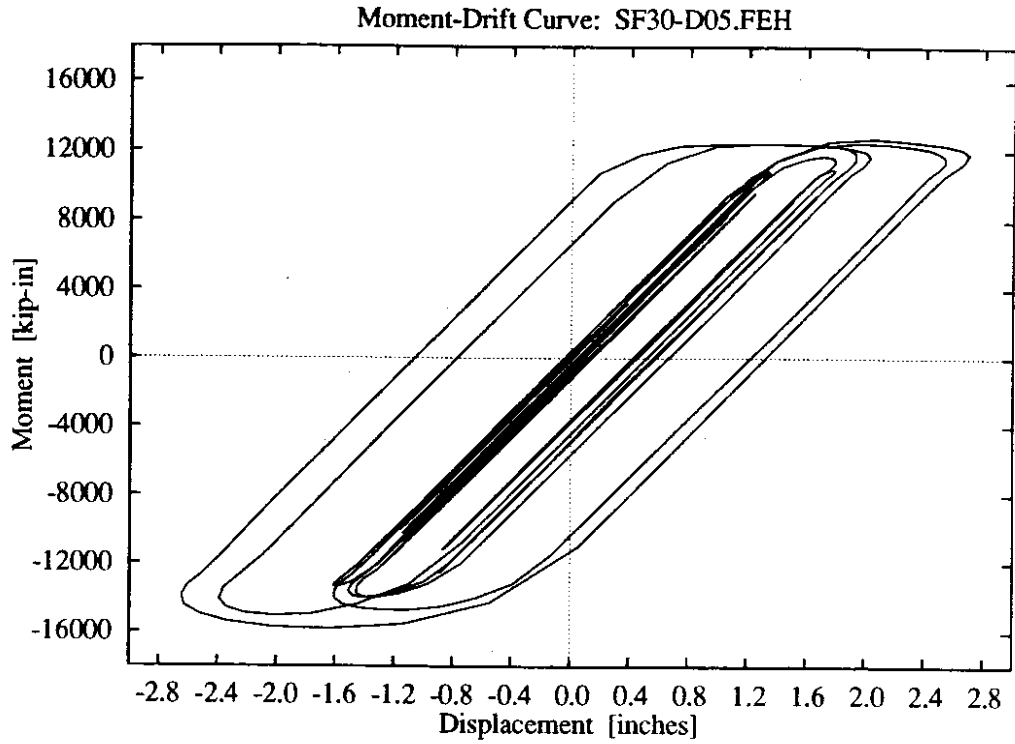


**Figure D-60:** 5 parameter foundation model, low soil stiffness, higher intensity El Centro.

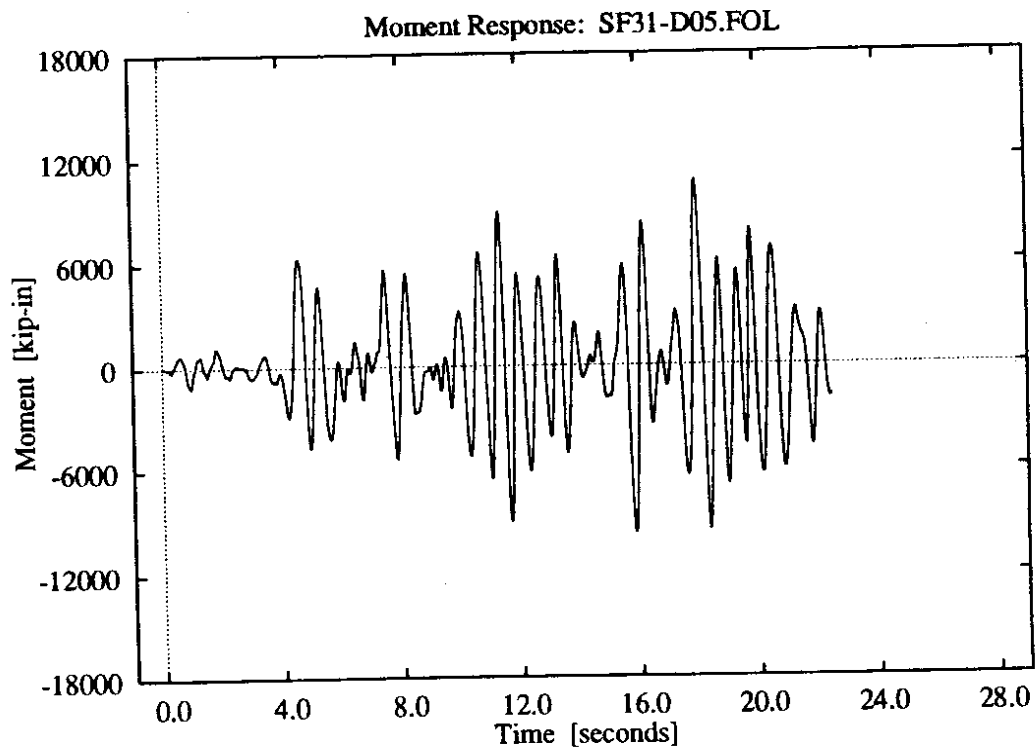
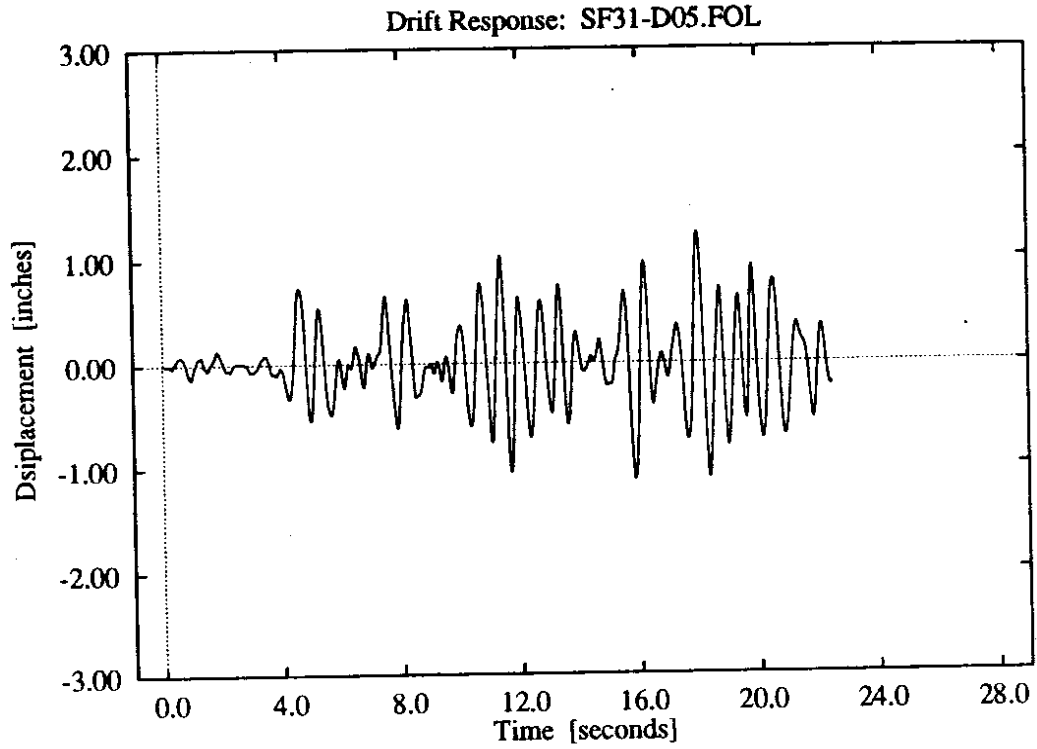


**Figure D-61: 5 parameter foundation model, low soil stiffness, lower intensity Olympia record.**

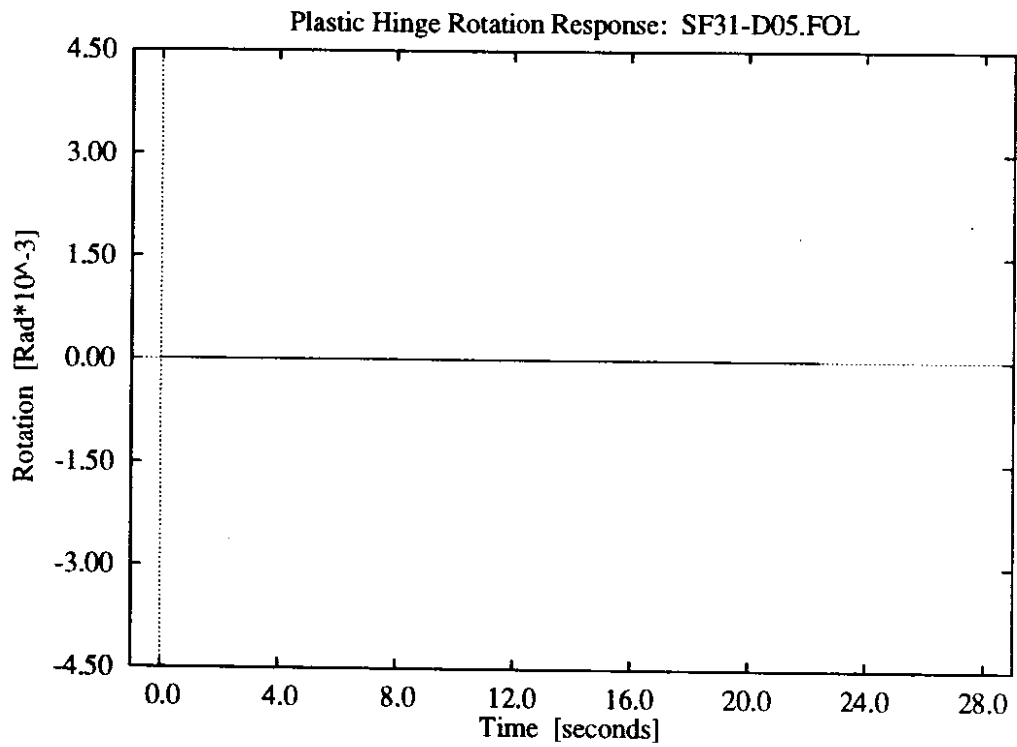
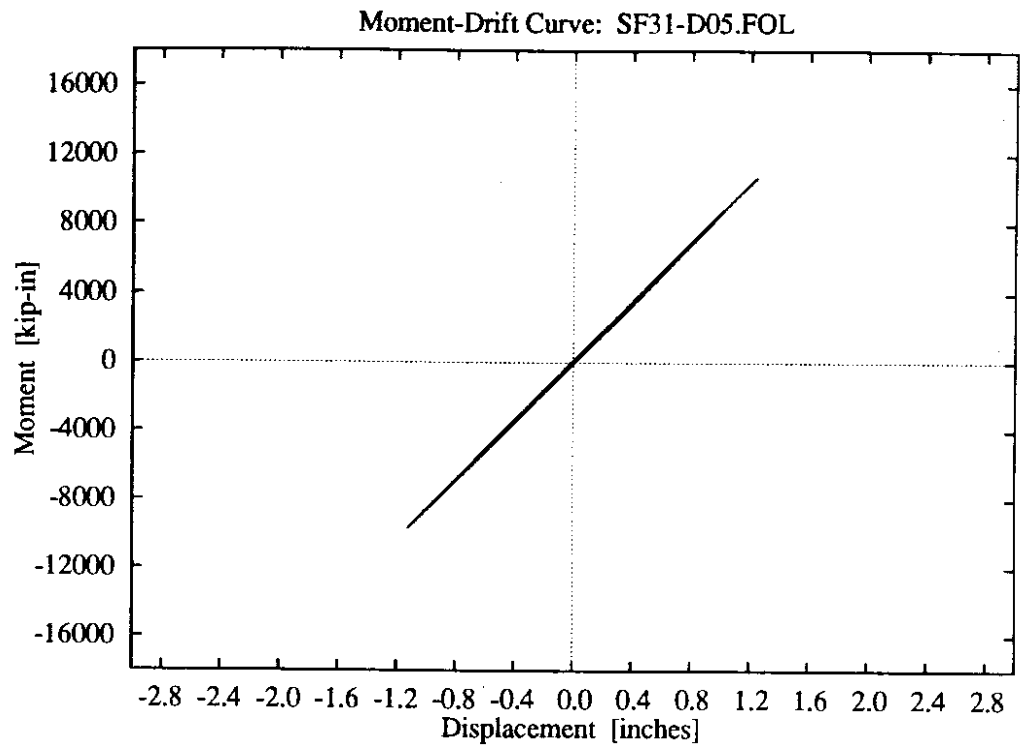


**Figure D-62:** 5 parameter foundation model, low soil stiffness, lower intensity Olympia record.



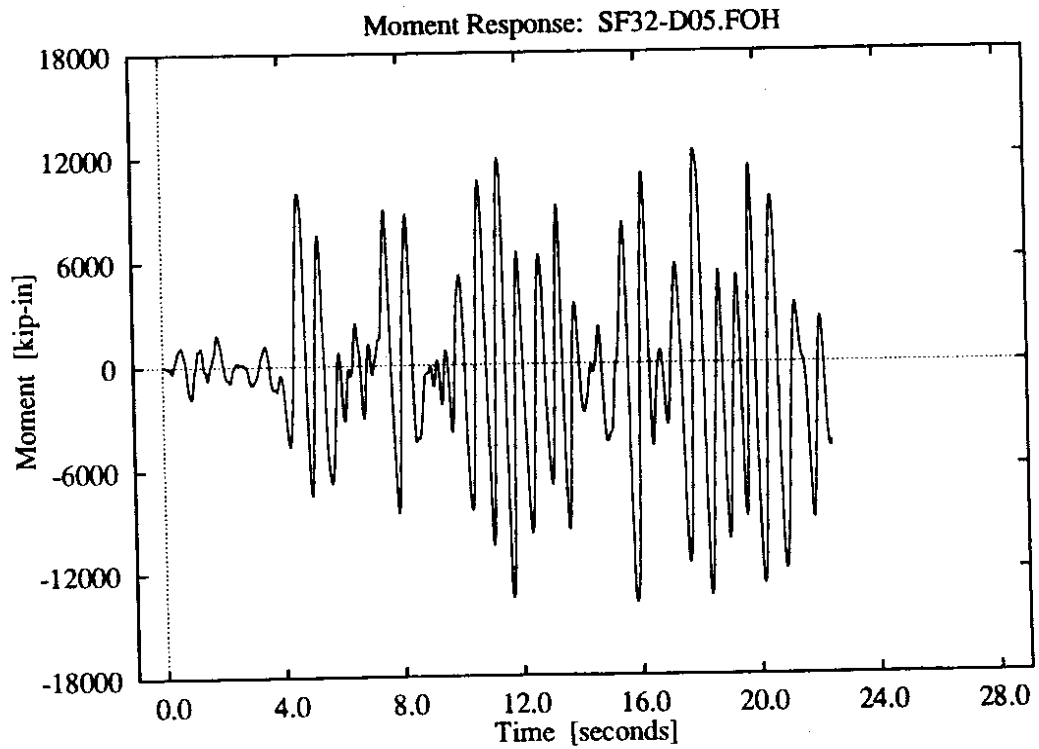
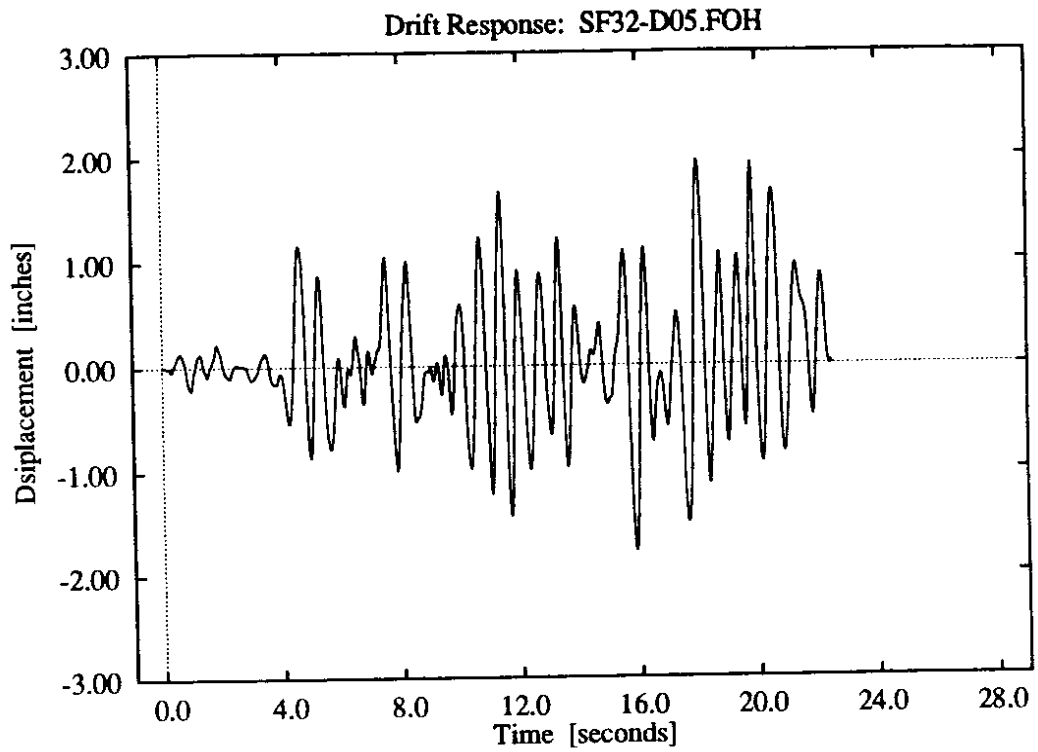


**Figure D-63:** 5 parameter foundation model, low soil stiffness, higher intensity Olympia record.

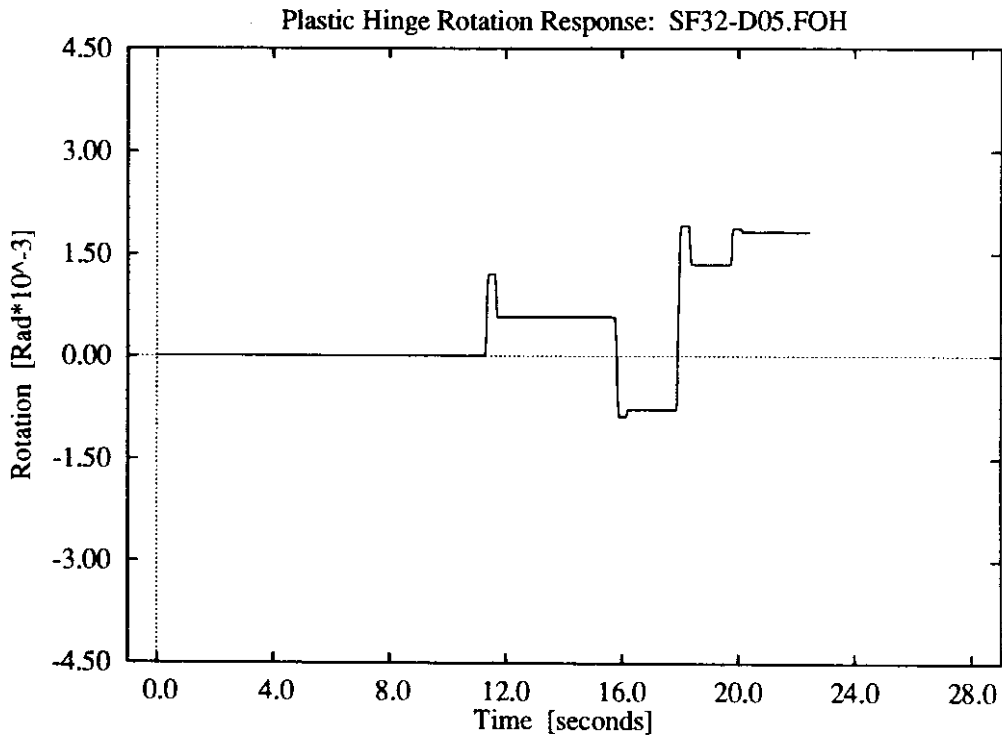
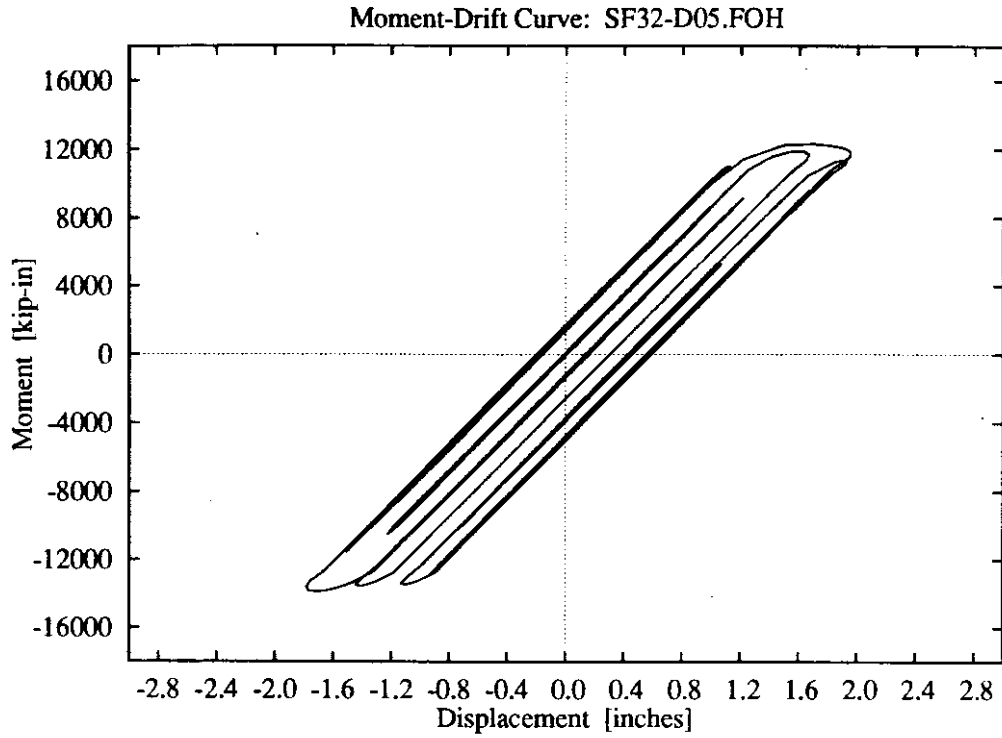


**Figure D-64:** 5 parameter foundation model, low soil stiffness, higher intensity Olympia record.

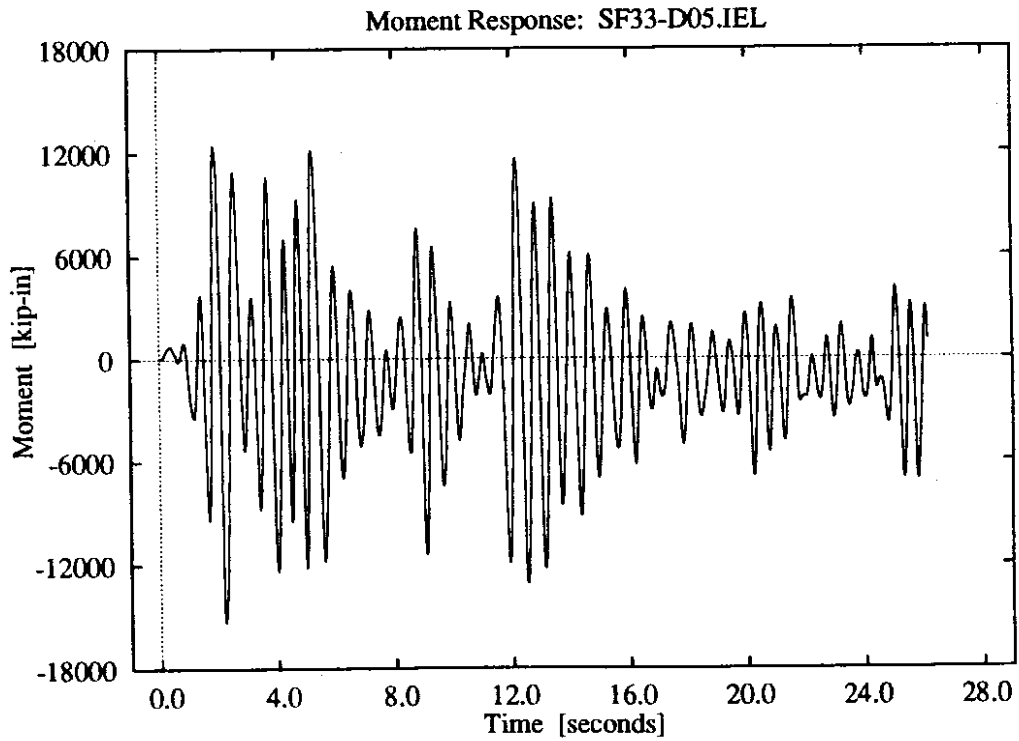
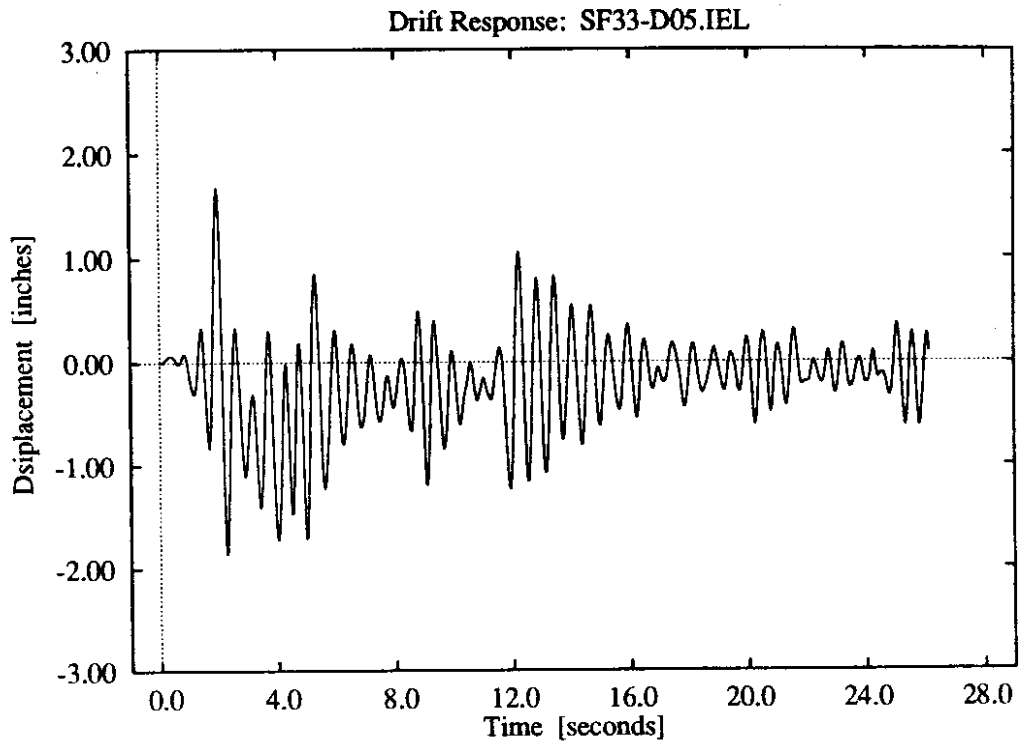


**Figure D-65:** 5 parameter foundation model, intermediate soil stiffness, lower intensity El Centro record.

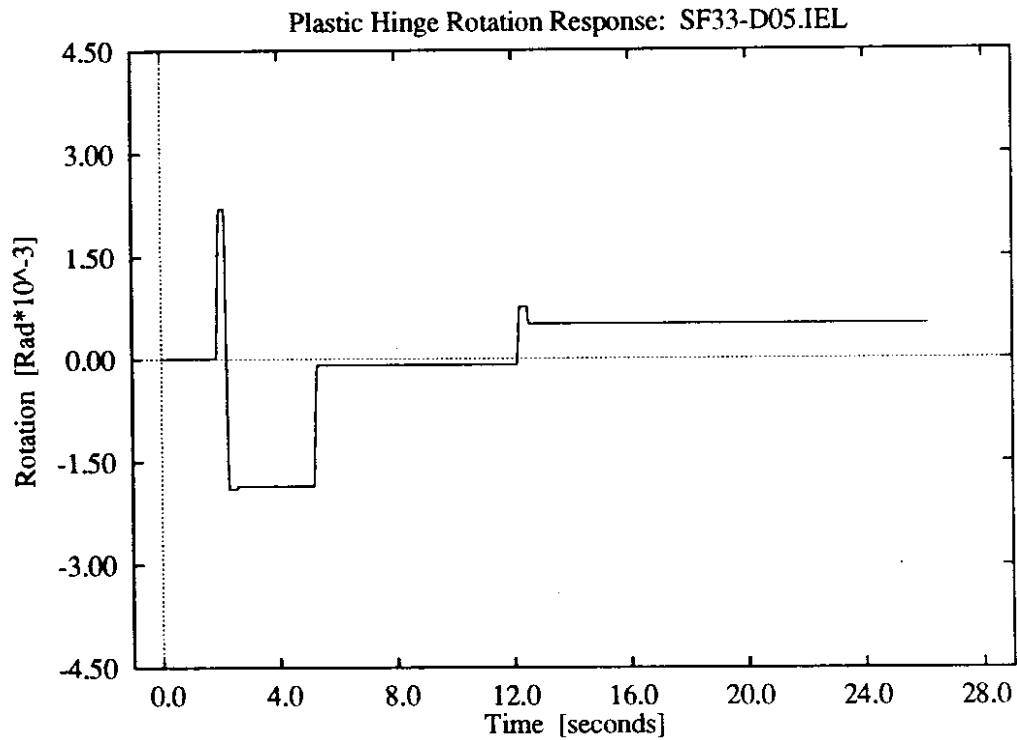
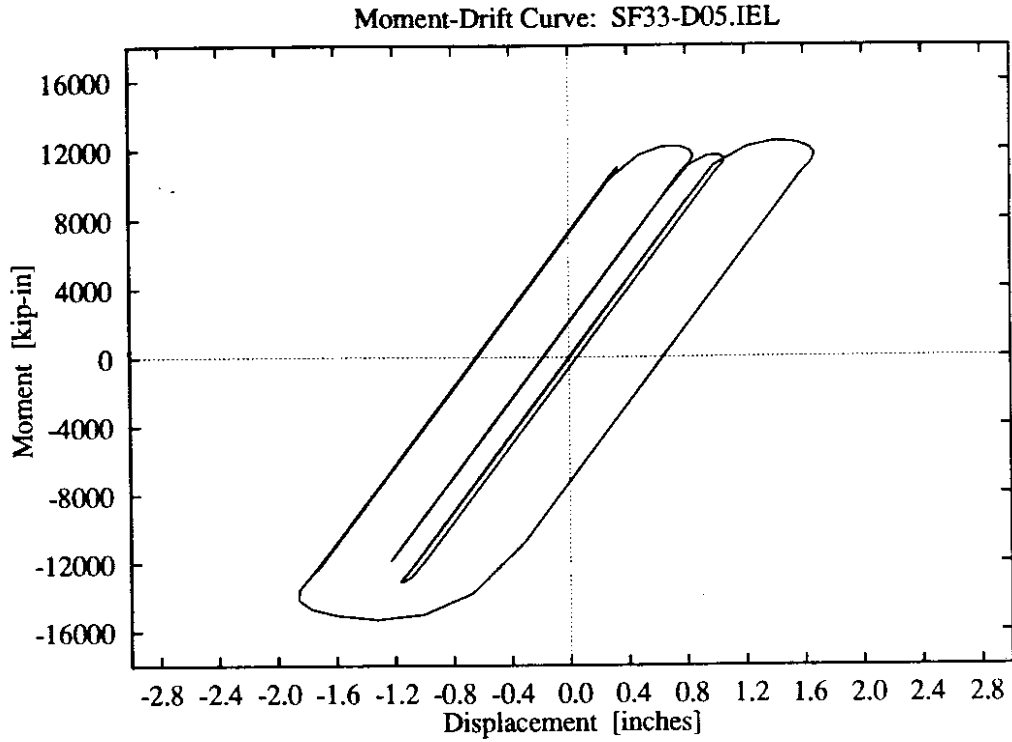


**Figure D-66:** 5 parameter foundation model, intermediate soil stiffness, lower intensity El Centro record.

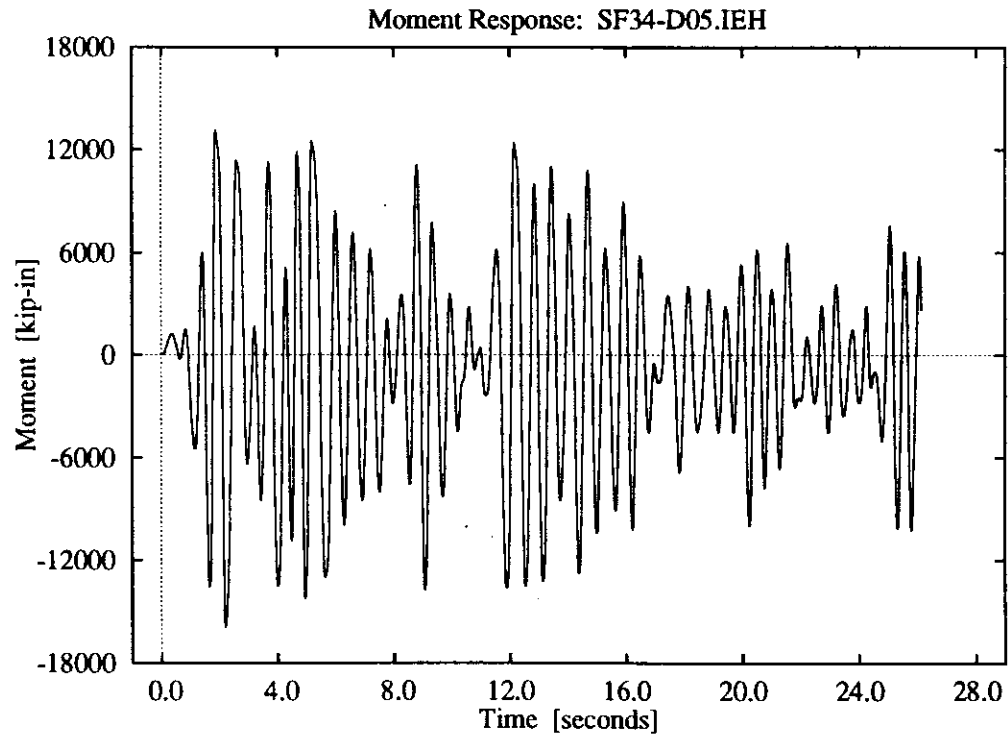
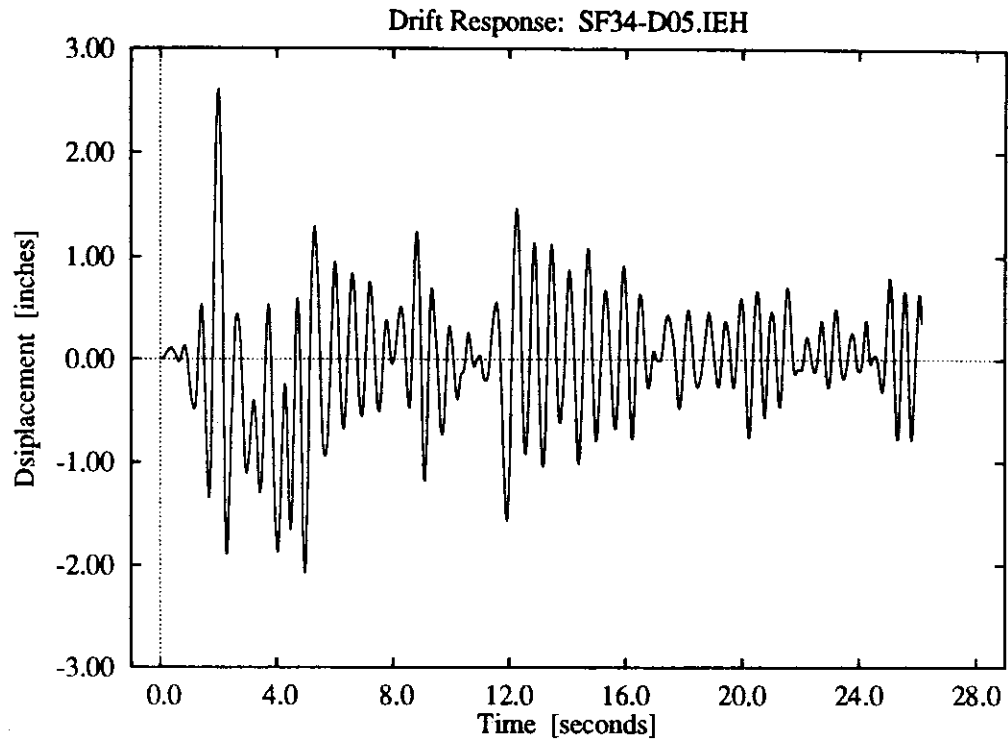


**Figure D-67:** 5 parameter foundation model, intermediate soil stiffness, higher intensity El Centro record.

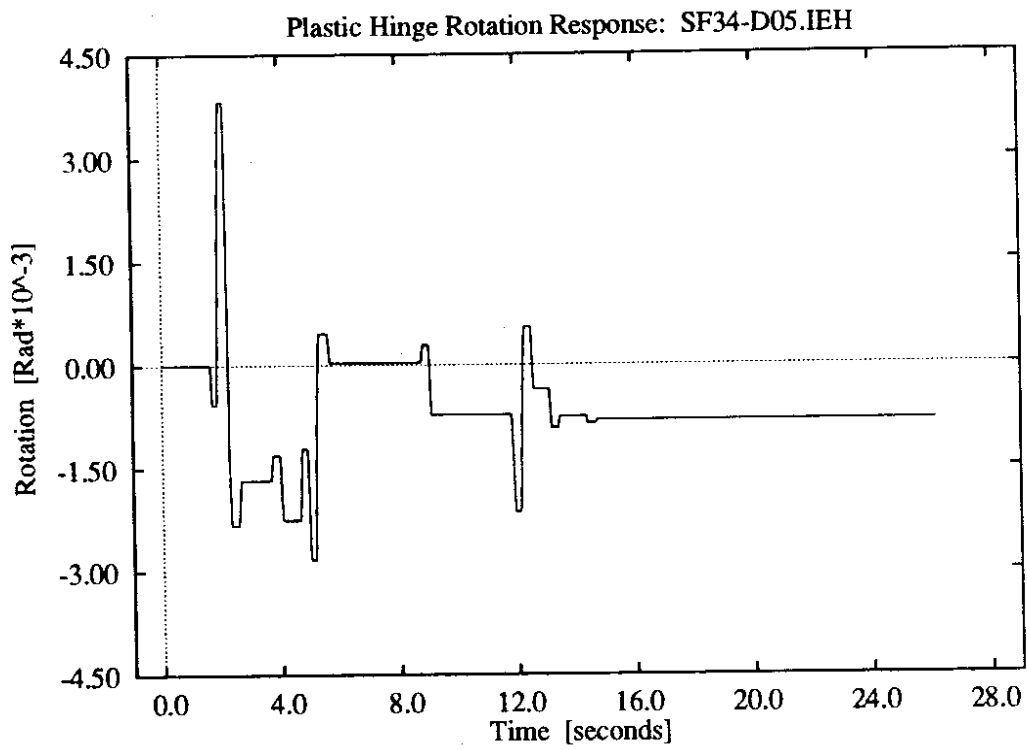
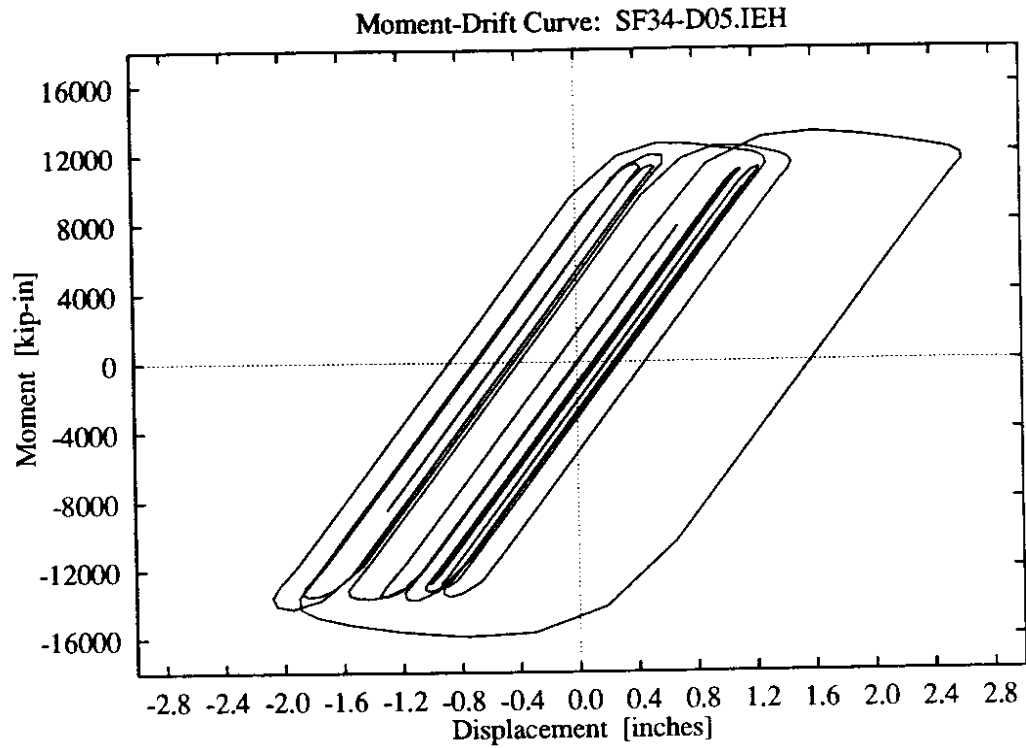


**Figure D-68:** 5 parameter foundation model, intermediate soil stiffness, higher intensity El Centro record.

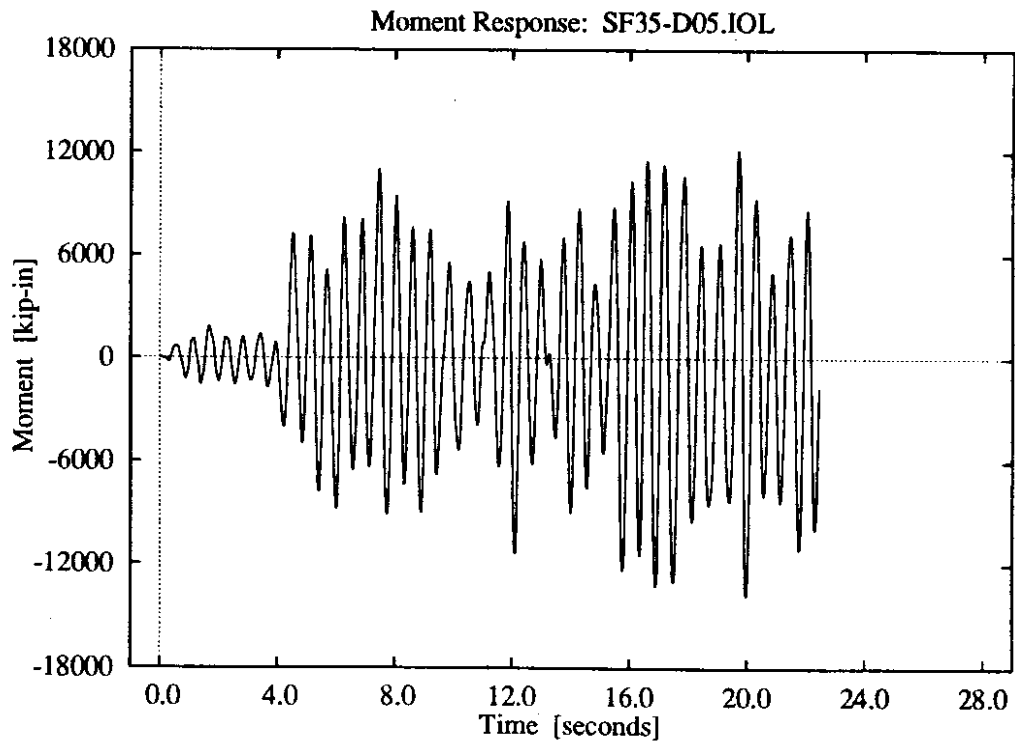
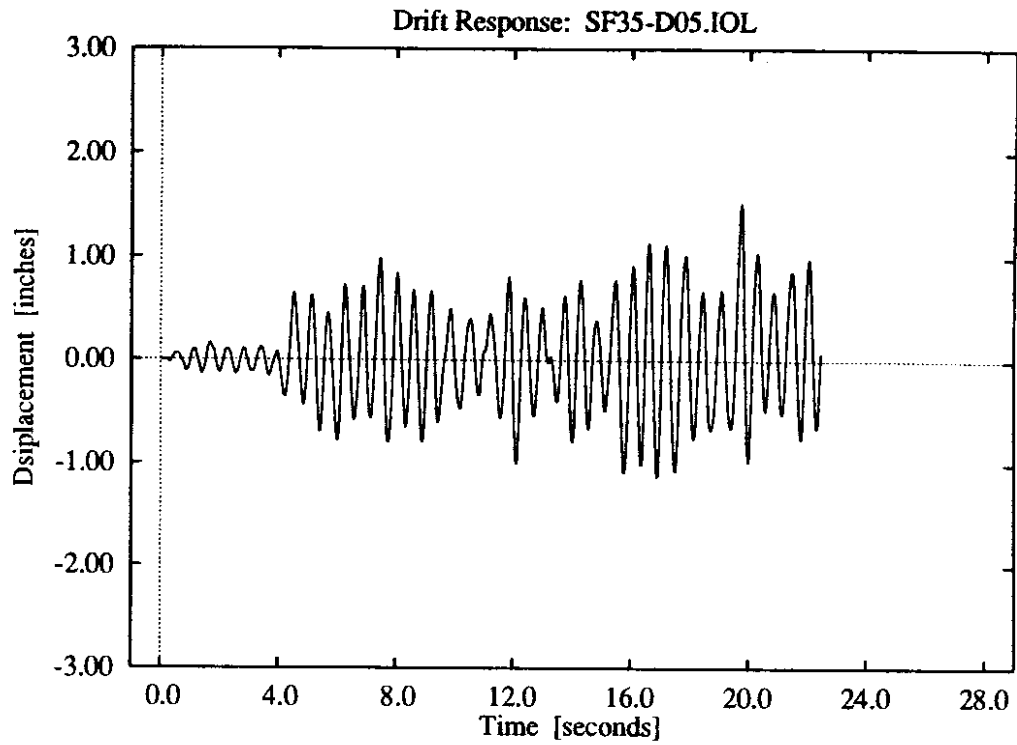


**Figure D-69:** 5 parameter foundation model, intermediate soil stiffness, lower intensity Olympia record.

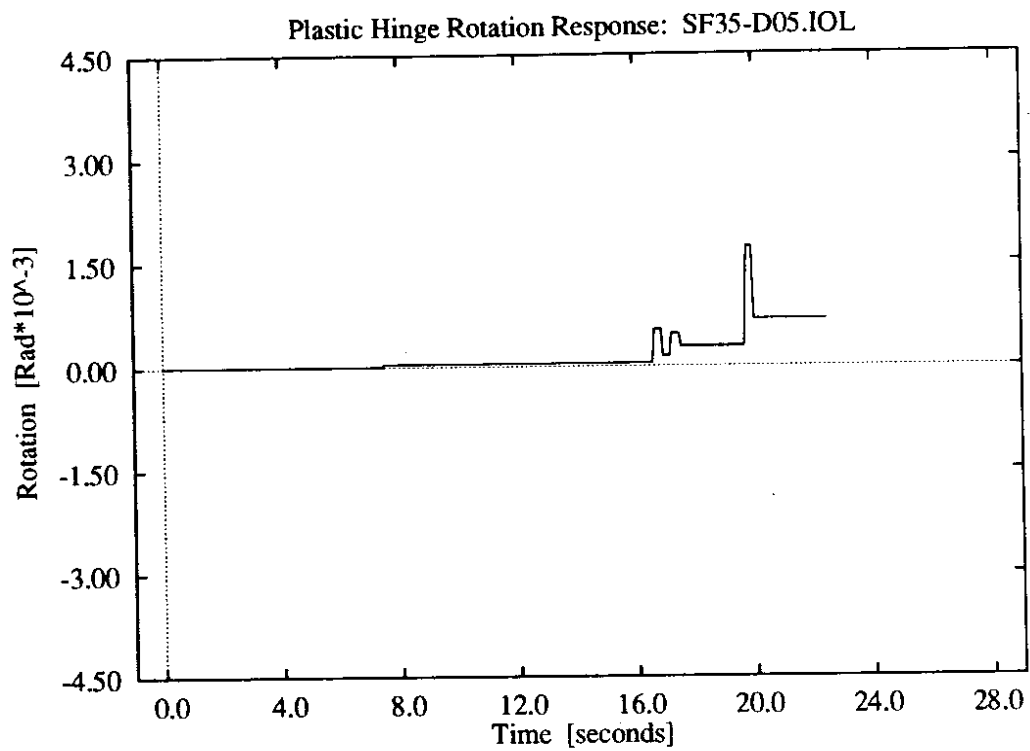
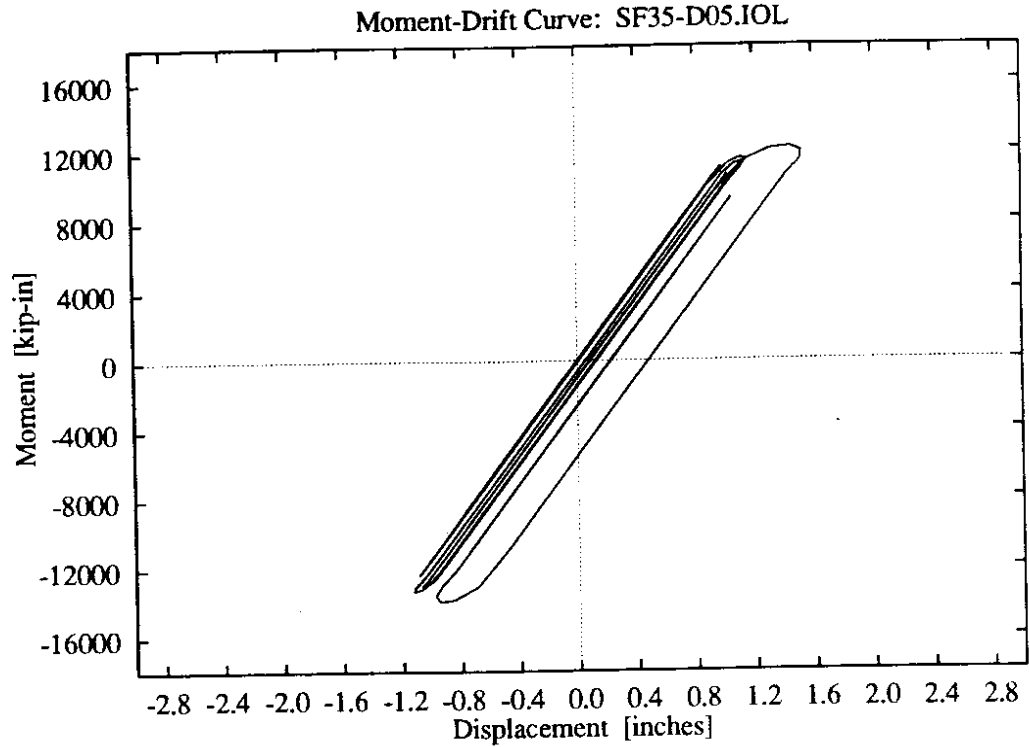


**Figure D-70:** 5 parameter foundation model, intermediate soil stiffness, lower intensity Olympia record.



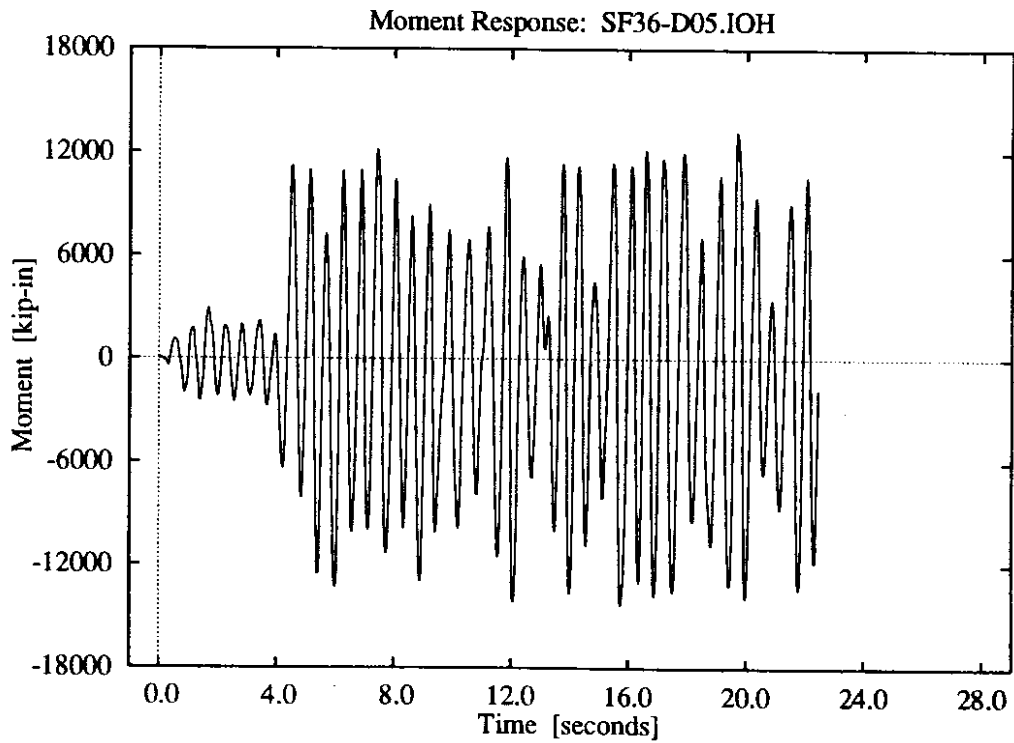
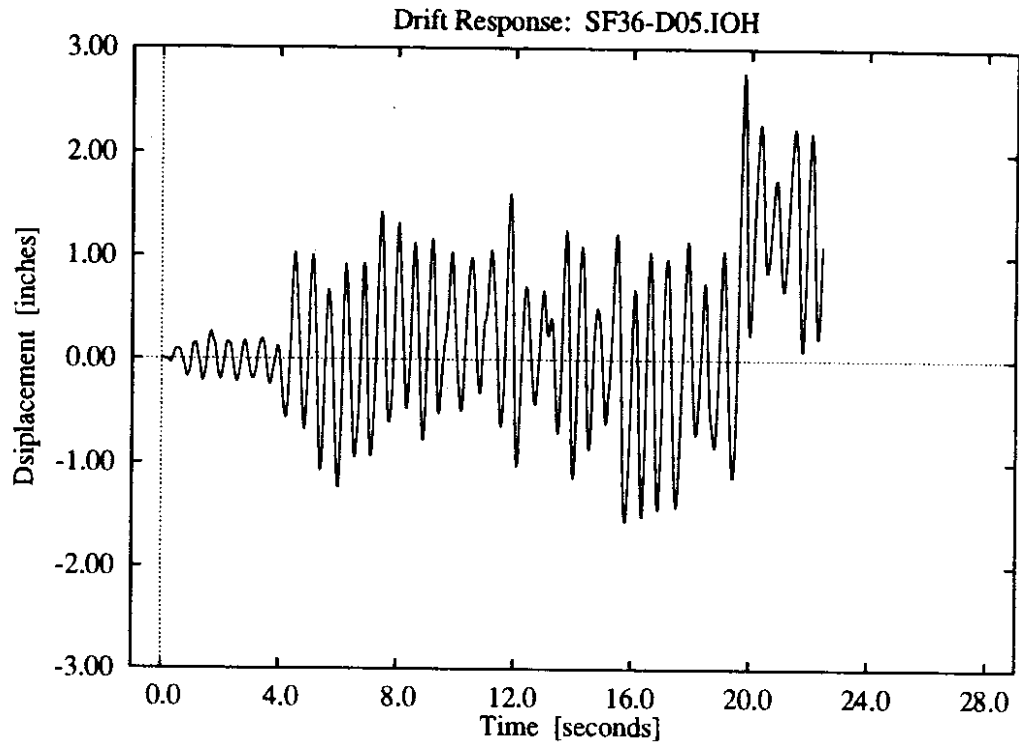


**Figure D-71:** 5 parameter foundation model, intermediate soil stiffness, higher intensity Olympia record.

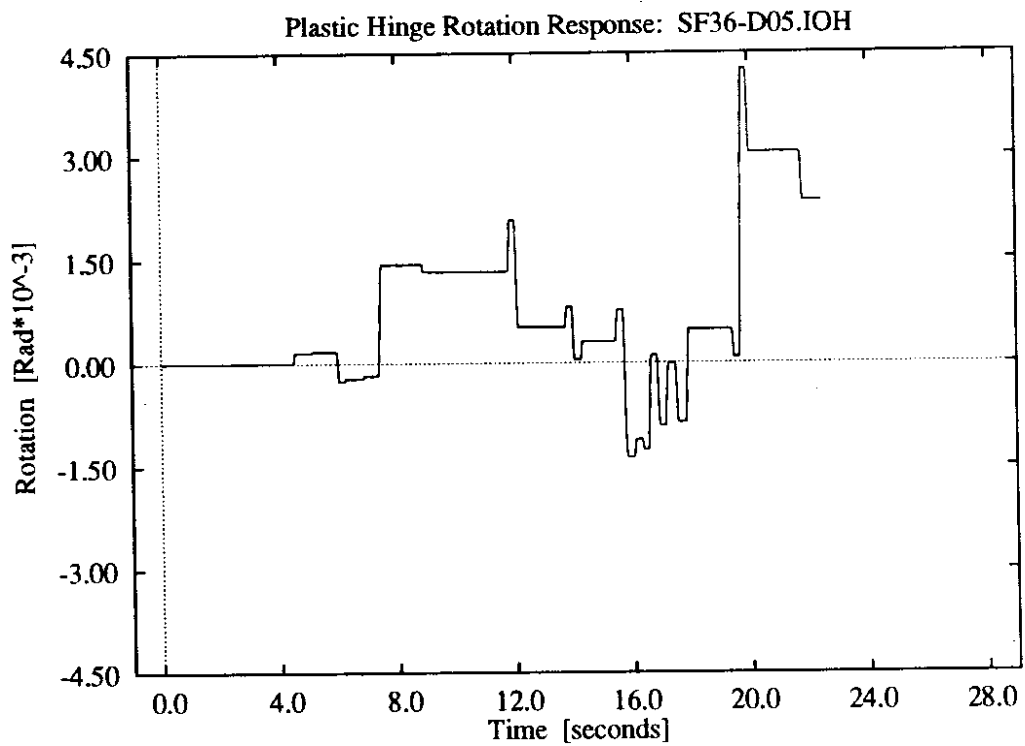
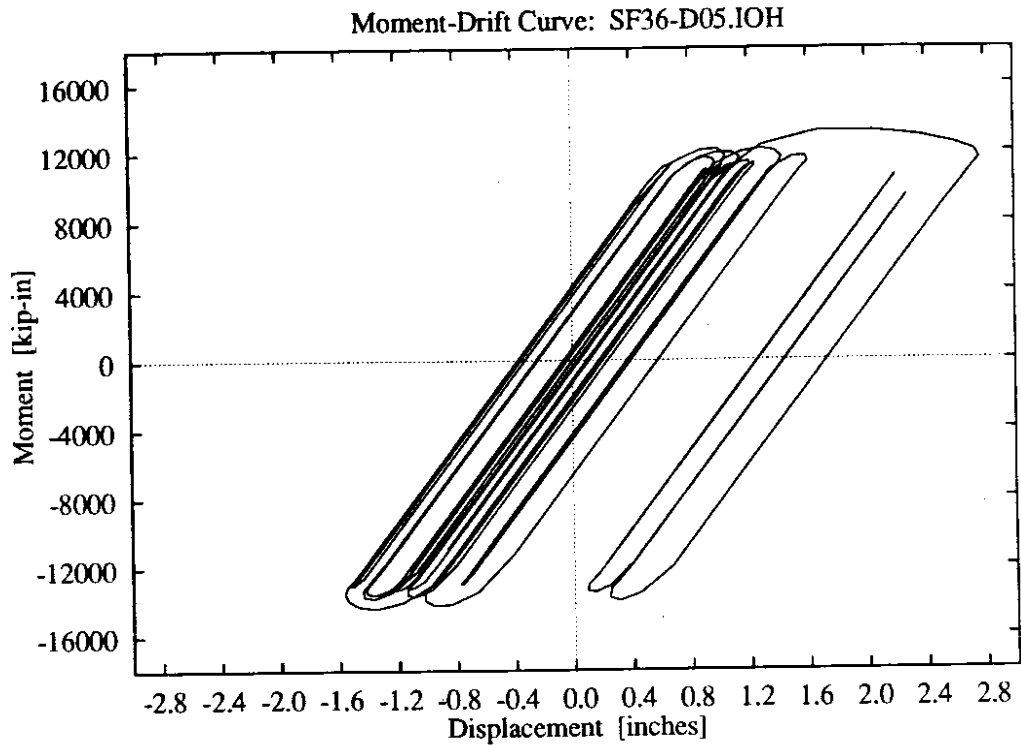


**Figure D-72:** 5 parameter foundation model, intermediate soil stiffness, higher intensity Olympia record.

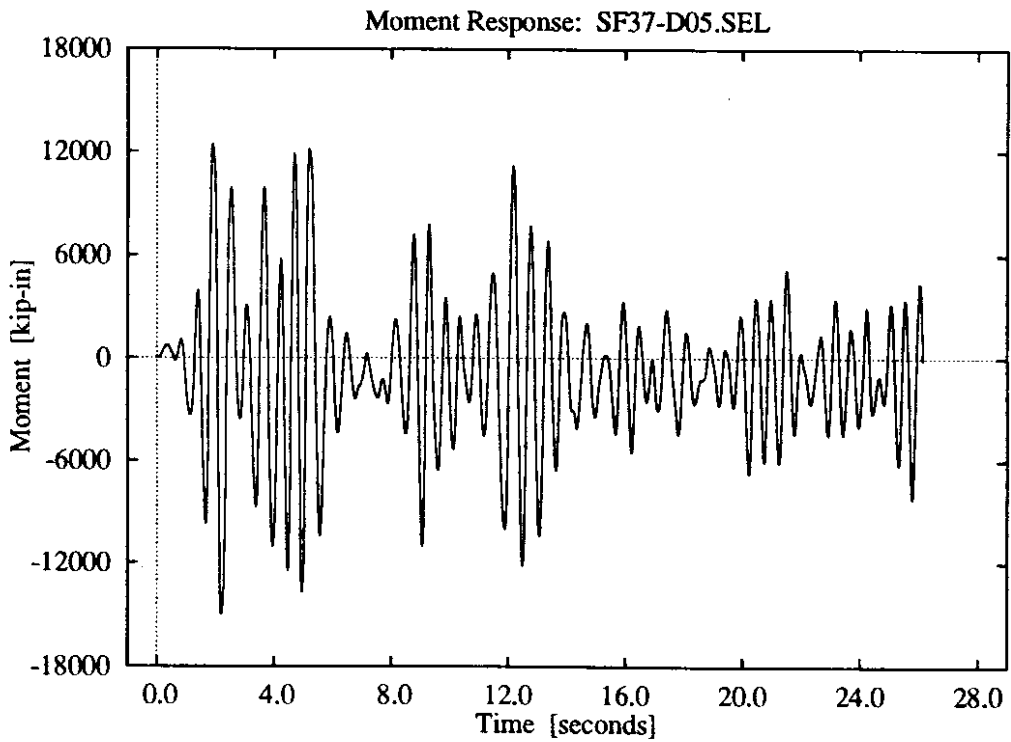
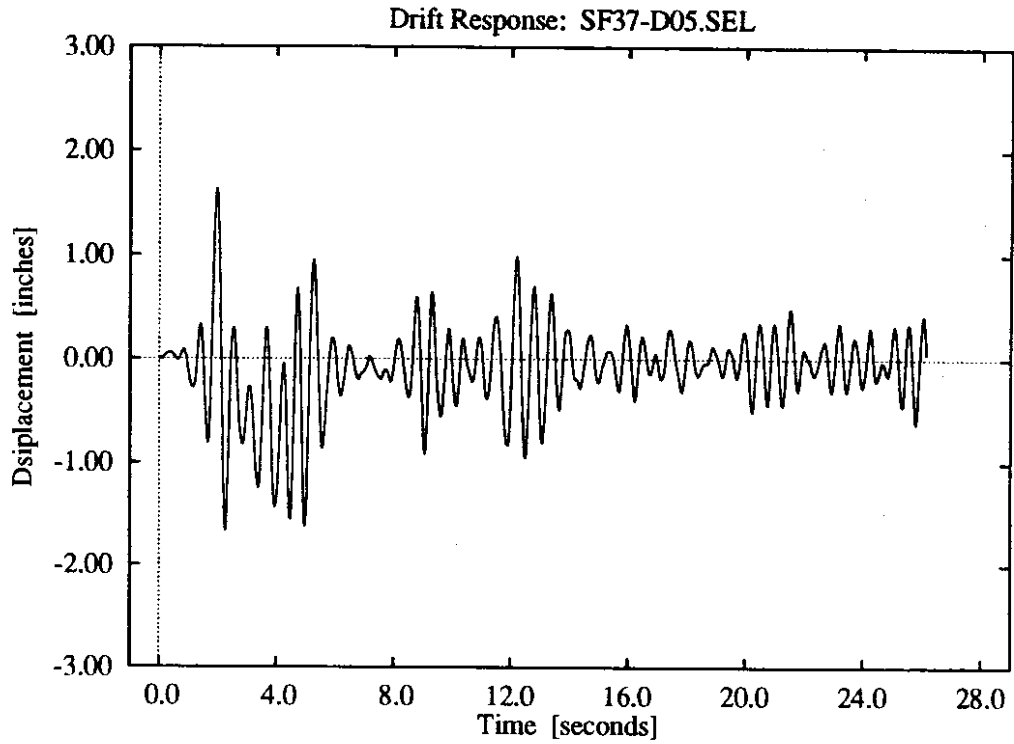


**Figure D-73:** 5 parameter foundation model, high soil stiffness, lower intensity El Centro record.

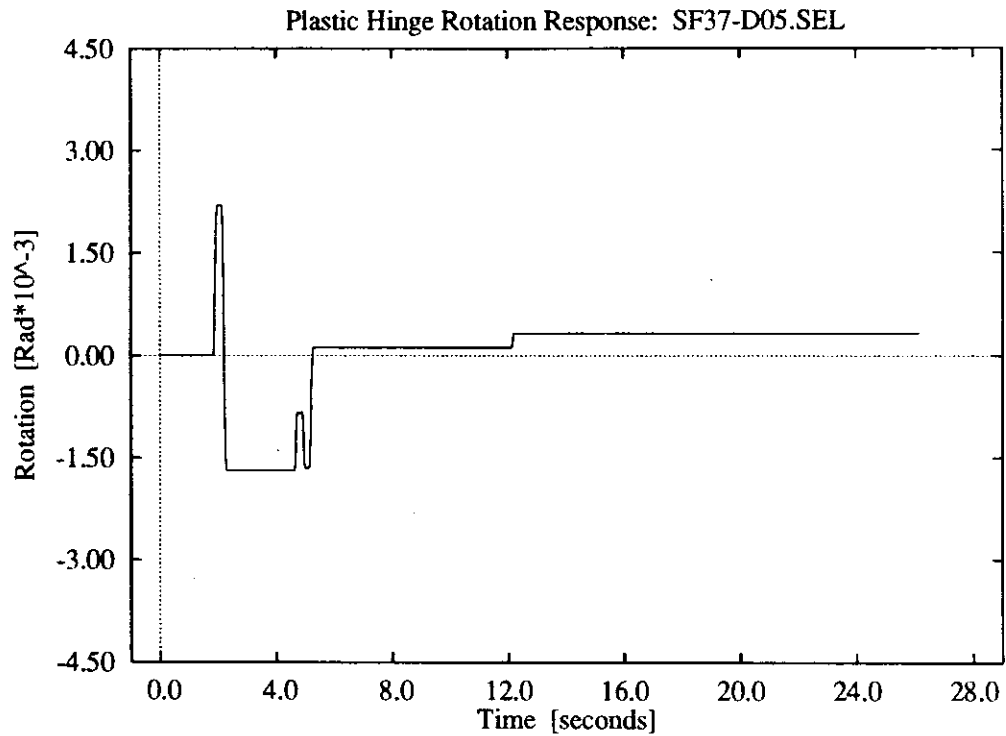
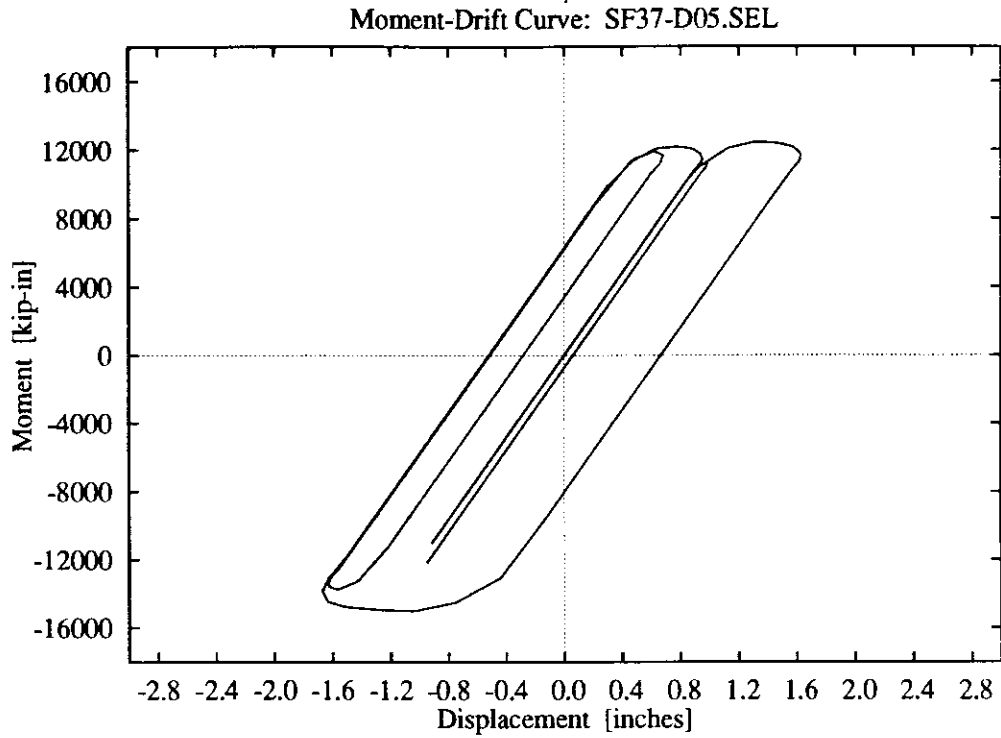


**Figure D-74:** 5 parameter foundation model, high soil stiffness, lower intensity El Centro record.

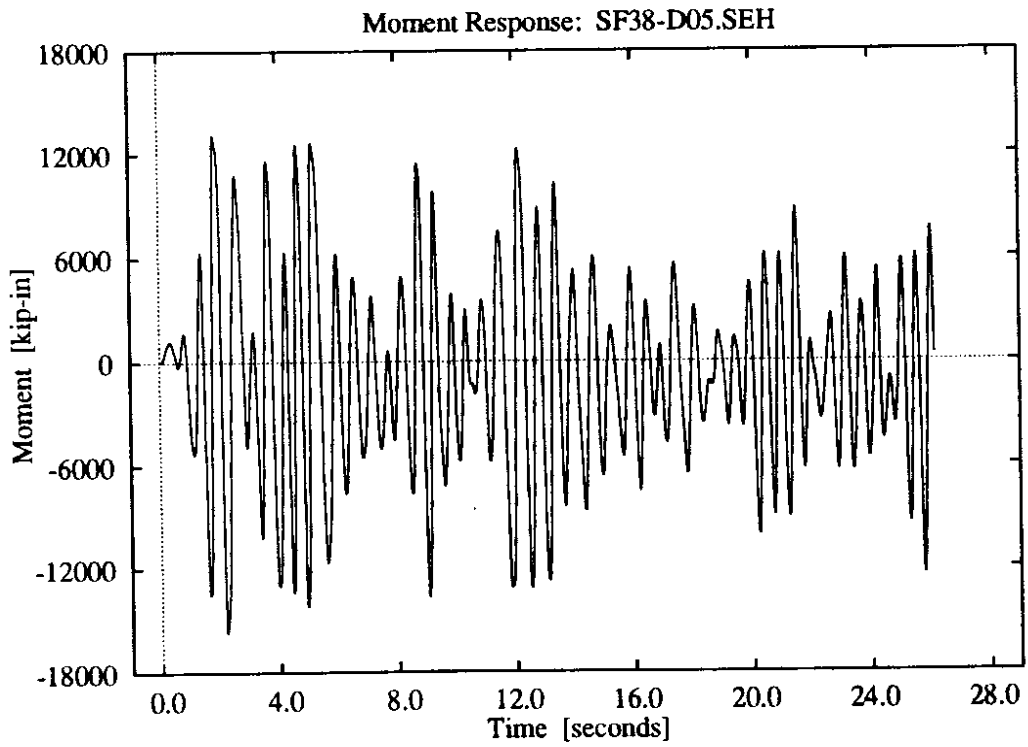
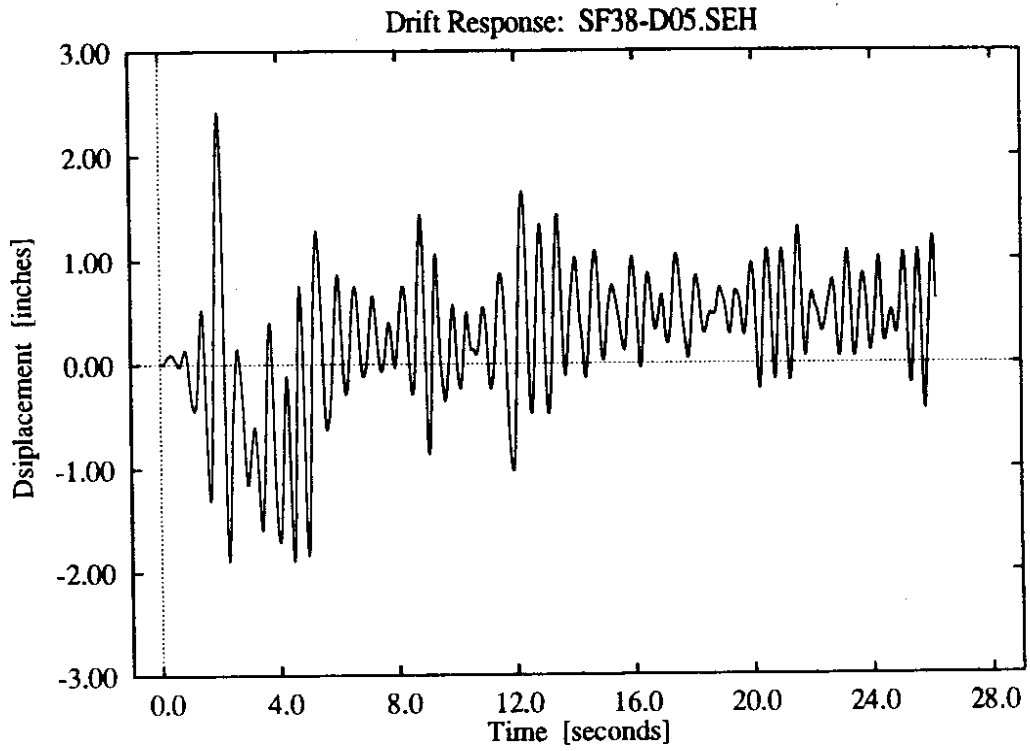


**Figure D-75: 5 parameter foundation model, high soil stiffness, higher intensity El Centro record.**

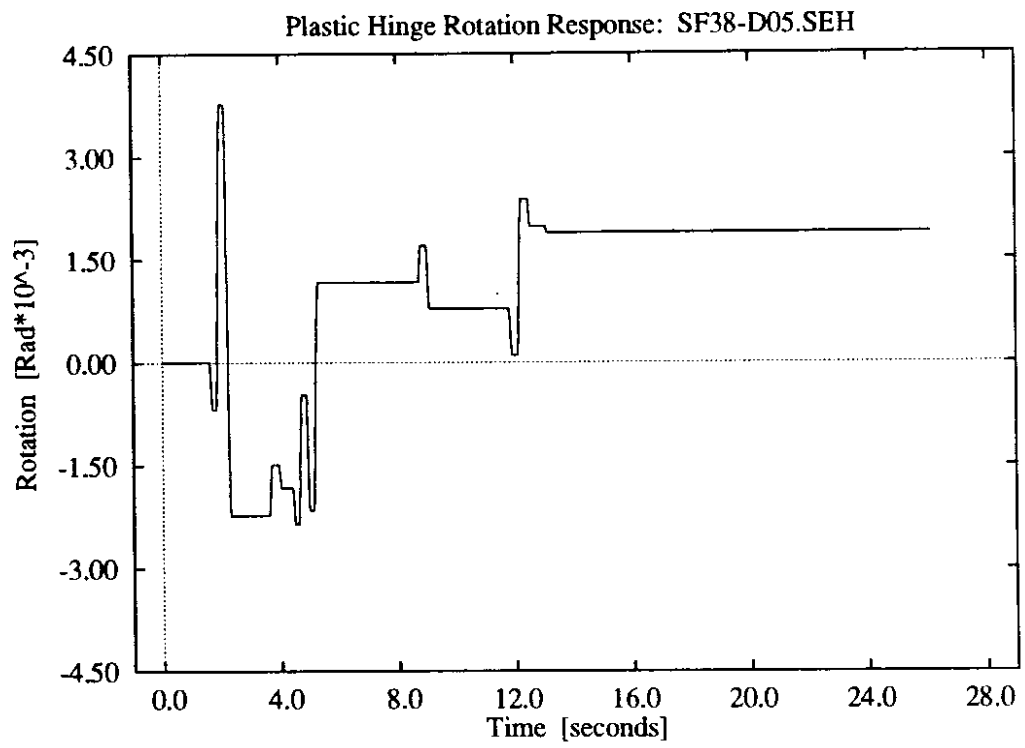
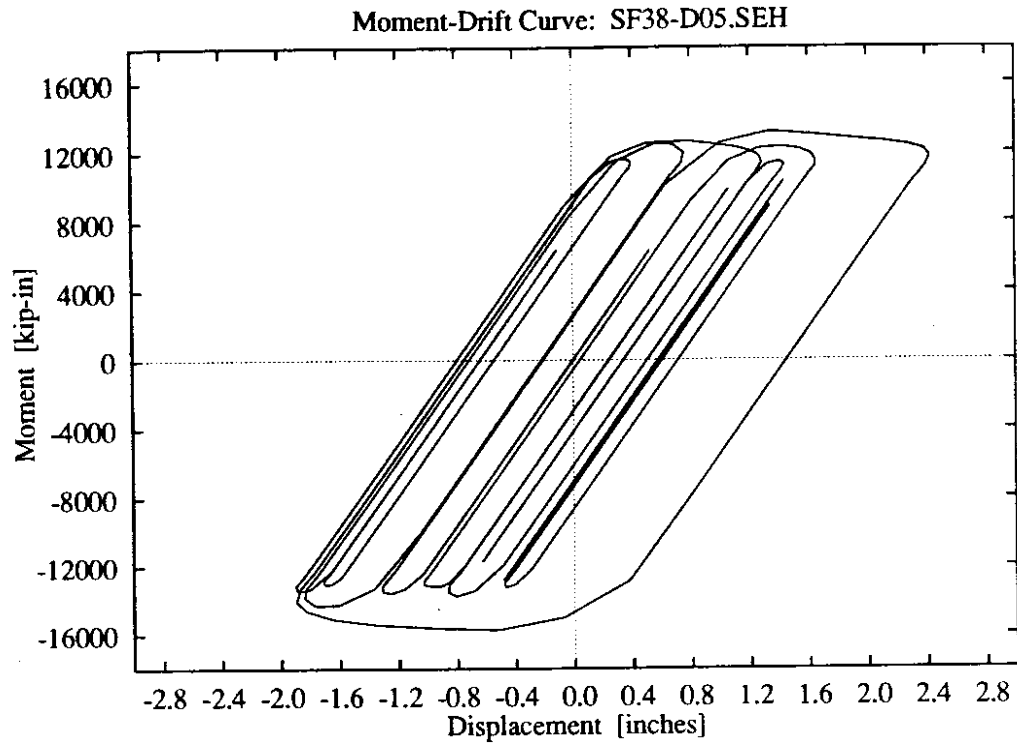


**Figure D-76:** 5 parameter foundation model, high soil stiffness, higher intensity El Centro record.

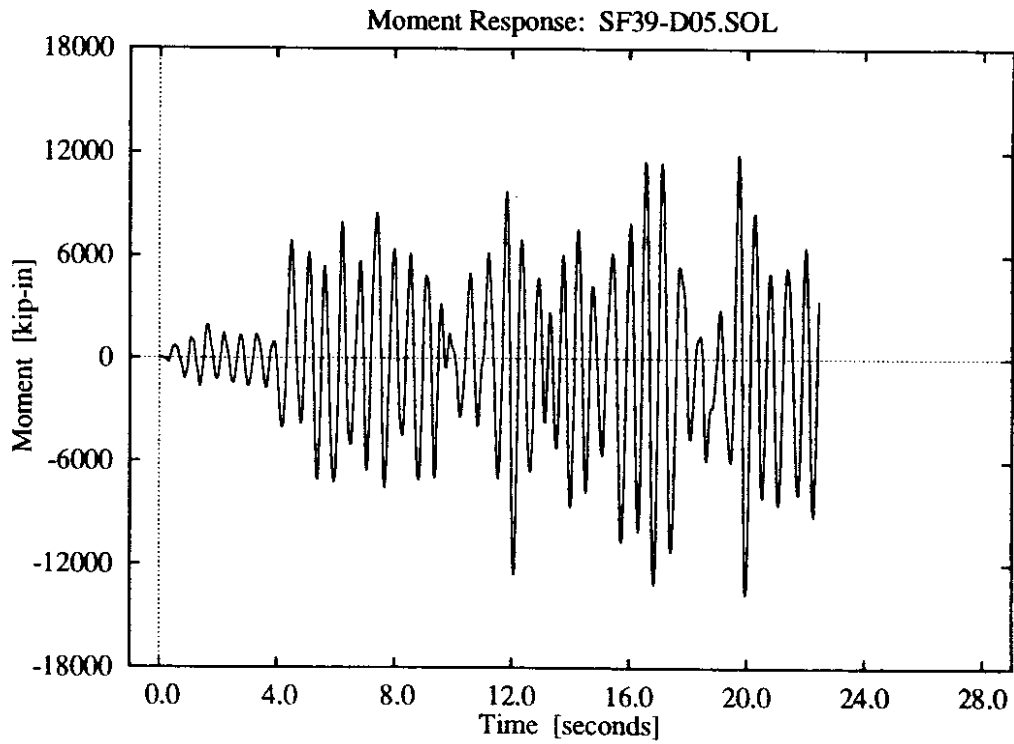
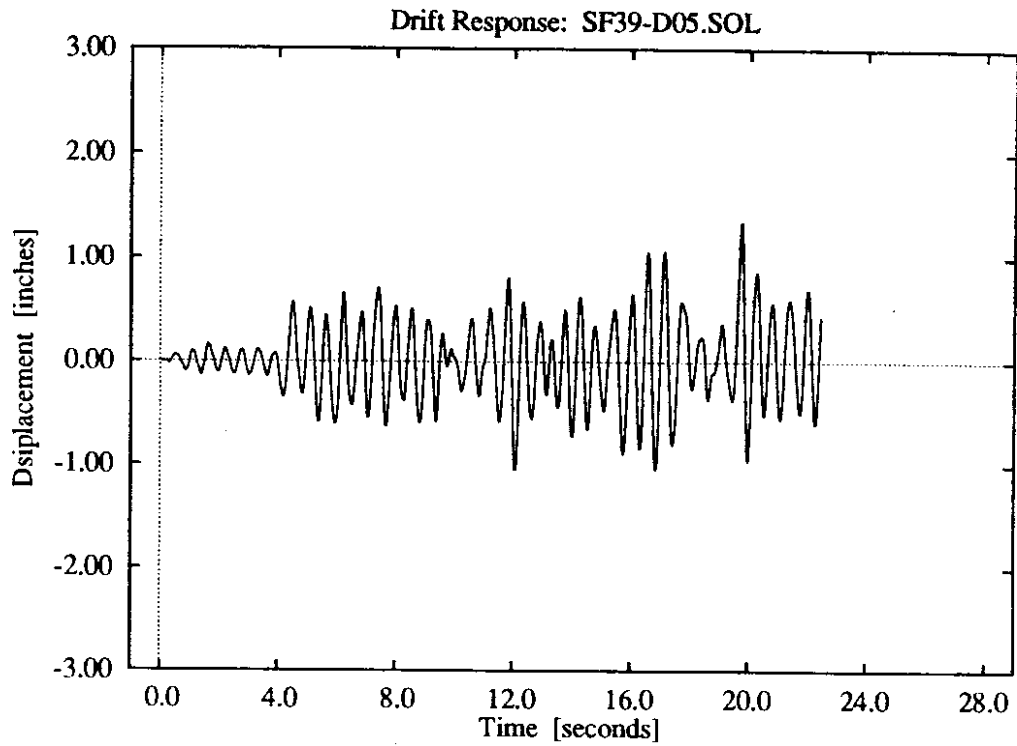


**Figure D-77:** 5 parameter foundation model, high soil stiffness, lower intensity Olympia record.

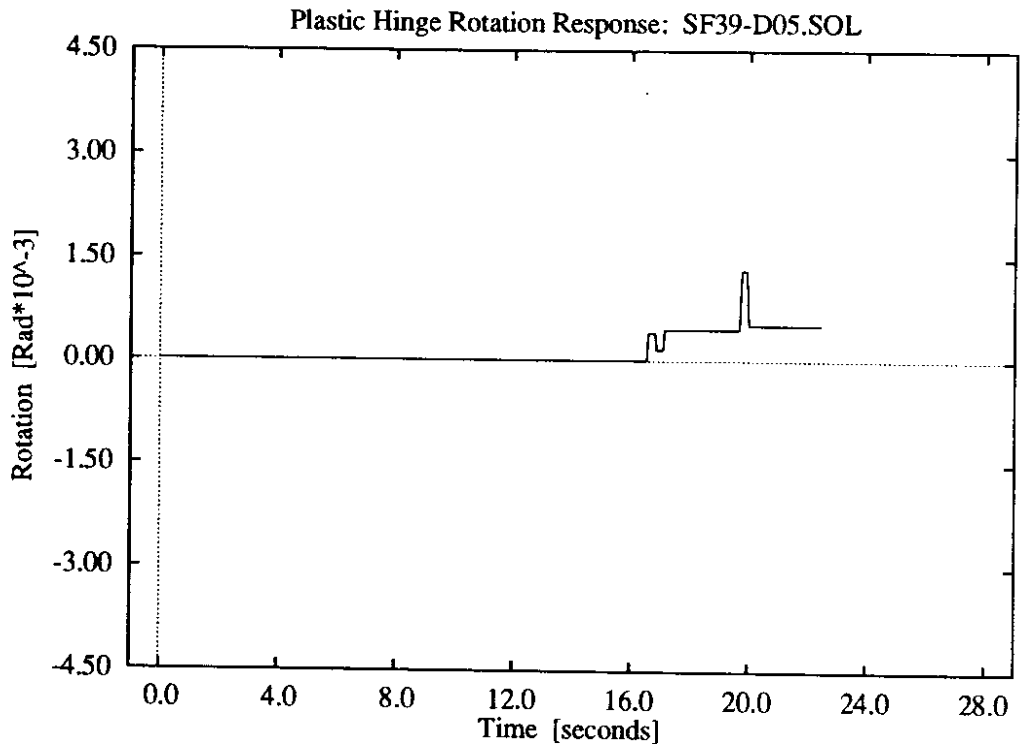
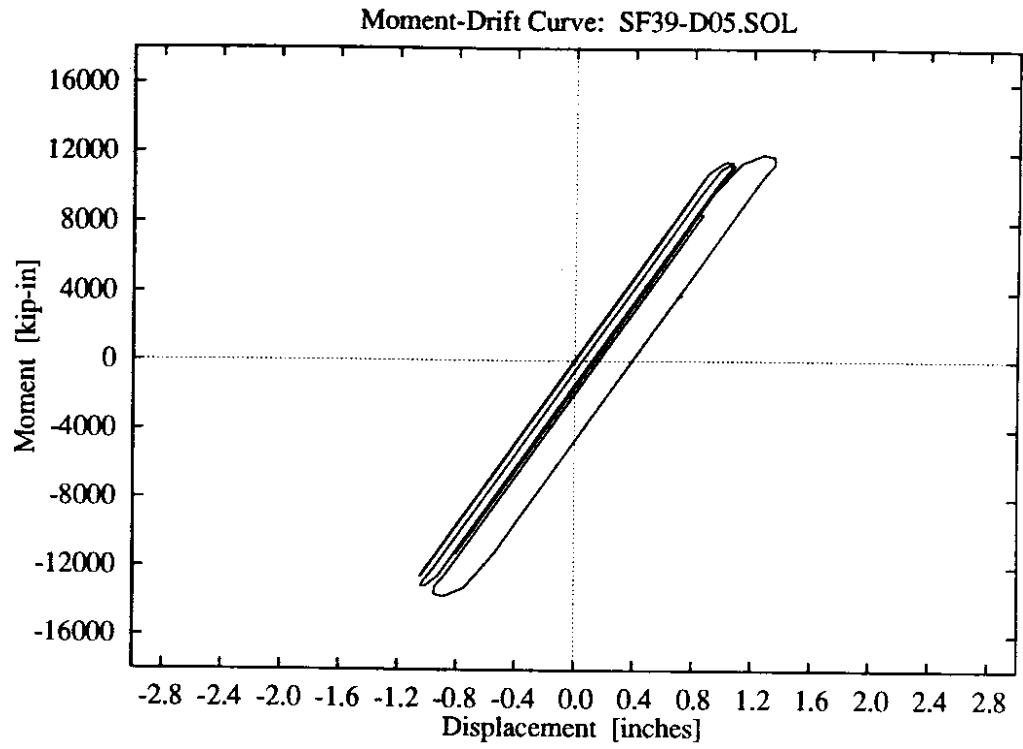


**Figure D-78:** 5 parameter foundation model, high soil stiffness, lower intensity Olympia record.



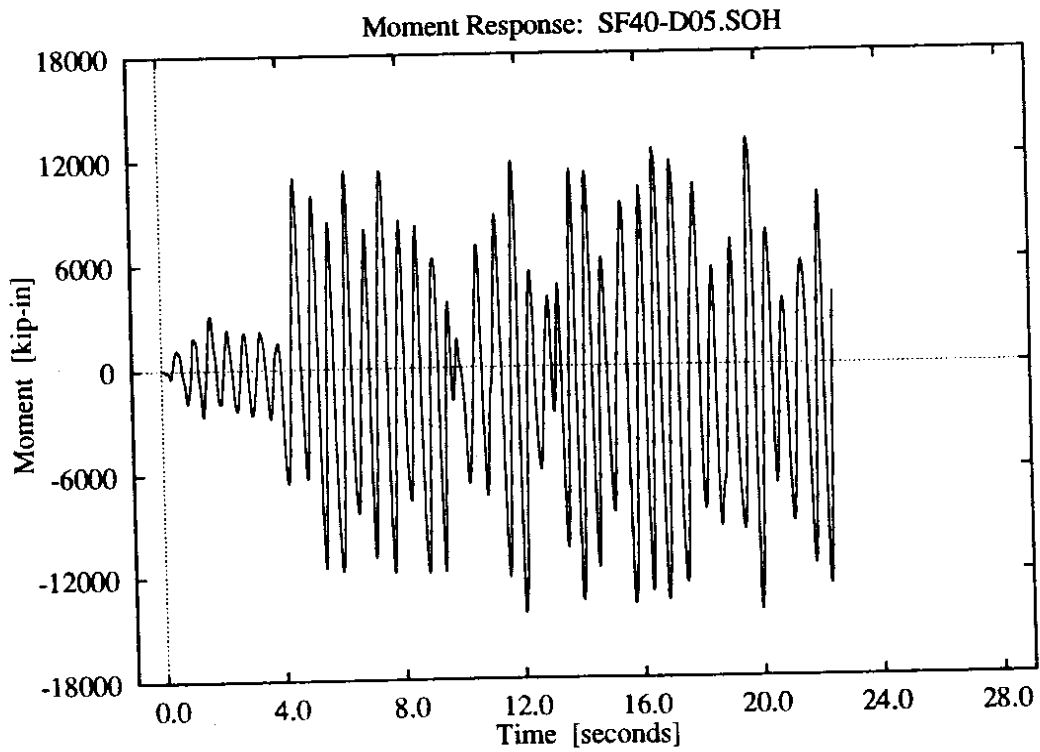
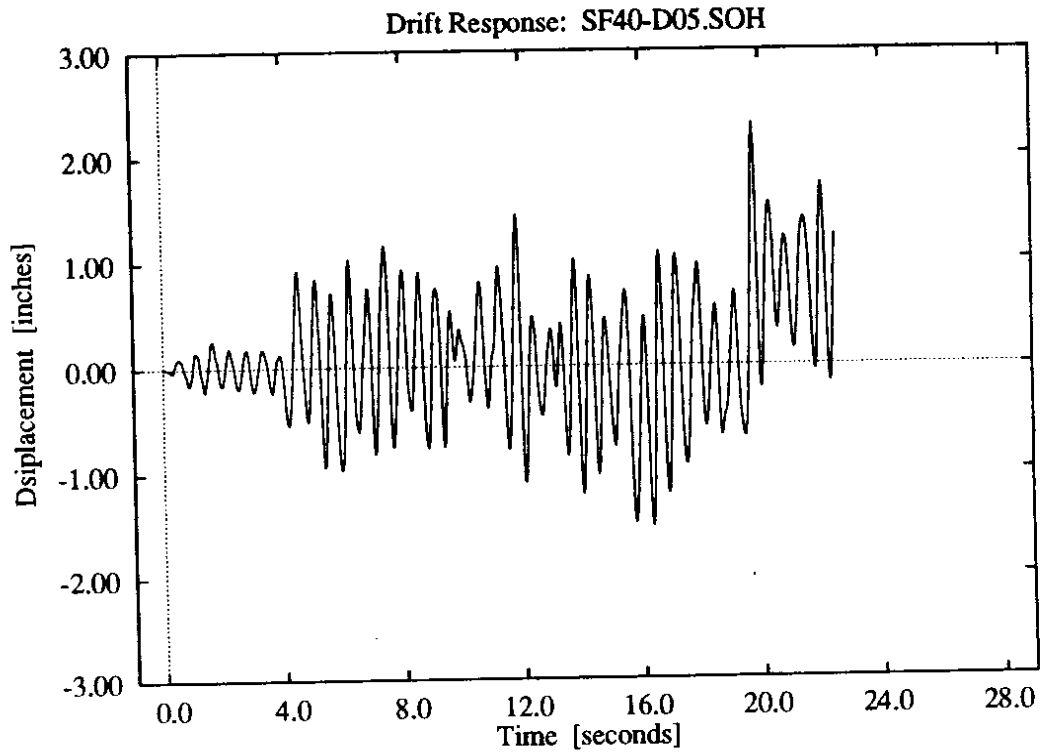


**Figure D-79: 5 parameter foundation model, high soil stiffness, higher intensity Olympia record.**

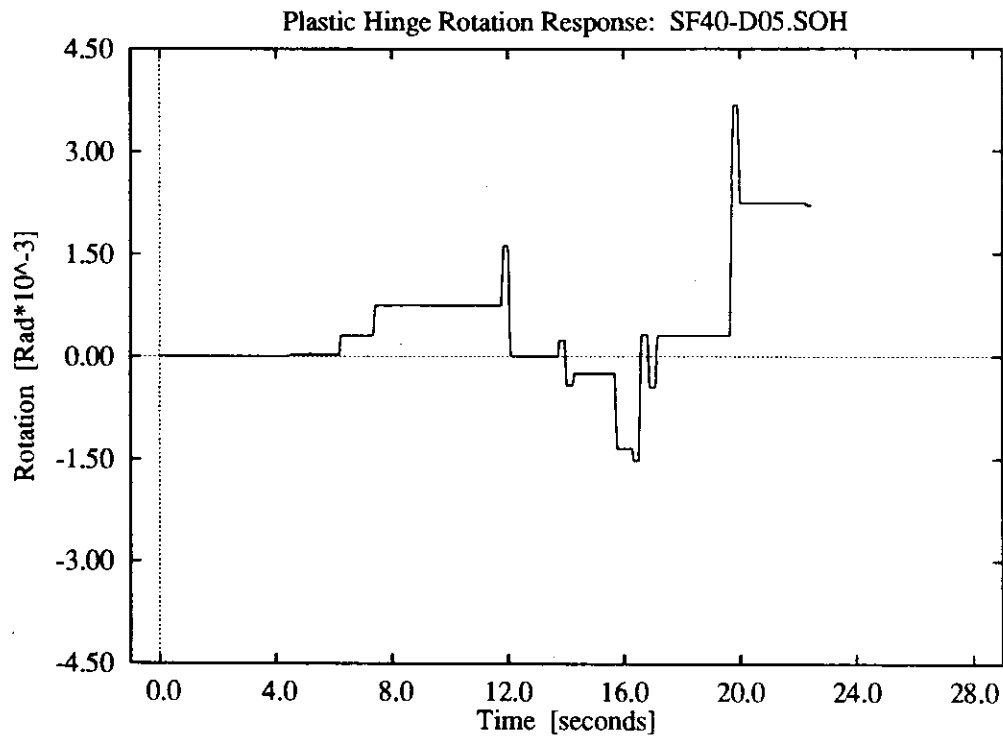
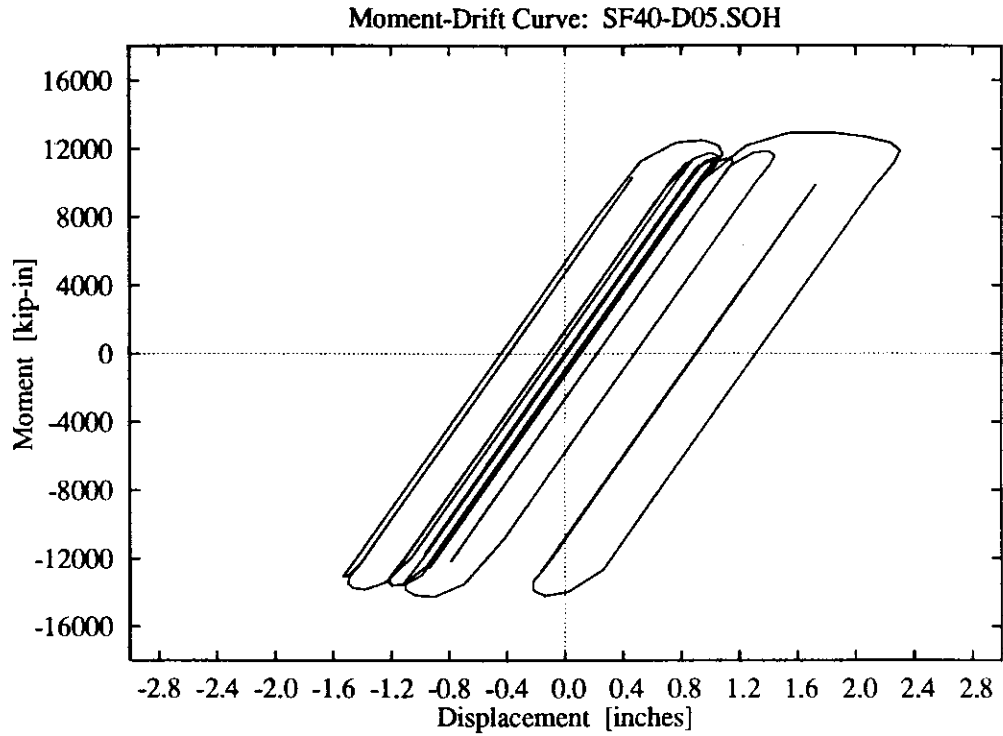


**Figure D-80:** 5 parameter foundation model, high soil stiffness, higher intensity Olympia record.

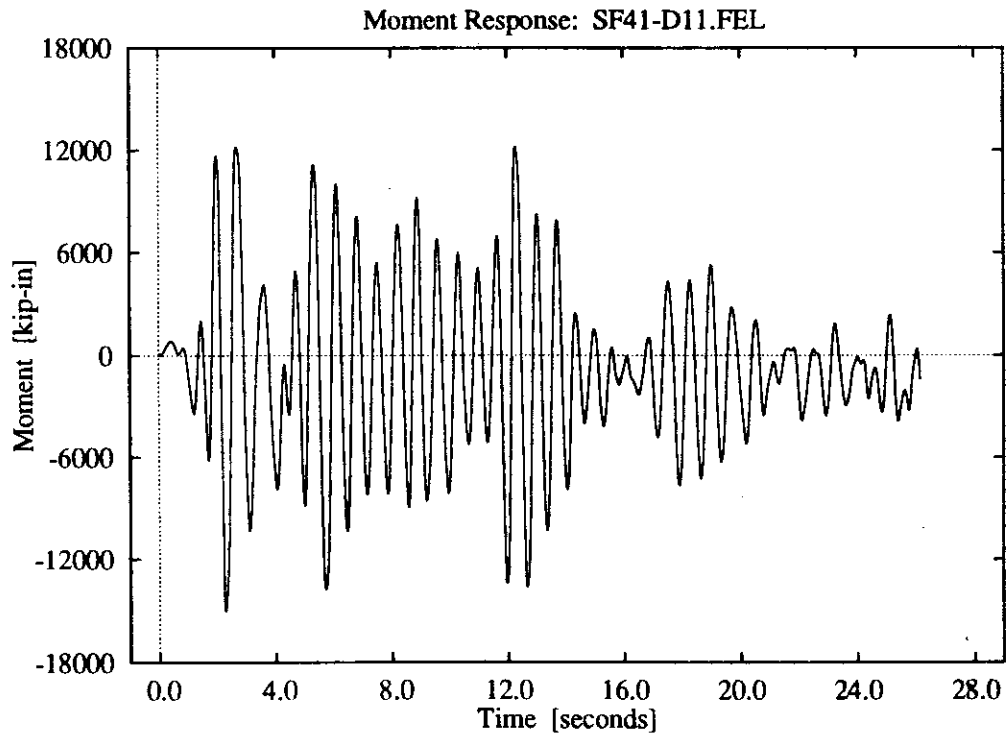
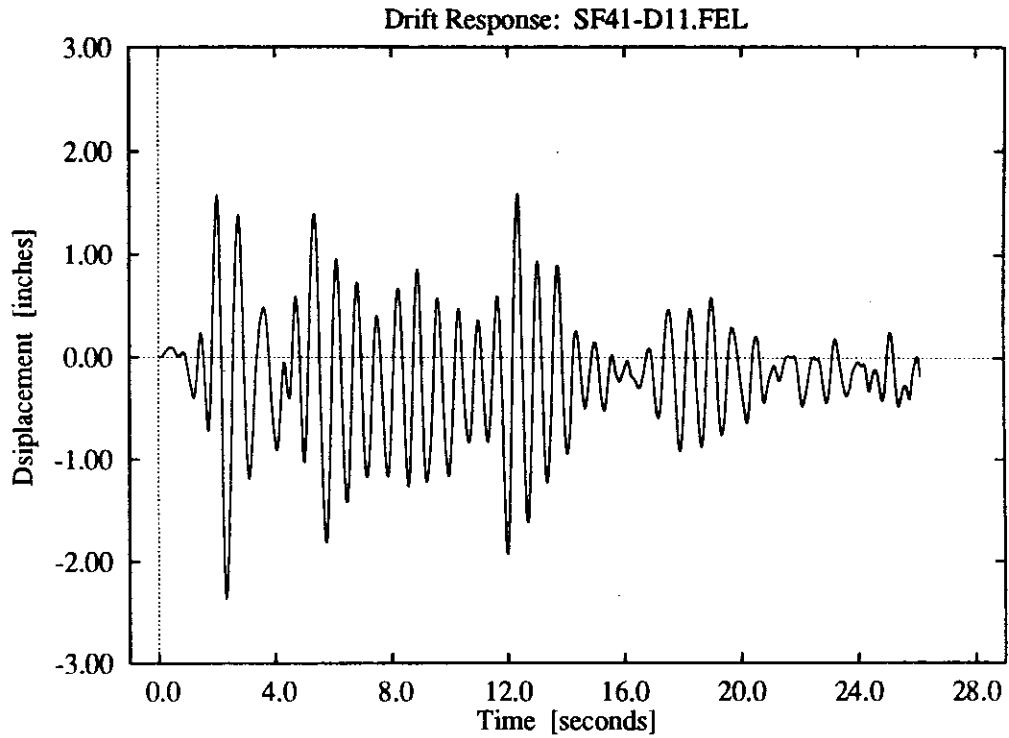


**Figure D-81:** 11 parameter foundation model, low soil stiffness, lower intensity El Centro record.

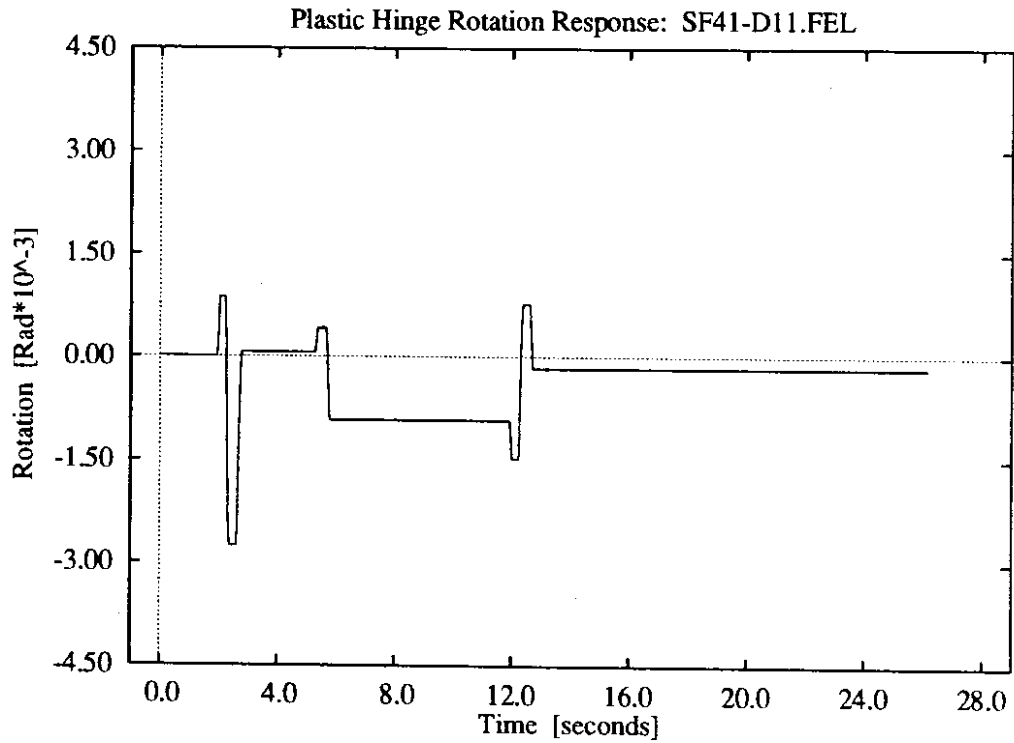
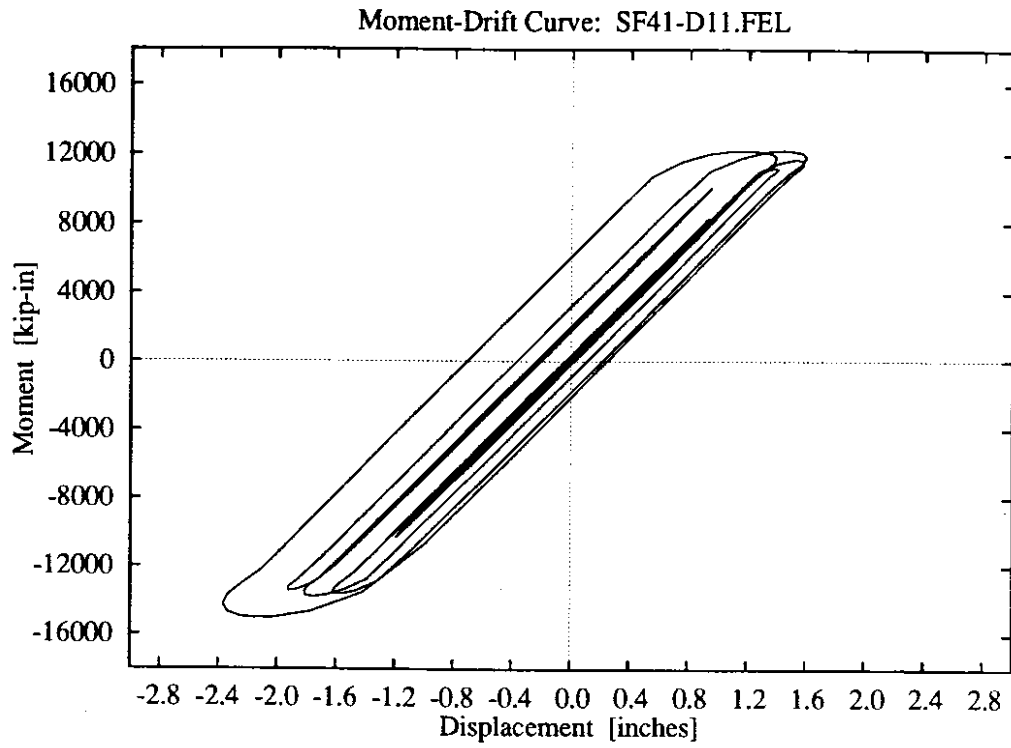


**Figure D-82:** 11 parameter foundation model, low soil stiffness, lower intensity El Centro record.

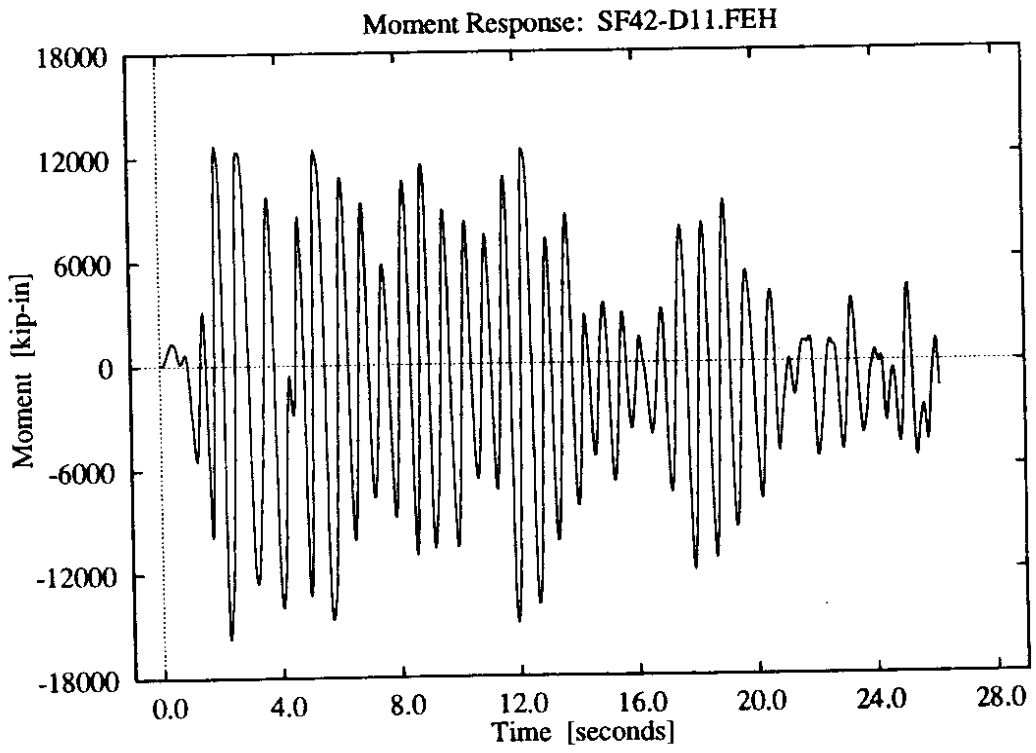
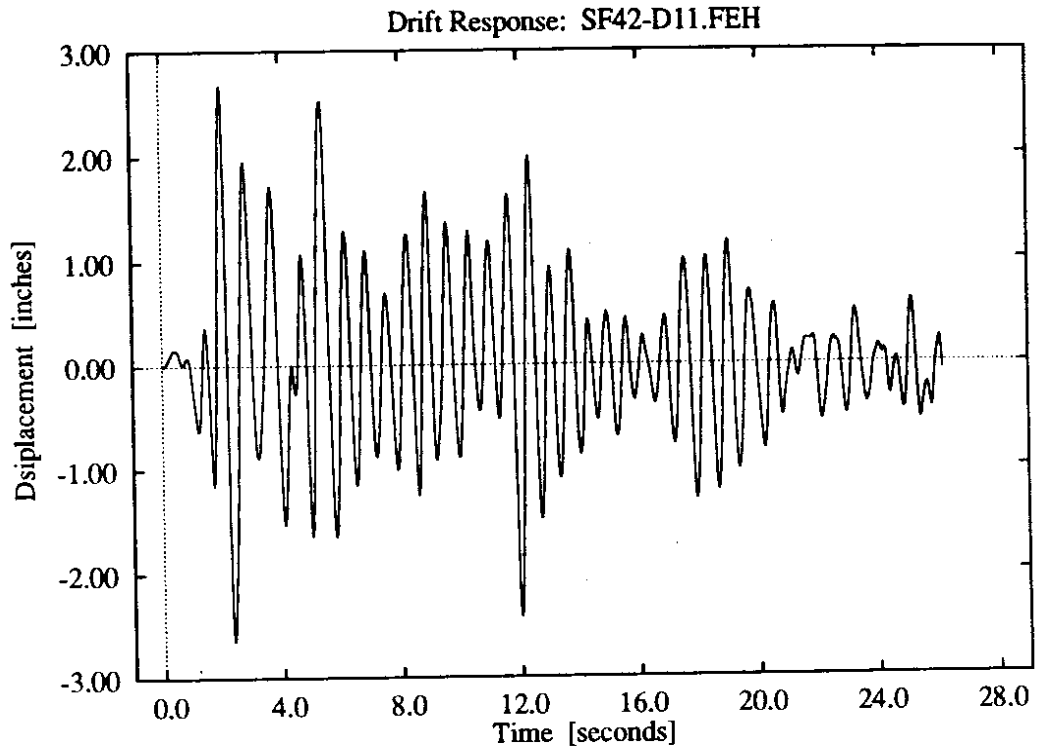


**Figure D-83:** 11 parameter foundation model, low soil stiffness, higher intensity El Centro record.

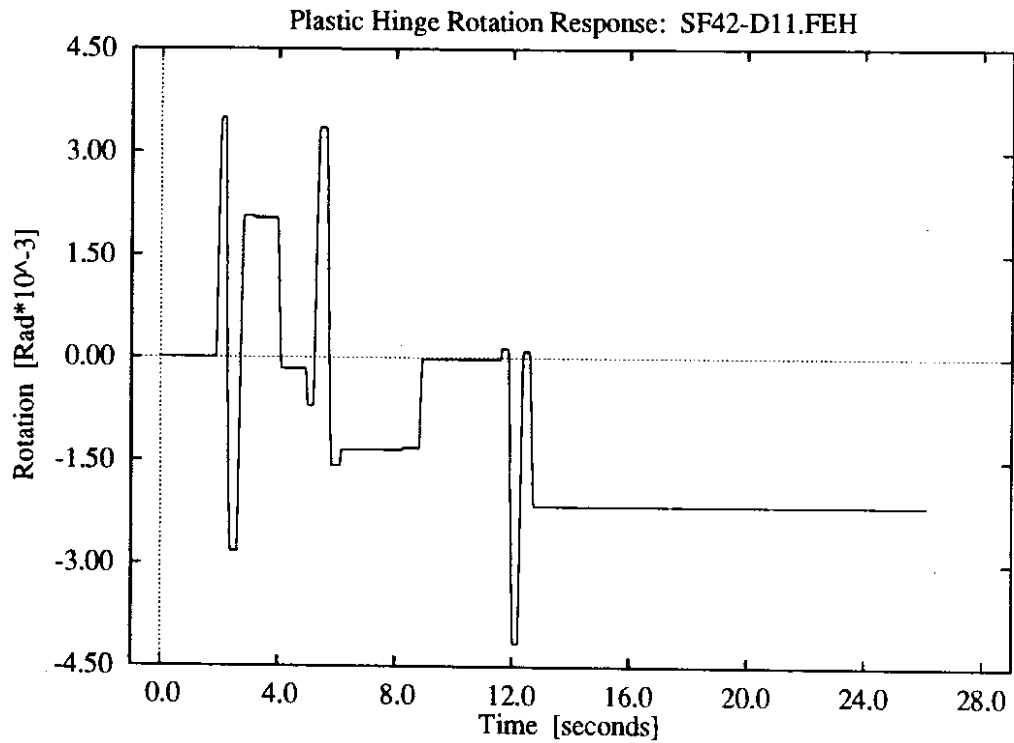
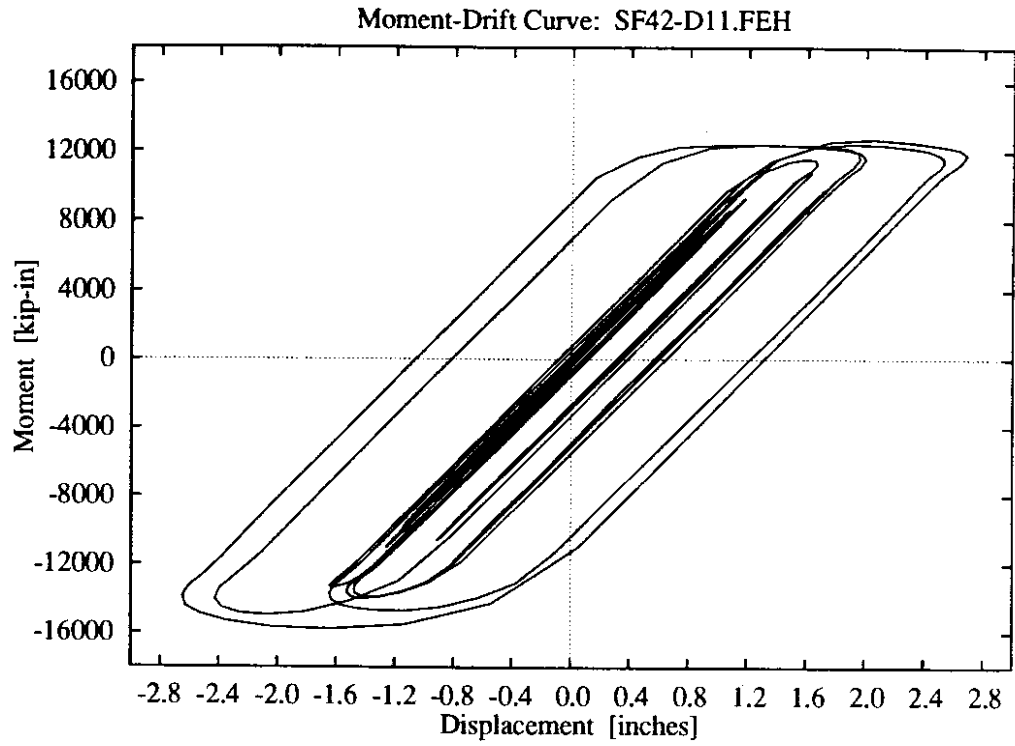


**Figure D-84:** 11 parameter foundation model, low soil stiffness, higher intensity El Centro record.

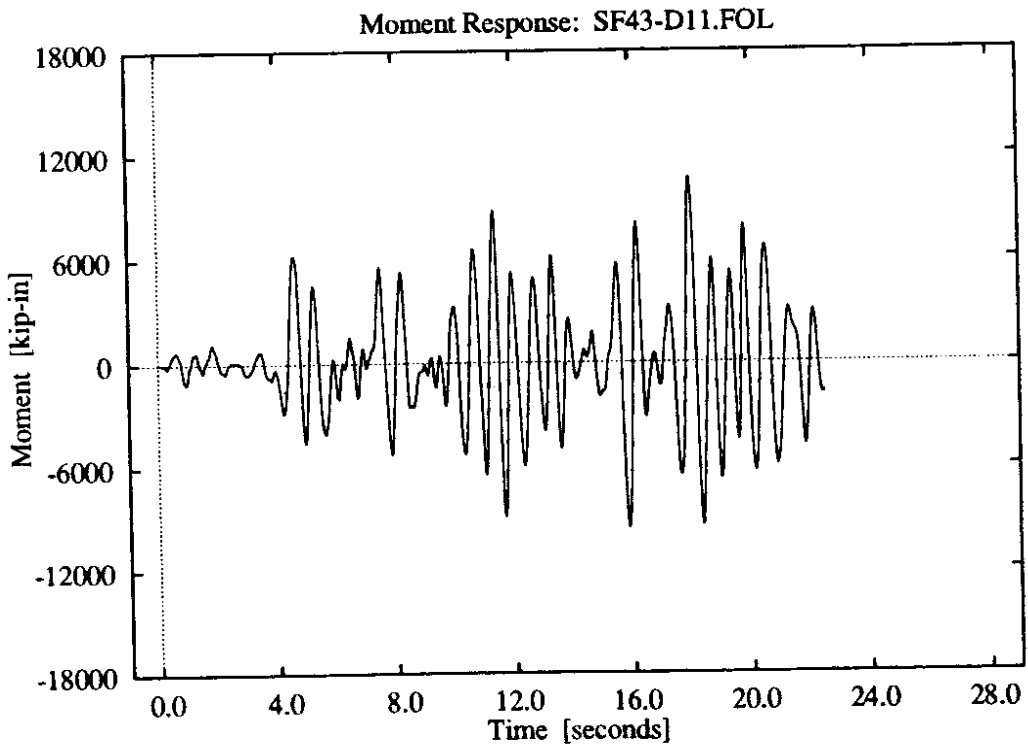
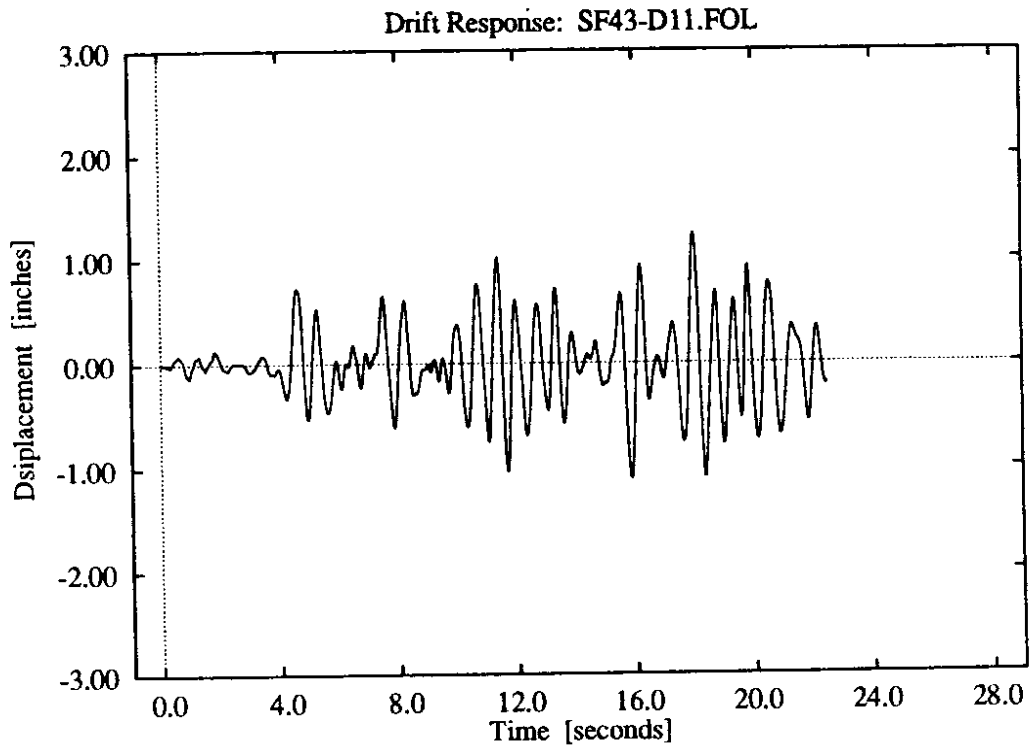


**Figure D-85:** 11 parameter foundation model, low soil stiffness, lower intensity Olympia record.

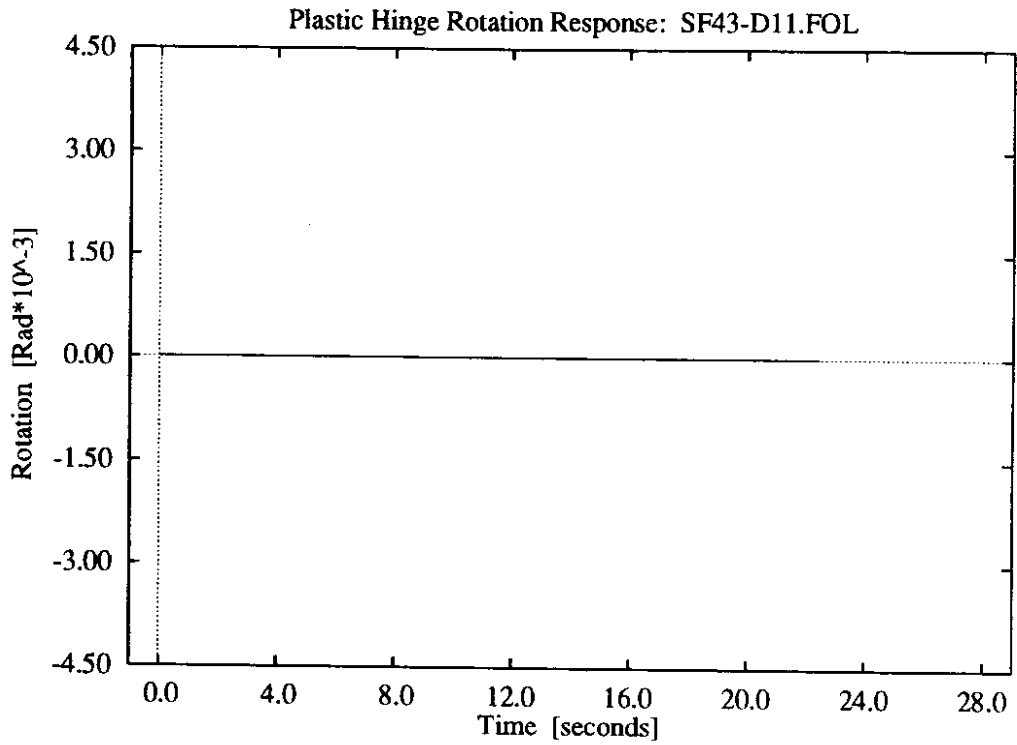
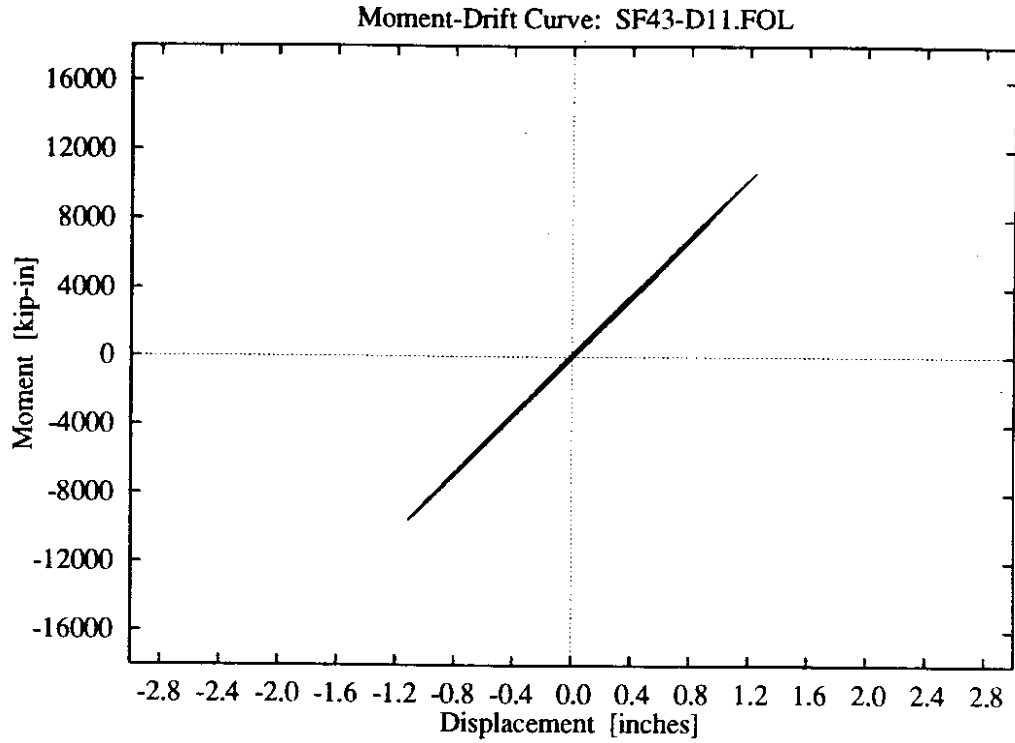


**Figure D-86:** 11 parameter foundation model, low soil stiffness, lower intensity Olympia record.



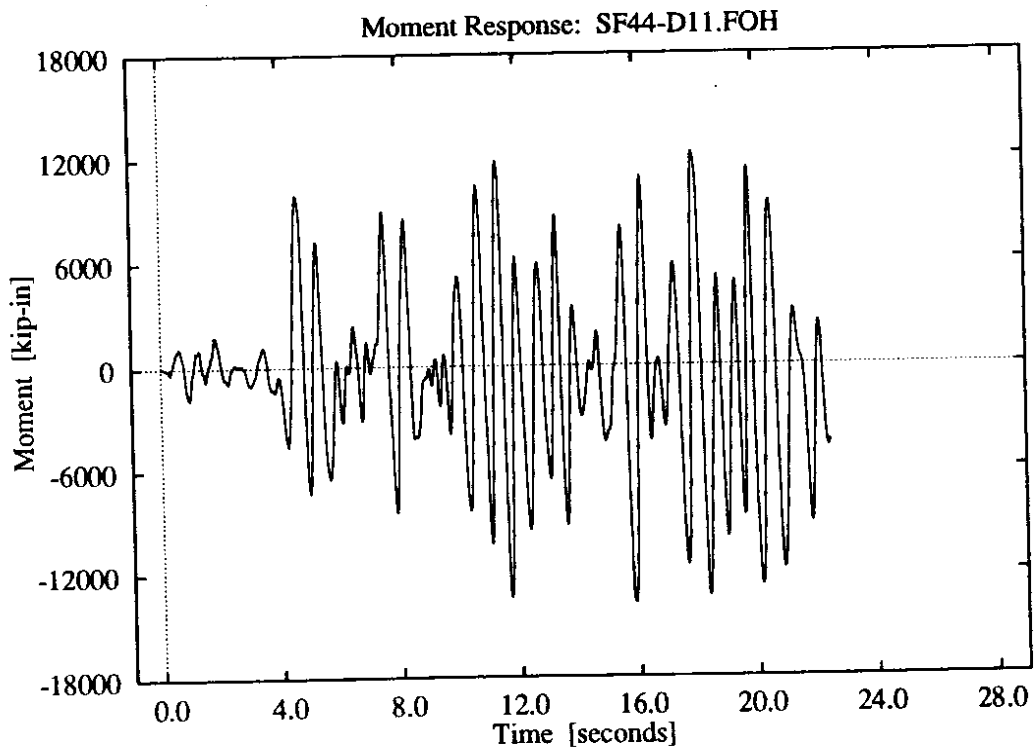
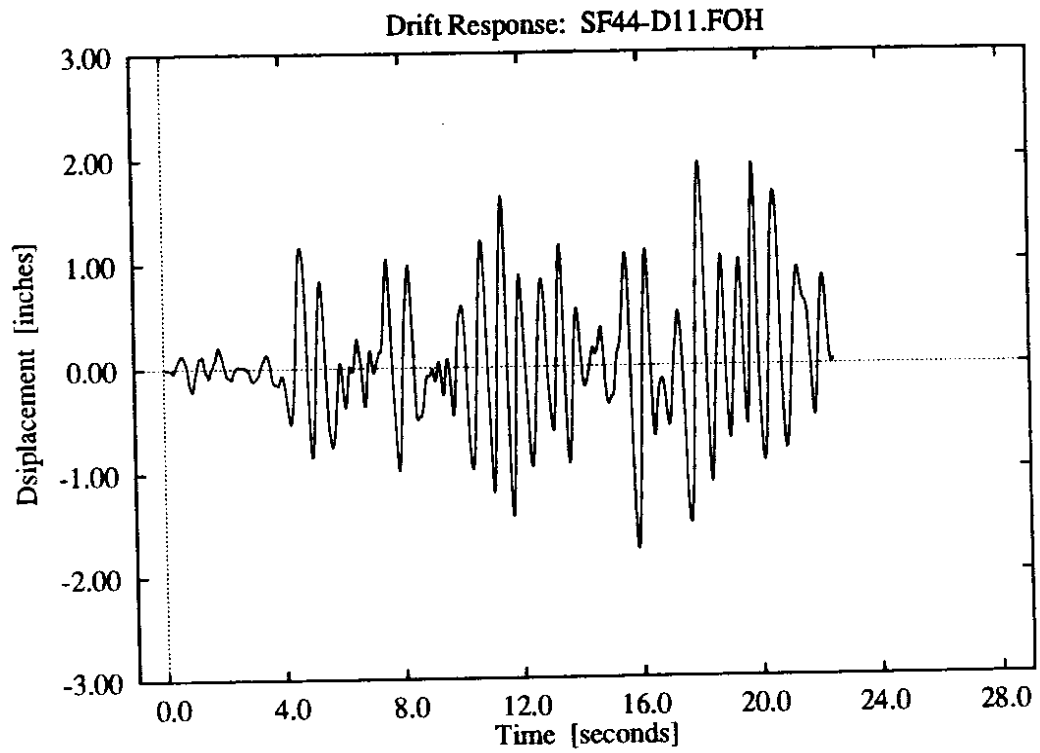


**Figure D-87:** 11 parameter foundation model, low soil stiffness, higher intensity Olympia record.

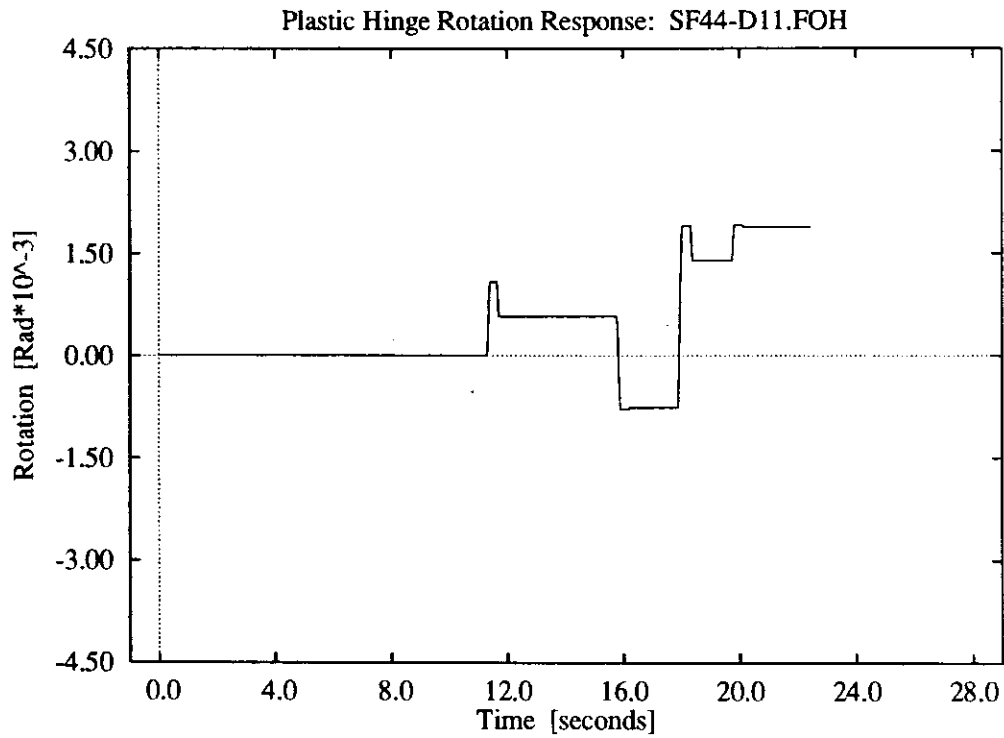
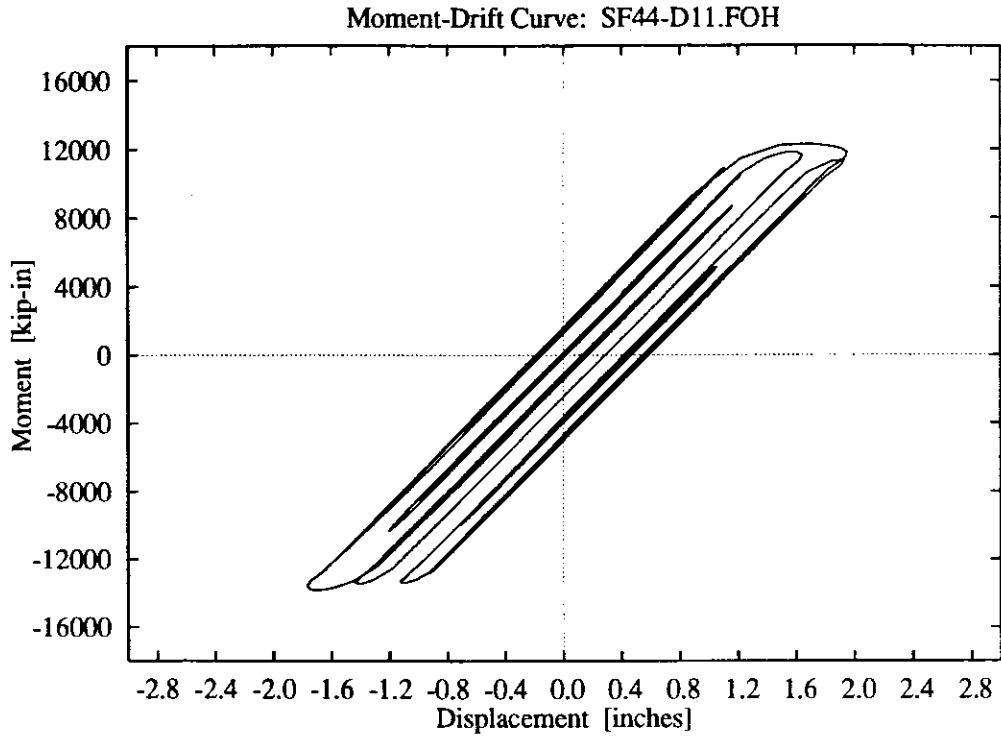


**Figure D-88:** 11 parameter foundation model, low soil stiffness, higher intensity Olympia record.

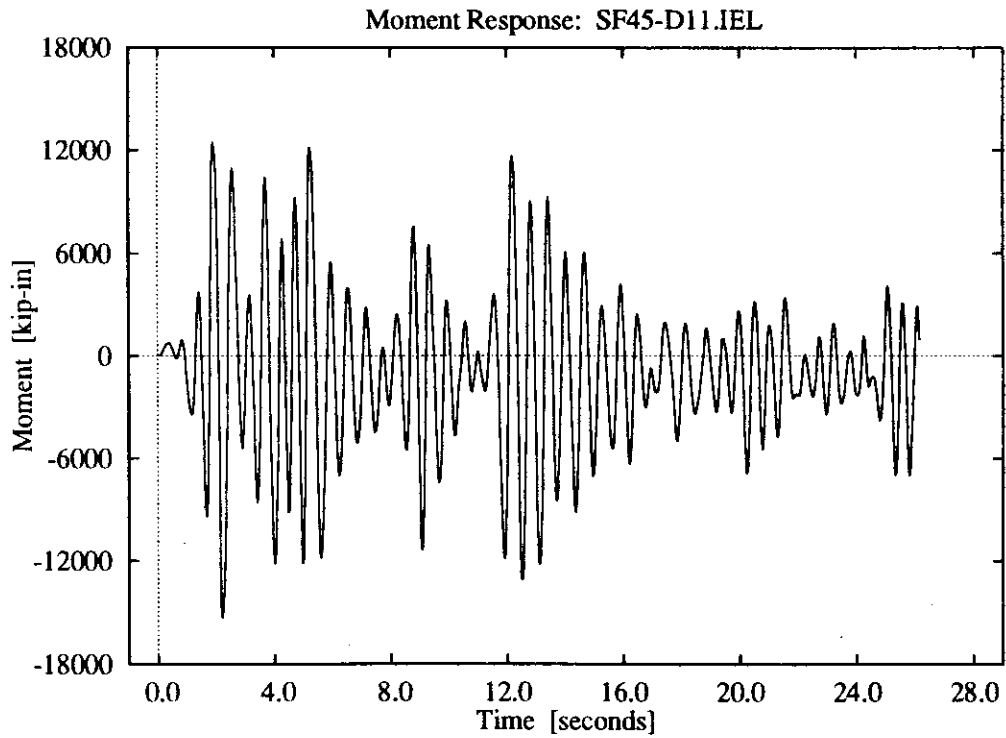
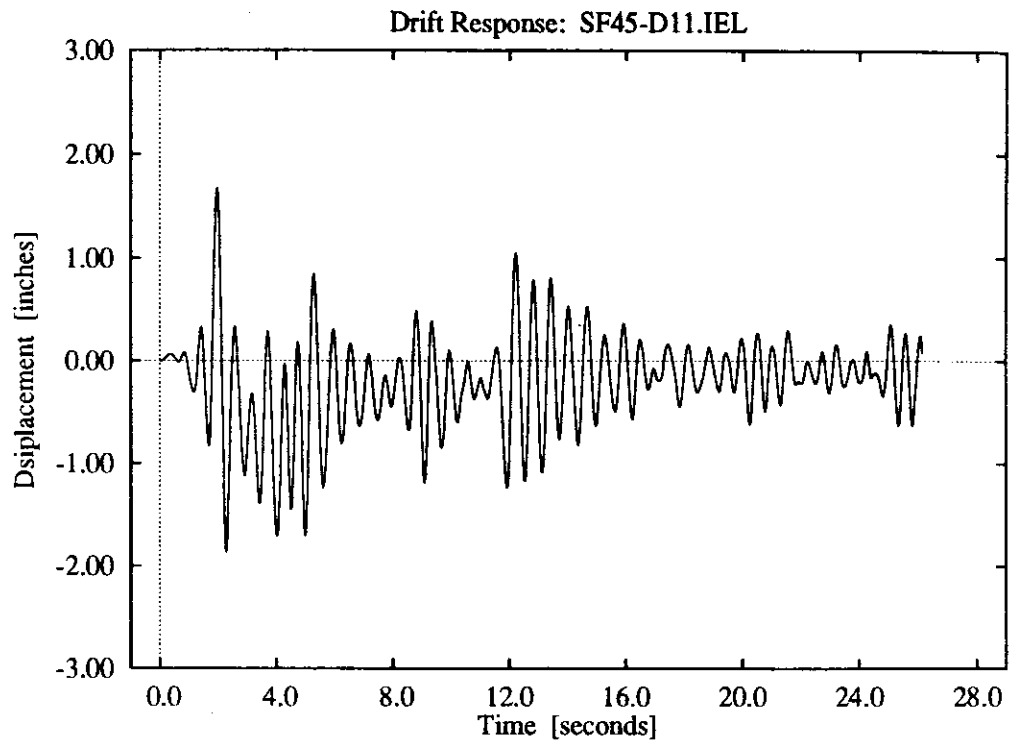


**Figure D-89:** 11 parameter foundation model, intermediate soil stiffness, lower intensity El Centro record.

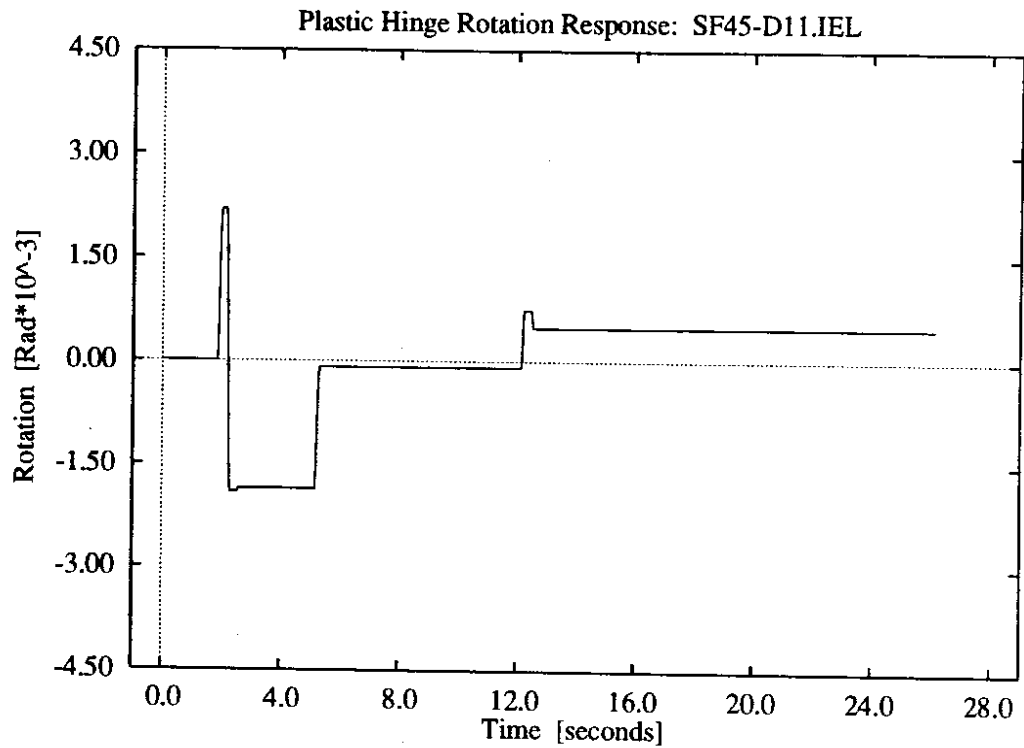
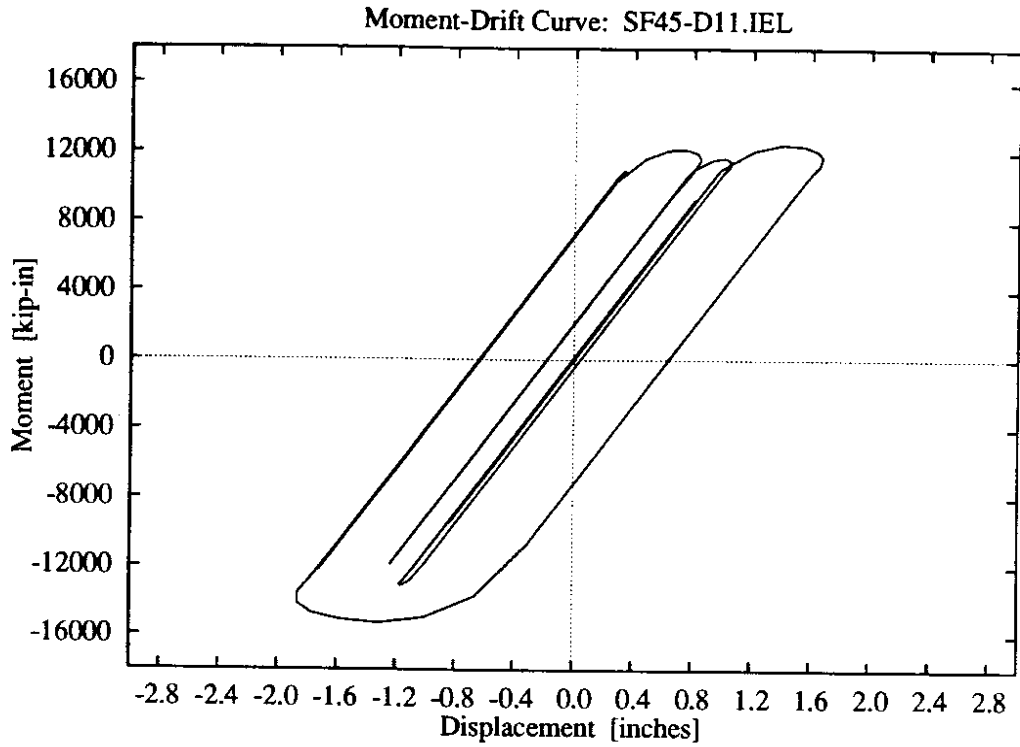


**Figure D-90:** 11 parameter foundation model, intermediate soil stiffness, lower intensity El Centro record.

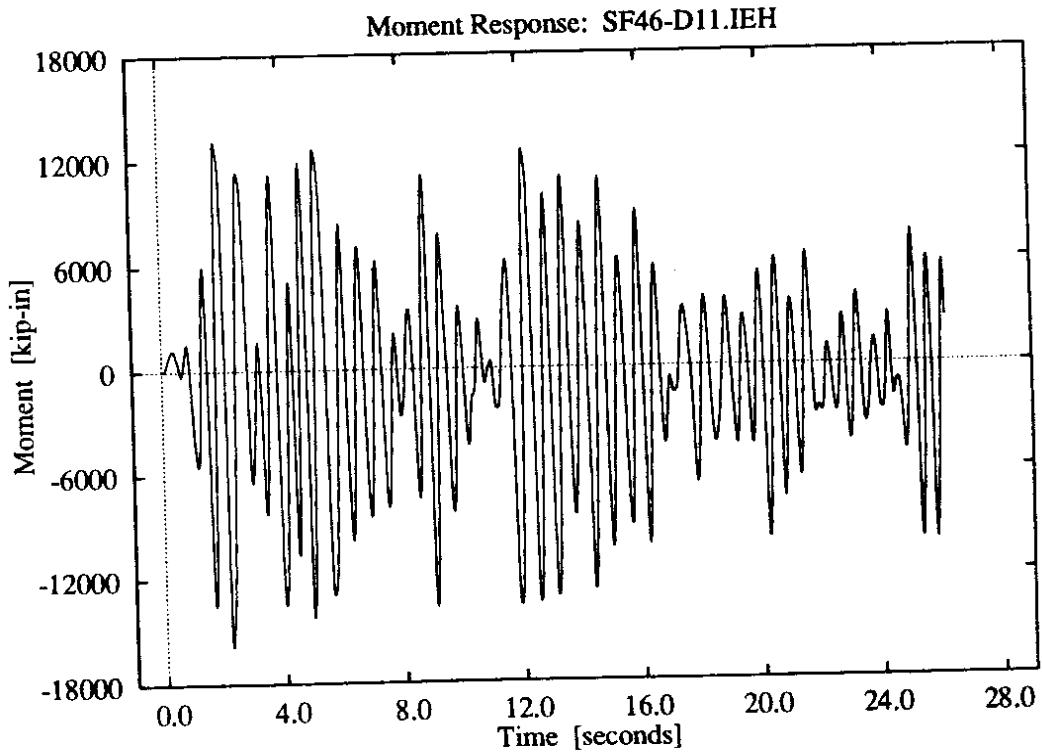
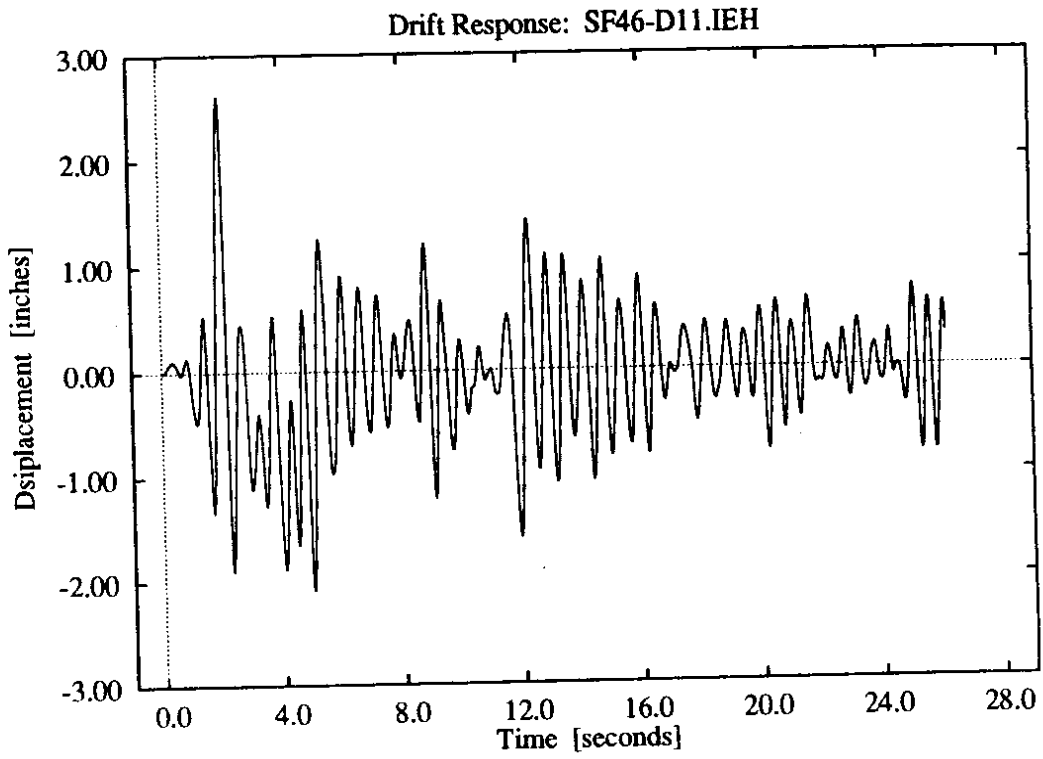


**Figure D-91:** 11 parameter foundation model, intermediate soil stiffness, higher intensity El Centro record.

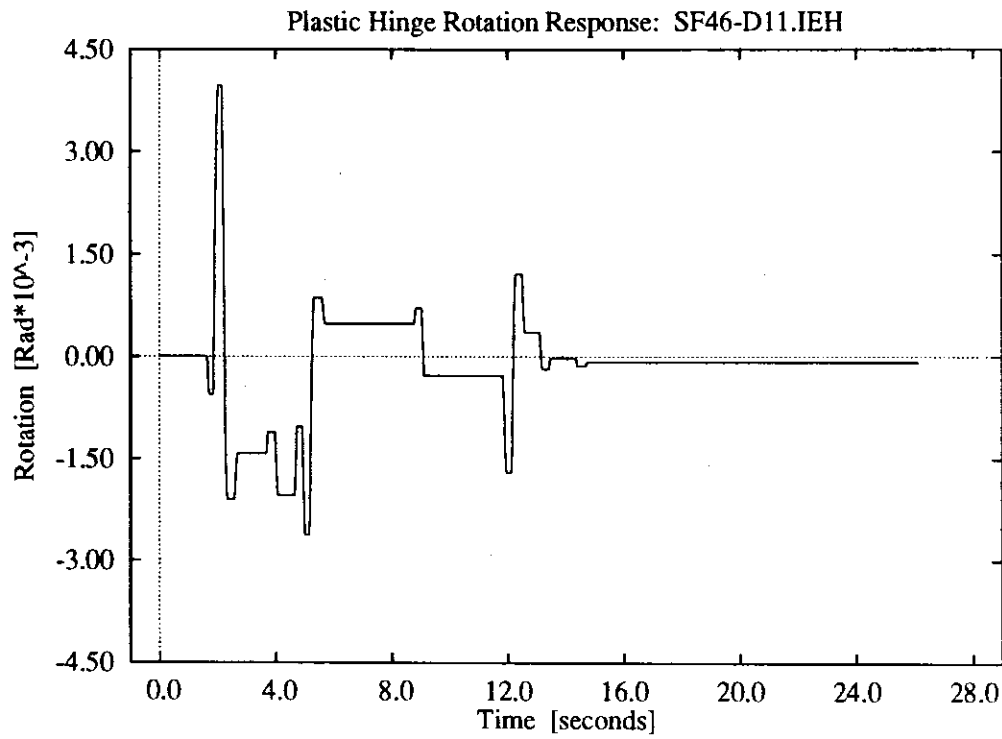
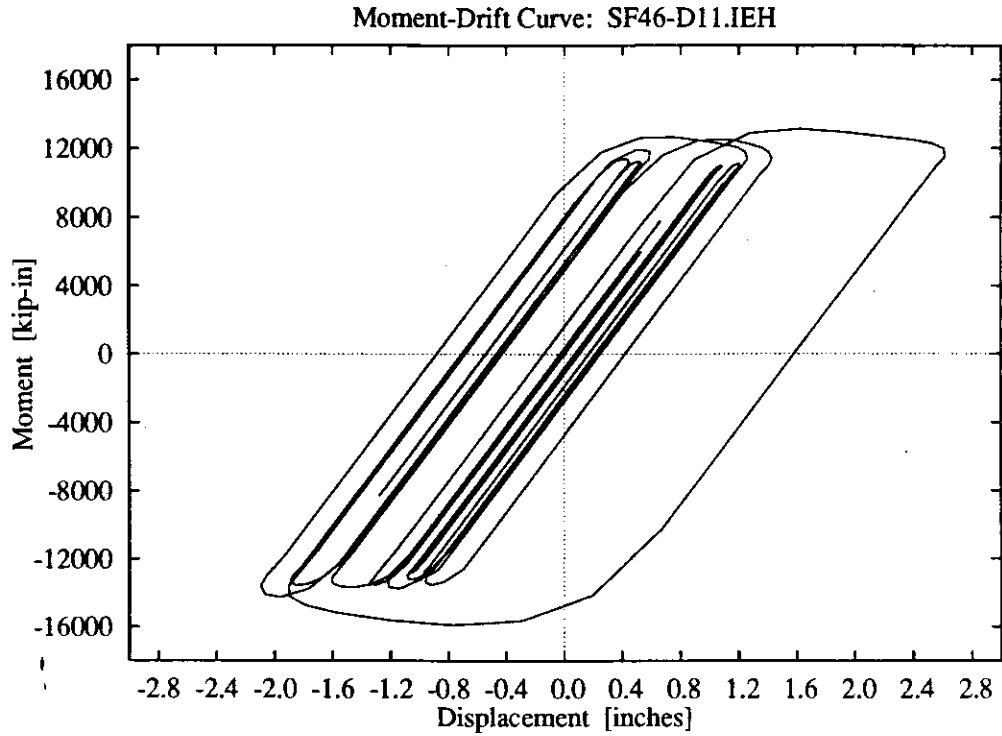


**Figure D-92:** 11 parameter foundation model, intermediate soil stiffness, higher intensity El Centro record.

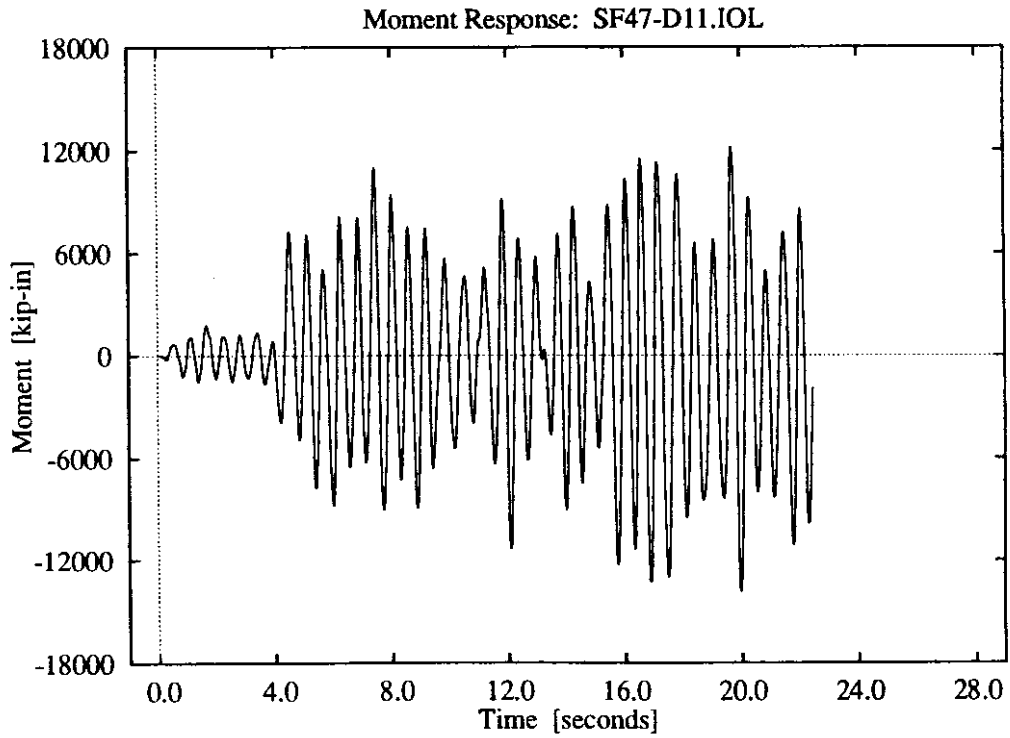
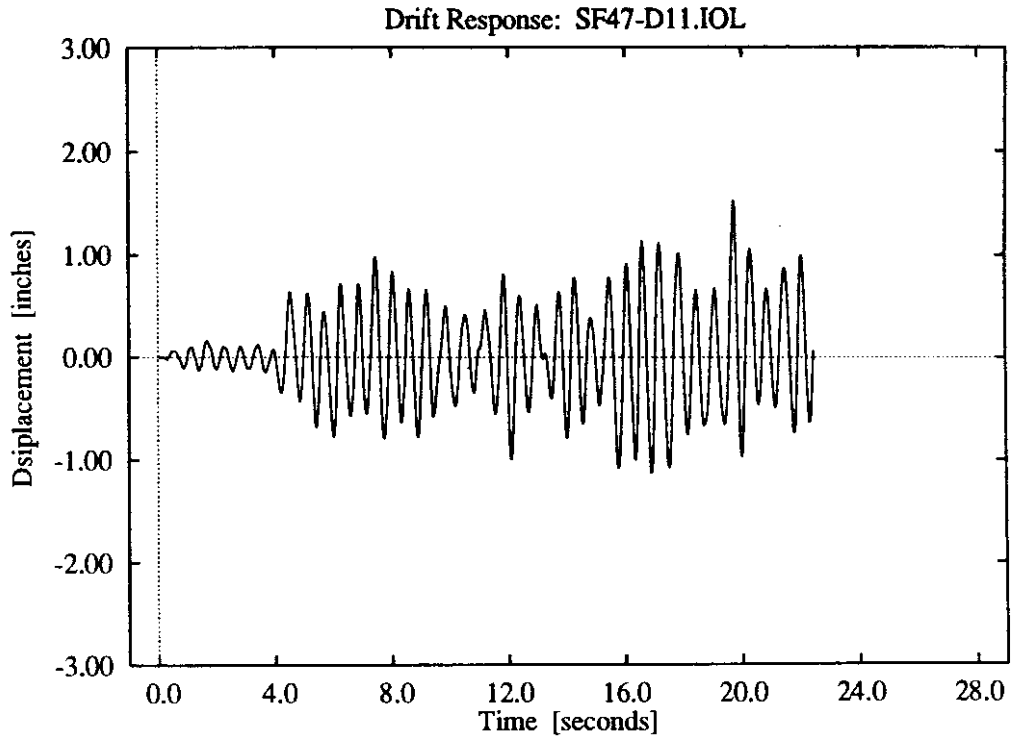


**Figure D-93:** 11 parameter foundation model, intermediate soil stiffness, lower intensity Olympia record.

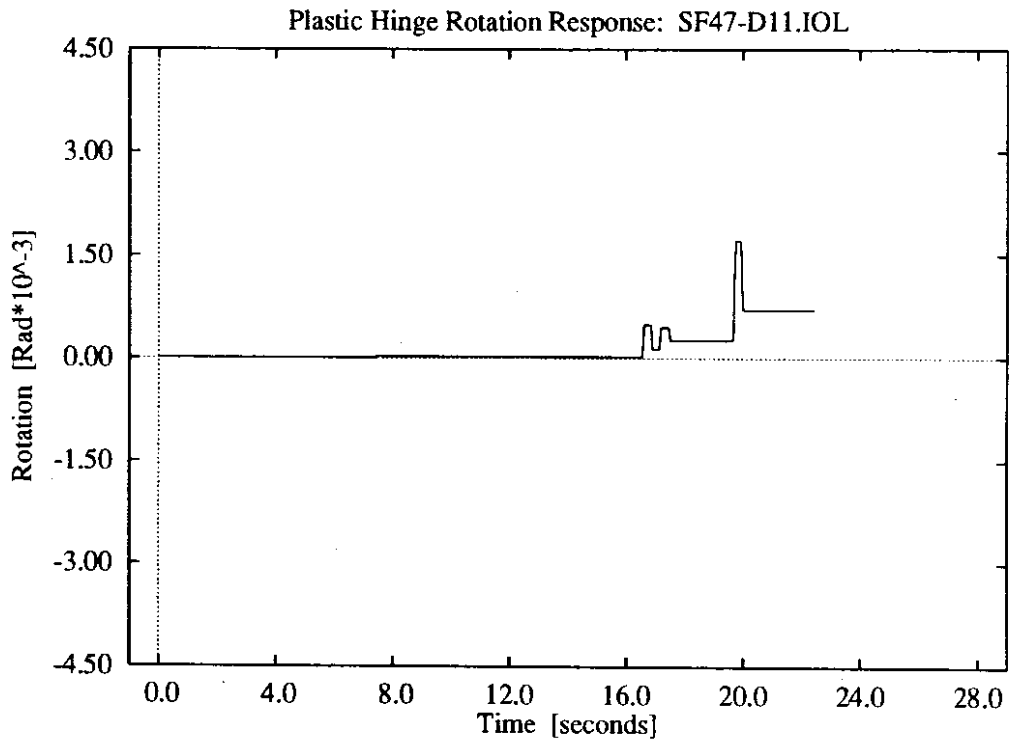
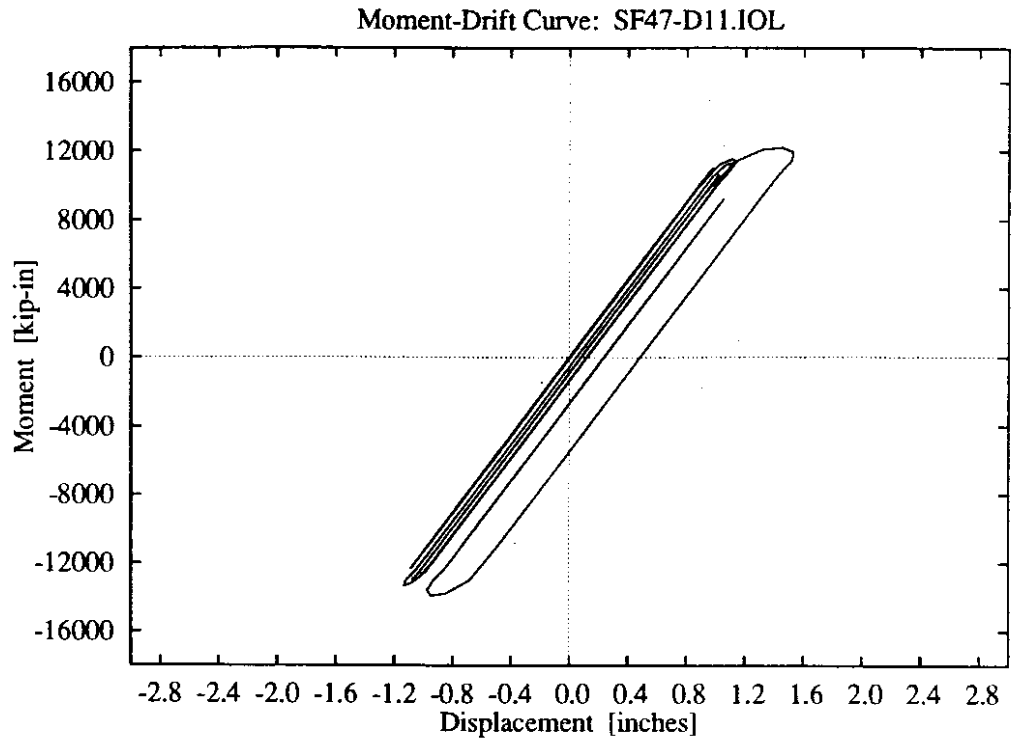


**Figure D-94:** 11 parameter foundation model, intermediate soil stiffness, lower intensity Olympia record.



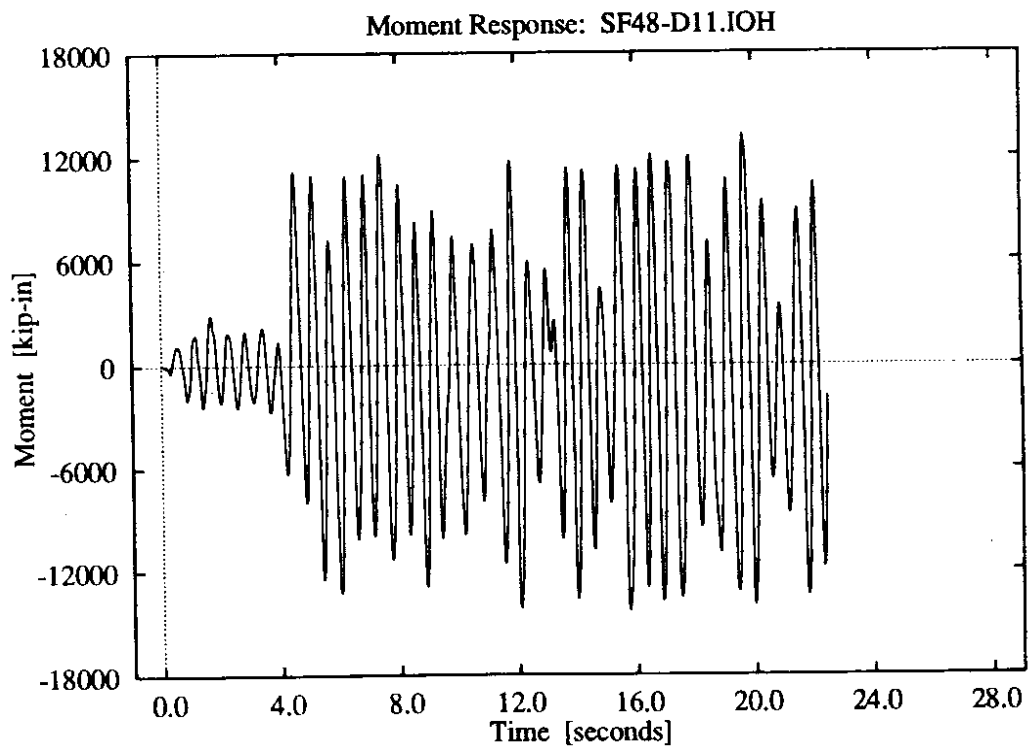
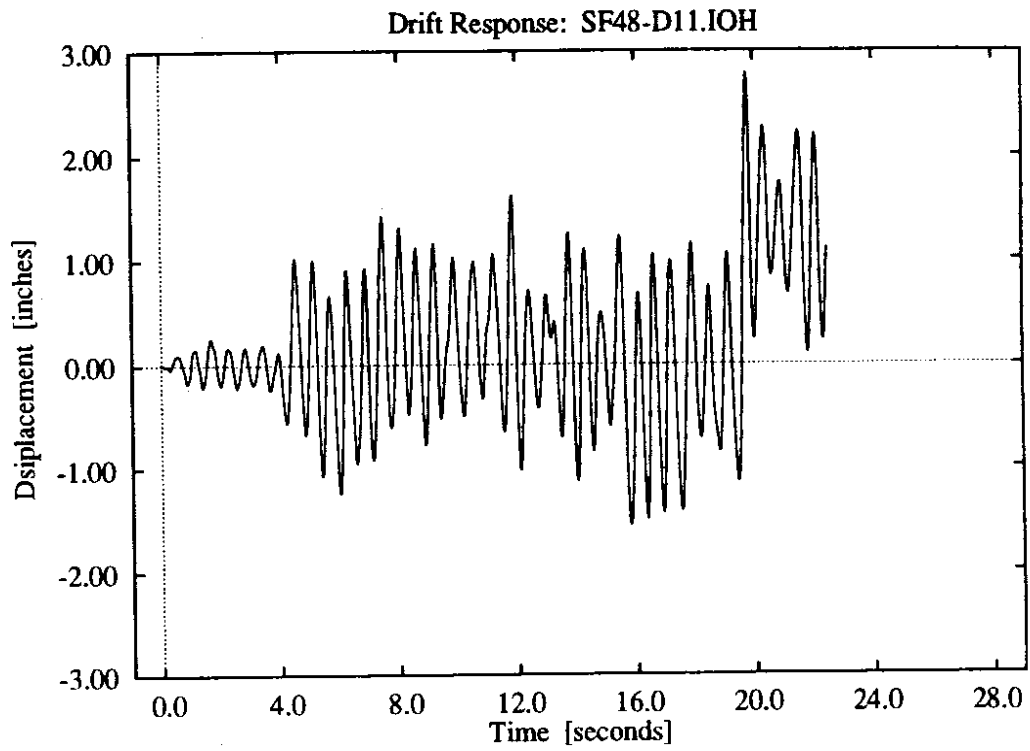


**Figure D-95:** 11 parameter foundation model, intermediate soil stiffness, higher intensity Olympia record.

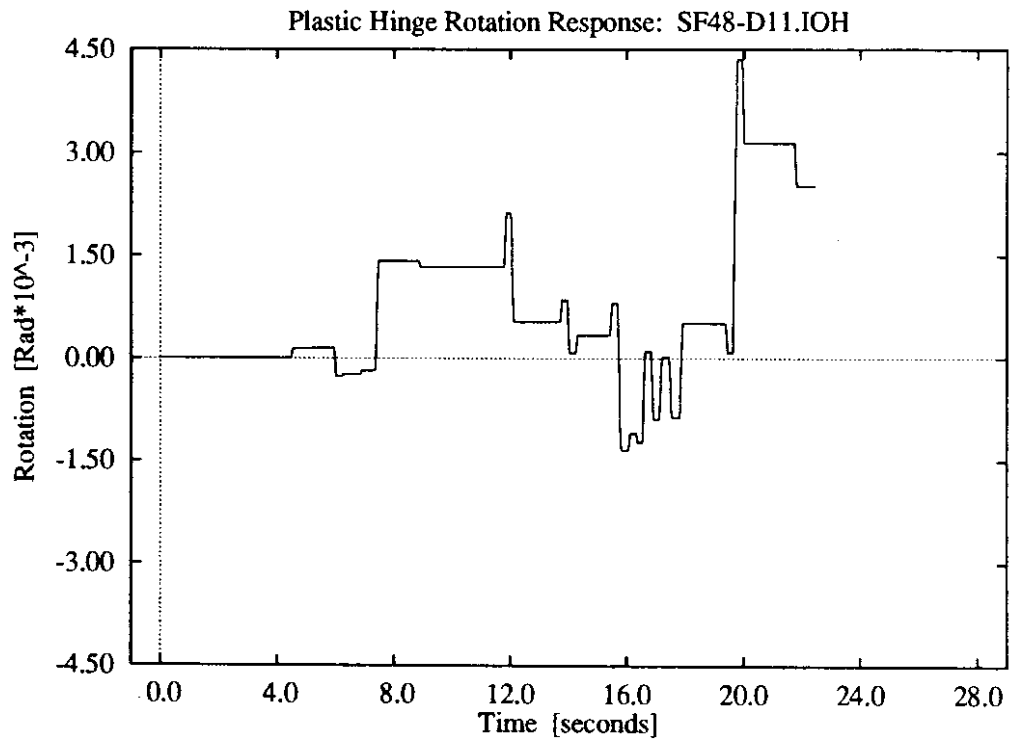
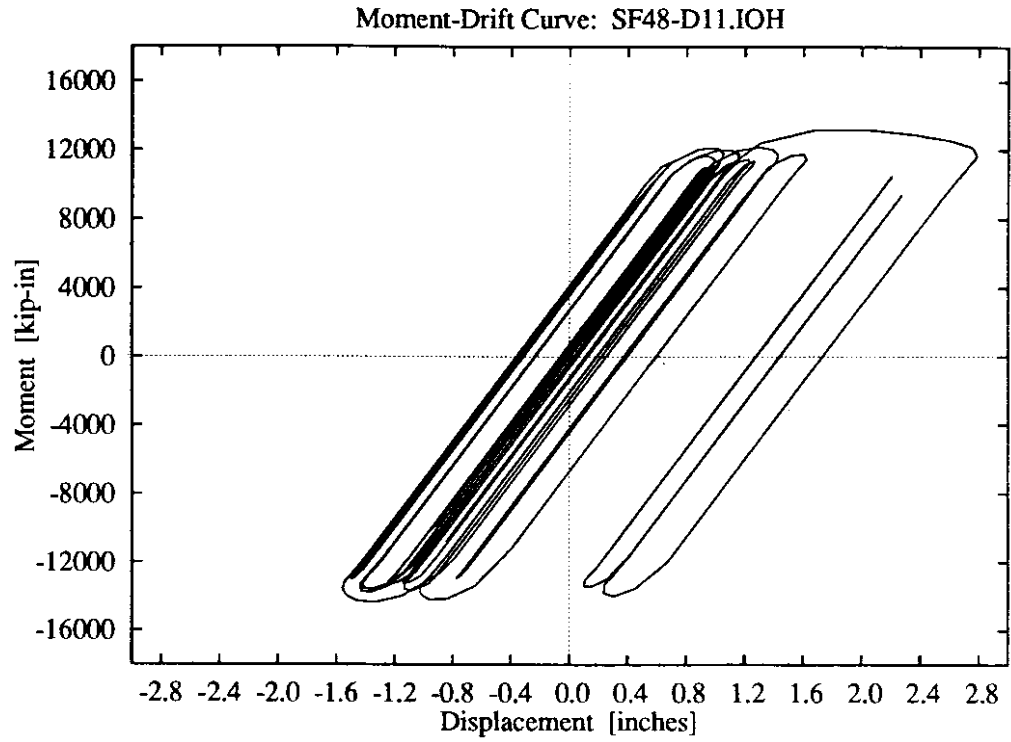


**Figure D-96:** 11 parameter foundation model, intermediate soil stiffness, higher intensity Olympia record.

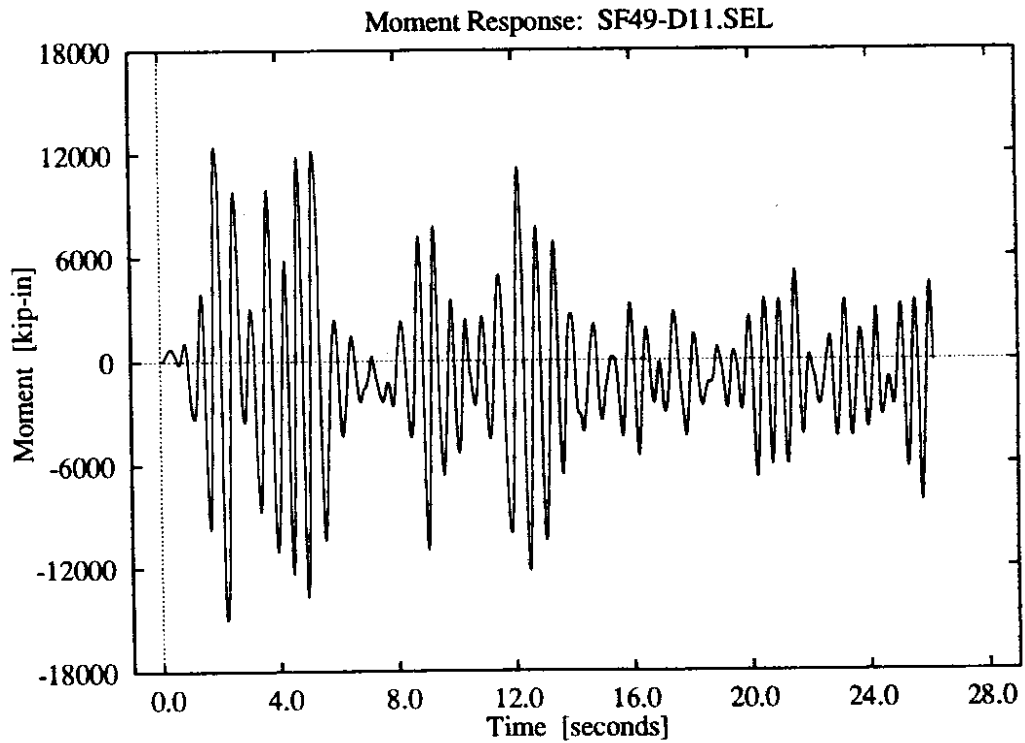
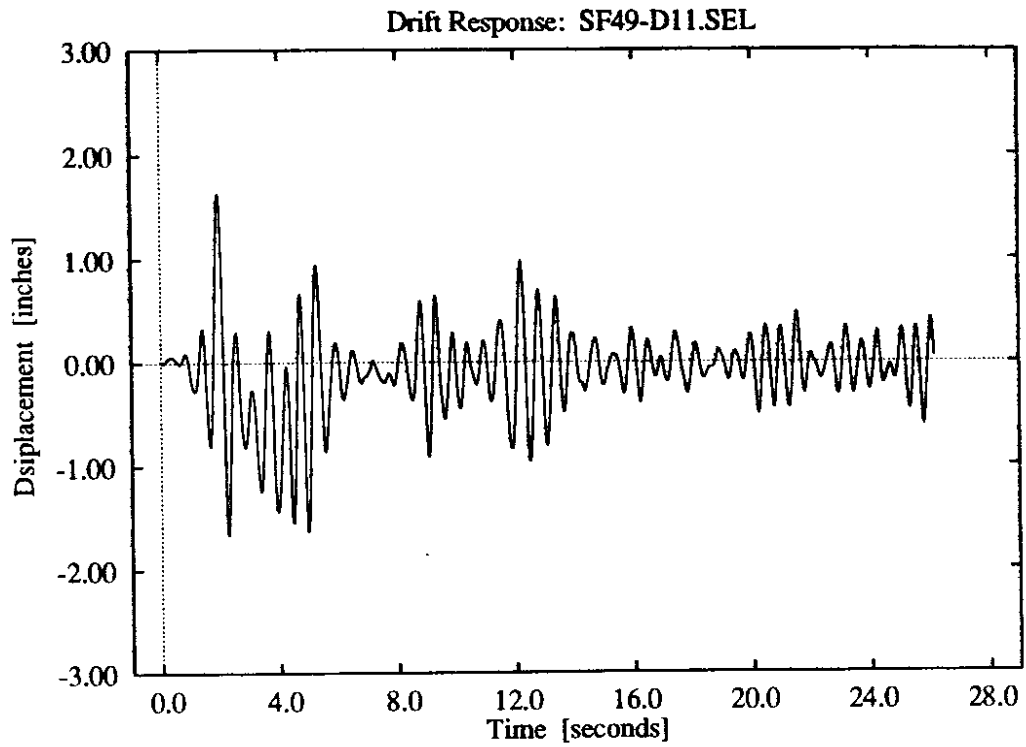


**Figure D-97: 11 parameter foundation model, high soil stiffness, lower intensity El Centro record.**

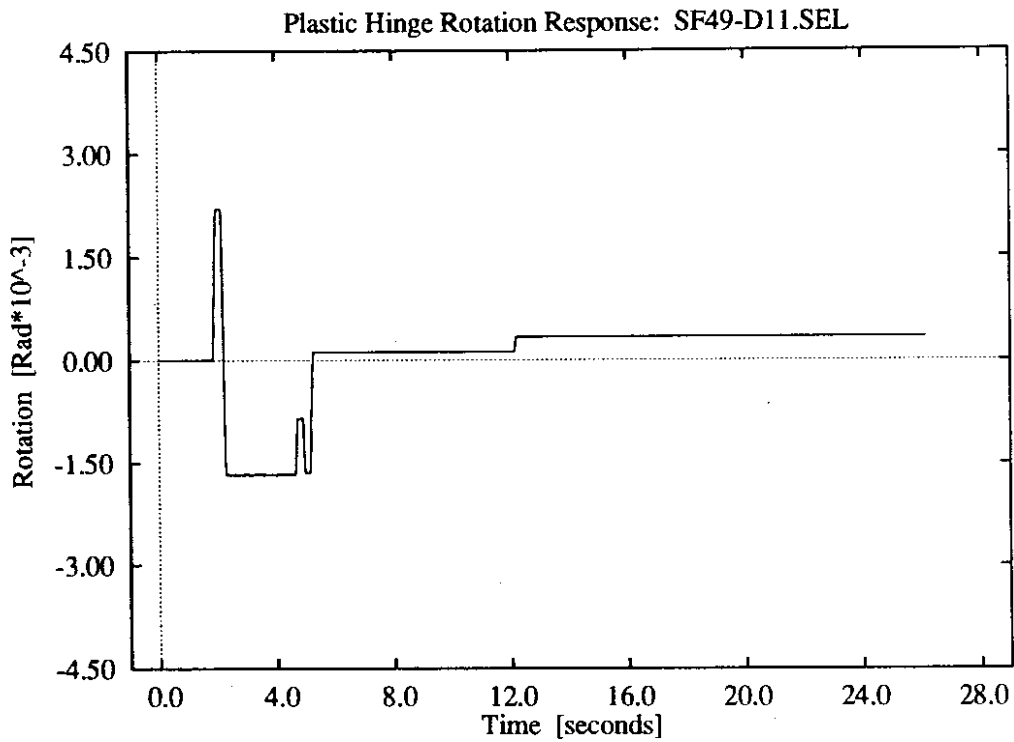
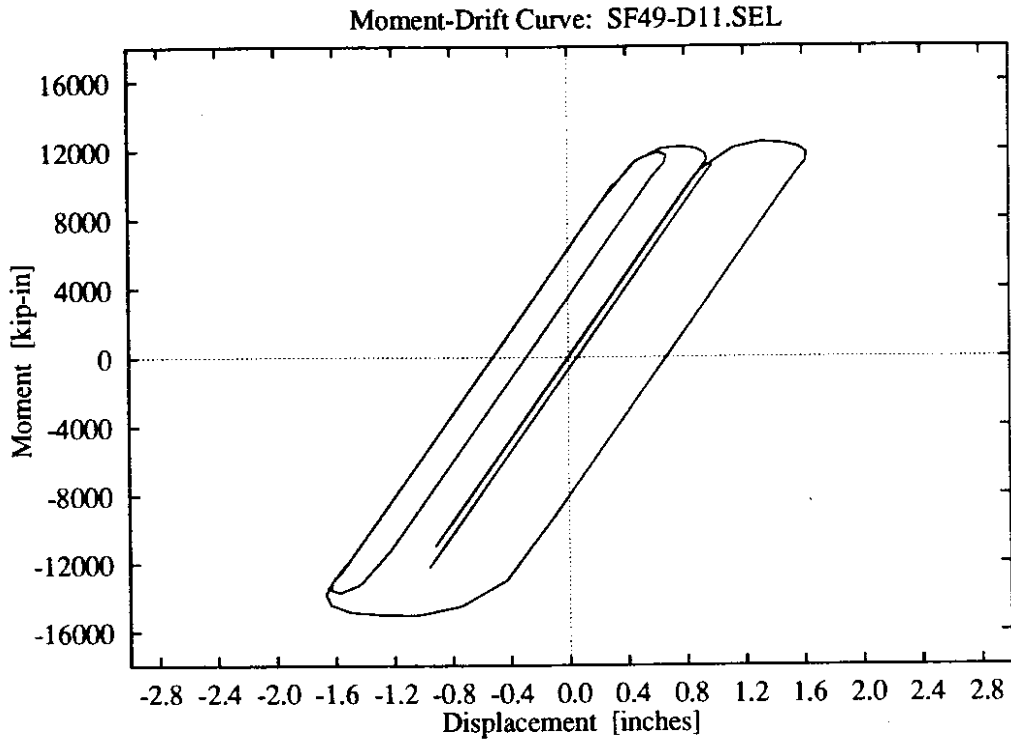


**Figure D-98:** 11 parameter foundation model, high soil stiffness, lower intensity El Centro record.

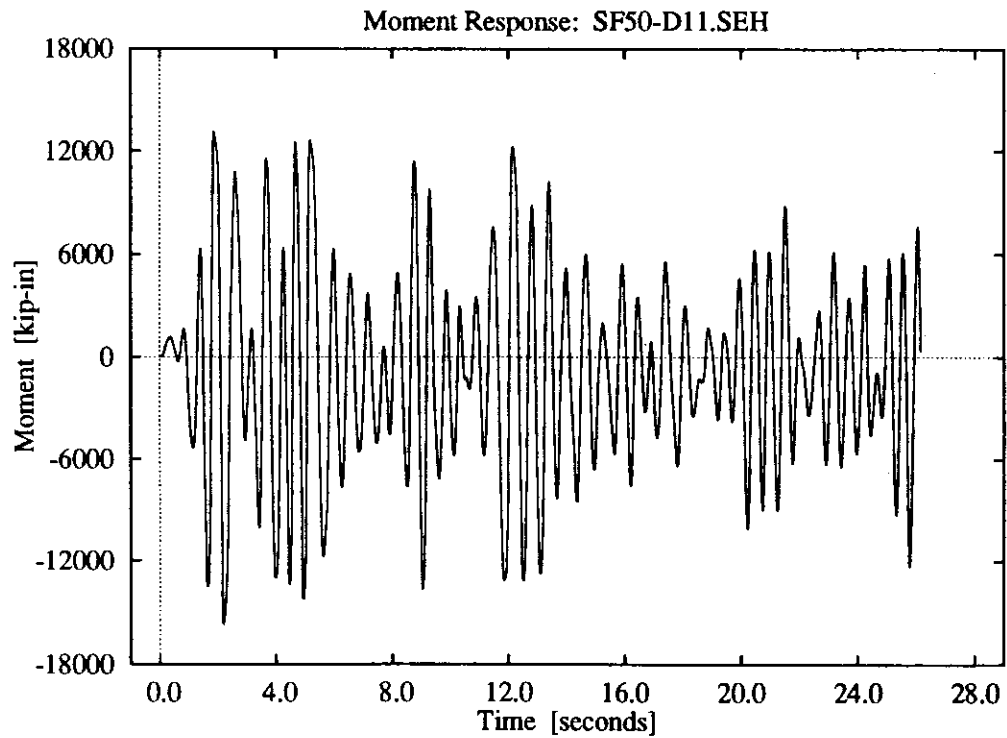
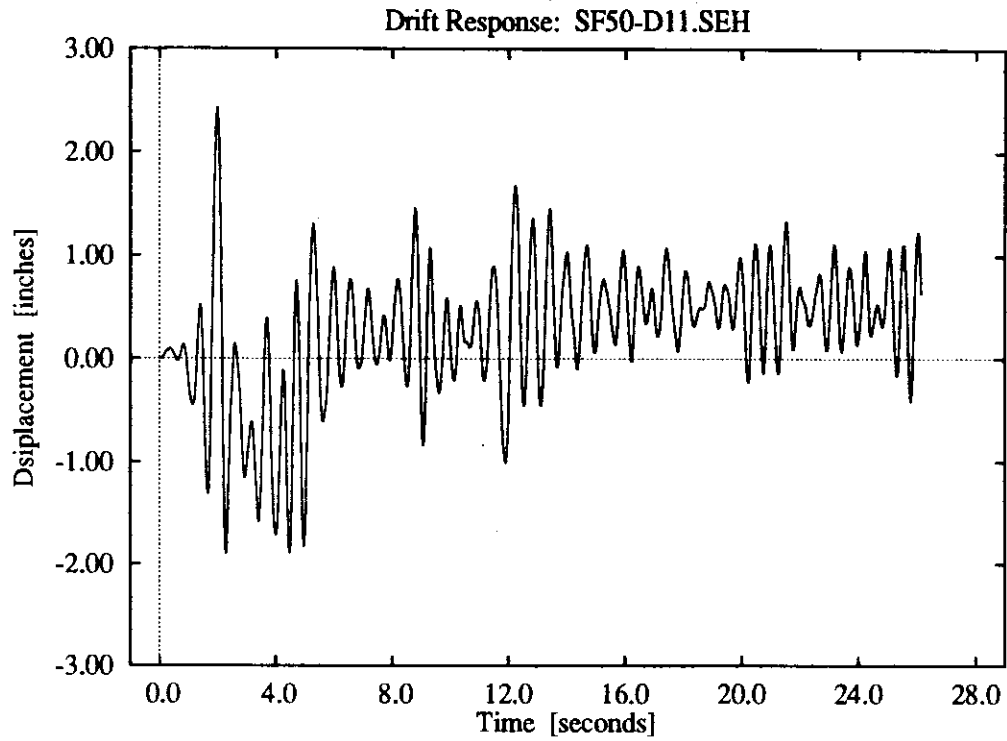


**Figure D-99: 11 parameter foundation model, high soil stiffness, higher intensity El Centro record.**

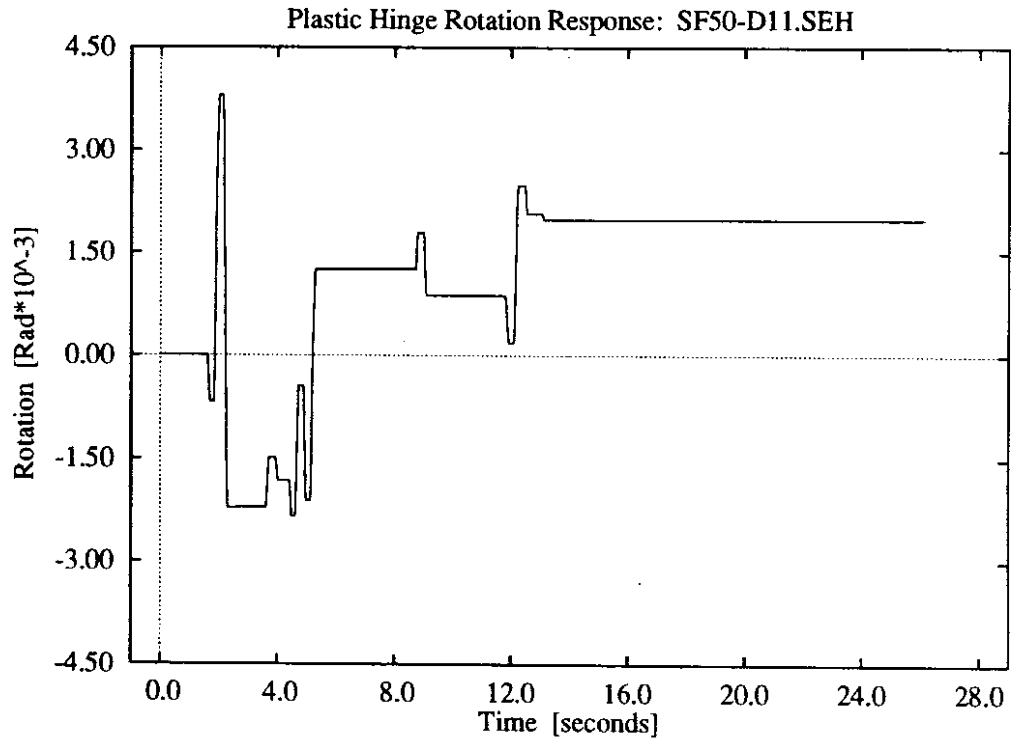
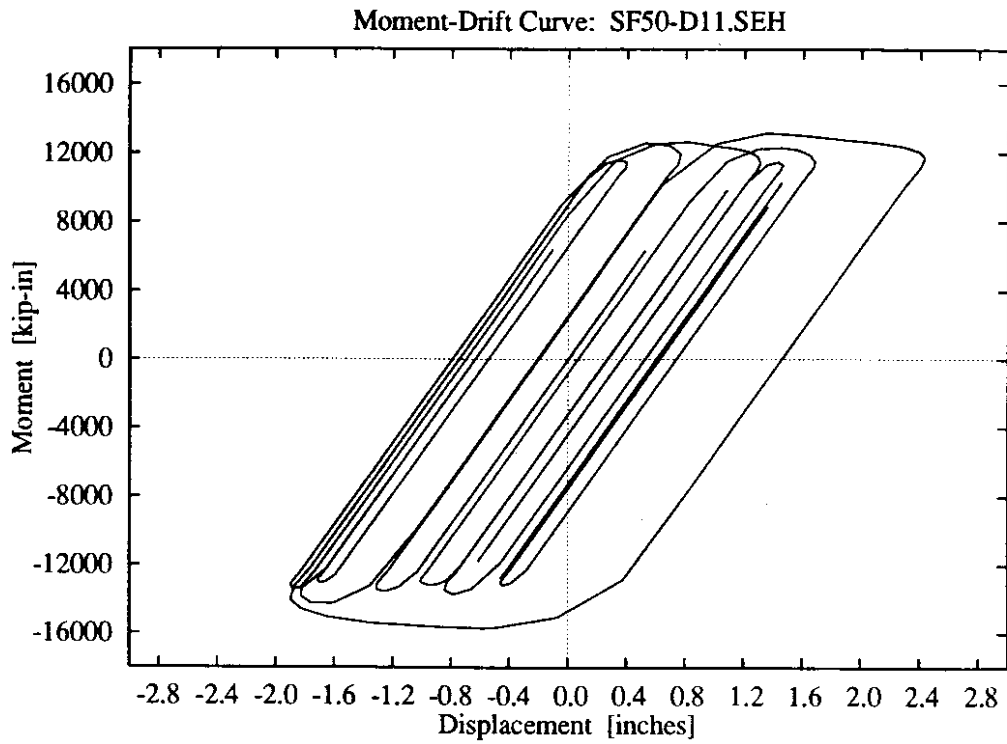


**Figure D-100:** 11 parameter foundation model, high soil stiffness, higher intensity El Centro record.

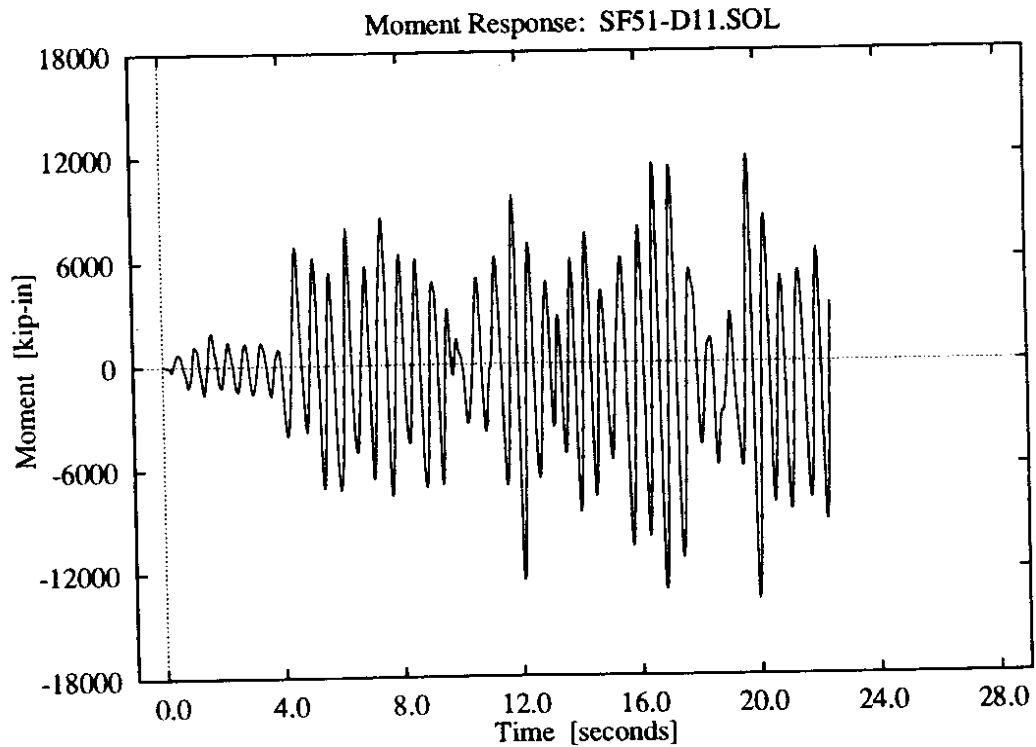
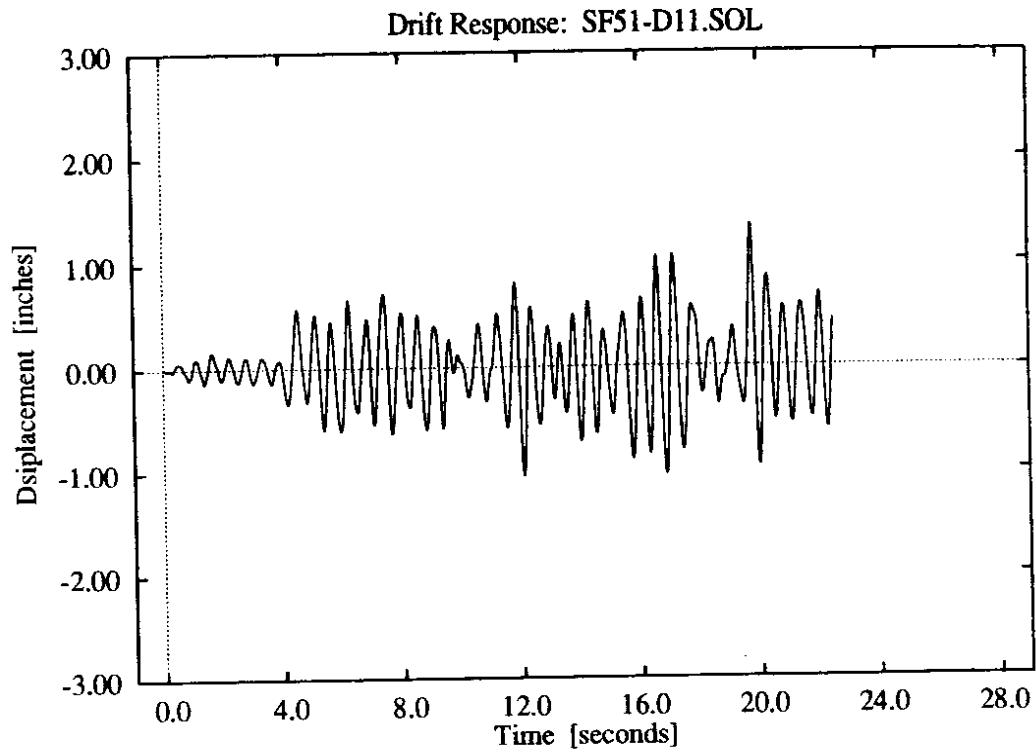


**Figure D-101:** 11 parameter foundation model, high soil stiffness, lower intensity Olympia record.

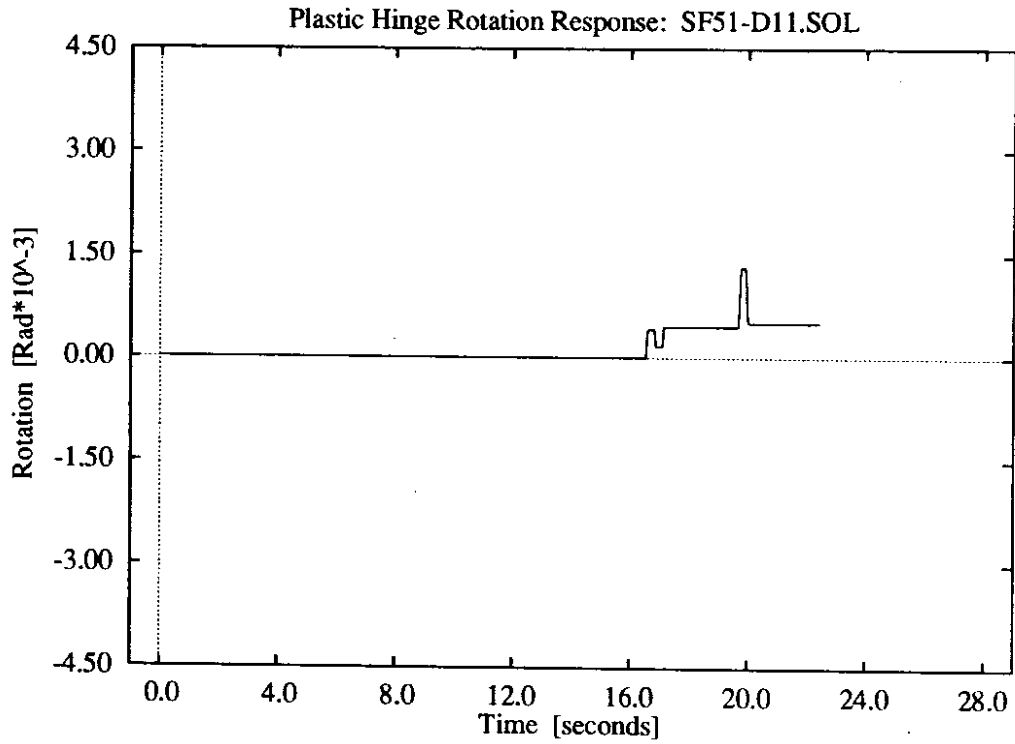
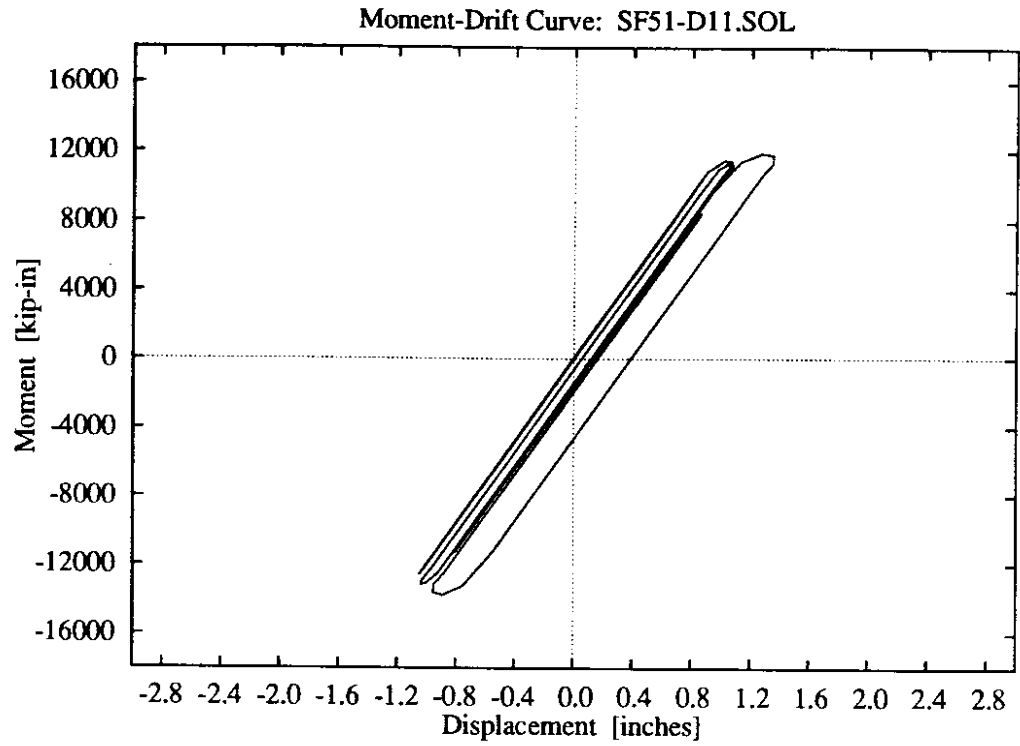


**Figure D-102:** 11 parameter foundation model, high soil stiffness, lower intensity Olympia record.



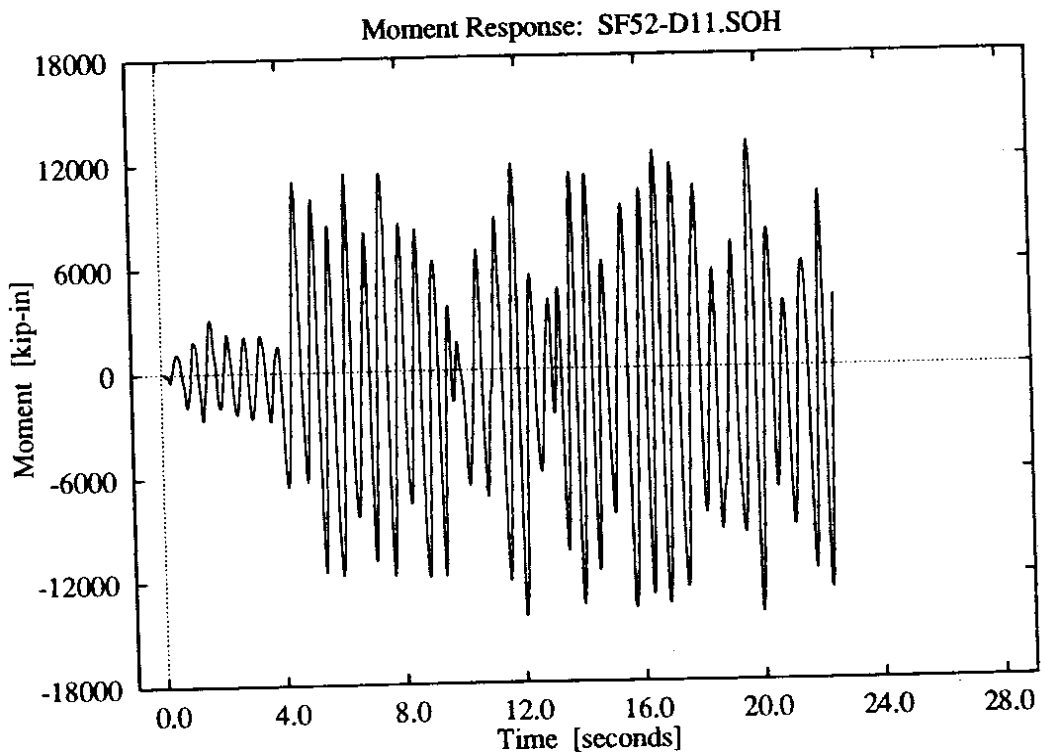
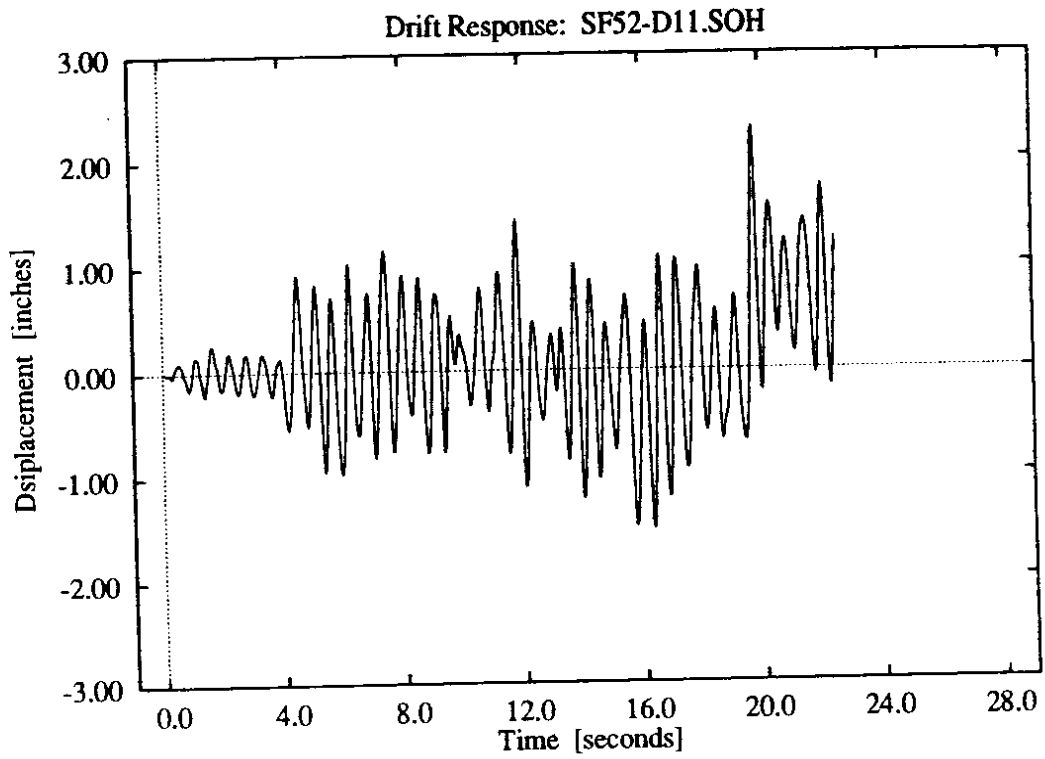


**Figure D-103:** 11 parameter foundation model, high soil stiffness, higher intensity Olympia record.

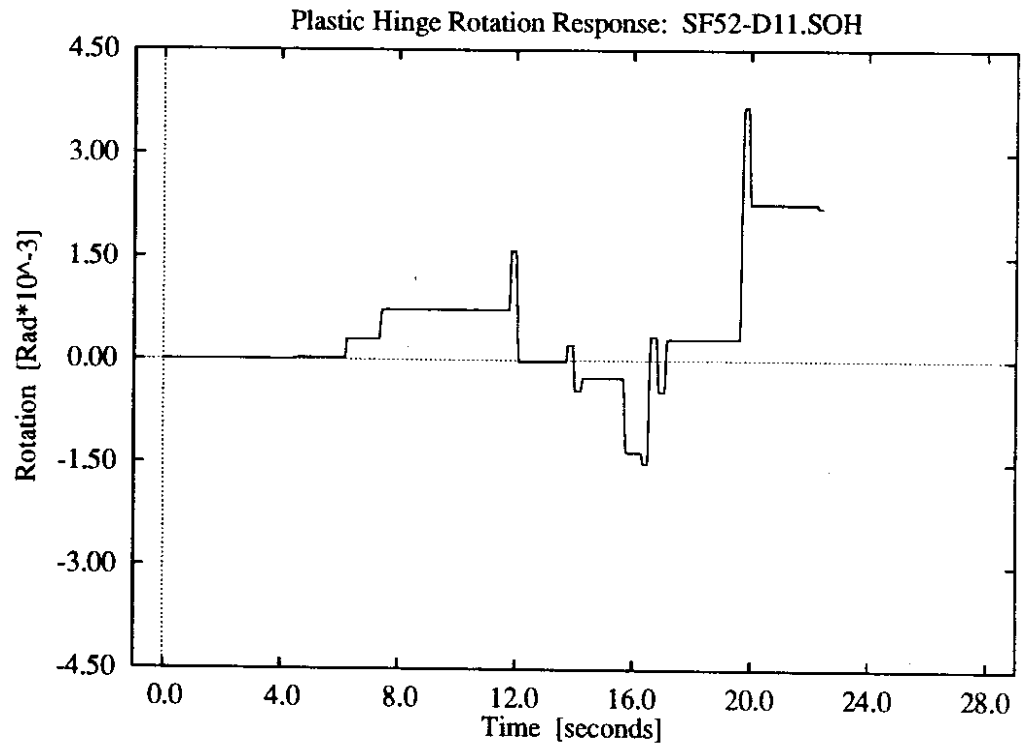
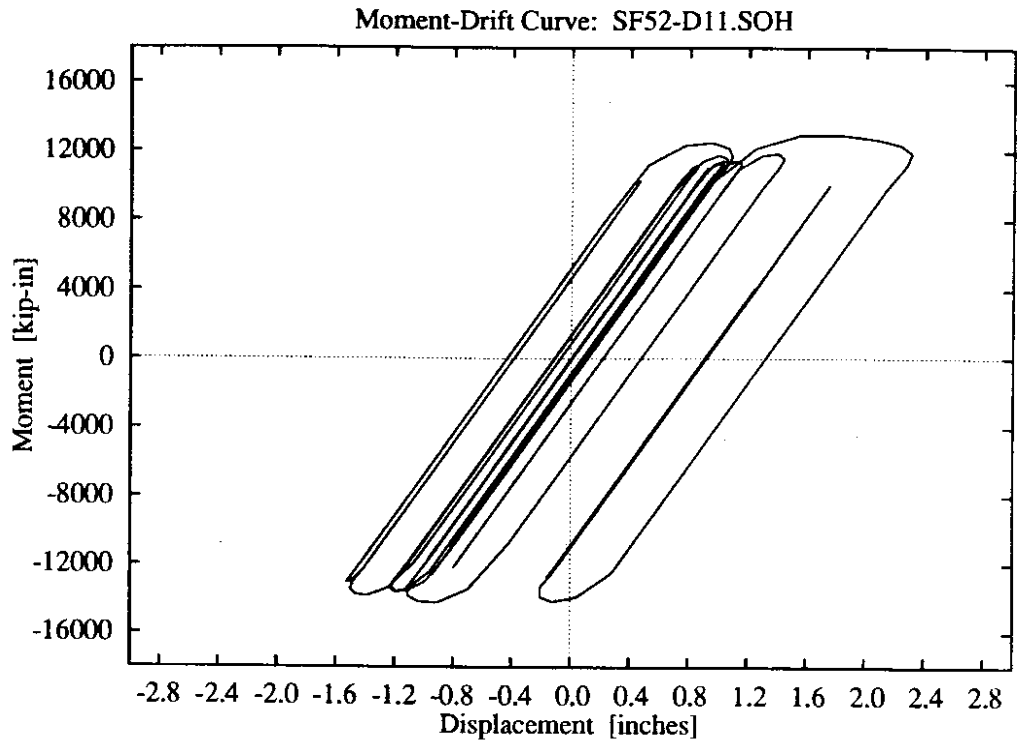


**Figure D-104:** 11 parameter foundation model, high soil stiffness, higher intensity Olympia record.

## Appendix E

### Pile Foundation Study

The 25 NEABS analyses performed in the parametric study of spread footing foundations are presented below in matrix form. Each run is identified by a name of the form "PF $nn$ - $fff.eee$ ," where  $nn$  is the run number,  $fff$  is the foundation model code, and  $eee$  is the applied seismic record code. The values of the foundation model parameters are given in this appendix, in terms of the model configurations shown in Figure 3.18 of Chapter Three. References of the publications which describe the procedures used to determine these parameters accompany the values. The results of the NEABS analyses are also presented in this appendix; the presentation order of the results follows the numbering of the analyses given in the matrix below.

	Filtered Records				Unfiltered Records	
	El Centro		Lake Hughes		El Centro	
	Zone 3	Zone 4	Zone 1	Zone 2	Lower Inten.	Higher Inten.
Fixed	PF01-FX_3EL	PF02-FX_4EL	PF03-FX_1LH	PF04-FX_2LH	PF05-FX_LEL	PF06-FX_HEL
DF1	PF07-DF1.3EL	PF08-DF1.4EL	PF09-DF1.1LH	PF10-DF1.2LH	PF11-DF1.LEL	PF12-DF1.HEL
DF2	PF13-DF2.3EL	PF14-DF2.4EL	PF15-DF2.1LH	PF16-DF2.2LH	PF17-DF2.LEL	PF18-DF2.HEL
DF3						PF19-DF3.HEL
WPF	PF20-WPF.3EL	PF21-WPF.4EL	PF22-WPF.1LH	PF23-WPF.2LH	PF24-WPF.LEL	PF25-WPF.HEL

## Pile Foundation Models: Parameter Values\*

All Models:

Elastic Rotational Pile Head Spring:  $k = 516,000$   
 Lateral Pile Head Damper (when used):  $c = 0.1625$

Pile Head Models:

	DF1	DF2	DF3
Elastic Stiffness	8.2	11.6	9.0
Yield Force	-	26.8	-
Plastic Stiffness	-	2.1	-

WPF Model:

depth	m	k1	c1	k2	c2	k3	c3
43	0.01060	68.28	43.90	69.50	9.756	107.3	3.634
105	0.01164	74.96	48.19	76.30	10.71	117.8	3.989
179	0.01306	84.08	54.06	85.59	12.01	132.1	4.475
266	0.01517	97.67	62.80	99.42	13.96	153.5	5.198
370	0.01884	121.3	77.98	123.5	17.33	190.6	6.455
515	0.02835	182.5	117.4	185.8	26.08	286.9	9.715

\* unit of force = kip; unit of length = inch; unit of rotation = radians; unit of time = second

DF1 Model: David I. McLean and Ian B. S. Cannon, *Seismic Analysis of the I-90 Mercer Slough Wesbound Lanes*, WSDOT Technical Report, 1992.

WPG Model: Toyoaki Nogami and K. Konagai, "Time Domain Flexural Response of Dynamically Loaded Single Piles," *Journal of Engineering Mechanics*, ASCE, Vol. 114, No. 9, September, 1988, pp. 1512-1525.

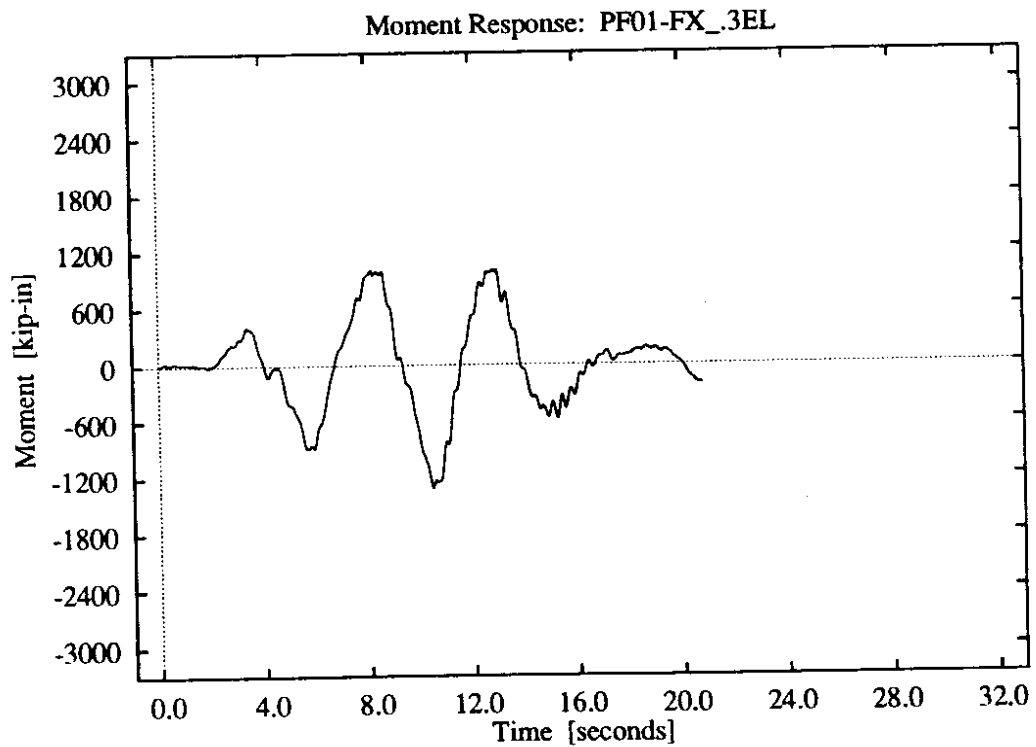
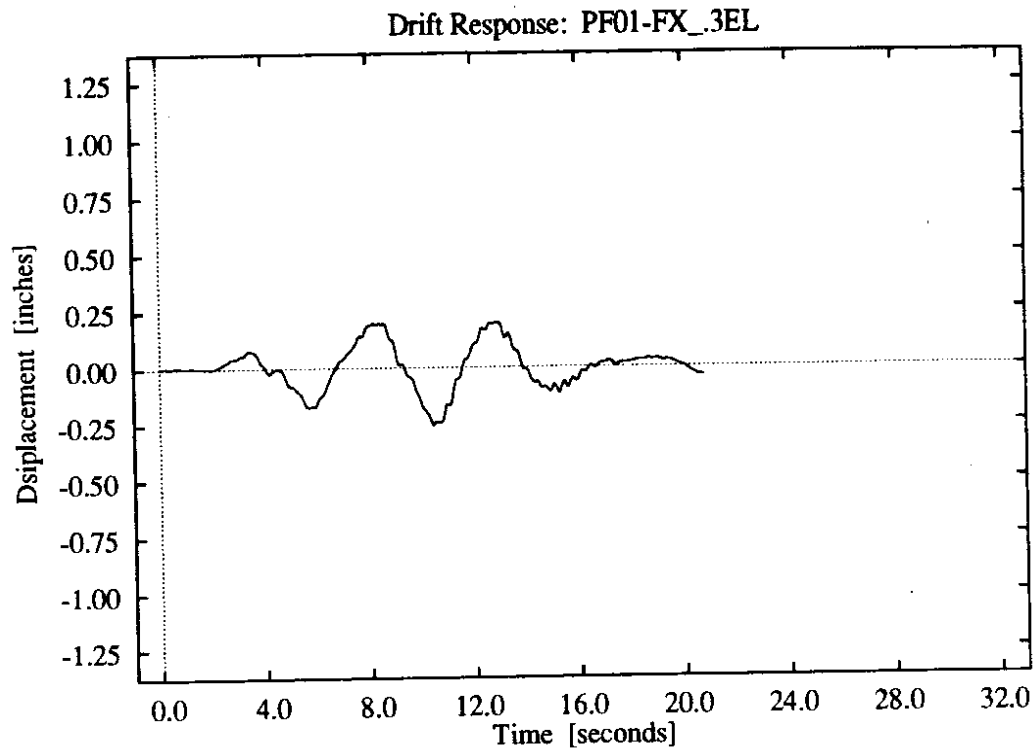


**Figure E-1: Fixed-base foundation, El Centro Z3 record.**

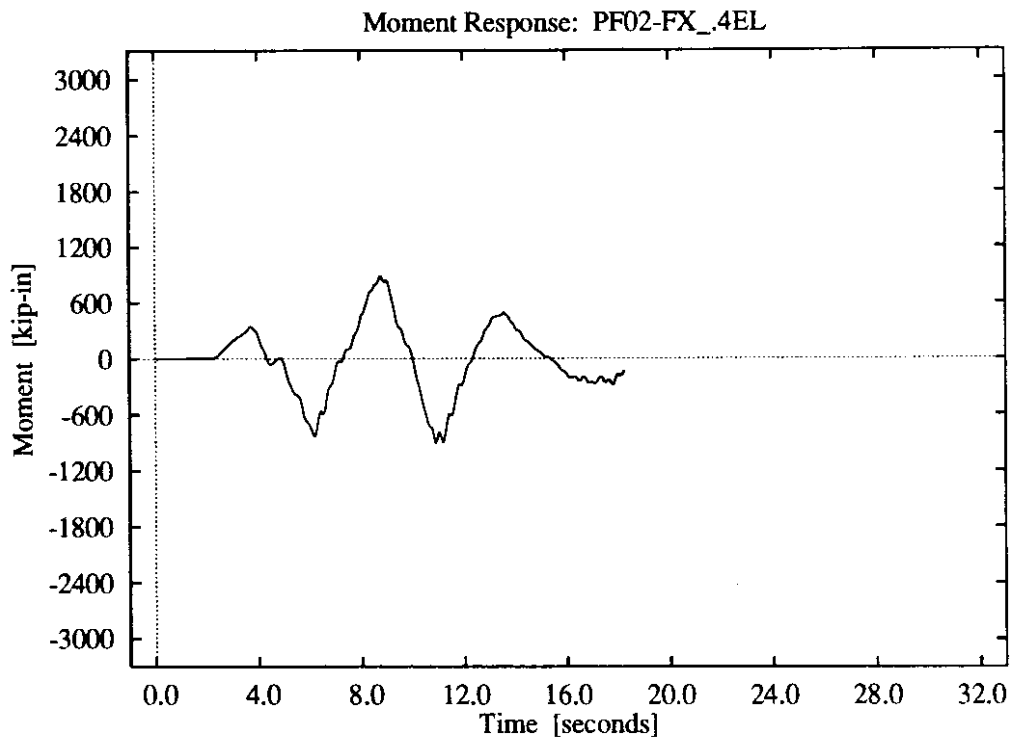
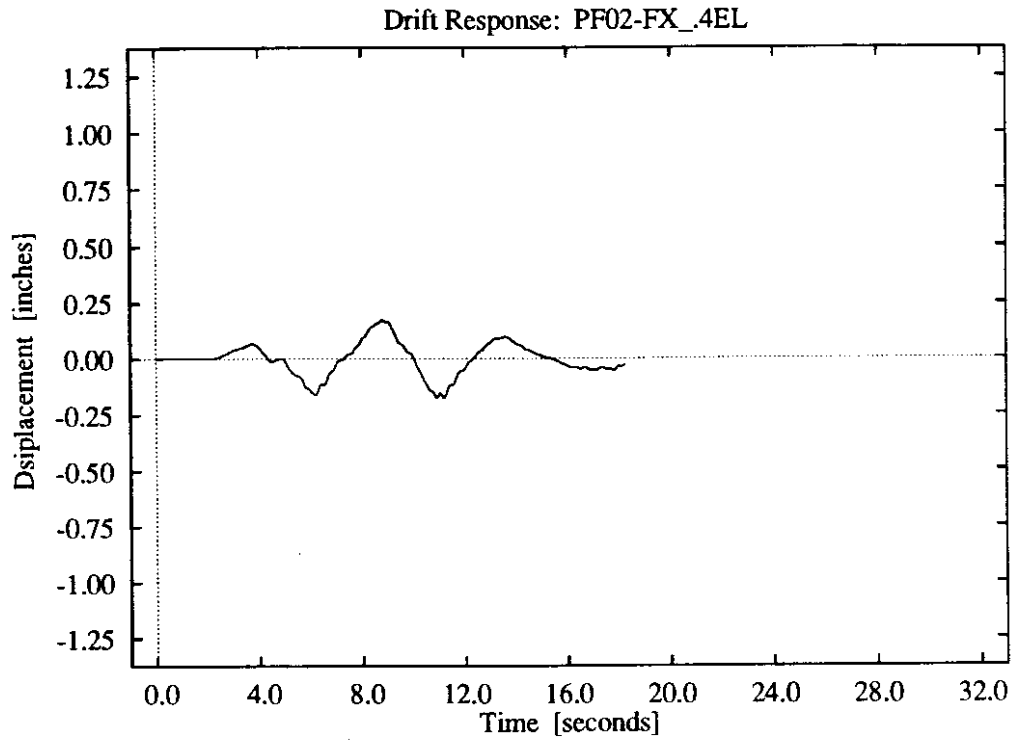


**Figure E-2:** Fixed-base foundation, El Centro Z4 record.

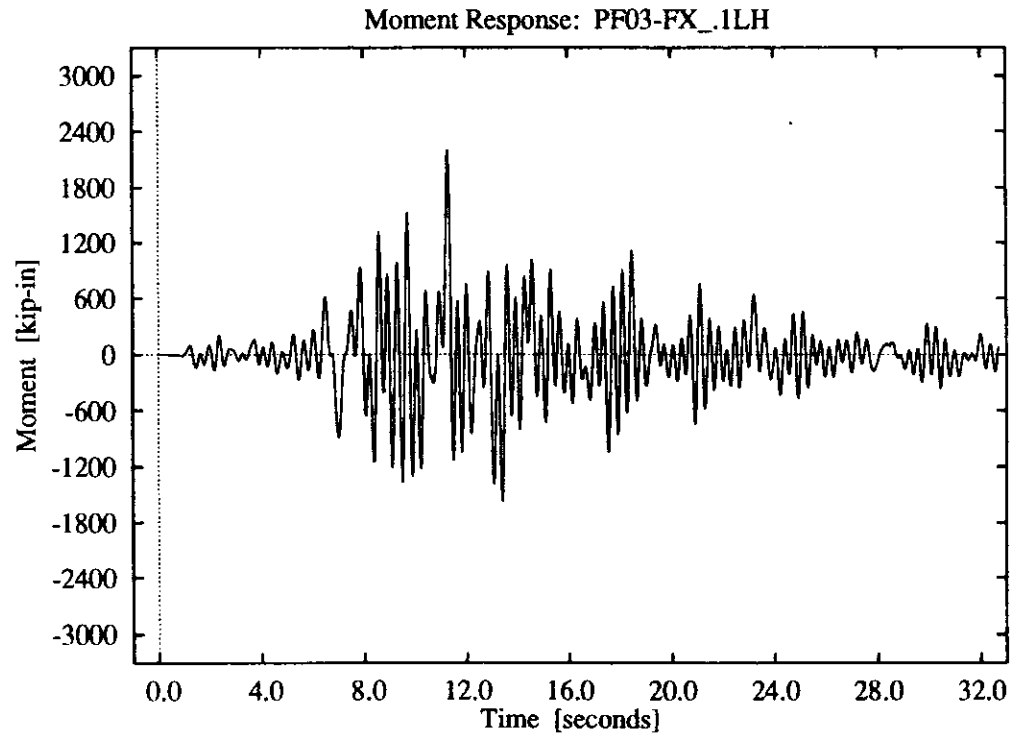
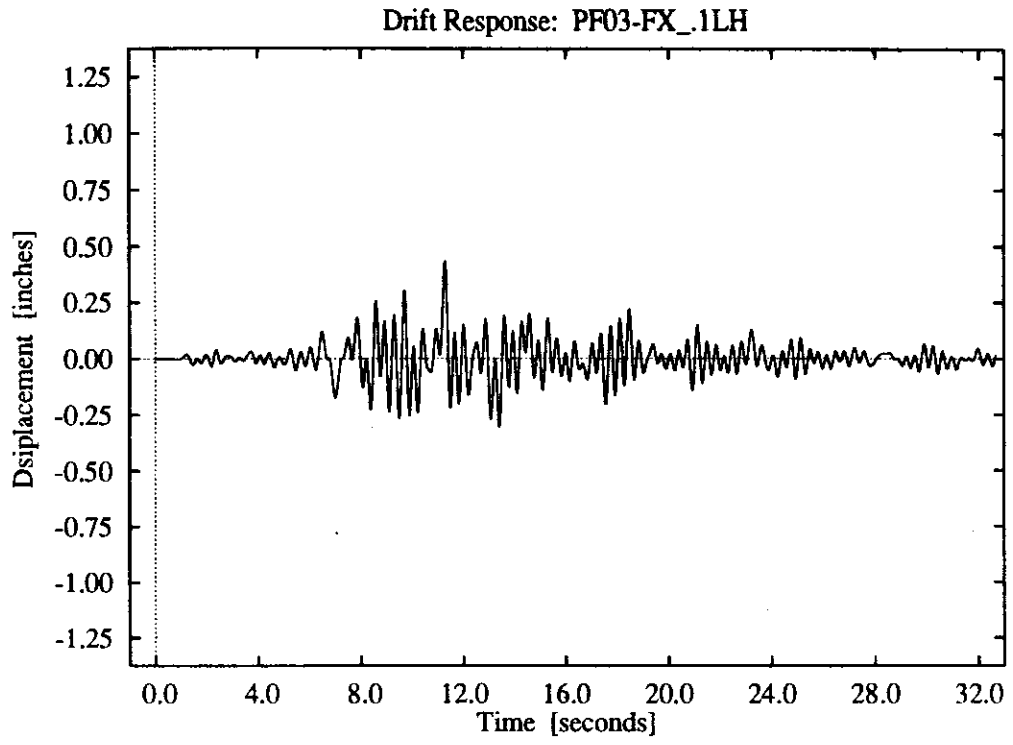


**Figure E-3:** Fixed-base foundation, Lake Hughes Z1 record.

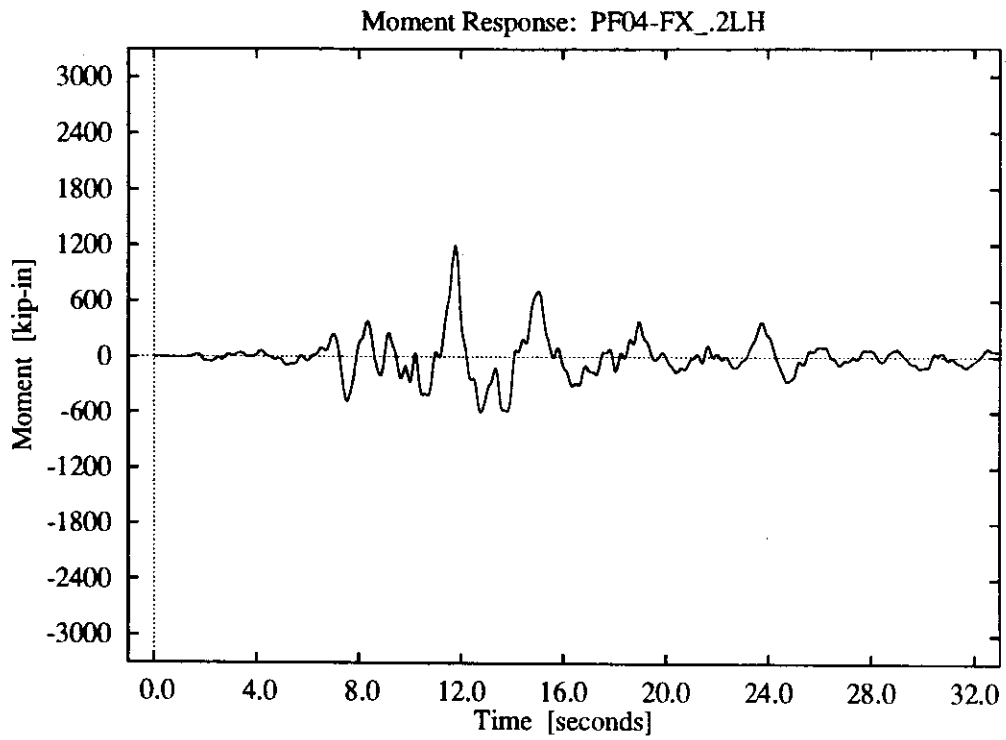
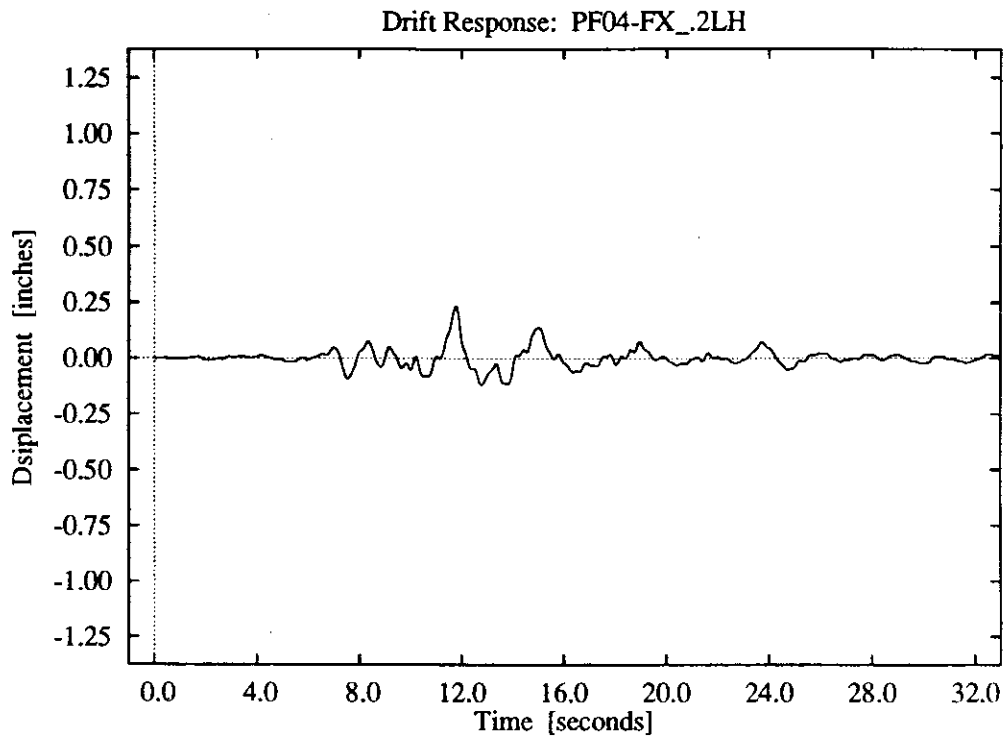


**Figure E-4:** Fixed-base foundation, Lake Hughes Z2 record.



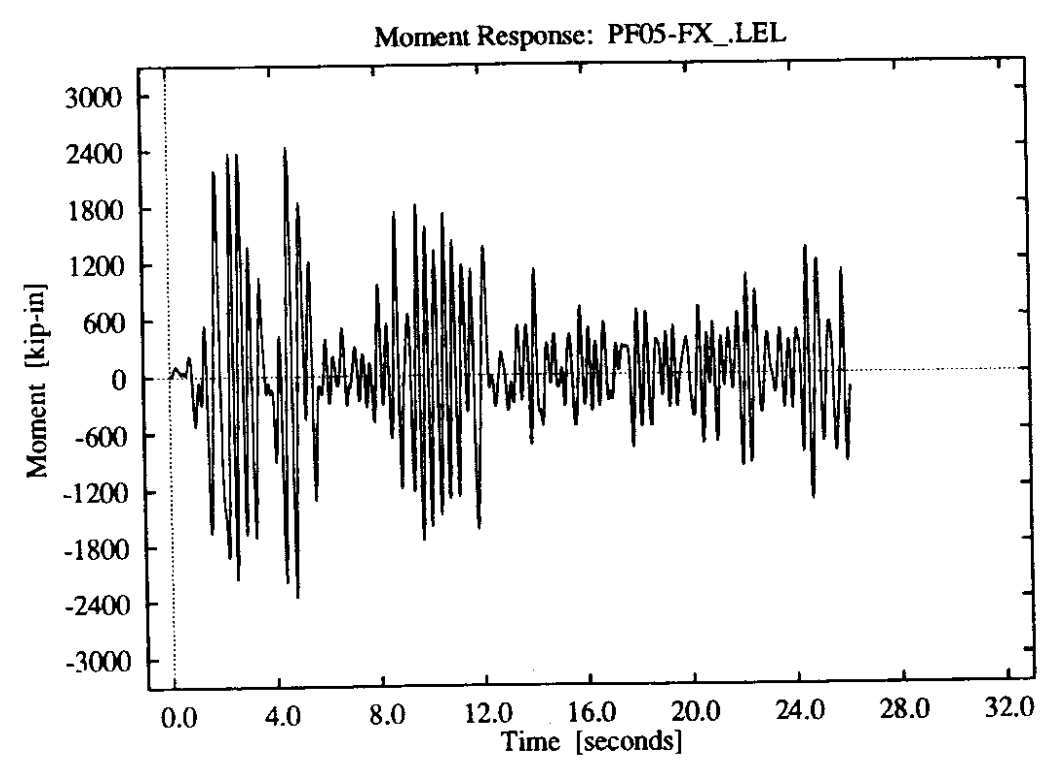
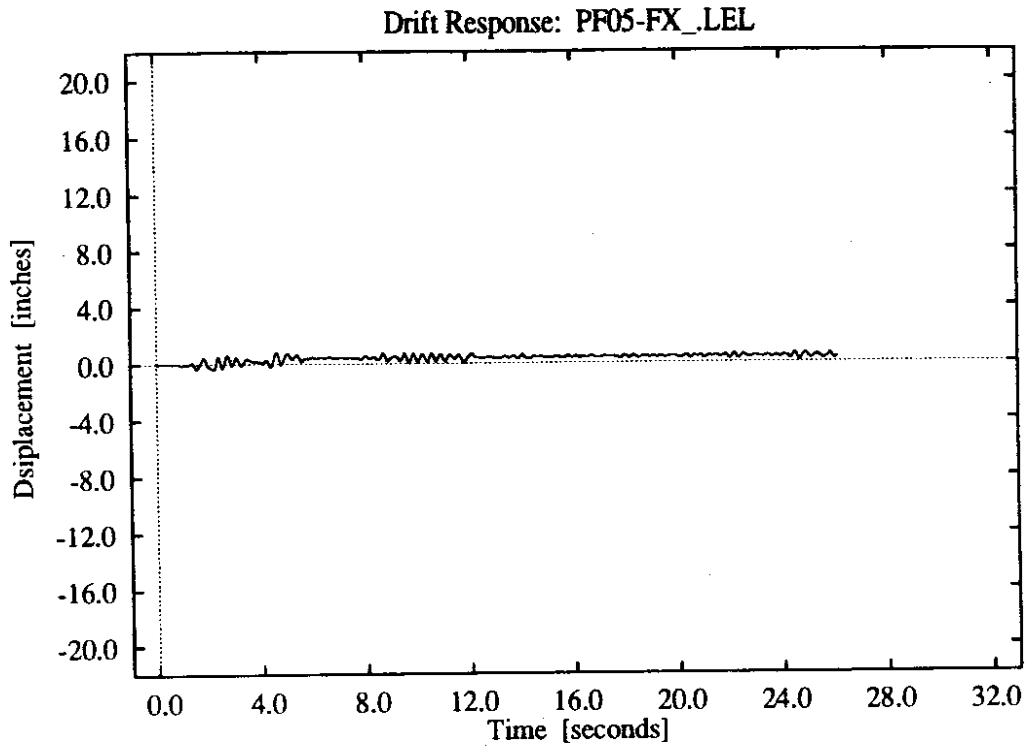


**Figure E-5: Fixed-base foundation, lower intensity El Centro record.**

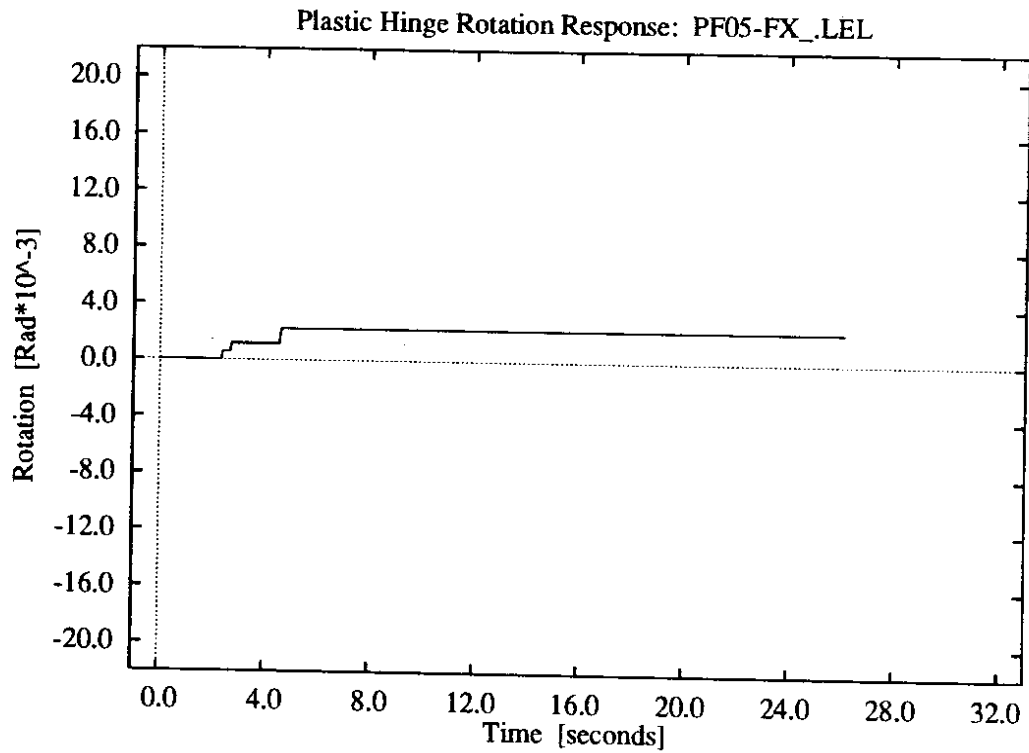
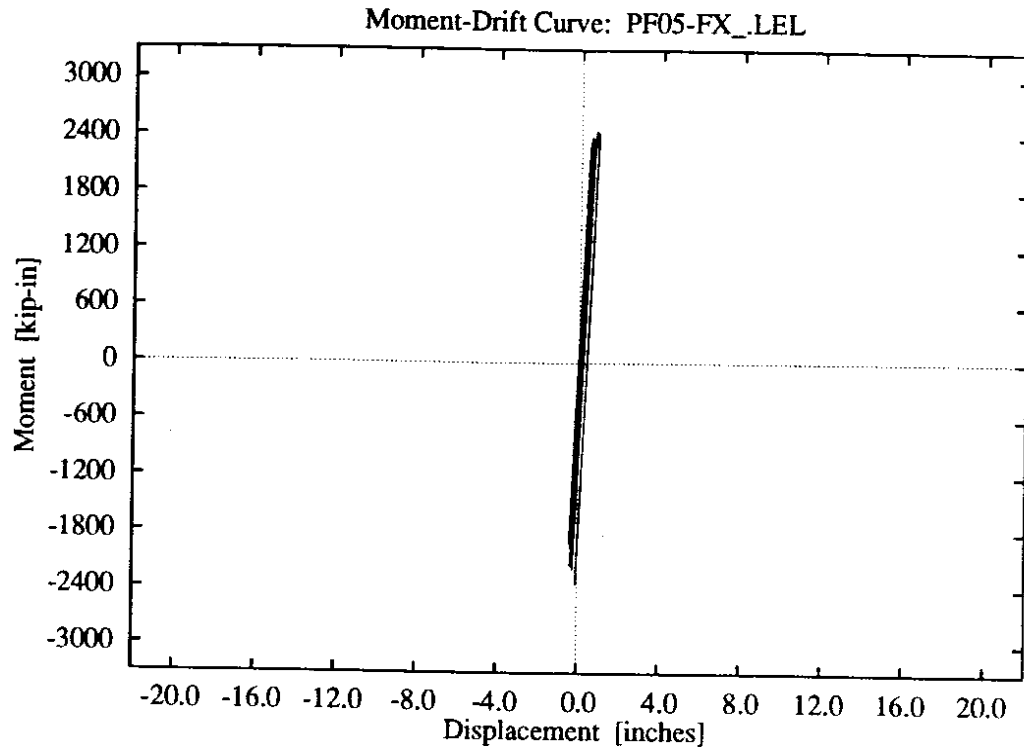


**Figure E-6:** Fixed-base foundation, lower intensity El Centro record.

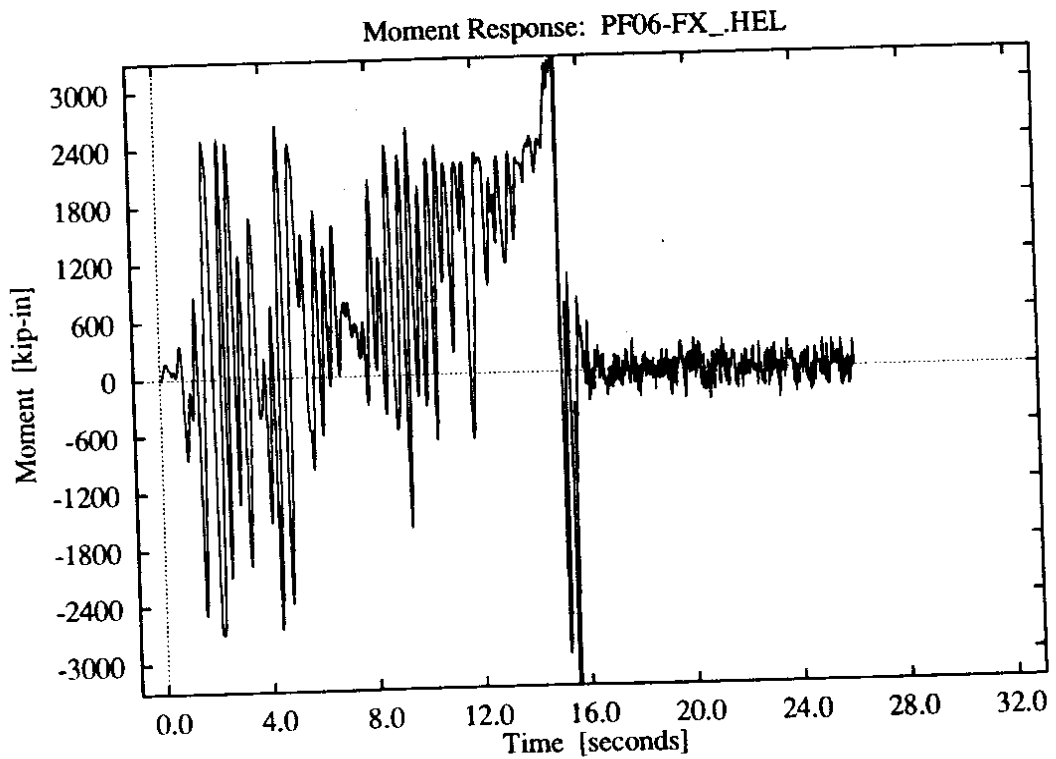
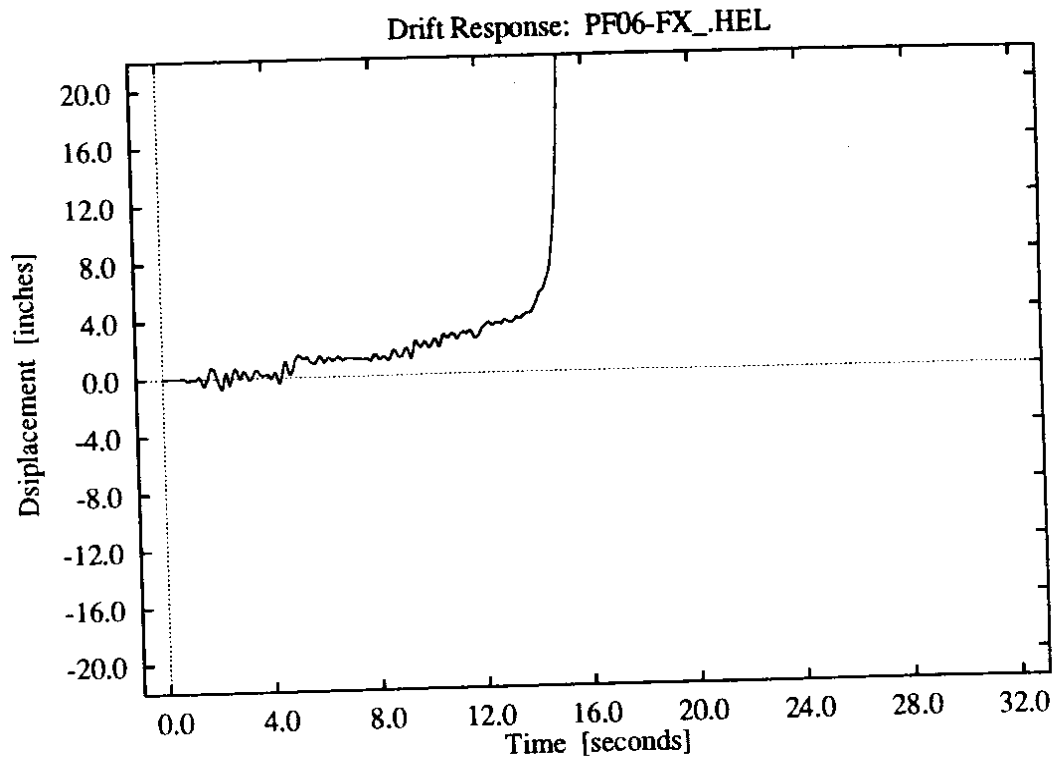


**Figure E-7:** Fixed-base foundation, higher intensity El Centro record.

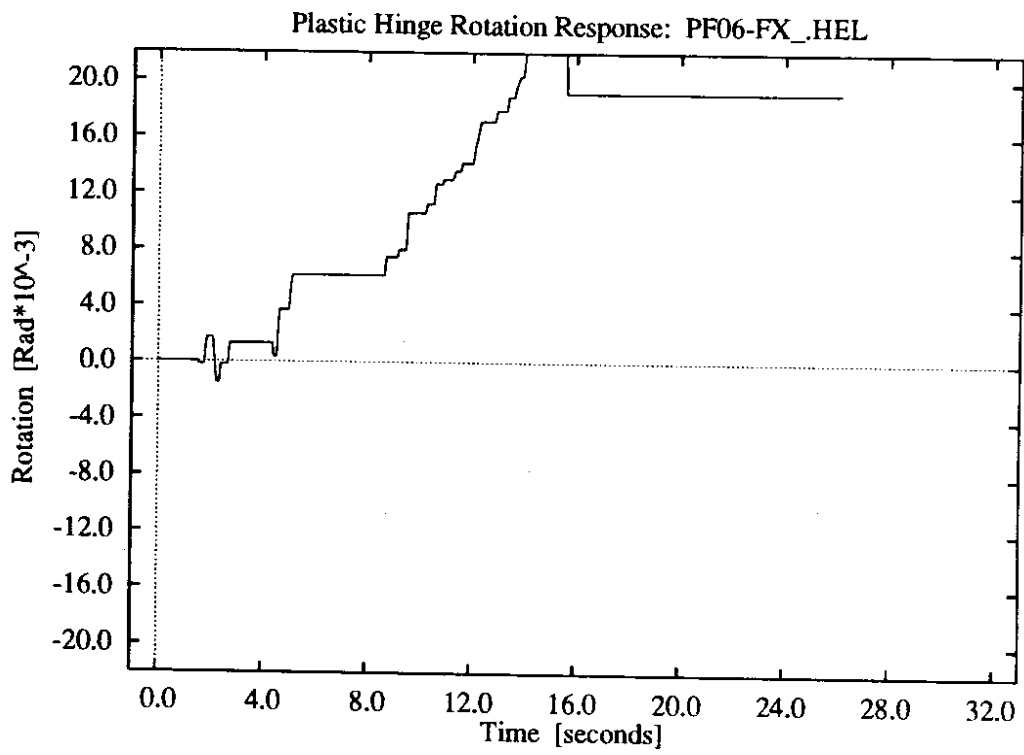
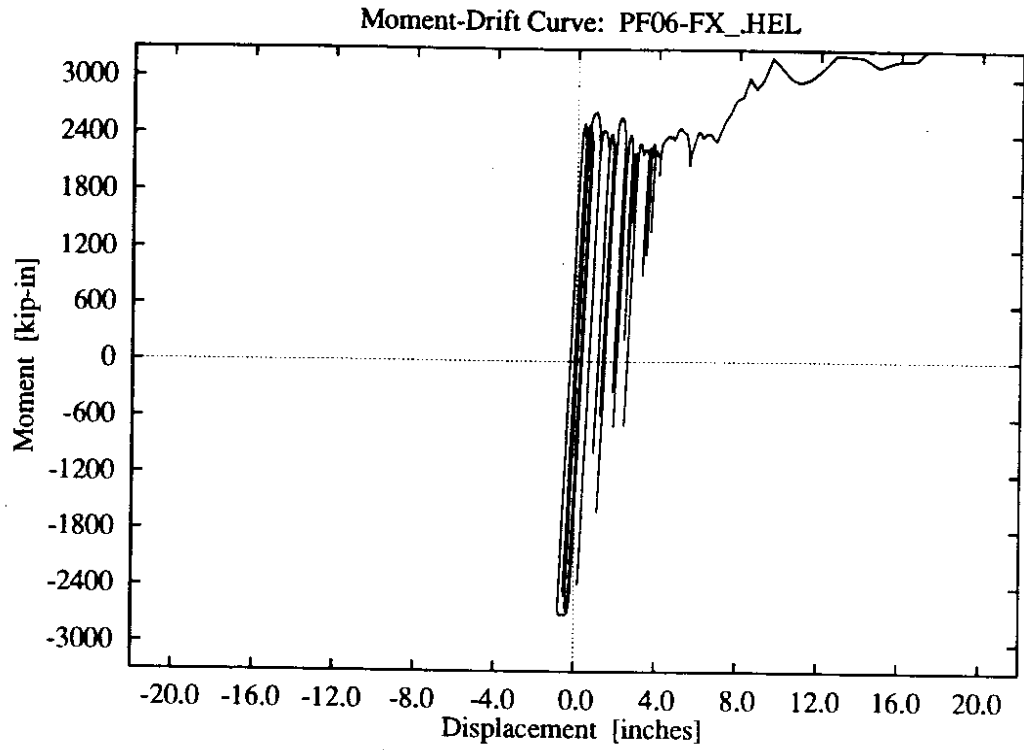


**Figure E-8:** Fixed-base foundation, higher intensity El Centro record.

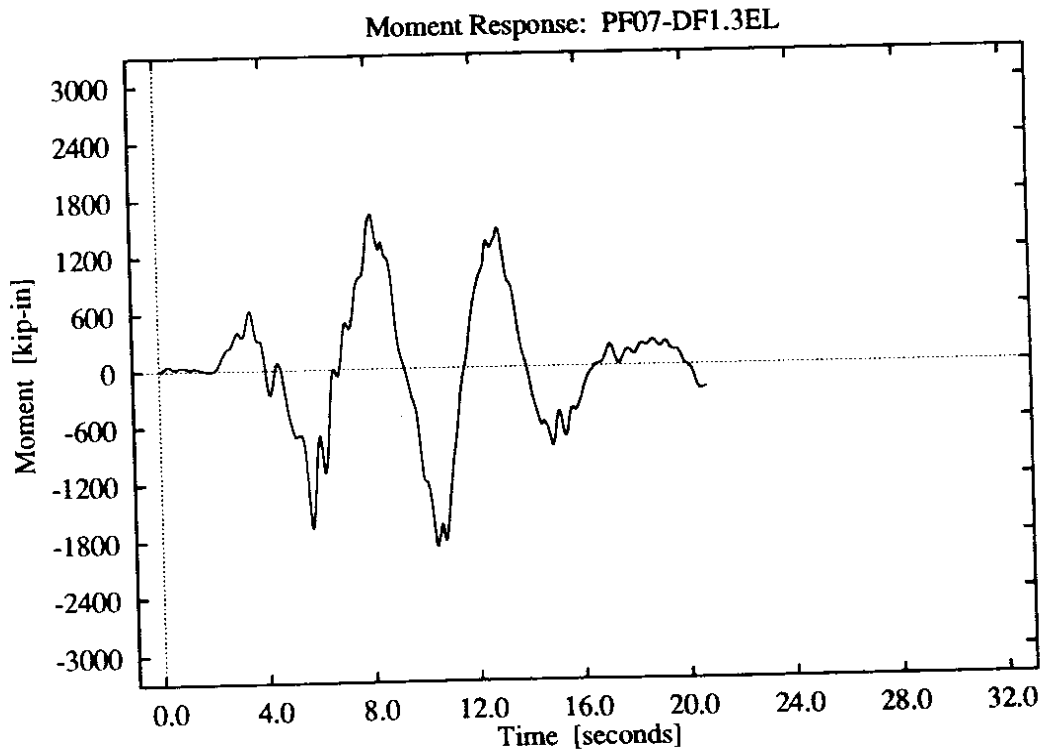
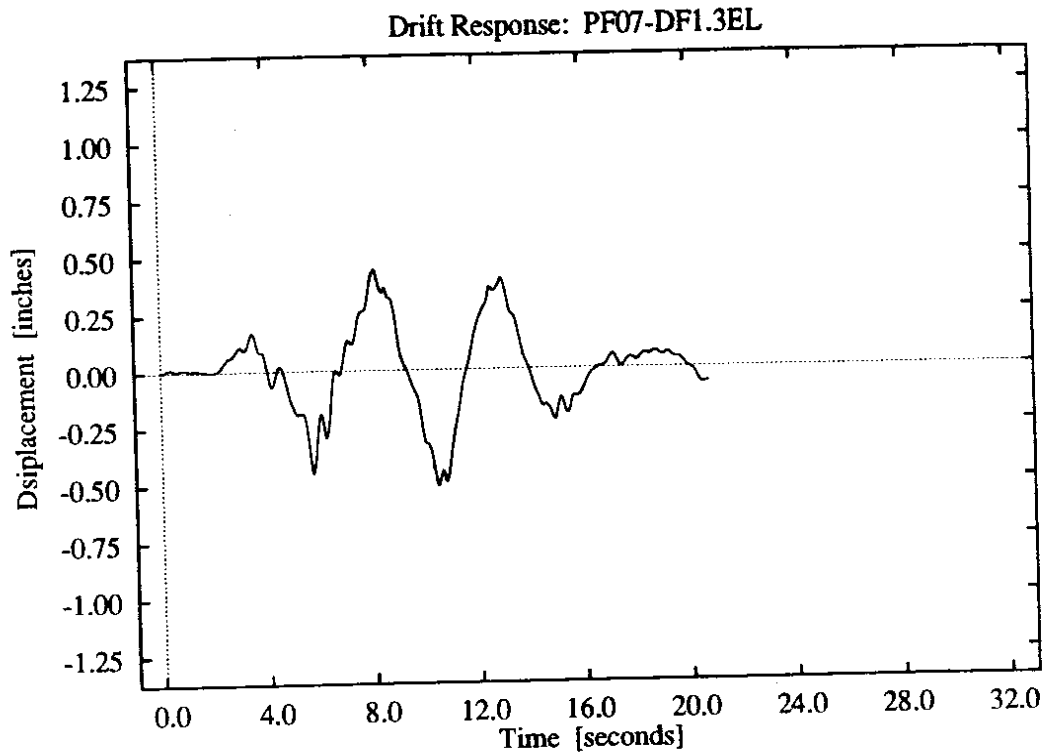


**Figure E-9: DF1 foundation model, El Centro Z3 record.**

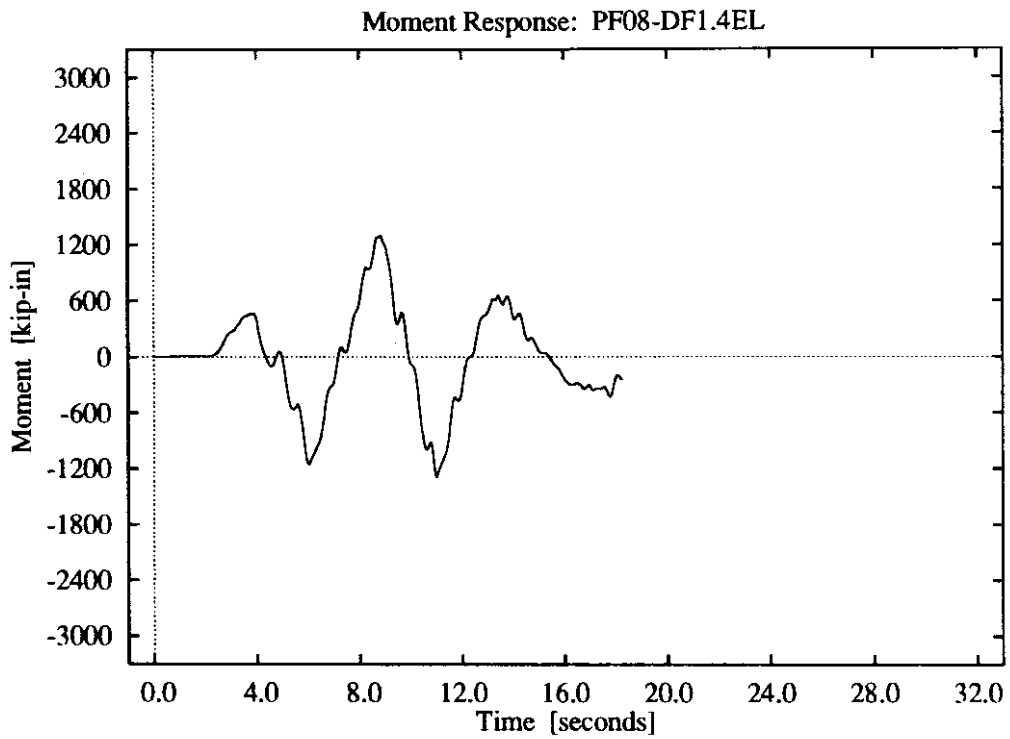
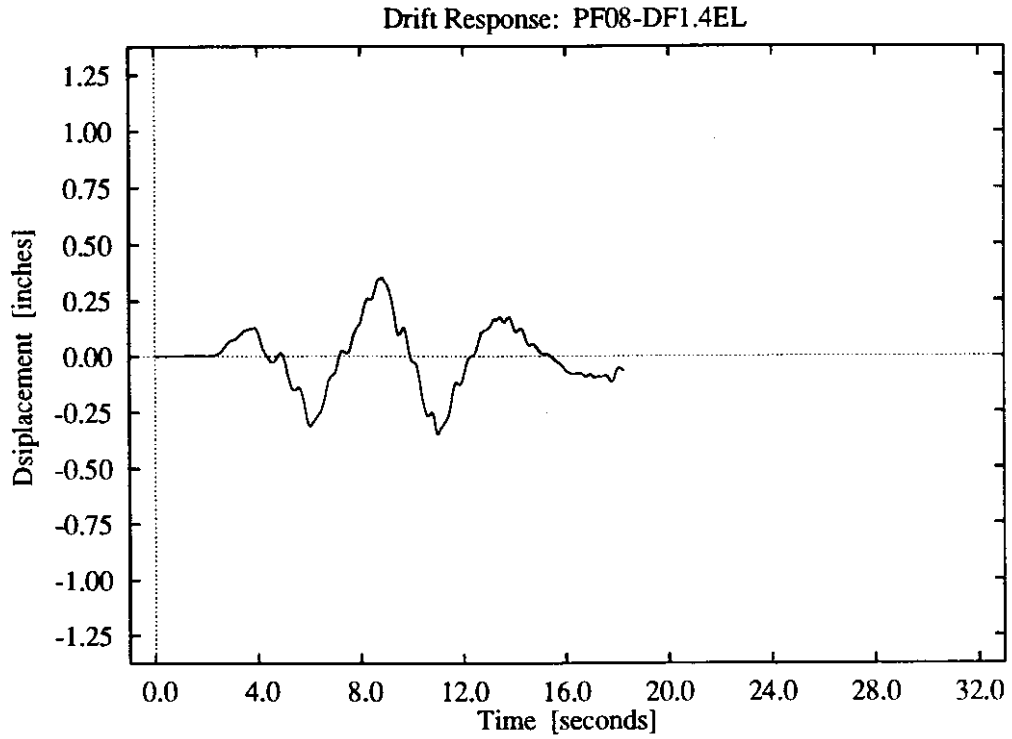


**Figure E-10:** DF1 foundation model, El Centro Z4 record.

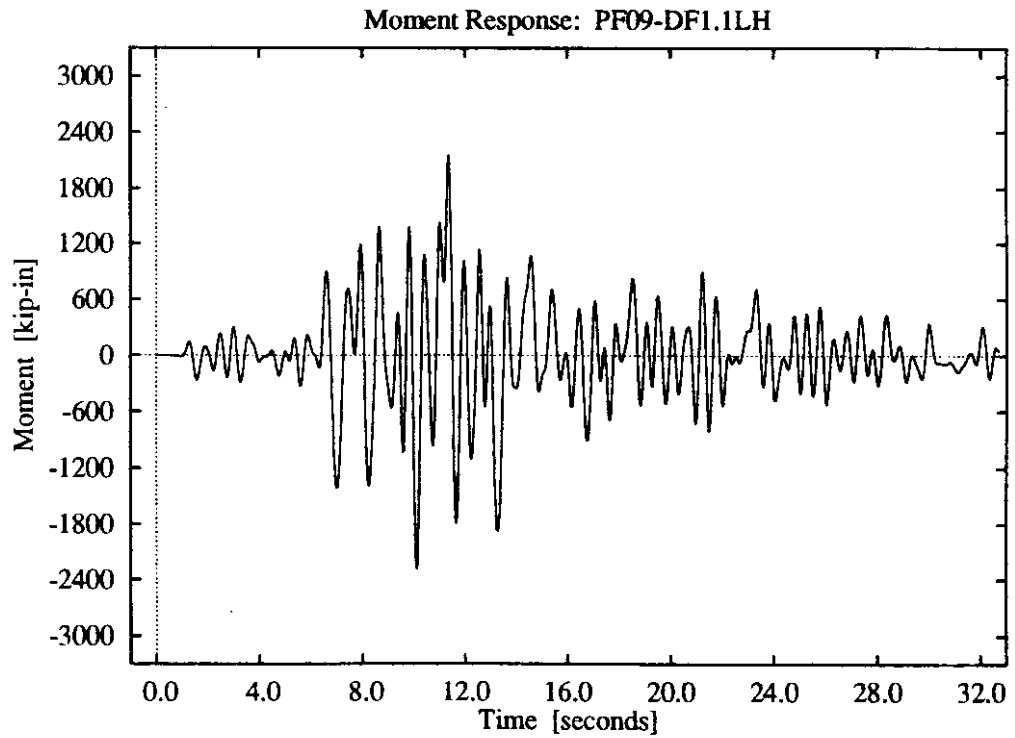
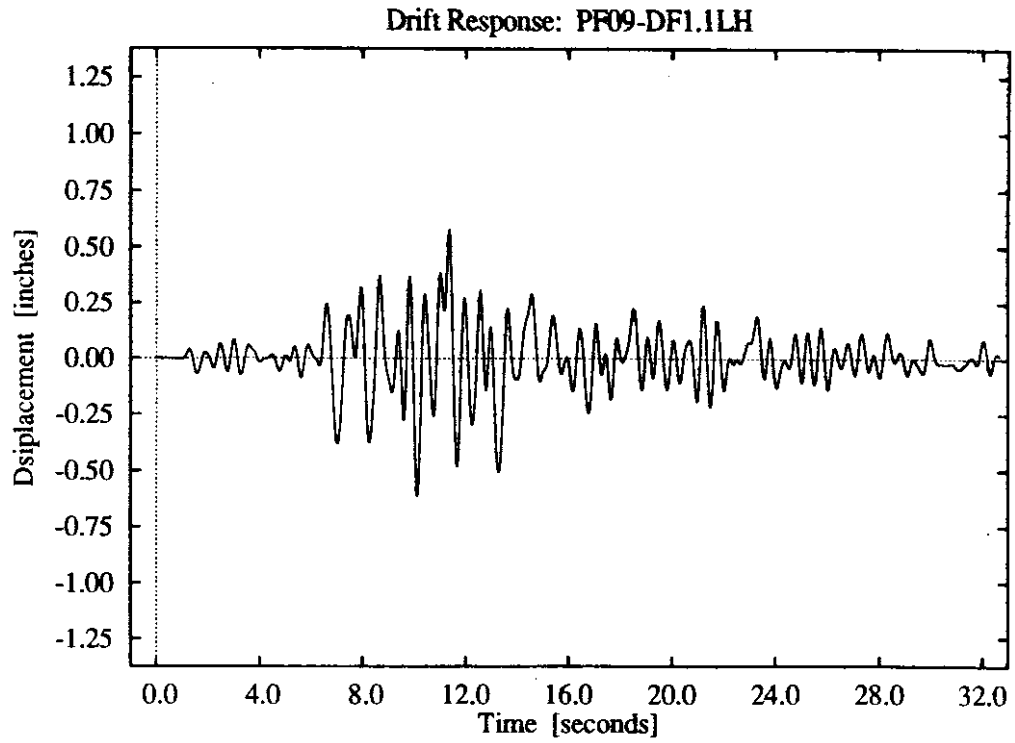


**Figure E-11: DF1 foundation model, Lake Hughes Z1 record.**

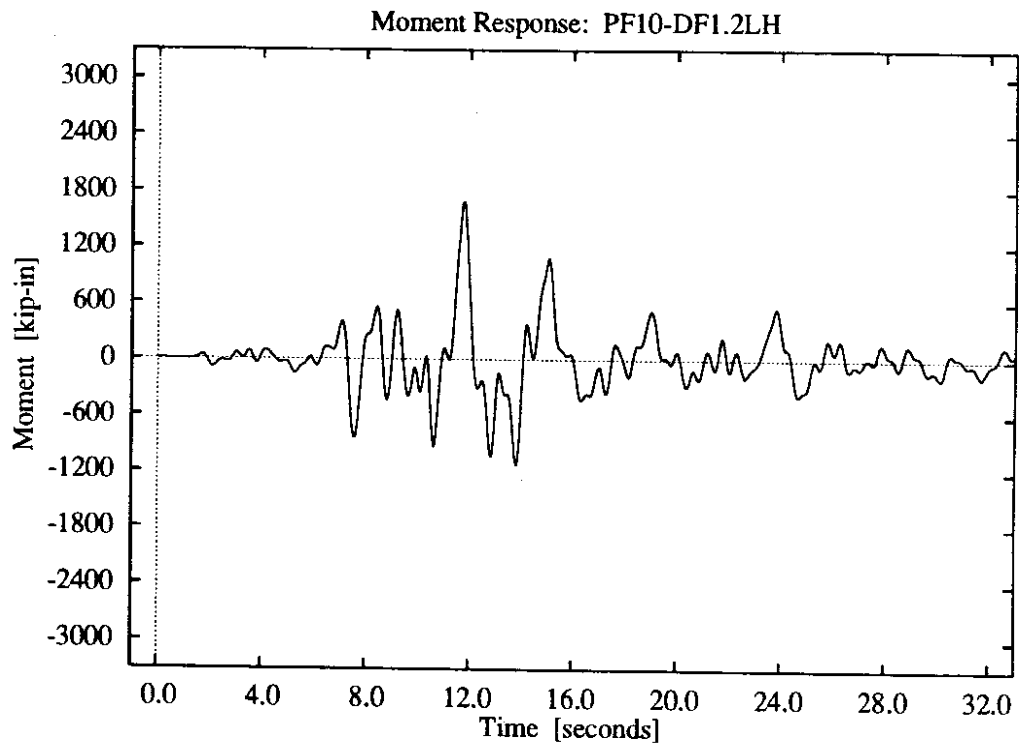
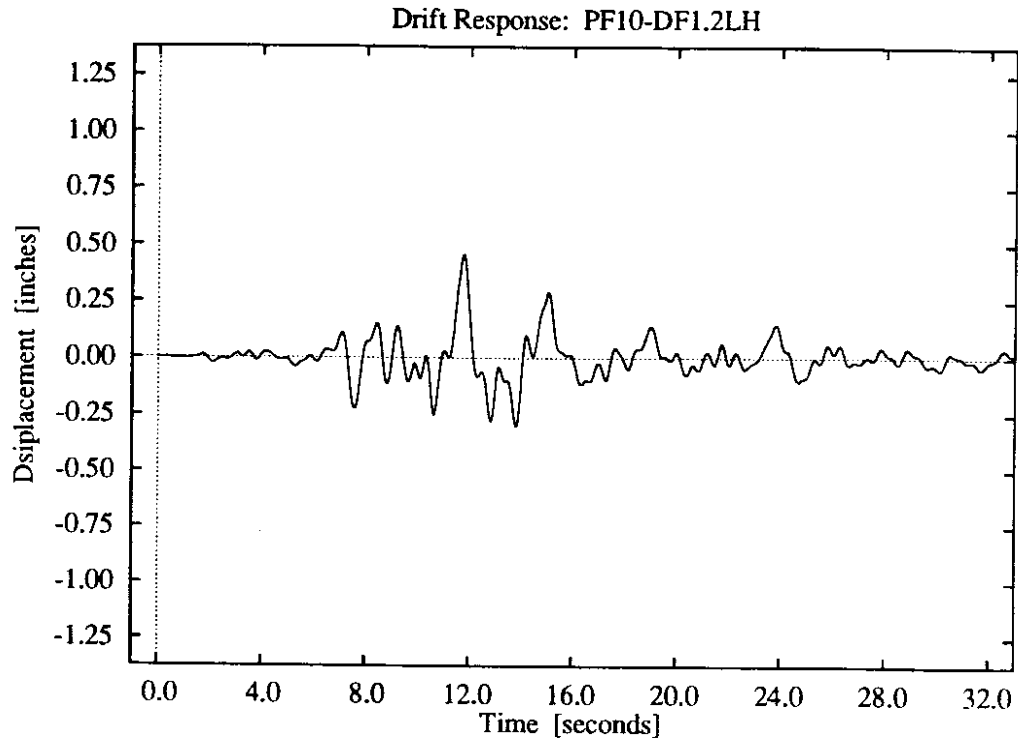


**Figure E-12:** DF1 foundation model, Lake Hughes Z2 record.



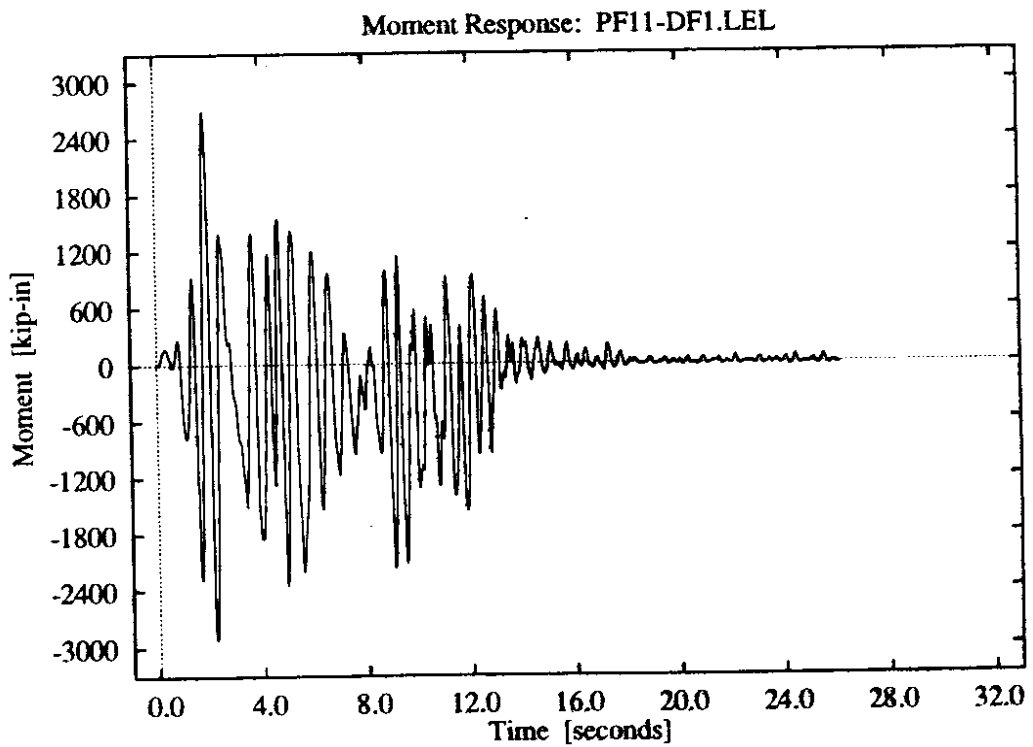
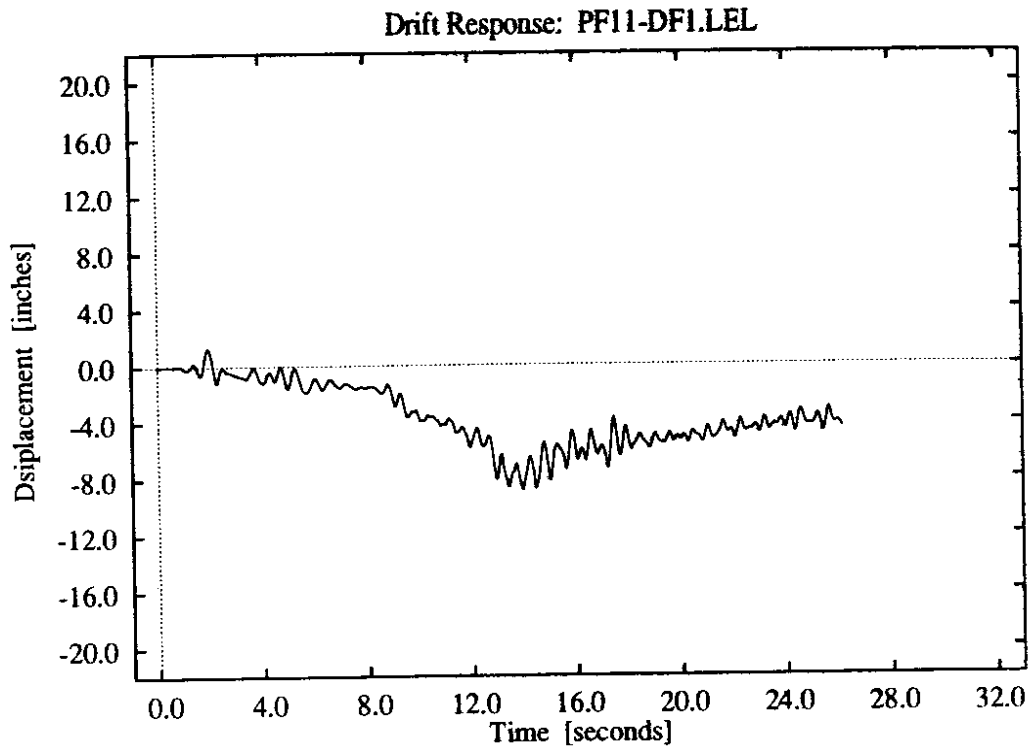


**Figure E-13:** DF1 foundation model, lower intensity El Centro record.

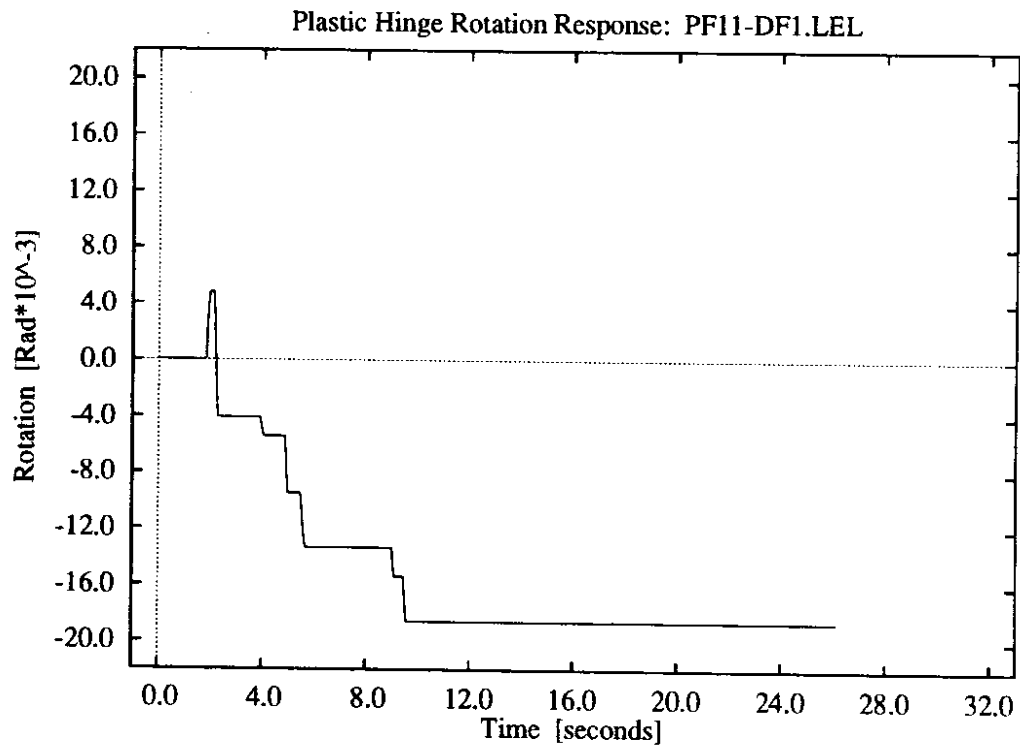
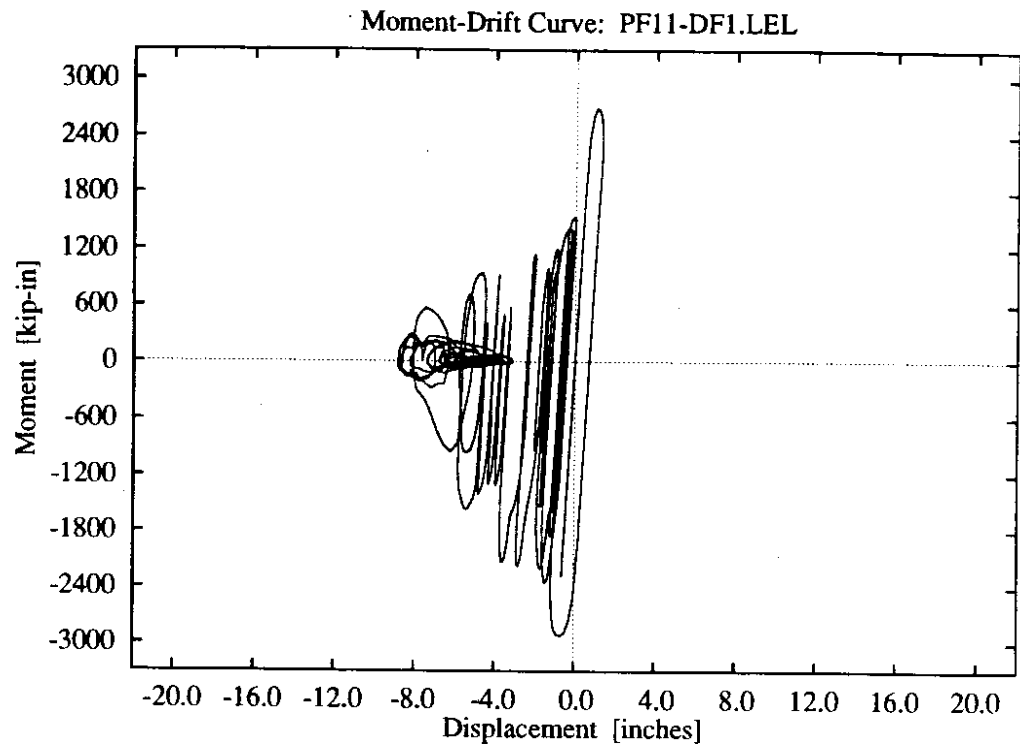


**Figure E-14:** DF1 foundation model, lower intensity El Centro record.

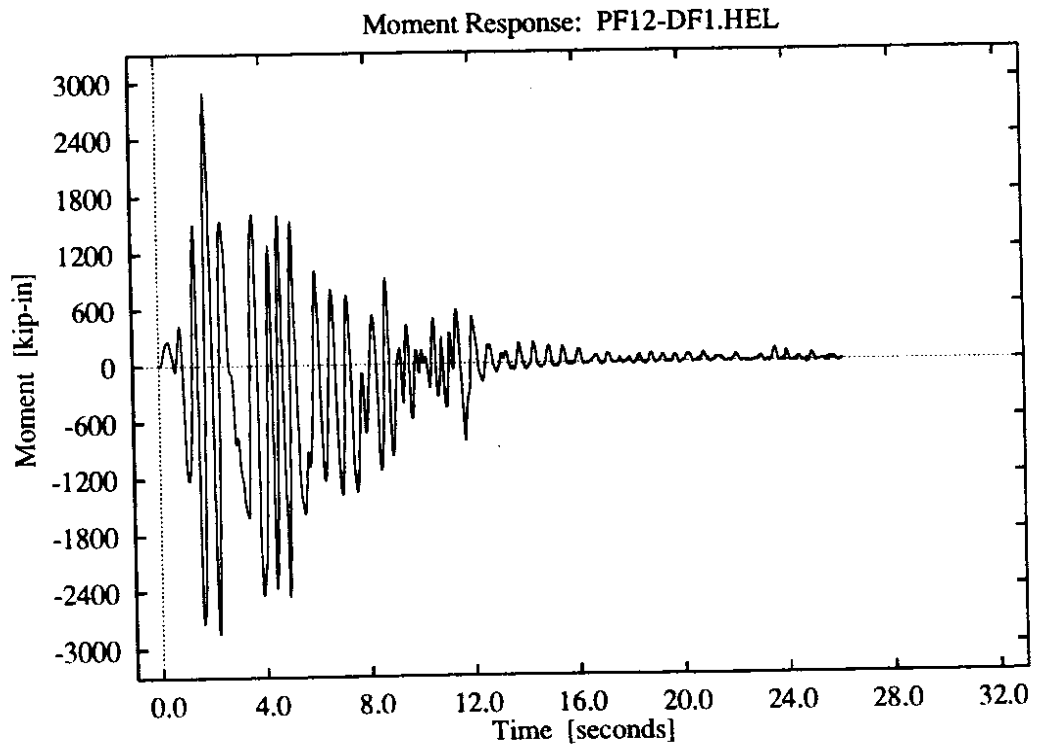
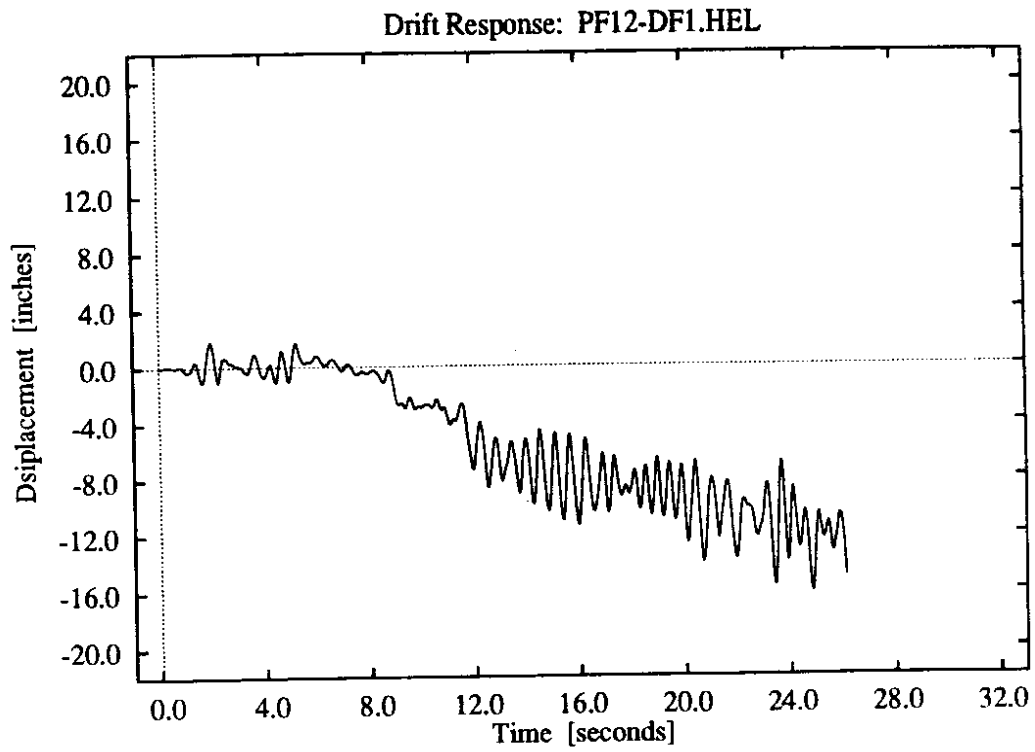


**Figure E-15:** DF1 foundation model, higher intensity El Centro record.

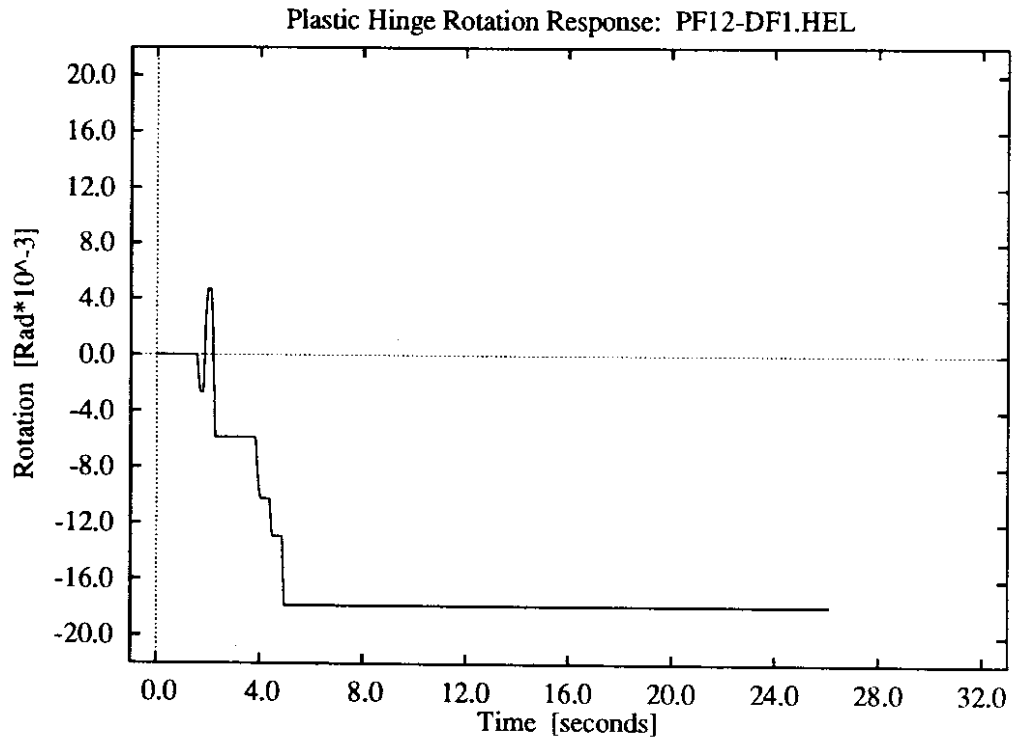
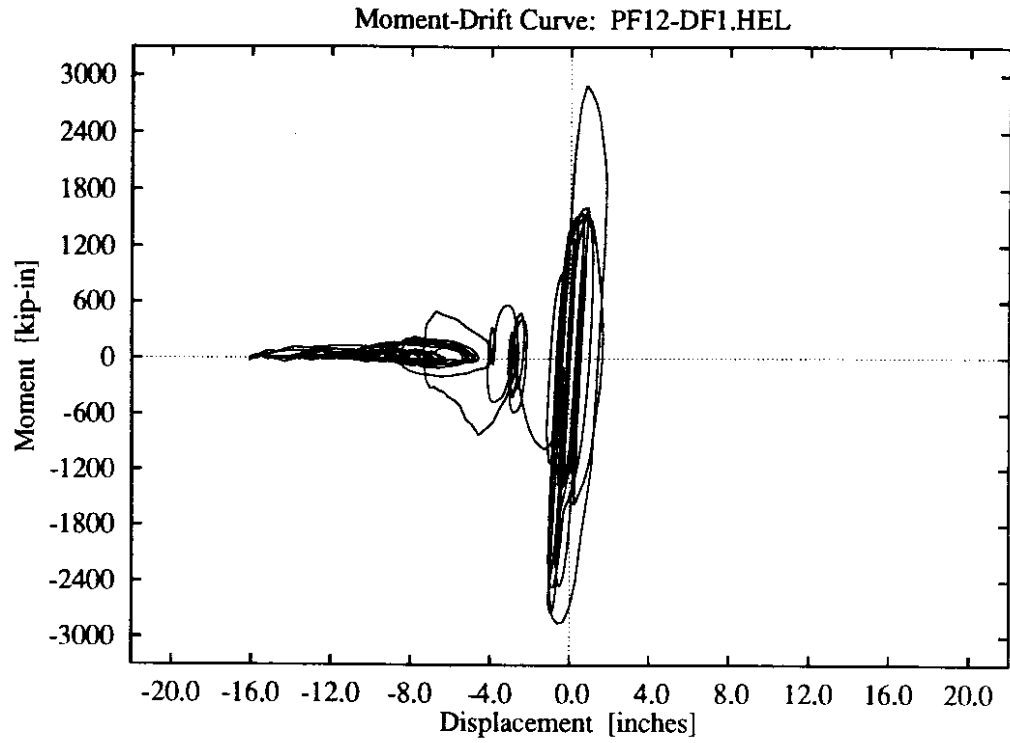


**Figure E-16:** DF1 foundation model, higher intensity El Centro record.

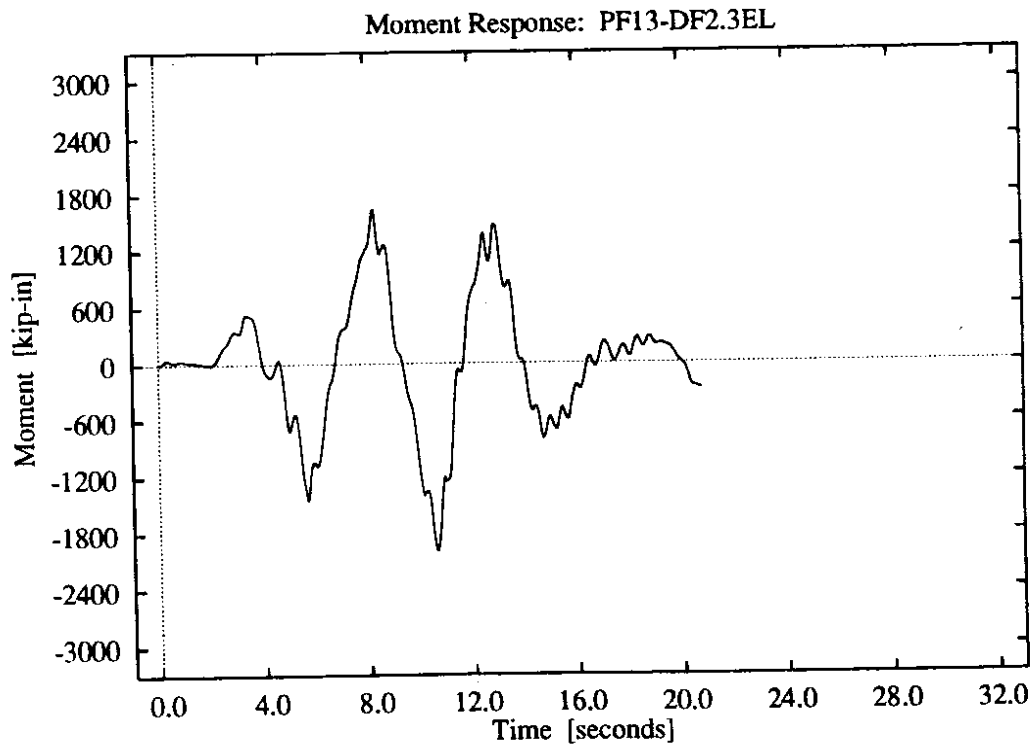
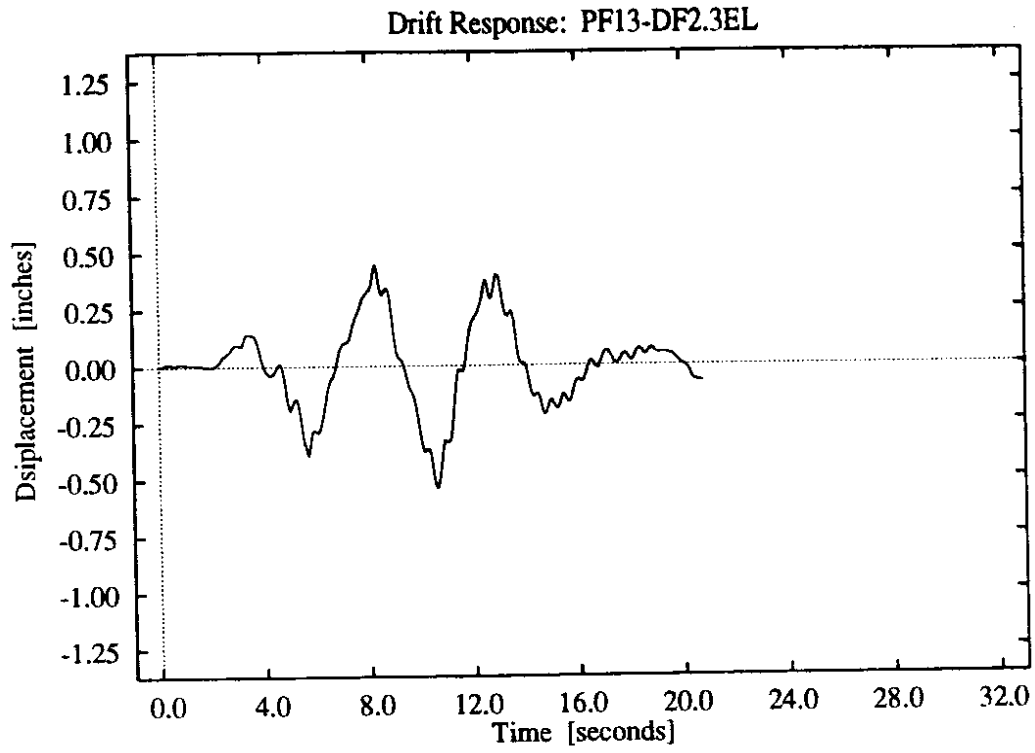


**Figure E-17:** DF2 foundation model, El Centro Z3 record.

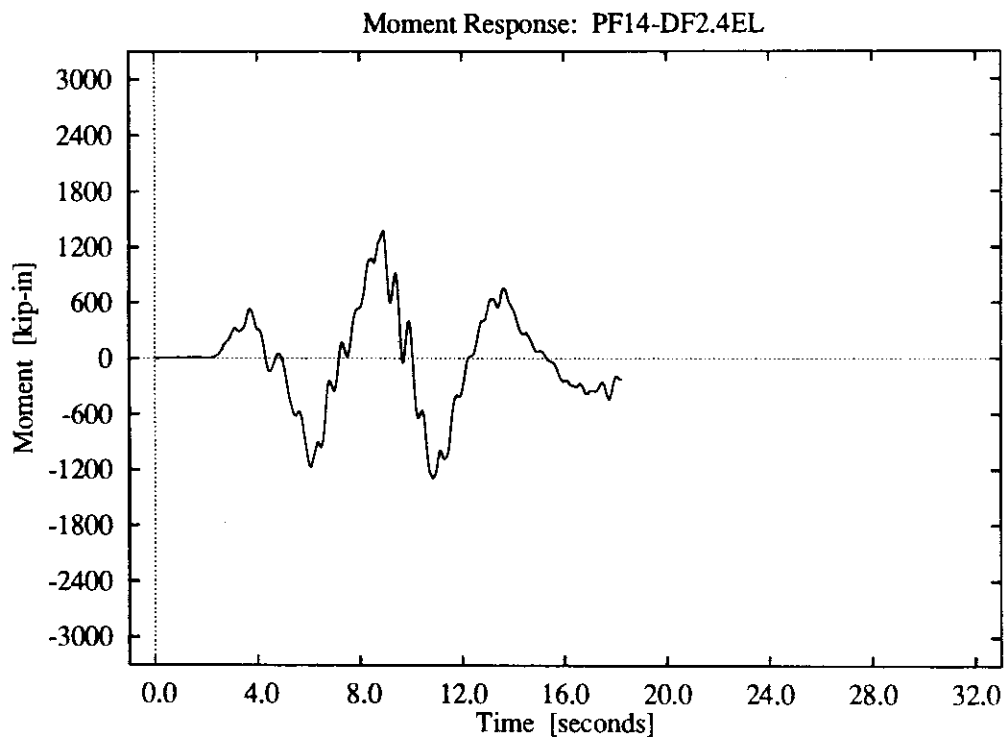
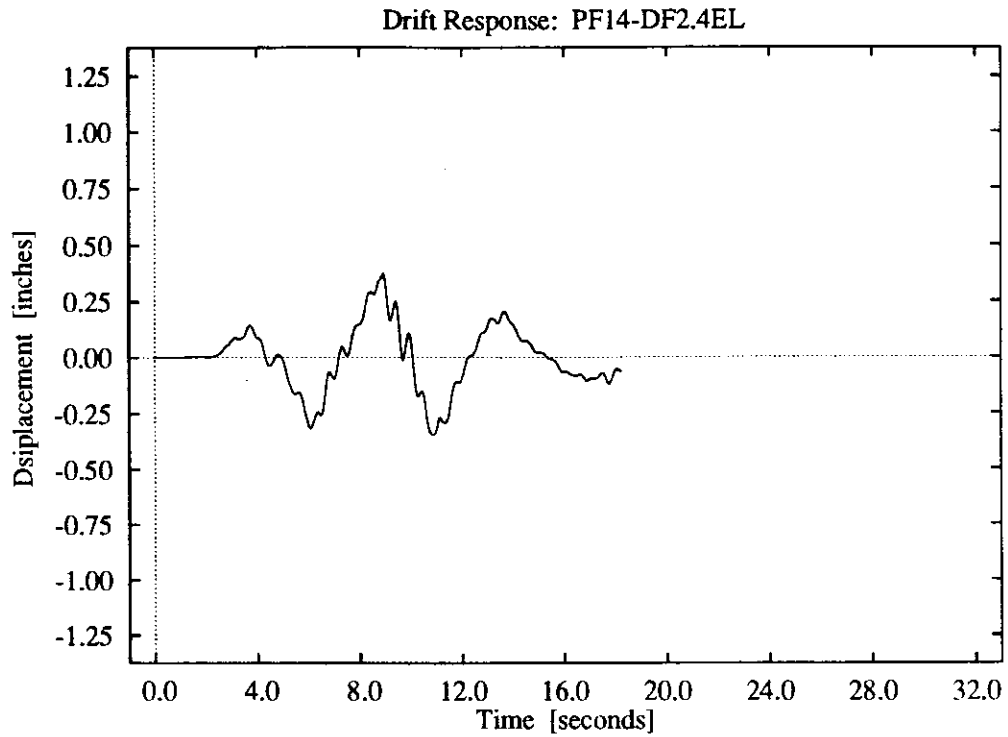


**Figure E-18:** DF2 foundation model, El Centro Z4 record.

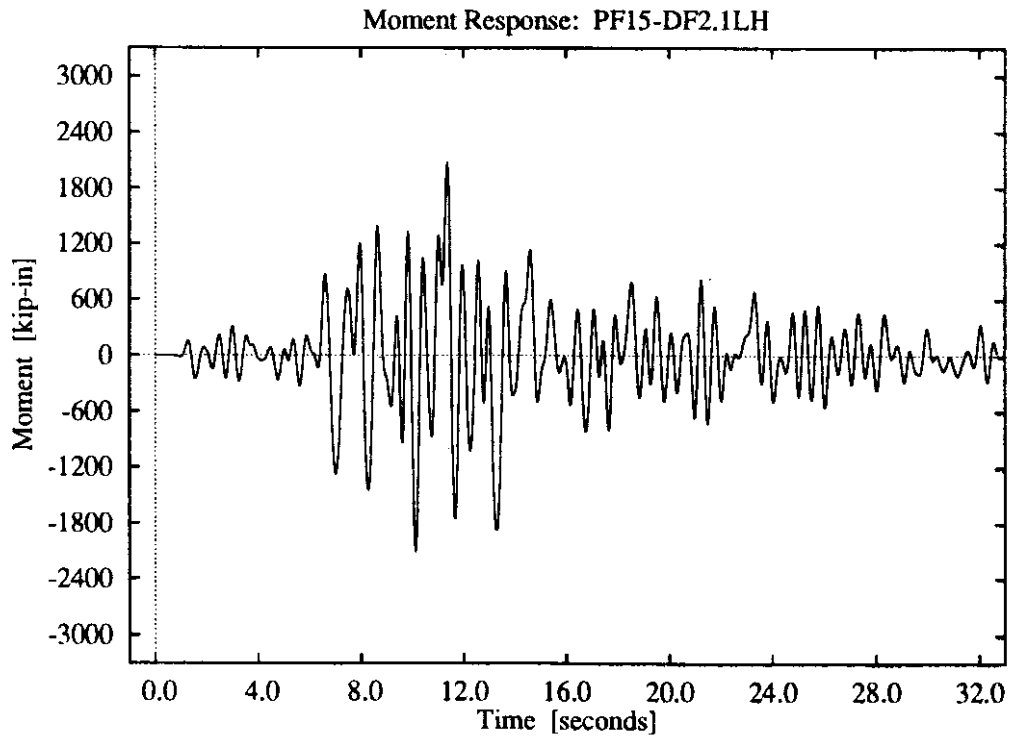
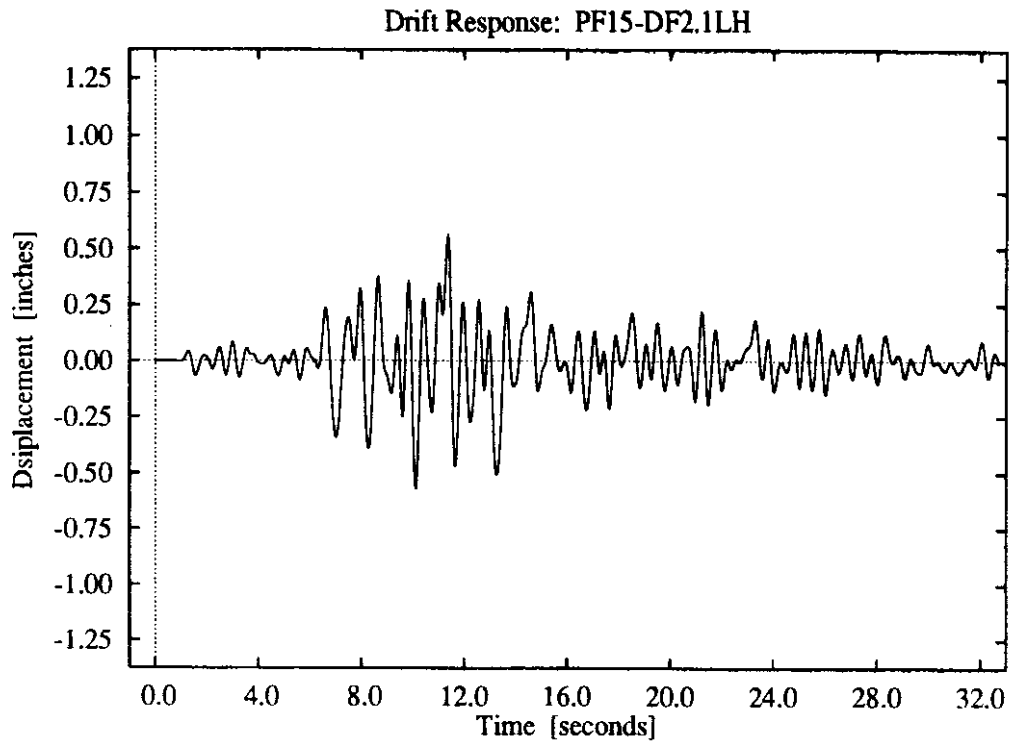


**Figure E-19:** DF2 foundation model, Lake Hughes Z1 record.

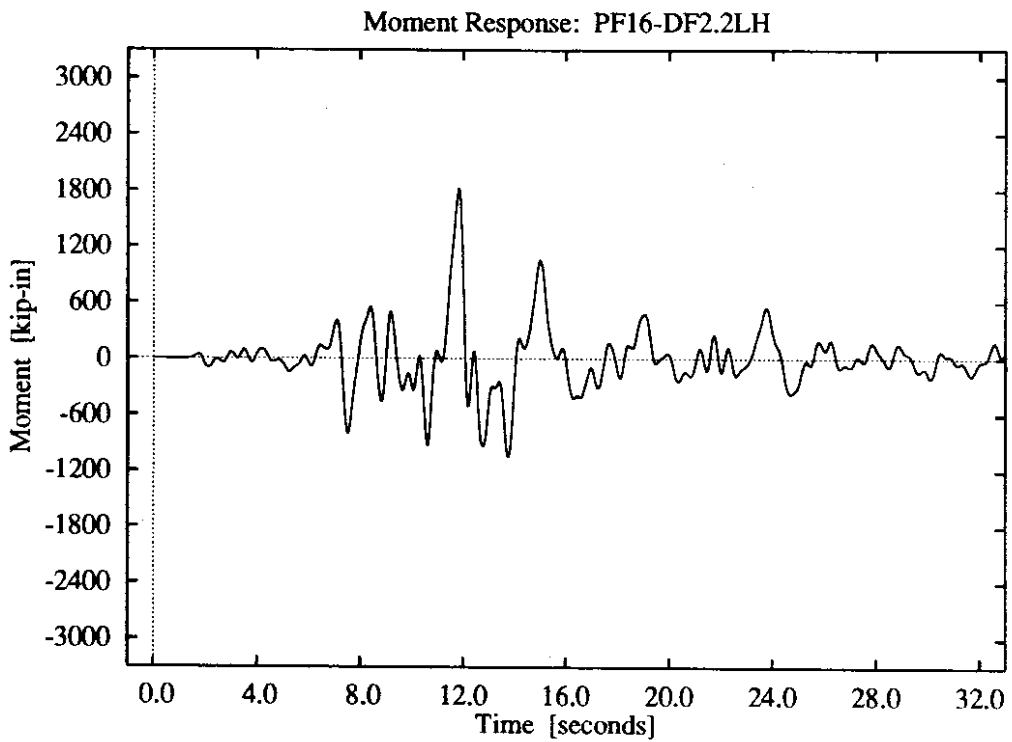
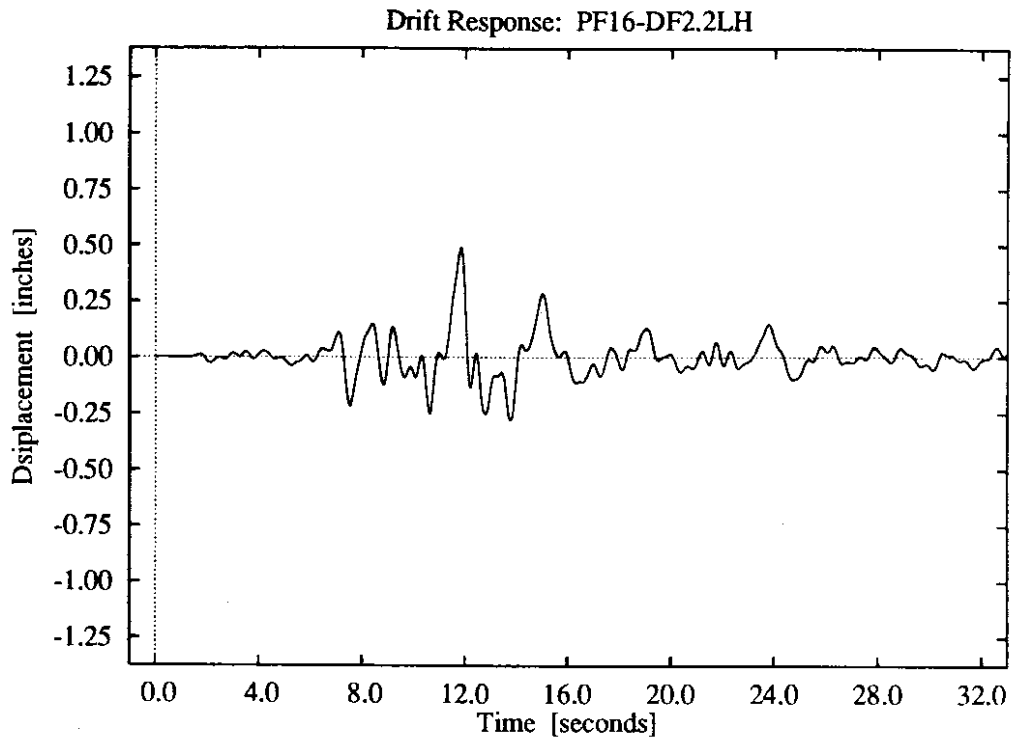


**Figure E-20: DF2 foundation model, Lake Hughes Z2 record.**



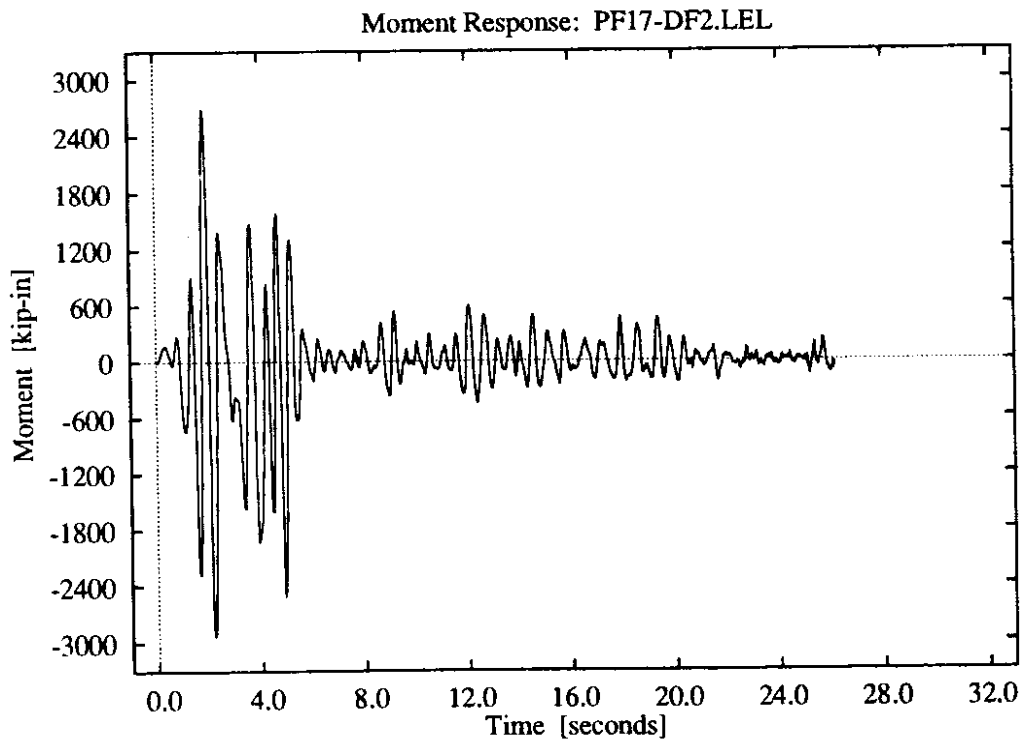
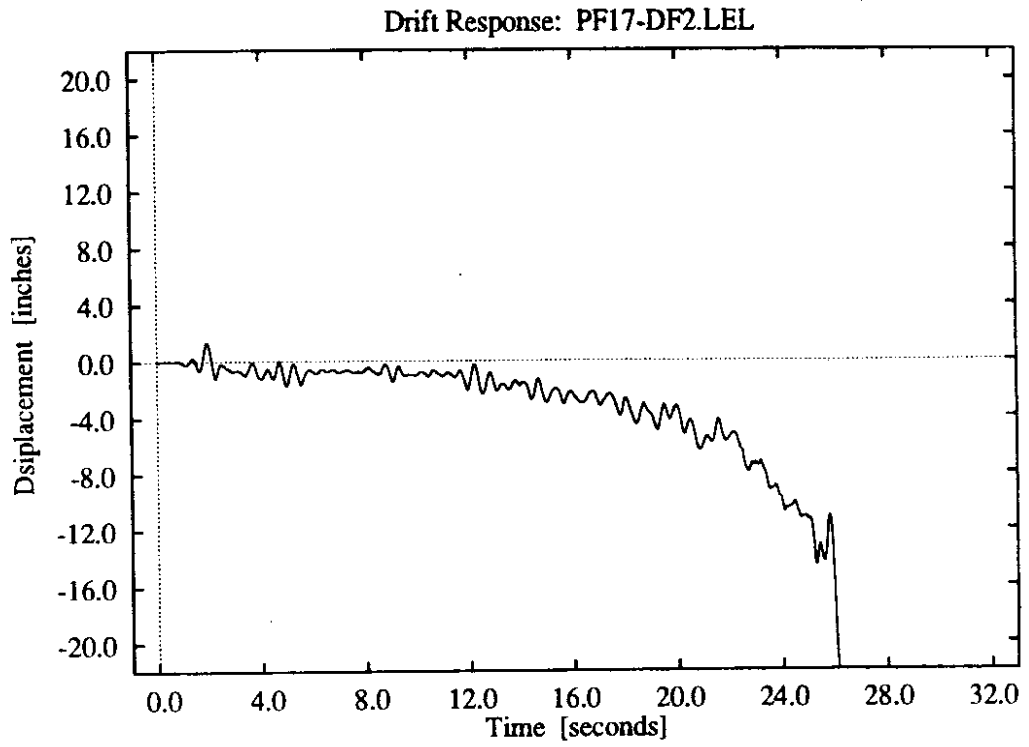


**Figure E-21:** DF2 foundation model, lower intensity El Centro record.

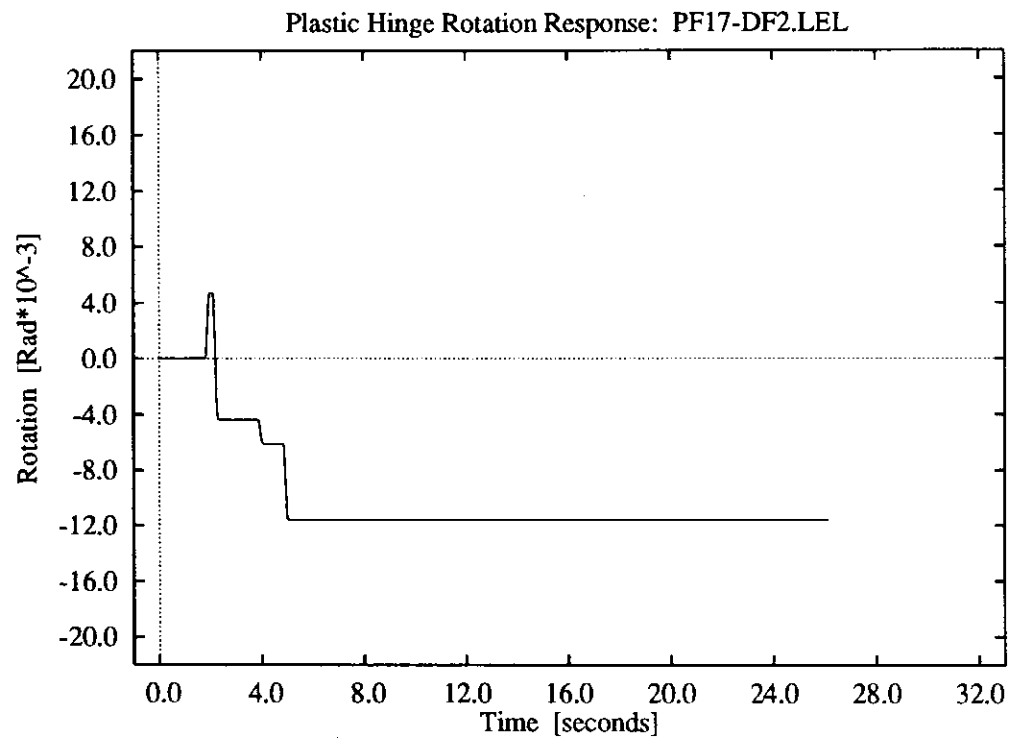
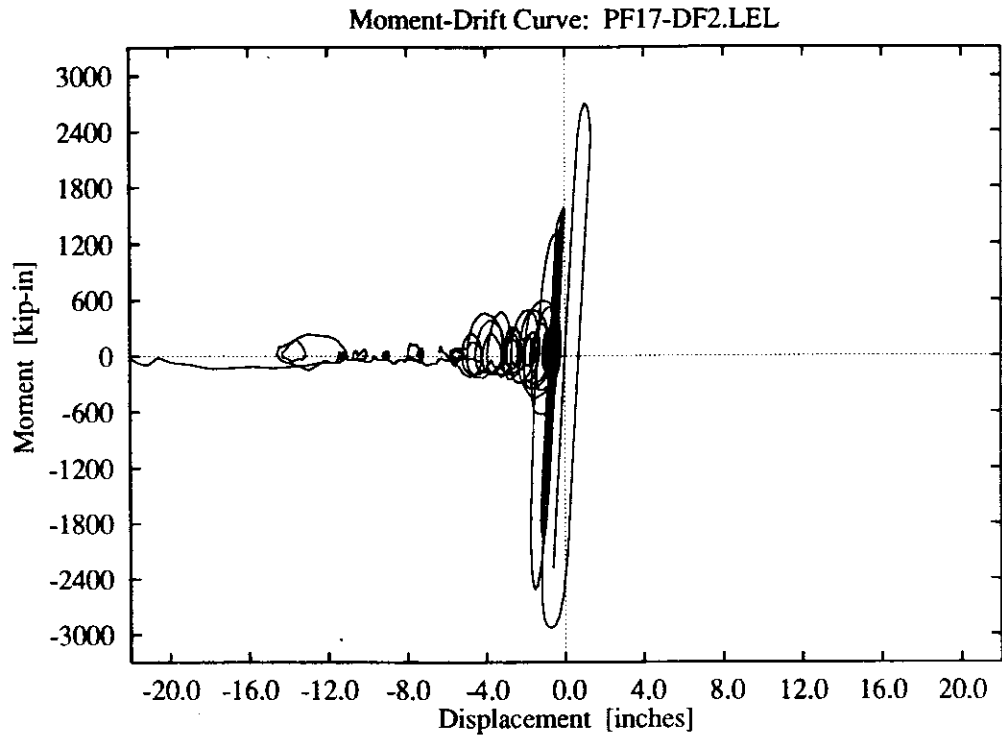


**Figure E-22:** DF2 foundation model, lower intensity El Centro record.

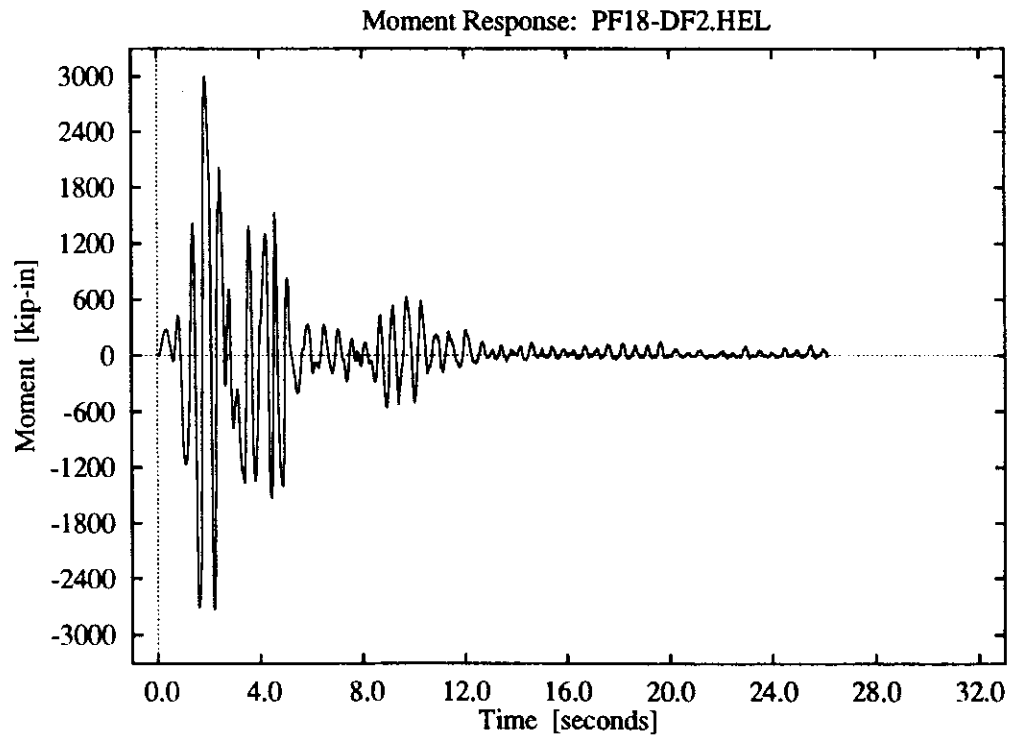
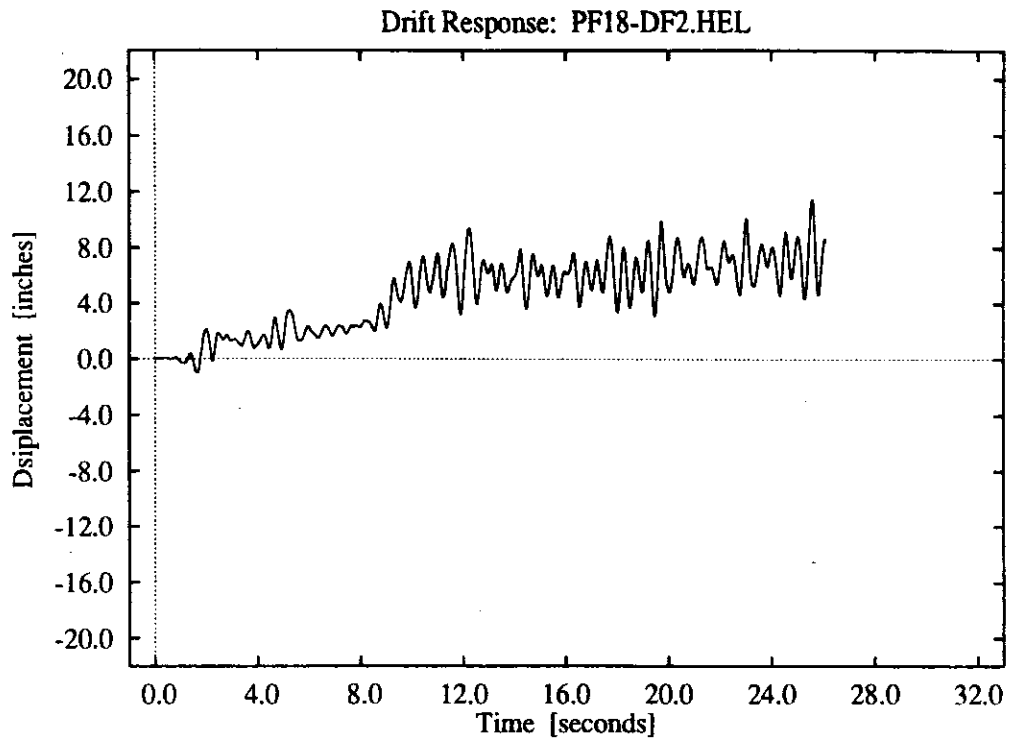


**Figure E-23:** DF2 foundation model, higher intensity El Centro record.

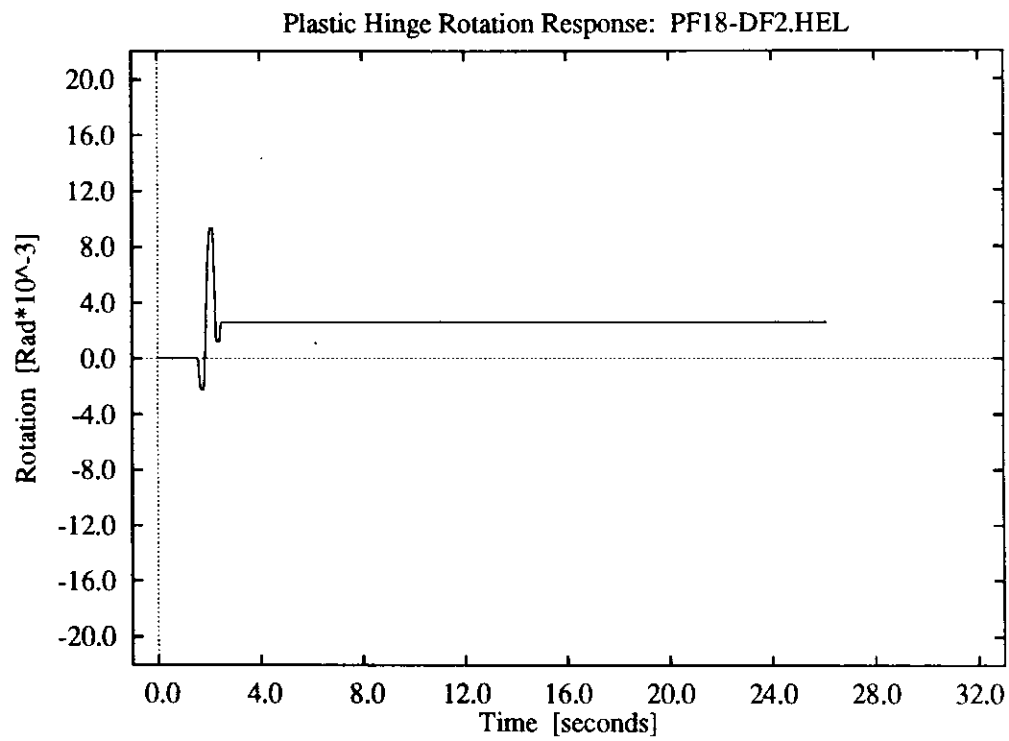
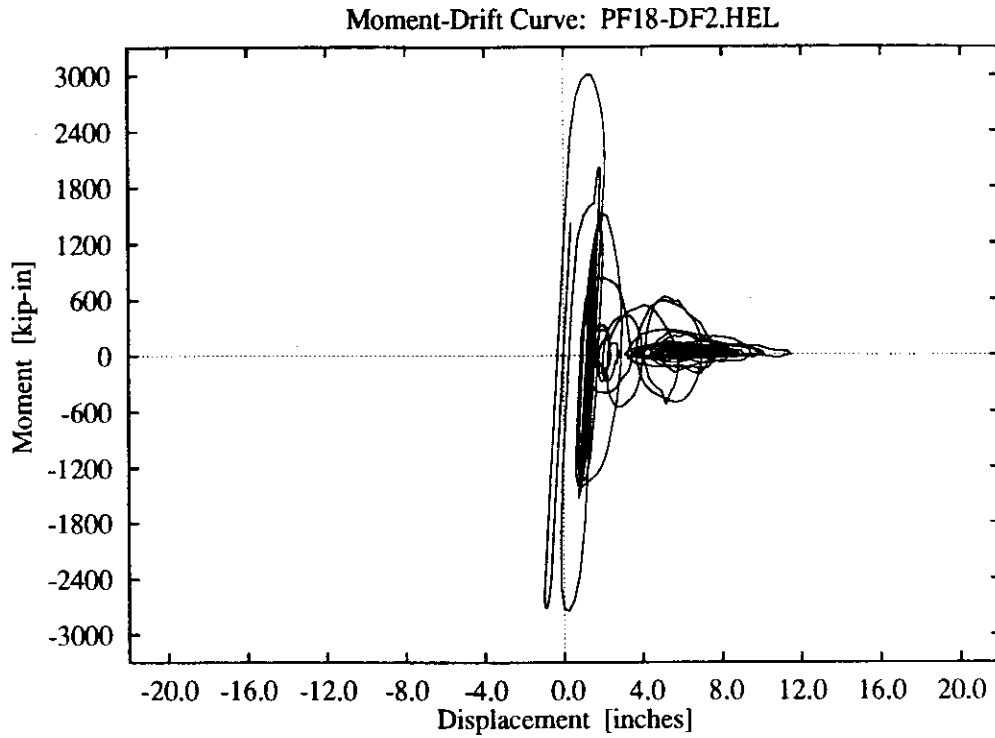


**Figure E-24:** DF2 foundation model, higher intensity El Centro record.

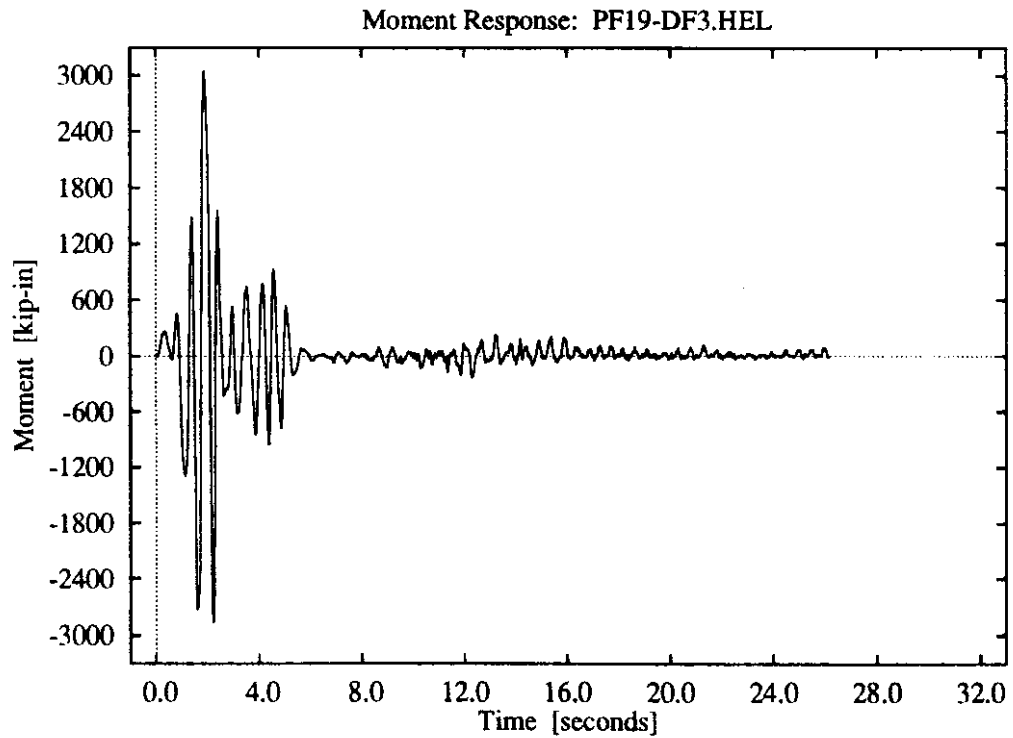
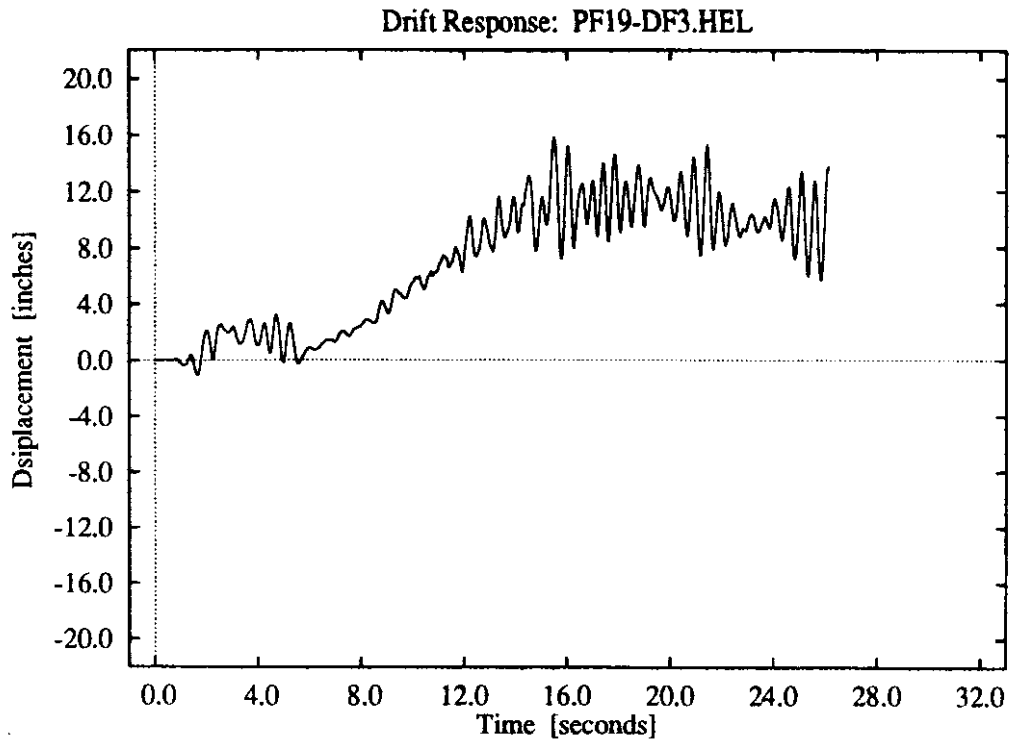


**Figure E-25: DF3 foundation model, higher intensity El Centro record.**

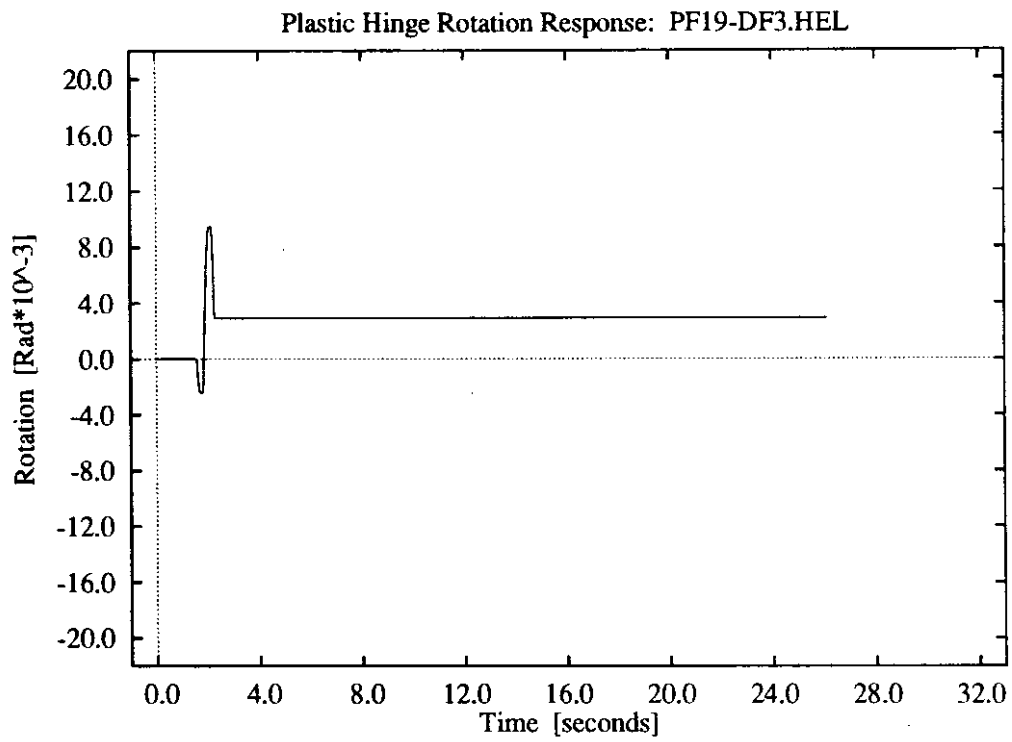
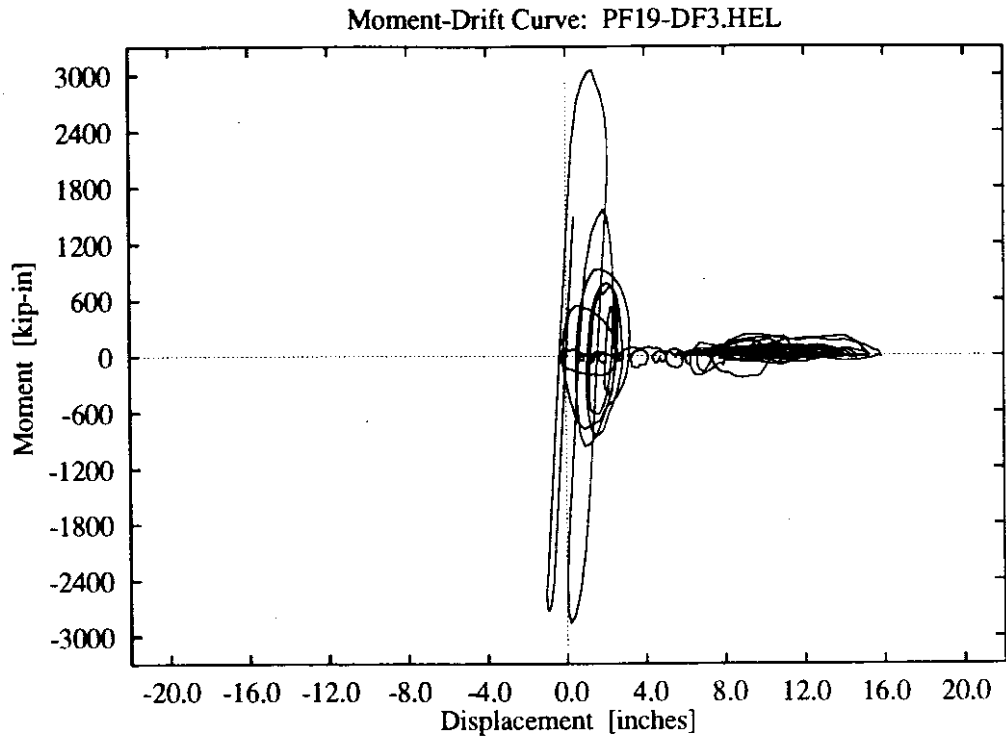


**Figure E-26:** DF3 foundation model, higher intensity El Centro record.

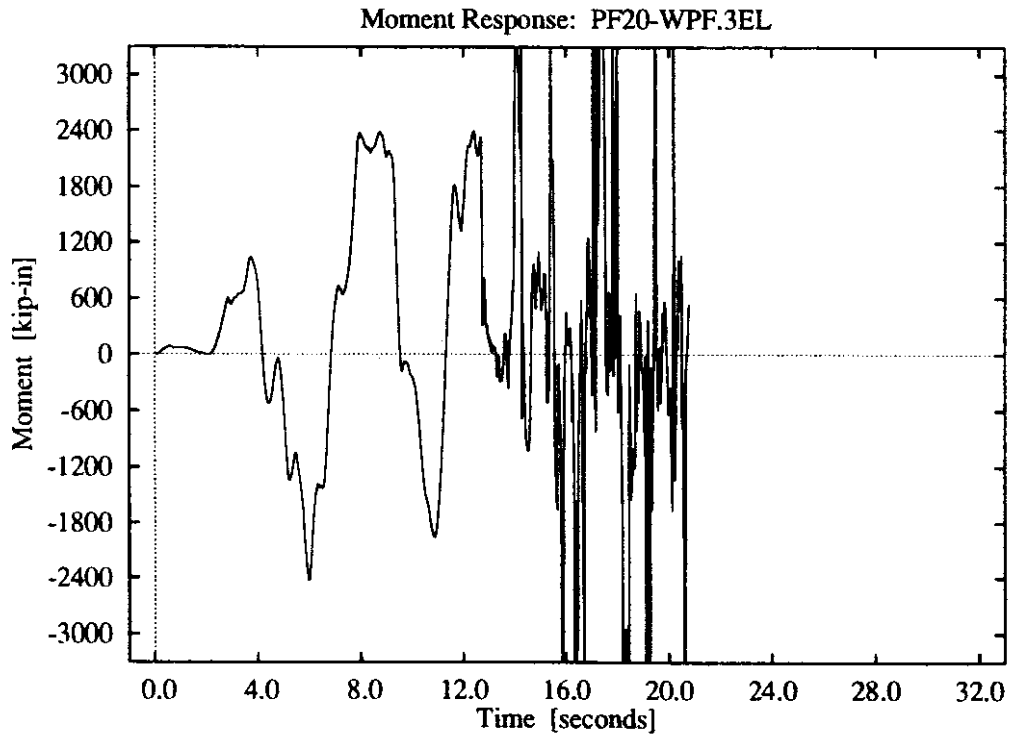
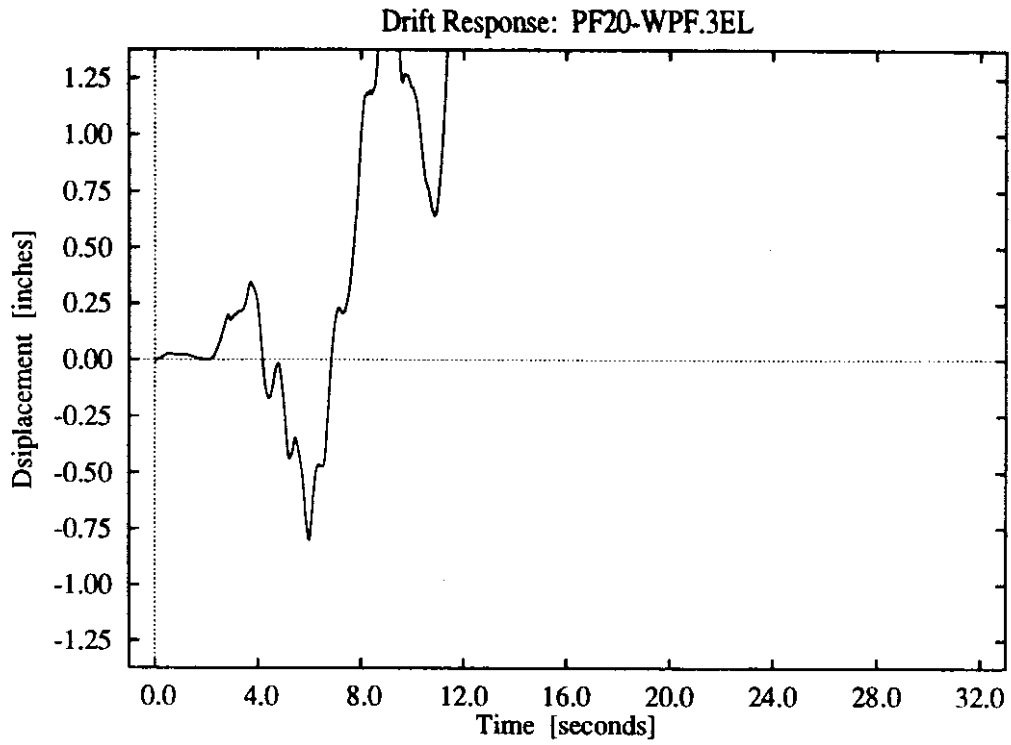


**Figure E-27:** WPF foundation model, El Centro Z3 record.

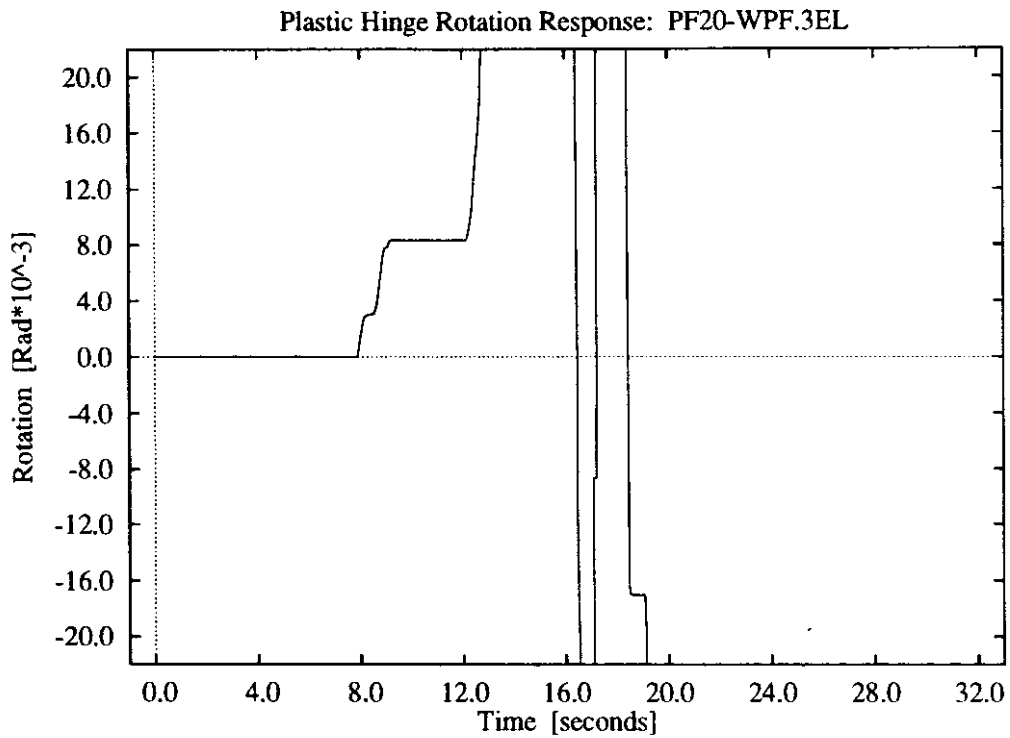
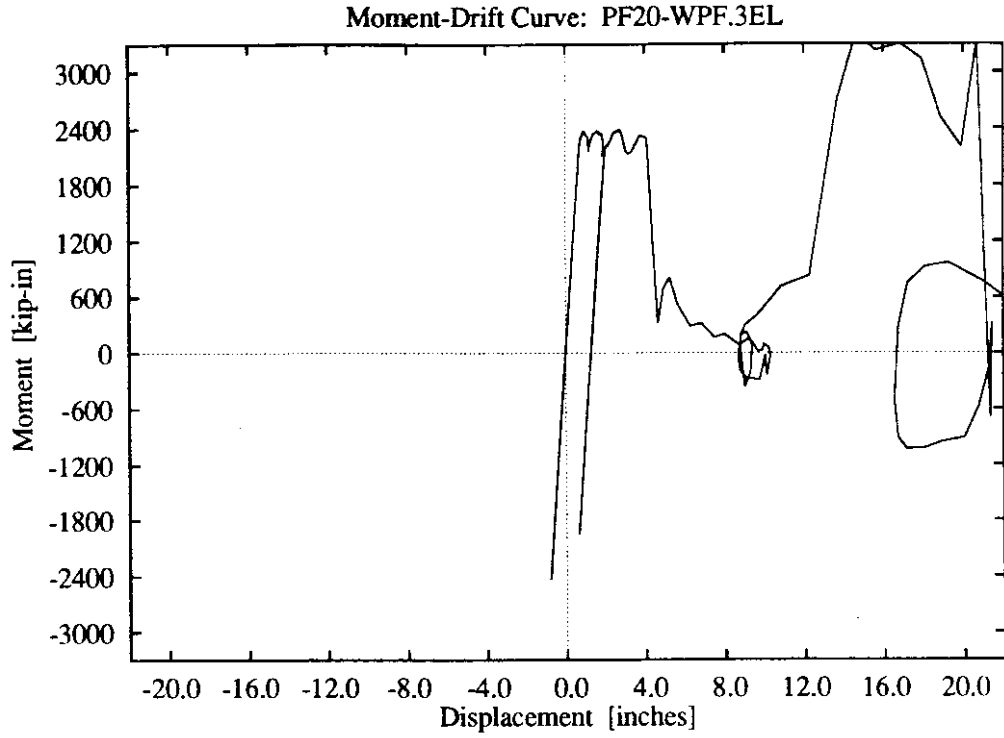


**Figure E-28:** WPF foundation model, El Centro Z3 record.



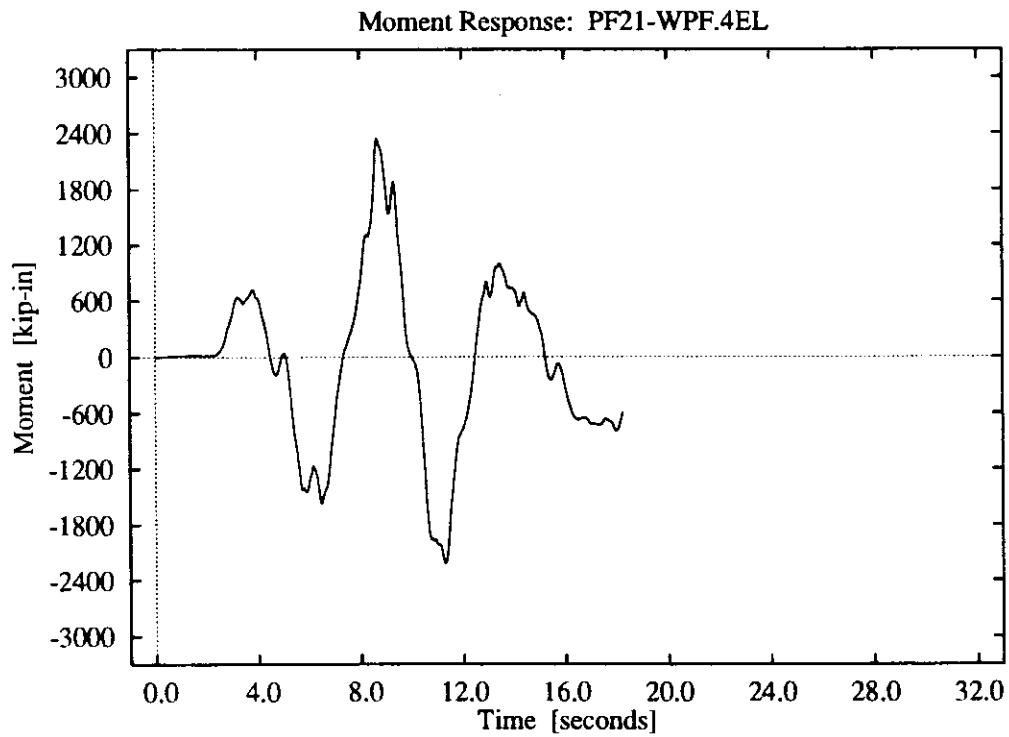
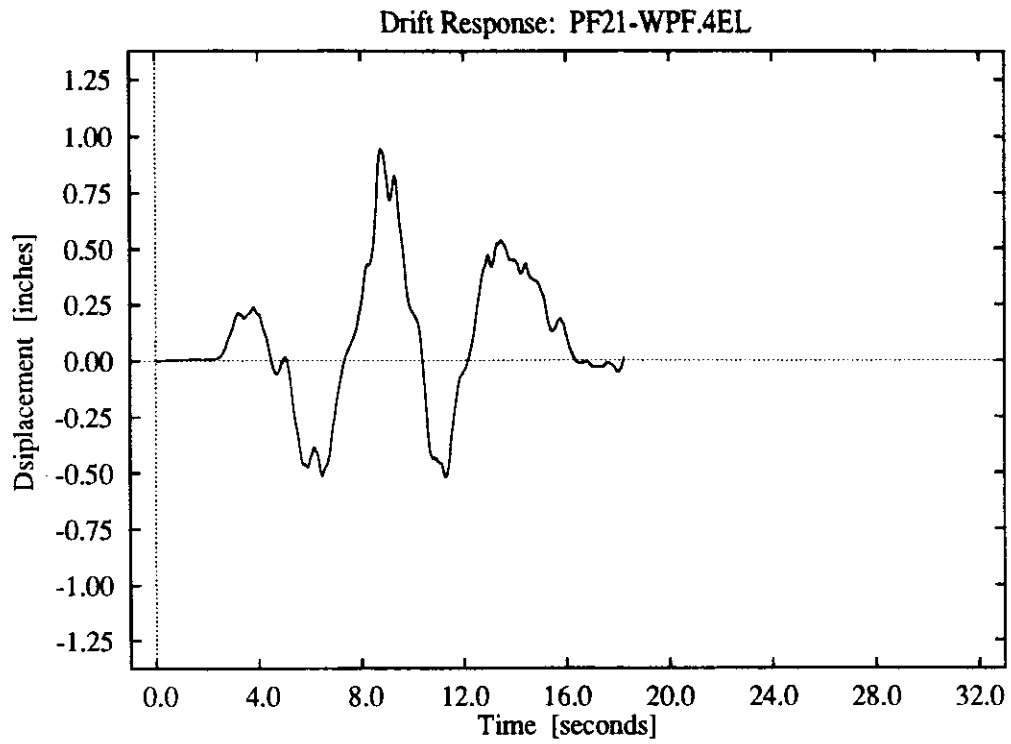


**Figure E-29:** WPF foundation model, El Centro Z4 record.

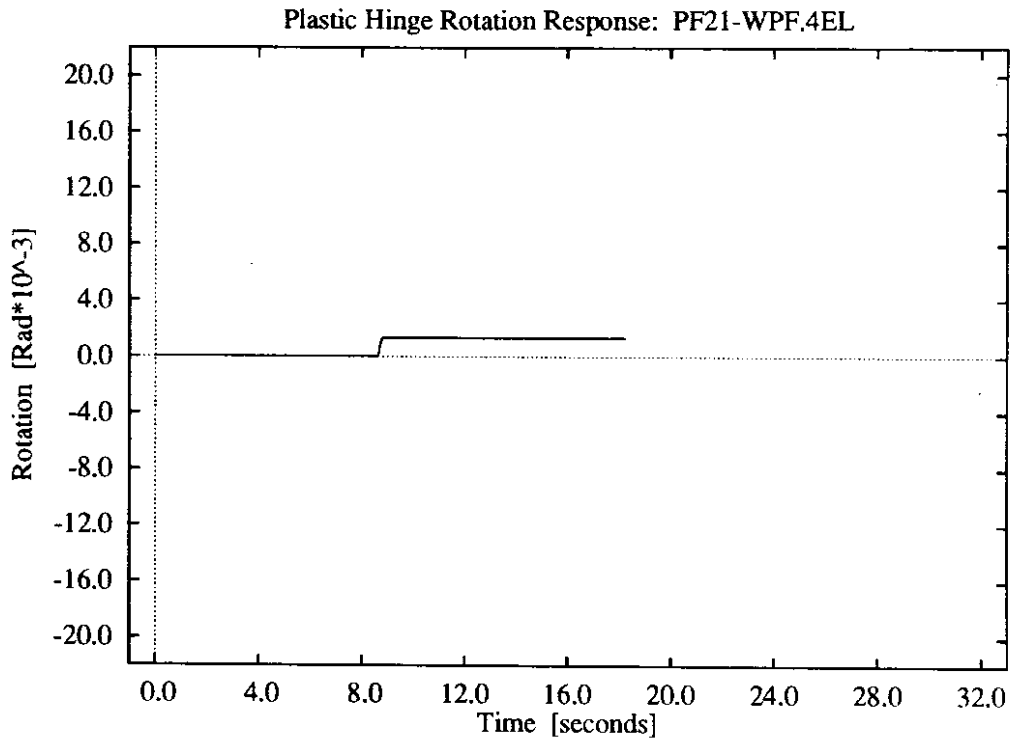
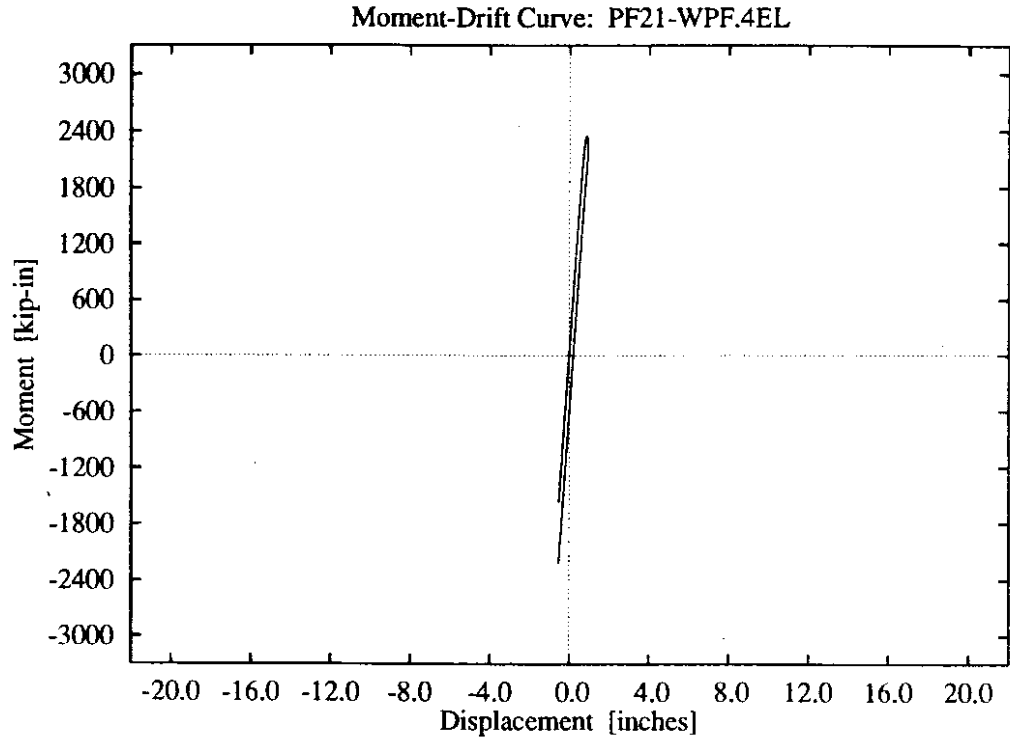


**Figure E-30:** WPF foundation model, El Centro Z4 record.

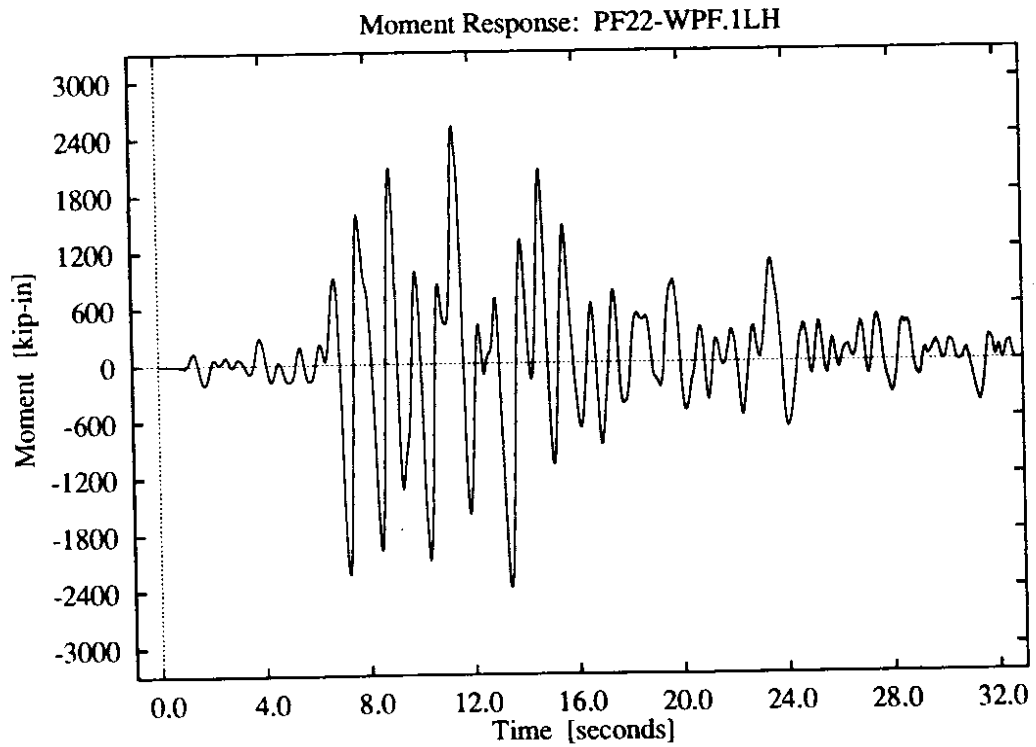
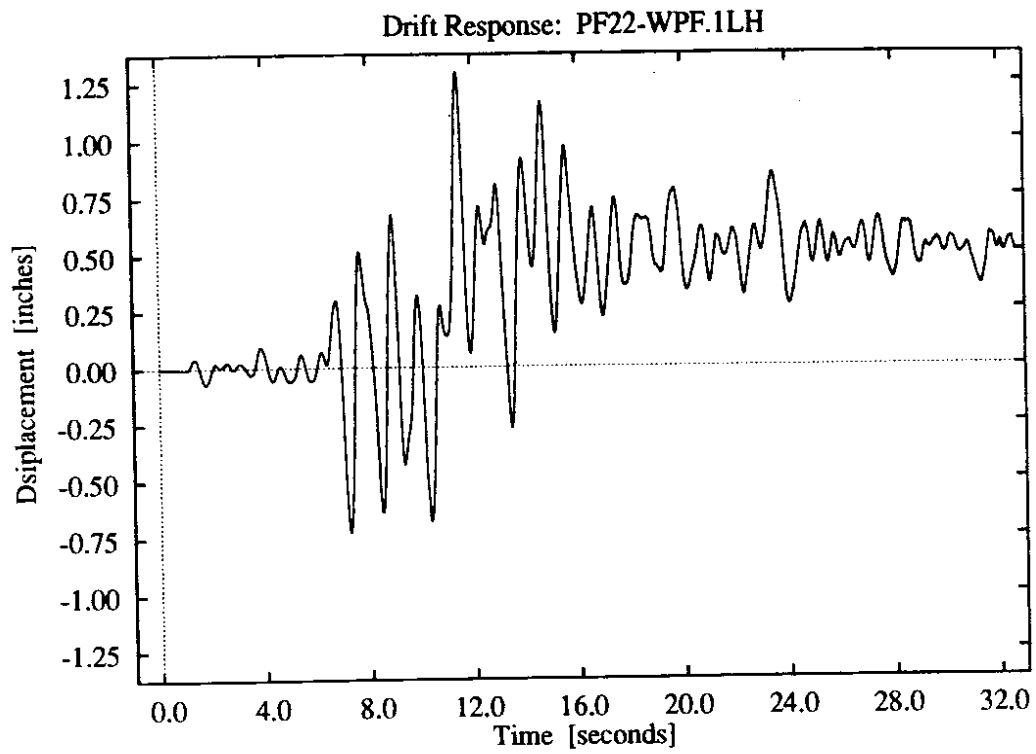


**Figure E-31: WPF foundation model, Lake Hughes Z1 record.**

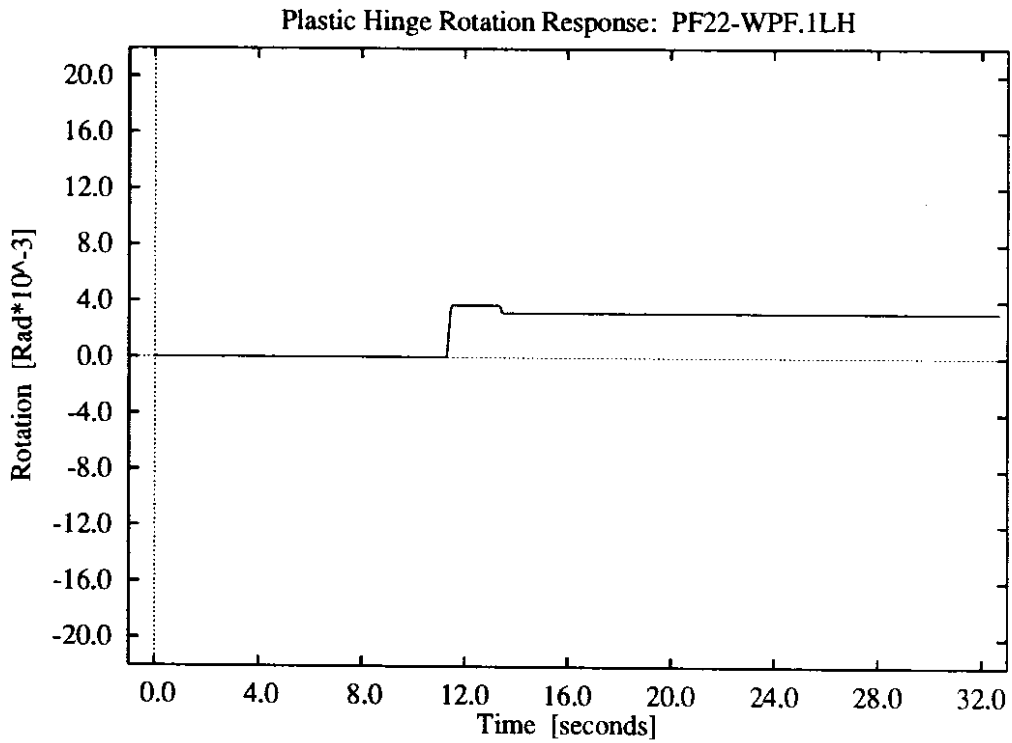
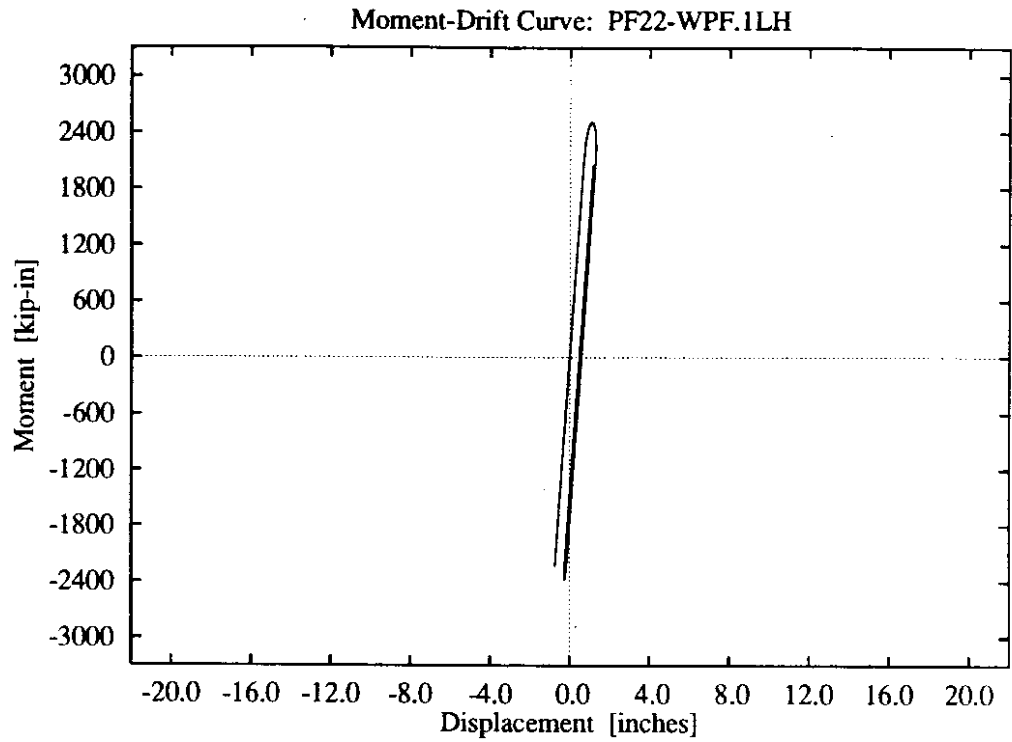


**Figure E-32:** WPF foundation model, Lake Hughes Z1 record.

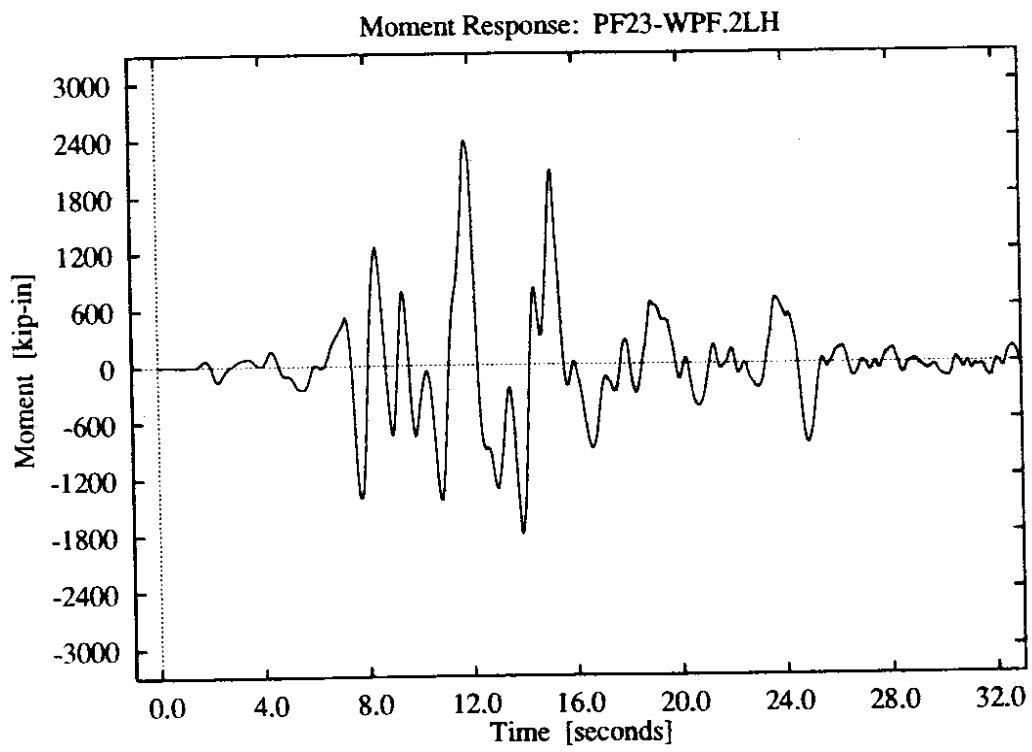
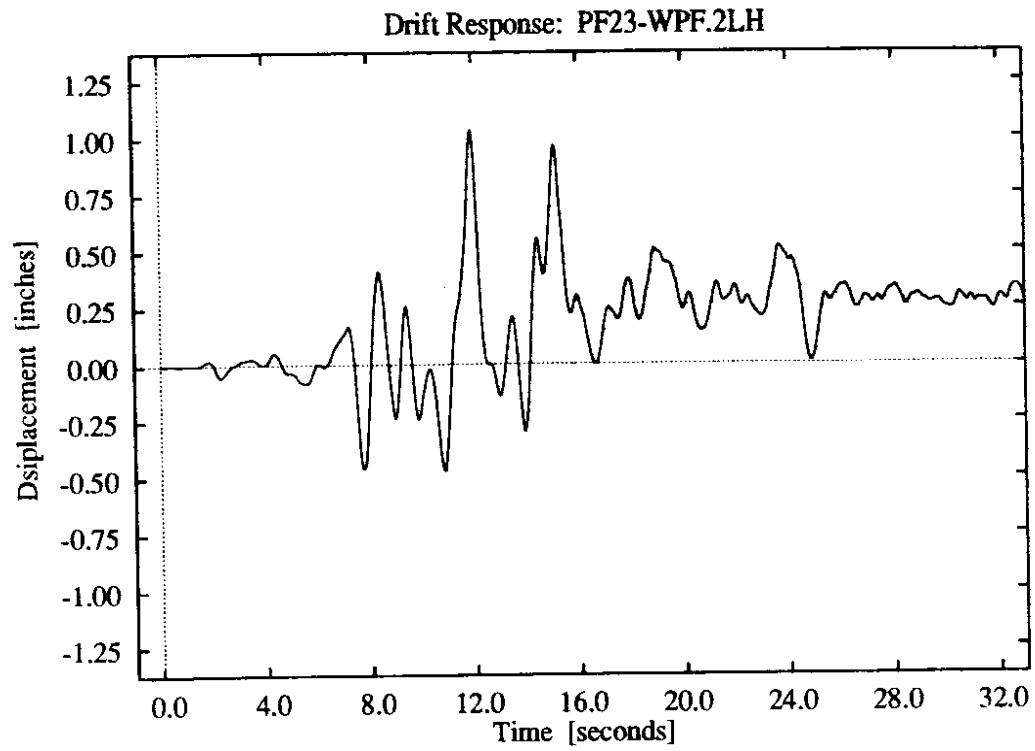


**Figure E-33: WPF foundation model, Lake Hughes Z2 record.**

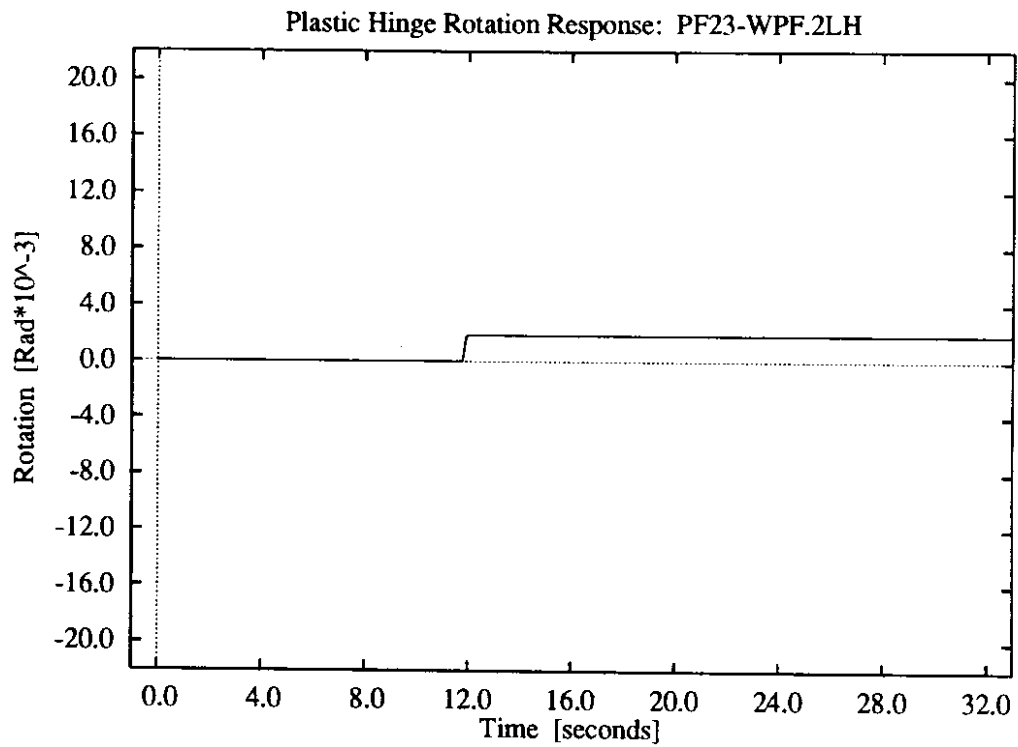
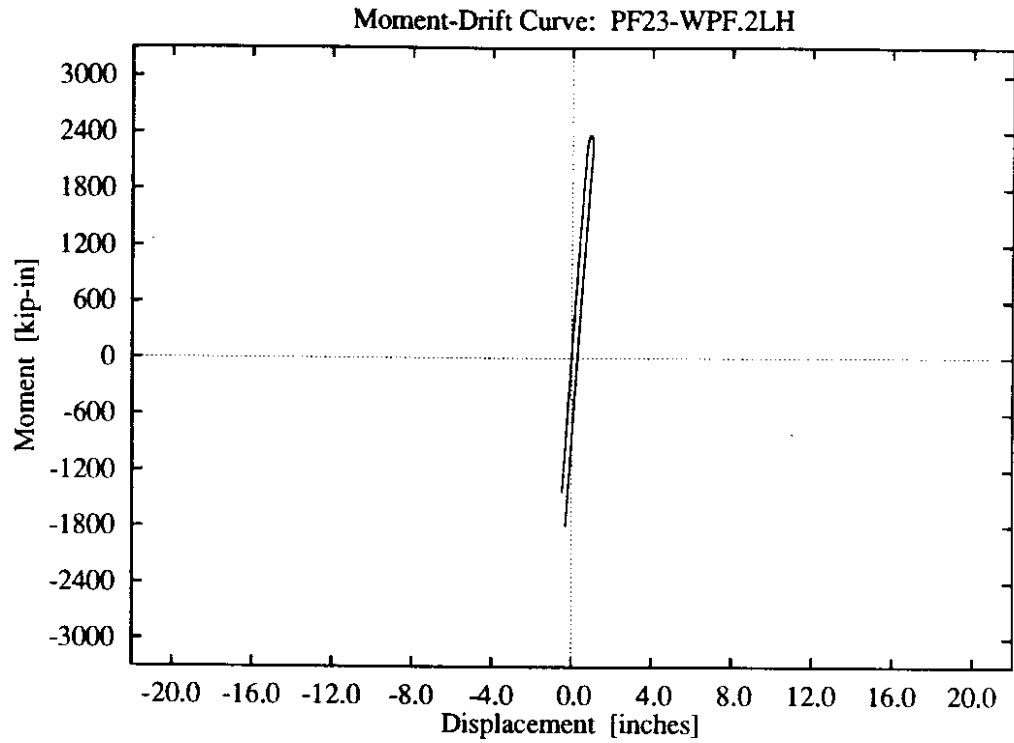


**Figure E-34:** WPF foundation model, Lake Hughes Z2 record.

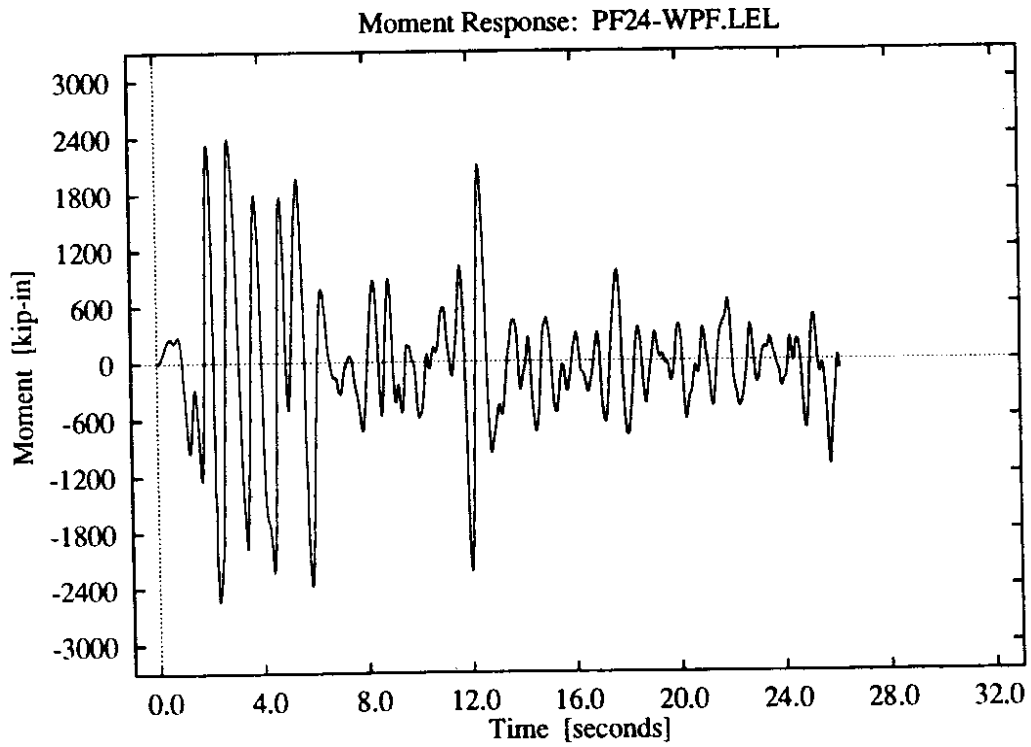
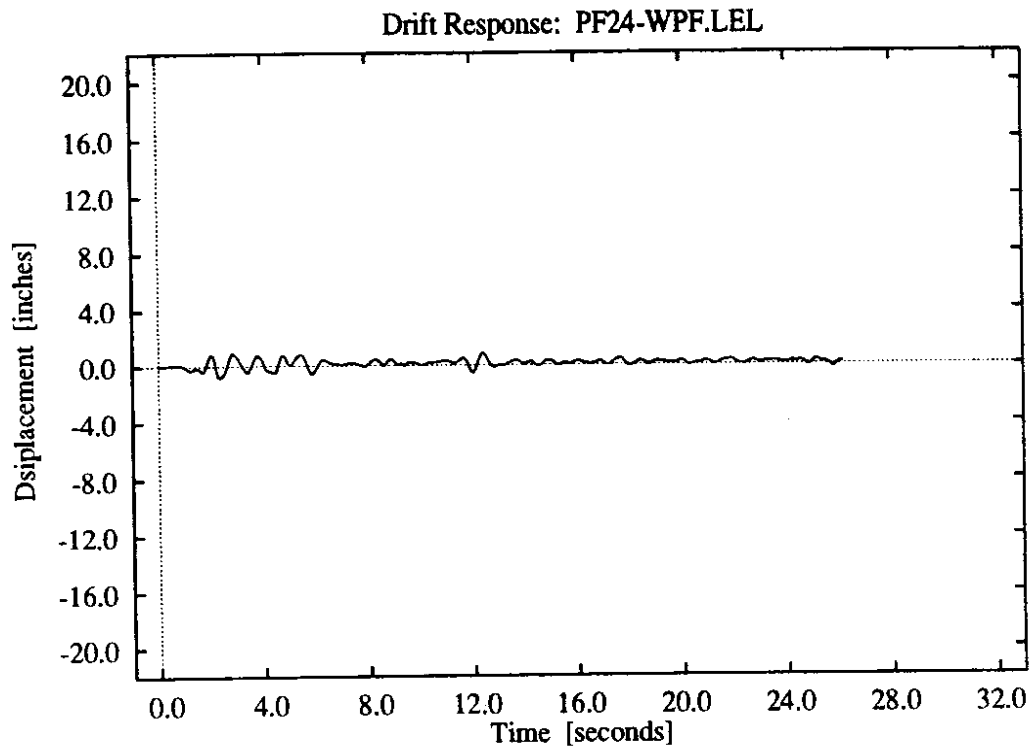


**Figure E-35:** WPF foundation model, lower intensity El Centro record.

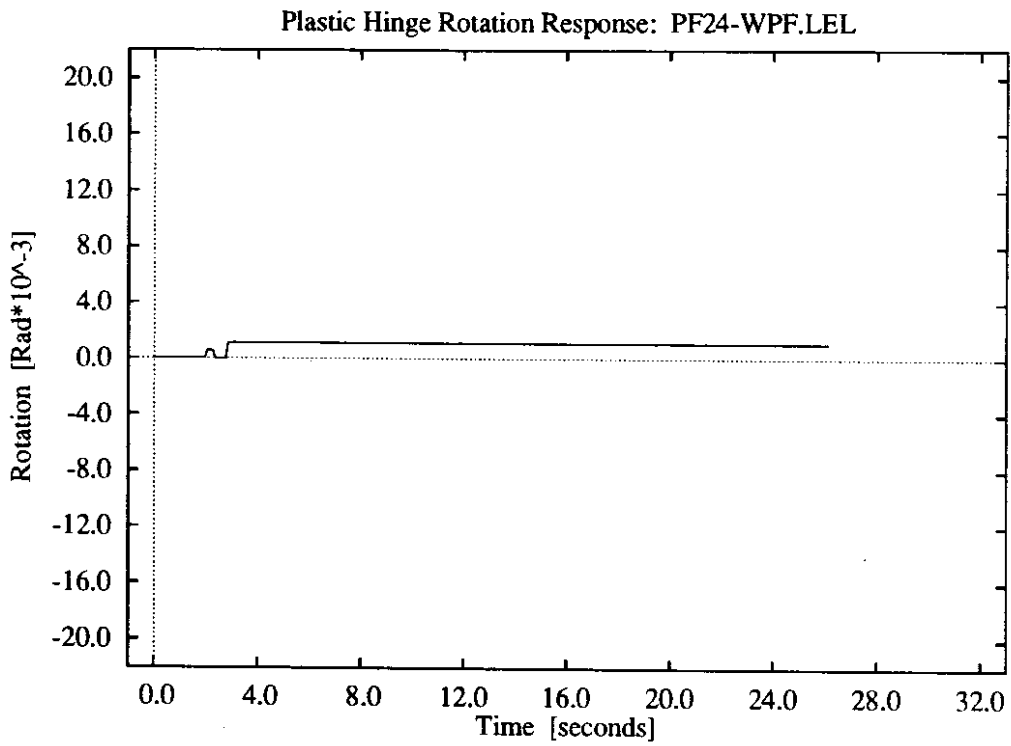
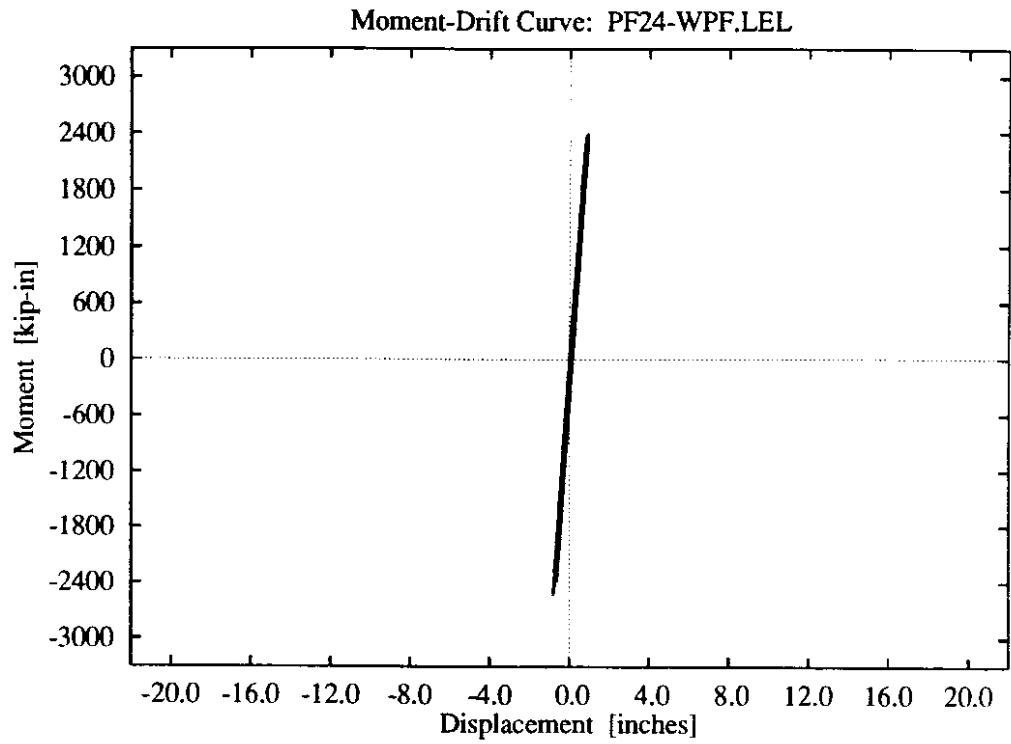


**Figure E-36:** WPF foundation model, lower intensity El Centro record.



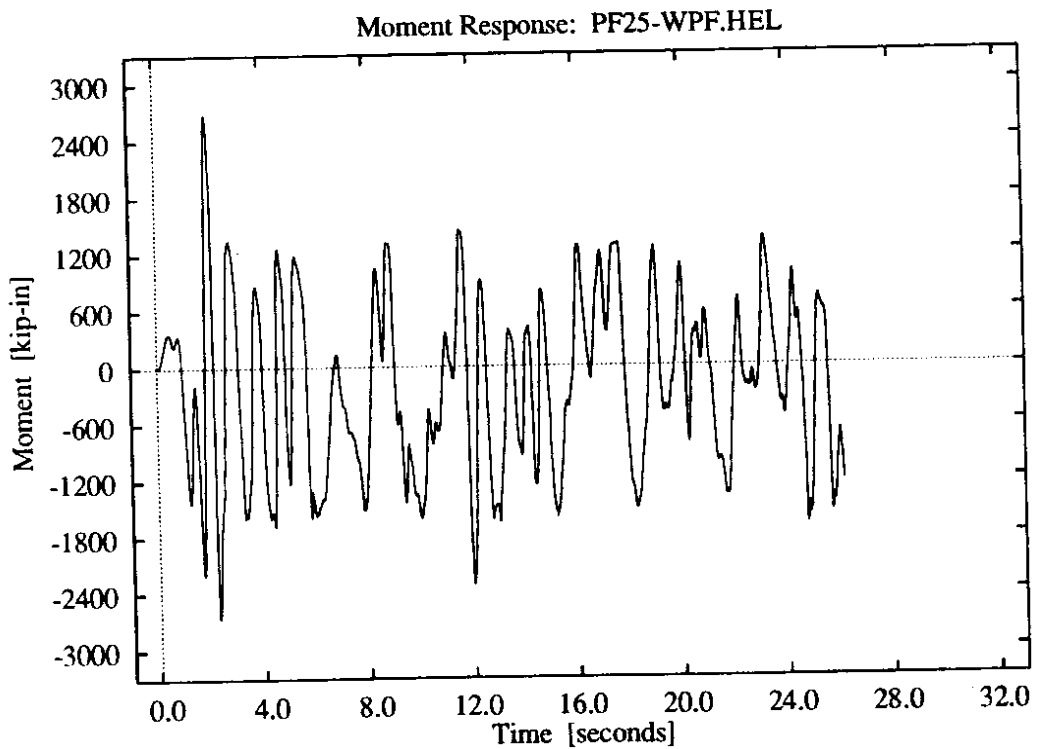
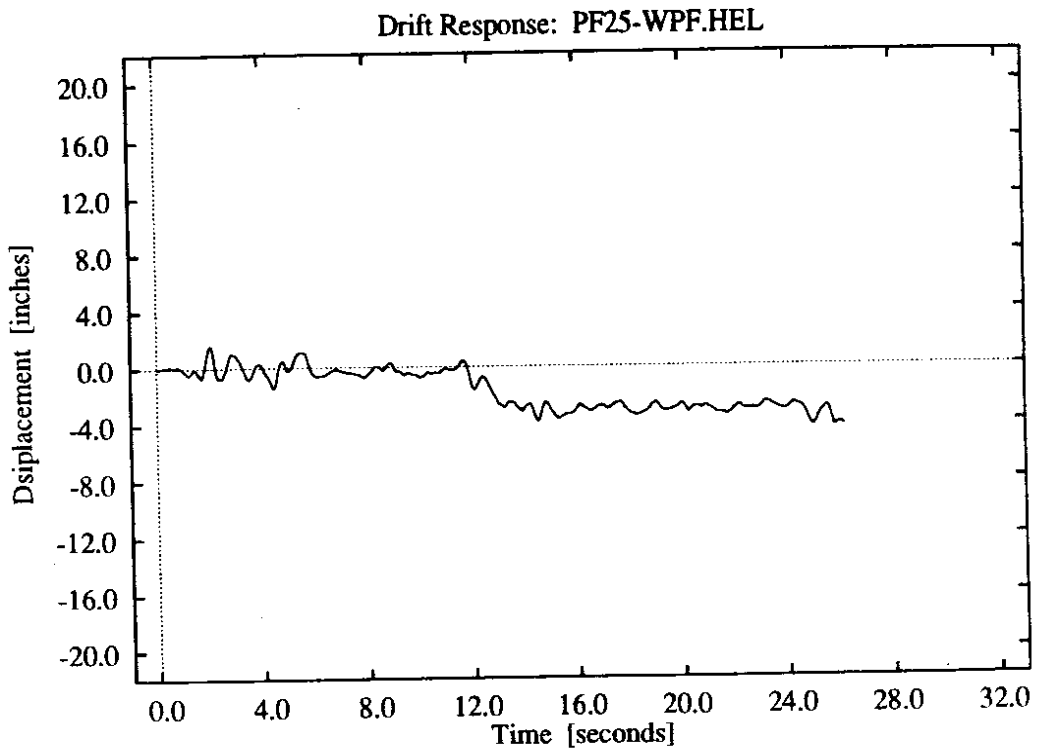


**Figure E-37:** WPF foundation model, higher intensity El Centro record.

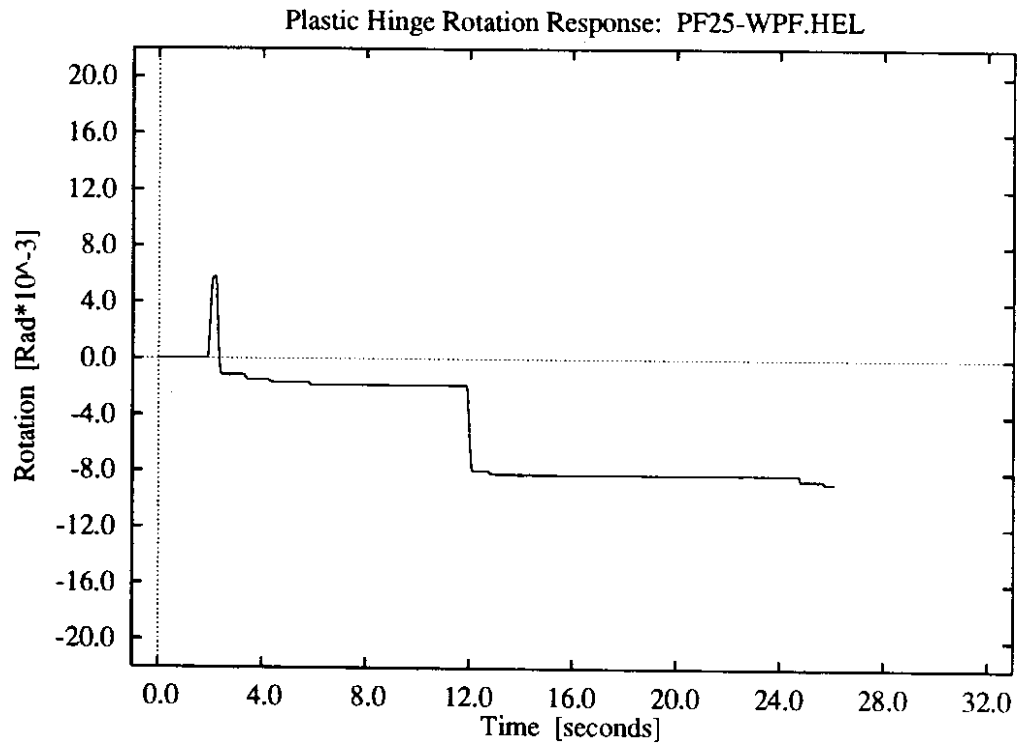
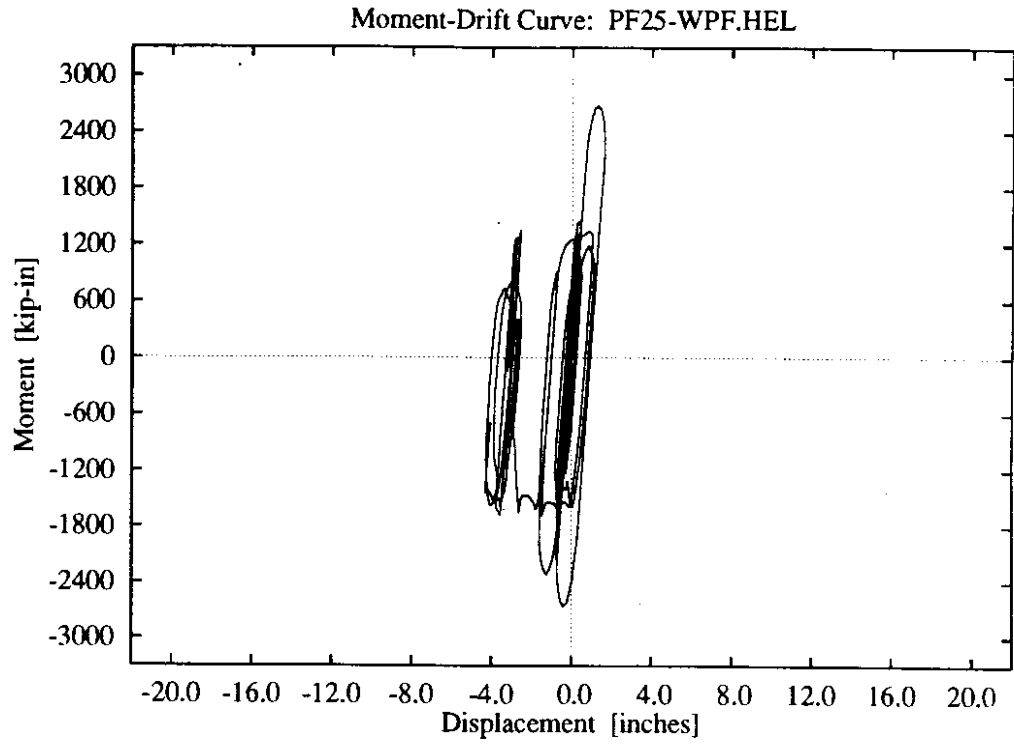


**Figure E-38:** WPF foundation model, higher intensity El Centro record.